Molecular Imaging Probes for N-Methyl-D-Aspartate Receptors

SIM, NEIL

Durham University
Department of Chemistry

Molecular Imaging Probes for *N*-Methyl-D-Aspartate Receptors

Neil Sim

A thesis submitted for the degree of Doctor of Philosophy

August 2014

Abstract

The non-invasive detection of neuronal transmission is of prime importance in order to understand brain function better. This will aid cognitive neuroscience, as well as medical science, in the early detection of diseased states. Herein, approaches to molecular imaging of the NMDA receptor, a receptor subtype of the excitatory neurotransmitter glutamate, through the use of targeted contrast agents, is described.

Initially, a series of NMDA receptor-targeted MRI contrast agents was developed based upon a known competitive NMDA receptor antagonist, appended to an *N*-linked 'Gd-DOTA' core that possesses a fast-exchanging water molecule. Their use as responsive MR imaging probes was evaluated *in vitro* using a neuronal cell line model, and three contrast agents showed large enhancements in cellular relaxation rates.

In order to confirm NMDA receptor localisation, derivatives of the lead compounds were also prepared. The derivatives contained a biotin moiety, which allowed direct visualisation of the cell-surface receptors, after addition of an AvidinAlexaFluor®-488 conjugate. Using these derivatives, the specificity and reversibility (in the presence of glutamate) of binding at the NMDA receptor was demonstrated in living cells using laser scanning confocal microscopy.

In an attempt to generate a single-component NMDA receptor-targeted optical imaging agent, a very bright europium complex conjugated to an NMDA receptor-binding moiety was synthesised. Unfortunately, upon incubation with a neuronal cell line model, complex localisation appeared to be dictated by the ligand structure and not by the receptor-binding moiety.

One emerging imaging technique with potential applications in neuronal imaging is photoacoustic imaging. Two NMDA receptor-targeted photoacoustic imaging agents were synthesised and their ability to label NMDA receptors assessed *in vitro*. Finally, preliminary *in vivo* evaluation of the most promising photoacoustic imaging agent is described.

Declaration

The research described herein was undertaken at the Department of Chemistry, Durham University between October 2011 and August 2014. All of the work is my own, except where specifically stated otherwise. No part has been previously submitted for a degree at this, or any other, university.

Statement of Copyright

Acknowledgements

I would like to begin by thanking my supervisor, Prof. David Parker, for giving me the opportunity to conduct my Ph.D within his group. His guidance and inspiration in a variety of aspects is greatly appreciated.

I would also like to extend my thanks to Dr. Anurag Mishra, for his constant ideas and enthusiasm towards the project, especially during his time in Durham.

For invaluable contributions from further afield, I would like to thank Dr. Sven Gottschalk and Dr. Jörn Engelmann.

At Durham, I would like to thank all the analytical staff and services for advice and assistance. Furthermore, I would like to thank Phil, Jeff and Tony in stores for always providing a bit of light relief from chemistry.

There are several members within the group, past and present, whom I would like to thank. First of all, Dr. Robert Pal for performing cell microscopy experiments. His intellect, persistence and enthusiasm in order to achieve the best results possible is greatly appreciated. Moreover, I recognise him as a great friend and thank him for three years of fun. Secondly, I thank Dr. Stephen Butler for making the lab an enjoyable place to work. Although he seems to keep forgetting to play golf with me, he never seems to forget any chemistry and I thank him for some invaluable advice. I would also like to thank Dr. Nicholas Evans and Dr. Bradley Waldron for keeping me company when working some weekends.

I must also mention all of my friends at home who think I work with Bunsen burners for a living. Thanks to them for always being there to give me a break from chemistry.

A very special thanks to my mum and dad, without whom, I would not be where I am today. Finally, I thank Katie for putting up with me when I've had a bad day, but more importantly, for her love.

Abbreviations

A	absorbance
Å	Ångstrom
Ac	acetate
AMPA	α-amino-3-hydroxy-5-methyl-4-isoxazole propionic acid
Ar	aromatic
ATD	amino terminal domain
ATP	adenosine triphosphate
BMS	bulk magnetic susceptibility
Boc	*tert*-butoxycarbonyl
br	broad
BSA	bovine serum albumin
°C	degrees celcius
cAMP	cyclic adenosine monophosphate
cm	centimetre
cm^{-1}	wavenumber
CN	coordination number
CNS	central nervous system
CT	computed tomography
CTD	carboy-terminal domain
cyclen	1,4,7,10-tetraazacyclododecane
d	doublet
dd	doublet of doublets
DMEM	dulbecco's modified eagle medium
DO3A	1,4,7-tris(carboxymethyl)-1,4,7,10-tetraazacyclododecane
DOTA	1,4,7,10-tetraazacyclododecane-1,4,7,10-tetraacetic acid
DTPA	Diethylenetriaminepentaacetic acid
EAAT	excitatory amino acid transporters
EC_{50}	half maximal effective concentration
ESI-MS	electrospray ionisation mass spectrometry
ε	molar extinction coefficient

FBP	folate binding protein
FPR	formyl peptide receptor
FR	folate receptor
g	gram
Glu	glutamate
h	hour
HATU	(1-[Bis(dimethylamino)methylene]-1H-1,2,3-triazolo[4,5-b]pyridinium 3-oxid hexafluorophosphate)
HBSS	hank's buffered saline solution
RP-HPLC	reverse-phase high-pressure liquid chromatography
HRMS	high resolution mass spectrometry
HSA	human serum albumin
HSQC	hetronuclear single quantum coherence
Hz	hertz
IC_{50}	half maximal inhibitory concentration
ICP-MS	Inductivley coupled plasma mass spectrometry
iGluRs	ionotropic glutamate receptors
IP_3	inositol 1,4,5-trisphosphate
IR	infrared
K	Kelvin
k_{ex}	water exchange rate
kg	kilogram
l	length
LBD	ligand binding domain
LD_{50}	half maximal lethal dose
LSCM	lasar-scanning confocal microscopy
λ	wavelength
M	molar
mg	milligram
mGluR	metabotropic glutamate receptor
mL	millilitres
mM	millimolar
mmol	millimole
MRI	magnetic resonance imaging

ms	millisecond
MSOT	multispectral optoacoustic tomography
MTT	3-(4,5-dimethylthiazol-2-yl)-2,5-diphenyltetrazolium bromide
NHS	national health service
nm	nanometre
nM	nanomolar
NMDA	*N*-methyl-D-aspartate
NMLA	*N*-methyl-L-aspartate
NMR	nuclear magnetic resonance
PET	positron emission tomography
ppb	parts per billion
ppm	parts per million
PR	progesterone receptor
PRE	proton relaxation enchancement
ps	picosecond
q	quartet
q	hydration number
QRN	glutamine-arginine-asparagine
r	relaxivity
R_1	longitudinal relaxation rate
R_2	transverse relaxation rate
$R_{1,\mathrm{cell}}$	cellular longitudinal relaxation rate
RF	radiofrequency
s	second
SAP	square antiprismatic
SPECT	single photon emission computed tomography
t	triplet
t	time
T	tesla
T_1	longitudinal relaxation time
T_2	transverse relaxation time
TIRF	total internal reflection fluorescence
TFA	trifluoroacetic acid

TLC	thin layer chromatography
TMD	trans membrane domain
TOF-MS	time of flight mass spectrometry
TSAP	twisted square antiprismatic
τ_c	effective correlation time
τ_e	electronic relaxation time
τ_m	lifetime of bound solvent
τ_R	rotational correlation time
μM	micromolar
US	ultrasound
UV-Vis	ultra-violet, visible
VGlut	vesicular glutamate transporters
9-*N*-3	triazacyclononane

Table of Contents

CHAPTER ONE

Introduction

1. Introduction

1.1 An Introduction to Molecular Imaging

Molecular imaging is defined as the non-invasive visualisation of biochemical events at the cellular and molecular level within cells, tissues or whole-bodied specimens.[1] It is one of the most rapidly expanding areas of scientific and medical research.

The beginning of molecular imaging can be traced to early nuclear medicine, whereby doctors would use hand-held Geiger counters to crudely measure the distribution of administered radionucleotides, as a method to facilitate patient diagnosis. Following this, the first instrument with the ability to capture images of different organs within the body was developed in the 1950's.[2]

Building on the advances in nuclear imaging, specifically Single Photon Emission Computed Tomography and Positron Emission Tomography (SPECT and PET, respectively), a variety of other imaging techniques has been developed, including Computed Tomography (CT), Ultrasound (US), Magnetic Resonance Imaging (MRI) and more recently Optical and Photoacoustic Imaging (*Figure 1*).[1]

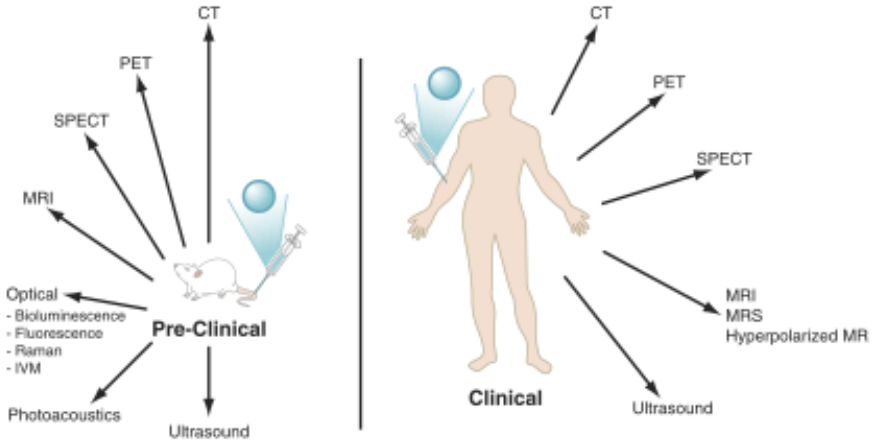

Figure 1. Key preclinical and clinical molecular imaging modalities.[1]

Historically, these methods were developed to image non-specific physiological changes. However, over the past twenty years, efforts have been made to identify specific molecular events *in vivo*, and this has led to the design and development of specific molecules, so-called contrast agents, to provide image contrast.

Labelled antibodies, peptides, proteins and small molecules have each been employed in this manner, but in general it is often difficult to obtain a large enough signal intensity change, due to the relatively low probe-target to background ratio. Furthermore, it is often the case that the target of interest is present in relatively low concentrations. Nevertheless, these issues can be overcome by improving the contrast agent's pharmacokinetics and affinity, coupled with the use of rapid and sensitive, high-resolution imaging techniques.

The selection of a particular molecular imaging modality is highly dependent upon the biochemical process that is to be visualised, and exactly what information is needed. The factors that need to be addressed include:

- The spatial resolution required;
- the sensitivity required i.e. the likely concentration of your target;
- whether dynamic information is needed;
- whether whole body or regional imaging is required;
- the temporal resolution;
- the depth of penetration needed.

By addressing these issues, it is possible to decide which is the best imaging technique to use.

The work carried out in this thesis describes the use of three molecular imaging modalities: magnetic resonance, optical and photoacoustic imaging to visualise a subclass of glutamate receptors, which are abundantly present in the brain. Glutamate is the most abundant excitatory neurotransmitter and activation of its receptors plays key roles in normal brain function. However, mis-regulation and overstimulation of receptors can often lead to cell death and disease.

The remainder of this chapter will focus on the role of glutamate as a neurotransmitter, including a description of its receptors, followed by a review of the use of targeted MRI contrast agents to image intra-and extra-cellular receptors.

1.2 Glutamate as a Neurotransmitter

Every organism relies on the transfer of chemical signals in order to function. The ability of glutamate to act as a chemical stimulant for neurons was first

demonstrated in 1960.[3] Due to its ability to activate nearly all neurons, many people were sceptical as to whether glutamate behaved as a specific neurotransmitter. But now, it is correctly regarded as the most abundant excitatory neurotransmitter in the mammalian central nervous system, with concentrations between 5-15 mmol/kg found in brain tissue.[4] Such a high concentration of glutamate means that approximately 90% of all neurons in the brain use glutamate as their neurotransmitter, with the concentration of cytoplasmic neuronal glutamate typically between 5-10 mM.[5]

Glutamate is unable to penetrate the blood brain barrier and is thus synthesised in neuronal mitochondria, via the transamination of α-ketoglutarate produced in the Krebs cycle from citrate. Glutamate then diffuses into the cytosol and is stored, at high concentration, in vesicles.[6, 7] Changes in cytosolic calcium levels, in response to an action potential, trigger the vesicles to fuse with the plasma membrane and release glutamate into the synaptic cleft. Glutamate actively diffuses across the synapse to interact with receptor proteins localised on the post-synaptic membrane, allowing transfer of the glutamatergic signals from pre- to post-synaptic cells (*Figure 1.1*).

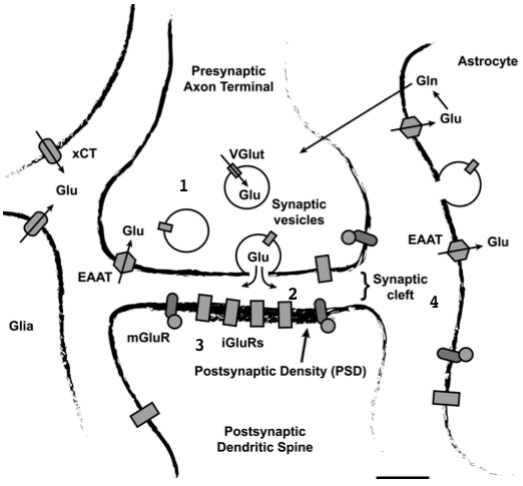

Figure 1.1. An atypical glutamatergic synapse. (1) Glutamate is synthesised in the mitochondria, stored in vesicles and pumped into the extracellular space upon vesicular fusion. (2) An increase in synaptic glutamate concentration is observed. (3) Glutamate diffuses and binds to receptors located on the post-synaptic membrane. (4) After signal transduction, glutamate is removed from synapse by EAATs.[8]

Glutamate does not undergo any metabolic transformation in the extracellular space and so is removed by excitatory amino acid transporters (EAAT's), which pump the glutamate into nearby astrocytes. The glutamate is converted into glutamine, exported back into the extracellular space and taken up by neurons. The glutamine is converted back to glutamate, which is again stored in the presynaptic vesicles.[8]

Despite synaptic transmission leading to a high local concentration of extracellular glutamate (0.5-5 mM), this local increase is transient and only present for a few milliseconds. The major source of extracellular glutamate is nonvesicular in nature and comes from neighbouring glia, giving rise to a steady background concentration of glutamate, of between 1-5 μM.[9] Given the difference in concentration between background and synaptic glutamate, it would seem reasonable to suggest that background glutamate has a negligible effect on the brain. However, changes in the concentration of this ambient extracellular glutamate have been associated with developmental, physiological and behavioural disorders.[9-11]

1.2.1 Glutamate Receptor Proteins

Located within the central nervous system are glutamate receptor proteins, which bind synaptic glutamate and conduct the transfer of glutamatergic signals. There are two categories of glutamate receptor; ligand-gated ionotropic receptors (iGluR's) and G-protein coupled metabotropic receptors (mGluR's). The iGluR family is classified into three subtypes: *N*-methyl-D-Aspartate (NMDA), α-amino-3-hydroxyl-5-methyl-4-isoazole-propionate (AMPA) and Kainate receptors. Similarly, the mGluR family is also divided into three groups, groups I-III, which possess the eight different mGluRs ($mGluR_{1-8}$) (*Figure 1.2*).[12]

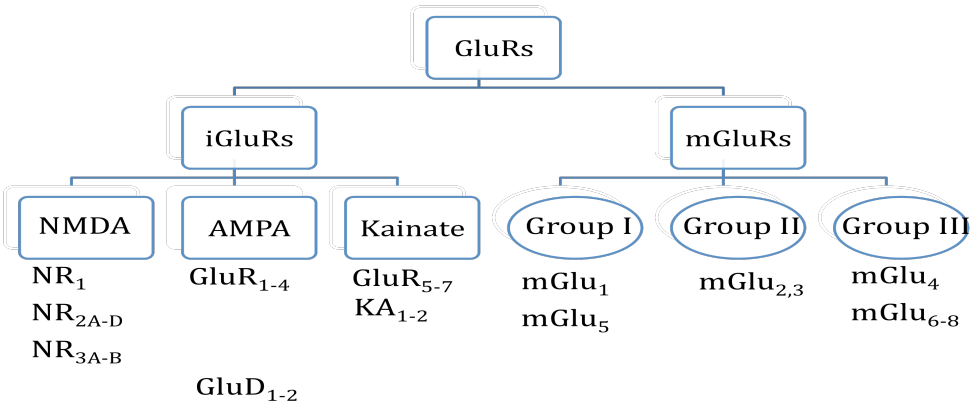

Figure 1.2. Classification of the glutamate receptor family.

The mGluRs play a modulatory role, regulating slow neuronal excitability and synaptic transmission through secondary messengers.[13] The mGluRs are classified into three groups according to their amino acid sequence, agonist pharmacology, and most importantly, their secondary messenger transduction pathways. Group I mGluRs couple via G_q/G_{11} to stimulate phospholipase C activity and increase the concentration of intracellular Ca^{2+}. Group II and group III mGluRs are linked via G_i/G_o to inhibit adenylate cyclase activity, slowing the conversion of ATP to cAMP and pyrophosphate.[4, 13, 14]

In common with other G-protein coupled receptors, the mGluRs comprise a large bi-lobed extracellular amino-termial domain (ATD), linked to a heptahelical transmembrane domain (TMD) and finally the intracellular *C*-terminus (CTD). Glutamate binds at the agonist-binding site in the ATD[15] whereas receptor activity is mediated at the CTD, through interaction with intracellular proteins.[16]

The mGluRs are expressed on both pre- and post-synaptic membranes, as well as neighbouring glial cells, with different group members exhibiting a distinct spatial distribution within the central nervous system. Group I mGluRs are predominantly located on the post-synaptic membrane, modulating the cells' synaptic sensitivity towards glutamate. In comparison, group II and group III mGluRs are pre-synaptic receptors that mediate glutamate release.[17-19] It should also be noted that $mGluR_6$ is the only receptor not located in the CNS, but is found in high density in the retina.[20]

Unlike the mGluR family, the iGluRs are responsible for the majority of fast excitatory neurotransmission in the brain.[12] The iGluR family of receptors comprises the NMDA, AMPA or Kainate receptors, which are grouped based on

their affinity for selective agonists, amino acid sequence and electrophysiological properties. There are a total of 18 different gene products (NR1, NR2A-D, NR3A-B, GluR1-4, GluR5-7, KA1-2 and GluD1-2), which give rise to a large degree of variation between ion channels.[21] Despite this, there are still similarities between every iGluR.

Each iGluR is a tetrameric complex, comprising more than one subunit to give rise to a central ion pore. A feature of the iGluRs is that different subunit combinations produce functionally different receptors. For example, all iGluRs transmit their currents using a variety of cations (K^+, Na^+ and Ca^{2+}).[22] Cation permeability is subunit specific in the AMPA and Kainate receptors, whereby the presence of the GluR2, GluK1 and GluK2 subunits renders the receptors impermeable to Ca^{2+}.[23, 24] A regional difference in expression of subunits illustrates the heterogenicity of the iGluRs, supporting the existence of multiple subtypes of NMDA, AMPA and Kainate receptors.[4]

A functional iGluR subunit comprises four main domains; the extracellular amino terminal domain (ATD), the extracellular ligand binding domain (LBD), the transmembrane domain (TMD) and an intracellular C-terminal domain (CTD) (*Figure 1.3*).

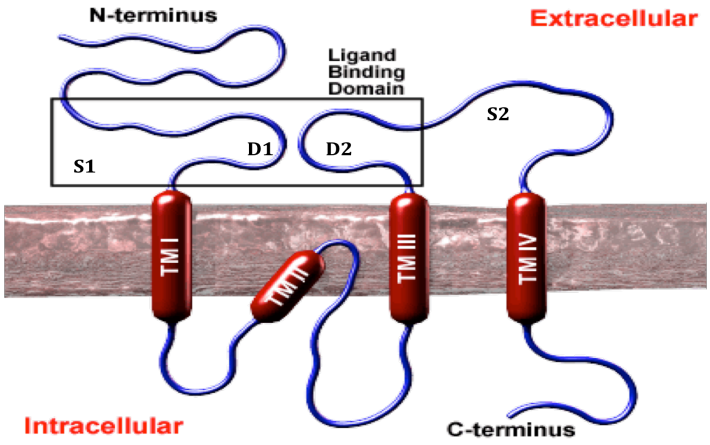

Figure 1.3. The general structure of an iGluR subunit.[25]

The ATD of iGluRs adopts a clamshell-like structure resembling that of the LBD of $mGluR_1$.[26] This suggests that the ATD could provide a secondary binding pocket for endogenous ligands. Indeed, this is the case for NMDA receptors.

However, no ions or small molecules are known to bind to the ATD of AMPA or Kainate receptors.[22]

Pore opening, deactivation and desensitisation of the receptor and regulation of subunit specific assembly are all dictated by the ATD.[27-30] Such behaviour is consistent with the observation that glycosylation of the ATD of AMPA and Kainate receptors leads to desensitisation and a drop in transduction current.[31]

Similar to the ATD, the LBD of iGluRs also adopt a clamshell-like conformation and is formed from two extracellular peptide strands, S1 and S2.[32] The cleft between these two peptide chains (D1 and D2) forms the agonist-binding pocket. The first step in activation of the iGluRs involves agonist binding, and this occurs when the α-amino and α-carboxylate fragments of the agonist interact with residues located inside D1. The residues responsible for binding these fragments of the agonist are fairly conserved throughout all iGluRs, with intrinsic selectivity for specific agonists towards a particular receptor gained from additional agonist functionalisation.[22]

The activation of iGluRs involves a conformational change in the LBD. Agonist binding induces a transition in the D2 lobes causing a rearrangement in the segments linking the ion-channel (TMD) to the LBD, resulting in channel opening (*Figure 1.4*).[33]

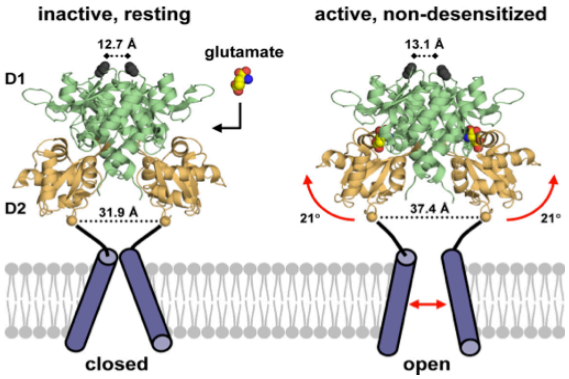

Figure 1.4. Conformational changes associated with activation of a functional AMPA receptor.[22]

The LBD is connected to three trans-membrane helices, M1, M3 and M4, which form the core of the ion channel. The M2-loop lines the inner cavity of the pore with M1 lining the outer cavity. It is generally thought that the presence of M1

and M2 form the gating mechanism that obstructs the flux of ions when the channel is closed.[22]

The intracellular CTD is the most diverse region of iGluR subunits, and very little is known about the structures between different subunits. Although the CTD is not essential for iGluR function, it is an important feature known to bind and interact with many intracellular proteins[34, 35] in order to modulate receptor signalling.

The three different iGluRs all have different functions and spatial locations. The AMPA receptors are located post-synaptically and are responsible for most of the fast excitatory information transfer in the CNS, with desensitisation of the receptor occurring around 1-2 ms after glutamate binding.[36, 37] Similarly, NMDA receptors are also post-synaptic receptors, but stay open for longer time periods then AMPA receptors, to allow for significant Ca^{2+} influx. However, Kainate receptors are located on both pre- and post-synaptic neurons, typically activated after only short bursts of pre-synaptic activity. In a similar manner to mGluRs, Kainate receptors serve to regulate vesicle formation and glutamate release.[38]

1.2.2 The NMDA Receptor: Structure, Function and Ligands

The NMDA receptor is the most characterised example within the iGluR family. Similar to the other iGluRs, the NMDA receptor is a tetrameric complex, composed of four of the possible seven subunits. The most common architecture consists of two GluN1 and two GluN2 subunits, organised as a dimer of dimers with an alternating pattern. The GluN1 and GluN2 subunits share a common topology with the other iGluRs, consisting of an extracellular ATD, an extracellular LBD, a TMD and an intracellular CTD.[39]

The NMDA receptor is a structurally more complex receptor ion channel compared to the AMPA and Kainate receptors, and possesses a variety of different ligand binding sites within its subunits (*Figure 1.5*).

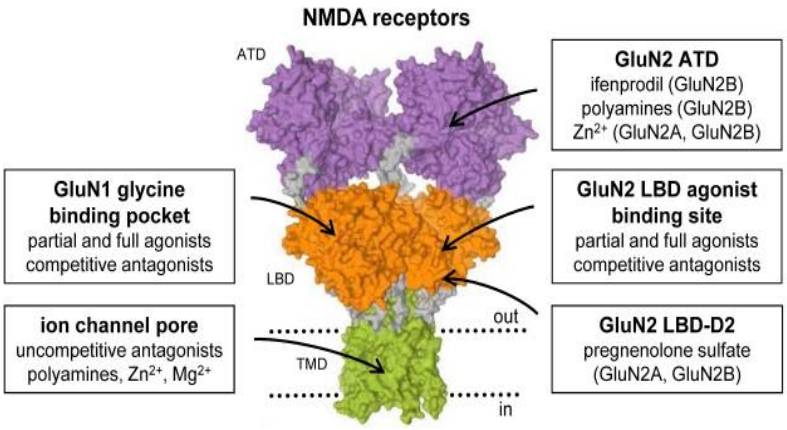

Figure 1.5. Locations of the various binding sites present on NMDA receptors.[22]

The ATD of GluN2 subunits contain binding sites for a variety of small molecules and ions. Divalent zinc ions have been shown to act as negative allosteric modulators by coordinating with high affinity (IC_{50} 10-30 nM), in a non-voltage dependent manner, to histidine and glutamic acid residues.[22] Coordination of Zn^{2+} is proposed to involve closure of the ATD, which destabilises the dimer interface of the LBD, leading to a decrease in glutamate affinity.[33]

Also present in the ATD are specific binding sites for polyamines and ifenprodil-like compounds. Ifenprodil and its higher affinity derivatives, which have increased subunit selectivity, are an important class of compounds currently providing preclinical data regarding the role of the GluN2B subunit in neuropathic pain and excitotoxicity.[40] These compounds are another class of negative allosteric modulators, which bind with a high affinity (150 nM) at an exclusive site on the ATD.[41] Ifenprodil binds at the interface between GluN1 and GluN2B subunit ATD dimers. The subunit selectivity for ifenprodil, over other iGluR ATD's, arises from the ability of the NMDA receptor subunits to form heterodimeric assemblies, with a slightly different orientation to the homodimers observed in other iGluR assemblies. The ifenprodil-binding site is buried deep within the interface (*Figure 1.6*), suggesting an induced-fit mechanism of binding, with dissociation likely to involve opening of the GluN2B ATD bi-lobed structure.[42]

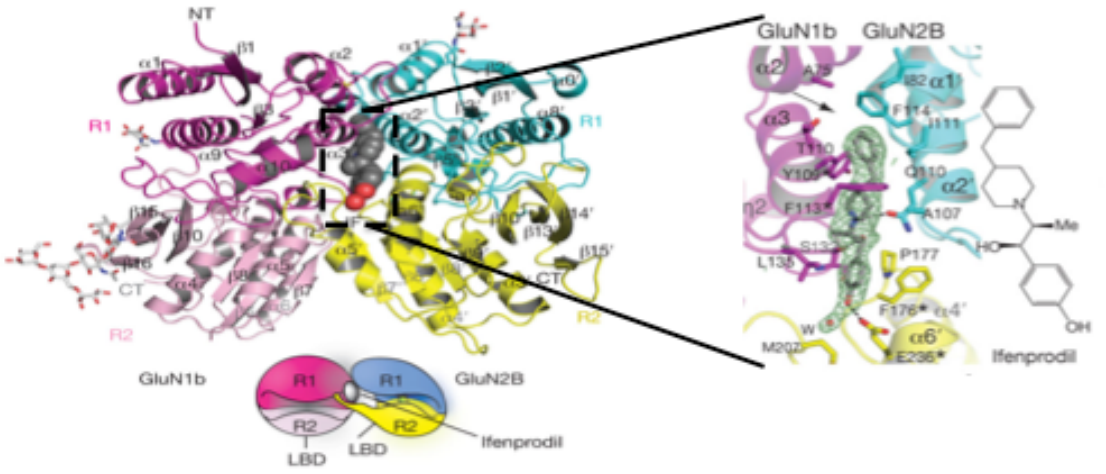

Figure 1.6. Crystal structure of the GluN1-GluN2B ATD in complex with ifenprodil, with an expansion of the phenylethanolamine-binding site.[42]

Polyamines such as spermine and spermidine act as positive allosteric modulators that can potentiate in either a glycine-independent or glycine-dependent manner. Glycine-independent potentiation occurs only for the GluN2B subunit in saturating glycine conditions. NMDA receptors are approximately 50% inhibited by protons at physiological pH, but polyamine binding can lead to a relief of this proton inhibition.[43] In contrast, the glycine-dependant mechanism involves the GluN2A-B subunits and potentiates via an enhancement of glycine binding.[44]

The NMDA receptor differs from other iGluRs in that it requires two separate ligands to bind simultaneously to the LBD for activation. Glutamate acts as the primary agonist and binds to the GluN2 subunit, whereas glycine is a co-agonist, binding at the LBD on GluN1 subunits.

The glutamate binding site is highly conserved between all GluN2 subunits, but differs between iGluRs. The α-carboxylate of glutamate interacts with an aspartate residue in a similar manner to the other iGluRs. A glutamate residue present in the agonist-binding site of AMPA and Kainate receptors is responsible for direct interaction with the α-amino group on the agonist. However, it is replaced by aspartate731 in NMDA receptors and the loss of the additional methylene group results in the α-amino group of glutamate being unable to form a direct ionic interaction. Instead, the α-amino group forms water-mediated hydrogen bonds to glutamate413 and tyrosine761, with displacement of the

water molecule accounting for the selectivity for NMDA binding to the GluN2 subunit. The γ-carboxylate of glutamate binds with tyrosine730, a residue conserved in GluN2 subunits, and this interaction coupled with an inter-domain hydrogen bond between tyrosine730 and glutamate413 is responsible for the high affinity binding of glutamate to the NMDA receptor (*Figure 1.7*).[45]

Glycine acts as the co-agonist and binds at the cleft between D1 and D2 domains in the GluN1 subunit. The carboxylate of glycine forms several hydrogen bonds to arginine522, threonine518 and serine688 and the amino group interacts with the carbonyl group of proline516, the carboxylate of aspartate732 and the hydroxyl of threonine518 (*Figure 1.7*).[46]

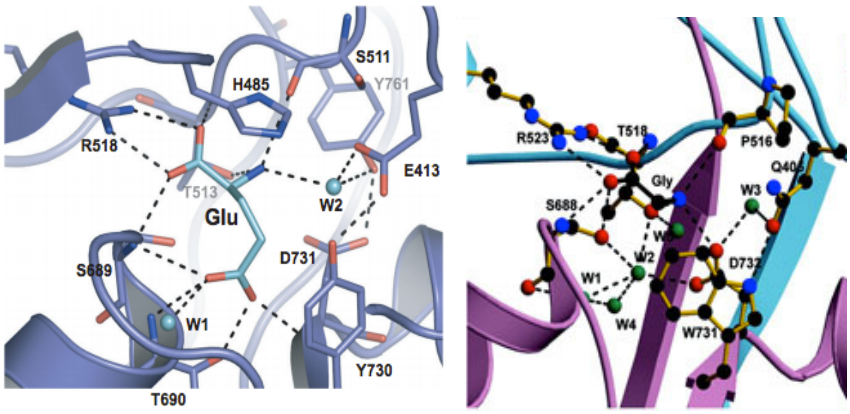

Figure 1.7. The structure of the agonist binding sites on GluN2A (*left*)[45] and GluN1 (*right*)[46] subunits.

The agonist-binding site in the GluN1 subunit shows high selectivity for glycine over glutamate due to two factors. First, the presence of tryptophan731 in GluN1 subunits increases the steric demand around the region where the γ-carboxylate of glutamate would potentially bind. Secondly, replacement of threonine690 by valine689 in GluN1 subunits leads to a loss of a hydrogen-bond donor, again destabilising γ-carboxylate binding.[46]

The TMD in NMDA receptors is structurally related to TMDs found in other iGluRs. The subtle difference is substitution of a key amino acid residue found in the re-entrant loop, M2. This region is called the QRN site as it is occupied by an asparagine (N) residue in GluN2 NMDA receptor subunits, and a glutamine (Q) or arginine (R) residue in non-NMDA receptors.[47] In NMDA receptors, the QRN site

is the home of the voltage-dependent Mg^{2+} block. At membrane potentials around -50 mV, the concentration of extracellular Mg^{2+} is sufficiently high to block NMDA receptor ion transport, despite the presence of glutamate and glycine 'activating' the neuron. However, as the membrane potential increases towards +40 mV, the affinity for the QRN site to bind Mg^{2+} decreases and the block becomes ineffective, allowing the influx of ions through the channel.[39, 48]

Activation of the NMDA receptor occurs when glutamate, released from the pre-synaptic neuron, and glycine bind at the GluN1 and GluN2 subunits simultaneously. Binding of these agonists induces a conformational change, such that the LBD adopts a closed conformation. Meanwhile, synaptically released glutamate also activates AMPA receptors on the post-synaptic neuron, which allows the flux of Na^{+} ions through the channel, depolarising the membrane. Concurrent membrane depolarisation and the change in conformation of the LBD induces opening of the NMDA receptor ion channel and relief of the voltage dependent Mg^{2+} blockade. Na^{+} and K^{+} ions flow into and out of the cell, respectively, through the NMDA receptor ion channel generating a short-lived excitatory post-synaptic potential. Ca^{2+} ions also permeate the ion channel to induce a long-lasting signal transmission enhancement, thought to be linked to synaptic plasticity, which underlies memory and learning. However, excessive Ca^{2+} transport also has an excitotoxic effect leading to neurodegradation.[39]

In contrast to other iGluRs, the NMDA receptor shows much slower gating kinetics, activating in milliseconds and deactivating over much longer periods, i.e. seconds, with little or no desensitisation. The kinetics of gating determines the time course of synaptic currents produced by the receptor and differs between each NMDA receptor subunit (*Table 1*).[22]

Table 1. Kinetic parameters describing glutamate activation of NMDA receptors.

	Deactivation/ ms [a,b]	**Desensitisation/ ms**	**Recovery/ ms**	**Open Time/ ms**
N1/N2A	22-230	386-750	618	1.3
N1/N2B	538-617	100	1014-2100	2-3.2
N1/N2C	260-382	59-719	NA	0.6
N1/N2D	1700-4408	NA	NA	0.9-2.6

[a] average AMPA deactivation time is 0.7 ms, [b] average Kainate deactivation time is 1.6-2.5 ms.

The long deactivation time course for NMDA receptors is a direct result of its increased affinity for glutamate, relative to other iGluRs.

1.2.2.1 Glutamate Binding-Site Ligands for the NMDA Receptor

Although it has been proposed that increasing the activity of the NMDA receptor can improve neurodegenerative disorders, over-stimulation of the receptor has a related high excitotoxicity. This has led to the development of a range of NMDA receptor agonists and antagonists that could potentially serve as therapeutic agents against neurodegredation.

Upon complexation of an agonist, the LBD undergoes a conformational switch to a closed state around the ligand, leading to channel opening. This means that the ligand is surrounded by the LBD, leaving little or no conformational freedom that could be exploited in the design of new agonist structures. Therefore, NMDA receptor agonists are generally α-amino acids, with one or two stereocentres. Furthermore, they contain at least three charged functional groups and possess a charged side-chain approximately 3.5-4 Å away from the amino acid group.[39, 49]

An important consideration when designing an NMDA receptor agonist is its stereochemistry. Although all iGluRs exhibit a stereospecific preference for (*S*)-agonists, the NMDA receptor is less strict and in some cases can bind (*R*)-agonists with a higher affinity (*Scheme 1, Table 1.1*).[50] These straight chain agonists do not exhibit high subunit selectivity, except for SYM2081. Unfortunately, SYM2081 activates all iGluRs with a preference for Kainate receptors.[51]

Table 1.1. Binding affinity of NMDA receptor agonists to different GluN2 subunits using an electrophysiological assay.[39]

		EC_{50} (μM)			
	IC_{50} (μM)	**GluN1/N2A**	**GluN1/N2B**	**GluN1/N2C**	**GluN1/N2D**
(S)-Glu	0.31	3.30	2.86	1.68	0.51
(R)-Glu	23.0	249	156	111	42.3
NMDA	3.68	94.10	29.5	21.7	7.30
NMLA	14.5	581	127	154	40
SYM2081	NA	144	25.1	18.2	3.15

Bioisosteric replacement of functional groups is a widely used strategy to obtain potent and selective ligands. Although the α-carboxylate group of glutamate is critical for high affinity ligands, the γ-carboxylate can tolerate changes and in some cases increased affinity and subunit selectivity has been observed (*Table 1.2*).[50] This phenomenon was observed for the agonist tetrazolylglycine (*Scheme 1*).

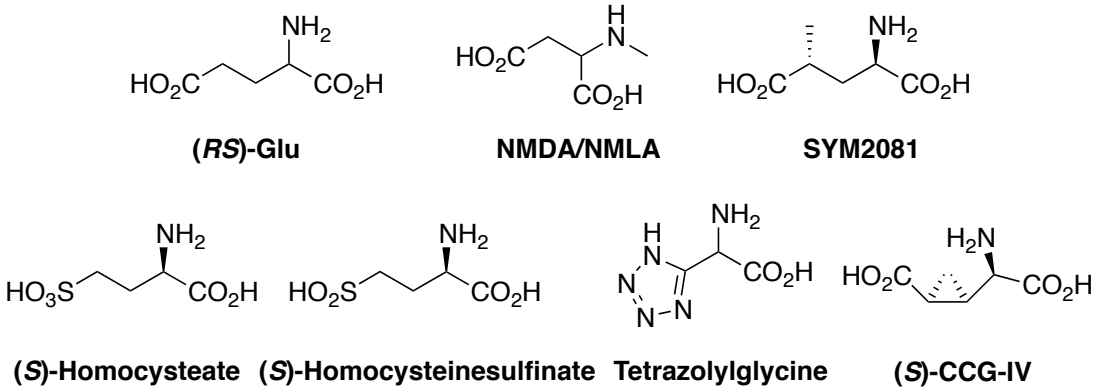

Scheme 1. Structures of NMDA receptor agonists.

One method used to obtain subunit specificity in agonist binding is to restrict the conformational flexibility of the endogenous ligand. Insertion of a cyclopropyl group between C3 and C4 of glutamate results in eight stereoisomers, four of which adopt the preferred 'folded' conformation. One of the folded isomers, (*S*)-CCG-IV (*Scheme 1*), has been shown to be the most potent NMDA receptor

agonist to date, with a three-fold selectivity for the GluN2B and GluN2D subunits (*Table 1.2*).[50]

Table 1.2. The effect of bioisosteric replacement and conformational restriction on the binding affinity of NMDA receptor agonists, using an electrophysiological assay.[39]

	EC_{50} (μM)			
	GluN1/N2A	**GluN1/N2B**	**GluN1/N2C**	**GluN1/N2D**
Homocysteate	34.1	8.09	11.6	3.35
Homocysteinesulfinate	73.2	17.9	13.7	6.19
Tetrazolylglycine	1.72	0.518	0.491	0.0993
(*S*)-CCG-IV	0.262	0.083	0.110	0.036

In comparison to NMDA receptor agonists, when antagonists bind at the glutamate binding-site, they stabilise the open conformation of the LBD to hinder ion channel activation. Stabilising the open conformation results in there being a larger volume for the antagonist to interact with.[39, 49]

Generally, the design of most NMDA receptor antagonists employs the same methods as for agonist design; the major difference is to increase the distance between the α- and distal carboxylate residues to approximately 5.1-6.6 Å.[49]

In the 1980's, two compounds, AP5 and AP7 (*Scheme 1.1*), were developed,[52, 53] which have since been used as the prototypical compounds to develop more potent and selective NMDA receptor antagonists. A stereochemical preference is found for (*R*)-enantiomers over (*S*)-enantiomers for antagonists that have been resolved, although there are a few exceptions to this generality.[54]

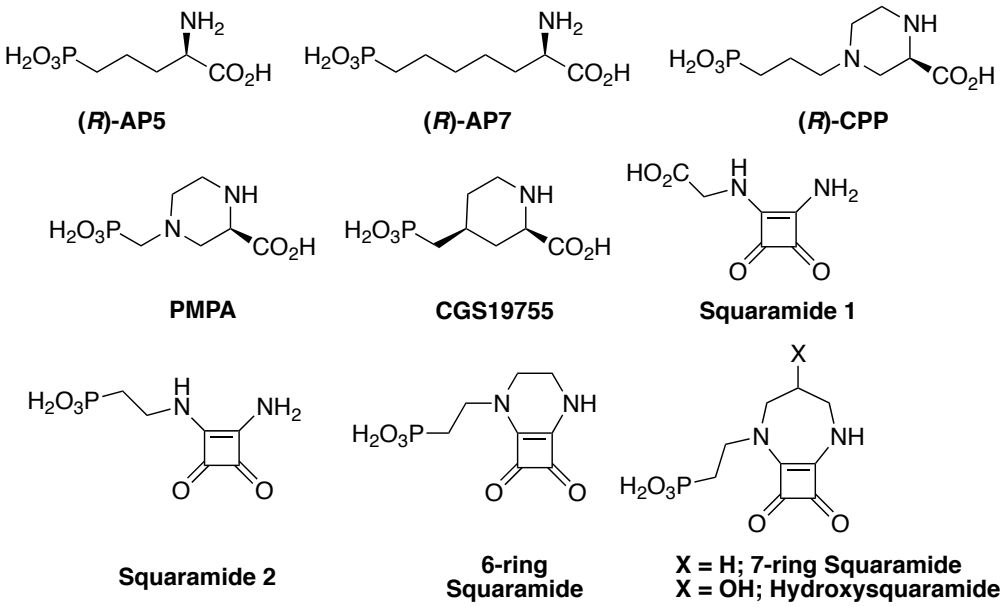

Scheme 1.1. Competitive NMDA receptor antagonists.

By reducing the conformational freedom of AP5 and AP7, cyclic derivatives such as (*R*)-CPP were developed (*Scheme 1.1*) in an attempt to increase NMDA receptor affinity and improve bioavailability.[55] This method proved successful and (*R*)-CPP was found to be a potent NMDA receptor antagonist (*Table 1.3*). It has approximately two-times higher affinity compared to its one-carbon homologue, PMPA. This is somewhat surprising, given that the piperidine analogue, CGS19755,[56] exhibits an even higher affinity than that of (*R*)-CPP (*Table 1.3*). The decrease in affinity of PMPA is most likely due to protonation of N4 in the piperazine ring, stabilising an unfavourable conformation.[57]

Table 1.3. Affinities of NMDA receptor antagonists measured by their ability to displace [^{3}H]CPP from the glutamate binding-site.[39]

	IC_{50} (μM)[a]		IC_{50} (μM)[a]
AP5	0.290	**Squaramide 1**	2.30
AP7	0.760	**Squaramide 2**	0.470
(*R*)-CPP	0.079	**6-ring Squaramide**	0.092
PMPA	0.320	**7-ring Squaramide**	0.030
CGS19755	0.065	**Hydroxysquaramide**	0.019

[a] IC_{50} of glutamate is 0.070-0.171 μM.

Bioisosteric replacement of functional groups has also been adopted for the development of NMDA receptor antagonists. The 3,4-diamino-3-cyclobutene-1,2-dione moiety represents an isosteric replacement of the α-amino-carboxylic acid functionality present in the majority of NMDA receptor agonists and antagonists. This cyclic group acts as an electronic mimic, possessing partial negative charges on the carbonyl oxygens and partial positive charges on the nitrogen atoms, generating a significant dipole moment. However, this bioisostere lacks other properties; it is not acidic or basic at physiological pH and the amino group is non-nucleophilic.[58]

Nevertheless, this isosteric replacement was shown to be active. The squaramide 1 (*Scheme 1.1*) was able to function in a displacement assay, albeit binding at the NMDA receptor with 30-times weaker affinity compared to glutamate. Further extension of the pendant arm and substitution of the distal carboxylic acid for a phosphonic acid gave weak NMDA receptor antagonists with affinity in the low micromolar range (*Table 1.3*).[59]

The 3,4-diamino-3-cyclobutene-1,2-dione moiety is known to adopt different rotameric forms, which could lead to internal hydrogen-bonding reducing the number of available hydrogen-bond donors and acceptors for the glutamate binding site. Based on the argument that a compound that is more freely available to hydrogen-bond to amino acid residues in the binding site should have a higher affinity for the NMDA receptor, bicyclic structures with further conformational restriction were developed.[60]

The six-membered ring derivative was found to exhibit a 5-times greater affinity for the NMDA receptor than its acyclic counterpart. Increasing the ring size from 6- to 7- increased the affinity further by a factor of 3. This was attributed to the presence of a larger dipole moment in the 7-ring system giving increased charge separation, resulting in an increase in NMDA receptor affinity. Also, by including a hydroxyl substituent to act as a hydrogen-bond donor, NMDA receptor affinity of this class of antagonists has been found to match the most potent antagonists to date.[60]

Detection and imaging of neuronal transmission and monitoring receptor activity is of prime importance in cognitive neuroscience. This could help neuroscientists better understand brain function, as well as potentially

diagnosing early stage diseases. Magnetic resonance imaging is a primary technique that could be used for these purposes.

1.3 Magnetic Resonance Imaging

Magnetic resonance imaging (MRI) is widely regarded as one of the most powerful imaging techniques used throughout clinical medicine, with over 2.4 million scans conducted by the NHS in the UK between 2012 and 2013. This represents a 12% growth in the use of MRI over a 10-year period, reflecting its diagnostic potential.[61] It has the ability to generate images with an impressive sub-millimetre spatial resolution, which can give accurate physiological and pathological information on various tissues and organs within the human body. Furthermore, it is a non-invasive technique without the need to employ harmful ionising radiation more commonly associated with other imaging modalities, such as X-ray scanning.[62]

The MRI technique is based upon fundamental NMR theory independently developed in 1946 by Bloch and Purcell, who later received the Nobel Prize in Physics in 1952.[63] Expansion of the field led to the discovery that different relaxation times could be used to generate images,[64, 65] and by 1977 the first MR scan on a human subject was performed.[66] The rapid rise and global importance of this diagnostic imaging tool was demonstrated in 2003 with the award of the Nobel Prize in Medicine jointly shared between Paul Lauterbur and Sir Peter Mansfield for their efforts in the development of MRI.

Proton MRI utilises the strong ^{1}H NMR signal of water to generate images. Protons possess spin angular momentum $I = ½$, and a magnetic moment, μ, due to the presence of the positively charged nucleus. When a sample of protons is placed inside an external magnetic field, B_0, they align themselves in definite directions, either parallel (+ ½) or anti-parallel (- ½) and precess around B_0 at the Larmor frequency (*Figure 1.8A*). The difference in energy between the two spin states is directly related to the strength of the external magnetic field, with the majority of spins aligned in the more energetically favourable parallel alignment. The vector sum of magnetic moments in the parallel state generates a

net macroscopic magnetisation, M_0, orientated along the z-axis, making M_z non-zero (*Figure 1.8B*).

Upon application of an RF pulse along the x-axis, the spins occupying the lower energy parallel state absorb energy and make the transition to the higher anti-parallel state, causing M_z to tip towards the x-y plane, if assuming a 90° pulse (*Figure 1.8C*). The degree of which M_z is rotated away from B_0 depends upon the time frame of the RF pulse (*Figure 1.8D*).[67]

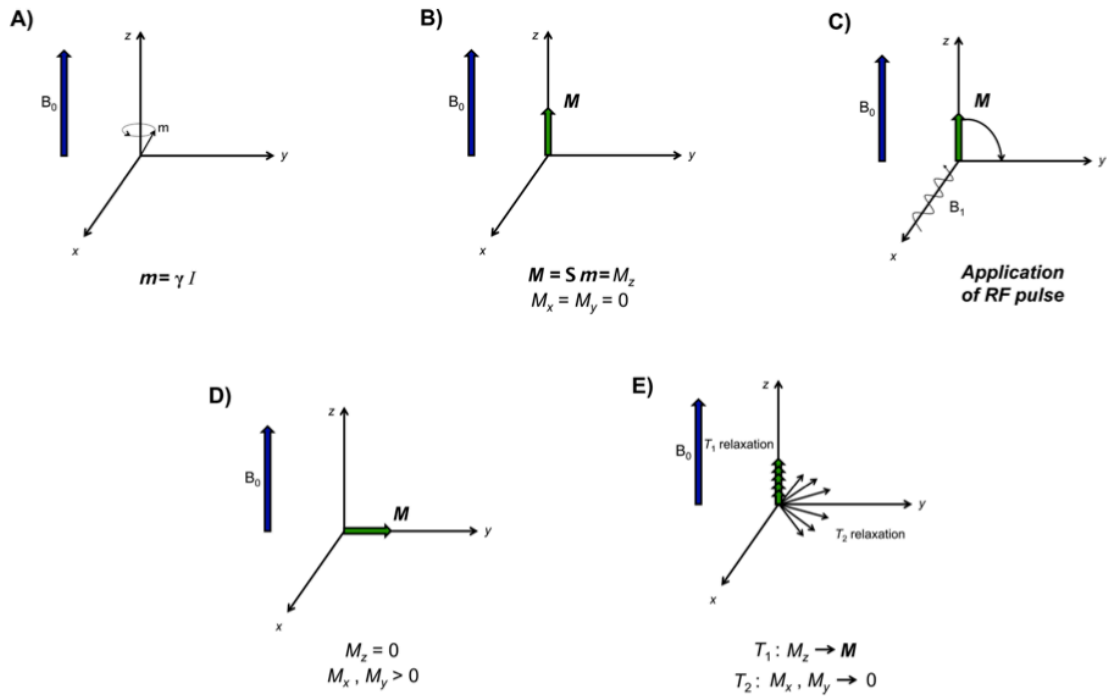

Figure 1.8. (A) The magnetic moment of each proton nucleus precesses around B_0 at the Larmor frequency. (B) The vector sum of magnetic moments generates a net macroscopic magnetization, M_0, orientated along the z-axis. (C) Application of an RF pulse along the x-axis generates a secondary magnetic field, causing M_z to tip away from z-axis. (D) Assuming a 90° pulse, the net magnetization will lie in the x-y plane. (E) Over time, relaxation processes recover the magnetization to its equilibrium values. T_1 relaxation is responsible for M_z recovery.[68]

Once the RF pulse is removed, the thermodynamic instability associated with the perturbed magnetic state results in the net magnetisation relaxing back to its equilibrium position along the z-axis, with characteristic time constants T_1 and T_2 (*Figure 1.8E*). Spin-lattice relaxation, T_1, involves the equilibrium return of the spin states via the stimulated emission of energy, through interaction with nearby fluctuating magnetic fields, present in molecules in the surrounding medium. This random process recovers M_0 in an exponential manner, such that

at time, $t = T_1$, the longitudinal magnetisation has recovered to 63% of its original value with almost full recovery achieved at $t = 5 \times T_1$.[67]

Differential T_1 and T_2 relaxation rates provide the basis for signal intensity modulation in MRI, whereby the protons of water molecules in various tissues relax back to equilibrium at different rates, providing image contrast.

1.3.1 Contrast Agents and Relaxivity

The main drawback of MRI is its intrinsically low sensitivity due to the fact that the technique is observing the protons from water molecules that are present at a concentration of 55 M.[69] Although there are changes in T_1 relaxation time between different tissues (i.e. healthy tissue has a significantly shorter T_1, 0.367 s, compared to malignant breast tissue, 1.080 s)[70], due to the large background of water it becomes difficult to detect changes in tissue types based on differences in longitudinal relaxation times. In order to induce additional contrast, synthetic compounds known as contrast agents are employed to affect the water protons' relaxation rate, R_i ($R_i = 1/T_i$; $i = 1,2$), such that differences in contrast are easier to observe.

Contrast agents are paramagnetic, superparamagnetic or ferromagnetic compounds that shorten both T_1 and T_2 relaxation times of nearby water protons. This shortening of T_1 and T_2 is due to a dipolar interaction between the electronic magnetic moment of the contrast agent and the nuclear magnetic moment of the proton. A contrast agent is classified as either a T_1 or T_2 agent depending on which relaxation time it affects the most. The majority of contrast agents are T_1 agents and these induce a positive contrast, whereas T_2 agents provide a reduction in signal intensity and a negative image contrast.[69]

The T_1 agents are typically paramagnetic compounds that employ Gd(III) chelates to increase the relaxation rates of water protons. The choice of Gd(III) is explained by its high spin paramagnetism and long electronic relaxation time (typically ms). Indeed, despite Dy(III) or Ho(III) having a larger magnetic moment, Gd(III) possesses a symmetrical S-state which gives a slower electronic relaxation time more tuned to the proton Larmor frequency of water, leading to an increase in relaxation rate.[71]

Similar to the rest of the lanthanide series, the free Gd(III) ion is highly toxic (LD_{50}~0.1 mM/ kg) and so must be encapsulated in a thermodynamic and kinetically stable multidentate ligand when administered as an MRI contrast agent.[71] There are countless examples of these coordinating ligands within the literature, and some will be reviewed later in this chapter. The first commercially approved Gd(III)-based MRI contrast agent was [Gd(DTPA)(H_2O)], marketed as Magnevist® in 1988. Since then, eight further Gd(III)-based contrast agents have been approved, with approximately 35% of all MRI scans employing one of these contrast agents.[72]

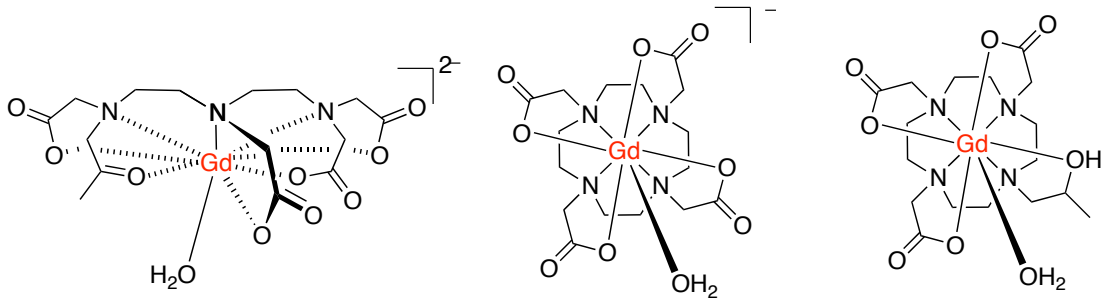

Magnevist® **Dotarem®** **Prohance®**

Scheme 1.2. Structures of selected clinically approved MRI contrast agents.

Upon administration of a Gd(III) contrast agent, the observed increase in solvent relaxation rate, $1/T_{1obs}$, is the sum of the diamagnetic ($1/T_{i,d}$) and paramagnetic ($1/T_{i,p}$) relaxation rates (*Equation 1*)[73];

$$\frac{1}{T_{i,obs}} = \frac{1}{T_{i,d}} + \frac{1}{T_{i,p}} \qquad i = 1,2 \qquad (1)$$

The ability of the Gd(III) contrast agent to enhance ($1/T_1$) or ($1/T_2$) is represented as relaxivity, r_1 or r_2 respectively, whereby proton relaxivity is the change in relaxation rate after introduction of the contrast agent, normalised to the concentration of the metal ion (*Equation 1.1*)[73];

$$\frac{1}{T_{i,obs}} = \frac{1}{T_{i,d}} + r_i[Gd(III)] \qquad i = 1,2 \qquad (1.1)$$

The relaxivity is a direct measure of the ability of a complex to enhance the rate of relaxation of the water protons and is sometimes thought of as a catalytic property of these contrast agents. A complex displaying a larger r_1 will increase the contrast of an MR image more effectively.

The presence of the paramagnetic species creates a strong local magnetic field, which can interact with the nuclear spins providing a more efficient relaxation mechanism for the water protons. However, this local magnetic field diminishes with distance and so specific chemical interactions coupled with random translational diffusion which bring water molecules in close proximity of the Gd(III) centre are crucial. This generally leads to the paramagnetic relaxation rate enhancement being divided into two contributions (*Equation 1.2, Figure 1.9*)[71, 73];

$$\frac{1}{T_{i,p}} = \left(\frac{1}{T_{i,p}}\right)^{IS} + \left(\frac{1}{T_{i,p}}\right)^{OS} \qquad i = 1,2 \qquad (1.2)$$

Inner sphere (IS) relaxation refers to the relaxation rate enhancement due to a water molecule binding in the first coordination sphere of the metal ion. Providing this water molecule is in fast exchange with the bulk solvent, propagation of the paramagenetic effect occurs. Outer sphere (OS) relaxation refers to the relaxation rate enhancement obtained by translational motion bringing bulk solvent molecules within close proximity of the Gd(III) metal ion. There is a further term, so-called second sphere relaxation, which is attributed to water molecules held in the second coordination sphere of the Gd(III) ion for a relatively long period of time through hydrogen bonding networks. However, this contribution to the overall relaxation rate enhancement is often either neglected or included within the outer sphere term.

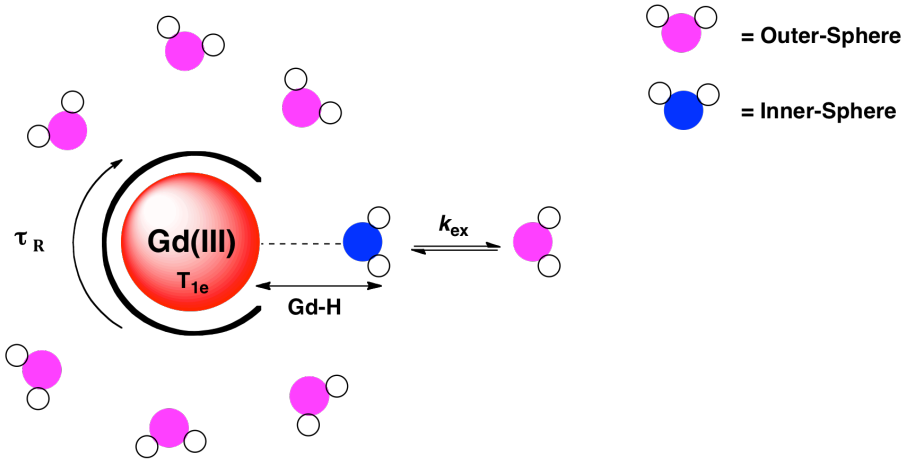

Figure 1.9. Schematic representation of a Gd(III) complex, highlighting the factors affecting its relaxivity.

1.3.1.1 Inner Sphere Relaxation

Although the overall contribution to relaxation rate enhancement is approximately equal for both inner and outer sphere mechanisms, the absence of detailed information on second and outer sphere water structure and exchange dynamics means that only the inner sphere term can be significantly controlled with confidence.[73]

Inner sphere relaxation is defined by (*Equation 1.3*);

$$\left(\frac{1}{T_1}\right)^{IS} = \frac{qP_m}{T_{1M} + \tau_m} \qquad (1.3)$$

where P_m is the mole fraction of bound water nuclei, q is the hydration number τ_m is the lifetime of the bound solvent molecule ($\tau_m = 1/k_{ex}$; where k_{ex} is the exchange rate of the solvent) and T_{1M} is the longitudinal proton relaxation time of the bound water.

It is possible to consider the relative importance of the factors that determine inner sphere relaxation. In the limiting case, where $\tau_m << T_{1M}$, the relaxation rate will depend directly on the relaxation rate of the coordinated water molecule. On the contrary, if $T_{1M} << \tau_m$, the exchange rate of the water molecule at the metal centre will govern proton relaxivity.

Increasing the hydration number of the contrast agent, such that *q* changes from 1 to 2 will result in an overall increase in inner sphere relaxation. However, an increase in hydration number effectively removes one permanent coordinating ligand donor from the Gd(III) centre, and as such results in a decrease in complex stability and compromises its kinetic inertness.[71, 73]

From the Solomon-Bloembergen-Morgan equations,[74-77] it is apparent also that the water proton to metal ion distance is a factor that governs inner sphere relaxation. Due to the r^{-6} distance dependence, a small increase of 0.2 Å results in a 50% decrease in proton relaxation.[71]

The dipole-dipole mechanism that dictates proton relaxation is governed by the effective correlation time, τ_{ci}, such that;[68, 78]

$$\frac{1}{\tau_{c,i}} = \frac{1}{T_{i,e}} + \frac{1}{\tau_m} + \frac{1}{\tau_R} \qquad i = 1,2 \qquad (1.4)$$

where T_{ie} is the electronic spin relaxation times, τ_M is the lifetime of the bound water molecule and τ_R is the rotational correlation time.

Theory predicts that the relaxivity maximum is attained when τ_{ci} equals the inverse of the proton Larmor frequency. However, τ_M also enters *equation 1.3* and predicts a higher inner sphere relaxation rate for a shorter τ_M. Consequently, τ_M needs to be optimised in a way that it does not begin to limit T_{1M}. The optimal relationship is:

$$\frac{1}{T_{1M}} < \frac{1}{\tau_m} < \frac{1}{\tau_R}; \frac{1}{T_{1e}} \qquad (1.5)$$

Contrast agents that are currently used do not possess relaxivities that are anywhere near the theoretically achievable value as their rotational correlation time, and proton exchange rates are not optimal. In the low to medium field range, τ_R is of the order of 100-200 ps, and when water exchange rate is reasonably fast (i.e. $\sim 10^7$ s^{-1}), this term dominates the water proton relaxivity.[78]

1.3.2 Receptor-Targeted Gd(III)-MR Contrast Agents

Throughout the literature there are widespread examples of Gd(III) contrast agents that have been designed to report upon local changes in pH, metal ion concentration and enzyme activity.[79-81] There are also detailed examples of contrast agents targeted towards abundantly present blood pool proteins, such as human serum albumin (HSA).[82] However, this review will focus only on the contrast agents that have been designed to change their relaxivity upon associating with cell-surface and intracellular receptors, of which there are few. There are only a handful of reports of these contrast agents due to the low sensitivity of the MRI method. Even with a low cellular diamagnetic relaxation rate, upon administration of the Gd(III) complex, it has been hypothesised that there needs to be a 10 μM local Gd(III) concentration to observe a 10% change in R_1 for a contrast agent which possesses a typical relaxivity of 5 mM^{-1} s^{-1}.[83] This makes it difficult to image the majority of cell surface receptors, as they are believed to be present in the nanomolar range.

1.3.2.1 Intracellular Receptor-Targeted Contrast Agents

Cancer cells are known to over-express a variety of receptors that are present on or in healthy cells. The higher concentration of these receptors allows targeted-contrast agents to overcome the inherent low sensitivity of MRI.

The progesterone receptor (PR) is a useful marker for cancer progression and is frequently used to predict patient prognosis. Historically, progesterone receptor levels are determined from *in vitro* immunohistochemistry assays of patient samples gained by invasive biopsies. However, Meade and co-workers have produced a series of reports on the development of progesterone receptor targeted MRI contrast agents, which could potentially report the degree of cancer progression.

Although their initial complex, **[Gd.L$^{1.0}$]** (*Scheme 1.3*), induced a 40% enhancement in R_1 upon incubation with progesterone receptor positive cells,

the complex had a relatively weak affinity for the progesterone receptor (IC_{50} = 1.91 μM).[84]

In an effort to increase relaxation rate enhancement, four further complexes were synthesised (*Scheme 1.3*), in order to optimise intracellular accumulation and progesterone receptor affinity. The effect of charge on the complex lipophilicity and cell permeability was assessed, along with the effect of the length of the spacer unit separating the progesterone motif and Gd(III) chelate.[85]

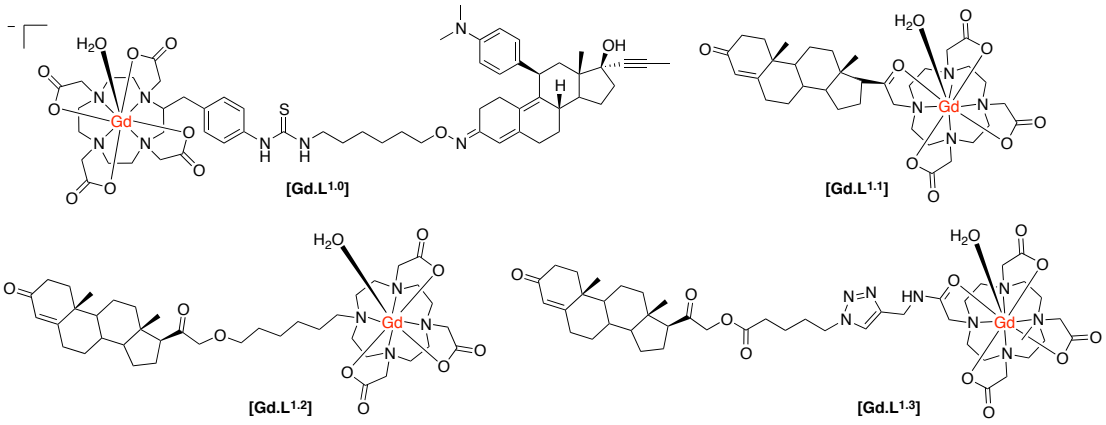

Scheme 1.3. Structures of progesterone receptor-targeted contrast agents (CN and *q* not specified for **[Gd.L$^{1.1\text{-}1.3}$]**).

In order to increase intracellular accumulation, it was rationalised that a complex with a more positive Log*P* value would assist in enhancing cell permeability. Therefore, the neutral complexes **[Gd.L$^{1.1}$]** and **[Gd.L$^{1.2}$]** were the lead complexes.

The length and nature of the spacer group also had an effect on the complexes' affinity for the progesterone receptor. Surprisingly **[Gd.L$^{1.1}$]** with no spacer exhibited the largest affinity for the progesterone receptor, suggesting the possibility for a favourable interaction between the hydrophilic Gd(III) chelate and the receptor binding site. However, all four complexes exhibited approximately 100-fold increase in progesterone receptor affinity over **[Gd.L$^{1.0}$]**, with IC_{50} values in the nanomolar range. Of the four compounds, **[Gd.L$^{1.2}$]** showed optimal charge and spacer properties and was subject to further evaluation.[85]

The complex, **[Gd.L$^{1.2}$]**, was internalised in both progesterone receptor positive and negative cells, with progesterone receptor positive cells exhibiting twice the accumulation over a 24 hour period. This suggested that **[Gd.L$^{1.2}$]** is retained longer in the progesterone receptor positive cells, through interaction with the intracellular receptor. The non-specific uptake into progesterone receptor negative cells was attributed to the high hydrophobicity and cell permeability of the complex.[86]

Retention of **[Gd.L$^{1.2}$]** in the uterus, ovaries and mammary over a 24 hour period demonstrated its ability to target progesterone receptor rich tissue. Importantly, **[Gd.L$^{1.2}$]** did not accumulate in the abdominal tissue or fat.

Finally, **[Gd.L$^{1.2}$]** was shown to enhance the contrast of progesterone receptor positive tumours in the presence of progesterone receptor negative tumours *in vivo*. Independent of the mode of administration (subcutaneous *vs.* intraperitoneal), a significant difference in the T_1-weighted MR images between the two tumours was evident 2-6 hours post injection.[86]

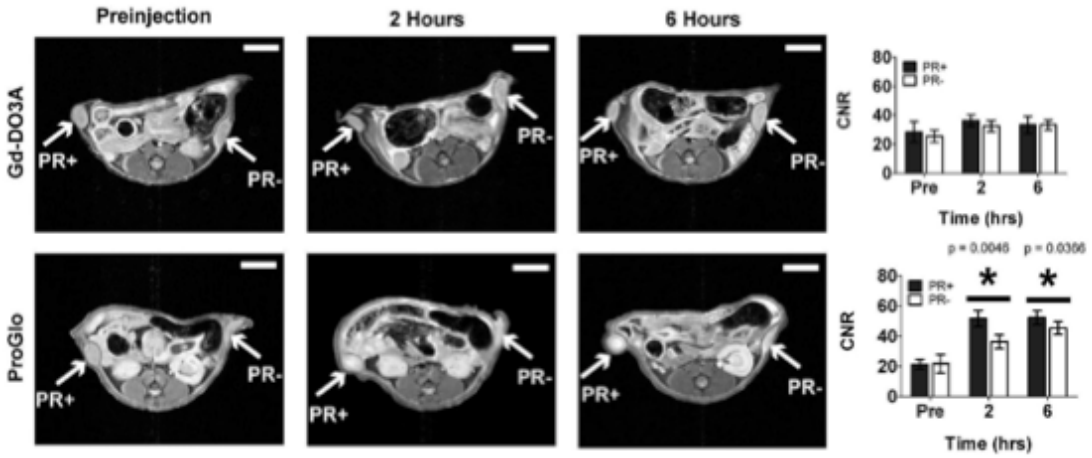

Figure 1.10. T_1-weighted MR images and contrast-to-noise plots (7 T) of xenografted mice intraperitoneally injected with **[Gd.DO3A]** or **[Gd.L$^{1.2}$]**. A significant contrast enhancement is observed in both progesterone receptor positive and negative tumours over a 6 hour period when injected with **[Gd.L$^{1.2}$]**.[86]

Despite the relative successes of **[Gd.L$^{1.2}$]**, it should be noted that this contrast agent is based on an *N*-alkyl-DO3A system. Such systems are likely to bind to protein non-specifically[87] (approximately 30% of **[Gd.L$^{1.2}$]** was found to reside in the membrane and not interact with the progesterone receptor), or to endogenous anions (e.g. bicarbonate or lactate), leading to displacement of the

coordinated water molecule. This will tend to reduce the relaxivity gain the authors observed upon receptor binding. Furthermore, the authors did not assess the effect of non-specific protein binding on cellular uptake, which could be the reason for their relatively poor 2:1 cellular uptake specificity. Finally, the poor water solubility and intracellular uptake of **[Gd.L$^{1.2}$]** resulted in a significant toxicity, most likely due to gadolinium retention.

In an attempt to reduce the toxicity associated with **[Gd.L$^{1.2}$]**, the lipophilicity of the complex was adjusted through modification of the linker unit.[88] As expected, no change in progesterone receptor affinity was observed. However, an increase in cellular uptake of **[Gd.L$^{1.3}$]** was achieved in progesterone positive tumours; 90% of the complex was found to localise in the cytoplasm, where one form of the progesterone receptor is located. Contrast-to-noise ratios in T_1-weighted MR measurements of **[Gd.L$^{1.3}$]** were comparable to that of **[Gd.L$^{1.2}$]**, but the increased water solubility resulted in an increase in cell viability.

Despite the improvements, **[Gd.L$^{1.3}$]** is based on a mono-amide-DO3A system. These types of system have inherently slower water exchange rates ($k_{ex} \sim 10^6$ s^{-1}) due to the presence of the weakly donating amide carbonyl and so relaxivity gain is limited. Furthermore, the receptor-targeting moiety is attached through an ester linkage, which is well known to be susceptible to hydrolysis *in vivo*. A chemical linkage that is more stable to *in vivo* conditions would possibly give increased cellular retention in progesterone positive tumours, leading to an enhancement in signal contrast.

1.3.2.2 Surface Receptor Targeted Contrast Agents

In 1995, a seminal paper by Meade and co-workers[89] described how Gd-DTPA chelates conjugated to polylysine, which were then loaded onto DNA containing transferrin, were able to label cells expressing the transferrin receptor. This resulted in a large enhancement in the T_1-weighted MR image contrast, compared to untreated cells. Furthermore, cells treated simultaneously with the Gd-DTPA loaded DNA-transferrin conjugate and also iron-loaded transferrin resulted in a negligible enhancement in T_1-weighted MR contrast, due to

competition for the receptor site. This demonstrated that internalisation of the contrast agent was mediated by the cell surface receptor.[89]

Folate is an essential vitamin for cells and binds with high affinity to the folate receptor present on the cell surface. Upon the binding of folate, the folate receptor-ligand conjugate undergoes receptor-mediated endocytosis to deliver folate to the cytosol. Following dissociation of folate, the receptor returns to the cell surface ready for the next ligand to bind.

There are several examples in the literature of polymeric, high molecular weight contrast agents that target the folate receptor.[90-92] One example of a low molecular weight complex is from Kalber and co-workers,[93] who synthesised a contrast agent by conjugation of folic acid to a monoamide GdDO3A chelate separated by an ethylene glycol spacer (*Figure 1.11*). Inductively coupled mass spectrometry (ICP-MS) measurements showed that the complex **[Gd.L$^{1.4}$]** was internalised readily by folate receptor positive (FR+) cells after 1 hour, with more than double the accumulation than in folate receptor negative (FR-) cells. Furthermore, the presence of free folic acid in the medium as a competitor resulted in a reduction in uptake of **[Gd.L$^{1.4}$]** into FR+ cells, suggesting receptor-mediated internalisation.

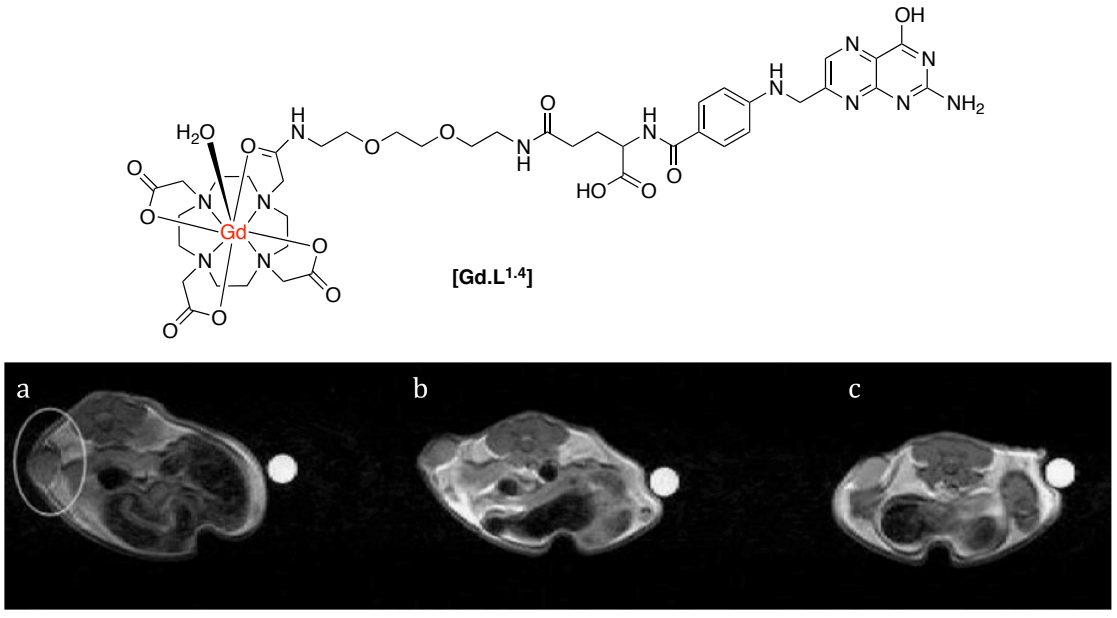

Figure 1.11. (Top) Structure of folate receptor-targeted contrast agent, **[Gd.L$^{1.4}$]**. (Bottom) T_1-weighted MR images (unknown field) of a FR+ tumour xenograft pre- (a), 2 h post (b) and 4 h post administration of **[Gd.L$^{1.4}$]** (c).[93]

Despite confirmation of cellular labelling by ICP-MS measurements, there was no increase in cellular relaxation rate *in vitro*, after incubation of **[Gd.L$^{1.4}$]**. Contrastingly, when **[Gd.L$^{1.4}$]** was administered to nude mice bearing a FR+ tumour xenograft, up to a 50% enhancement in R_1 was observed over a 14 hour period, resulting in an increase in T_1-weighted MR contrast (*Figure 1.11*). In comparison, there was no increase in R_1 for tumour xenografts baring FR- cells, or when the non-targeted **[Gd.DOTA]** was used.

The contrasting *in vitro* and *in vivo* results are rather surprising. The authors suggest a significant degree of cellular variation in folate receptor expression as a possible reason for the contrasting results. This is a plausible assumption, although it is very difficult to determine the real mechanism by which R_1 increases *in vivo*. The intracellular fate of the complex is key. Once the complex is bound to the folate receptor, internalisation is likely to be quick resulting in the contrast agent residing in the cytosol. It can then theoretically bind non-specifically to intracellular proteins, modulating τ_R, and increasing R_1. However, the expected relaxivity gain *in vitro* could be quenched if the contrast agent is trapped in a sub-cellular vesicle/endosome after internalisation, limiting k_{ex}.[94] Whatever the reasons for the discrepancies, the design of the complex could also limit the expected relaxivity gain. Monoamide Gd(III) chelates possess a sub-optimal k_{ex} approximately four-times slower than a tetra-carboxylate derivative, resulting in a decrease in R_1.

One further example of a folate receptor-targeted contrast agent is from some unpublished work in Durham.[95] In a similar approach to that outlined above, folic acid was conjugated to a Gd(III) chelate. However, the choice of ligand used to encapsulate the Gd(III) ion was derived from a tetra-carboxy-substituted DOTA ligand, giving the complex an overall negative charge. This complex was found to exhibit an 80% increase in R_1 in the presence of folate binding protein (FBP), in comparison to a negligible increase in the presence of BSA. The use of carboxylate donors results in the complex having a fast water exchange rate (k_{ex} ~ 10^7 s^{-1}). This coupled with the overall negative charge, which hinders non-specific protein binding, results in a large R_1 enhancement in the presence of FBP.

The formyl peptide receptors (FPRs) are a class of G-protein-coupled receptors present on the surface of neutrophils. Their main function is to mediate migration of neutrophils to a site of injury causing an inflammatory response. Long and co-workers[96] synthesized a FPR-1-targeted MR contrast agent based on the hexapeptide, cFLFLFK, known to be an antagonist for this receptor. Conjugation of the peptide fragment to the Gd(IIII) chelate through the lysine residue did not disrupt the affinity of the antagonist towards the receptor, with the apparent binding affinity only slightly decreasing (K_d = 4.5 vs 2 nM for **[Gd.L$^{1.5}$]** and native peptide, respectively).

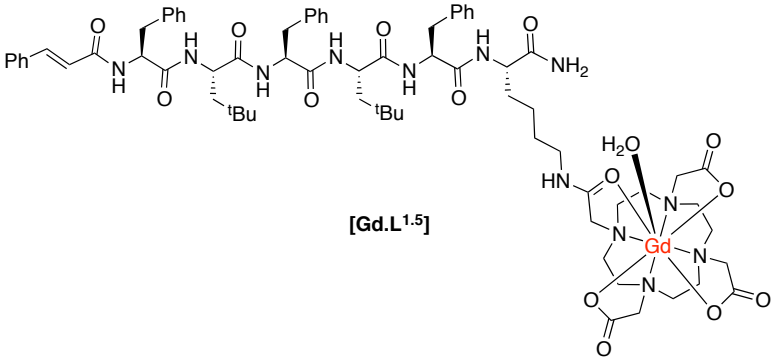

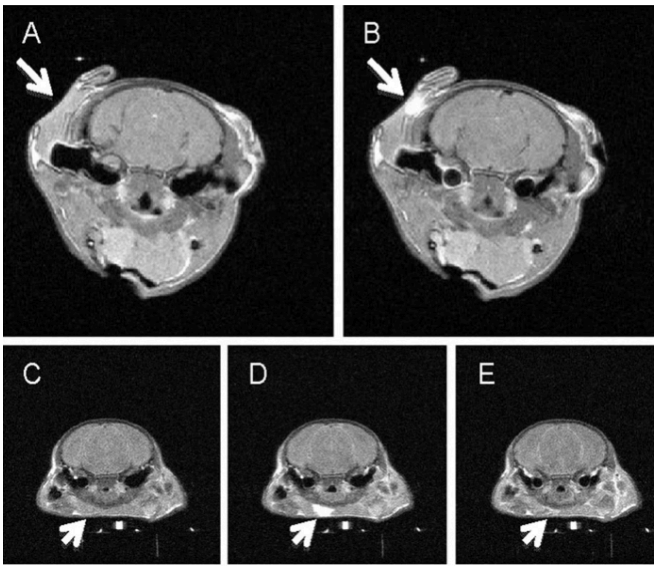

Figure 1.12. T_1-weighted MR images (9.4 T) of a mouse brain pre injection (a) and 80 minutes post injection of **[Gd.L$^{1.5}$]** (b). In comparison, pre (c), 1 minute post (d) and 80 minutes post injection of the control **[Gd.DOTA]**.[96]

The complex **[Gd.L$^{1.5}$]** was then intravenously administered to mice (1 mmol/kg), which had been pre-injected with an inflammatory agent for 24 hours. Upon administration, a significant increase in T_1-weighted MR contrast ensued and was visible for up to 80 minutes post injection at the site of inflammation (*Figure 1.12A-B*). In comparison, the non-targeted **[Gd.DOTA]**$^-$ shows an initial increase in T_1-weighted contrast after 1 minute, but is totally undetectable 80 minutes post injection (*Figure 1.12 C-E*). The authors attribute this difference in time-dependent, T_1-weighted contrast to specific targeting and binding of **[Gd.L$^{1.5}$]** to the neutrophils' FPR-1 receptor, prolonging the contrast agent's lifetime at the site of inflammation.

Of the examples of receptor-targeted MR contrast agents in the literature, there are very few that are targeted towards cell surface receptors. Dopamine is an abundant neurotransmitter in the central nervous system and mediates its affects through metabotropic dopamine receptors. The dopaminergic system is related to many neurological and psychological disorders. The D2/D3 dopamine receptors are the primary sites for anti-Parkinsonic and anti-psychotic drugs.

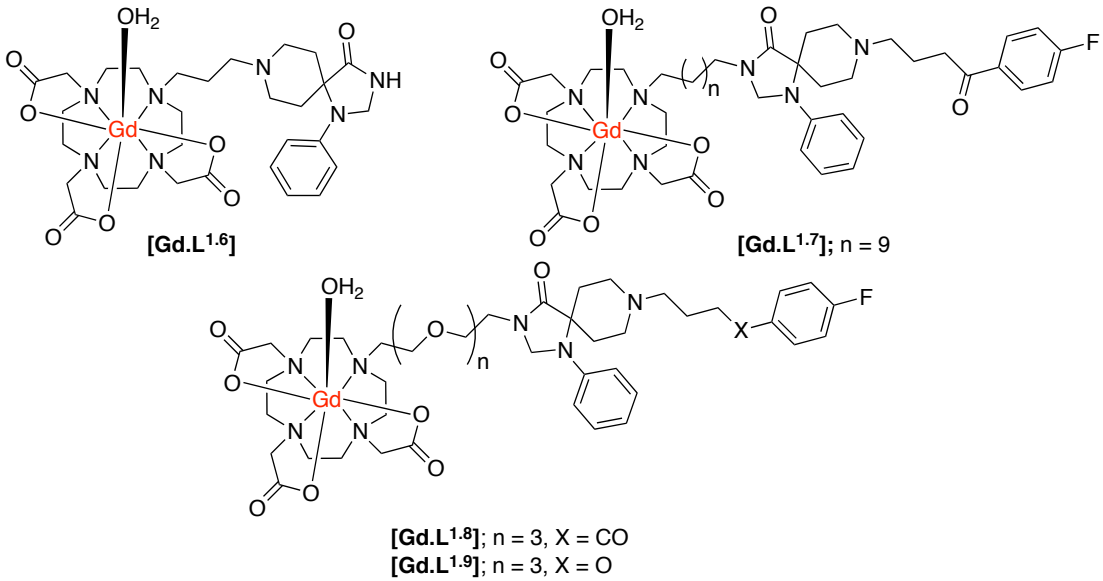

Scheme 1.4. Structures of potential dopamine receptor-targeted MR contrast agents (*q*-values not determined; possibly *q* = 2).

Cohen and co-workers[97, 98] synthesised a small series of D2/D3 receptor-targeted MR contrast agents based on an *N*-alkyl-DO3A system conjugated to

modified dopamine receptor ligands (*Scheme 1.4*). In an inhibition assay, complex **[Gd.L$^{1.6}$]** was shown to possess a large decrease in binding affinity for the dopamine D2-receptor, relative to the radiolabeled ligand, with an IC_{50} for **[Gd.L$^{1.6}$]** of approximately 10 μM. The decrease in affinity reflects the large modification made to the spiperone ligand, inhibiting receptor binding. In an attempt to increase receptor affinity, further complexes were synthesised, reducing the number of structural modifications to the spiperone ligand and varying the length and nature of spacer. This resulted in an increase in D2 receptor binding affinity for **[Gd.L$^{1.7\text{-}1.8}$]**, demonstrating the need for the entire ligand moiety to be present in order to maintain affinity.

Table 1.4. Comparative binding affinities and relaxivity values (9.4 T, H_2O/D_2O 1:1, 298 K) of dopamine receptor-targeted contrast agents.[97, 98]

	[Gd.L$^{1.6}$]	**[Gd.L$^{1.7}$]**	**[Gd.L$^{1.8}$]**	**[Gd.L$^{1.9}$]**
IC_{50}/ M	$1x10^{-5}$	$5x10^{-9}$	$1x10^{-8}$	$1x10^{-6}$
r_1/ $mM^{-1}s^{-1}$	5.9	5.5	7.8	*n.d*

Despite demonstrating the ability of these conjugates to bind at the dopamine D2 receptor, there is a significant amount of work missing to fully characterise **[Gd.L$^{1.6\text{-}1.9}$]** as dopamine-receptor targeted contrast agents. Firstly, there are no *in vitro* studies that demonstrate a change in relaxivity of these complexes upon binding to the dopamine receptor. The degree of relaxivity enhancement upon receptor binding would be limited due to the choice of the Gd(III) chelate, since *N*-alkyl-DO3A systems are likely to bind non-specifically to endogenous protein or anions.[87] This leads to displacement of the coordinated water molecule, reducing the relaxivity gain. Furthermore, specifically in **[Gd.L$^{1.8\text{-}1.9}$]**, the ligand moiety is positioned at a considerable distance from the Gd(III) chelate. Although this will inevitably increase the affinity of the complex for the receptor based on steric arguments, it could hinder the relaxivity gain upon receptor binding. The expected increase in R_1 is modulated by the rotational correlation time, τ_R. Therefore, the large spacer in these systems may induce independent motion of the slowly tumbling macromolecule and the Gd(III) chelate, resulting in a decrease in relaxivity enhancement.

1.4 Molecular Imaging of Glutamate Receptors

There have been several molecular imaging approaches used for the visualisation of glutamate receptors. The following summarises the current literature relating to the use of PET/SPECT, optical and MR for imaging glutamate receptors.

1.4.1 PET and SPECT Radiotracers for Glutamate Receptors

PET and SPECT are both radionuclide-imaging techniques, which rely on the decay of radioactive isotopes via emission of a positron or gamma ray, respectively. Both techniques possess very high sensitivity (10^{-11} – 10^{-12} M) and can be used to image whole bodied live subjects.[1]

There have been several reports on the synthesis and application of PET and SPECT tracers for glutamate receptors.[99] The majority of these tracers are derived from well-known ligands of glutamate receptors, with the incorporation of either an $^{18}F/^{11}C$ radiolabel for PET tracers and $^{123}I/^{111}In$ labels for SPECT. Of the examples in the literature, the most characterised PET tracer for $mGluR_5$ receptors is [^{18}F]SP203 (*Scheme 1.5*).[100] This tracer was synthesised in a high radiochemical yield through nucleophillic substitution of the bromomethyl analogue with [^{18}F]KF,[101] resulting in a ligand with an extremely high affinity (IC_{50} = 0.036 nM) and selectivity for $mGluR_5$. Rapid uptake into the brain of rhesus monkeys was observed, with accumulation residing in $mGluR_5$-rich regions. Although a moderate amount of radioactivity accumulated in the skull during the *in vivo* experiments with monkeys,[102] this was not observed in a pilot study with seven healthy human subjects.

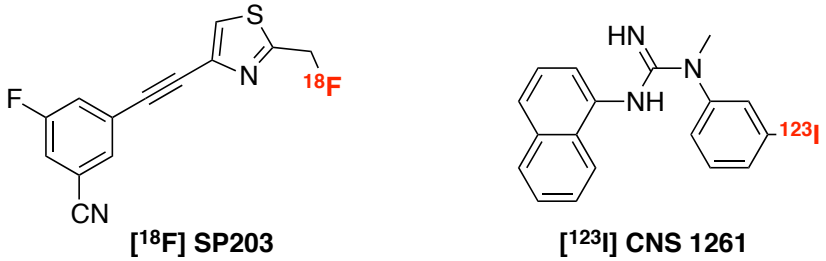

[^{18}F] SP203 **[^{123}I] CNS 1261**

Scheme 1.5. Structures of PET and SPECT agents for glutamate receptor imaging.

Among the iGluR imaging agents, there has been little progress in imaging the AMPA and Kainate receptors. However, of the several radiotracers synthesized for NMDA receptors, the SPECT ligand, [^{123}I]CNS 1261 (*Scheme 1.5*) has shown the most potential.[103] In human experiments, this tracer showed high distribution volumes in regions consistent with high NMDA receptor concentrations. Specific binding to the NMDA receptor was confirmed in a competition experiment with ketamine, but due to high degree of non-specific binding, the ability to detect small changes in receptor availability was limited.

Although there has been some success in the development of radiotracers for PET and SPECT imaging of glutamate receptors, there are many limitations associated with these methods. First, the resolution of these techniques is between 1-10 mm, which limits the ability to observe small changes at a receptor site. Furthermore, these methods rely on efficient chemical synthesis of radio-labelled-tracers. This requires the use of a nearby cyclotron to generate the short-lived radionuclide, which must be quickly reacted with a substrate in a high yielding reaction. The use of a radiotracer exposes both the patient and chemist to potentially harmful ionising radiation.

1.4.2. Optical Imaging of Glutamate Receptors

Similar to PET and SPECT, optical imaging is endowed with excellent sensitivity (10^{-9} - 10^{-12} M) and can be used to image biomolecules, which are present in lower concentrations, such as the ionotropic glutamate receptors. Further to their sensitivity, fluorescently labelled ligands are superior to radioligands as they are generally safer and easier to handle. However, the major limitation of optical imaging is the poor tissue penetration of photons in the range of 400-900 nm; no more than a cm or so is possible.

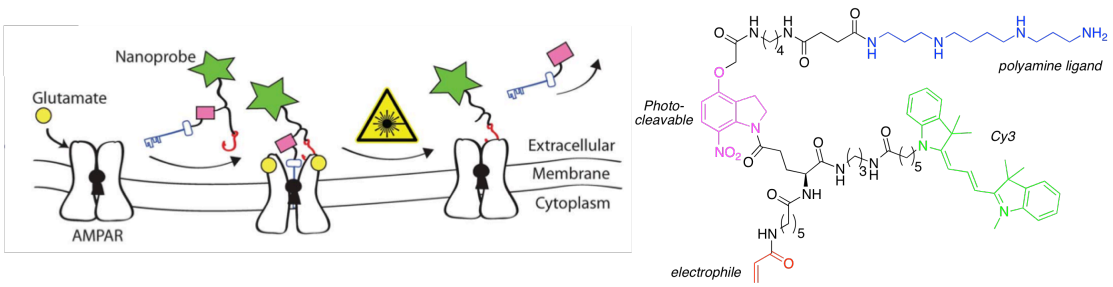

Figure 1.13. Schematic representation of the mechanism of action of Cy3 probe.[104]

Chambers and co-workers have developed a four-component molecular probe for visualisation of AMPA receptors.[104] The design of the molecule is based on a polyamine ligand (known to bind in the AMPA channel), conjugated to a Cy3 fluorescent reporter via a photo-cleavable linker. The molecule also bears an electrophilic acrylamide moiety, which can undergo reaction with a nucleophilic partner, such as an amino acid side chain present on the AMPA receptor, to anchor the probe to the receptor (*Figure 1.13*). The probe was found to block functional AMPA receptors in electrophysiology experiments, with removal of the polyamine block restoring the receptor to its native state after irradiation with 380 nm light.

When cells were treated with Cy3-probe for 2 mins and then continuously perfused with fresh buffer, fluorescence was observed around the synaptic junction, consistent with the expected distribution of AMPA receptors (*Figure 1.14A-B*). The fluorescence intensity was time dependent, decreasing rapidly over a 7 minute period (*Figure 1.14C*). In comparison, incubation of the Cy3 unit missing the targeting ligand showed no cellular localisation in microscopy studies, suggesting that the acrylamide moiety does not react promiscuously with any nucleophile.[104]

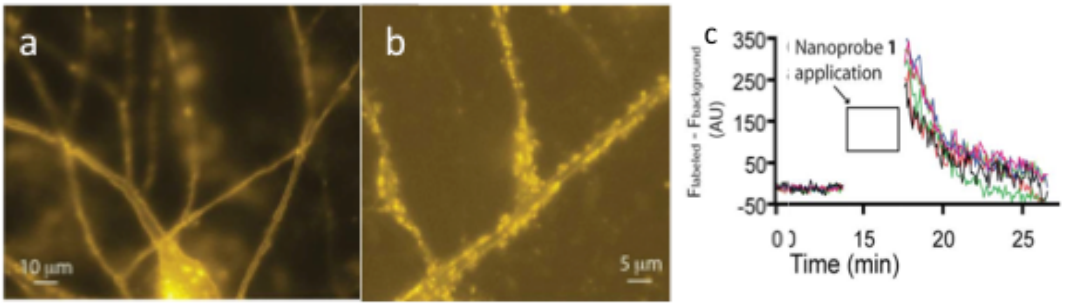

Figure 1.14. (A) Fluorescent images of neurons 30 seconds after incubation of Cy3 probe. (B) Magnified region after 5 minutes of washing with buffer. (C) Quantitative analysis showing a decrease in fluorescence intensity from the neuronal cells over a short period of time.[104]

Despite the visualisation of AMPA receptors, there are some discrepancies within this article. The authors do not state whether or not the imaging is performed after photo-dissociation of the polyamine ligand, and whether they are visualising the Cy3 unit directly bound to the AMPA receptor. The fact the

fluorescence decreases over time suggests that the positively charged polyamine is also non-specifically labelling the plasma membrane, which can then be washed out over time. It is also unclear as to whether the probe is selective for labelling AMPA receptors, with all iGluRs possessing a polyamine-binding site.

Another example exploiting the use of fluorescently labelled channel blockers is from Stromgaard and co-workers,[105] who systematically replaced the aromatic head-group of polyamine iGluR channel blockers with fluorescent labels of varying size. It was found that as the size of the fluorophore increased, the compounds affinity for the AMPA and NMDA receptor decreased. Furthermore, the size of the fluorophore had an impact on the selectivity of the probes toward different receptors but, in general, a higher affinity for the AMPA receptor was observed.

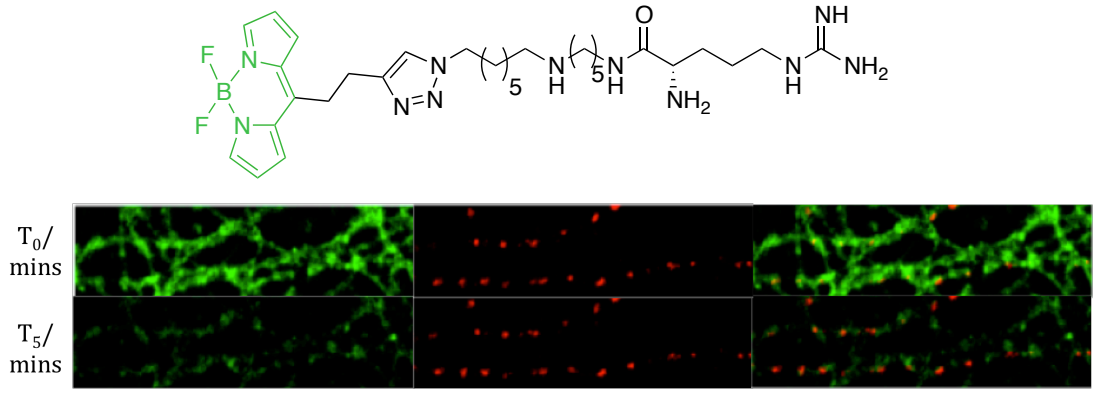

Figure 1.15. (Top) Structure of iGluR-targeted BODIPY probe. (Bottom) Confocal microscopy images of neurons expressing mCherry-tagged NMDA receptors (red fluorescence). Cells were treated for 2 minutes with 50 nM of BODIPY probe (green fluorescence) and then imaged at beginning of washing stage (T_0) and following five minutes continuous washing (T_5).[105]

The most promising BODIPY probe (*Figure 1.15*) was used in cellular staining experiments of NMDA receptors transfected with the red fluorescent protein, mCherry. Upon incubation of BODIPY1, a considerable degree of non-specific binding was observed due to interaction of the positively charged polyamine with the plasma membrane. However, following a continuous five minute washing period, the non-specific staining was removed to reveal punctate fluorescence, overlapping with mCherry emission along the dendrites (*Figure 1.15*). In contrast, cells which were treated with a similar compound with a much

weaker affinity for the NMDA receptor showed no cellular localisation after the 5 minute washing period.[105]

Recently, Perrio and co-workers have synthesised three series of NMDA receptor NR2B subunit specific optical imaging probes by conjugation of fluoroscein to derivatives of the non-competitive antagonist, ifenprodil.[106, 107]

The point of attachment and length of spacer unit connecting the fluorophore to the ligand moiety was found to strongly dictate probe affinity towards the NMDA receptor. By measuring Ca^{2+} influx transients in a competitive assay, optimal affinity was demonstrated when conjugation occurred through modification of the benzylic hydroxyl of ifenprodil. Generally, a longer spacer also increased affinity for the NR2B subunit, although IC_{50} values were approximately 6-fold higher as compared to ifenprodil. Other pharmacological properties, such as subunit selectivity and neuroprotective effects were not compromised by the conjugation of the fluorophore.

When neuronal cells expressing DS-red labelled NMDA receptors were treated with fluoroscein-ifenprodil, a punctate fluorescence was observed from the fluoroscein moiety (*Figure 1.16B*). This fluorescence overlayed with the red fluorescence from the genetically labelled NMDA receptors, demonstrating co-localisation of fluroscein-ifenprodil at the NMDA receptor (*Figure 1.16C*). Furthermore, when cells were pre-treated with ifenprodil and then loaded with fluoroscein-ifenprodil, no fluorescence was observed, suggesting fluoroscein-ifenprodil localises and binds in the same position on NMDA receptors as the native ligand (*Figure 1.16D-F*).

Despite the increased sensitivity and resolution associated with optical imaging methods, this technique is limited by light scattering and absorbance in soft tissue, and has a low effective imaging depth of the order of 10 mm or so.

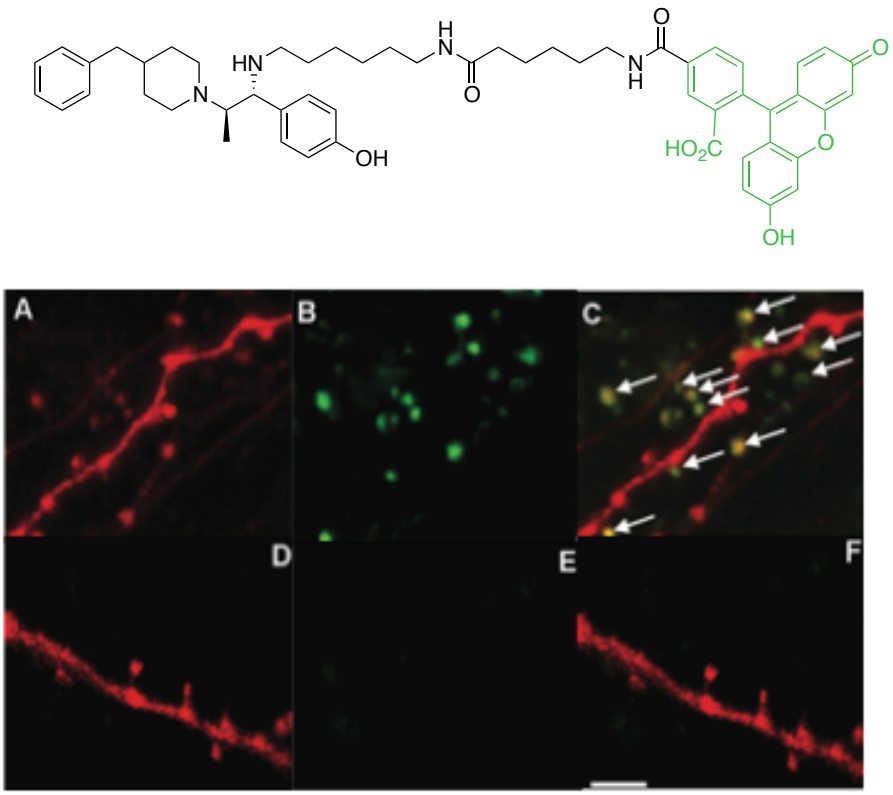

Figure 1.16. (Top) Structure of fluoroscein-ifenprodil. (Bottom) Confocal microscopy imaging of DS-red labelled NMDA receptors (red fluorescence). (A) DS-red emission; (B) Visualisation of fluoroscein emission after incubation of fluorscein-ifenprodil (10 μM, 15 mins); (C) Merge image showing co-localization. (D, E, F) are same as (A, B, C) but with a pre-incubation of ifenprodil (10 μM, 15 mins).[106]

1.4.3 Gd(III)-MRI Contrast Agents for Glutamate Receptors

Despite its lower sensitivity, MRI offers a non-invasive, whole body method for imaging glutamate receptors. Previous work in Durham has shown targeting of $mGluR_5$ receptors by novel MR imaging probes.[108] The imaging probes are derived from a $[Gd.DOTA]^-$ complex linked via a glutarate arm to various selective and specific $mGluR_5$ antagonists (*Scheme 1.6*).

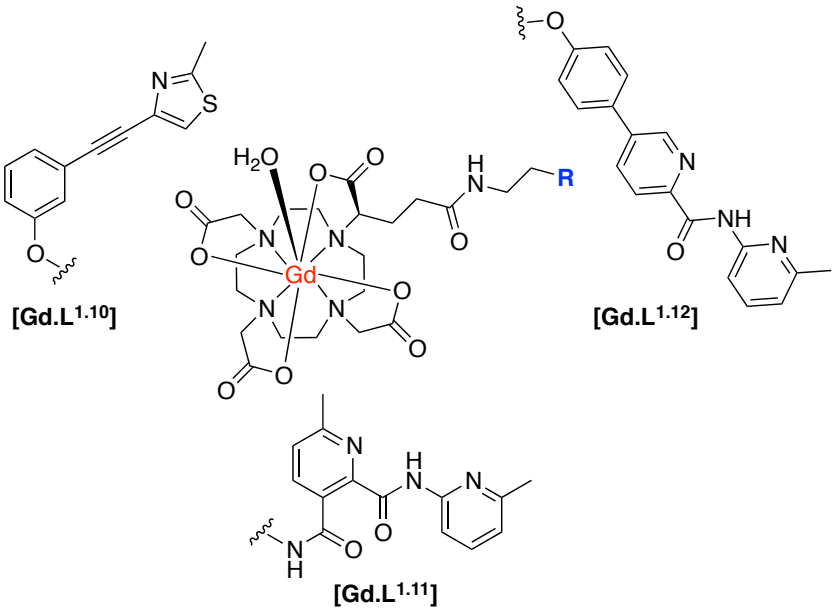

Scheme 1.6. Structures of $mGluR_5$ receptor-targeted contrast agents.

Since appending a Gd(III) complex to an antagonist represents a substantial modification to the chemical structure of the antagonist, the antagonistic effect of the modified probes was investigated. Based on changes in intracellular Ca^{2+} levels, only three complexes **[Gd.L$^{1.10}$]**, **[Gd.L$^{1.11}$]** and **[Gd.L$^{1.12}$]** maintained a significant antagonist effect.[109]

A complete study of the concentration-dependence on the cellular relaxation rate ($R_{1,cell}$) enhancement of primary rat astrocytes expressing $mGluR_5$ receptors was undertaken for all eight compounds, by recording T_1-weighted MR images at 3 T. The complex derived from the most potent antagonist gave rise to the largest enhancement in $R_{1,cell}$ (35% at 200 μM). However this complex did not exhibit any antagonist effect, leading to **[Gd.L$^{1.10}$]** ($R_{1,cell}$ = 33% at 200 μM) being identified as a lead compound from the alkyne-based contrast agents. Of the dipyridyl amide systems, **[Gd.L$^{1.12}$]** exhibited the largest enhancement in $R_{1,cell}$ (30% at 200 μM) and possessed a significant antagonist effect (*Figure 1.17*). This was attributed to the antagonist moiety being able to adopt a planar conformation, essential for $mGluR_5$ affinity.[109]

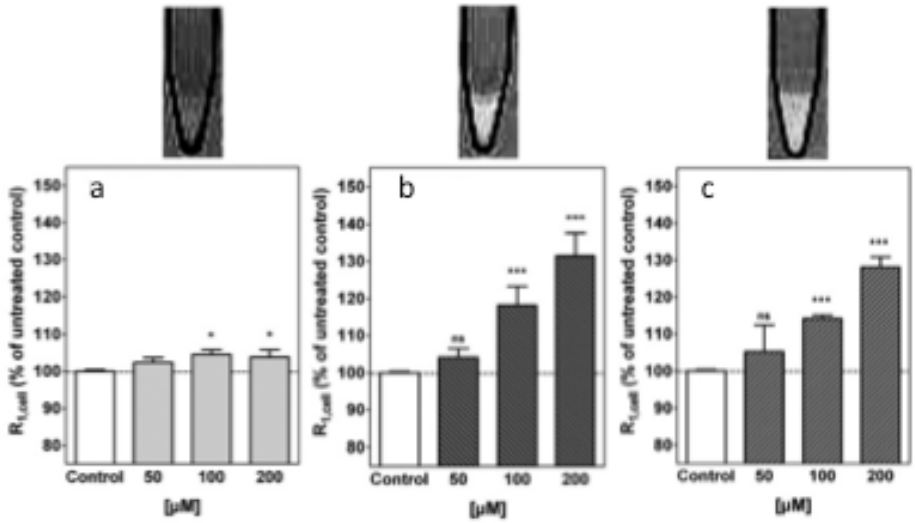

Figure 1.17. (Top) Representative T_1-weighted MR images (3 T) of 1 x 10^7 cells. (Bottom) Cellular relaxation rates, $R_{1,cell}$, after treatment of primary rat astrocytes with (a) **[Gd.DOTA]**, (b) **[Gd.L$^{1.10}$]** and (c) **[Gd.L$^{1.12}$]** (all 200 μM, 45 mins).[109]

Following MR experiments, the cells treated with **[Gd.L$^{1.10}$]** and **[Gd.L$^{1.12}$]** were subject to ICP-MS measurements to determine the total Gd(III) content. Between 6-60 x 10^7 Gd(III) ions per cell were present, which is well above the detection limit of modern MRI experiments. However, the cellular relaxivites were found to differ substantially (2.9 mM^{-1} s^{-1} and 7.4 mM^{-1} s^{-1}, for **[Gd.L$^{1.10}$]** and **[Gd.L$^{1.12}$]**, respectively), suggesting a different mechanism for $R_{1,cell}$ enhancement. The enhancement due to **[Gd.L$^{1.10}$]** can be assigned to the huge increase in cell-associated Gd(III), whereas **[Gd.L$^{1.12}$]** induces a comparable enhancement with only one third Gd(III) present. This suggests that **[Gd.L$^{1.12}$]** induces $R_{1,cell}$ enhancement due to its higher affinity for the $mGluR_5$ receptor.[109]

The enhancements in $R_{1,cell}$ were tentatively assigned to an increase in the τ_R value of the complex upon receptor binding. This is reflected in the ability of **[Gd.L$^{1.12}$]** to bind reversibly to cells possessing $mGluR_5$ in the presence of glutamate, when studied by fluorescence spectroscopy.[108]

Internalisation of the contrast agents was ruled out by performing control experiments, where competition assays in the presence of unmodified antagonists resulted in no significant increase in $R_{1,cell}$. Furthermore, derivatives of the lead compounds were synthesised which included a remote biotin tag. These derivatives were shown to label $mGluR_5$ receptors on the surface of

primary rat astrocytes using confocal and TIRF microscopy after co-incubation with AvidinAlexafluor®-488 conjugate (*Figure 1.18*).[110]

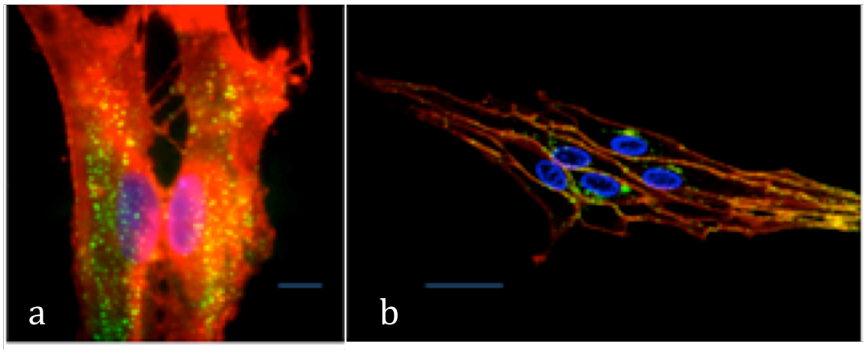

Figure 1.18. (A) TIRF and (B) confocal microscopy images of primary rat astrocytes after incubation with biotin derivative of **[Gd.L$^{1.12}$]** showing predominate cell surface localisation. Green emission (avidinalexafluor®-488) is labelled $mGluR_5$ receptors; orange emission (cell mask orange) is plasma membrane staining and blue emission (Hoechst) highlights the nucleus.[110]

1.5 Aims and Objectives

The aim of this project is to design, synthesise and evaluate a series of molecular imaging contrast agents that specifically target the NMDA receptor, with the majority focused towards MRI.

Glutamate is the most abundant excitatory neurotransmitter in the mammalian central nervous system, having roles in a variety of neuronal processes. The NMDA receptor is an abundantly present glutamate receptor located on the post-synaptic membrane and is responsible for excitatory neurotransmission, memory and learning. However, mis-regulation and over stimulation of the receptor can often lead to a variety of neurodegenerative disorders. Therefore, NMDA receptor-targeted MR contrast agents could provide a neurological tool, functioning both as a marker of receptor density and an indicator of neuronal activity.

The design of these contrast agents must consider the following:

i) The contrast agent should contain an MR-active core, conjugated to a known NMDA receptor ligand.

ii) There should be minimal/no pertubation to the receptor upon binding of the contrast agent.

iii) The contrast agent should bind to the receptor in a reversible manner and with competative affinity to the endogenous ligand, glutamate.

iv) The relaxivity enhancement upon receptor binding should be large enough to allow distinction between bound and unbound contrast agent.

v) The contrast agent should exhibit a fast water exchange rate, such that τ_R limits the relaxivity enhancement, and not the rate of water exchange on/off the Gd ion.

Chapters 2 and 3 describe the design, synthesis, characterisation and *in cellulo* evaluation of a number of NMDA receptor-targeted MRI contrast agents. In *chapter 4*, derivatives of lead compounds were synthesised to allow for direct visualisation of NMDA receptors by optical microscopy. *Chapter 5* describes the synthesis of a NMDA receptor-targeted Eu(III)-complex for time-gated visualisation of these receptors. Finally, *chapter 6* focuses on an emerging imaging modality, photoacoustic imaging, and details the design and synthesis of novel NMDA receptor-targeted photoacoustic imaging agents.

1.6 References

1. M. L. James and S. S. Gambhir, *Physiol. Rev.*, 2012, **92**, 897-965.
2. L. E. Williams, *Med. Phys.*, 2008, **35**, 3020-3029.
3. D. R. Curtis, J. W. Phillis and J. C. Watkins, *J. Physiol.*, 1960, **150**, 656-682.
4. G. J. Siegel, R. W. Albers, S. T. Brady, D. L. Price, *Basic Neurochemistry: Molecular, Cellular amd Medical Aspects*, Elsevier Acadmeic Press, Burlington, 2006.
5. N. C. Danbolt, *Prog. Neurobiol.*, 2001, **65**, 1-105.
6. S. R. Takamori, S. Jeong, C. Rosenmund, J. Reinhard, *Nature*, 2000, **407**, 189-193.
7. S. Takamori, *Neurosci. Res.*, 2006, **55**, 343-351.
8. D. E. Featherstone, *ACS Chem. Neurosci.*, 2009, **1**, 4-12.
9. D. E. Featherstone and S. A. Shippy, *The Neuroscientist*, 2008, **14**, 171-181.
10. Y. Grosjean, M. Grillet, H. Augustin, J. F. Ferveur, D. E. Featherstone, *Nat. Neurosci.*, 2008, **11**, 54-61.
11. K. Chen, H. Augustin and D. E. Featherstone, *J. Comp. Physiol. A*, 2009, **195**, 21-29.
12. C. G. Rousseaux, *J. Toxicol. Pathol.*, 2008, **21**, 25-51.
13. J. N. C. Kew and J. A. Kemp, *Psychopharmacology*, 2005, **179**, 4-29.
14. P. J. Conn and J.P. Pin, *Ann. Rev. Pharmacol. Toxicol.*, 1997, **37**, 205-237.
15. P. Malherbe, F. Knoflach, C. Broger, S. Ohresser, C. Kratzeisen, G. Adam, H. Stadler, J. A. Kemp and V. Mutel, *Mol. Pharmacol.*, 2001, **60**, 944-954.
16. J.-P. Pin, T. Galvez and L. Prézeau, *Pharmacology & Therapeutics*, 2003, **98**, 325-354.
17. D. D. Schoepp, *Neurochem. Int.*, 1994, **24**, 439-449.
18. S. Ozawa, H. Kamiya and K. Tsuzuki, *Prog. Neurobiol.*, 1998, **54**, 581-618.
19. J. Q. Wang, L. Mao, N. K. Parelkar, Q. Tang, Z. Liu, S. Sarwar and E. Choe, *Curr. Neuropharmacol.*, 2003, **1**, 1-20.
20. Y. Nakajima, H. Iwakabe, C. Akazawa, H. Nawa, R. Shigemoto, N. Mizuno and S. Nakanishi, *J. Biol. Chem.*, 1993, **268**, 11868-11873.
21. J. Kumar and M. L. Mayer, *Ann. Rev. Physiol.*, 2013, **75**, 313-337.
22. S. F. Traynelis, L. P. Wollmuth, C. J. McBain, F. S. Menniti, K. M. Vance, K. K. Ogden, K. B. Hansen, H. J. Yuan, S. J. Myers and R. Dingledine, *Pharmacol. Rev.*, 2010, **62**, 405-496.
23. R. Hume, R. Dingledine and S. Heinemann, *Science*, 1991, **253**, 1028-1031.
24. N. Burnashev, H. Monyer, P. H. Seeburg and B. Sakmann, *Neuron*, 1992, **8**, 189-198.
25. http://www.bristol.ac.uk/synaptic/receptors/, 2002
26. N. Kunishima, Y. Shimada, Y. Tsugi, T. Sato, M. Yamamoto, T. Kumasaka, S. Nakanishi, H. Jingami, K. Morikawa, *Nature*, 2000, **407**, 7.
27. W. D. Leuschner and W. Hoch, *J. Biol. Chem.*, 1999, **274**, 16907-16916.
28. G. Ayalon and Y. Stern-Bach, *Neuron*, **31**, 103-113.
29. G. Ayalon, E. Segev, S. Elgavish and Y. Stern-Bach, *J. Biol. Chem.*, 2005, **280**, 15053-15060.
30. H. Yuan, K. B. Hansen, K. M. Vance, K. K. Ogden and S. F. Traynelis, *J. Neurosci.*, 2009, **29**, 12045-12058.

31. P. L. Chazot, M. Cik and F. A. Stephenson, *Mol. Membr. Biol.*, 1995, **12**, 331-337.
32. Y. Stern-Bach, B. Bettler, M. Hartley, P. O. Sheppard, P. J. O'Hara and S. F. Heinemann, *Neuron*, 1994, **13**, 1345-1357.
33. M. L. Mayer, *Nature*, 2006, **440**, 456.
34. S. S. Correia, C. B. Duarte, C. J. Faro, E. V. Pires and A. L. s. Carvalho, *J. Biol. Chem.*, 2003, **278**, 6307-6313.
35. F. Gardoni, A. Caputi, M. Cimino, L. Pastorino, F. Cattabeni and M. Di Luca, *J. Neurochem.*, 1998, **71**, 1733-1741.
36. D. T. Monaghan and R. J. Wenthold, *The Ionotropic Glutamate Receptors*, Humana Press, Totowa, 1997.
37. H. W. Kessels and R. Malinow, *Neuron*, 2009, **61**, 340-350.
38. P. Pinheiro and C. Mulle, *Cell Tissue Res.*, 2006, **326**, 457-482.
39. C. Bonaccorso, N. Micale, R. Ettari, S. Grasso and M. Zappala, *Curr. Med. Chem.*, 2011, **18**, 5483-5506.
40. A. M. Van Dongen, *Biology of the NMDA Receptor*, CRC Press, Boca Raton, 2009.
41. L. Mony, J. N. C. Kew, M. J. Gunthorpe and P. Paoletti, *Br. J. Pharmacol.*, 2009, **157**, 1301-1317.
42. E. Karakas, N. Simorowski and H. Furukawa, *Nature*, 2011, **475**, 249-U170.
43. T. Masuko, K. Kashiwagi, T. Kuno, N. D. Nguyen, A. J. Pahk, J.-i. Fukuchi, K. Igarashi and K. Williams, *Mol. Pharmacol.*, 1999, **55**, 957-969.
44. R. W. Ransom and N. L. Deschenes, *Synapse*, 1990, **5**, 294-298.
45. H. Furukawa, S. K. Singh, R. Mancusso and E. Gouaux, *Nature*, 2005, **438**, 185-192.
46. H. G. E. Furukawa, *EMBO J.*, 2003, **22**, 2873-2885.
47. N. Burnashev, R. Schoepfer, H. Monyer, J. Ruppersberg, W. Gunther, P. Seeburg and B. Sakmann, *Science*, 1992, **257**, 1415-1419.
48. L. Nowak, P. Bregestovski, P. Ascher, A. Herbet and A. Prochiantz, *Nature*, 1984, **307**, 462-465.
49. I. G. Tikhonova, I. I. Baskin, V. A. Palyulin, N. S. Zefirov and S. O. Bachurin, *J. Med. Chem*, 2002, **45**, 3836-3843.
50. K. Erreger, M. T. Geballe, A. Kristensen, P. E. Chen, K. B. Hansen, C. J. Lee, H. Yuan, P. Le, P. N. Lyuboslavsky, N. Micale, L. Jørgensen, R. P. Clausen, D. J. A. Wyllie, J. P. Snyder and S. F. Traynelis, *Mol. Pharmacol.*, 2007, **72**, 907-920.
51. S. D. Donevan, A. Beg, J. M. Gunther and R. E. Twyman, *J. Pharmacol. Exp. Ther.*, 1998, **285**, 539-545.
52. M. N. Perkins, T. W. Stone, J. F. Collins and K. Curry, *Neurosci. Lett.*, 1981, **23**, 333-336.
53. H. J. Olverman, A. W. Jones and J. C. Watkins, *Nature*, 1984, **307**, 460-462.
54. H. Bräuner-Osborne, J. Egebjerg, E. Ø. Nielsen, U. Madsen and P. Krogsgaard-Larsen, *J. Med. Chem.*, 2000, **43**, 2609-2645.
55. E. W. Harris, A. H. Ganong, D. T. Monaghan, J. C. Watkins and C. W. Cotman, *Brain Res.*, 1986, **382**, 174-177.
56. J. Lehmann, A. J. Hutchison, S. E. McPherson, C. Mondadori, M. Schmutz, C. M. Sinton, C. Tsai, D. E. Murphy, D. J. Steel and M. Williams, *J. Pharmacol. Exp. Ther.*, 1988, **246**, 65-75.

57. S. J. Hays, C. F. Bigge, P. M. Novak, J. T. Drummond, T. P. Bobovski, M. J. Rice, G. Johnson, L. J. Brahce and L. L. Coughenour, *J. Med. Chem.*, 1990, **33**, 2916-2924.
58. R. Ian Storer, C. Aciro and L. H. Jones, *Chem. Soc. Rev.*, 2011, **40**, 2330-2346.
59. W. A. Kinney, N. E. Lee, D. T. Garrison, E. J. Podlesny, J. T. Simmonds, D. Bramlett, R. R. Notvest, D. M. Kowal and R. P. Tasse, *J. Med. Chem.*, 1992, **35**, 4720-4726.
60. W. A. Kinney, M. Abou-Gharbia, D. T. Garrison, J. Schmid, D. M. Kowal, D. R. Bramlett, T. L. Miller, R. P. Tasse, M. M. Zaleska and J. A. Moyer, *J. Med. Chem.*, 1998, **41**, 236-246.
61. http://www.england.nhs.uk/statistics/wp-content/uploads/sites/2/2013/04/KH12-release-2012-13.pdf, 2012
62. R. B. Lauffer, *Chem. Rev.*, 1987, **87**, 901-927.
63. F. Bloch, *Nature*, 1952, 911-912.
64. P. C. Lauterbur, *Nature*, 1973, **242**, 190-191.
65. R. Damadian, *Science*, 1971, **171**, 1151-1153.
66. R. Damadian, L. Goldsmith, and L. Minkoff, *Physiol. Chem. Phys*, 1977.
67. P. J. Hore, *Nuclear Magnetic Resonance*, Oxford University Press Inc, New York, 1995.
68. M. C. Heffern, L. M. Matosziuk and T. J. Meade, *Chem. Rev.*, 2013.
69. P. Caravan, *Chem. Soc. Rev.*, 2006, **35**, 512-523.
70. R. Damadian, K. Zaner, D. Hor and T. DiMaio, *Proc. Nat. Acad. Sci.*, 1974, **71**, 1471-1473.
71. P. Caravan, J. J. Ellison, T. J. McMurry and R. B. Lauffer, *Chem. Rev.*, 1999, **99**, 2293-2352.
72. M. Bottrill, L. Kwok and N. J. Long, *Chem. Soc. Rev.*, 2006, **35**, 557-571.
73. A. E. Merbach and E. Toth, *The chemistry of contrast agents in medical magnetic resonance imaging*, Wiley, New York, Chichester, 2001.
74. I. Solomon, *Phys. Rev.*, 1955, **99**, 559-565.
75. N. Bloembergen and L. O. Morgan, *J. Chem. Phys.*, 1961, **34**, 842-850.
76. N. Bloembergen, E. M. Purcell and R. V. Pound, *Phys. Rev.*, 1948, **73**, 679-712.
77. N. Bloembergen, *J. Chem. Phys.*, 1957, **27**, 572-573.
78. P. Caravan, C. T. Farrar, L. Frullano and R. Uppal, *Contrast Media Mol. Imaging*, 2009, **4**, 89-100.
79. M. P. Lowe, D. Parker, O. Reany, S. Aime, M. Botta, G. Castellano, E. Gianolio and R. Pagliarin, *J. Am. Chem. Soc.*, 2001, **123**, 7601-7609.
80. E. L. Que and C. J. Chang, *Chem. Soc. Rev.*, 2010, **39**, 51-60.
81. J. L. Major and T. J. Meade, *Acc. Chem. Res.*, 2009, **42**, 893-903.
82. P. Caravan, *Acc. Chem. Res.*, 2009, **42**, 851-862.
83. P. Caravan and Z. Zhang, *Eur. J. Inorg. Chem.*, 2012, **2012**, 1916-1923.
84. J. Lee, M. J. Zylka, D. J. Anderson, J. E. Burdette, T. K. Woodruff and T. J. Meade, *J. Am. Chem. Soc.*, 2005, **127**, 13164-13166.
85. J. Lee, J. E. Burdette, K. W. MacRenaris, D. Mustafi, T. K. Woodruff and T. J. Meade, *Chem. Biol.*, 2007, **14**, 824-834.
86. P. A. Sukerkar, K. W. MacRenaris, T. J. Meade and J. E. Burdette, *Mol. Pharm.*, 2011, **8**, 1390-1400.

87. S. Aime, E. Gianolio, E. Terreno, G. B. Giovenzana, R. Pagliarin, M. Sisti, G. Palmisano, M. Botta, M. P. Lowe and D. Parker, *J. Biol. Inorg. Chem.*, 2000, **5**, 488-497.
88. P. A. Sukerkar, K. W. MacRenaris, T. R. Townsend, R. A. Ahmed, J. E. Burdette and T. J. Meade, *Bioconjugate Chem.*, 2011, **22**, 2304-2316.
89. J. Faiz Kayyem, R. M. Kumar, S. E. Fraser and T. J. Meade, *Chem. Biol.*, 1995, **2**, 615-620.
90. S. D. Konda, M. Aref, S. Wang, M. Brechbiel and E. C. Wiener, *Magn. Reson. Mat. Phys. Biol. Med.*, 2001, **12**, 104-113.
91. O. Saborowski, G. H. Simon, H.-J. Raatschen, M. F. Wendland, Y. Fu, T. Henning, R. Baehner, C. Corot, M.-H. Chen and H. E. Daldrup-Link, *Contrast Media Mol. Imaging*, 2007, **2**, 72-81.
92. Z. Sideratou, D. Tsiourvas, T. Theodossiou, M. Fardis and C. M. Paleos, *Bioorg. Med. Chem. Lett.*, 2010, **20**, 4177-4181.
93. T. L. Kalber, N. Kamaly, P.-W. So, J. A. Pugh, J. Bunch, C. W. McLeod, M. R. Jorgensen, A. D. Miller and J. D. Bell, *Mol. Imag. Biol.*, 2011, **13**, 653-662.
94. S. Aime, C. Cabella, S. Colombatto, S. Geninatti Crich, E. Gianolio and F. Maggioni, *J. Magn. Res. Imag.*, 2002, **16**, 394-406.
95. D. Messeri, *Targeted and High Relaxivity Contrast Agents*, PhD Thesis, Durham, 2002.
96. G. J. Stasiuk, H. Smith, M. Wylezinska-Arridge, J. L. Tremoleda, W. Trigg, S. K. Luthra, V. M. Iveson, F. N. E. Gavins and N. J. Long, *Chem. Commun.*, 2013, **49**, 564-566.
97. I. Zigelboim, D. Offen, E. Melamed, H. Panet, M. Rehavi and Y. Cohen, *J. Incl. Phenom. Macrocycl. Chem.*, 2007, **59**, 323-329.
98. I. Zigelboim, A. Weissberg and Y. Cohen, *J. Org. Chem.*, 2013, **78**, 7001-7012.
99. V. J. Majo, J. Prabhakaran, J. J. Mann and J. S. D. Kumar, *Drug Discovery Today*, 2013, **18**, 173-184.
100. A. K. Brown, Y. Kimura, S. S. Zoghbi, F. G. Siméon, J.-S. Liow, W. C. Kreisl, A. Taku, M. Fujita, V. W. Pike and R. B. Innis, *J. Nucl. Med.*, 2008, **49**, 2042-2048.
101. F. G. Siméon, A. K. Brown, S. S. Zoghbi, V. M. Patterson, R. B. Innis and V. W. Pike, *J. Med. Chem.*, 2007, **50**, 3256-3266.
102. Y. Kimura, F. Siméon, J. Hatazawa, P. D. Mozley, V. Pike, R. Innis and M. Fujita, *Eur. J. Nucl. Med. Mol. Imaging*, 2010, **37**, 1943-1949.
103. J. Stone, K. Erlandsson, E. Arstad, L. Squassante, V. Teneggi, R. Bressan, J. Krystal, P. Ell and L. Pilowsky, *Psychopharmacology*, 2008, **197**, 401-408.
104. D. Vytla, R. E. Combs-Bachmann, A. M. Hussey, I. Hafez and J. J. Chambers, *Org. Biomol. Chem.*, 2011, **9**, 7151-7161.
105. N. G. Nørager, C. B. Jensen, M. Rathje, J. Andersen, K. L. Madsen, A. S. Kristensen and K. Strømgaard, *ACS Chem. Biol.*, 2013.
106. P. Marchand, J. Becerril-Ortega, L. Mony, C. Bouteiller, P. Paoletti, O. Nicole, L. Barré, A. Buisson and C. Perrio, *Bioconjugate Chem.*, 2011, **23**, 21-26.
107. M. Dhilly, J. Becerril-Ortega, N. Colloc'h, E. T. MacKenzie, L. Barré, A. Buisson, O. Nicole and C. Perrio, *Chem. Bio. Chem.*, 2013, **14**, 759-769.
108. A. Mishra, S. Gottschalk, J. Engelmann and D. Parker, *Chem. Sci.*, 2012, **3**, 131-135.

109. S. Gottschalk, J. Engelmann, G. A. Rolla, M. Botta, D. Parker and A. Mishra, *Org. Biomol. Chem.*, 2013, **11**, 6131-6141.
110. A. Mishra, R. Mishra, S. Gottschalk, R. Pal, N. Sim, J. Engelmann, M. Goldberg and D. Parker, *ACS Chem. Neurosci.*, 2013, **5**, 128-137.

CHAPTER TWO

First Generation NMDA Receptor-Targeted MRI Contrast Agents

2. First Generation NMDA Receptor-Targeted MRI Contrast Agents

2.1 Introduction

The specification at the end of *chapter 1* outlines key criteria to consider in the design of NMDA receptor-targeted MRI contrast agents. Firstly, the receptor-binding moiety must be a known ligand, with sufficient affinity to induce a detectable enhancement in relaxation rate. However, the affinity should not be too high so that it binds reversibly in competition with glutamate. The receptor-binding moiety must also bind in such a way as to minimise perturbation of receptor homeostasis.

The receptor-binding moiety should be linked to a paramagnetic core. A larger enhancement in relaxation rate upon receptor binding will be observed if the most paramagnetically stable ion, Gd(III), is used. The high toxicity of the free metal results in the need for a multidentate, macrocyclic ligand to encapsulate the Gd(III) ion. The resultant complex should possess fast water exchange and some degree of motional coupling to optimise changes in inner sphere relaxation.

Thus, the spacer unit linking the paramagnetic core to the receptor-binding moiety must be of optimal length, so rotational motion between the two sites does not become decoupled. The target structures that were designed are shown below (*Scheme 2*).

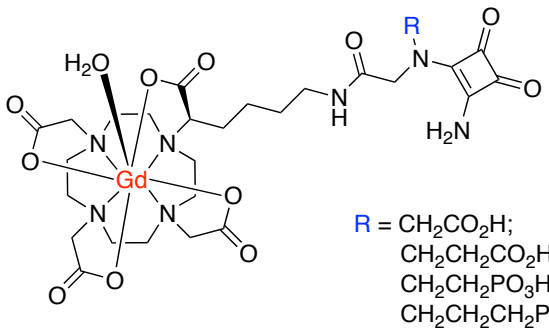

Scheme 2. Structures of potential NMDA receptor-targeted MRI contrast agents.

The target compounds are based on a [Gd.DOTA] core conjugated to derivatives of known competitive antagonists for the NMDA receptor.[1] A competitive antagonist was selected as it was expected to compete with glutamate for the ligand-binding site, whilst not activating the NMDA receptor. As described in *chapter 1*, the 3,4-diamino-3-cyclobutene-1,2-dione moiety acts as an isosteric replacement of the α-amino carboxylic acid functionality found within the majority of competitive NMDA receptor antagonists. Antagonists based on this structure are able to bind to the NMDA receptor with a lower affinity than glutamate, fulfilling the specification outlined in *chapter 1*. Furthermore, the Gd(III) ion is encapsulated in the DOTA structure, with this ligand system chosen in order to maximise the water exchange rate, k_{ex}, and minimise non-specific protein binding. The linker unit is derived from lysine, and was chosen because the receptor-binding moiety is sufficiently spaced from the Gd(III) chelate in order to maintain antagonist affinity and yet retain some coupled rotational motion.

2.2 Synthetic Details

2.2.1 Receptor-Binding Moieties of [Gd.L[1]] and [Gd.L[2]]

The synthesis of the receptor binding moieties of **[Gd.L[1]]** and **[Gd.L[2]]** began with commercially available 3,4-cyclobutene-1,2-dione. Mono-amination was achieved by stirring with an ethanolic ammonia solution overnight at room temperature.[2] Trituration with cold hexane revealed the free amine ***1***, which was then protected as the carbamate using di-*tert*-butyl-dicarbonate in anhydrous DCM, in the presence of triethylamine as a base (*Scheme 2.1*). The product ***2*** was isolated as a stable yellow solid.

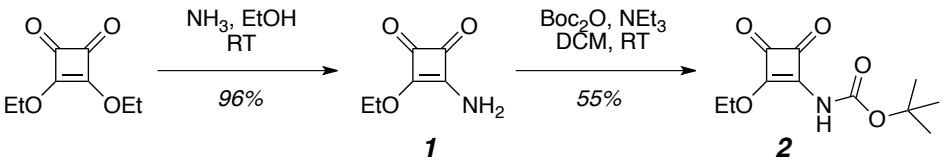

Scheme 2.1.

With compound ***2*** in hand, a divergent approach was adopted (*Scheme 2.2*). For the synthesis of **[Gd.L¹]**, a Michael addition-elimination reaction between *tert*-butyl (2-ethoxy-3,4-dioxocyclobut-1-en-1-yl)carbamate (***2***) and the hydrochloride salt of *tert*-butyl glycine was conducted in anhydrous EtOH with diisopropylethylamine present to neutralise the hydrochloride salt. After removal of the solvent under reduced pressure, the crude residue was purified by column chromatography to afford ***3***, in a high yield.

The final step in the synthesis of the receptor-binding moiety of **[Gd.L¹]** involved introduction of a small linker, which would provide the point of attachment to the macrocyclic core. This was achieved through *N*-alkylation of ***3*** in dry DMF at 40 °C, with methyl bromoacetate in the presence of NaH. Following work-up and purification by column chromatography, the fully protected receptor-binding moiety (***4***) was isolated as a light green oil.

Due to the orthogonal nature of the protecting group strategies employed in the synthesis of ***4***, this compound was subject to basic conditions in order to selectively remove the methyl ester. Rapid methyl ester hydrolysis was confirmed by ^{1}H NMR spectroscopy, with loss of the methyl singlet at 3.76 ppm to give ***5***.

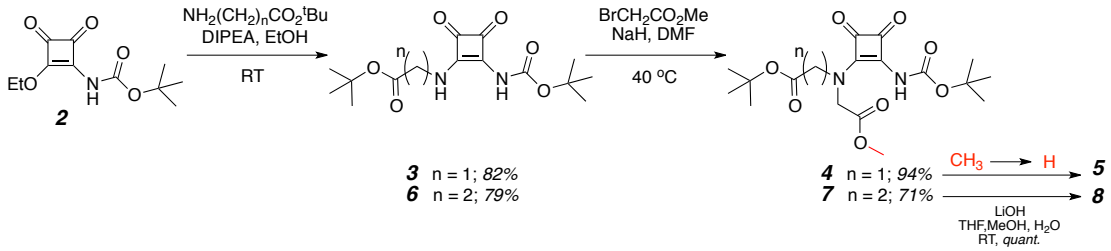

Scheme 2.2.

Using the same approach as described for the synthesis of compound ***5***, the receptor-binding moiety of **[Gd.L²]** was also achieved by replacing glycine *tert*-butyl ester with the hydrochloride salt of *β*-alanine *tert*-butyl ester (*Scheme 2.2*).

2.2.2 Receptor-Binding Moieties of [Gd.L^3] and [Gd.L^4]

The majority of NMDA receptor antagonists contain a phosphonic acid group to replace the distal carboxylic acid. This often leads to the antagonist possessing an increased NMDA receptor affinity, as was the case of AP5 and AP7 (*chapter 1*).[3] Similarly, in the original work describing the squaramide derived NMDA receptor antagonists, it was observed that substitution of the distal carboxylic acid with a phosphonic acid moiety resulted in a 3-fold enhancement in receptor affinity.[1] Baring this in mind, it was reasoned that the use of a higher affinity receptor-binding moiety would offset the expected decrease in overall affinity upon conjugation to the relatively large Gd(III) chelate.

The synthesis of the receptor-binding moieties of **[Gd.L^3]** and **[Gd.L^4]** followed a similar route to that used in the synthesis of compounds ***5*** and ***8***. Initially, the synthesis of the β- and γ-amino phosphonates was undertaken and were used in subsequent Michael addition-elimination reactions with ***2***. Following standard Gabriel synthesis methods,[4] the corresponding β- and γ-bromo phosphonates were stirred with potassium phthalamide and NaH in DMF at 100 °C. For the γ-bromo phosphonate, the corresponding phthalamide-phosphonate (***9***) was prepared in a reasonable yield after work-up. Subsequent unmasking of the primary amine (***10***) was achieved in excellent yield, upon stirring with hydrazine in refluxing ethanol (*Scheme 2.3*).

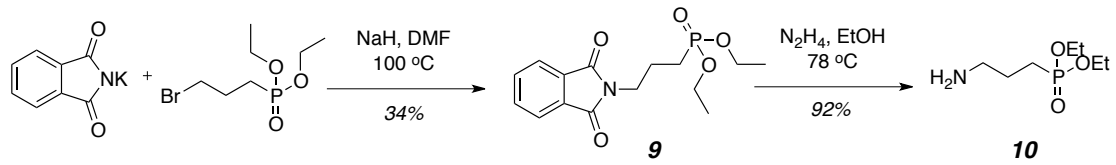

Scheme 2.3.

However, under the conditions employed, the β-bromo phosphonate underwent a competing elimination reaction to form predominantly diethyl vinyl phosphonate, as identified by ^{1}H and ^{31}P NMR spectroscopy. With this in mind,

the commercially available diethyl (2-amino ethyl) phosphonate oxalate was considered a better precursor for the Michael addition-elimination reaction.

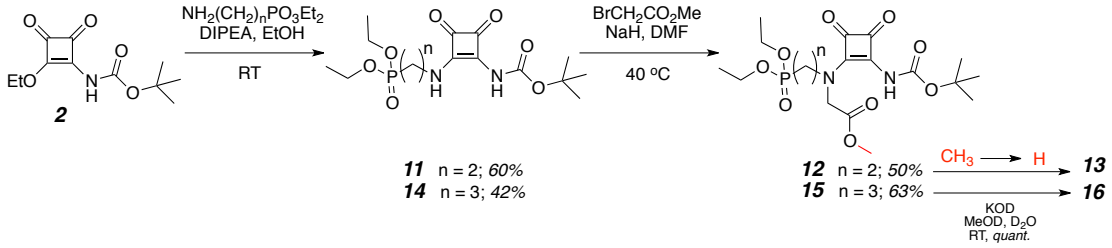

Scheme 2.4.

The remaining steps followed the previous route used for the synthesis of the receptor-binding moieties of **[Gd.L^1]** and **[Gd.L^2]**, giving the free carboxylic acids, ***13*** and ***16*** (*Scheme 2.4*), ready for conjugation to the macrocycle.

2.2.3 Linker and Macrocycle Synthesis

The linker between the Gd(III) core and pendant NMDA receptor-binding moiety was derived from the commercially available amino acid derivative, ε-Cbz-protected L-lysine. Derivitisation via diazotisation of the α-amino group, followed by *in-situ* bromination gave the brominated derivative (***17***), with the reaction proceeding with overall retention of configuration. After work-up, the yellow oil was esterified using *tert*-butyl acetate in the presence of a catalytic amount of acid, to give orthogonally protected ***18*** (*Scheme 2.5*).

The macrocycle ***19*** was synthesised in a reasonable yield using an established literature procedure.[5] Alkylation of ***19*** with ***18*** to afford ***20*** was achieved by stirring in anhydrous acetonitrile, at 80 °C, overnight. Two equivalents of K_2CO_3 and a small volume of solvent were used in order to accelerate the reaction. Finally, removal of the carbamate protecting group was achieved through $Pd(OH)_2$/C-catalysed, high pressure hydrogenation. Filtration and evaporation of the solvent revealed the hygroscopic primary amine, ***21*** (*Scheme 2.5*).

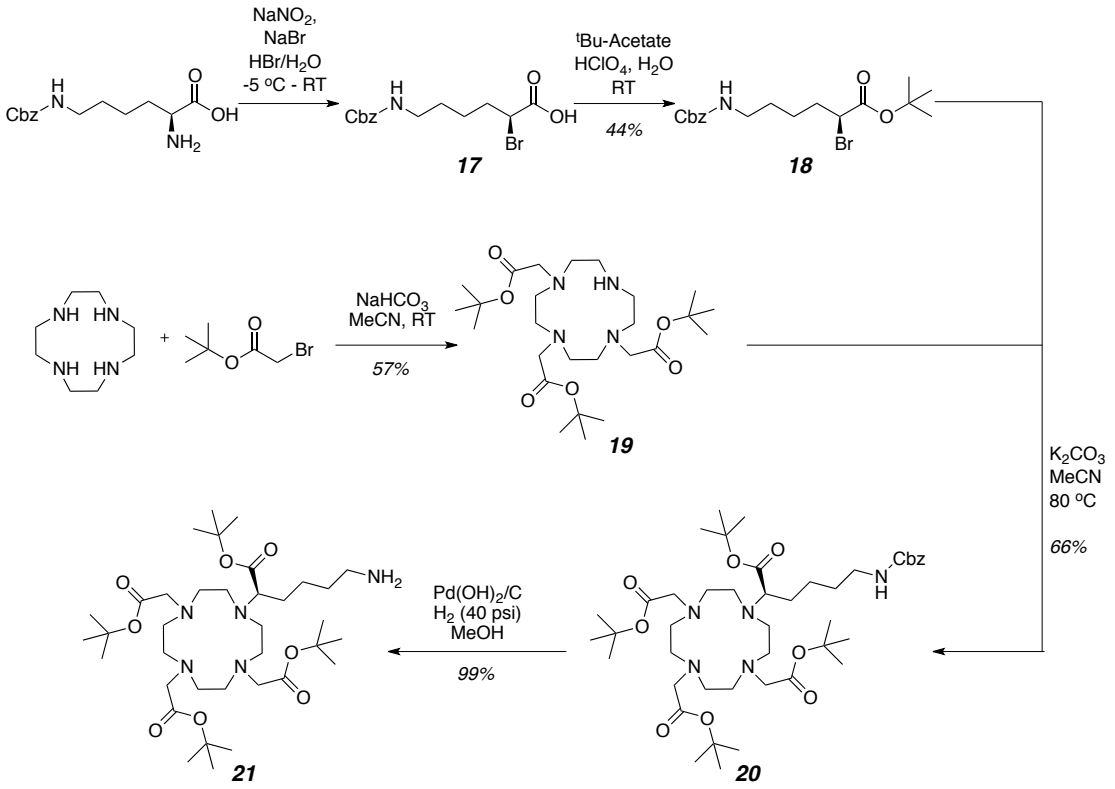

Scheme 2.5.

2.2.4 Conjugates and Complexes

With each of the four receptor-binding moieties and the macrocyclic amine in hand, the next step was to join the two fragments together. Conjugation of the coupling partners was achieved as outlined in *scheme 2.6*. Compounds ***5***, ***8***, ***13*** and ***16*** were dissolved in a minimum amount of anhydrous DMF along with EDC.HCl and HOBt, and stirring was commenced for 20 minutes to allow the formation of the active ester *in-situ*. After this period, a pre-formed solution of ***21*** and *N*-methyl-morpholine (NMM) in a small volume of DMF was added dropwise to the reaction mixture. Slow formation of the desired conjugates was observed by ESI-MS after stirring at room temperature for 48 hours. After work-up and purification by column chromatography, **[conjugates 1-4]** (***22-25***), were isolated as viscous oils, albeit in low yields.

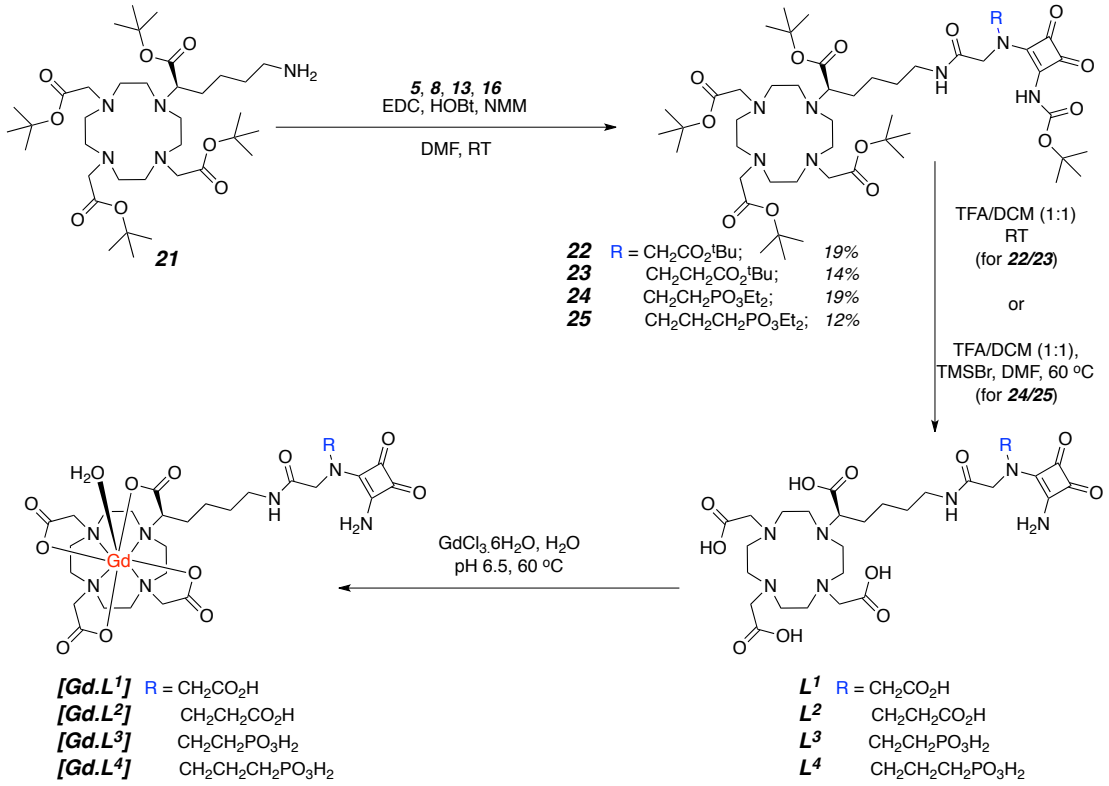

Scheme 2.6.

Cleavage of the carbamate and *tert*-butyl protecting groups of ***22*** and ***23*** was achieved using a 1:1 mixture of trifluoroacetic acid and DCM at room temperature overnight. Analysis of the crude product by ^{1}H NMR and mass spectrometry provided confirmation of the formation of ***L¹*** and ***L²***.

In a similar manner, cleavage of the carbamate and *tert*-butyl esters of ***24*** and ***25*** was undertaken in a 1:1 mixture of trifluoroacetic acid and DCM. The crude phosphonate ethyl ester was dissolved in DMF and heated to 60 °C in the presence of an excess of bromotrimethylsilane. Analysis of the ^{31}P NMR spectrum of ***L⁴*** showed a characteristic shift to lower frequency after 16 hours, indicating complete hydrolysis to the corresponding phosphonic acid.

Finally, complexation of the corresponding TFA salts of ***L¹⁻⁴*** was carried out by reaction with $GdCl_3.6H_2O$ in H_2O (pH 6-6.5) at 60 °C overnight (*Scheme 2.6*). A slight excess of the Gd(III) salt was used to ensure complete complexation. Upon completion, the excess Gd(III) was removed by the addition of Chelex-100™ resin. After 30 minutes, syringe filtration of the resin from the aqueous solution revealed the complexes **[Gd.L$^{1-4}$]$^{-}$** after lyophilisation.

In order to confirm the presence of complexes **[Gd.L$^{1-4}$]**, high-resolution mass spectrometry analysis was undertaken. Gadolinium has six stable isotopes, giving an observable characteristic isotope pattern in mass spectrometry. The presence of the isotope pattern of **[Gd.L^{4}]** is shown (*Figure 2*), comparing theoretical and experimental distrubutions.

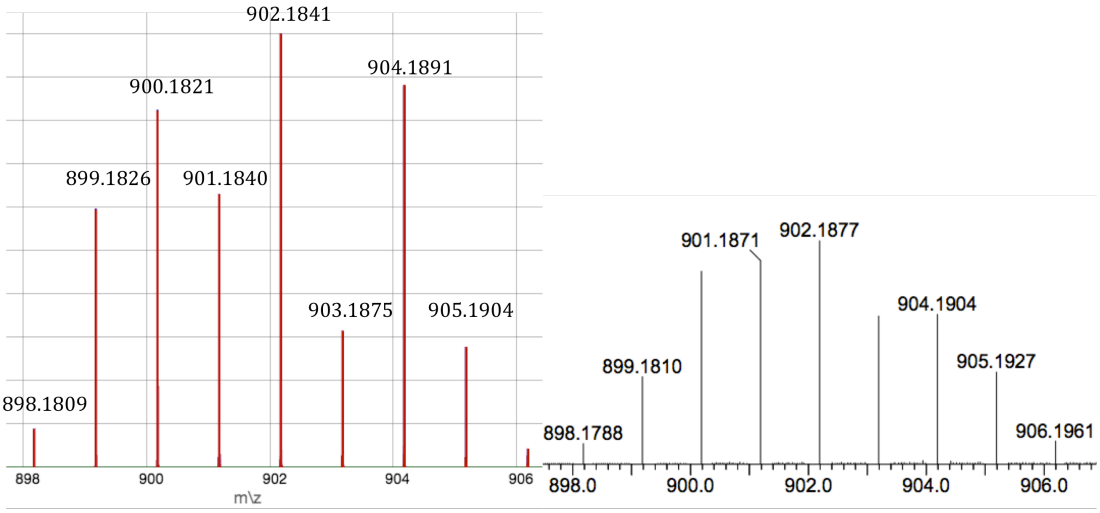

Figure 2. (Left) Calculated and (Right) observed high-resolution electrospray mass spectrum of **[Gd.L^{4}]**, showing the characteristic Gd-isotope pattern; TOF-MS negative mode.

2.3 Relaxivity Properties

The aqueous synthesis of complexes **[Gd.L$^{1-4}$]** results in contamination of these samples with various salts, which renders it difficult to obtain accurate weights of the complexes. Therefore, the Evans' bulk magnetic susceptibility (BMS) method[6] was employed to determine total complex concentration in a given volume. This NMR method relies on the phenomenon that a paramagnetic species can induce a chemical shift in nuclear frequencies via three general mechanisms, one of which is the BMS mechanism. The sample is dissolved in D_2O (containing 1% *tert*-butanol) and placed inside an NMR tube. A co-axial tube containing the same solvent mixture (minus the paramagnetic species) provides a reference point and the frequency difference ($\Delta\delta_{ppm}$) between the two *tert*-butanol resonances represents the BMS shift (Δ_x). To a good approximation, the BMS shift is related to the total paramagnetic concentration (c) by *equation 2*;[7]

$$\Delta\delta_{ppm} = \Delta_x = \frac{4\pi c}{3T}\left(\frac{\mu_{eff[Gd]}}{2.84}\right)^2 \times 10^3 \quad (2)$$

where T is the temperature and $\mu_{eff[Gd]}$ is the effective magnetic moment of the Gd(III) ion.

Following the determination of the complex concentration, the water proton relaxation times, T_1, were measured in aqueous solution (pH 7.4), at 310 K and 1.4 T, on a Bruker Minispec mq60 instrument (*Table 2*). The mean value of three independent measurements was recorded and averaged. Relaxivities, r_{1p}, of the complexes **[Gd.L$^{1\text{-}4}$]** were calculated as the slope of the function shown in *equation 1.1*, with $T_{1,d}$ calculated to be 4000 ms. The relaxivities for **[Gd.L$^{1\text{-}4}$]** were 5.2 (±0.3), 5.3 (±0.3), 4.7 (±0.2) and 4.8 (±0.2) mM^{-1} s^{-1}, respectively at 60 MHz. These values are typical and lie in the expected range for mono-aqua gadolinium species of this molecular weight, where relaxivity scales with molecular volume as a function of τ_R.[8]

2.3.1 The Effects of Albumin on Complex Relaxivity

In the low to medium field range, the relaxivity of **[Gd.L$^{1\text{-}4}$]** is largely dictated by τ_R. Upon interaction with the NMDA receptor, the complexes **[Gd.L$^{1\text{-}4}$]** should increase their relaxivity leading to an increase in water proton relaxation rate. This is due to disruption of the rotational dynamics of the complex upon formation of a non-covalent conjugate with the receptor.

In order to assess the relaxivity properties of the receptor-bound contrast agent, a relatively large concentration (typically high μM range) of isolated NMDA receptors is needed. Since this is impractical and expensive, it was decided that assessment of protein interaction would be conducted with a more readily available model protein. Human serum albumin (HSA) is a large globular protein and constitutes approximately 4.5% of plasma. It contains a number of different binding sites for a variety of endogenous ligands and drug molecules, transporting them throughout the vascular network.[9] There is a large amount of data in the literature describing the interaction of this protein with various Gd(III) complexes.[10, 11] In this study, the non-covalent relaxation enhancement

may reflect, to some extent, that which may occur through non-specific binding to endogenous protein. At least, it may set the lower limit of enhancement when the complexes are bound to the NMDA receptor.

Using the proton relaxation enhancement (PRE) technique,[11] incremental additions of up to 1.6 mM of HSA to aqueous solutions of **[Gd.L$^{1\text{-}4}$]** (all 1 mM) were made and the resulting relaxivity measured at 310 K and 1.4 T. Association constants were then estimated assuming a 1:1 stoichiometry of interaction from the 'best-fit' of an iterative least squares fitting (*Figure 2.1 and Table 2*).

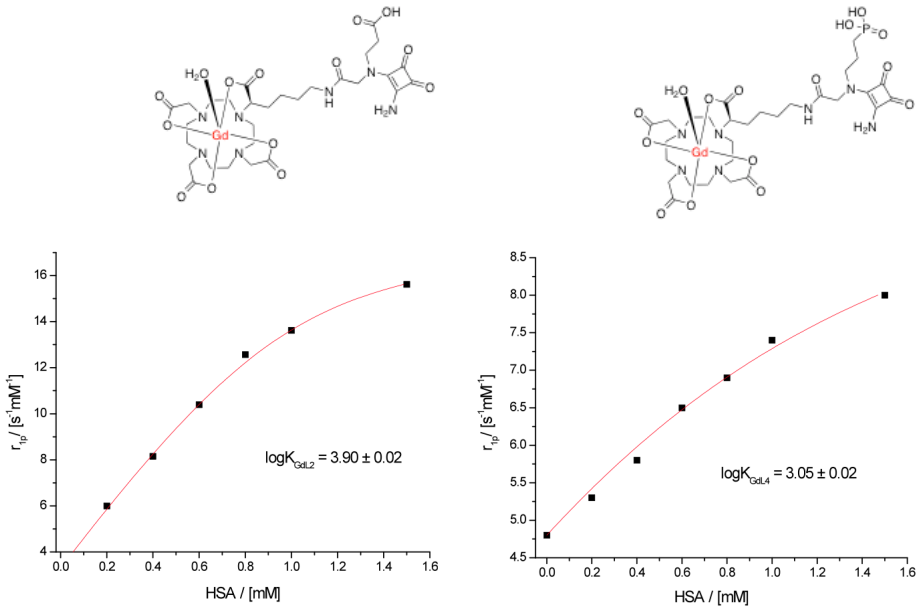

Figure 2.1. Binding constant determination of **[Gd.L$^{2\&4}$ vs HSA]** showing the fit(line) to the data derived by iterative least squares fitting, assuming a 1:1 binding interaction. Errors quoted are statistical errors in the fitting (1.4 T, pH 7, 310 K).

Table 2. Binding affinities to serum albumin, [a,b,c] and relaxation properties of the complexes reported herein (310 K, pH 7.4, 1.4 T).

	[Gd.L^1]	**[Gd.L^2]**	**[Gd.L^3]**	**[Gd.L^4]**
log *K*	3.50^a	3.90^b	2.50^a	3.05^b
$r_{1p}^{initial}$/mM^{-1} s^{-1}	5.2	5.3	4.7	4.8
r_{1p} at 0.7 mM HSA/ mM^{-1} s^{-1}	7.6	11.4	5.6	6.7
r_{1p}^{limit}/ mM^{-1} s^{-1}	11	18	14	11

^{a} error is ± 0.03 mM^{-1} s^{-1}; ^{b} error is ± 0.02 mM^{-1} s^{-1} ; ^{c} the relative affinities (IC_{50} values, i.e. not the 1: 1 binding constant), for the NMDA binding moiety in L$^{1\text{-}4}$ are 2.3, 1.6, 0.47 and 2.6 μM respectively.[1]

Log *K* for **[Gd.L$^{1\text{-}4}$]** with HSA were 3.50 (±0.03), 3.90 (± 0.02), 2.50 (±0.03) and 3.05 (± 0.02), respectively (Table 2). These values are consistent with relatively weak binding, similar to that reported for a [Gd.DOTA] derivative with three benzyloxymethelene pendant groups (log*K* = 3.2).[11] By comparing each pair (**[Gd.L$^{1\text{-}2}$]** vs. **[Gd.L$^{3\text{-}4}$]**) it is apparent that increasing the chain length of the pendant acidic arm enhances the binding interaction between the complex and the protein. In the case of **[Gd.L^{2}]**, the limiting relaxivity value is significantly higher than the other complexes, as a direct result of a greater τ_R modulation. This is reflected in the larger association constant (*cf*. closer to that of MS-325; log*K* = 4.05 at 310 K),[9] which is consistent with a stronger complex-protein interaction. However, this interaction is relatively weak (K_d =100 μM). This is promising, as it is expected that a larger relaxivity gain will be observed when the complexes bind to the NMDA receptor, which can be distinguished from the weaker non-specific binding interaction examined here.

2.4 Probe-Receptor Binding Studies

2.4.1 Development of a Neuronal Cell-line Model

To investigate the ability of **[Gd.L$^{1\text{-}4}$]** to act as NMDA receptor-targeted MR contrast agents, a neuronal cell line model expressing functional NMDA receptors was needed. The majority of cell lines in the literature which possess glutamate receptors, are grown through differentiation of tumour cells. However, these cells do not fully represent a neuronal cell. In 2000, Manning and co-workers described the development of a glutamate-sensitive hybrid cell-line, derived from the fusion of motor-neuron enriched mouse spinal cord and neuroblastoma cells.[12] After differentiation, these cells were reported to express the NR1 and NR2A/B subunits that are responsible for the formation of functional NMDA receptors. These differentiated NSC-34 cells were also reported to express function AMPA and Kainate receptor subunits. In the original report, undifferentiated NSC-34 cells did not express any glutamate receptor density in immunofluorescence staining experiments, so it was envisaged that they could provide a negative control in the cellular labelling experiments.

Cell culture of both undifferentiated and differentiated NSC-34 cells was performed by Dr. Joern Engelmann and Dr. Sven Gottschalk at the Max Planck Institute for Biological Cybernetics in Tuebingen. Cells were cultured in a 1:1 mixture of Dulbecco's modified Eagle's (DMEM) and Hams' F12 media, supplemented with fetal bovine serum (10%). At approximately 90% confluence, differentiation of the cells was induced through gradual serum depletion (10 to 1%). The cells were allowed to proliferate over the course of 7 days to allow for the growth of functional NMDA receptors.

The expression of NMDA receptors was demonstrated on differentiated NSC-34 cells using immunofluorescence techniques. The cells were fixed to microscope slides and incubated for 2 hours with the primary antibodies for the NMDA receptor subunits, NR1 and NR2B. After washing, the secondary antibody was loaded (2 hours), followed by incubation with the nuclear stain, Hoechst. Visualisation of the differentiated NSC-34 cells by fluorescence microscopy demonstrated the presence of both NMDA receptor subunits, indicating functional NMDA receptors (*Figure 2.2*).

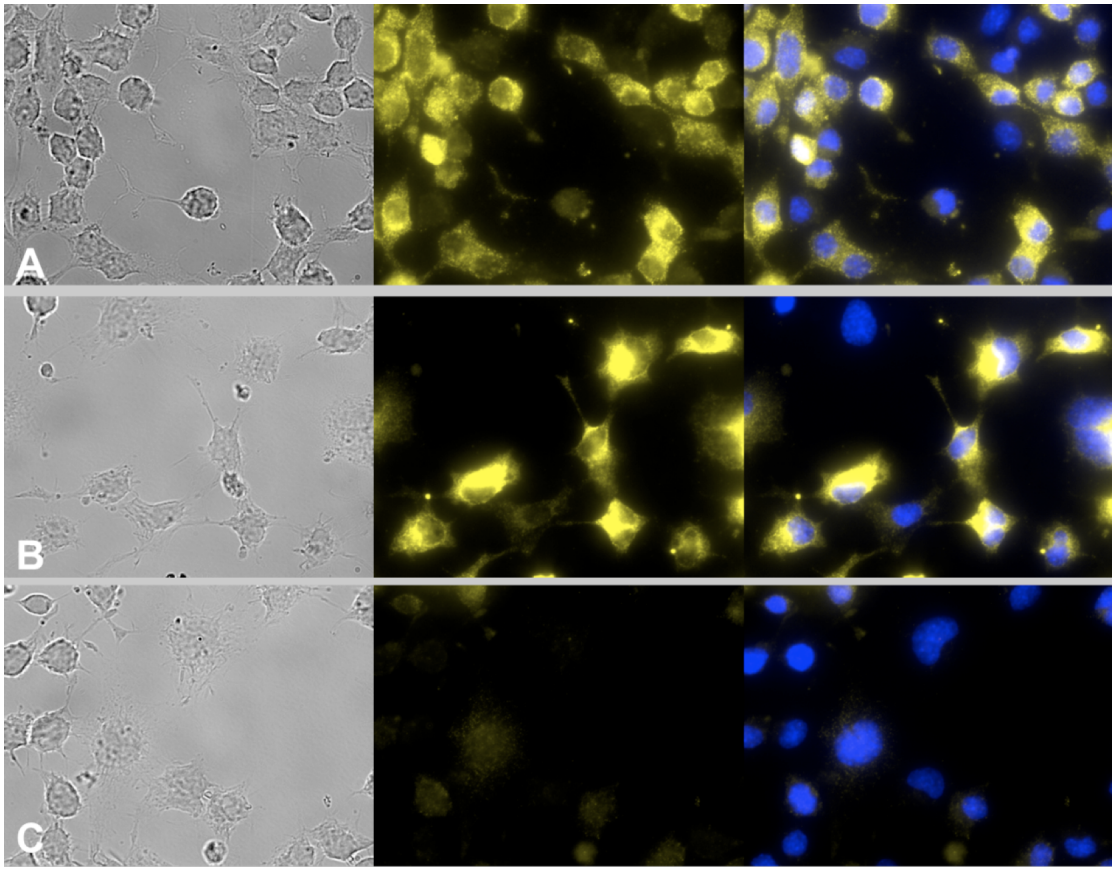

Figure 2.2. Immunostaining of differentiated NSC-34 cells. (A) From left to right: differential interference contrast image showing cell morphology, NMDA NR2B (yellow,

Cy 3™) visualised after staining with specific antibodies and overlay with counterstained cell nuclei (blue, Hoechst 33342). (B) as (A) but with specific antibodies for the NMDAR1 subunit on different cells. (C) Control staining for non-specific binding of the 2nd antibody (goat anti-rabbit-Cy 3™). The middle image was normalized to the brightness and contrast of the Cy 3™ image in (A), demonstrating very low non-specific binding of the 2nd antibody. [Carried out at MPI, Germany].

2.4.2 MRI Analysis of Cell Suspensions *In vitro*

Following the positive expression of NMDA receptors, cellular labelling of differentiated and undifferentiated (control) NSC-34 cells with **[Gd.L$^{1\text{-}4}$]** was assessed by measuring the longitudinal relaxation time, T_1, of the cells on a 3 T Siemens human whole body MR scanner, which allowed the calculation of cellular relaxation rates, $R_{1,cell}$. All MR experiments were performed by Dr. Sven Gottschalk at the Max Planck, Tuebingen. Differentiated and undifferentiated NSC-34 cells were treated with 200 μM solutions of the complexes **[Gd.L$^{1\text{-}4}$]** for 45 minutes at 310 K and 5% CO_2. After this period, the cells were washed thoroughly with Hank's buffered saline solution (HBSS) to remove any unbound complex, re-suspended in fresh buffer and the T_1-weighted MR images were acquired overnight, using a spin-echo inversion recovery method. Untreated cells and cells treated with the non-targeted, clinically approved contrast agent, [Gd.DOTA], were also imaged to serve as controls.

By normalising the untreated cells to 100% it was then possible to determine the influence of each complex on $R_{1,cell}$. Initial studies showed positive signs of cellular labelling by **[Gd.L^1]**, **[Gd.L^2]** and **[Gd.L^4]** on differentiated NSC-34 cells, represented as a percentage increase in cellular relaxation rate of 120%, 195% and 170%, respectively. However, treatment of the same concentration of these three complexes induced increases in $R_{1,cell}$ of 130%, 186% and 115% on undifferentiated NSC-34 cells. This suggests that these complexes either possessed the ability to label cells through non-specific interactions, or that undifferentiated NSC-34 cells also possessed NMDA receptor density, reducing their potential as a control cell line. In order to elucidate which was the more likely, immunofluorescence techniques were performed on undifferentiated NSC-34 cells, to look for the expression of NMDA receptors.

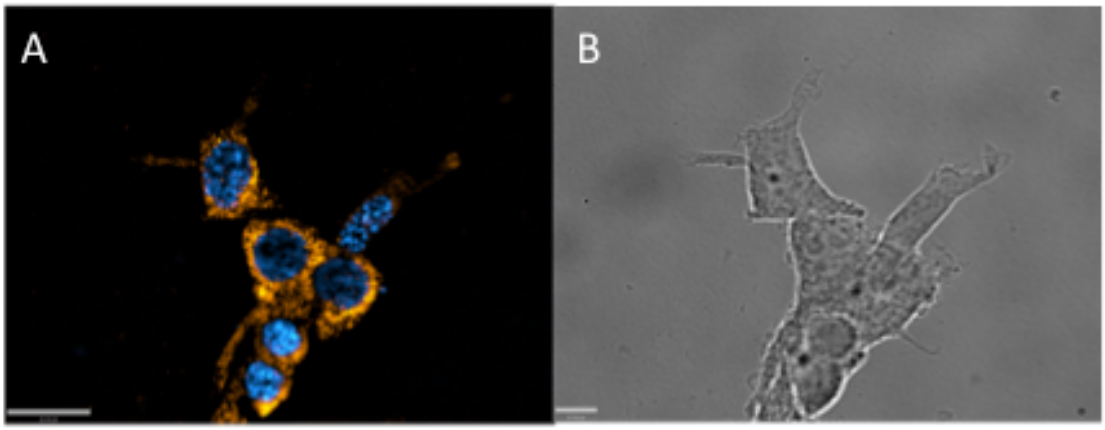

Figure 2.3. (A) Visualisation of the NMDA receptor NR2B subunit after staining undifferentiated NSC-34 cells with NR2B specific antibodies and overlaying with nuclear stain, Hoechst. (B) Transmission image.

In contrast to the report by Manning and co-workers,[12] undifferentiated NSC-34 cells were found to express both NMDA receptor subunits, NR1 and NR2B (*Figure 2.3*). This explains the observed increases in $R_{1,cell}$ for the undifferentiated cells which were incubated with **[Gd.L^1]**, **[Gd.L^2]** and **[Gd.L^4]**. Since there is no way to quantify the receptor density present on each cell type, it was thought best to avoid the use of the undifferentiated cells as a control. The differentiated NSC-34 cells should possess a higher NMDA receptor density and therefore, more closely resemble the *in vivo* situation.

To allow for a statistically relevant measure of $R_{1,cell}$ enhancement for each complex, T_1 measurements were conducted several times on differentiated NSC-34 cells, that were continuously cultured before differentiation. However, each time the T_1 was measured, a much lower value of $R_{1,cell}$ was found in comparison to the previous measurement, resulting in a statistically lower average $R_{1,cell}$ enhancement for each complex. This suggested that the receptor density decreased over prolonged cell culture periods. Taking this into account, the continuous growth of cells before differentiation was stopped. The cell culture protocol was modified so that fresh, undifferentiated NSC-34 cells were grown and then differentiated for each T_1-measurment, and this led to reproducible changes in $R_{1,cell}$ (*Figure 2.4*).

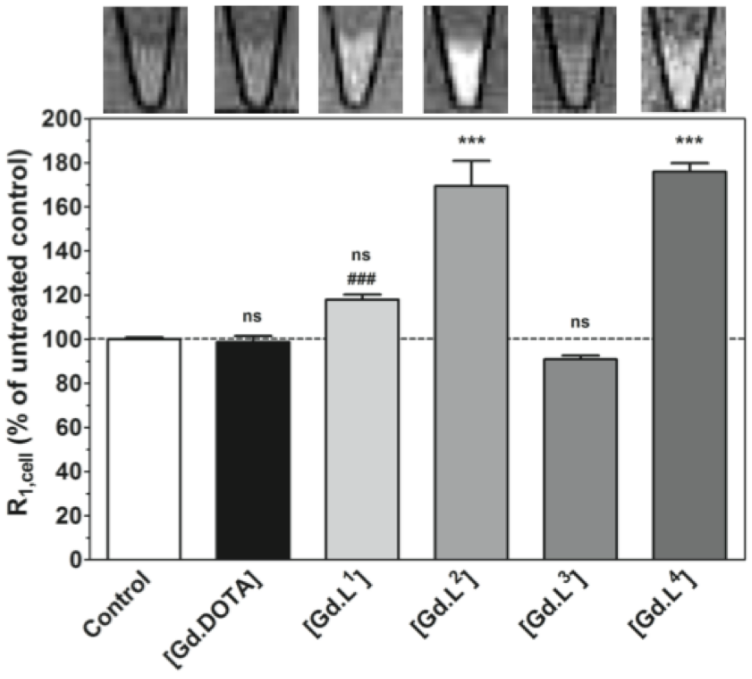

	[Gd.DOTA]	**[Gd.L^1]**	**[Gd.L^2]**	**[Gd.L^3]**	**[Gd.L^4]**
$R_{1,cell}$/ % control	99±1%	118±2%	170±11%	91±2%	176±4%

Figure 2.4. (Top) Representative T_1-weighted MR-images of 1 x 10^7 untreated differentiated cells (control) and differentiated cells treated for 45 min with 200 μM of **[Gd.DOTA]** or **[Gd.L$^{1-4}$]**. (Bottom) Cellular ^{1}H MR relaxation rates $R_{1,cell}$ in cell suspensions (3 T, 298 K) after treatment of differentiated NSC-34 cells with 200 μM **[Gd.DOTA]** or **[Gd.L$^{1-4}$]** for 45 min. **[Gd.DOTA]** served as a negative control. Values are mean ± SEM (n=3-6). ns: not significant, ***P<0.001 ANOVA with Bonferroni's multiple comparison post test. ###P<0.001 Student's t-test. Both tests vs. untreated control using Graphpad Prism 5.02.[Carried out at MP, Germany].

The presence of an α-amino carboxylic acid functionality is essential for a compound to serve as an NMDA receptor antagonist. The complexes **[Gd.L$^{1-4}$]** contain an isosteric replacement for the α-amino carboxylic acid functionality, linked to a pendant acidic group of varying length, which gives the NMDA receptor-binding moiety of these contrast agents. The complexes **[Gd.L$^{1-2}$]** employ a carboxylic acid with a one or two carbon spacer, as the pendant acidic group. Although **[Gd.L^1]** induces an increase in $R_{1,cell}$ when incubated with differentiated NSC-34 cells (118% of control), the two-carbon homologue, **[Gd.L^2]**, displays a statistically higher increase in $R_{1,cell}$ (170% of control). This suggests that **[Gd.L^2]** binds to the NMDA receptor with a greater affinity than

that of **[Gd.L^1]**, and this is consistent with the reported trend in affinity constants of the small molecule antagonists.[1]

The original small molecule work suggested that substitution of the pendant carboxylic acid with phosphonic acid results in a NMDA receptor-binding motif with a greater affinity. Therefore, it was expected that **[Gd.L$^{3\text{-}4}$]** should bind to the NMDA receptor with a greater affinity, leading to a larger enhancement of $R_{1,cell}$. Interestingly, **[Gd.L^3]** showed no apparent receptor specific interaction ($R_{1,cell}$ = 91% of control), despite the antagonist it was derived from being reported as the most potent of the series.[1] In contrast, **[Gd.L^4]**, with the three-carbon linker induces a large enhancement in $R_{1,cell}$ (176% of control) when incubated with differentiated NSC-34 cells.

Previous work in the Durham group has shown that appending a sterically demanding Gd(III) chelate to a known receptor-binding moiety can result in a marked decrease in affinity for a specific receptor.[13] It is possible that this is the reason for the lack of binding of **[Gd.L^3]** to the NMDA receptor. However, it is also plausible that the squaramide moiety in **[Gd.L^3]** adopts an unfavourable conformation for receptor binding. Due to rotation around the C-N bond, several rotameric forms of squaramides exist.[14] This can give rise to 8/9-ring chelates that are stabilised through intramolecular hydrogen bonding, which will decrease the likelihood of intermolecular bonding to specific residues present on the NMDA receptor (*Scheme 2.7*).[15]

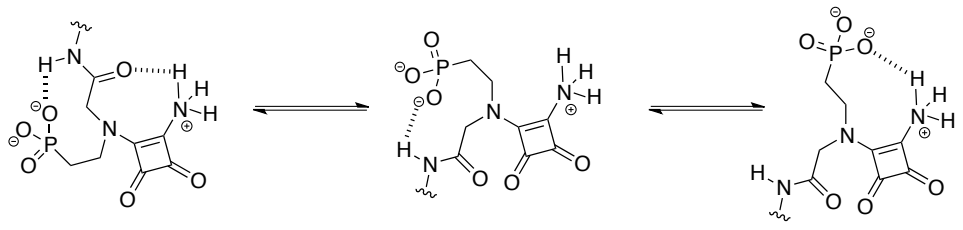

Scheme 2.7. Possible rotameric forms of the receptor-binding moiety of **[Gd.L^3]**.

Nevertheless, **[Gd.L^2]** and **[Gd.L^4]** were identified to be promising candidates as NMDA receptor-targeted MR contrast agents.

2.4.3 Analysis of Metal Ion Concentration *In Cellulo*

In the receptor-labelling experiments, **[Gd.L^4]** induced the largest enhancements in $R_{1,cell}$. In order to assess whether the large *in vitro* changes in $R_{1,cell}$ could be visible *in vivo*, the number of **[Gd.L^4]** complexes per cell was determined.

It has been proposed that in order to observe a 10% increase in the water proton relaxation rate, R_1, for a contrast agent possessing a typical relaxivity of 5 mM^{-1} s^{-1}, a 10 μM local concentration of the contrast agent is needed. This corresponds to 10^7 Gd(III) chelates per cell, suggesting that this is the required NMDA receptor density needed to observe a 10% change in MR contrast.[16] At present, there is no typical value reported for the NMDA receptor density. However, even if the bulk receptor density is low, the receptors can still be imaged successfully at below 10 μM local concentration if the receptors cluster together and form microdomains in high concentrations.[17]

Therefore, the cell pellets that were incubated with **[Gd.L^4]** were digested by heating to 50 °C overnight, in the presence of aqueous HNO_3. The cell associated Gd(III) content was then measured by ICP-MS, giving an average Gd(III) content of 2022 ppb. Using this number it was possible to estimate the number of **[Gd.L^4]** complexes per cell;

Average Gd(III) content = 2022 ppb = 2.022 ppm = 2.022 mg/L

Using ^{157}Gd (mass = 157000 mg/mol),

$$\text{Concentration} = \frac{2.022 mg/L}{157000 mg/mol} = 1.29 \times 10^5 \text{ mol dm}^{-3},$$

Number of moles = 1.29 x 10^5 mol dm^{-3} x 0.0012 dm^3 = 1.55 x 10^{-8} moles,

Number of complexes = 1.55 x 10^{-8} mols x 6.022 x 10^{23} mol^{-1} = 9.32 x 10^{15} complexes.

Using 1 x 10^7 cells.

$$\text{Complexes/cell} = \frac{9.32 \times 10^{15} complexes}{1 \times 10^7 cells} = 9.3 \times 10^8 \text{ complexes/cell.}$$

By using an estimate for the volume of each cell (5000 μm^3),[18] the number of **[Gd.L^4]** complexes per cell revealed an estimated local Gd(III) concentration of

310 μM. This value is well beyond the proposed theoretical detection limit, and is consistent with the large enhancement in $R_{1,cell}$ observed for **[Gd.L^4]**.

2.5 Toxicity Studies

When designing imaging probes for use with live cells, a critical property that the probe must posses is that it be non-toxic towards the cell in any way, and should minimally perturb cell homeostasis. The concentration dependence of the toxicity is also important, as all compounds are toxic to some degree, if used at a high enough concentration. However, it is the applied concentration that is the dominant factor.

There are several assays available to deduce whether a compound is toxic.[19] The MTT assay[20] is a colorimetric assay that measures the reducing potential of a cell. Mitochondrial reductase enzymes of viable cells reduce MTT into an insoluble purple formazan product. This can be solubilised and its concentration quantified spectrophotometrically. The amount of formazan produced is proportional to the number of viable cells.

Utilizing the MTT assay, approximately 5 x 10^3 differentiated NSC-34 cells in 100 μL culture medium were seeded into each well of flat-bottomed 96-well plates and allowed to attach overnight. Complex solutions were added to triplicate wells to give final concentrations over a 2-log range. Following 24 h incubation, MTT (1.0 mM) was added to each well, and the plates incubated for a further 4 h. The culture medium was removed, and DMSO was added to solubilise the formazan product. The plates were shaken for 20 seconds and the absorbance measured immediately at 540 nm in a microplate reader.

To process the results, the percentage viability of a well was calculated from the relative absorbance of the well, compared to a well containing untreated cells. IC_{50} values were determined as the probe concentration required to reduce the absorbance to 50% of that in the untreated, control wells, and represent the mean for data from at least three independent experiments (*Table 2.1*).

Table 2.1. Observed absorbance at 540 nm of **[Gd.L$^{1\text{-}4}$]** at varying concentrations giving IC_{50} > 200 μM. (control blank wells and untreated cells (7 well each) gave an averaged absorbance value of 0.26 and 1.69, respectively).

Concentration/ μM	[Gd.L^1]	[Gd.L^2]	[Gd.L^3]	[Gd.L^4]
5	1.75	1.61	1.63	1.82
10	1.59	1.80	1.76	1.55
30	1.50	1.43	1.49	1.82
50	1.43	1.47	1.46	1.68
100	1.49	1.76	1.78	1.43
150	1.82	1.77	1.55	1.48
200	1.65	1.49	1.85	1.72

For each of the four complexes, **[Gd.L$^{1\text{-}4}$]**, IC_{50} values were found to be greater than 200 μM, which is the concentration used throughout the MR-experiments. Therefore, it can be assumed that the probes are non-toxic, under these conditions.

2.6 Conclusions

The initial aim of this chapter was to design, synthesise and evaluate the *in vitro* behaviour of a small series of NMDA receptor-targeted MR contrast agents. The contrast agents, **[Gd.L$^{1\text{-}4}$]**, use an antagonist-mediated approach, with the aim of binding competitively at the glutamate-binding site located on the NMDA receptor. These compounds have been fully characterised, including a study on their potential to bind non-specifically to a model protein, HSA.

Of the four compounds synthesised, **[Gd.L^2]** and **[Gd.L^4]** induced large enhancement in cellular relaxation rate (170 and 176%, respectively), upon incubation with differentiated NSC-34 cells, possessing functional NMDA receptors. These enhancements in $R_{1,cell}$ have been tentatively assigned to the contrast agent binding to the NMDA receptor, modulating τ_R. This is in keeping with the observation that none of the complexes exhibited any cytotoxic effects

on these cells, up to 200 μM, suggesting that the complexes do not penetrate the cells and instead remain attached to the cell-surface receptor.

It was surprising that the most potent receptor-binding motif used in **[Gd.L^3]** did not result in any enhancement in $R_{1,cell}$. This has been tentatively attributed to the formation of stable chelates through intramolecular hydrogen bonding, as previously described.

In order to further increase affinity and potentially gain further enhancements in $R_{1,cell}$, *chapter 3* will discuss the synthesis of higher affinity receptor-binding moieties and their conjugation to Gd(III) chelates, to give a series of second-generation NMDA receptor-targeted MRI contrast agents.

2.7 References

1. W. A. Kinney, N. E. Lee, D. T. Garrison, E. J. Podlesny, J. T. Simmonds, D. Bramlett, R. R. Notvest, D. M. Kowal and R. P. Tasse, *J. Med. Chem.*, 1992, **35**, 4720-4726.
2. C.-W. Lee, H. Cao, K. Ichiyama and T. M. Rana, *Bioorg. Med. Chem. Lett.*, 2005, **15**, 4243-4246.
3. C. Bonaccorso, N. Micale, R. Ettari, S. Grasso and M. Zappala, *Curr. Med. Chem.*, 2011, **18**, 5483-5506.
4. P. Bakó, T. Novák, K. Ludányi, B. Pete, T. László and G. Keglevich, *Tetrahedron: Asymmetry*, 1999, **10**, 2373-2380.
5. D. A. Moore, *Org. Synth.*, 2008, 2.
6. D. M. Corsi, C. Platas-Iglesias, H. van Bekkum and J. A. Peters, *Magn. Reson. Chem.*, 2001, **39**, 723-726.
7. K. C. Chu, Y. Xu, J. A. Balschi and C. S. Springer, *Magn. Reson. Med.*, 1990, **13**, 239-262.
8. A. E. Merbach and E. Toth, *The chemistry of contrast agents in medical magnetic resonance imaging*, Wiley, New York, Chichester, 2001.
9. P. Caravan, N. J. Cloutier, M. T. Greenfield, S. A. McDermid, S. U. Dunham, J. W. M. Bulte, J. C. Amedio, R. J. Looby, R. M. Supkowski, W. D. Horrocks, T. J. McMurry and R. B. Lauffer, *J. Am. Chem. Soc.*, 2002, **124**, 3152-3162.
10. S. Aime, E. Gianolio, E. Terreno, G. B. Giovenzana, R. Pagliarin, M. Sisti, G. Palmisano, M. Botta, M. P. Lowe and D. Parker, *J. Biol. Inorg. Chem.*, 2000, **5**, 488-497.
11. S. Aime, M. Botta, M. Fasano, S. G. Crich and E. Terreno, *J. Biol. Inorg. Chem*, 1996, **1**, 312-319.
12. C. J. Eggett, S. Crosier, P. Manning, M. R. Cookson, F. M. Menzies, C. J. McNeil and P. J. Shaw, *J. Neurochem.*, 2000, **74**, 1895-1902.
13. A. Mishra, S. Gottschalk, J. Engelmann and D. Parker, *Chem. Sci.*, 2012, **3**, 131-135.
14. R. I. Storer, C. Aciro and L. H. Jones, *Chem. Soc. Rev.*, 2011, **40**, 2330-2346.
15. W. A. Kinney, M. Abou-Gharbia, D. T. Garrison, J. Schmid, D. M. Kowal, D. R. Bramlett, T. L. Miller, R. P. Tasse, M. M. Zaleska and J. A. Moyer, *J. Med. Chem.*, 1998, **41**, 236-246.
16. P. Caravan and Z. Zhang, *Eur. J. Inorg. Chem.*, 2012, **2012**, 1916-1923.
17. K. Hanaoka, A. J. M. Lubag, A. Castillo-Muzquiz, T. Kodadek and A. D. Sherry, *Magn. Reson. Imaging*, 2008, **26**, 608-617.
18. E. J. New, A. Congreve and D. Parker, *Chem. Sci.*, 2010, **1**, 111-118.
19. T. L. Riss, A. L. Niles, *Assay Guidance Manual*, Bethesda, 2013.
20. J. Carmichael, W. G. Degraff, A. F. Gazdar, J. D. Minna and J. B. Mitchell, *Cancer Res.*, 1987, **47**, 936-942.

CHAPTER THREE

Second Generation NMDA Receptor-Targeted MRI Contrast Agents

3. Second-Generation NMDA Receptor-Targeted MRI Contrast Agents

3.1 Introduction

The first-generation series of NMDA receptor targeted MRI contrast agents showed that employing a modified NMDA receptor antagonist as the receptor-binding moiety allowed for cellular labelling of differentiated NSC-34 cells. Two complexes, **[Gd.L^2]** and **[Gd.L^4]**, exhibited large enhancements in $R_{1,cell}$, consistent with modulation of the rotational dynamics of these contrast agents upon NMDA receptor-binding.

Surprisingly, **[Gd.L^3]**, the contrast agent bearing the most potent antagonistic moiety, appeared to show no receptor-specific interactions, leading to no enhancement in $R_{1,cell}$. This was attributed to the squaramide motif adopting several rotameric conformations, stabilised by internal hydrogen bonding.[1] Based on the assumption that a molecule that does not undergo significant hydrogen bonding would be more available to hydrogen bond to complementary sites on the NMDA receptor, and so possess a greater binding affinity, a second series of NMDA receptor-binding moieties has been derived (*Scheme 3*). These are again based on competitive NMDA receptor antagonists first reported by Kinney. The bicyclic nature rigidifies the compound and restricts it to a conformational form that is similar in structure to several other highly potent NMDA receptor antagonists.

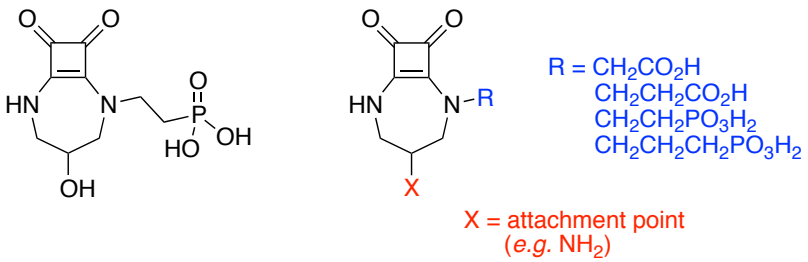

Scheme 3. (Left) Kinney's NMDA receptor antagonist (IC_{50} = 19 nM)[1] and (right) structures of the modified receptor-binding moieties of the second generation contrast agents.

The macrocyclic Gd(III) core was chosen to be similar to that used for the complexes **[Gd.L$^{1-4}$]**, since tetra-carboxylate macrocyclic complexes possess fast water exchange rates and help minimise non-specific protein binding. However, the length of the spacer that links the Gd(III) chelate to the NMDA receptor binding moiety has been varied. A varying chain length was used in an attempt to study the effect of chain length on the binding affinity of each complex to the receptor, and how this modulates τ_R.

3.2 Synthetic Details

3.2.1 Synthetic Approaches to Second-Generation Receptor-Binding Moieties

Initial work was based on Kinney's antagonist (*Scheme 3*), allowing modification of the free alcohol to an amine in the final step, which would provide the linkage point to the macrocycle. Therefore, the initial synthetic pathway to ***29***, the precursor to Kinney's antagonist followed the literature method (*Scheme 3.1*).[1]

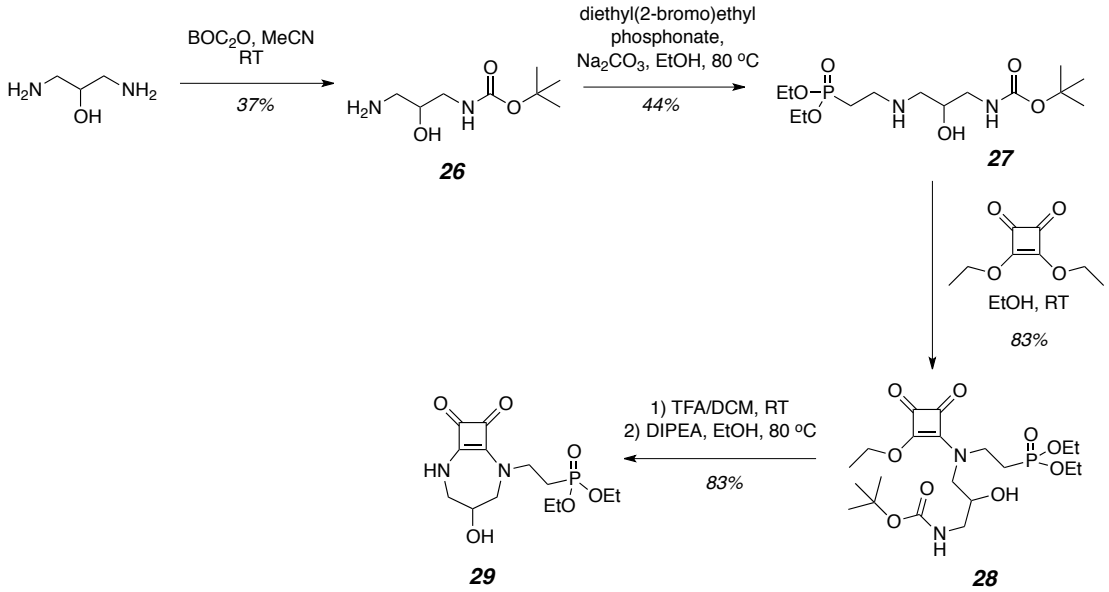

Scheme 3.1.

Mono-Boc protection of 1,3-diamino-propan-2-ol was achieved, albeit in a modest yield, by reaction with 0.3 equivalents of di-*tert*-butyl-dicarbonate in anhydrous acetonitrile.[2] The phosphonate group was introduced through *N*-alkylation of ***26*** with diethyl-(2-bromo)-ethyl phosphonate, under basic conditions, to afford the secondary amine ***27***, after purification by column chromatography. The amine ***27*** was subjected to a Michael addition-elimination reaction with 3,4-diethoxy-3-cyclobutene-1,2-dione, which afforded ***28***, in an excellent yield, as a clear viscous oil. Due to the restricted rotation around the C-N bond, compound ***28*** was observed as a pair of rotamers in solution. The ratio of the rotamers was deduced to be 1.1:1 by ^{31}P NMR spectroscopy. Finally, the *N*-Boc group of ***28*** was cleaved under acid conditions, and the resulting crude TFA salt treated with an excess of diisopropylethylamine in refluxing ethanol overnight, to give the bicyclic compound ***29***, in a high yield.

With compound ***29*** in hand, it was thought that direct conversion of the alcohol to an azide, followed by a mild reduction, would yield the desired primary amine which could be coupled to a pendant carboxylic acid on the macrocycle. The alcohol was subject to Mitsunobu conditions (*Scheme 3.2*), in which ***29*** was dissolved in anhydrous THF under an atmosphere of argon. The solution was cooled to 0 °C and triphenylphosphine, diphenylphosphorylazide and diethyl azadicarboxylate were added sequentially. The reaction was allowed to warm to room temperature and was monitored by ESI-MS over a period of 48 hours. However, no reaction was observed, even after warming to 40 °C, and the starting alcohol ***29*** was recovered.

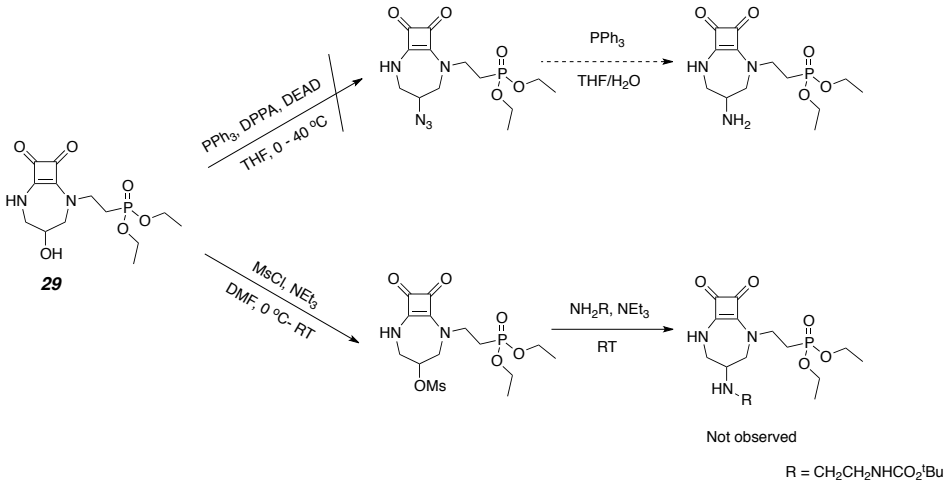

Scheme 3.2.

With the no reaction of ***29*** observed under the Mitsunobu conditions, an attempt to functionalise via substitution of the alcohol was performed (*Scheme 3.2*). To this end, ***29*** was dissolved in DMF and treated with methanesulfonyl chloride and triethylamine at 0 °C. Mesylation reactions usually proceed very quickly in near quantitative yields, but formation of the mesylated product never surpassed 80%, even after prolonged reaction times. Nevertheless, the *in-situ* generated mesylate was treated with *N*-Boc ethylenediamine and triethylamine and the reaction allowed to warm to room temperature overnight. The reaction progress was monitored by ESI–MS. Analysis of the ESI-MS data after one hour showed the presence of only one major product, with *m/z* = 633.9. This corresponded to the doubly alkylated product, with no mono-substitution observed by ESI-MS, even after shorter reaction periods.

With activation and substitution of the alcohol in ***29*** proving difficult, a new synthetic route was devised, which incorporates the amine earlier in the synthetic sequence (*Scheme 3.3*).

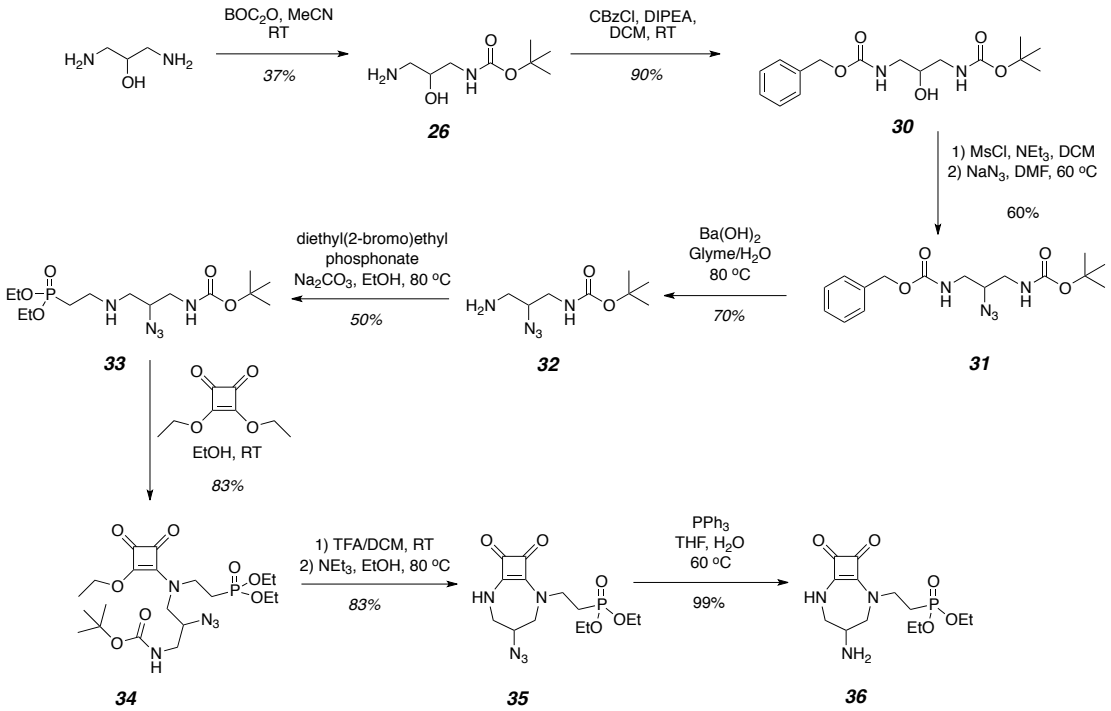

Scheme 3.3.

(3-Amino-2-hydroxypropyl)carbamic acid-1,1-dimethylethylester, ***26***, was synthesised as described above. Orthogonal protection of the second amine was achieved through reaction with benzyl chloroformate and diisopropylethylamine in anhydrous DCM, to give ***30*** in a high yield. With both amine groups protected, selective activation and substitution of the alcohol moiety of ***30*** was conducted through generation of the mesylate. After work-up, the mesylate was dissolved in anhydrous DMF and treated with sodium azide at 60 °C, overnight. After work-up and purification by column chromatography, the azide, ***31*** (which would serve as a 'masked amine') was isolated in a good yield.

A reagent for the selective removal of the Cbz protecting group from ***31*** was then needed. This ruled out the use of standard deprotection methods, such as hydrogenation over a palladium catalyst, as this would also reduce the azide group. Instead, $Ba(OH)_2$ in refluxing aqueous glyme was employed.[3] This basic hydrolysis step yielded the free amine ***32*** after subsequent work-up and purification through adjustment of the pH. Following the methods outlined above, the primary amine, ***32***, was alkylated with diethyl-(2-bromo)ethyl phosphonate under basic conditions to give the secondary amine, ***33***. This was subject to a Michael addition-elimination reaction with 3,4-diethoxy-3-cyclobutene-1,2-dione to obtain ***34*** as a pair of rotamers, in a 1:1.2 ratio as deduced by ^{31}P NMR spectroscopy. Cyclisation to ***35*** was achieved in a high yield by selective acidic hydrolysis of the *N*-Boc group to yield the TFA salt, which was then treated with an excess of triethylamine in refluxing ethanol. Triethylamine was employed over diisopropylethylamine in order to simplify the purification step. By studying the ^{1}H NMR spectrum of the cyclised azide, ***35*** (*Figure 3*), it was possible to deduce that the conformation adopted by this and related bicyclic intermediates in solution involves preferential population of a twist-chair isomer.

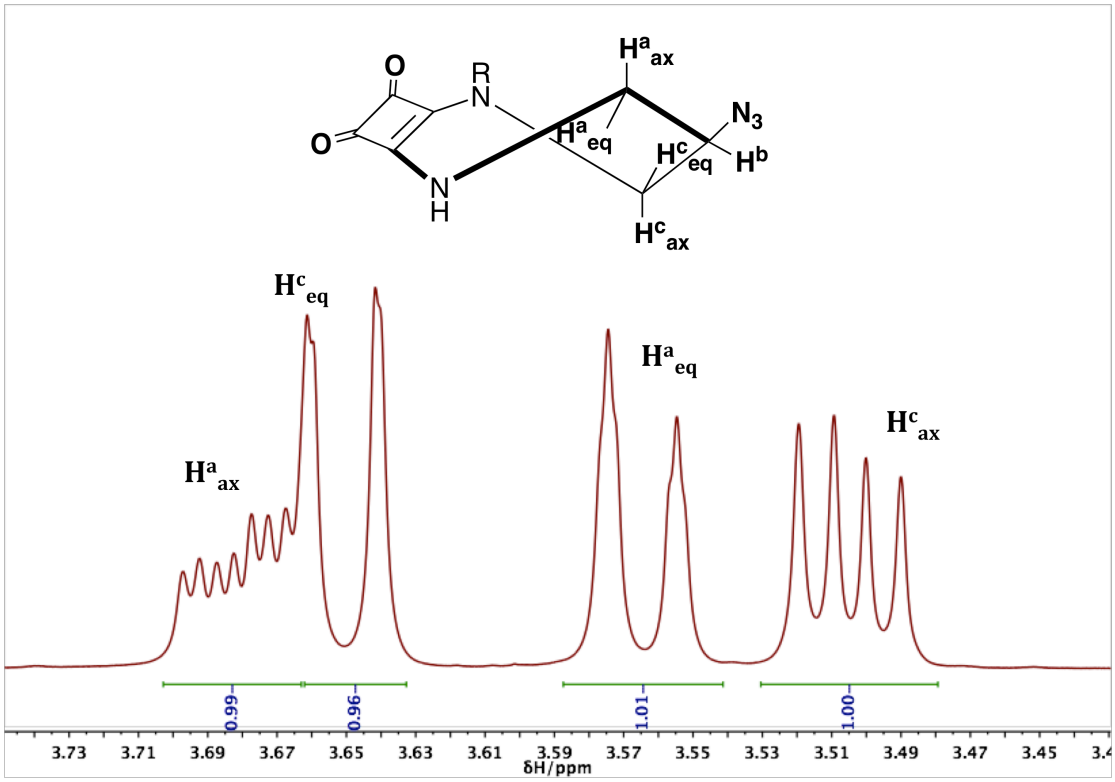

Figure 3. Partial ^{1}H NMR spectrum of the bicyclic azide, ***35*** (295 K, $CDCl_3$, 700 MHz), showing the twist chair conformation of the ring that is likely to be preferentially populated.

Heterocyclic seven-membered rings can adopt several conformations, of which the twist-chair is normally lowest in energy, with bulky substituents in the six-position preferring the equatorial site.[4] Based on this, the conformation in *figure 3* is proposed. The axial proton, H^a_{ax}, is coupled to the equatorial proton, H^a_{eq}, with a coupling constant of -14 Hz. It is also coupled to H^b with a 3-bond coupling of 7 Hz, and finally to the NH proton with a 3-bond coupling of 4 Hz. This splitting pattern gives H^a_{ax} as a ddd, observed at around 3.68 ppm.

Using 2D ^{1}H-^{13}C HSQC NMR spectroscopy, it was possible to identify H^a_{eq} as the doublet at 3.55 ppm. A coupling constant of 14 Hz represents that of the two-bond coupling to H^a_{ax}. There also appeared to be some fine splitting associated with the peak at 3.55 ppm, and this reflects the small coupling to either H^b or NH due to the twisted nature of the 7-ring.

Since H^c_{ax} is almost eclipsing H^b, it becomes apparent that the doublet of doublets at 3.49 ppm corresponds to H^c_{ax}. This arises due to the coupling with H^c_{eq} and H^b.

Finally, with H^{c}_{eq} close to 90° in correlation to H^{b}, no real coupling is observed between these two resonances, and this is reflected in the very small degree of fine splitting in the H^{c}_{eq} resonance at 3.64 ppm.

With the azide ***35*** in hand and characterised, a mild selective reduction of the azide group to unmask the primary amine functionality was accomplished using a standard Staudinger reduction reaction, which employed triphenylphosphine in a THF/H_2O solvent mixture. The H_2O is present in order to hydrolyse the intermediate iminophosphorane. This reaction proceeded efficiently and non-stereospecifically, to yield ***36*** as a pair of enantiomers, after simple purification.

With this synthetic route providing access to the functionalised receptor-binding fragment, the same route was repeated for the synthesis of the C1- and C2-carboxylate and C3-phosphonate analogues (*Scheme 3.4*).

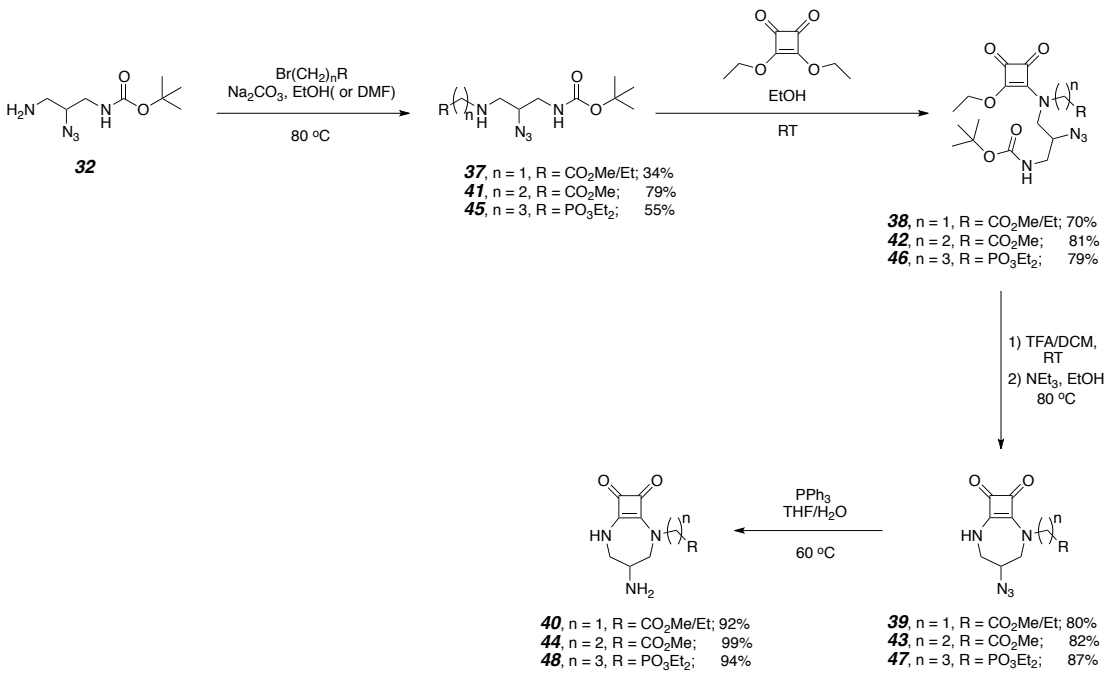

Scheme 3.4.

During the synthesis of the amine, ***40***, the ethyl ester was also synthesised along with the methyl ester. This was due to transesterification from the ethanol solvent that was used in the alkylation step, during the formation of ***37***. However, exclusive formation of the methyl ester could be achieved by exchanging the solvent for DMF, as was the case for the synthesis of ***41***.

During the synthesis of these small molecule NMDA receptor-binding moieties, a pair of rotamers is formed upon the Michael addition-elimination reaction onto 3,4-diethoxy-3-cyclobutene-1,2-dione. An example of this is in the formation of compound ***46***, wherein at room temperature, two resonances are present in the ^{31}P NMR spectrum. The pair of rotamers arises due to the donation of the nitrogen lone pair into the cyclobutene moiety, leading to restricted rotation around the C-N enamine bond.

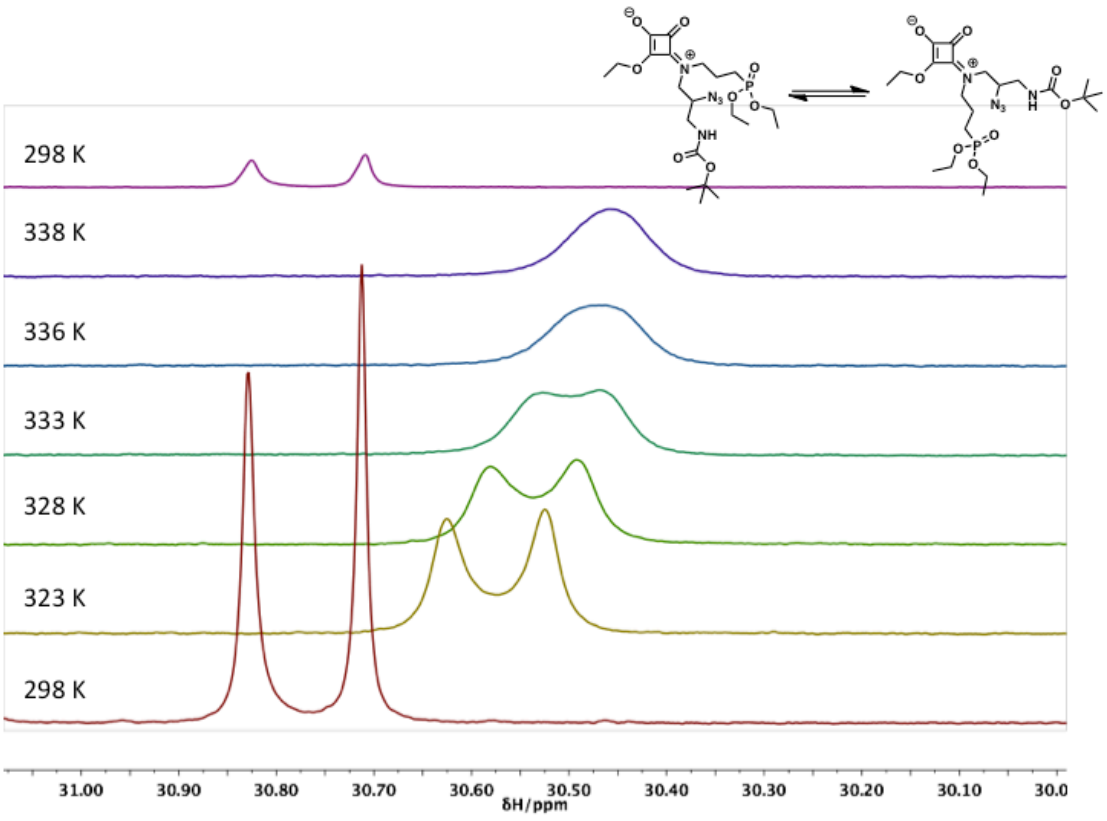

Figure 3.1. Variable temperature ^{31}P NMR spectra of ***46*** (DMSO-d_6, 700 MHz). The upper spectrum shows the two resonances reappearing upon cooling from 338 to 298K.

Variable temperature ^{31}P NMR spectroscopy was used to examine the behaviour of the rotamers and deduce the free energy of rotation around the C-N bond (*Figure 3.1*). Upon warming from 298 to 348 K, the two phosphorus resonances begin to broaden and coalescence was observed with T_c estimated to be 337 K. At this temperature, the rate constant for interconversion, k_c was calculated, using *equation 3*, to be 180 s^{-1}.

$$k_c = \frac{\pi \Delta v}{\sqrt{2}} \quad (3)$$

Using *equation 3.1*, an estimate of the free energy of activation (ΔG_c) associated with this dynamic process could be made.

$$\Delta G_c = RT_c\left(23.7 + 2.3\log\left(\frac{T_c}{\Delta v}\right)\right) \quad (3.1)$$

where R is the molar gas constant, T_c is the coalescence temperature and Δv is the difference in frequencies. Based on an Eyring analysis, the free energy of activation was estimated to be 70.4 ± 0.2 kJ mol^{-1}. This relatively high energy of activation reflects the significant degree of double bond character associated with the C-N bond.

3.2.2 Linker and Macrocycle Synthesis

In order to determine the optimal length of the linker between the Gd(III) core and the pendant NMDA receptor binding moiety, two varying spacer units were used. The first linker was derived from the commercially available (*S*)-glutamic acid 5-benzyl ester. Derivitisation via diazotisation of the α-amino group, followed by *in-situ* bromination gave the (*S*)-brominated derivative, ***49***. After purification, the free carboxylic acid was esterified using *tert*-butyl acetate in the presence of a catalytic amount of acid, to give the orthogonally protected ester, ***50***.[5]

Alkylation of ester ***50*** onto DO3A^{t}Bu, ***19***, was performed in a similar manner as in the synthesis of compound ***20***. Finally, the benzyl-protecting group of ***51*** was removed under high-pressure hydrogenation, in the presence of a Pd/C catalyst. Filtration of the catalyst and removal of the solvent yielded the hygroscopic carboxylic acid, ***52*** (*Scheme 3.5*).[6]

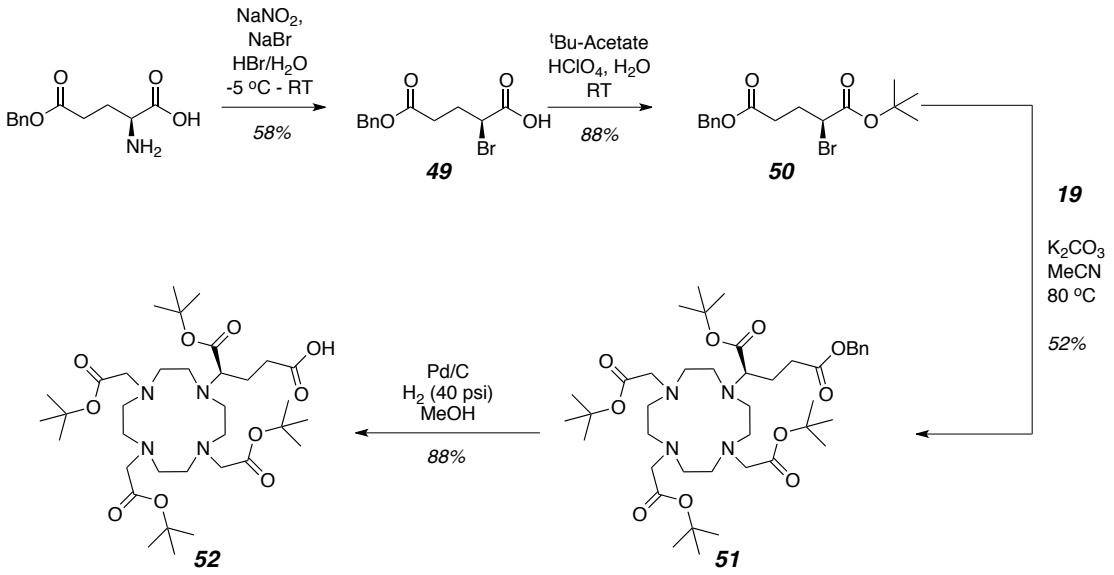

Scheme 3.5.

The second macrocycle and linker unit was derived from compound ***21***. Chain extension of the pendant free amine was performed through nucleophilic attack onto succinic anhydride, leading to ring opening of the anhydride. This gave ***53*** with an elongated chain possessing a terminal carboxylic acid (*Scheme 3.6*).

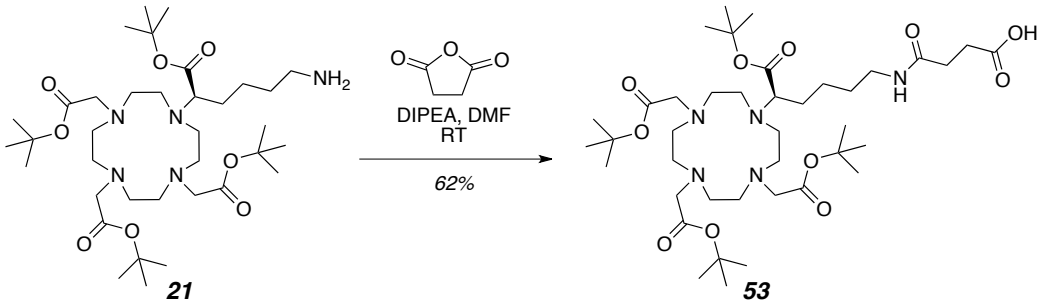

Scheme 3.6.

3.2.3 Synthesis of Conjugates and Complexes

With all four bicyclic NMDA receptor binding moieties to hand, the final step in the synthesis of **[conjugates 5-10]** involved formation of an amide bond between the primary amine of compounds ***36***, ***40***, ***44*** and ***48*** and the carboxylic

acid of ***52*** or ***53*** (*Scheme 3.7*). This was achieved by stirring ***52*** or ***53*** as a solution in anhydrous DMF with EDC.HCl and HOBt for 20 minutes. After formation of the active ester, a solution of the amine and NMM was added dropwise and the reaction monitored by ESI-MS. Formation of the conjugates appeared to proceed more quickly than previously observed for that of **[conjugates 1-4]**. After work-up and purification by column chromatography, **[conjugates 5-10]** (***54-59***), were isolated as pairs of diasteroisomers, in a slightly greater yield than for **[conjugates 1-4]**.

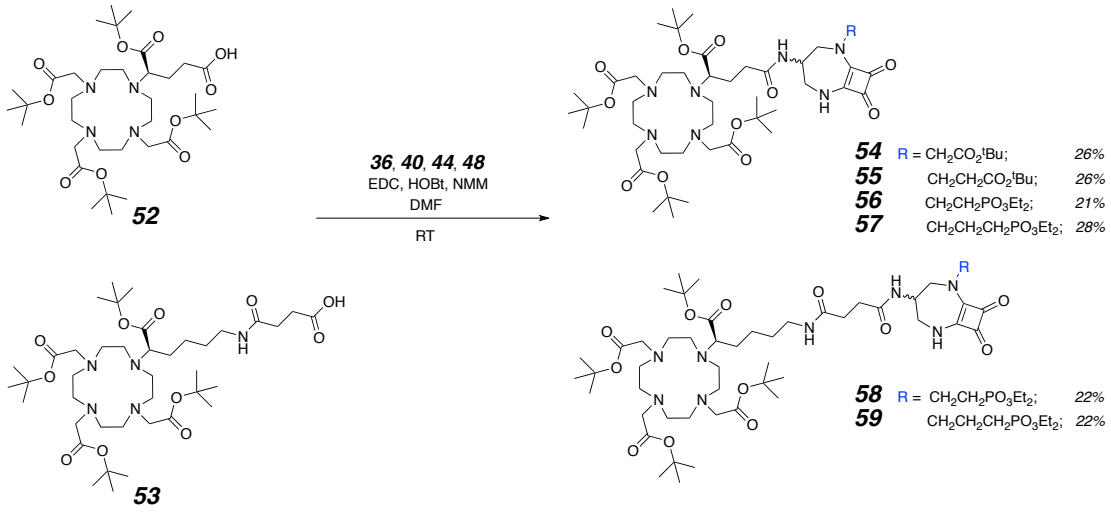

Scheme 3.7.

Characterisation of **[conjugates 5-10]** (***54-59***) was undertaken using ^{1}H, ^{13}C, and when applicable, ^{31}P NMR spectroscopies, as well as HRMS, with each technique consistent with the formation of the desired product. The final two steps in the synthesis of ***L*$^{5\text{-}10}$** before metal complexation involved global deprotection of the protecting groups.

In the case of ***L*^{5}** and ***L*^{6}**, methyl/ethyl ester hydrolysis was achieved under standard basic conditions, utilising NaOH in an aqueous methanol solvent. The crude carboxylic acids were then subject to *tert*-butyl ester cleavage using a 1:1 mixture of trifluoroacetic acid and DCM at room temperature, overnight (*Scheme 3.8*). Confirmation of the formation of ***L*^{5}** and ***L*^{6}** was provided through analysis of the mass spectra (684.7 and 698.3, $[M+H]^{+}$, respectively).

For ***L*$^{7\text{-}10}$**, hydrolysis of the *tert*-butyl ester groups of **[conjugates 7-10]** (***56-59***) was achieved using a 1:1 mixture of trifluoracetic acid and DCM. The crude phosphonate ethyl ester was dissolved in DMF and heated to 60 °C in the presence of an excess of bromotrimethylsilane (*Scheme 3.8*). Complete hydrolysis was again confirmed through analysis of the mass spectra (734.9, 748.7, 833.7 and 847.8, $[M+H]^+$, for ***L*$^{7\text{-}10}$**, respectively).

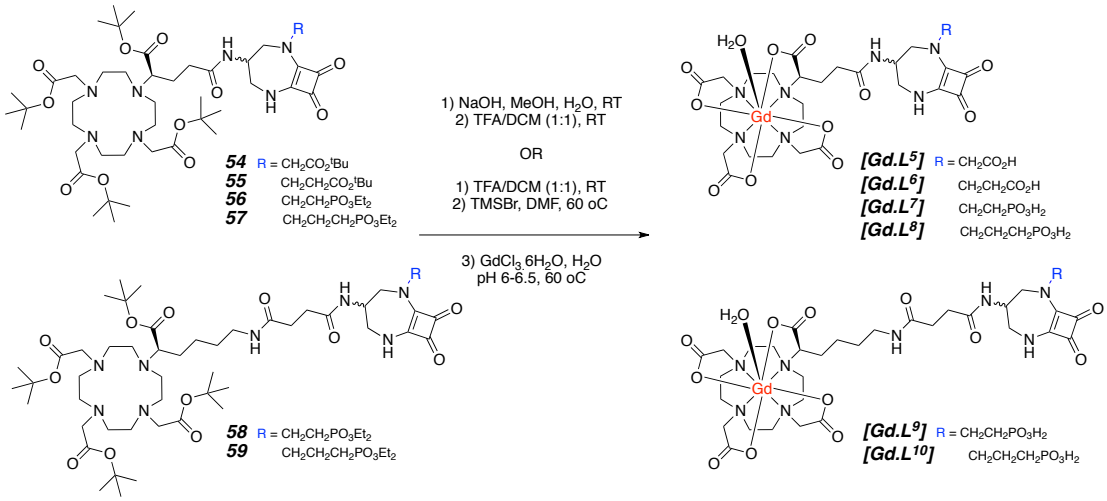

Scheme 3.8.

Finally, complexation of the corresponding TFA salts of ***L*$^{5\text{-}10}$** was achieved by reaction with $GdCl_3.6H_2O$ in H_2O (pH 6-6.5) at 60 °C, overnight (*Scheme 3.8*). Upon completion, the excess Gd(III) was removed through chelation to Chelex-100™ resin, and the complexes were eluted by syringe filtration. Final purification was achieved using RP-HPLC, to give the complexes **[Gd.L$^{5\text{-}10}$]**, isolated as a diastereoisomeric mixture. The presence of the desired complexes was confirmed through analysis of the high-resolution mass spectra, with comparison of the theoretical and observed isotope distribution of **[Gd.L^6]** shown below (*Figure 3.2*).

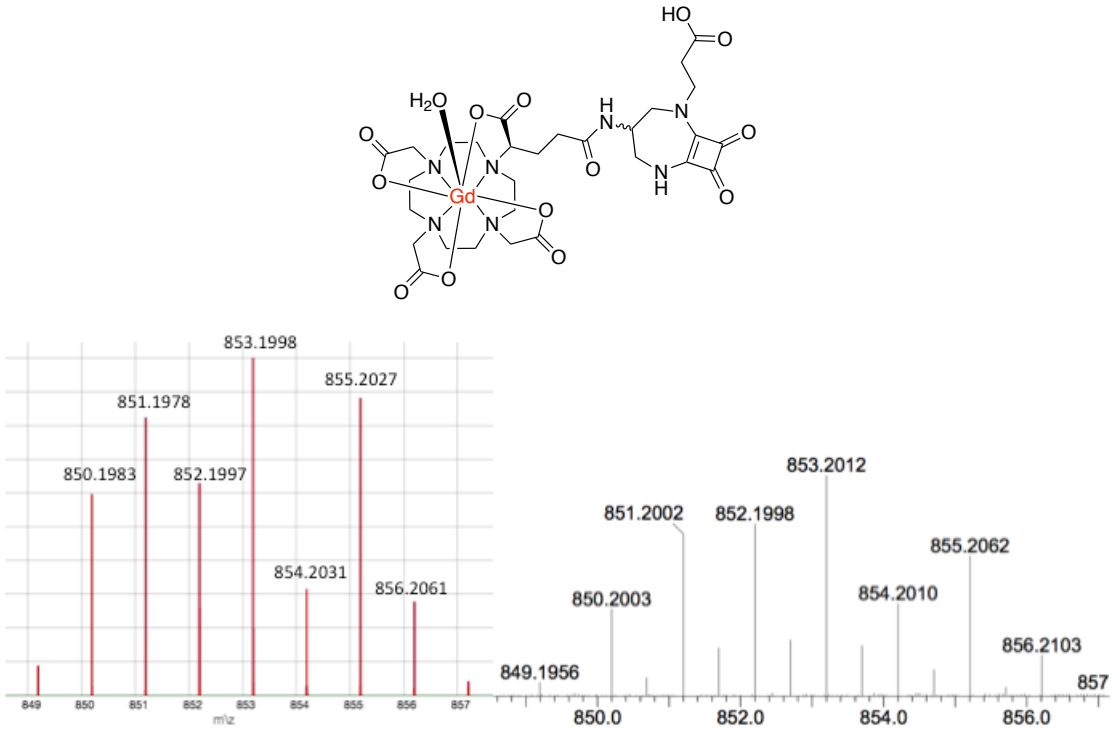

Figure 3.2. Calculated (*left*) and observed (*right*) high-resolution electrospray mass spectra of **[Gd.L^{6}]**, showing the characteristic Gd-isotope pattern; TOF-MS positive mode.

3.3 Relaxivity Properties

3.3.1 Complex Isomeric Ratio in Solution

For octadentate Gd(III) complexes, the primary mechanism of water exchange is dissociative.[7] This means that the rate-determining step in inner-sphere water exchange has a high activation energy, and so any factor which weakens the Gd-O_{H2O} bond will tend to enhance k_{ex} and increase relaxivity. There are two methods to weaken the Gd-O_{H2O} bond. First, by employing a negative donor group to coordinate to the Gd(III) ion, as is the case in **[Gd.L$^{5\text{-}10}$]**, this will reduce the electropositive nature of the metal centre and weaken its interaction with the O_{H2O} lone pair, thus weakening the Gd-O_{H2O} bond.

Secondly, increasing the degree of steric compression around the Gd(III) ion also destabilises the Gd-O_{H2O} bond. It is well known that Gd(III) chelates, based on a DOTA-type structure, can adopt two diastereomeric conformations; square antiprismatic (SAP) and twisted square antiprismatic (TSAP) (*Figure 3.3*). The

two isomers are distinguishable by the angle between the N_4 and O_4 planes, with the TSAP angle approximately 25°, compared to the SAP angle, which is larger at 40°.[8] As a result of the increased steric repulsion between the chelating nitrogen and oxygen atoms in the TSAP conformation, the distance between the N_4 and O_4 planes is greater.[9] This means that the inner-sphere water molecule must come in close proximity to the plane of negatively charge oxygen atoms, or the Gd-O_{H2O} bond must increase, when binding to the Gd(III) centre. This has resulted in it being widely accepted that the TSAP isomer possesses a greater k_{ex} than that of the SAP isomer, leading to a greater relaxivity for the TSAP conformation.

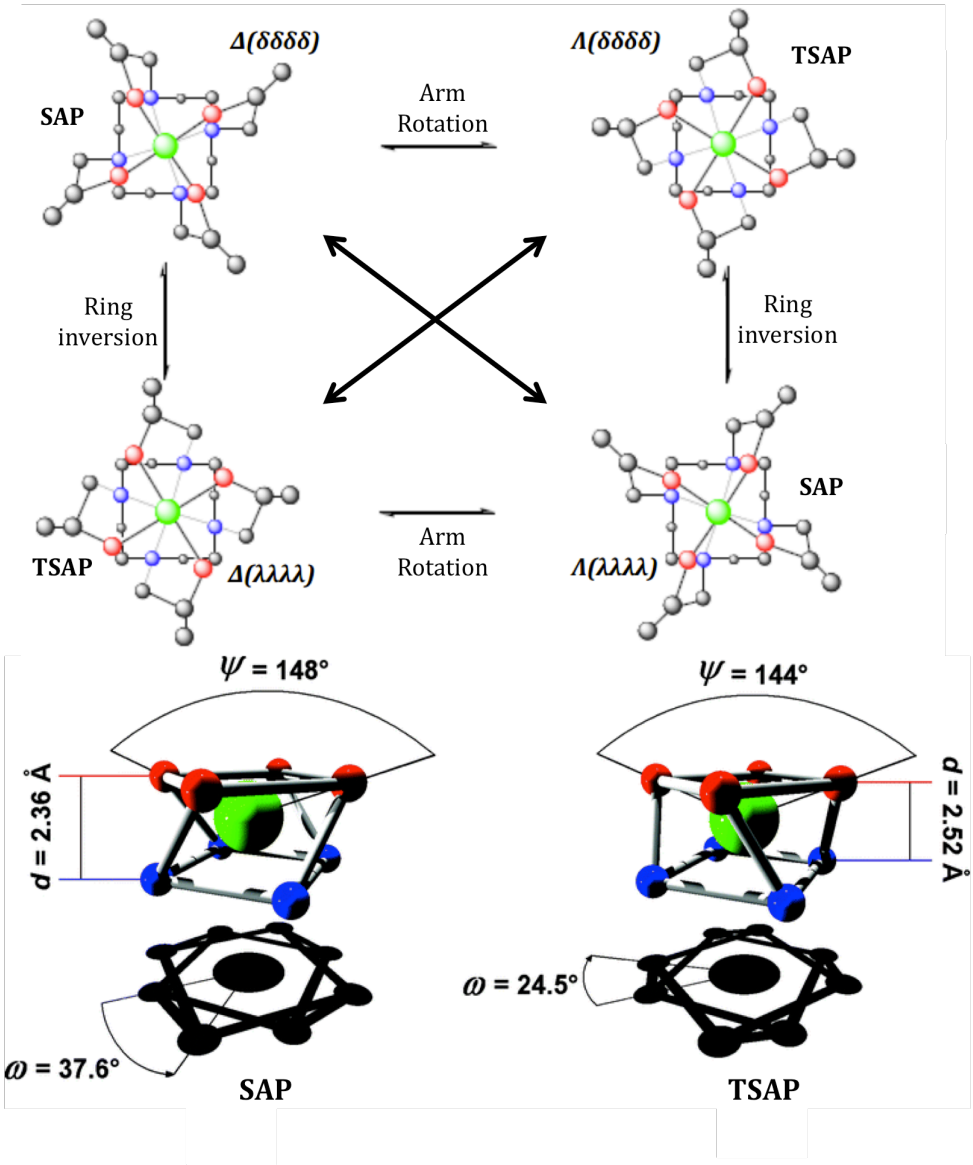

Figure 3.3. (Top) Possible isomers for Ln(III) complexes of DOTA-like ligands; (Bottom) The coordination polyhedra of the SAP and TSAP isomers, showing the average angle rotations between the N_4 (blue) and O_4 (red) planes.[9]

Despite this, recent studies by Woods and co-workers[10] has shown that a greater relaxivity can be obtained from the SAP isomer of structurally related Gd(III) complexes. This is due to the TSAP isomer possessing a lower hydration state (q/r_{GdH}^6), which limits the overall relaxivity of the complex. On the other hand, the SAP isomer possesses a greater hydration state leading to a greater relaxivity. Therefore it is not just water exchange rate, but also the Gd-H_{H2O} distance of a complex that has a profound effect on relaxivity.[10]

Bearing the above in mind, the isomeric ratio of SAP and TSAP conformations of a Eu(III) complex of a structurally related ligand to that of ***L*^5-8^** was deduced by ^{1}H NMR spectrometry. SAP complexes are known to exhibit a larger paramagnetic shift (for q=1 complexes), and the most shifted axial ring protons of SAP isomers of EuDOTA-type complexes resonate between 30-50 ppm. In contrast, the corresponding TSAP resonances are at approximately 20 ppm.[11]

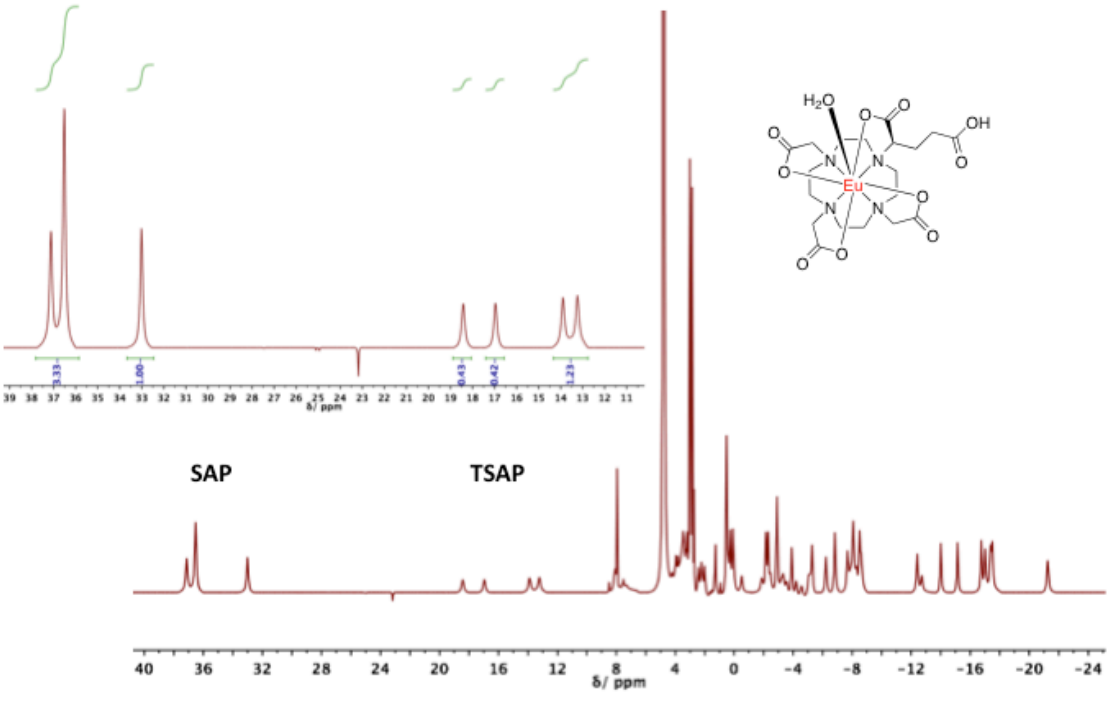

Figure 3.4. ^{1}H NMR spectrum of **[EuDOTAGlu]** (298 K, D_2O, 700 MHz). (*Inset*) Enlarged region showing the most shifted axial protons of each isomer.

Analysis of the ^{1}H NMR spectrum of **[EuDOTAGlu]** (*Figure 3.4*) shows a ratio of SAP to TSAP isomers in solution that is slightly greater than 2:1. This is a good

approximation of the likely isomer distribution of complexes **[Gd.L$^{5\text{-}10}$]**, which all bear the same core structure as **[EuDOTAGlu]**.

3.3.2 Relaxivities of [Gd.L$^{5\text{-}10}$] in Aqueous Solution and the Effect of Added Protein

The longitudinal proton relaxivities of the six Gd(III) complexes, **[Gd.L$^{5\text{-}10}$]**, were measured in water at 1.4 T and 310 K (*Table 3*). The values fell in the expected range for such mono-aqua complexes of molecular weight in the range of 850 to 1450, for which the relaxivity value increases with molecular volume, as it scales with the overall rotational correlation time.[12]

Table 3. Relaxation properties of **[Gd.L$^{5\text{-}10}$]** and their estimated binding affinities for serum albumin[a, b] (310 K, pH 7.4, 1.4 T).

	[Gd.L^5]	**[Gd.L^6]**	**[Gd.L^7]**	**[Gd.L^8]**	**[Gd.L^9]**	**[Gd.L^{10}]**
log K	2.16 (±0.01)	1.91 (±0.01)	3.69 (±0.04)	1.60 (±0.01)	1.61 (±0.01)	3.68 (±0.04)
$r_{1p}^{initial}$/mM^{-1} s^{-1}	4.9 (±0.2)	4.5 (±0.2)	5.8 (±0.3)	5.2 (±0.3)	5.0 (±0.3)	5.2 (±0.3)
r_{1p}^{limit}/ mM^{-1} s^{-1}	18.0	22.0	7.50	30.0	25.0	8.50
r_{1p}/mM^{-1} s^{-1} (0.7 mM HSA)	6.0 (±0.3)	5.4 (±0.3)	6.6 (±0.3)	5.9 (±0.3)	5.5 (±0.3)	6.8 (±0.3)

[a] the r_{1p}^{limit} values were derived from the iterative least-squares fitting analysis; values for the complexes of L^8 and L^9 are subject to the largest error; [b] the relative affinity constant (IC_{50} values, i.e. not the 1: 1 binding constant that is assumed here in the data analysis) for a structurally similar NMDA binding moiety (Kinney's antagonist) was reported to be 19 nM, determined using a radiolabelled competition assay.[1]

The contrast agents, **[Gd.L$^{5\text{-}10}$]**, can each bind non-specifically to protein to some extent, which will disrupt their rotational dynamics and lead to an enhancement of the longitudinal water proton relaxation rate. As discussed in *section 2.3.1*, HSA is the major protein constituent in the circulatory system. Therefore, as a control experiment, the effect of added HSA on the measured relaxivity of **[Gd.L$^{5\text{-}10}$]** (each at 1 mM) was assessed at 1.4 T, following incremental addition of up to

2 mM HSA. Increases in r_{1p} were observed and the association constants were estimated by assuming a 1:1 stoichiometry of interaction.

The association constants for **[Gd.L$^{5\text{-}10}$]** with HSA were 2.16 (±0.01), 1.91 (±0.01), 3.69 (±0.04), 1.60 (±0.01), 1.61 (±0.01) and 3.68 (±0.04), respectively (*Table 3*). These are all much lower values than those calculated for the acyclic analogues **[Gd.L$^{1\text{-}4}$]**, with **[Gd.L^{7}]** and **[Gd.L^{10}]** the only two complexes to show any apparent binding to HSA. No particular trend was evident correlating log *K* values with molecular structure; indeed the weakest interaction occurred with the phosphonates, **[Gd.L^{8}]** and **[Gd.L^{9}]**, whilst the analogues with one less and one more methylene groups, **[Gd.L^{7}]** and **[Gd.L^{10}]**, respectively, bound to albumin 100 times more strongly in each case.

The concentration of HSA in plasma is approximately 0.67 mM.[13] At a protein concentration of 0.7 mM, the highest relaxivity values were measured to be 6.63 and 6.82 mM^{-1} s^{-1} for **[Gd.L^{7}]** and **[Gd.L^{10}]**, reflecting their higher binding affinities for HSA. This constitutes a small 15 and 32% enhancement in r_{1p}, which is promising as a much greater enhancement should be expected when these complexes bind to the cell surface NMDA receptor. Of course, such behaviour requires that non-specific binding of the probes be minimal and that they bind to the NMDA receptors with high selectivity.

3.4 Toxicity Studies

The NMDA receptor-targeted MR contrast agents, **[Gd.L$^{5\text{-}10}$]**, were assessed for their toxicity. The MTT assay, as described in *chapter 2*, was performed on differentiated NSC-34 cells with incubations of up to 200 μM of each complex. As found for the first-generation NMDA receptor-targeted MR contrast agents, no significant toxicity was observed for the probe concentrations used, giving an IC_{50} value for **[Gd.L$^{5\text{-}10}$]** greater than 200 μM. Such behaviour is consistent with the absence of probe internalisation.

3.5 MRI Analysis of Cell Suspensions *In Vitro*

A neuronal cell line model expressing functional NMDA receptors was established in *chapter 2*. The cellular labeling of differentiated NSC-34 cells with **[Gd.L$^{5\text{-}10}$]** was assessed by measuring the longitudinal relaxation times, T_1, of the water signal in cell suspensions using a Siemens human whole body MR scanner, equipped with a head coil operating at 3 T. These measurements allowed the calculation of cellular relaxation rates, $R_{1,cell}$. Following the same procedure outlined in *chapter 2*, differentiated NSC-34 cells were incubated with 200 μM **[Gd.L$^{5\text{-}10}$]** for 45 minutes. The cells were washed with HBSS to remove any unbound complex, re-suspended in fresh buffer and T_1-weighted MR images acquired overnight. Analysis of the T_1-weighted images allowed calculation of $R_{1,cell}$ (*Figure 3.5*).

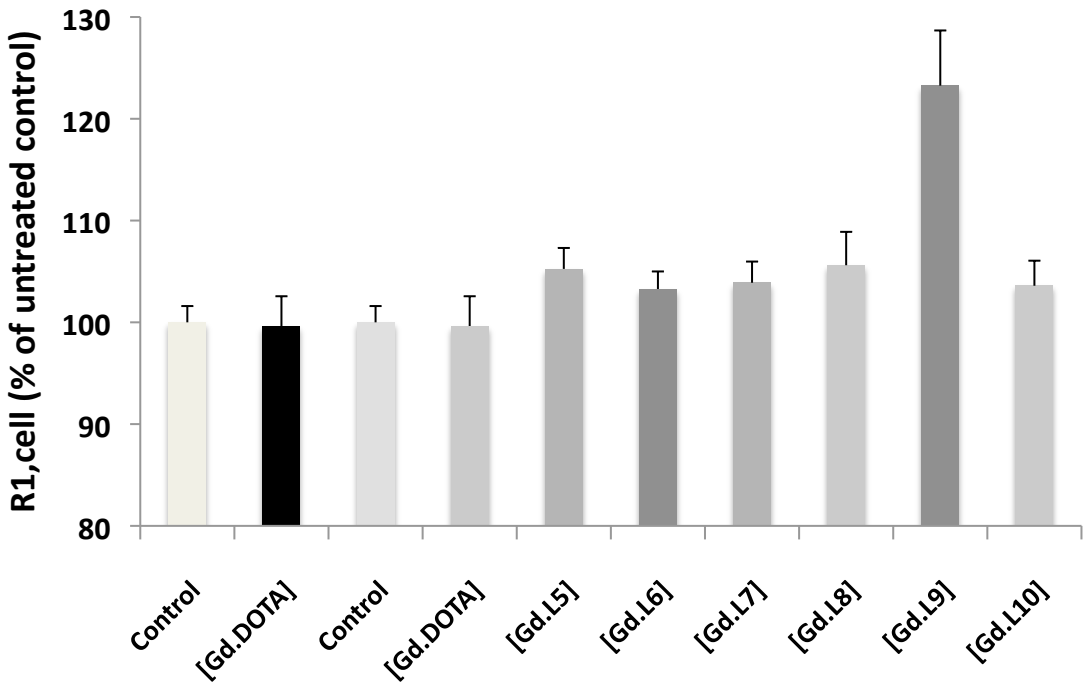

Figure 3.5. Cellular ^{1}H MR relaxation rates $R_{1,cell}$ in cell suspensions (3 T, 298 K) after treatment of differentiated NSC-34 cells with 200 μM **[Gd.DOTA]** or **[Gd.L$^{5\text{-}10}$]** for 45 min. **[Gd.DOTA]** served as a negative control. Values are mean ± STD (n=3-4). [Carried out at MPI, Germany].

The four complexes **[Gd.L$^{5\text{-}8}$]** are all based on a Gd(III) complex of DOTAGlu, conjugated to the novel bicyclic NMDA receptor-binding moieties, with varying

pendant acidic groups. When incubated with the differentiated NSC-34 cells, these four complexes induced negligible enhancements in $R_{1,cell}$ of 105, 103, 104 and 106%, respectively. These enhancements are not significantly distinguishable from the enhancements gained when using the clinically approved, non-targeted contrast agent, [Gd.DOTA].

The complexes, **[Gd.L^{9}]** and **[Gd.L^{10}]** incorporate the same receptor binding moieties as **[Gd.L^{7}]** and **[Gd.L^{8}]**, respectively, but have a longer spacer unit between the NMDA receptor binding moiety and the Gd(III) chelate. The complex **[Gd.L^{9}]** induces a relatively large enhancement in $R_{1,cell}$ of 123%, whereas the addition of a single methylene group to the targeting moiety results in only a 104% enhancement in $R_{1,cell}$ for **[Gd.L^{10}]**.

Since the set of complexes, **[Gd.L$^{5\text{-}8}$]**, each gave less than 6% enhancement in $R_{1,cell}$, it suggests that these complexes could be inhibited in binding to the cell surface NMDA receptor. This could either be due to the alteration made to the NMDA receptor binding moieties, leading to decreased affinities towards the receptor, or that the sterically demanding Gd(III) chelate is too close to the targeting moiety to allow for receptor binding. Given that **[Gd.L^{9}]**, with the longer spacer induces a significant enhancement in $R_{1,cell}$, it suggests that the targeting moieties do possess reasonable affinity for the NMDA receptor. Therefore, it must be that receptor binding is inhibited for **[Gd.L$^{5\text{-}8}$]** due to the close proximity of the Gd(III) chelate. The lower $R_{1,cell}$ observed for **[Gd.L^{10}]** is in keeping with the lower receptor affinity of such antagonists in the small molecule work.[1]

Despite the observable enhancement in $R_{1,cell}$ for **[Gd.L^{9}]**, it is much lower than the enhancements observed for **[Gd.L^{2}]** and **[Gd.L^{4}]**, notwithstanding the fact that the receptor binding moiety is reported to possess an increased NMDA receptor affinity. This is most likely due to the length of the spacer unit linking the targeting moiety to the Gd(III) chelate, which is longer in the case of **[Gd.L^{9}]**. This could lead to a decrease in the rotational coupling between the Gd(III) chelate and the receptor bound targeting moiety, resulting in the global τ_R not being modulated as much.

3.6 Conclusions

The aim of this chapter was to build on the results from *chapter 2*. The goal was to develop a second generation of NMDA receptor-targeted MR contrast agents, with an improved receptor affinity, by using the modified bicyclic antagonist proposed by Kinney. A novel route has been designed to synthesise the four new receptor-binding moieties, and they have been conjugated to Gd(III) chelates to give the complexes **[Gd.L$^{5\text{-}10}$]**. In order to study the effect of linker length on relaxivity gain, the complexes **[Gd.L$^{5\text{-}8}$]** possess a linker derived from glutaric acid, whereas **[Gd.L$^{9\text{-}10}$]** incorporate a longer chain which further separates the receptor-binding moiety and the Gd(III) chelate. The compounds were fully characterised and their potential to bind non-specifically to HSA has been assessed.

Upon incubation with a neuronal cell line model, the complexes **[Gd.L$^{5\text{-}8}$]** induced an increase in cellular relaxation rate of no more than 106%. In contrast, **[Gd.L^{9}]**, with the longer spacer, induced an enhancement in $R_{1,\text{cell}}$ of 123%. This suggests that the complexes **[Gd.L$^{5\text{-}8}$]** are unable to bind to the NMDA receptor, most likely due to the close proximity of the large Gd(III) chelate. However, **[Gd.L^{9}]** can bind to the cell surface NMDA receptor, modulating τ_R of the complex leading to an increase in $R_{1,\text{cell}}$. Whilst an enhancement in $R_{1,\text{cell}}$ is observed for **[Gd.L^{9}]**, it is much smaller than that observed for **[Gd.L^{2}]** and **[Gd.L^{4}]**. This is either due to the receptor-binding moiety of **[Gd.L^{9}]** possessing a lower receptor affinity, or the increased spacer length in **[Gd.L^{9}]** leads to a greater degree of decoupled rotation, limiting the relaxivity gain.

At present, the variation in $R_{1,\text{cell}}$ of NSC-34 cells when incubated with **[Gd.L^{2}]**, **[Gd.L^{4}]** and **[Gd.L^{9}]** is consistent with an increase in τ_R that is associated with slower molecular tumbling of the complex when bound to the cell surface NMDA receptor. However, internalisation of the complex via receptor-mediated endocytosis or non-specific binding to the cell membrane are also possible mechanisms that could lead to an increase in $R_{1,\text{cell}}$. In order to establish which of these possibilities was responsible for the observed increases in $R_{1,\text{cell}}$, direct

visualisation of the complex on the cell surface is needed. Due to the limiting resolution associated with MRI, a different imaging technique was needed.

Chapter 4 will discuss the design and synthesis of two new NMDA receptor-targeted conjugates for optical imaging. Based on the structures of **[Gd.L^4]** and **[Gd.L^9]**, a comparative study of the new conjugates was performed which determined the localisation profile, reversibility and cellular specificity of binding, as well as the relative affinities of the two receptor-binding moieties used.

3.7 References

1. W. A. Kinney, M. Abou-Gharbia, D. T. Garrison, J. Schmid, D. M. Kowal, D. R. Bramlett, T. L. Miller, R. P. Tasse, M. M. Zaleska and J. A. Moyer, *J. Med. Chem.*, 1998, **41**, 236-246.
2. W. S. Saari, J. E. Schwering, P. A. Lyle, S. J. Smith and E. L. Engelhardt, *J. Med. Chem.*, 1990, **33**, 97-101.
3. L. E. Overman and M. J. Sharp, *Tetrahedron Lett.*, 1988, **29**, 901-904.
4. D. Parker and B. P. Waldron, *Org. Biomol. Chem.*, 2013, **11**, 2827-2838.
5. D. Parker, L. Laurent and C. Montgomery, *Pyridyl-aza(thio)xanthone sensitizer comprising lanthanide (III) ion complexing compounds, their luminescent lanthanide (III) ion complexes and use thereof as fluorescent labels*, IPO WO 2010/084090 A1, 2010.
6. A. Mishra, S. Gottschalk, J. Engelmann and D. Parker, *Chem. Sci.*, 2012, **3**, 131-135.
7. L. Helm and A. E. Merbach, *Chem. Rev.*, 2005, **105**, 1923-1960.
8. S. Aime, M. Botta and G. Ermondi, *Inorg. Chem.*, 1992, **31**, 4291-4299.
9. P. Hermann, J. Kotek, V. Kubicek and I. Lukes, *Dalton Trans.*, 2008, 3027-3047.
10. S. Avedano, M. Botta, J. S. Haigh, D. L. Longo and M. Woods, *Inorg. Chem.*, 2013, **52**, 8436-8450.
11. M. Woods, S. Aime, M. Botta, J. A. K. Howard, J. M. Moloney, M. Navet, D. Parker, M. Port and O. Rousseaux, *J. Am. Chem. Soc.*, 2000, **122**, 9781-9792.
12. A. E. Merbach and E. Toth, *The chemistry of contrast agents in medical magnetic resonance imaging*, Wiley, New York, Chichester, 2001.
13. P. Caravan, N. J. Cloutier, M. T. Greenfield, S. A. McDermid, S. U. Dunham, J. W. M. Bulte, J. C. Amedio, R. J. Looby, R. M. Supkowski, W. D. Horrocks, T. J. McMurry and R. B. Lauffer, *J. Am. Chem. Soc.*, 2002, **124**, 3152-3162.

CHAPTER FOUR

Direct Visualisation of NMDA Receptors by Optical Microscopy

4. Direct Visualisation of NMDA Receptors By Optical Microscopy

4.1 Introduction

Ten NMDA receptor-targeted MRI contrast agents have been synthesised, of which three, **[Gd.L^2]**, **[Gd.L^4]** and **[Gd.L^9]**, showed considerable enhancements in $R_{1,cell}$ when incubated with a neuronal cell line model possessing functional NMDA receptors. The variation of $R_{1,cell}$ of differentiated NSC-34 cells in the presence of these three contrast agents is consistent with an increase in τ_R that is associated with slower molecular tumbling of the complex when bound to the cell-surface receptor. However, due to the intrinsic insensitivity of MR imaging, direct visualisation of the complexes is prohibited, meaning there is no direct proof of cell-surface receptor localisation. The observed increases in $R_{1,cell}$ could also result from internalisation of the complex, via receptor-mediated endocytosis, or through the complex non-specifically binding to the cell membrane. In order to establish which mechanism is responsible for the increases in $R_{1,cell}$, two new complexes were designed and synthesised, allowing complex visualisation using high-resolution laser-scanning confocal microscopy.

As discussed in *chapter 1*, appending a fluoroscein label to a non-competitive antagonist has recently been shown to allow for the direct visualisation of the NR2B subunit.[1, 2] However, work by Barton and co-workers[3, 4] and within the Durham group[5-8] has shown that appending a relatively lipophilic fluorescent moiety to a complex can perturb cell uptake mechanisms, promoting non-specific cellular-uptake. In order to target and visualise NMDA receptors on the cell surface selectively, the structures of **[Gd.L^2]**, **[Gd.L^4]** and **[Gd.L^9]** needed to be perturbed minimally, limiting the changes to overall complex charge and hydrophilicity.

The new complexes, **[Gd.L^{11}]** and **[Gd.L^{12}]**, comprise the receptor-binding moieties of the most promising MRI contrast agents, **[Gd.L^4]** and **[Gd.L^9]** (largest increases in $R_{1,cell}$ for each series), with a *trans*-substituted D-biotin moiety appended to the macrocyclic core. This design was based on the hypothesis that if the cell-surface NMDA receptor-binding is responsible for the increases in

$R_{1,cell}$ of **[Gd.L^{4}]** and **[Gd.L^{9}]**, the receptor-binding moieties of **[Gd.L$^{11\text{-}12}$]** would interact with the NMDA receptors. The remote biotin moiety would then act as a tag, binding to an added AvidinAlexaFluor®488 conjugate, which would allow visualisation of the avidin-biotin conjugate by optical microscopy.

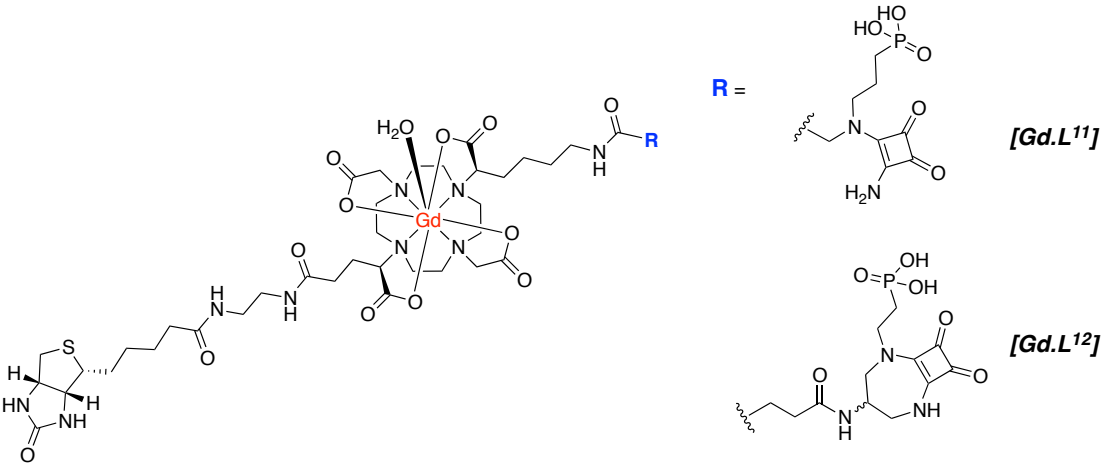

Scheme 4. Structures of the target complexes, **[Gd.L^{11}]** and **[Gd.L^{12}]**.

4.2 Synthetic Details

4.2.1 Synthesis of [Conjugate 11]

The ligand macrocyclic framework was built up over a series of protection, alkylation and deprotection steps (*Scheme 4.1*). Starting from cyclen, bis-protection in the 1,7- positions under pH control, using benzyl chloroformate afforded compound ***60***, which was then subject to *N*-alkylation in the 4- and 10-positions using *tert*-butyl bromoacetate. Removal of the benzyl protecting groups under high-pressure hydrogenation over a Pd/C catalyst, afforded ***62***, as previously reported.[9]

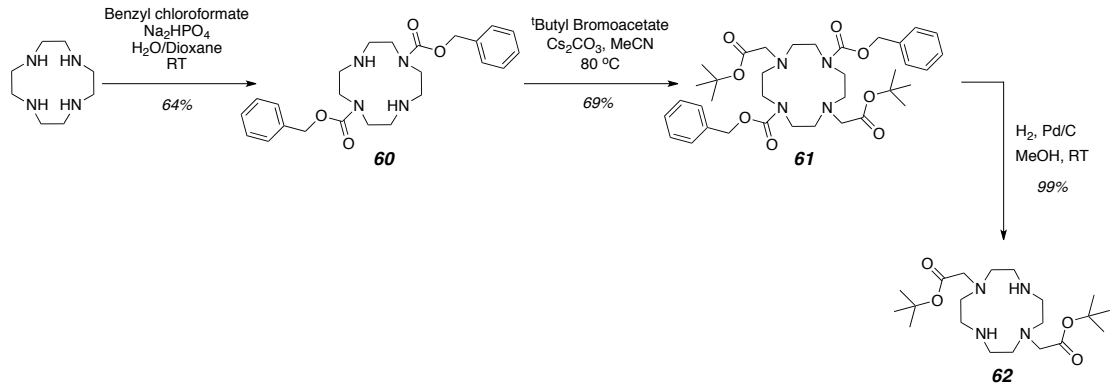

Scheme 4.1

As shown in *scheme 4.2*, mono-alkylation of ***62*** was undertaken in anhydrous acetonitrile at 80 °C, using 0.9 equivalents of α-bromo ester, ***18***, in the presence of Na_2CO_3.[10] Separation of the tri-substituted cyclen from the tetra-substituted derivative by column chromatography afforded ***63*** in a reasonable yield. The free amine ***63*** was subject to *N*-alkylation with a slight excess of the bromoglutarate derivative, ***50***, in the presence of K_2CO_3, to give the tetra-substituted cyclen, ***64***, as a pale yellow oil after purification by column chromatography.[11] The orthogonal nature of the protecting groups allowed for selective hydrolysis of the benzyl ester group of ***64*** under mild basic conditions.[11] Concurrent synthesis of ***67*** was achieved through amide bond formation between the carboxylic acid of D-biotin and the amine of *N*-Boc ethylene diamine, to give ***66*** as a white solid.[12] This was subsequently deprotected under acidic conditions to afford the TFA salt of the amine, ***67***.

The carboxylic acid, ***65***, was stirred as a solution in a small amount of anhydrous DMF with EDC.HCl and HOBt for 20 minutes. After this period, a solution of the TFA salt of ***67*** and NMM in a minimal amount of DMF was added and the reaction monitored by ESI-MS. After stirring at room temperature overnight, the introduction of the biotin moiety to the macrocycle was confirmed through analysis of the crude mass spectrum. After work-up and purification by column chromatography, compound ***68*** was isolated as a viscous brown oil in 30% yield. Removal of the Cbz protecting group from the *N*-terminus of the pendent lysine arm by high-pressure hydrogenation over a palladium hydroxide catalyst gave the free amine, which was used directly in the coupling step to the receptor binding moiety of **[Gd.L^4]** (***16***). Employment of the same amide bond formation

techniques as previously used gave **[conjugate 11]** (***69***), in a poor yield, after subsequent work up and purification by preparative RP-HPLC.

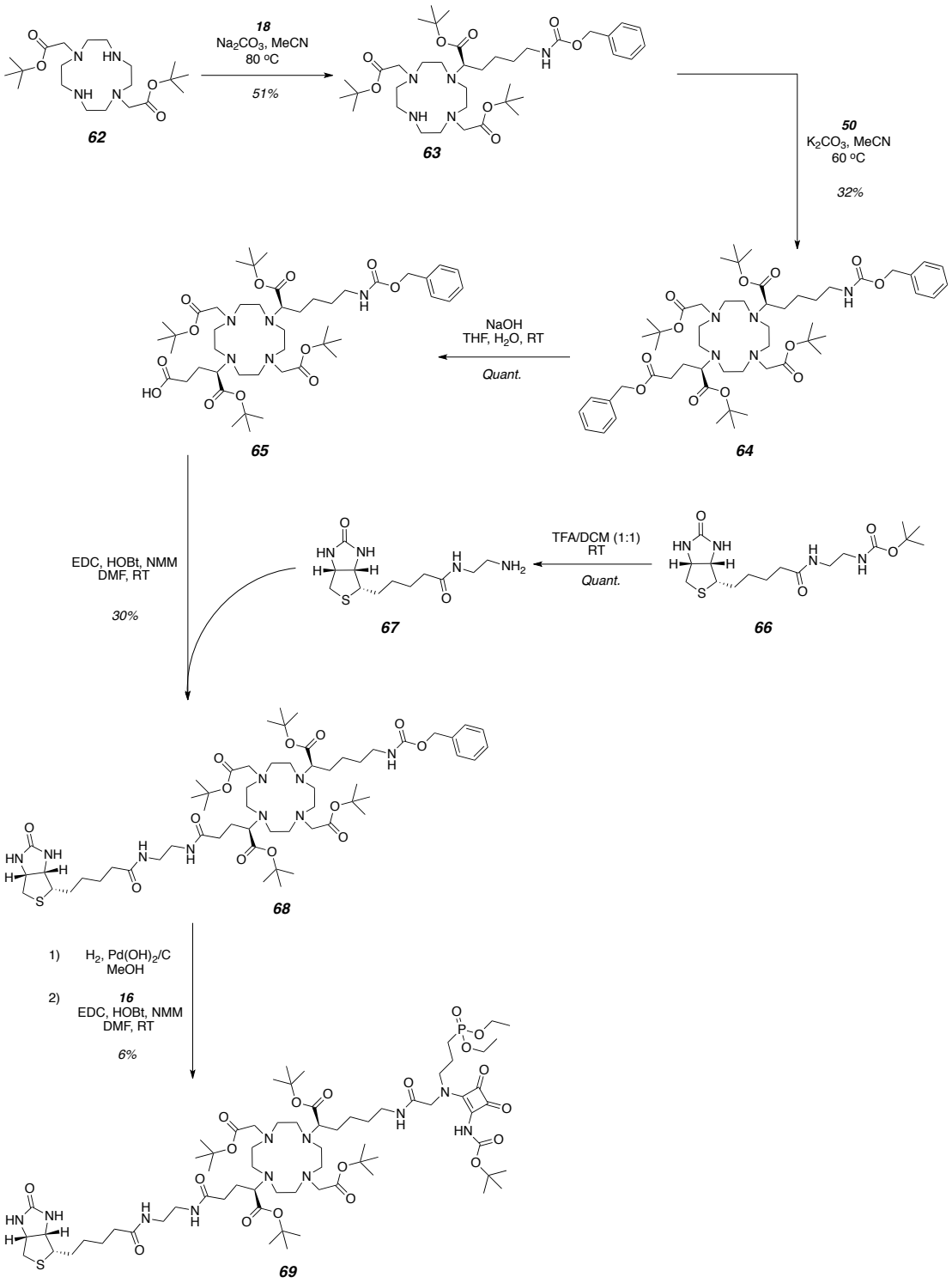

Scheme 4.2

4.2.2 Synthesis of [Conjugate 12]

During the synthesis of **[conjugate 11]** (***69***), the hydrogenation step to remove the Cbz protecting group was slow, taking several days for complete deprotection. This was attributed to the presence of the sulfur atom of the biotin moiety, which may possibly poison the catalyst and decrease the reaction rate. The synthesis of **[conjugate 12]** (***75***) followed a modified route (*Scheme 4.3*), which would allow for incorporation of the biotin moiety in the final step of the conjugate synthesis. Therefore, there was a slight change in the protecting group strategies employed.

A simple methyl ester group replaced the benzyl-protecting group of the bromoglutarate arm. This compound was synthesised from the commercially available (*S*)-glutamic acid 5-methyl ester. Diazotisation of the α-amino group, followed by *in-situ* bromination gave the brominated derivative ***70***, after purification by column chromatography. Subsequent esterification of the carboxylic acid group, using *tert*-butyl acetate in the presence of a catalytic amount of acid, gave the orthogonally protected ester, ***71***. *N*-alkylation of ***63*** by ***71*** was achieved by stirring in anhydrous acetonitrile at 60 °C in the presence of K_2CO_3. Removal of the Cbz protecting group from the *N*-terminus of the penta-ester, ***72***, followed by chain extension via reaction with succinic anhydride gave the free carboxylic acid, ***73***, after purification by column chromatography. The acid, ***73***, was then coupled to the primary amine of the receptor-binding moiety of **[Gd.L^9]** (***36***), using the amide bond forming techniques previously established, to yield ***74*** as a diastereoisomeric mixture. Finally, methyl ester hydrolysis under ambient basic conditions, followed by a second amide bond formation with the TFA salt of biotin ethylene diamine, ***67***, gave **[conjugate 12]** (***75***), albeit in a low yield, after purification by column chromatography.

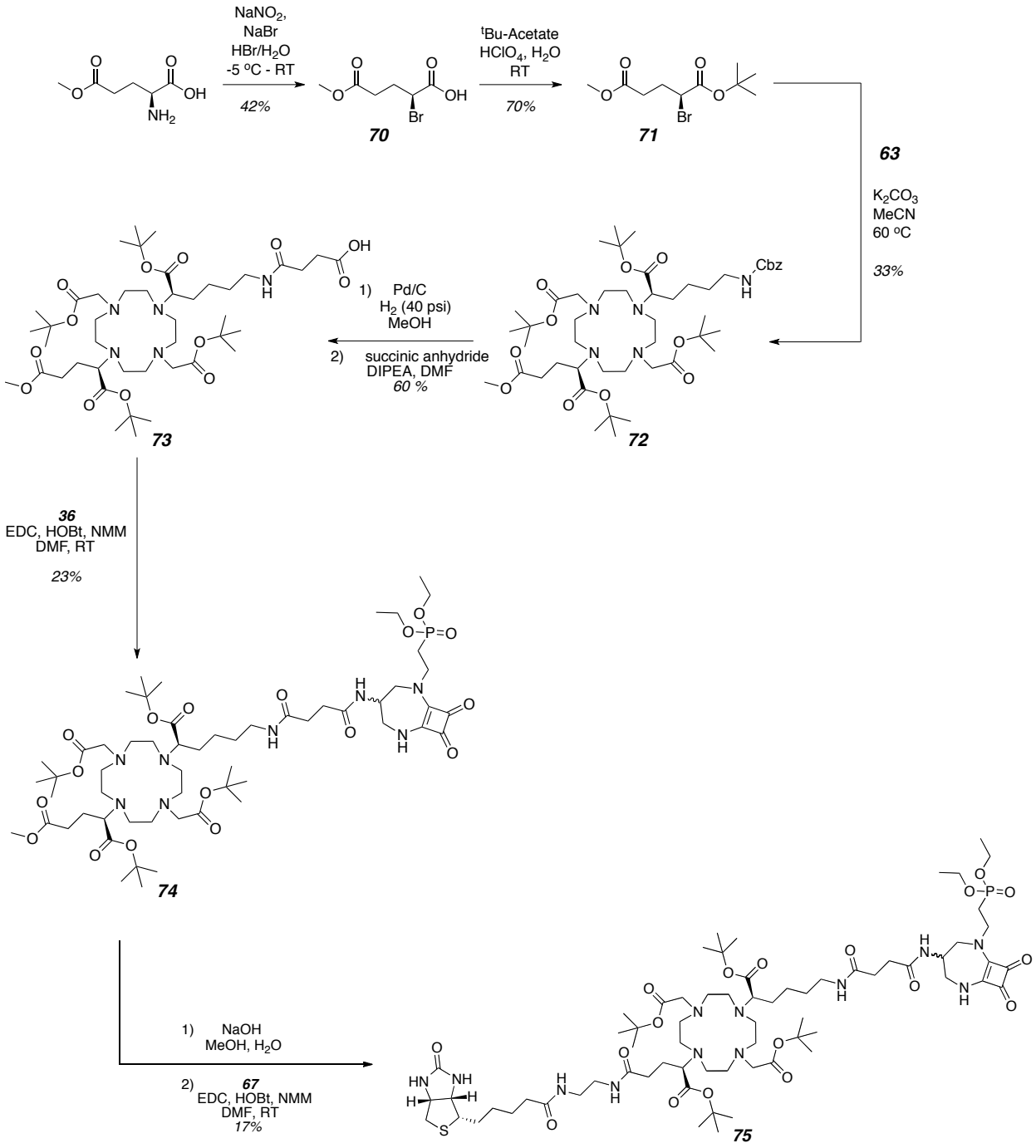
NaNO2, NaBr HBr/H2O -5 °C - RT
42%
70
tBu-Acetate HClO4, H2O RT
70%
71
63
K2CO3 MeCN 60 °C
33%
72
1) Pd/C H2 (40 psi) MeOH
2) succinic anhydride DIPEA, DMF 60 %
73
36 EDC, HOBt, NMM DMF, RT
23%
74
1) NaOH MeOH, H2O
2) 67 EDC, HOBt, NMM DMF, RT 17%
75

Scheme 4.3

4.2.3 Complex Synthesis and Characterisation

With **[conjugates 11-12]** in hand, the final step before metal complexation involved global hydrolysis of all protecting groups (*Scheme 4.4*). In the formation of ***L*^{11}**, basic hydrolysis of the phosphonate ethyl esters was undertaken by stirring in THF with aqueous KOH at 60 °C for four hours. Removal of the phosphonate ethyl esters after this time was verified by ESI-MS, at which point the crude phosphonic acid was dissolved in a 1:1 mixture of trifluoroacetic acid and DCM and stirred at room temperature overnight. Complete removal of the *tert*-butyl ester and carbamate protecting groups gave ***L*^{11}**, with its presence confirmed through analysis of the crude mass spectrum (545.1, $[M+2H]^{2+}$).

In the synthesis of ***L*^{12}**, it was decided that a better approach was to hydrolyse the *tert*-butyl ester protecting groups first. This was again achieved using a 1:1 solution of trifluoroacetic acid and DCM. Following hydrolysis of the *tert*-butyl esters, the crude phosphonate ethyl ester was dissolved in DMF and heated to 60 °C in the presence of an excess of bromotrimethylsilane. Global hydrolysis was confirmed after 16 hours, through analysis of the mass spectrum (587.0, $[M+2H]^{2+}$).

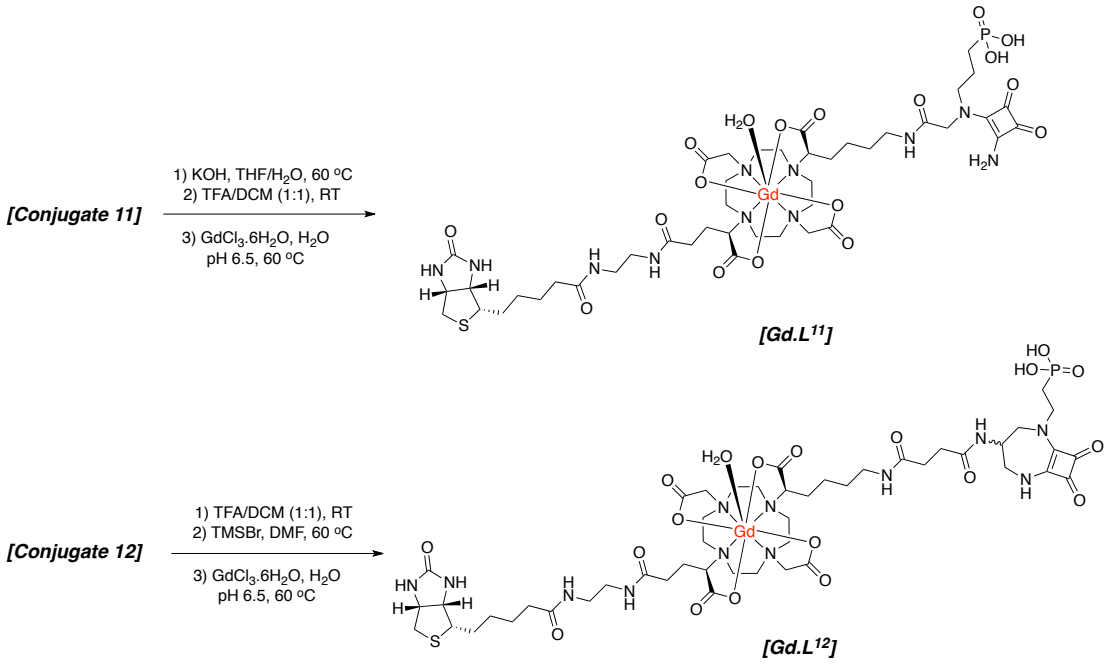

Scheme 4.4

Finally, complexation of the corresponding TFA salts of ***L*$^{11\text{-}12}$** was carried out by reaction with $GdCl_3.6H_2O$ in H_2O (pH 6-6.5) at 60 °C overnight (*Scheme 4.4*). A slight excess of the gadolinium salt led to rapid complexation. Upon completion, the excess Gd(III) was removed via complexation to Chelex-100™ resin, and the complexes **[Gd.L$^{11\text{-}12}$]** purified by preparative RP-HPLC. Confirmation of the presence of the complexes **[Gd.L$^{11\text{-}12}$]** was achieved using high-resolution mass spectrometry analysis. The theoretical and experimental mass distributions for **[Gd.L^{12}]** showed good agreement (*Figure 4*).

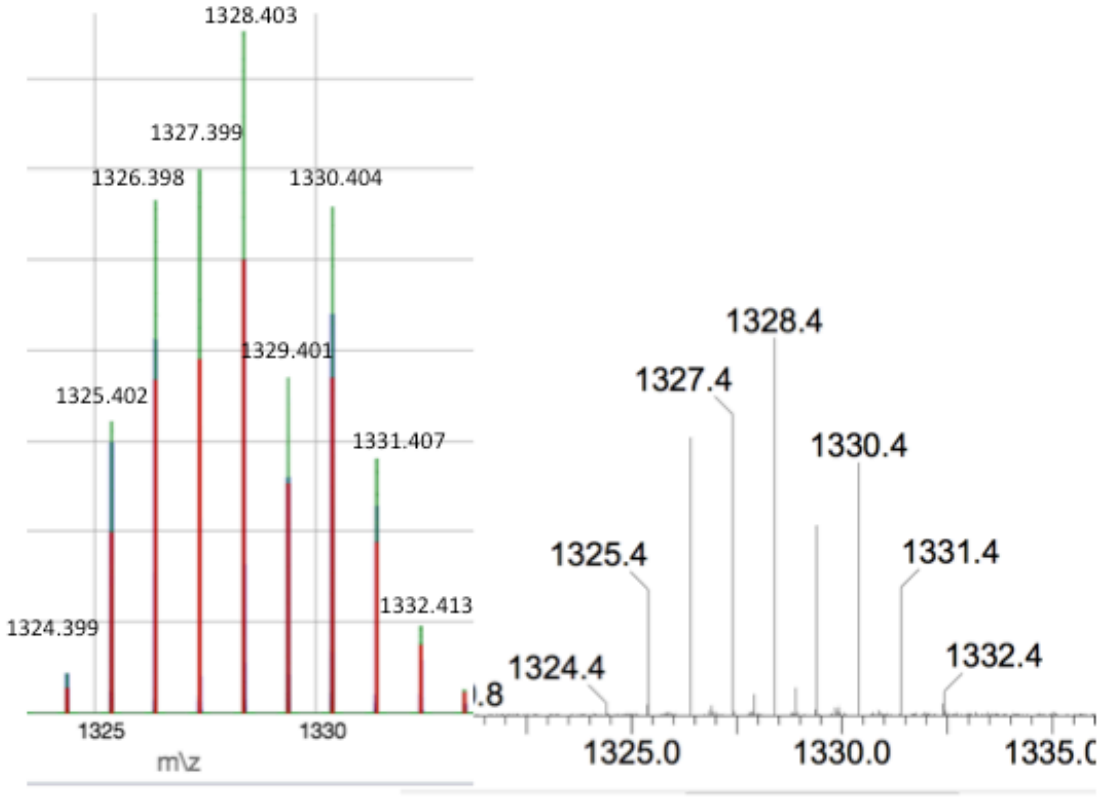

Figure 4. Calculated (left) and observed (right) high-resolution electrospray mass spectra of **[Gd.L^{12}]**, showing the characteristic Gd-isotope pattern; TOF positive mode.

The longitudinal proton relaxivities of **[Gd.L$^{11\text{-}12}$]** were measured in water at 1.4 T and 310 K. The relaxivities of **[Gd.L$^{11\text{-}12}$]** were both 7.2 (± 0.4) mM^{-1} s^{-1}. In contrast to the parent compounds, these higher relaxivity values are associated with an increased molecular volume of the complexes, giving rise to a slower rotational correlation time. Also, there is an increased likelihood of second sphere hydration through multiple hydrogen bonding interactions, which also tends to increase r_{1p}.[13]

4.3 Comparative Studies Using Confocal Microscopy

4.3.1 Localisation Studies

In order to study the localisation profiles of **[Gd.L$^{11\text{-}12}$]**, live-cell laser scanning confocal microscopy (LSCM) imaging studies were carried out using a Leica SP5 II microscope by Dr Robert Pal, Durham University. Differentiated NSC-34 cells expressing functional NMDA receptors were grown (as described in *chapter 2*) on specially designed microscope slides, comprising a 100 μL flow-through channel and subjected to various experimental conditions.

Initially, differentiated NSC-34 cells were incubated simultaneously with solutions of **[Gd.L^{11}]** or **[Gd.L^{12}]** (10 μM) and AvidinAlexaFluor® 488 conjugate (2.5 μM), for 10 minutes at 37 °C and 5% CO_2. After this time, the cells were washed three times with fresh buffer to remove any unbound complex and imaged. Both **[Gd.L^{11}]** and **[Gd.L^{12}]** showed a localisation profile resembling 'pit-like' regions at the cell surface (*Figure 4.1 A and D*). By keeping the microscope settings constant throughout all imaging studies, a comparison of the fluorescence intensities gave an idea of the relative affinities of each complex. Cells that were treated with **[Gd.L^{12}]** appeared 38% brighter than those treated with **[Gd.L^{11}]**. This suggests that the receptor-binding moiety of **[Gd.L^{12}]** has a higher affinity for the NMDA receptor than the acyclic analogue used in **[Gd.L^{11}]**, which is in keeping with the relative affinities of the small molecule antagonists.[14] Unequivocal evidence of the selective localisation of **[Gd.L$^{11\text{-}12}$]** at the cell membrane was obtained using the commercially available dye, CellMask™ Orange, which non-specifically stains the plasma membrane. A repeat of the simultaneous loading experiments of **[Gd.L^{11}]** or **[Gd.L^{12}]** (10 μM) and AvidinAlexaFluor® 488 conjugate (2.5 μM, 10 mins) on differentiated NSC-34 cells, with a co-incubation of CellMask™ Orange (5 μg/mL, 5 mins), demonstrated that the signal from the complex-Avidin conjugate was residing at the cell surface, with no intracellular staining observed at all (*Figure 4.1 A-F*).

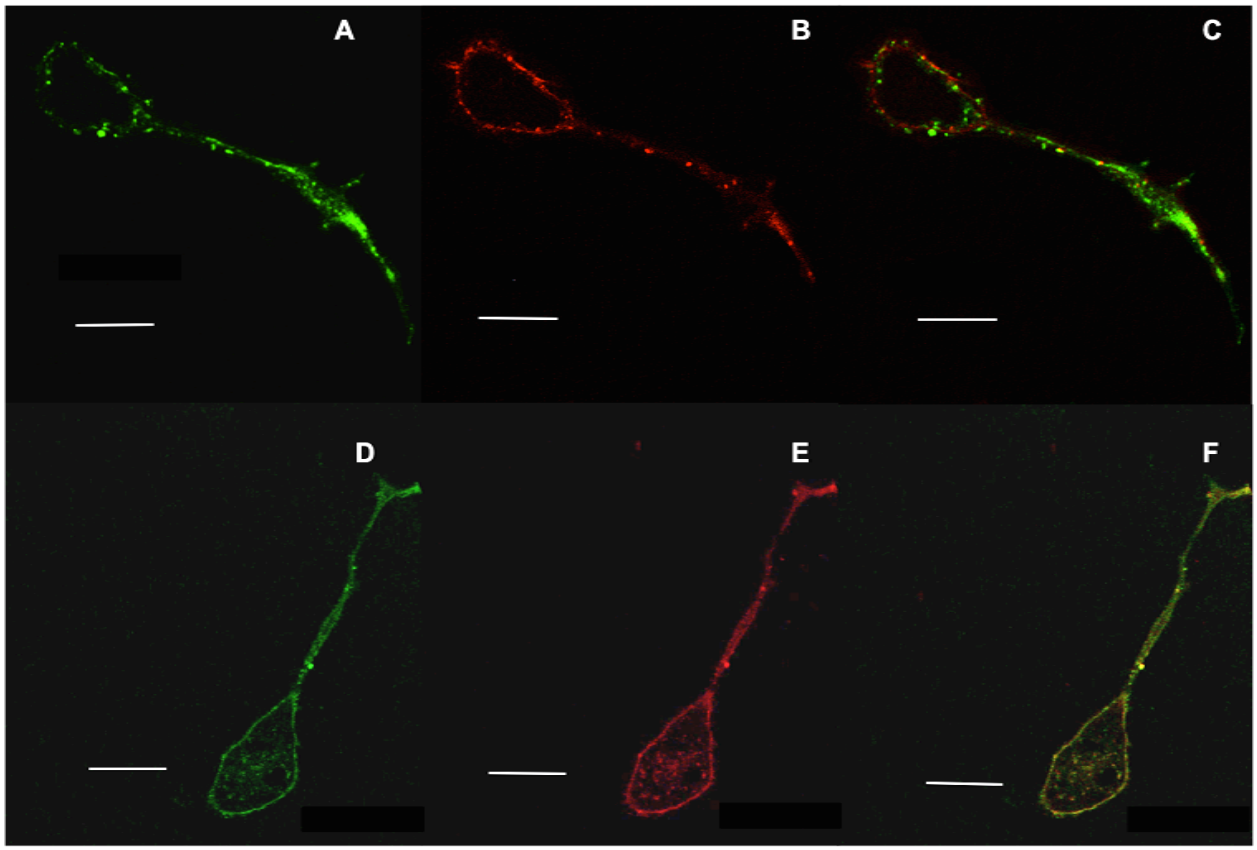

Figure 4.1. Live cell LSCM images of differentiated NSC-34 cells following treatment with **[Gd.L$^{11\text{-}12}$]** showing cell surface localisation. (A) Simultaneous loading of **[Gd.L^{11}]** (10 μM), and AvidinAlexaFluor® 488 conjugate (2.5 μM, 10 mins) allowing visualisation of AvidinAlexaFluor® 488 conjugate $\lambda_{ex}/\lambda_{em}$ =488/505-555 nm; (B) As (A) but with a 5 minute CellMask™ Orange incubation allowing visualisation of CellMask™ Orange $\lambda_{ex}/\lambda_{em}$ = 543/550-660 nm; (C) RGB merge showing co-localisation of the AvidinAlexaFluor® 488 conjugate and CellMask™ Orange on the cell surface; (D-F) As images (A-C) but using **[Gd.L^{12}]**. Scale bars are 17.0 μm for (A-C) and 20.0 μm for images (D-F).

In order to confirm that the fluorescence profiles are due to the strong biotin-avidin interaction between the complexes **[Gd.L^{11}]** and **[Gd.L^{12}]** and the AvidinAlexaFluor® 488 conjugate, three control experiments were carried out (*Figure 4.2*). First, in order to demonstrate that the observed fluorescence was not due to cellular autofluorescence, untreated differentiated NSC-34 cells were imaged. Secondly, to demonstrate that AvidinAlexaFluor® 488 conjugate was not able to bind to differentiated NSC-34 cells, these cells were treated only with a solution of AvidinAlexaFluor® 488 conjugate (2.5 μM, 10 mins). Finally, in order to show that the complexes **[Gd.L$^{11\text{-}12}$]** are non-fluorescent themselves, differentiated NSC-34 cells were treated with solutions of these complexes alone

(10 μM, 10 mins). In every case, no observable fluorescence signal in the visible region of the spectrum was detected, indicating that the fluorescence observed in *figure 4.1 A and D* is due to the strong (logK_a >15) biotin-avidin interaction between the gadolinium complexes and the fluorescent conjugate.

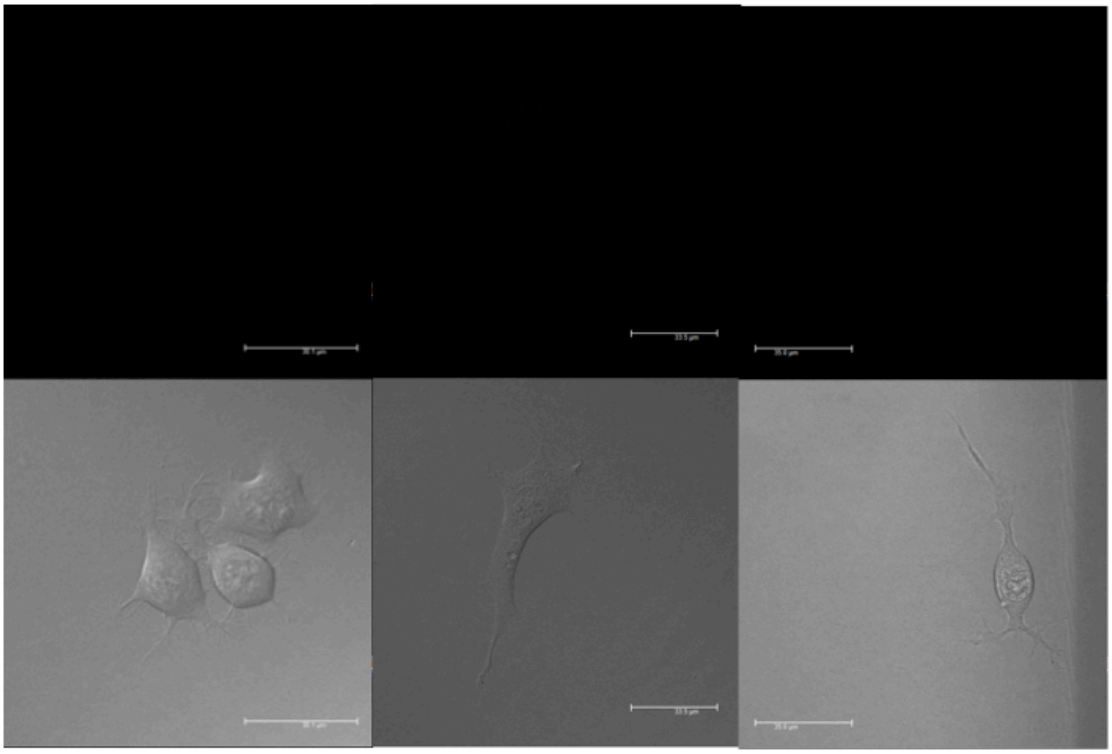

Figure 4.2. (*Top*) No observable fluorescence signal from cells; (*bottom*) transmission image, showing cell morphology. (*Left to right*) Untreated differentiated NSC-34 cells, cells treated with AvidinAlexaFluor® 488 conjugate alone (2.5 μM, 10 mins), and cells treated with **[Gd.L^{12}]** alone (10 μM, 10 mins).

The cell surface localisation of the Avidin conjugates of **[Gd.L$^{11\text{-}12}$]** was found to be independent of the loading concentration (up to 100 μM), time (up to 45 minutes) and the order of addition of AvidinAlexaFluor® 488 conjugate (stepwise vs simultaneous).

4.3.2 Establishing Cellular Specificity of Binding

The potential of **[Gd.L^4]** and **[Gd.L^9]** to bind non-specifically to endogenous protein was studied in *chapters 2 and 3*, using HSA as a model. However, a key characteristic needed for these contrast agents is to have cellular specificity of

binding, meaning that they can only bind to cells expressing functional NMDA receptors. Therefore, the potential of **[Gd.L$^{11\text{-}12}$]** to bind to NMDA receptor-negative cells was assessed. NIH-3T3 cells are mouse skin fibroblasts, and do not express any NMDA receptors. These cells were incubated simultaneously with solutions of **[Gd.L^{11}]** or **[Gd.L^{12}]** (10 μM) and AvidinAlexaFluor® 488 conjugate (2.5 μM) for 10 minutes, washed three times with fresh buffer to remove any unbound complex and then imaged. No localisation profile of any kind (cell surface or intracellular) was observed, strengthening the argument of a receptor-mediated localisation effect observed when **[Gd.L$^{11\text{-}12}$]** were incubated with NSC-34 cells. This behaviour further suggests that the enhancements in $R_{1,\text{cell}}$ of NSC-34 cells which were incubated for **[Gd.L^{4}]** and **[Gd.L^{9}]** results from the complexes binding to the NMDA receptor, modulating τ_R of the complexes, as opposed to non-specific membrane labelling.

4.3.3 Assessing the Reversibility of Binding

One of the key design characteristics needed for an NMDA receptor-targeted contrast agent was for it to possess the ability to bind to the NMDA receptor in a reversible manner, with a competitive affinity to the endogenous ligand glutamate. Since optical microscopy has a superior sensitivity and resolution, it was thought best to assess the ability of **[Gd.L^{4}]** and **[Gd.L^{9}]** to bind reversibly at the NMDA receptor by visualising the fate of their fluorescent-conjugate analogues, **[Gd.L$^{11\text{-}12}$]**, after a simulated 'glutamate burst'.

Differentiated NSC-34 cells were simultaneously incubated with solutions of **[Gd.L^{11}]** or **[Gd.L^{12}]** (10 μM) and AvidinAlexaFluor® 488 conjugate (2.5 μM) for 10 minutes, washed three times with fresh buffer to remove any unbound complex and then imaged. The average image intensity for each complex was assessed as triplicates using three cells (excluding the axon), which gave rise to a maximum contrast transfer function (CTF) displaying a Gaussian distribution. The CTFs of **[Gd.L^{11}]** and **[Gd.L^{12}]** were found to be 173 and 239 counts (out of 256), demonstrating that **[Gd.L^{12}]** is 38% brighter than that of **[Gd.L^{11}]** (*Figure 4.3 A and D*). These cells were then washed with five successive aliquots (V_{tot} = 500 μL) of a glutamate-rich (1 mM) culture media and imaged again. A ten- and

nine-fold drop in fluorescence intensity was observed for cells treated with **[Gd.L^{11}]** and **[Gd.L^{12}]**, respectively, compared to the original cell staining experiment (*Figure 4.3 B and E*). Furthermore, when cells were sequentially treated with the avidin/biotin components and with five volumetric aliquots of a glutamate-rich (1 mM) culture media, then washed with normal culture media and finally re-incubated with solutions of **[Gd.L^{11}]** or **[Gd.L^{12}]** (10 μM) and AvidinAlexaFluor® 488 conjugate (2.5 μM) for 10 minutes, 35% and 38% of the fluorescence signal was recovered for **[Gd.L^{11}]** and **[Gd.L^{12}]**, respectively (*Figure 4.3 C and F*). The fluorescence intensity could be almost fully recovered (98% of the original intensity) when prolonging the re-incubation of **[Gd.L^{12}]** to 45 minutes.

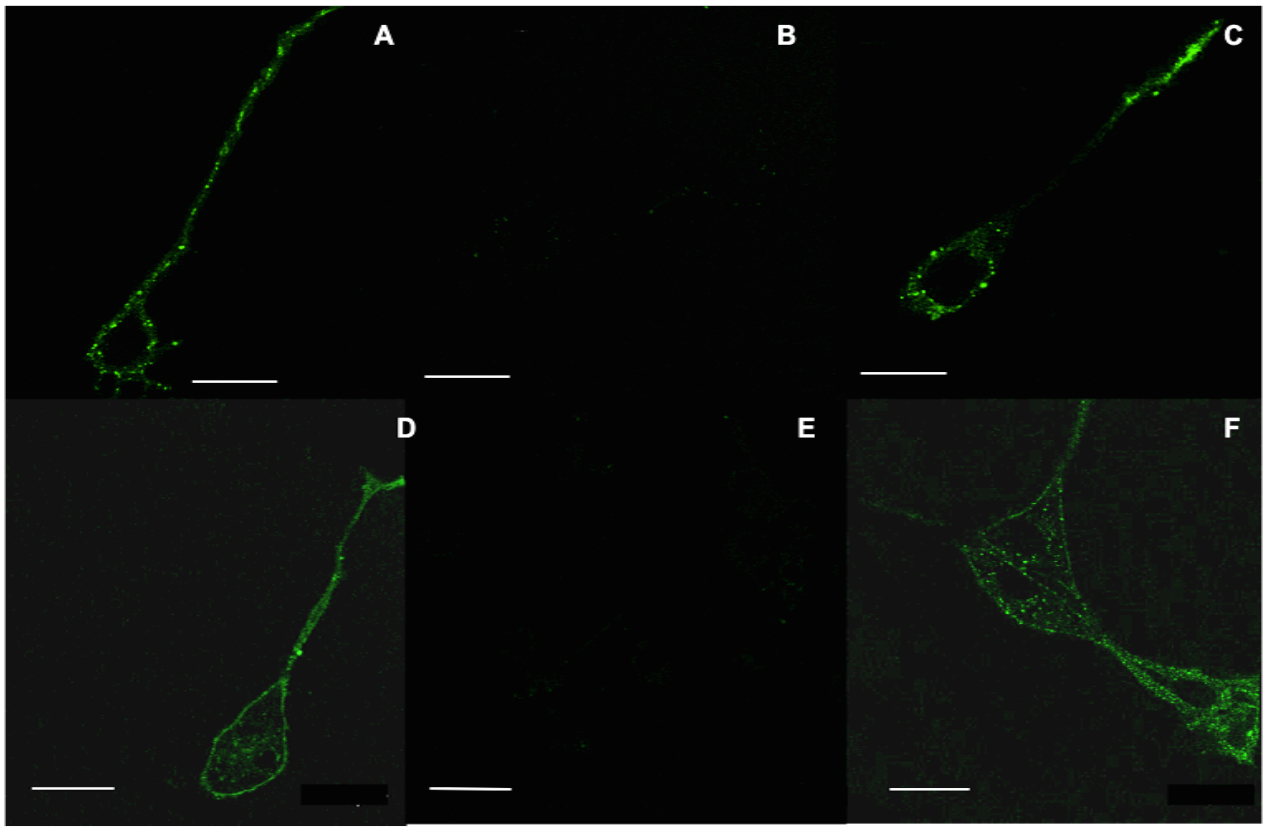

Figure 4.3. Live cell LSCM images of differentiated NSC-34 cells following treatment with **[Gd.L$^{11\text{-}12}$]**. (A) Simultaneous loading of **[Gd.L^{11}]** (10 μM), and AvidinAlexaFluor® 488 conjugate (2.5 μM, 10 mins) allowing visualisation of AvidinAlexaFluor® 488 conjugate $\lambda_{ex}/\lambda_{em}$ =488/505-555 nm; (B) As (A) but with a post glutamate (1 mM) wash showing **[Gd.L^{11}]** is removed from the cell surface; (C) As image (B) and then simultaneous loading of **[Gd.L^{11}]** (10 μM), and AvidinAlexaFluor® 488 conjugate (2.5 μM, 10 mins) showing signal recovery; (D-F) As images (A-C) but using **[Gd.L^{12}]**. Scale bars are 17.0 μm for (A-C) and 20.0 μm for images (D-F).

Aspartate is a weaker natural agonist for the NMDA receptor[15] and should also possess the ability to displace the contrast agents from the glutamate-binding site. A repeat of the simulated glutamate burst experiment detailed above, with substitution of glutamate with aspartate in the washing step, led to the fluorescence intensity decreasing to 38% and 50% of the original intensity for **[Gd.L^{11}]** and **[Gd.L^{12}]**, respectively. This result is in keeping with the fact that aspartate has a lower affinity than glutamate for the NMDA receptor, and cannot fully displace the contrast agents from the binding site.[i] Also, since **[Gd.L^{11}]** is removed by aspartate to a larger extent, this reflects the lower affinity of the receptor-binding moiety of **[Gd.L^{11}]** with respect to the receptor-binding moiety of **[Gd.L^{12}]**.

These results further suggest that these contrast agents are binding to the glutamate binding site, present on the NMDA receptor. The results also demonstrate that the contrast agents are displaced easily enough by glutamate, and can compete to bind again after a simulated pre-synaptic glutamate burst.

4.3.4 Competition Experiments Involving [Gd.L^{12}]

Since **[Gd.L^{12}]** appeared to possess a higher affinity for the NMDA receptor over **[Gd.L^{11}]**, and in order to further confirm cell surface NMDA receptor tagging, competitive binding experiments were conducted with **[Gd.L^{12}]**.

At the outset it was expected that appending a sterically demanding Gd(III) chelate to a known NMDA receptor antagonist would result in a drop in the affinity of that antagonist towards the receptor. The complex **[Gd.L^{12}]** is derived from Kinney's antagonist, ***76***, which was synthesised in one step from compound ***29*** (*Scheme 4.5*).[14]

[i] The IC50 value of glutamate and aspartate are 0.31 and 1.18 μM, respectively.[15]

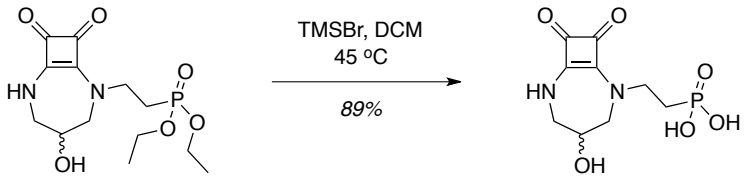

29 ***76***

Scheme 4.5.

The competitive antagonist, ***76***, binds to the NMDA receptor with a dissociation constant of the order of 20 nM. In order to study the effect of conjugation of a Gd(III) chelate to a known antagonist, on the antagonist's NMDA receptor affinity, a series of competition experiments was performed. First, differentiated NSC-34 cells were incubated simultaneously with a solution of **[Gd.L^{12}]** (10 μM) and AvidinAlexaFluor® 488 conjugate (2.5 μM) for 10 minutes, washed with fresh buffer and then incubated with compound ***76*** (10 μM, 10 mins). After this period, the cells were washed with buffer and imaged, giving rise to less than 5% signal intensity, compared to the original cell staining experiment (*Figure 4.4 A*). Reversing the order of incubation by first loading compound ***76*** (10 μM, 10 mins) and then incubating a solution of **[Gd.L^{12}]** (10 μM) and AvidinAlexaFluor® 488 conjugate (2.5 μM, 10 mins), led to less than 7% of the original signal intensity being observed (*Figure 4.4 B*). In a final experiment, differentiated NSC-34 cells were incubated with compound ***76*** (10 μM, 10 mins), washed with a glutamate-rich (1 mM) culture media and then incubated with **[Gd.L^{12}]** (10 μM) and AvidinAlexaFluor® 488 conjugate (2.5 μM) for 10 minutes. This increased the observed signal intensity to 18% (*Figure 4.4 C*).

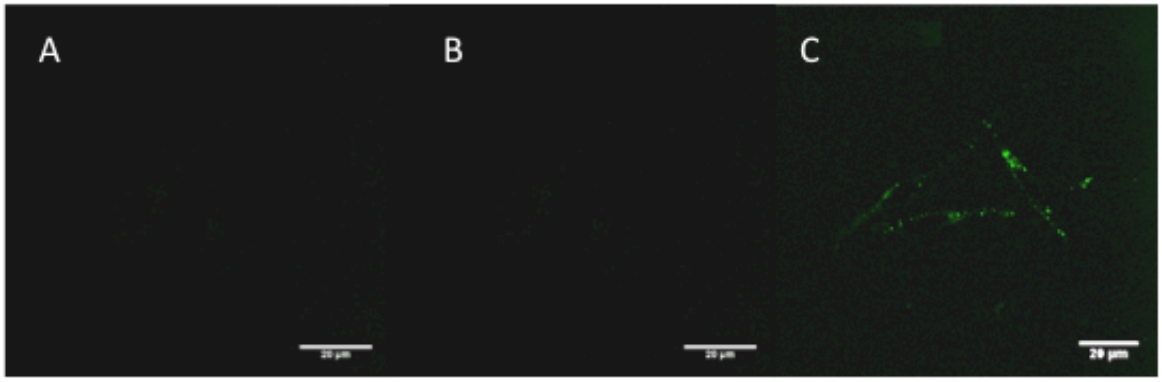

Figure 4.4. Live cell LSCM images of differentiated NSC-34 cells. (A) Loading of **[Gd.L^{12}]** (10 μM) and AvidinAlexaFluor® 488 conjugate (2.5 μM) for 10 minutes, washed with fresh buffer and then incubated with compound ***76*** (10 μM, 10 mins), showing <5% of

original intensity; (B) As image (A) but order of addition reversed, giving <7% of original intensity; (C) As image (B) but with a glutamate wash before loading **[Gd.L^{12}]** (10 μM) and AvidinAlexaFluor® 488 conjugate (2.5 μM), showing 18% of the original intensity.

Evidently, these results suggest that compound ***76*** has a higher affinity for the NMDA receptor than **[Gd.L^{12}]**, but the restoration of some signal (18%) after the glutamate wash suggests that it is important not to have a probe which is bound too tightly, or glutamate will not compete for receptor binding. The ability of **[Gd.L^{12}]** to bind reversibly in the presence of glutamate suggests this complex possesses an affinity for the NMDA receptor with the correct order of magnitude. The complex **[Gd.L^{12}]** is derived from the parent complex, **[Gd.L^{9}]**, but comprises a pendant biotin moiety in the *trans*-position. In order to establish if the biotin moiety is influencing the localisation profile of **[Gd.L^{12}]**, and more importantly to determine if **[Gd.L^{12}]** acts as a suitable model and binds at the same place as **[Gd.L^{9}]**, a second series of competition experiments were performed.

First, when differentiated NSC-34 cells were incubated with a solution of **[Gd.L^{9}]** (10 μM, 10 mins), washed with fresh buffer and then incubated simultaneously with a solution of **[Gd.L^{12}]** (10 μM) and AvidinAlexaFluor® 488 conjugate (2.5 μM) for 10 minutes, the signal intensity dropped to 25% of the original cell staining experiment (*Figure 4.5 A*). A complete recovery of the fluorescence signal could be obtained when the cells were washed with a glutamate-rich culture media (1 mM) and then re-incubated with a solution of **[Gd.L^{12}]** (10 μM) and AvidinAlexaFluor® 488 conjugate (2.5 μM) for 45 minutes.

In a similar experiment, when differentiated NSC-34 cells were first treated with a solution of **[Gd.L^{12}]** (10 μM) and AvidinAlexaFluor® 488 conjugate (2.5 μM) for 10 minutes, washed with fresh buffer and then incubated with a solution of **[Gd.L^{9}]** (10 μM, 10 mins), the signal intensity was 62%, compared to the original cell staining experiment (*Figure 4.5 B*). These results suggest that **[Gd.L^{9}]** and **[Gd.L^{12}]** have a comparable affinity for the NMDA receptor, and this was confirmed when a simultaneous incubation of all components (**[Gd.L^{12}]**, AvidinAlexaFluor® 488 and **[Gd.L^{9}]**) led to an intensity drop to 56% of the original signal (*Figure 4.5 C*). The observation that approximately 50% of the

original signal remains is consistent with the hypothesis that **[Gd.L^{9}]** and **[Gd.L^{12}]** bind at the same place on the NMDA receptor with similar affinities.

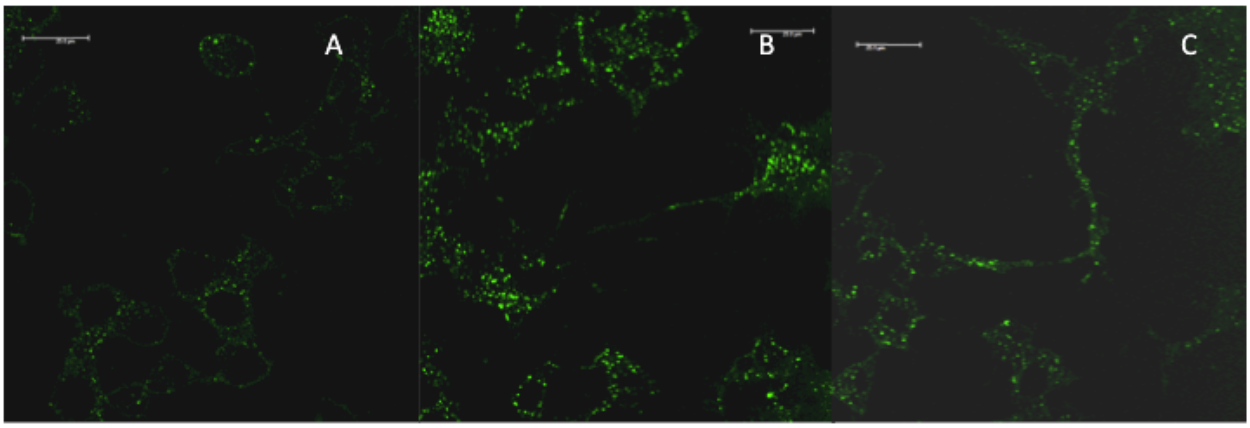

Figure 4.5. Live cell LSCM images of differentiated NSC-34 cells. (A) Cells loaded with **[Gd.L^{9}]** (10 μM, 10 mins), washed with buffer and then incubated with **[Gd.L^{12}]** (10 μM) and AvidinAlexaFluor® 488 conjugate (2.5 μM) for 10 minutes, showing 25% of original intensity; (B) As image (A) but order of addition reversed, giving 62% of original intensity; (C) Simultaneous loading of **[Gd.L^{12}]** (10 μM) and AvidinAlexaFluor® 488 conjugate (2.5 μM) and **[Gd.L^{9}]**, showing 56% of the original intensity.

The complex **[Gd.L^{12}]** also possesses the same NMDA receptor-binding moiety as **[Gd.L^{7}]**. However, the relatively short chain between the receptor-binding moiety and sterically demanding Gd(III) chelate in **[Gd.L^{7}]** brings the two into close proximity. In the MRI experiments, **[Gd.L^{7}]** induced a negligible (104%) enhancement in $R_{1,\text{cell}}$ when incubated with differentiated NSC-34 cells. This was attributed to the close proximity of the Gd(III) chelate to the NMDA receptor-binding moiety, inhibiting receptor-binding. In order to verify whether this conclusion is reasonable, one final series of competition experiments was performed between **[Gd.L^{12}]** and **[Gd.L^{7}]**.

First, differentiated NSC-34 cells were incubated with a solution of **[Gd.L^{7}]** (10 μM, 10 mins), washed with fresh buffer and then incubated simultaneously with a solution of **[Gd.L^{12}]** (10 μM) and AvidinAlexaFluor® 488 conjugate (2.5 μM) for 10 minutes. This led to a signal intensity drop to 7% of the original cell staining experiment (*Figure 4.6 A*). A complete recovery of the fluorescence signal could be obtained when the cells were washed with a glutamate-rich culture media (1 mM) and then re-incubated with a solution of **[Gd.L^{12}]** (10 μM) and AvidinAlexaFluor® 488 conjugate (2.5 μM) for 45 minutes.

Reversing the order of addition, when differentiated NSC-34 cells were first treated with a solution of **[Gd.L^{12}]** (10 μM) and AvidinAlexaFluor® 488 conjugate (2.5 μM) for 10 minutes, washed with fresh buffer and then incubated with a solution of **[Gd.L^{7}]** (10 μM, 10 mins), the signal intensity was 88% compared to the original cell staining experiment (*Figure 4.6 B*). Finally, a simultaneous incubation of all components (**[Gd.L^{12}]**, AvidinAlexaFluor® 488 and **[Gd.L^{7}]**) with differentiated NSC-34 cells led to an intensity drop to 43% of the original signal (*Figure 4.6 C*).

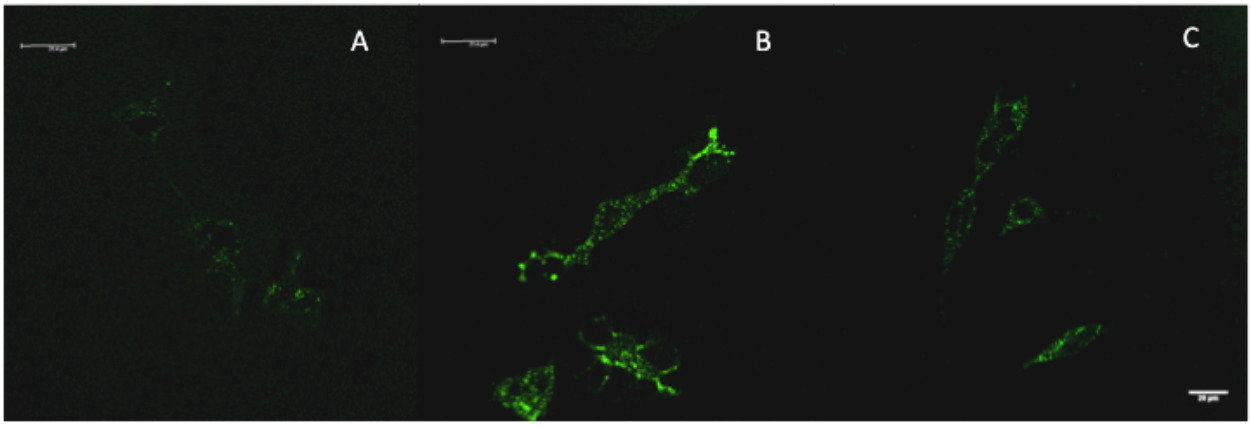

Figure 4.6. Live cell LSCM images of differentiated NSC-34 cells. (A) Cells loaded with **[Gd.L^{7}]** (10 μM, 10 mins), washed with buffer and then incubated with **[Gd.L^{12}]** (10 μM) and AvidinAlexaFluor® 488 conjugate (2.5 μM) for 10 minutes, showing 7% of original intensity; (B) As image (A) but order of addition reversed, giving 88% of original intensity; (C) Simultaneous loading of **[Gd.L^{12}]** (10 μM) and AvidinAlexaFluor® 488 conjugate (2.5 μM) and **[Gd.L^{7}]**, showing 43% of the original intensity.

Surprisingly, these results suggest that **[Gd.L^{7}]** has a comparable affinity, and binds at the same place on the NMDA receptor as **[Gd.L^{12}]**, despite there being no observed increase in $R_{1,\text{cell}}$ during the MR experiments. Without further more detailed studies, the explanation of this behaviour is difficult to rationalise. However, one potential explanation is that upon NMDA receptor-binding, the short spacer limits the flexibility of the Gd(III) chelate, which becomes buried in the receptor-binding cavity and shielded from the bulk solvent. This could inhibit the Gd(III) core from being sufficiently hydrated to allow for fast water exchange, which may limit the expected relaxivity gain upon τ_R modulation.

4.4 Conclusions and Summary

The aim of this chapter was to gain further insight into the origins of the enhancements in $R_{1,cell}$ when **[Gd.L^{2}]**, **[Gd.L^{4}]** and **[Gd.L^{9}]** were incubated with differentiated NSC-34 cells. Due to the inherently low sensitivity and resolution associated with MRI, optical microscopy was employed in order to directly observe whether the complexes were bound to the cell surface NMDA receptor. Two new conjugates, **[Gd.L^{11}]** and **[Gd.L^{12}]**, have been synthesised based on the most promising contrast agents, **[Gd.L^{4}]** and **[Gd.L^{9}]**, but with a *trans*-substituted biotin moiety to allow for complex visualisation by optical microscopy, following addition of an AvidinAlexaFluor® 488 conjugate. The complexes **[Gd.L$^{11\text{-}12}$]** were studied under a variety of experimental conditions using live-cell laser scanning confocal microscopy (LSCM) on differentiated NSC-34 cells expressing functional NMDA receptors.

Simultaneous loading of either **[Gd.L^{11}]** or **[Gd.L^{12}]** and AvidinAlexaFluor® 488 conjugate on differentiated NSC-34 cells gave a 'pit-like' localisation at the cell surface, with no intracellular staining observed. The complex **[Gd.L^{12}]** appeared 38% brighter, indicating this complex possesses a higher affinity than **[Gd.L^{11}]** for the NMDA receptor. The lower $R_{1,cell}$ enhancement for **[Gd.L^{9}]** compared to **[Gd.L^{4}]** must therefore be a result of the increased length between the Gd(III) chelate and the NMDA receptor-binding moiety, leading to a drop in rotational coupling.

The ability of **[Gd.L^{11}]** and **[Gd.L^{12}]** to bind only to cells which express functional NMDA receptors was demonstrated through a repeat of the simultaneous loading experiment with AvidinAlexaFluor® 488 conjugate, on NIH 3T3 mouse skin fibroblast cells, whereby no fluorescence signal was observed. This result is promising, indicating that **[Gd.L^{4}]** and **[Gd.L^{9}]** should only give rise to an enhancement in $R_{1,cell}$ upon binding to cells which possess NMDA receptor density.

It was also demonstrated that **[Gd.L^{11}]** and **[Gd.L^{12}]** are displaced from their binding site after a simulated glutamate burst, suggesting they bind at the NMDA receptor, at the same site as glutamate but with a lower affinity. However, the affinity is sufficient such that **[Gd.L^{11}]** and **[Gd.L^{12}]** were able to displace

glutamate from the binding site, leading to a restoration of the initial signal intensity after 45 minutes.

Finally, several competition experiments showed that the modifications made in the design of **[Gd.L^{12}]** have not perturbed its localisation behaviour away from the parent complex, **[Gd.L^{9}]**. Both complexes were shown to localise in the same place, with a comparable affinity, demonstrating that **[Gd.L^{12}]** acts as a suitable optical imaging derivative of the MR contrast agent, **[Gd.L^{9}]**.

As detailed at the end of *chapter 1*, one of the main goals of this thesis was to design and synthesise a series of NMDA receptor-targeted MRI contrast agents. Of the ten complexes made, three, **[Gd.L^{2}]**, **[Gd.L^{4}]** and **[Gd.L^{9}]**, were able to induce large measureable enhancements in cellular relaxation rates when incubated with a neuronal cell line model. Derivatives of **[Gd.L^{4}]** and **[Gd.L^{9}]** allowed further studies of these complexes using optical microscopy. These complexes, **[Gd.L^{11}]** and **[Gd.L^{12}]**, reside on the cell surface and bind specifically to cells which possess NMDA receptor density. They also bind reversibly at the NMDA receptor after a simulated glutamate burst, and can displace glutamate competitively upon restoration of equilibrium. Taken together, the results gained throughout *chapters 2, 3 and 4* suggest that the gadolinium complexes of ***L^{2}***, ***L^{4}*** and ***L^{9}*** are promising MR contrast agents for reporting or monitoring NMDA receptor density, and possess the ability to report on synaptic glutamate activity.

Chapter 5 follows on from the promising optical microscopy work detailed in this chapter, and focuses on replacing the biotin-avidin conjugate approach with a single compound. A bright Eu(III) complex for NMDA receptor visualisation has been synthesised which incorporates the receptor-binding moiety of **[Gd.L^{9}]**, as this has been shown to be the motif with the highest affinity.

4.5 References

1. P. Marchand, J. Becerril-Ortega, L. Mony, C. Bouteiller, P. Paoletti, O. Nicole, L. Barré, A. Buisson and C. Perrio, *Bioconjugate Chem.*, 2011, **23**, 21-26.
2. M. Dhilly, J. Becerril-Ortega, N. Colloc'h, E. T. MacKenzie, L. Barré, A. Buisson, O. Nicole and C. Perrio, *Chem. Bio. Chem.*, 2013, **14**, 759-769.
3. C. A. Puckett and J. K. Barton, *Biochem.*, 2008, **47**, 11711-11716.
4. C. A. Puckett and J. K. Barton, *J. Am. Chem. Soc.*, 2009, **131**, 8738-8739.
5. F. Kielar, A. Congreve, G.-l. Law, E. J. New, D. Parker, K.-L. Wong, P. Castreno and J. de Mendoza, *Chem. Commun.*, 2008, **0**, 2435-2437.
6. C. P. Montgomery, B. S. Murray, E. J. New, R. Pal and D. Parker, *Acc. Chem. Res.*, 2009, **42**, 925-937.
7. E. J. New, D. Parker and R. D. Peacock, *Dalton Trans.*, 2009, **0**, 672-679.
8. E. J. New, A. Congreve and D. Parker, *Chem. Sci.*, 2010, **1**, 111-118.
9. D. Parker, L. Laurent and C. Montgomery, *Pyridyl-aza(thio)xanthone sensitizer comprising lanthanide (III) ion complexing compounds, their luminescent lanthanide (III) ion complexes and use thereof as fluorescent labels*, IPO WO 2010/084090 A1,2010.
10. S. M. Vibhute, J. Engelmann, T. Verbic, M. E. Maier, N. K. Logothetis and G. Angelovski, *Org. Biomol. Chem.*, 2013, **11**, 1294-1305.
11. A. Mishra, R. Mishra, S. Gottschalk, R. Pal, N. Sim, J. Engelmann, M. Goldberg and D. Parker, *ACS Chem. Neurosci.*, 2013, **5**, 128-137.
12. A. Eisenführ, P. S. Arora, G. Sengle, L. R. Takaoka, J. S. Nowick and M. Famulok, *Bioorg. Med. Chem.*, 2003, **11**, 235-249.
13. M. Botta, *Eur. J. Inorg. Chem.*, 2000, **2000**, 399-407.
14. W. A. Kinney, M. Abou-Gharbia, D. T. Garrison, J. Schmid, D. M. Kowal, D. R. Bramlett, T. L. Miller, R. P. Tasse, M. M. Zaleska and J. A. Moyer, *J. Med. Chem.*, 1998, **41**, 236-246.
15. C. Bonaccorso, N. Micale, R. Ettari, S. Grasso and M. Zappala, *Curr. Med. Chem.*, 2011, **18**, 5483-5506.

CHAPTER FIVE

A Bright Europium Complex for NMDA Receptor Visualisation

5. A Bright Europium Complex for NMDA Receptor Visualisation

5.1 Introduction

The previous chapter discussed the synthesis and direct visualisation of two NMDA receptor-targeted optical imaging probes, which were able to mimic the behaviour and elucidate the mechanism of the $R_{1,cell}$ enhancements observed with the most promising MRI contrast agents. The complexes **[Gd.L$^{11\text{-}12}$]** are structurally related to the parent complexes, **[Gd.L^{4}]** and **[Gd.L^{9}]**, with a *trans*-substituted biotin moiety, which allowed complex visualisation on differentiated NSC-34 cells upon addition of the fluorescent conjugate, AvidinAlexaFluor® 488. Although this approach worked well and allowed deduction of complex localisation, reversibility and cellular specificity of binding, it was desirable to devise a single component optical imaging probe.

The potential limitations of appending a fluorescent motif to a complex were briefly discussed in *chapter 4*. Instead, a new approach was investigated whereby conjugation of the most potent NMDA receptor-binding moiety to a hydrophilic Eu(III) complex would generate a single component NMDA receptor-targeted optical imaging probe. Not only could this be useful for NMDA receptor visualisation, but also it could be highly advantageous in numerous biological assays, through replacement of standard radiolabelled ligands.

5.1.1 A Brief Introduction to Lanthanide Photochemistry

Luminescence from the lanthanide series involves *f-f* transitions and so, with the exception of lanthanum and lutetium which do not possess any unpaired electrons, all lanthanide(III) ions are luminescent. However, *f-f* transitions are very weak as they are formally Laporte forbidden. This cannot be overcome through ligand field interactions because of the high degree of shielding of the *f*-orbitals by the filled 5p and 5s/6s sub-shells. Despite this, a major advantage of the contracted nature of the *f*-orbitals is that the excited state lifetime is

prolonged (ms in the case of Eu(III)), allowing time-gated studies which can distinguish lanthanide emission from the short-lived background biological fluorescence. This is highly advantageous in the design of an optical probe for NMDA receptor visualisation. Unfortunately, the forbidden *f-f* transitions give rise to low molar extinction coefficients for Ln(III) ions, leading to inefficient population of the lanthanide excited states following irradiation. In order to circumvent this, sensitised emission (also known as the antenna effect) can be employed, which utilises a proximal sensitiser group to absorb light efficiently and then transfer the energy to the lanthanide excited state.[1] Initially, the sensitiser absorbs a photon and is excited to a vibrationally excited state. Non-radiative decay quickly relaxes this to the lowest lying excited state, S_1. The sensitiser then undergoes intersystem crossing to the longer-lived triplet excited state, T_1, which can transfer energy to one of the excited states of the Ln(III) ion. Non-radiative decay brings this to the lowest emissive manifold of the Ln(III) excited state, before emission of photons occurs via transitions to the ^7F ground state (*Figure 5*).[2, 3]

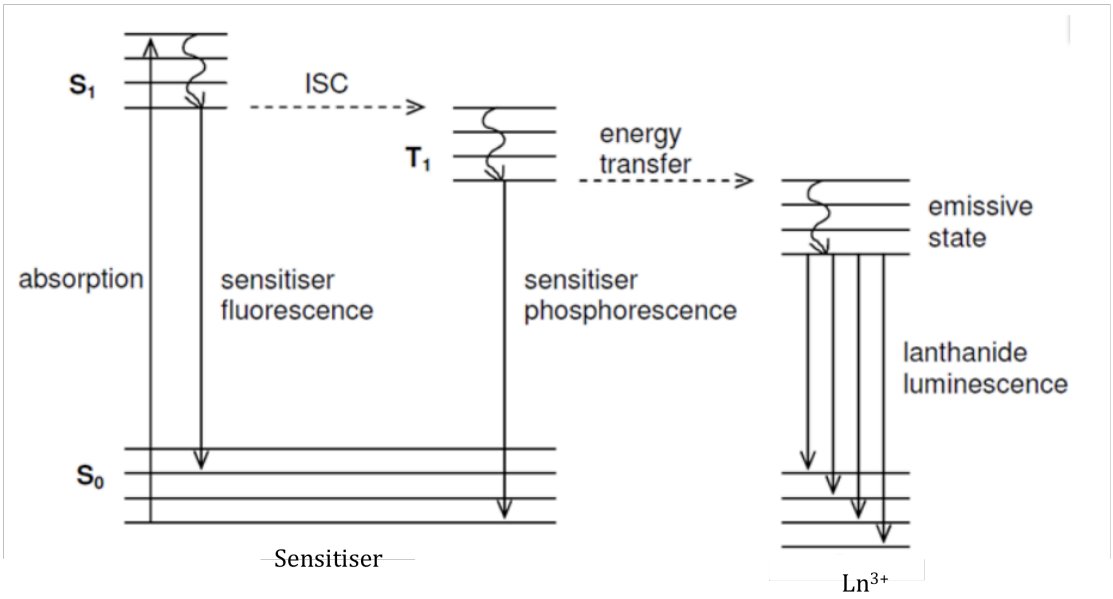

Figure 5. A simplified Jablonski diagram demonstrating sensitised Ln(III) emission.

The Eu(III) ion is one of the most studied of the lanthanide series with respect to luminescence. It possesses a ^7F ground state, which is split into seven manifolds. The non-degenerate electronically excited state, $^5D_0$, resides at approximately

17,200 cm^{-1} and radiative decay from $^5D_0 \rightarrow {}^7F_n$ (n = 0-4) results in emission spectra with several transitions, denoted by their ΔJ value (*Figure 5.1*).[4] Generally, the contracted nature of the *f*-orbitals means that the emission spectra of Eu(III) complexes are sharp and relativley independent of coordination environment. However, fine-structure can be observed within some emission bands and is known to be dependent on local symmetry and the nature of the coordinating group to the Eu(III) centre.

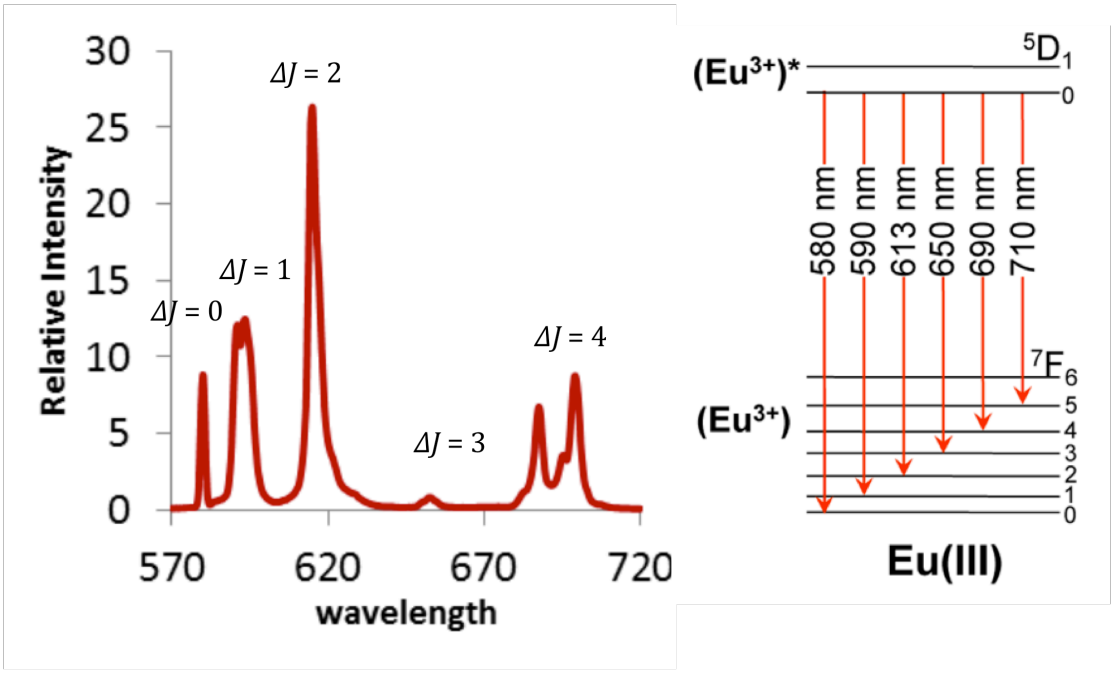

Figure 5.1. Typical emission spectrum and partial energy level diagram for Eu(III).[3]

5.1.2 Design of a NMDA Receptor-Targeted Eu(III) Complex

Recently, the Durham group has designed a series of Eu(III) complexes to act as alternative organelle stains for cellular imaging.[5, 6] These C_3-symmetrical Eu(III) complexes were all based on the 9-*N*-3-tris-arylalkynylpyridyl ligand, with conjugation of a targeting vector to the periphery of one of the chromophore arms allowing selective localisation of the complexes to specific sub-cellular compartments. These complexes exhibited large molar extinction coefficients (55-60,000 M^{-1} cm^{-1} at 330-350 nm) and quantum yields in the region of 20-38% in H_2O. Drawing inspiration from this, the NMDA receptor-targeted complex, **[Eu.L^{13}]**, was designed (*Scheme 5*).

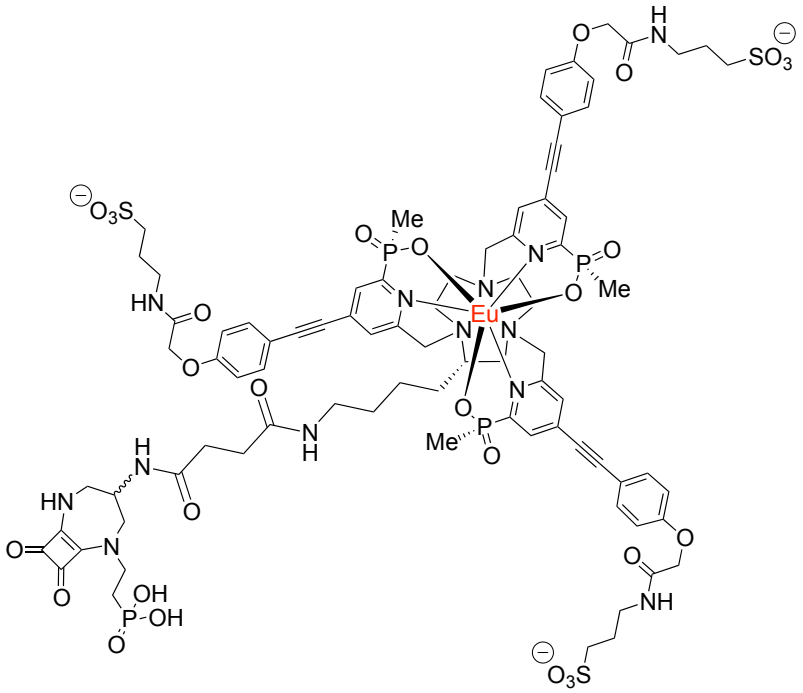

Scheme 5. Structure of **[Eu.L^{13}]**.

The complex **[Eu.L^{13}]** has several features. First, the Eu(III) ion is encapsulated by the conformationally rigid 9-*N*-3 macrocycle. The stability of the complex towards metal ion dissociation is further enhanced through coordination of three negatively charged pyridyl phosphonate groups, which interact strongly with the trivalent europium cation. This gives the europium centre a coordination number of nine, which inhibits the coordination of any water molecules and increases the efficiency of sensitised emission. The three electron-rich arylalkynylpyridyl chromophores each have a triplet energy in the region of 21,300 cm^{-1}, which is sufficiently high to allow population of the Eu(III) excited state and minimise back energy transfer, resulting in a very bright complex.[7] The presence of the sulfonate groups at the periphery of each chromophore enhances water solubility and should reduce the potential for non-specific binding to endogenous proteins. Finally, the NMDA receptor-binding moiety was conjugated to the Eu(III) complex using a similar linker to that used for the successful MRI contrast agent, **[Gd.L^{9}]**.

5.2 Synthetic Details

5.2.1 Macrocycle Synthesis

The synthesis of the macrocycle[8, 9] started from the commercially available hydrochloride salt of (2*S*)-lysine ethyl ester (*Scheme 5.1*). The ethyl ester was reacted with neat ethylenediamine at 120 °C for three hours. After this time, purification by vacuum distillation afforded the amide, ***77***, as a yellow oil in a good yield. The degree of racemisation during this step has previously been analysed using ^{1}H NMR spectroscopy.[10] Addition of the chiral solvating agent, R-*O*-acetyl mandelic acid (1.2 equivalents), to a sample of the amide, ***77***, in $CDCl_3$ showed the presence of only one amide NH resonance around 8.52 ppm (*Figure 5.2*). This was consistent with the presence of only one enantiomer. Racemisation would have led to the formation of two diasteroisomeric salts in which the amide NH protons are (up to) 0.25 ppm non-equivalent.[10]

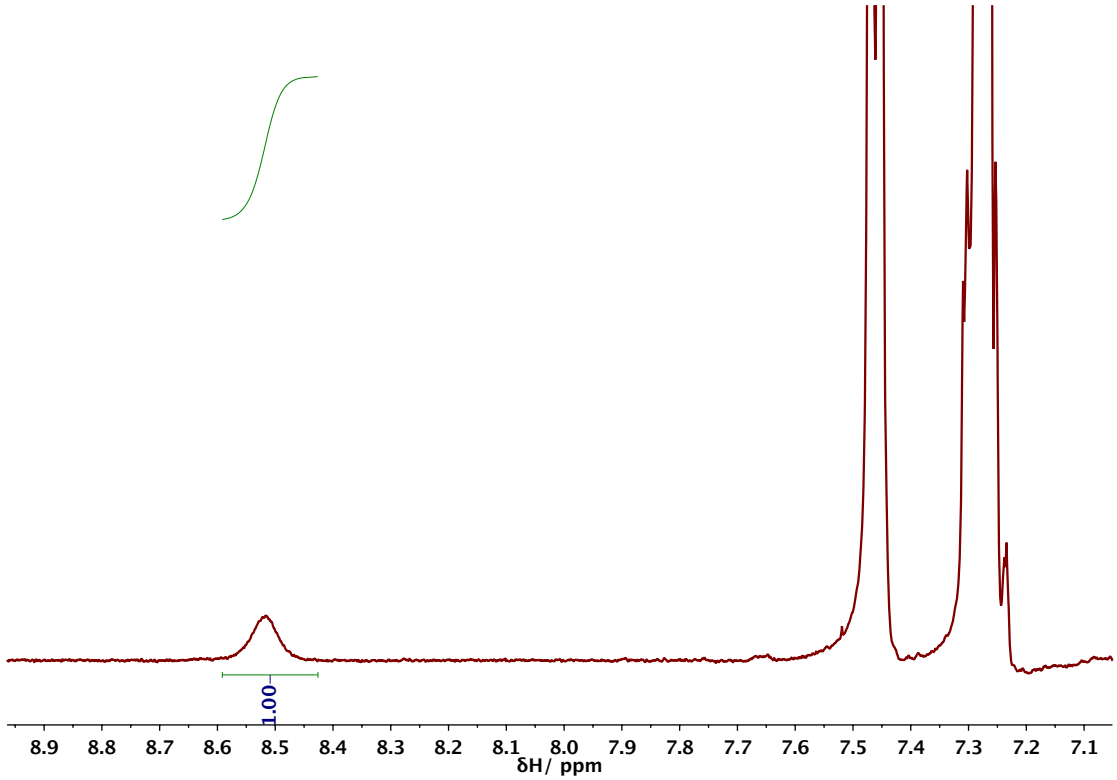

Figure 5.2. Partial ^{1}H NMR spectrum of ***77*** in the presence of R-*O*-mandelic acid, showing the presence of only one amide resonance.

Reduction of the amide, ***77***, was achieved by stirring at 70 °C with BH_3-THF for 24 hours. Completion of the reaction was verified using IR spectroscopy, with no carbonyl stretch observed between 1700-1900 cm^{-1}. After stirring the amino-borane complex in refluxing HCl overnight, compound ***78*** was isolated as the tetrahydrochloride salt. The next step involved selective protection of the distal amine. This was undertaken through reaction of the diethylenetriamine unit of ***78*** with basic copper carbonate at 50 °C. The intense blue solution confirmed the presence of a copper(II) complex. The solution was cooled to 0 °C and treated with benzoyl chloride, maintaining the pH between 8 and 9 by the addition of KOH. This procedure permitted selective acylation of the remote amino group. Treatment of the copper complex with H_2S allowed isolation of the benzamide, ***79***, after exhaustive extraction. Tosylation of the primary and secondary amines using a slight excess of 4-toluenesulfonyl chloride in anhydrous DCM, under basic conditions, afforded the tritosylamide, ***80***, after purification by column chromatography.

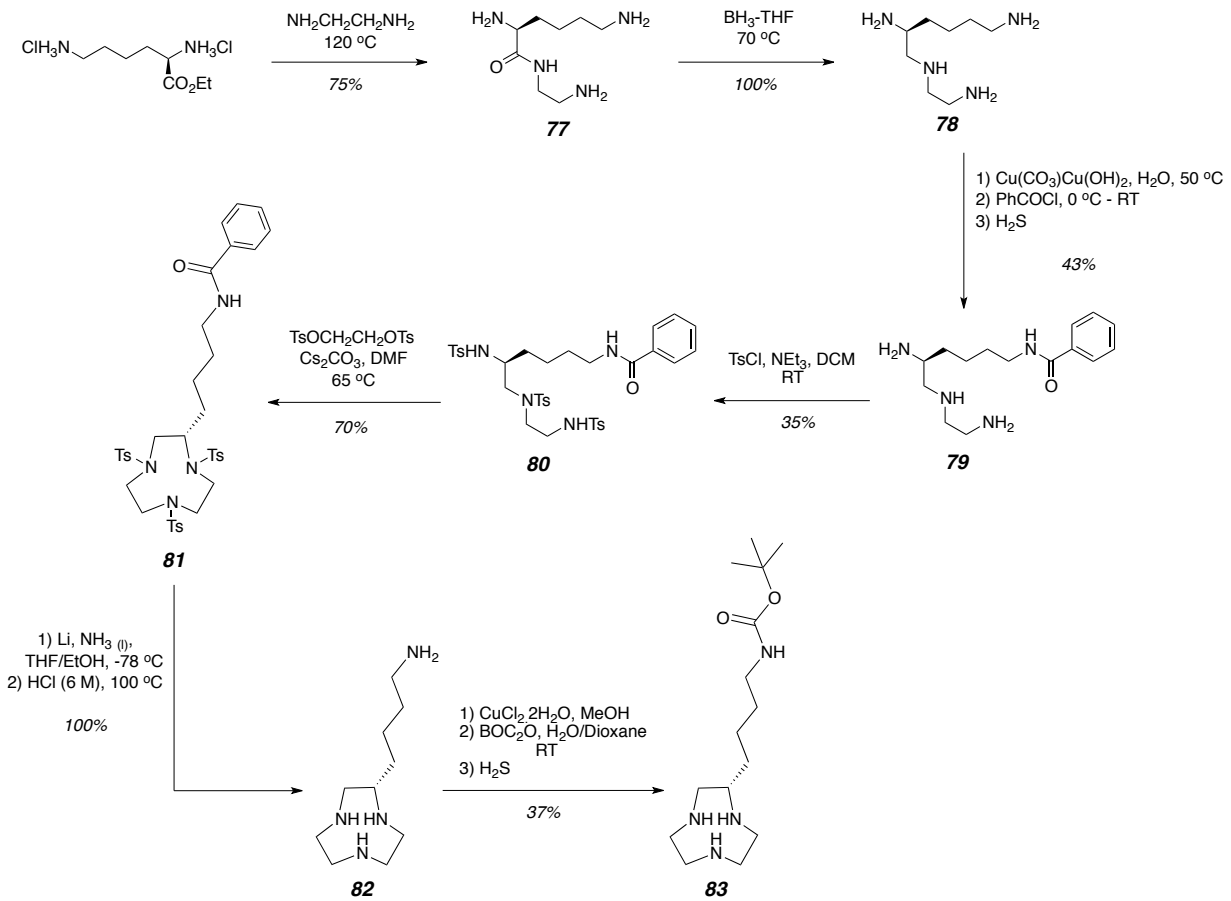

Scheme 5.1

Cyclisation to the 9-membered macrocycle was achieved through condensation of ***80*** with ethylene glycol distosylate in the presence of Cs_2CO_3 in anhydrous DMF at 65 °C. Purification of the crude product by column chromatography afforded ***81***, which was subject to global deprotection. Dissolving metal reduction conditions, which generate solvated electrons through the reaction of lithium in liquid ammonia, led to efficient detosylation. However, this was also accompanied by partial reduction of the aromatic ring in the benzoyl group, as observed by ESI-MS and ^{1}H NMR spectroscopy, and so the crude triamine was stirred in refluxing HCl to complete hydrolysis and furnish ***82*** as the tetrahydrochloride salt. Finally, differentiation of the macrocyclic triamine was achieved by selective protection of the remote amino group. Again, copper was employed to complex the triazacyclononane core, allowing Boc-protection of the free amine to be carried out using an excess of di-*tert*-butyl-dicarbonate in a water-dioxane mix. Decomplexation of the copper using H_2S, followed by adjustment of the pH and exhaustive extraction into DCM and chloroform afforded the free triamine, ***83***, in a 37% yield.

5.2.2 Chromophore Synthesis

A simple retrosynthetic analysis shows that the extended chromophore can be synthesised from a Sonogashira cross coupling between the *para*-bromopyridine platform and the *para*-substituted alkyne (*Scheme 5.2*).

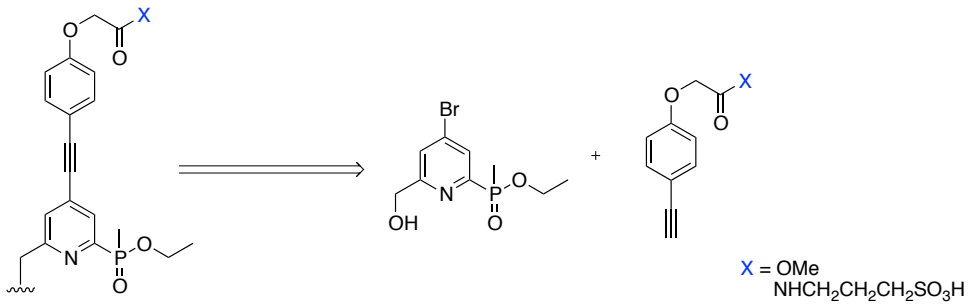

Scheme 5.2

Synthesis of the alkyne moiety resulted from deprotection of the trimethylsilane-protected alkyne[i] using a slight excess of triethylammonium dihydrofluoride in anhydrous THF at 35 °C (*Scheme 5.3*).[6] After purification by column chromatography, the alkyne, ***84***, was isolated as a colourless oil in a 72% yield. A palladium-catalysed Sonogashira cross-coupling reaction[6] with the *para*-bromo pyridine was undertaken next.[ii] A solution of the pyridine in anhydrous THF was degassed using a freeze-pump-thaw cycle, before the addition of ***84***, $Pd(dppf)Cl_2$ and NEt_3. The solution was further degassed, CuI added and the resultant mixture heated to 65 °C under argon for 18 hours. After subsequent work-up and purification by column chromatography, the extended chromophore, ***85***, was isolated in 55% yield. Finally, the hydroxyl group was activated towards nucleophilic substitution, through generation of the mesylate, ***86***, by reaction with methanesulfonyl chloride under basic conditions in anhydrous THF.[6]

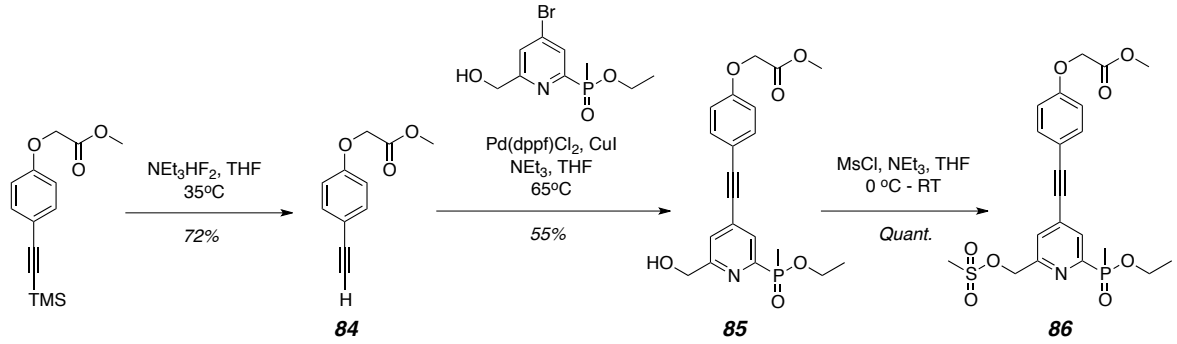

Scheme 5.3

5.2.3 Ligand and Complex Synthesis

Alkylation of ***83***, with 2.9 equivalents of the mesylate, ***86***, was followed by basic hydrolysis of the methyl and phosphinate ethyl esters before complexation with $Eu(OAc)_3$ (*Scheme 5.4*).[11] The alkylation step was conducted in anhydrous acetonitrile at 60 °C under an inert atmosphere of argon, with the reaction progress monitored by ESI-MS. Although the major product was the desired tri-

[i] *The TMS-protected alkyne was provided by Martina Delbianco.*

[ii] *The para-bromo pyridine was provided by Dr. Brian McMahon.*

substituted compound, ***87***, some mono- and di-substituted products were observed in the crude mass spectrum, and account for the moderate (30%) yield of ***87*** after column chromatography. The hydrolysis of the methyl and phosphinate ethyl esters was carried out using KOH in a mixture of MeOD and D_2O, which allowed the reaction to be monitored by ^{1}H and ^{31}P NMR spectroscopy. Complete hydrolysis of the phosphinate ethyl esters was confirmed by a characteristic shift in the ^{31}P NMR spectrum from 39.2 to 26.4 ppm. Once hydrolysis was complete, the pD of the solution was adjusted to 7 and $Eu(OAc)_3.H_2O$ was added. The reaction mixture was heated to 60 °C overnight, at which point the solvent was removed and the crude product purified by RP-HPLC (mobile phase comprising $MeOH/H_2O$ + 0.1% formic acid), to give the Eu(III) complex, ***88***, as a white solid.

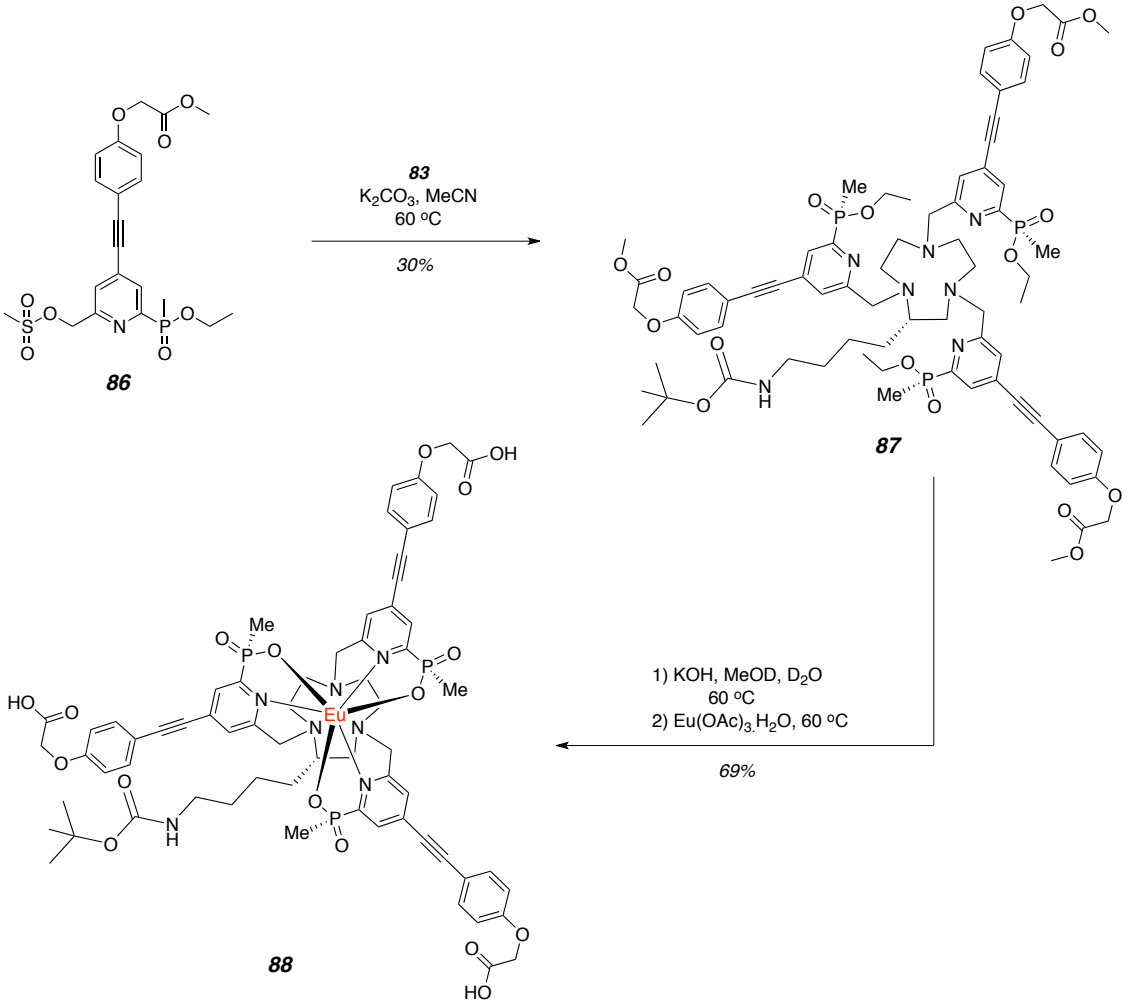

Scheme 5.4.

The sulfonate groups were introduced around the periphery of the complex via amide bond formation between the three carboxylates of ***88*** and 3-amino-1-propanesulfonic acid.[11] Rapid tris-sulfonation was achieved using approximately two equivalents of amine per carboxyate, in the presence of HATU in DMSO. The crude reaction mixture was purified by RP-HPLC (mobile phase comprising 25 mM triethylammonium acetate buffer and acetonitrile), to give the mono-Boc triethylammonium salt of the tris-sulfonate Eu(III)-complex, ***89***, as a white solid (*Scheme 5.5*).

Concurrent synthesis of the NMDA receptor-binding moiety was undertaken by reaction of ***36*** with succinic anhydride, in the presence of diisopropylethylamine in anhydrous DMF (*Scheme 5.5*). Complete conversion was observed by analysis of the crude mass spectrum after one hour, at which point an excess of bromotrimethylsilane was added. The reaction was heated to 60 °C and the hydrolysis monitored by ESI-MS. After three hours, complete hydrolysis was achieved and the crude product purified by preparative RP-HPLC, to give the free phosphonic acid, ***90***.

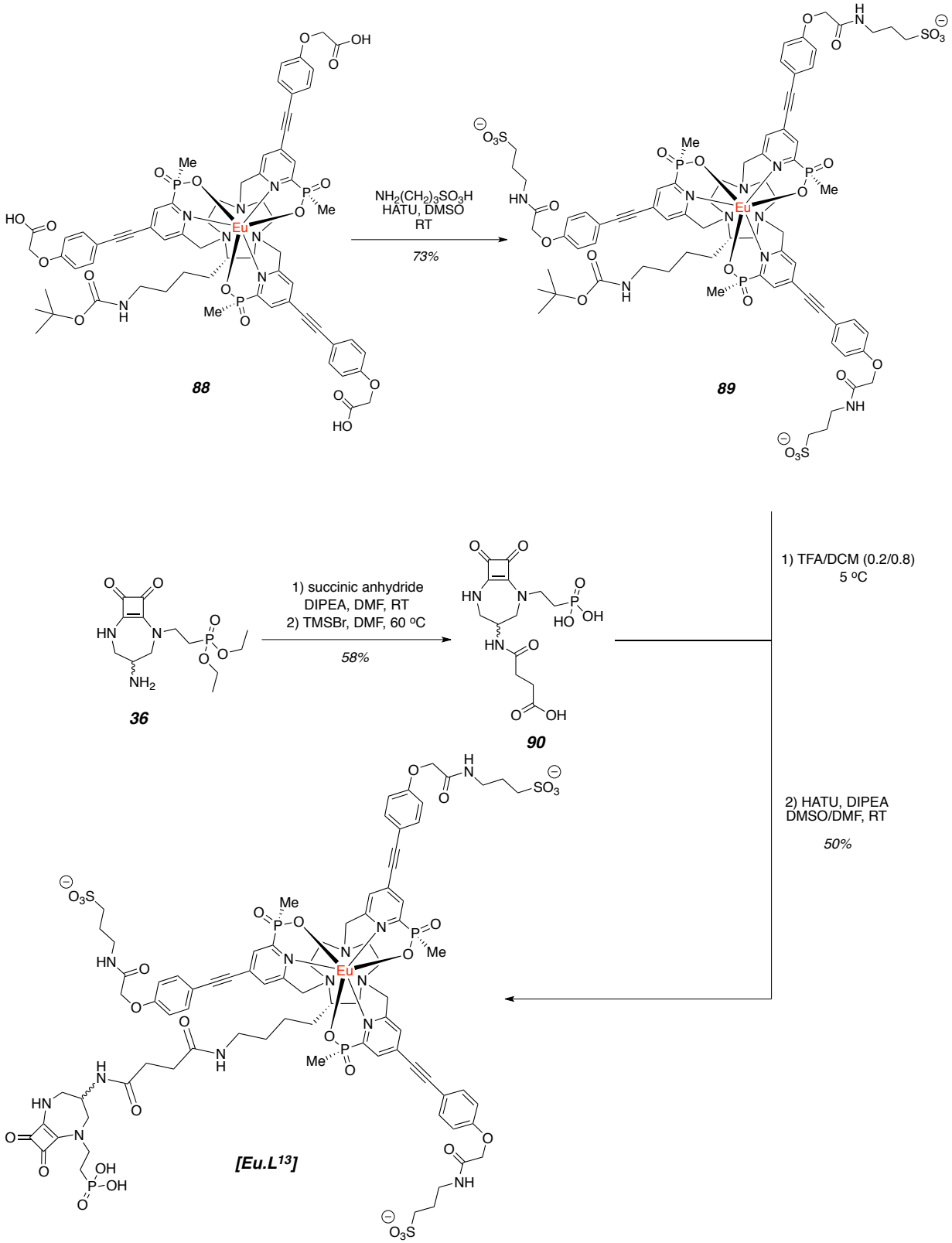
NH2(CH2)3SO3H
HATU, DMSO
RT
73%
88
89
1) succinic anhydride
DIPEA, DMF, RT
2) TMSBr, DMF, 60 ºC
58%
36
90
1) TFA/DCM (0.2/0.8)
5 ºC
2) HATU, DIPEA
DMSO/DMF, RT
50%
[Eu.L13]

Scheme 5.5.

Finally, the complex, **[Eu.L^{13}]**, was synthesised by conjugation of ***90*** to the Eu(III) complex, ***89***. Initially, the Boc-protecting group of the remote amine moiety on ***89*** was hydrolysed using dilute TFA in anhydrous DCM at 5 °C. The solution was stirred for twenty minutes at this temperature before the solvents were removed under reduced pressure on a high vacuum line. Excess TFA was removed by repeated addition and removal of DCM. This yielded the TFA salt of the Eu(III) amino complex, which was taken up into DMSO and added to a solution of ***90***, HATU and diisopropylethylamine in anhydrous DMF. The solution was stirred at room temperature overnight and then diluted with H_2O. The crude product was subject to purification by preparative RP-HPLC (mobile phase comprising 25 mM triethylammonium acetate buffer and acetonitrile), to give **[Eu.L^{13}]** as a white solid. Confirmation of the presence of **[Eu.L^{13}]** was demonstrated by comparison of the theoretical and experimental high-resolution mass distributions (*Figure 5.3*).

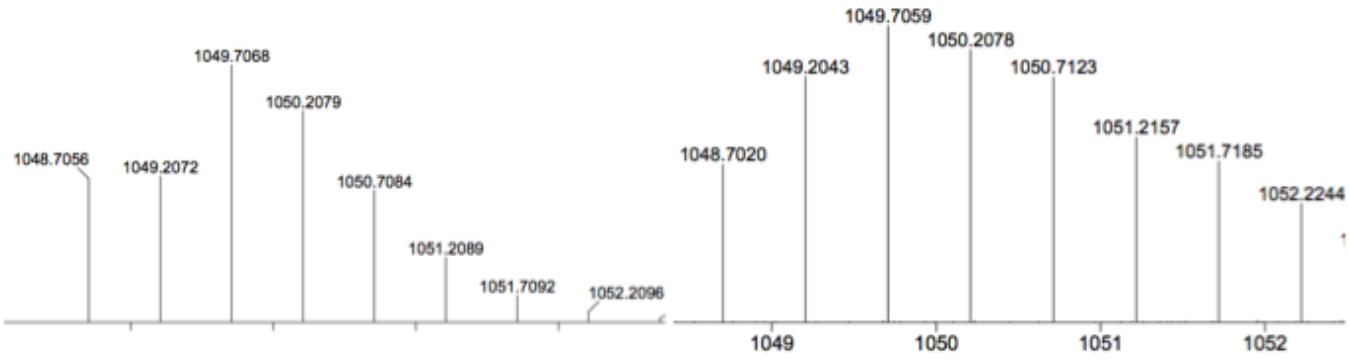

Figure 5.3. Observed (*left*) and calculated (*right*) high-resolution mass spectra of **[Eu.L^{13}]**; TOF negative.

5.3 Photophysical Characterisation

The photophysical characterisation of **[Eu.L^{13}]** was carried out in water. The absorption spectrum of **[Eu.L^{13}]** shows a broad absorption band centred at 328 nm, with a slight shoulder at 338 nm (*Figure 5.4*). This is characteristic of an ICT transition, with electrons flowing from the aryl oxygen to the pyridyl nitrogen. The extinction coefficient of **[Eu.L^{13}]** at 328 nm was estimated to be 58,000 M^{-1}

cm^{-1}, which is similar to reported systems that lack the receptor-binding moiety.[11]

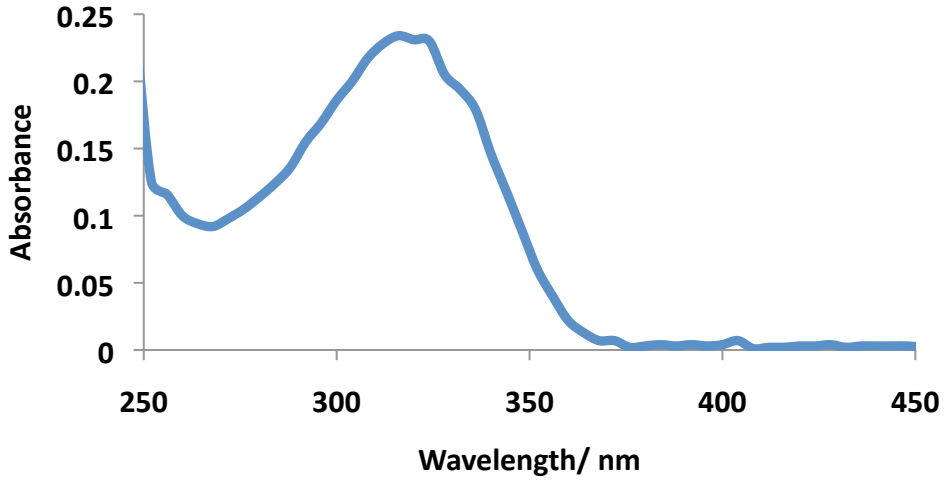

Figure 5.4. Absorption spectrum of **[Eu.L13]** (H_2O, λ_{ex} = 328 nm, 295 K).

The emission spectrum of **[Eu.L13]** was measured following excitation at 328 nm (*Figure 5.5*). No fluorescence was observed below 500 nm, indicating that the chromophore effectively populated the Eu(III) excited state. The form of the emission spectrum is relatively simple, and is again comparable to similar structures[11] demonstrating that the presence of the NMDA receptor-binding moiety does not impact on the spectral form. The lifetime of the europium emission in water was calculated to be 1.08 (±0.05) ms, reflecting the intense emission observed upon irradiation and is consistent with effective shielding of the europium ion excited state from vibrational deactivation by solvent.

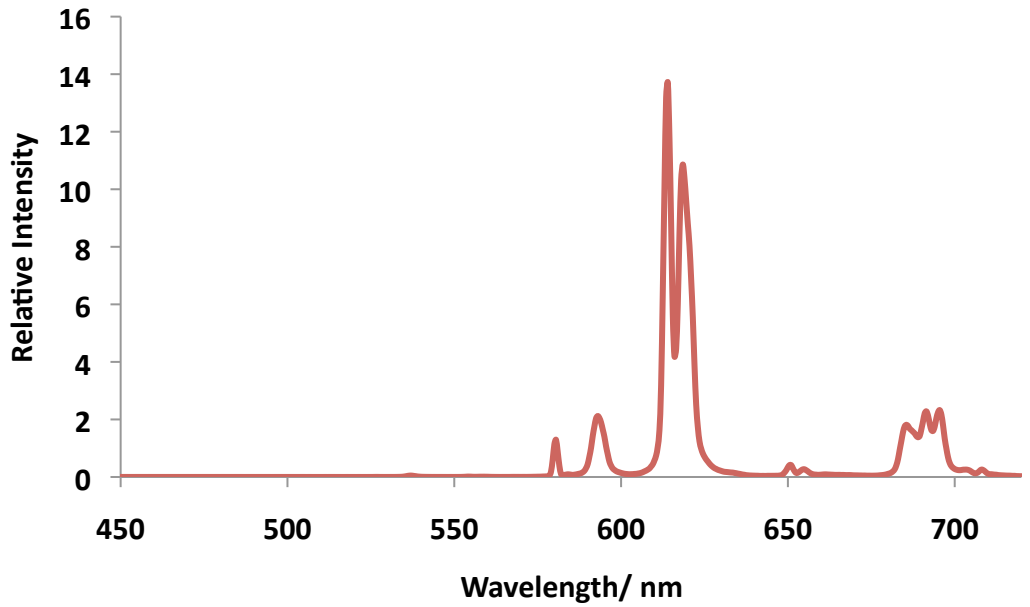

Figure 5.5. Emission Spectrum of **[Eu.L^{13}]** (H_2O, λ_{ex} = 328 nm, 295 K).

5.4 Cellular Localisation Studies

In order to study the localisation profile of **[Eu.L^{13}]**, live-cell laser scanning confocal microscopy imaging studies were carried out on a Leica SP5 II microscope by Dr Robert Pal, Durham University. In the same manner as described in *chapter 4*, differentiated NSC-34 cells expressing NMDA receptors were grown on specially designed microscope slides, comprising a 100 μL flow-through channel.

Initially, differentiated NSC-34 cells were incubated with a 10 μM solution of **[Eu.L^{13}]** for 10 minutes at 37 °C. After this time, the cells were washed three times with fresh buffer to remove any unbound complex and imaged. No cell surface localisation was observed for **[Eu.L^{13}]** after this time period, with a very small amount of complex internalisation observed. In an attempt to try and increase cell-surface localisation, the above experiment was repeated with a longer incubation time (45 minutes), but this proved ineffective with only complex internalisation being observed (*Figure 5.6*).

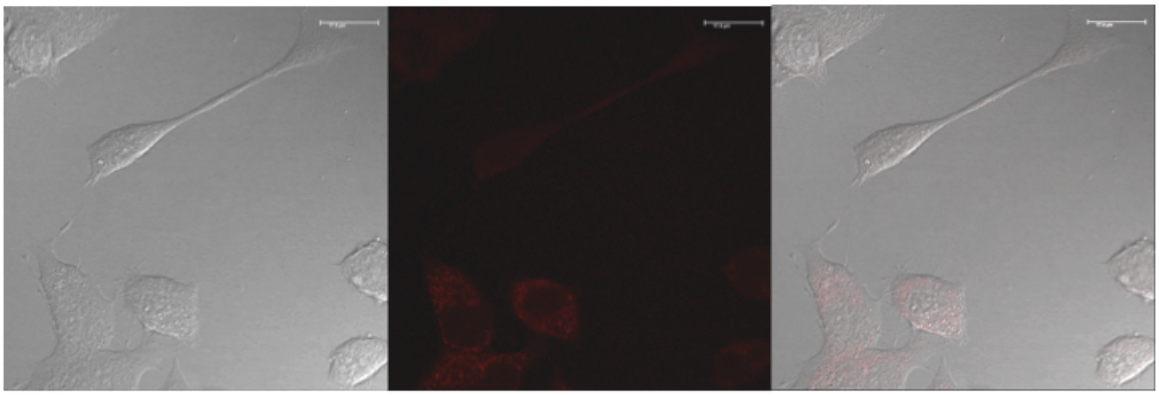

Figure 5.6. LSCM images of differentiated NSC-34 cells upon incubation of **[Eu.L^{13}]** (10 μM, 45 mins), showing a small amount of intracellular localisation. (Left to right) Transmission image, visualisation of europium emission and merge image ($\lambda_{ex}/\lambda_{em}$ = 355 nm/ 605-720 nm).

In order to gain insight into whether the small amount of internalisation of **[Eu.L^{13}]** in differentiated NSC-34 cells was NMDA receptor-mediated, three control experiments were undertaken. Firstly, a competition experiment was designed using Kinney's NMDA receptor antagonist, ***76***. It was envisaged that if receptor-mediated uptake was the primary internalisation mechanism, then blocking the NMDA receptor with compound ***76*** before incubation of **[Eu.L^{13}]** would lead to a decrease in signal intensity from within the cells. Therefore, differentiated NSC-34 cells were treated with a solution of compound ***76*** (10 μM, 10 mins), washed three times, and then incubated with a solution of **[Eu.L^{13}]** (10 μM, 45 mins). After washing, the cells were imaged but there appeared to be no change in signal intensity from within the cells (*Figure 5.7*), as compared to the original cell staining experiment, suggesting that any cell uptake is not receptor-mediated.

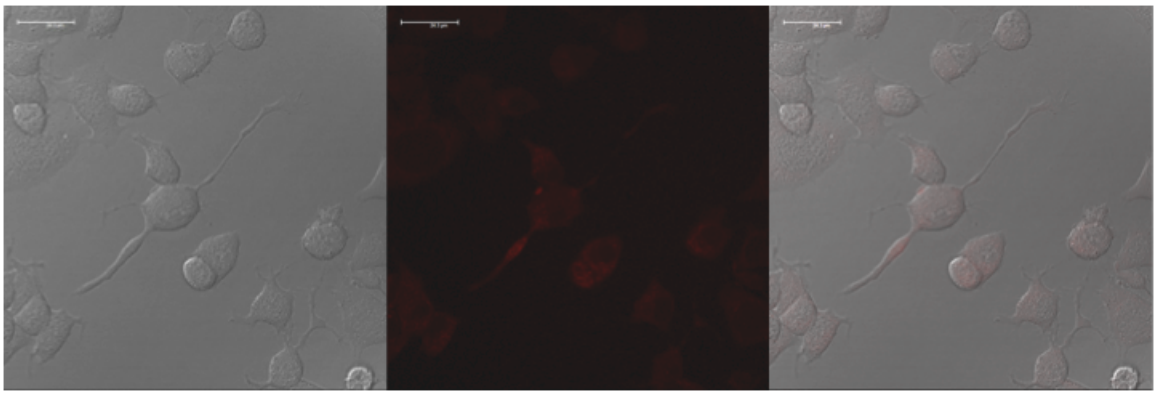

Figure 5.7. LSCM images of differentiated NSC-34 cells upon incubation of Kinney's antagonist, ***76*** (10 μM, 10 mins), followed by washing the cells and then incubating **[Eu.L^{13}]** (10 μM, 45 mins). There is no change in intracellular signal intensity as compared to *figure 5.6*. (Left to right) Transmission image, visualisation of europium emission and merge image ($\lambda_{ex}/\lambda_{em}$ = 355 nm/ 605-720 nm).

Secondly, NIH-3T3 skin fibroblast cells, which do not express any NMDA receptors, were incubated with a 10 μM solution of **[Eu.L^{13}]** for 45 minutes. As expected, no cell surface localisation was observed, but there was a discernible intracellular distribution of **[Eu.L^{13}]**, further strengthening the argument of a competitive non-receptor-mediated uptake mechanism (*Figure 5.8*).

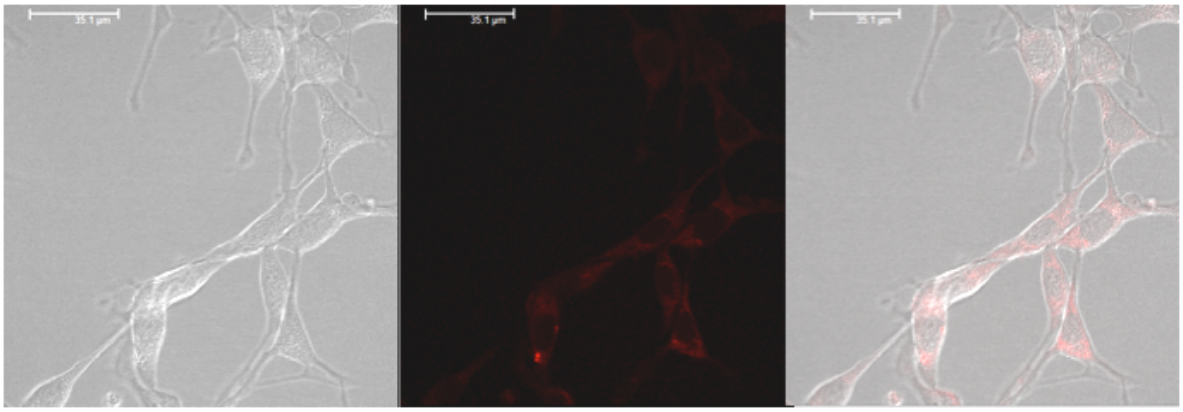

Figure 5.8. LSCM images of NIH-3T3 cells upon incubation of **[Eu.L^{13}]** (10 μM, 45 mins). (Left to right) Transmission image, visualisation of europium emission and merge image ($\lambda_{ex}/\lambda_{em}$ = 355 nm/ 605-720 nm).

Finally, a structurally related europium complex lacking the NMDA receptor-binding moiety was synthesised (*Scheme 5.6*) and incubated with differentiated NSC-34 cells. Incubation of **[Eu.L^{14}]** (10 μM, 45 mins) with differentiated NSC-34 cells again showed no cell surface localisation, as expected. However, there was

an increased intracellular localisation of this complex as compared to **[Eu.L^{13}]**, with 68% more signal observed from within the cells (*Figure 5.9*). Taken together, these results suggest that the overall structure of the Eu(III) complex, and not the relatively small NMDA receptor binding moiety, is dictating the localisation profile of **[Eu.L^{13}]**.

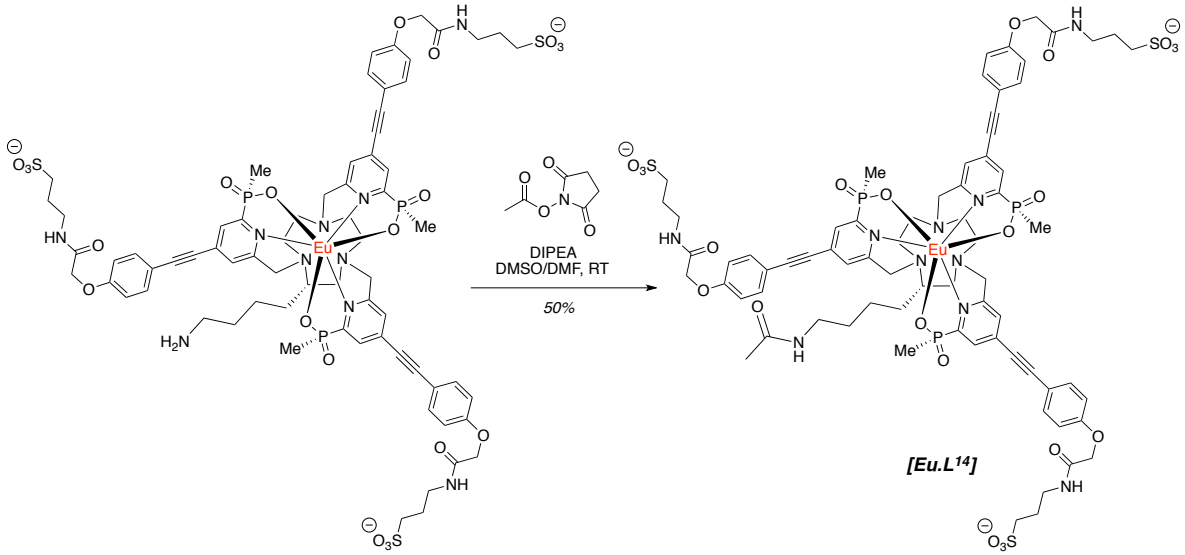

Scheme 5.6.

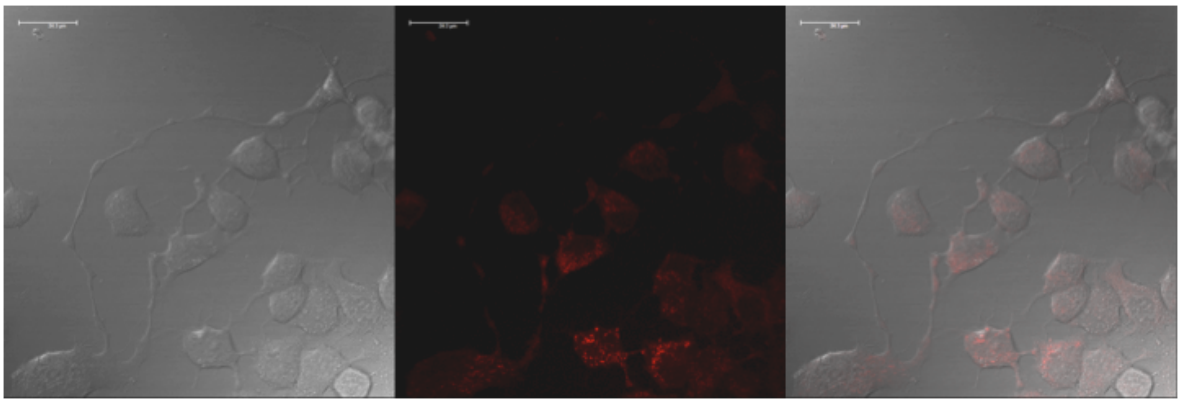

Figure 5.9. LSCM images of differentiated NSC-34 cells upon incubation of **[Eu.L^{14}]** (10 μM, 45 mins), showing an intracellular localisation with 68% more signal than what was observed for **[Eu.L^{13}]**. (Left to right) Transmission image, visualisation of europium emission and merge image ($\lambda_{ex}/\lambda_{em}$ = 355 nm/ 605-720 nm).

Notwithstanding the fact that **[Eu.L^{13}]** exhibited a distinct intracellular distribution, the observed signal was relatively weak for a Eu(III) complex of this type.[6, 11, 12] Such behaviour may either be due to complex emission being

quenched, or can be ascribed to poor complex accumulation. To investigate whether the europium emission was being quenched, the emission spectrum of **[Eu.L^{13}]** was measured in cell culture media and in an aqueous solution of HSA, and compared to that measured in water (*Figure 5.10*).

The **[Eu.L^{13}]** emission spectra were measured using a modified Zeiss Axiovert 200M inverted microscope.[13] Using the same concentrations of **[Eu.L^{13}]**, it is apparent that the relative intensity of the europium emission is quenched in cell culture media to approximately 30% of the intensity when measured in water. Human serum albumin is a major constituent of the cell culture media and it was thought that non-specific binding of **[Eu.L^{13}]** to HSA could be the reason for the quenched emission of the complex in the cell culture media. However, the relative intensity of **[Eu.L^{13}]** in an aqueous HSA solution remained at approximately 90%, suggesting a different component of the cell culture medium is responsible for quenching the europium emission.

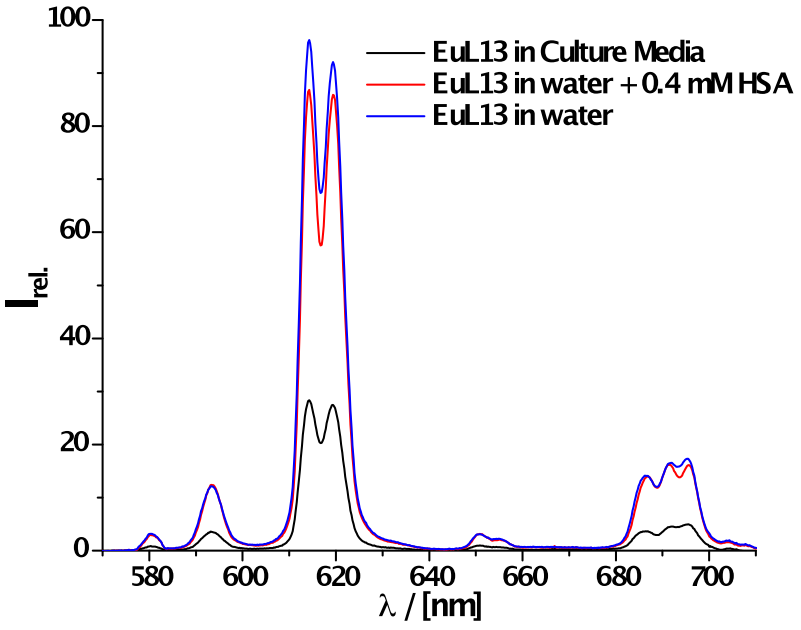

Figure 5.10. Emission spectra of **[Eu.L^{13}]** (10 μM) in water, in the presence of 0.4 mM HSA and in cell culture media, showing a significant drop in emission intensity in the cell culture medium.

In order to confirm that the NMDA receptor-binding moiety of **[Eu.L^{13}]** was not influencing the emission properties, the complex, **[Eu.L^{14}]**, was subject to the same comparative analysis. Again, the emission intensity dropped significantly in

cell culture media, as compared to in water, with HSA binding again not being the reason for the decreased emission (*Figure 5.11*).

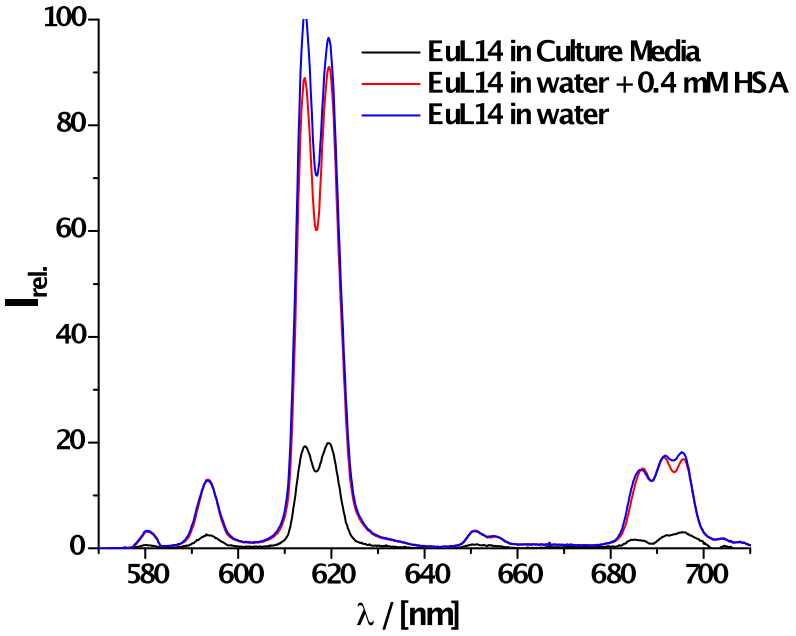

Figure 5.11. Emission spectra of **[Eu.L^{14}]** (10 μM) in water, in the presence of 0.4 mM HSA and in cell culture media, showing a significant drop in emission intensity the in cell culture medium.

5.5 Conclusions

The aim of this chapter was to build on the work discussed in *chapter 4*, and develop a single component probe for NMDA receptor visualisation. Luminescent lanthanide complexes offer a superior alternative to standard organic fluorophores and so the main goal was to develop an NMDA receptor-targeted Eu(III) complex.

The new complex, **[Eu.L^{13}]**, is derived from a series of previously studied Eu(III) complexes with three arylalkynylpyridyl chromophores. These complexes are inherently bright and have been shown to be useful as alternative organelle stains, or to detect ligand binding using time-resolved FRET.[6, 11] The Eu(III) complex was conjugated to the most potent NMDA receptor-binding moiety via a similar spacer unit to that used in the design of **[Gd.L^{12}]**, which was considered to sufficiently space the receptor-binding motif from the large complex core. The

presence of the NMDA receptor-binding moiety did not perturb the photophysical properties of the complex, with **[Eu.L^{13}]** showing similar absorption and emission profiles as the parent compounds.

The localisation profile of **[Eu.L^{13}]** was studied by live-cell laser scanning confocal microscopy on differentiated NSC-34 cells expressing NMDA receptors. Disappointingly, incubation of **[Eu.L^{13}]** on differentiated NSC-34 cells for up to 45 minutes led to no cell-surface localisation. Instead a small degree of complex internalisation was observed. The mechanism of cellular uptake was partially investigated through a series of control experiments, and found not to be receptor-mediated.

Following the observation of some weak intracellular fluorescence, the emission properties of **[Eu.L^{13}]** were recorded in the cell culture medium and compared to those recorded in water. It was found that the emission of **[Eu.L^{13}]** is significantly quenched in the cell culture medium to approximately 30% of the observed signal intensity in water. It was initially thought that if HSA were able to bind to the rod-like arms of the chromophore, this would be the most likely quencher of excited state emission. However, the emission intensity and spectral form of **[Eu.L^{13}]** did not change upon the addition of a large excess of HSA to an aqueous solution of the complex. This suggested that a different constituent of the cell culture medium, led to quenching of the europium emission. Without a full investigation into the effect of each component of the medium on the photophysical properties, it is difficult to decipher what is causing this effect.

Nevertheless, it is reasonable to hypothesise that the localisation profile of **[Eu.L^{13}]** is dominated by the large nature of the parent Eu(III) complex and not by the small NMDA receptor-binding moiety. It is likely that the complex binds non-specifically to a protein in the cell culture medium, via the rod-like chromophore units, and is then trafficked into the cell through some endocytocic mechanism, leading to the observed intracellular localisation.

In *Chapter 6* an emerging imaging technique is described and work is detailed towards an NMDA receptor-targeted NIR probe for optoacoustic imaging. Two new optoacoustic imaging contrast agents have been designed and synthesised and their potential to bind and image NMDA receptors is evaluated *in vitro* and *in vivo*.

5.6 References

1. J.-C. G. Bunzli and C. Piguet, *Chem. Soc. Rev.*, 2005, **34**, 1048-1077.
2. C. M. G. dos Santos, A. J. Harte, S. J. Quinn and T. Gunnlaugsson, *Coord. Chem. Rev.*, 2008, **252**, 2512-2527.
3. M. C. Heffern, L. M. Matosziuk and T. J. Meade, *Chem. Rev.*, 2013.
4. D. Parker, *Coord. Chem. Rev.*, 2000, **205**, 109-130.
5. J. W. Walton, A. Bourdolle, S. J. Butler, M. Soulie, M. Delbianco, B. K. McMahon, R. Pal, H. Puschmann, J. M. Zwier, L. Lamarque, O. Maury, C. Andraud and D. Parker, *Chem. Commun.*, 2013, **49**, 1600-1602.
6. S. J. Butler, L. Lamarque, R. Pal and D. Parker, *Chem. Sci.*, 2014, **5**, 1750-1756.
7. M. Soulié, F. Latzko, E. Bourrier, V. Placide, S. J. Butler, R. Pal, J. W. Walton, P. L. Baldeck , B. Le Guennic, C. Andraud, J. M. Zwier, L. Lamarque, D. Parker and O. Maury, *Chem. Eur. J.*, 2014, **20**, 8636-8646.
8. A. S. Craig, I. M. Helps, K. J. Jankowski, D. Parker, N. R. A. Beeley, B. A. Boyce, M. A. W. Eaton, A. T. Millican, K. Millar, A. Phipps, S. K. Rhind, A. Harrison and C. Walker, *J. Chem. Soc. Chem. Commun.*, 1989, 794-796.
9. J. P. L. Cox, A. S. Craig, I. M. Helps, K. J. Jankowski, D. Parker, M. A. W. Eaton, A. T. Millican, K. Millar, N. R. A. Beeley and B. A. Boyce, *J. Chem. Soc. Perkin Trans. 1*, 1990, 2567-2576.
10. D. Parker and R. J. Taylor, *Tetrahedron*, 1987, **43**, 5451-5456.
11. M. Delbianco, V. Sadovnikova, E. Bourrier, G. Mathis, L. Lamarque, J. M. Zwier and D. Parker, *Angew. Chem.*, 2014, Accepted.
12. S. J. Butler, M. Delbianco, L. Lamarque, B. K. McMahon, E. R. Neil, R. Pal, D. Parker, J. W. Walton and J. M. Zwier, *Dalton Trans.*, 2014.
13. R. Pal and A. Beeby, *Methods and Applications in Fluorescence*, 2014, Accepted.

CHAPTER SIX

NMDA Receptor-Targeted Photoacoustic Contrast Agents

6. NMDA Receptor-Targeted Photoacoustic Contrast Agents

6.1 Introduction

The two previous chapters have described the development of optical imaging probes for visualisation of NMDA receptors. Although the antagonist approach for NMDA receptor visualisation was demonstrated using the biotin-avidin conjugates, **[Gd.L$^{11\text{-}12}$]**, the localisation profile of the bright europium complex, **[Eu.L^{13}]**, appeared to be dictated by the overall complex structure and not directed by the NMDA receptor-binding moiety. Nevertheless, the exceptional sensitivity and resolution associated with optical imaging has provided a complementary technique, giving information on the reversibility and specificity of binding of the NMDA receptor-targeted MRI contrast agents. However, the major drawback associated with optical imaging, which limits its *in vivo* use, is its lack of deep tissue penetration.

One emerging imaging modality with the potential to limit the problems associated with the issue of depth penetration, is photoacoustic (also known as optoacoustic) imaging. Photoacoustic imaging is claimed to have a penetration depth of up to 5 cm,[1] which is far superior to most optical techniques. Furthermore, it possesses good spatial and temporal resolution by encoding optical contrast information onto acoustic waves.[1] Photoacoustic imaging offers another complementary imaging modality to MRI, for imaging and studying NMDA receptors *in vivo*.

6.1.1 Principles of Photoacoustic Imaging

The basic principles of photoacoustic imaging are shown below (*Figure 6*). First, a pulsed laser light, lasting several nanoseconds, is directed at a point of interest. Providing that the light is absorbed quickly at the region of interest by a photoabsorber, there is an increase in local pressure and temperature. This thermoelastic expansion releases energy in the form of acoustic waves, which then propagate back to the detector due to the elastic nature of tissue. The

acoustic waves are detected in close proximity to the illuminated tissue and can be mathematically decoded and reconstructed to form images.[2]

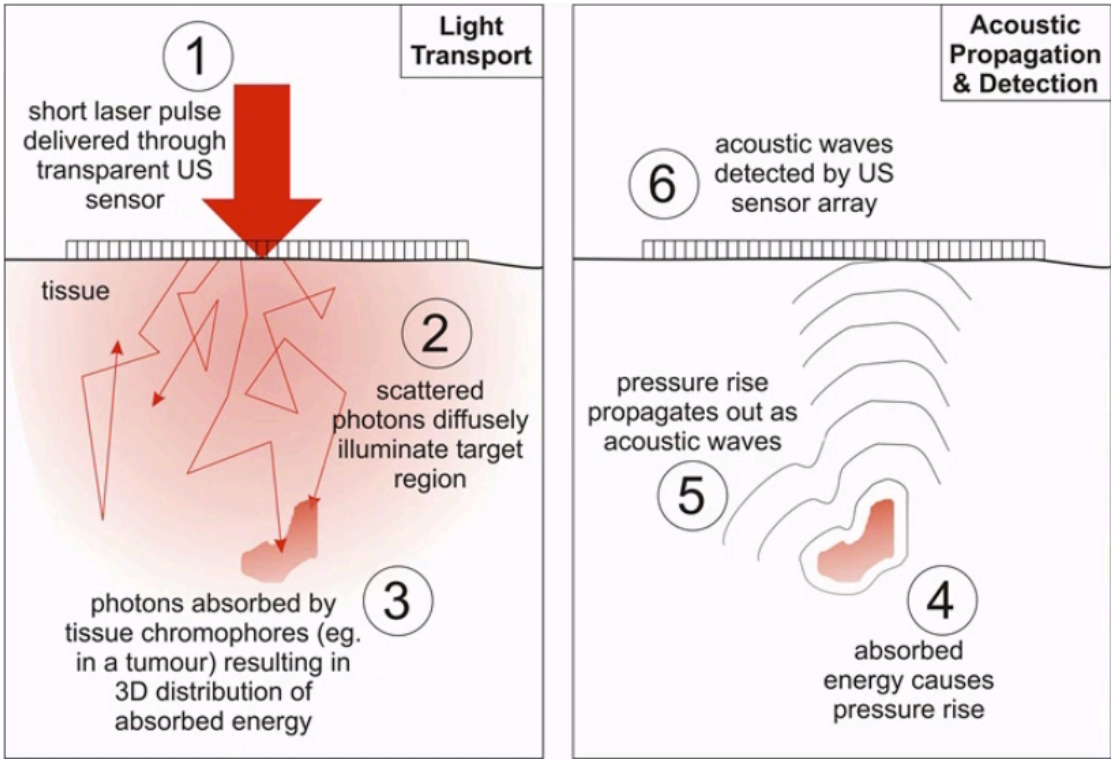

Figure 6. Basic principle of photoacoustic imaging.[3]

Although the photoacoustic phenomenon was first discovered by Alexander Graham Bell in 1880,[4] its utilisation in biomedical spectrometry and imaging has only been considered over the past few decades.[5] Photoacoustic imaging relies on efficient photoabsorbing agents, such as oxygenated and deoxygenated haemoglobin, and the majority of the literature to date utilises these endogenous photoabsorbers for visualising and imaging blood vessels with high resolution.[2] In addition to haemoglobin, a variety of other intrinsic tissue photoabsorbers exist, such as melanin, lipids and water, which each generate their own photoacoustic signal.

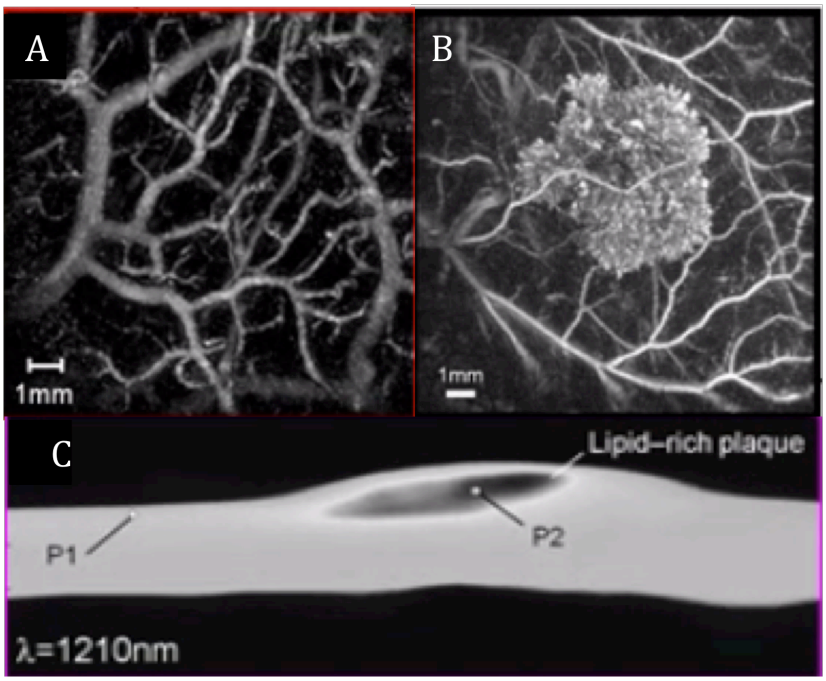

Figure 6.1. Images of (A) arteries, (B) a melanoma and (C) a lipid plaque from within a mouse, generated by photoacoustic imaging of oxygenated haemoglobin (blood), melanin and lipid, respectively.[3]

Although the presence of endogenous photoabsorbers can be used to generate high-quality images (*Figure 6.1*), they can also give rise to a large amount of background noise. However, this can be overcome by using multispectral optoacoustic tomography (MSOT). Employing a synthetic photoabsorbing agent and using light pulses of different wavelengths, allows the photoacoustic signals of the endogenous and synthetic photoabsorbers to be differentiated, giving rise to an increased sensitivity. Furthermore, by conjugating a targeting vector onto the photoabsorber, image specificity can be enhanced.

6.1.2 Design of an NMDA Receptor-Targeted Photoacoustic Contrast Agent

In order to provide sufficient contrast, a synthetic photoabsorbing agent must possess different absorption properties to the endogenous photoabsorbers.

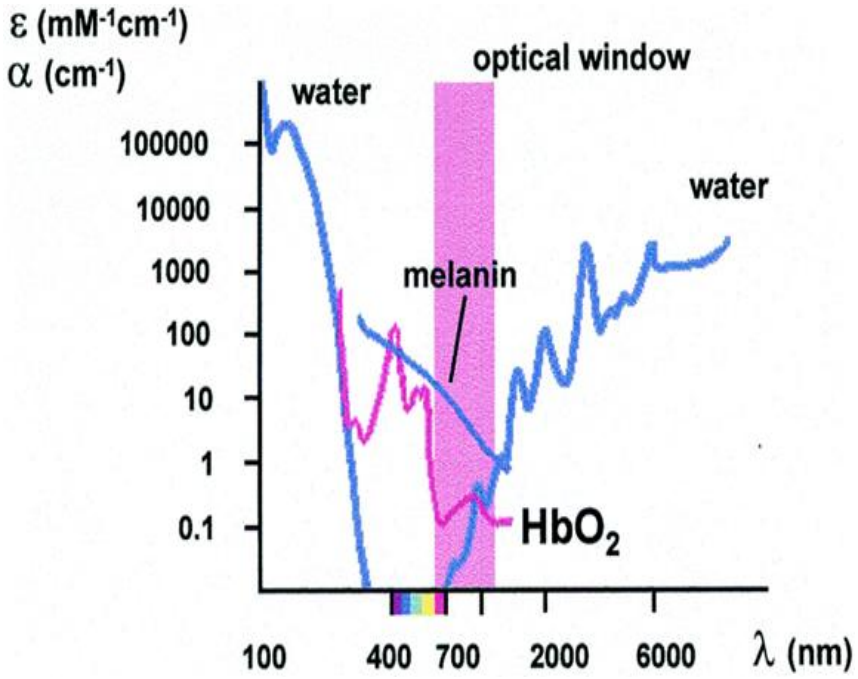

Figure 6.2. Absorption spectra of the major endogenous photoabsorbers.

The absorption spectrum of each of the major endogenous photoabsorbers (*figure 6.2*) demonstrates that between 600 and 900 nm, the majority of the endogenous photoabsorbers do not absorb light very well, providing an optical window in which to image. Also in this region, light scattering is relatively low, resulting in greater light penetration allowing images to be obtained from deeper within the body. Therefore, the major requirements for synthetic photoabsorbers for photoacoustic imaging are that they absorb light within the optical window, with a high molar absorption coefficient allowing detection above the intrinsic photoacoustic tissue signal.[6]

Recently, various gold nanostructures[7, 8] and single-walled carbon nanotubes[9], have been conjugated to specific antibodies and directing vectors and have been employed as photoacoustic contrast agents. Their selection was made because they possess exceptionally high molar absorption coefficients. However, they are relatively large and the concentration-normalised absorptivity (representing the optical absorption coefficient using a concentration of 1 mg/mL) of these structures is actually quite low.[2] In comparison, although organic dyes tend to have lower molar absorption coefficients, they possess a greater concentration-

normalised absorptivity and can out-perform the nanostructures as photoacoustic contrast agents.[2]

With this background in mind, we have set out to synthesise and evaluate two NMDA receptor-targeted photoacoustic contrast agents, **[NIR-1]** and **[NIR-2]**. Their structures are shown below (*Scheme 6*).

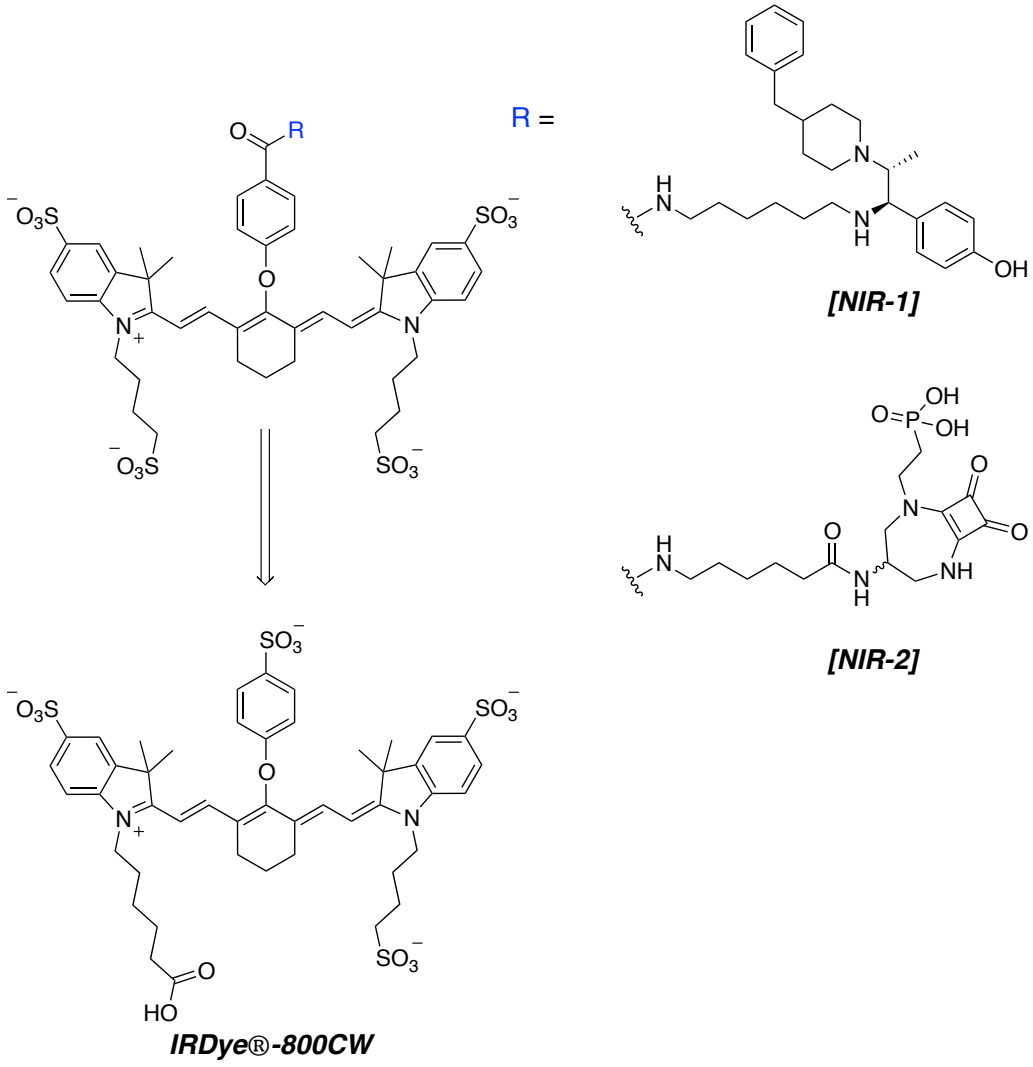

Scheme 6.

The two compounds, **[NIR-1]** and **[NIR-2]**, are based on a heptamethine cyanine dye conjugated to either the negative allosteric modulator, ifenprodil[10] or the NMDA receptor-binding moiety of **[Gd.L^{12}]**. Ifenprodil was chosen as it has recently been shown that this compound can be conjugated to a pentamethine cyanine dye and retain functionality at the NMDA receptor.[11] The IC_{50} values of the two NMDA receptor-binding moieties of **[NIR-1]** and **[NIR-2]** towards the

NMDA receptor are 150[12] and 19 nM[13], respectively. However, these values are not directly comparable due to the different methods used in their determination (the IC_{50} for ifenprodil was determined by voltage clamp recordings, whereas the IC_{50} of the alcohol derivative of the NMDA receptor-binding moiety of **[NIR-2]** was determined using a radiolabel displacement assay).[12, 13]

The heptamethine cyanine dye is derived from the commercially available dye, IRDye®-800CW (*Scheme 6*). This dye is well suited to act as a synthetic photoacoustic absorber. It possesses an extremely large molar absorption coefficient of approximately 240,000 M^{-1} cm^{-1}, with an absorption maximum centred around 790 nm, which is located well within the optical window.[14] Furthermore, the quantum yield of IRDye®-800CW is approximately 5-10%, meaning that the energy build up from the absorption of the pulsed light has a greater probability of leading to thermal elastic expansion and releasing acoustic waves, rather than being dissipated as fluorescence. Finally, the presence of the sulfonate groups around the periphery of the dye enhances the water solubility and should reduce the potential to bind non-specifically to endogenous proteins.[15]

6.2. Synthetic Details

6.2.1 Synthesis of the Heptamethine Cyanine Dye

The synthesis of the heptamethine cyanine dye began with construction of the hetrocyclic indole ring, using standard Fischer indole synthesis conditions (*Scheme 6.1*).[16] Hydrazinobenzene sulfonic acid and 3-methyl-2-butanone were stirred in acetic acid at 120 °C for three hours, at which point the solvent was removed to give the crude indole. Purification by precipitation of the potassium salt gave ***91*** in a 75% yield. This was then subject to an *N*-alkylation through reaction with 1,4-butanesultone in anhydrous toluene at 100 °C for twelve hours.[17] Upon completion of the reaction, as confirmed by ESI-MS, the solvent was decanted from the purple precipitate. Trituration with cold propan-2-ol yielded the quaternary ammonium salt, ***92***, as a free flowing pink powder.

Classical syntheses of heptamethine cyanine dyes involve condensation of the 2-methyl substituted quaternary indole with a bis-aldehyde, and this strategy was employed here. The bis-aldehyde was synthesised according to a literature procedure.[18] Initially, anhydrous DMF and $POCl_3$ were stirred as a solution in anhydrous DCM at 0 °C to allow for *in-situ* formation of the Vilsmeier-Haak reagent. To this solution was added cyclohexanone and the resulting mixture was heated to 80 °C and reaction progress monitored by TLC. Complete conversion was achieved after 3 hours, at which point the reaction was cooled to room temperature and poured onto ice and left overnight.

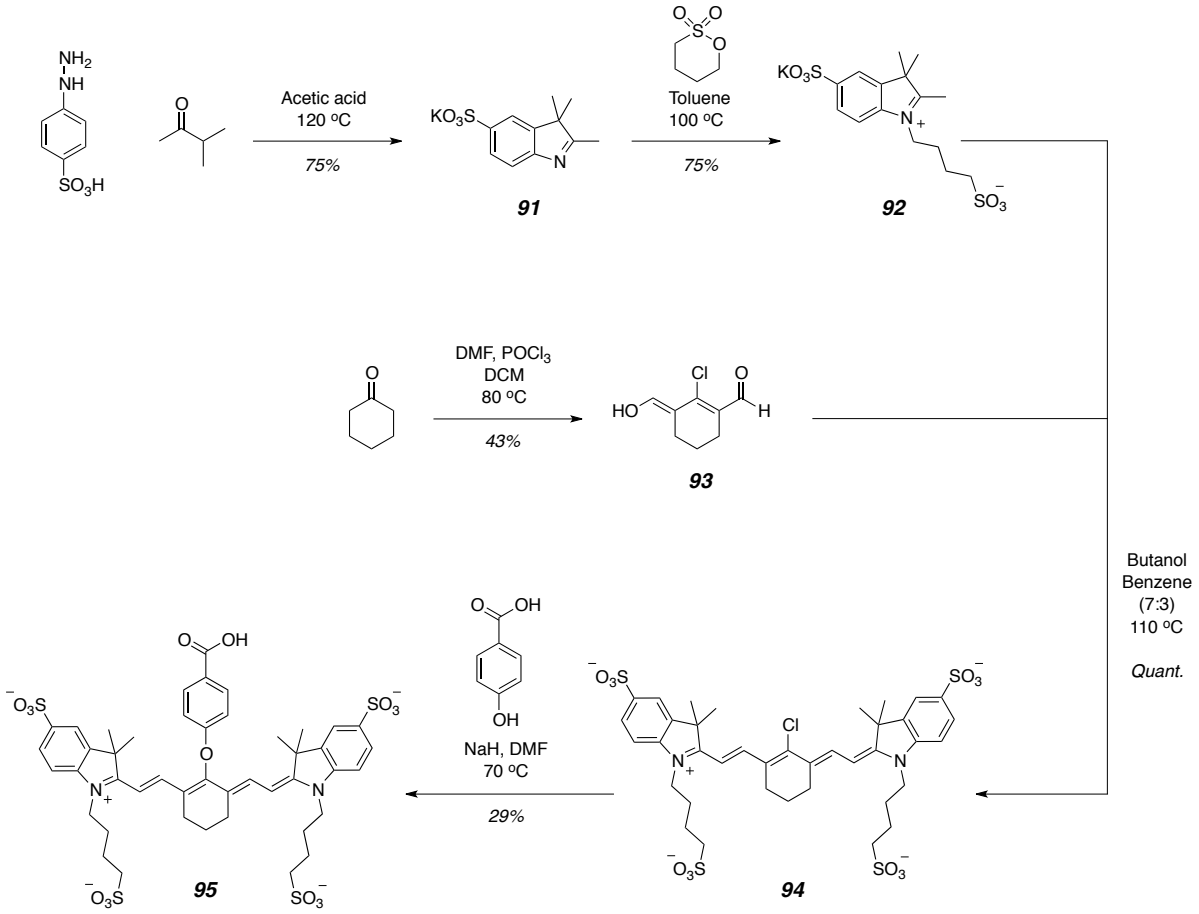

Scheme 6.1.

Complete hydrolysis of the iminium ion intermediate gave the bis-aldehyde, ***93***, as bright yellow crystals. Next, condensation of ***93*** with 2.2 equivalents of ***92*** gave the conjugated heptamethine cyanine dye. This reaction was undertaken by stirring the two compounds in a mixture of anhydrous butan-1-ol and anhydrous benzene at 110 °C, overnight. After this time, a green solution and a green

precipitate formed. The presence of the desired compound was confirmed through observation of an absorption band centred around 784 nm, which is consistent with heptamethine cyanine dyes of this nature. Removal of the solvent and washing with diethyl ether gave the chloro-substituted heptamethine cyanine dye, ***94***, as a green powder.[19]

Due to the electron-deficient nature of the π-system, the chlorine group at the meso-position of the cyclohexyl ring in heptamethine dyes is known to be susceptible to nucleophillic substitution. Compound ***94*** was subject to nucleophillic displacement by reaction with 4-hydroxy benzoic acid in the presence of an excess of NaH in anhydrous DMF at 70 °C [note: may take several additions of reagents]. The likely mechanism of this reaction involves an $S_{NR}1$ pathway, initiated by a single electron transfer from the nucleophile to the cationic π-system.[20] The progress of the reaction was monitored by analytical RP-HPLC and upon completion of the reaction, the solvent was removed and the crude residue purified by preparative RP-HPLC (mobile phase comprising 25 mM triethylammonium acetate buffer and acetonitrile), to give the heptamethine cyanine dye, ***95***, as a green powder. Confirmation of the substitution of the chlorine atom was achieved by comparison of the maximum absorption wavelength of ***95*** and ***94***. A hypsochromic shift of 12 nm was observed for ***95***, consistent with substitution by an electron rich ether group.[21]

6.2.2 Synthesis of the NMDA Receptor-Binding Moieties

The synthesis of the NMDA receptor-binding moiety of **[NIR-1]** followed the reported literature method (*Scheme 6.2*).[22] Initially, the benzyl-protected 4-hydroxypropiophenone underwent α-bromination, via reaction with molecular bromine in anhydrous diethyl ether. After stirring at room temperature for 30 minutes, a colour change was observed and the reaction was quenched by the addition of water. After work-up and subsequent purification by column chromatography, compound ***96*** was isolated in an 82% yield. Reaction of ***96*** with 4-benzylpiperidine was carried out in refluxing ethanol overnight.[23] The progress of the reaction was monitored by TLC and upon completion, the solvent was removed to give the crude product. Purification by column chromatography

afforded ***97*** as a yellow oil, which was then reduced to the corresponding alcohol, ***98***. Ketone reduction was carried out using two equivalents of $LiAlH_4$ in anhydrous THF at 0 °C. These conditions had previously been reported to give only the *threo*-diastereoisomer of ifenprodil, whereas $NaBH_4$ reduction often led to diastereoisomeric mixtures.[23] Upon completion of the reaction, as verified by ESI-MS, the reaction was quenched and the lithium salts removed. Compound ***98*** was isolated as a white solid in a 76% yield. Confirmation of the presence of only the *threo*-diastereoisomer was based on ^1H NMR analysis, by comparison to the reported literature data (*Figure 6.3*).[23] The proton next to the hydroxyl group resonated at 4.28 ppm, and split into a doublet through coupling to the adjacent proton, with a coupling constant of 10 Hz. If the *erythro* diastereoisomer had been present, the doublet would have been shifted to higher frequency by approximately 0.90 ppm, with a much smaller coupling constant due to the relative position of the nearest proton.[23]

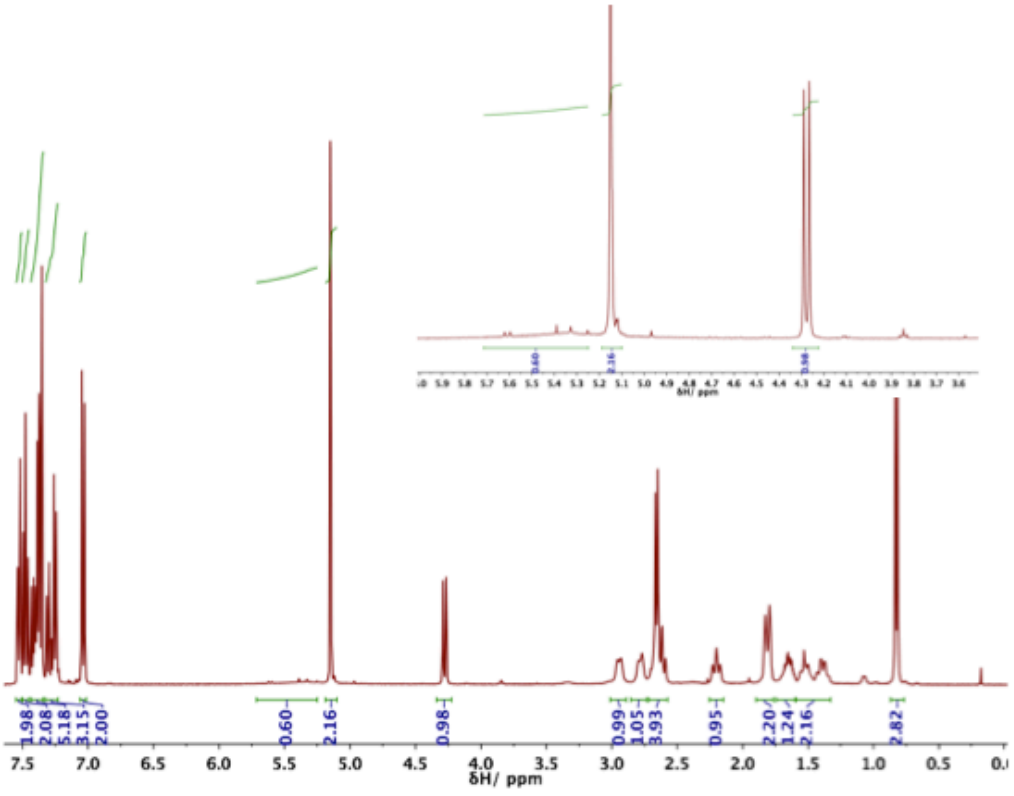

Figure 6.3. ^1H NMR spectrum of compound ***98*** showing the presence of only one diastereoisomer. (*Inset*) Expanded region between 3.50-6.00 ppm showing the presence of the doublet at 4.28 ppm (J = 10 Hz) assigned to the proton adjacent to the hydroxyl group in benzyl-protected *threo* ifenprodil, ***98***. (Literature data for ***98***: δH 4.1-4.2 ppm, J = 8.5-10 Hz).[23]

Racemic benzyl-protected *threo*-ifenprodil, ***98***, was subjected to a stereospecific mesylation-amination sequence to form ***99***.[11] The alcohol, ***98***, was first activated towards nucleophilic substitution via *in-situ* formation of the reactive mesylate, by reaction with methanesulfonylchloride in anhydrous THF under basic conditions. The presence of the mesylate was confirmed by TLC analysis after 30 minutes. After this time, *N*-Boc-1,6-hexyldiamine and triethylamine were added and the resulting solution stirred at room temperature overnight. Work-up and subsequent purification by column chromatography gave ***99*** in a 63% yield. Confirmation of a stereospecific reaction was again obtained through analysis of the proton resonances at the asymmetric centres, using ^{1}H NMR spectrometry, similar to the conformational analysis of ***98***. Finally, compound ***99*** was subject to acidic double deprotection to remove the benzyl and carbamate protecting groups. This was achieved by stirring ***99*** in aqueous HBr at 100 °C overnight, which gave the free amine, ***100***, as a pale yellow solid after purification by column chromatography.[11]

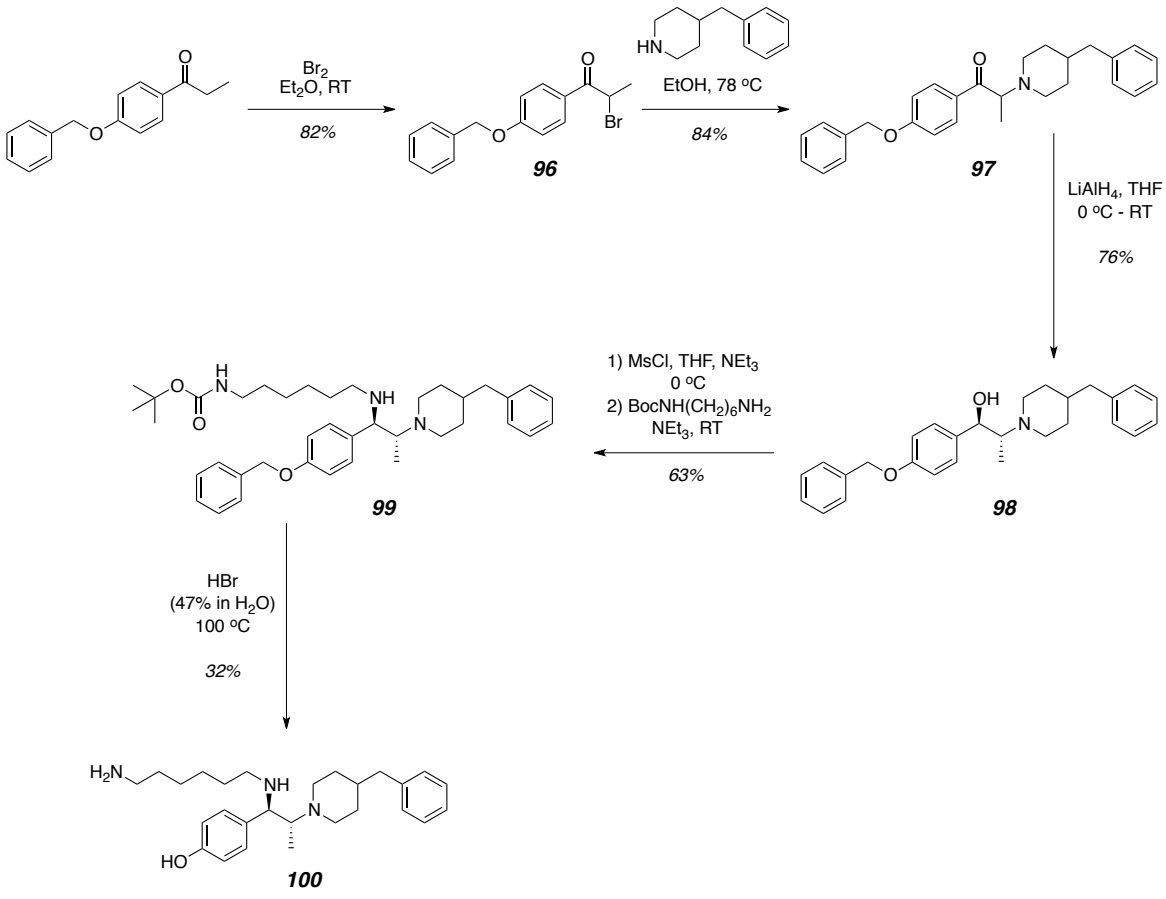

Scheme 6.2.

The synthesis of the NMDA receptor-binding moiety of **[NIR-2]** followed the sequence shown in *scheme 6.3*. First, the primary amine, ***36***, underwent amide bond formation with *N*-Boc-6-aminohexanoic acid to form ***101***. This reaction was undertaken by stirring the acid as a solution in anhydrous DMF with HDC.HCl and HOBt for 20 minutes. After this time, a solution of the amine, ***36***, and NMM was added dropwise and the reaction progress monitored by ESI-MS. Upon consumption of the starting materials after five hours, the solvent was removed to give the crude product. After work-up and purification by column chromatography, the carbamate, ***101***, was isolated as a yellow oil in a 43% yield. The final step before conjugation to the heptamethine cyanine dye, ***95***, involved hydrolysis of the carbamate protecting group. This was achieved using a 1:1 mixture of trifluoroacetic acid and DCM at room temperature for 30 minutes, at which point the solvent was removed under reduced pressure. Excess TFA was removed via repeated addition and removal of DCM under reduced pressure. This yielded the TFA salt of the amine, which was used directly in the coupling to ***95***, without further purification.

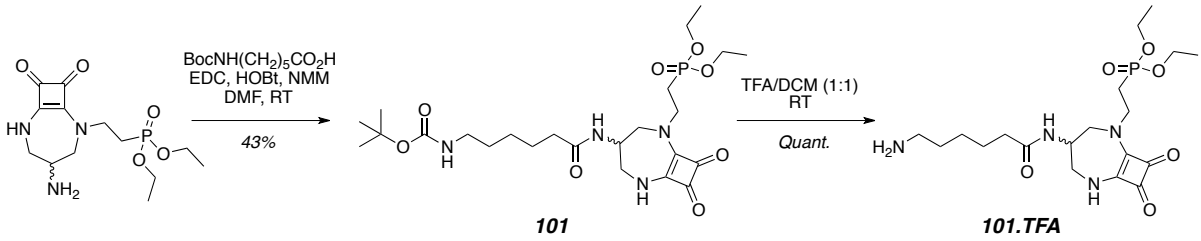

Scheme 6.3.

6.2.3 Synthesis of [NIR-1] and [NIR-2]

With each component in hand, the final step in the synthesis of the NMDA receptor-targeted contrast agents, **[NIR-1]** and **[NIR-2]**, involved conjugation of the receptor-binding moieties, ***100*** and ***101.TFA***, to the heptamethine cyanine dye, ***95*** (*Scheme 6.4*). In each case, conjugation was undertaken through amide bond formation, utilising HATU as a coupling reagent in the presence of diisopropylethylamine in anhydrous DMF. The reactions were stirred at room temperature and the progress monitored by analytical RP-HPLC. Once no further

reaction of the starting materials was observed, the solvent was removed and the crude residue that remained purified by preparative RP-HPLC (mobile phase comprising 25 mM triethylammonium acetate buffer and acetonitrile). In the case of **[NIR-2]**, one final step was carried out in which hydrolysis of the phosphonate ethyl esters occurred by reaction with an excess of bromotrimethylsilane in anhydrous DMF at 60 °C. This step was conducted prior to the final HPLC purification. Accordingly, the compounds, **[NIR-1]** and **[NIR-2]**, were obtained as green solids.

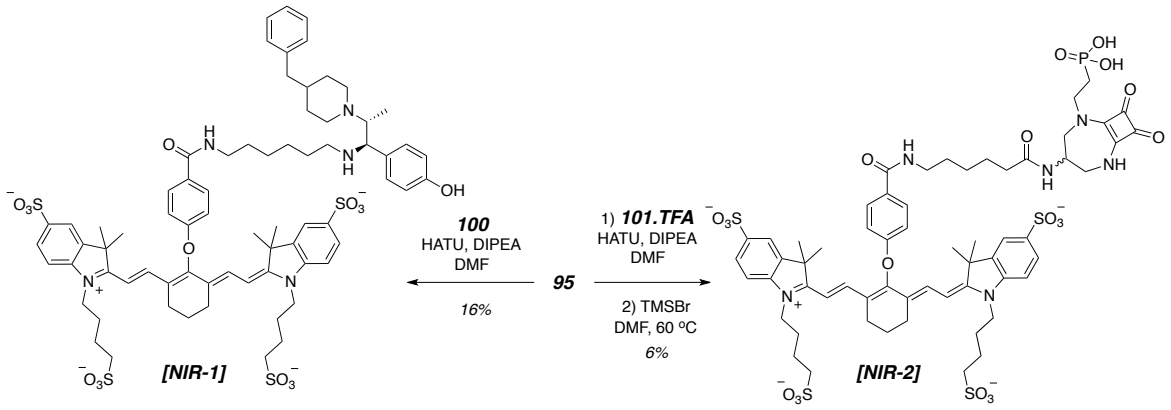

Scheme 6.4

The presence of the desired conjugates was confirmed through analysis of their high-resolution mass spectra, with comparison of the theoretical and observed mass distrubutions of **[NIR-1]** shown below (*Figure 6.4*).

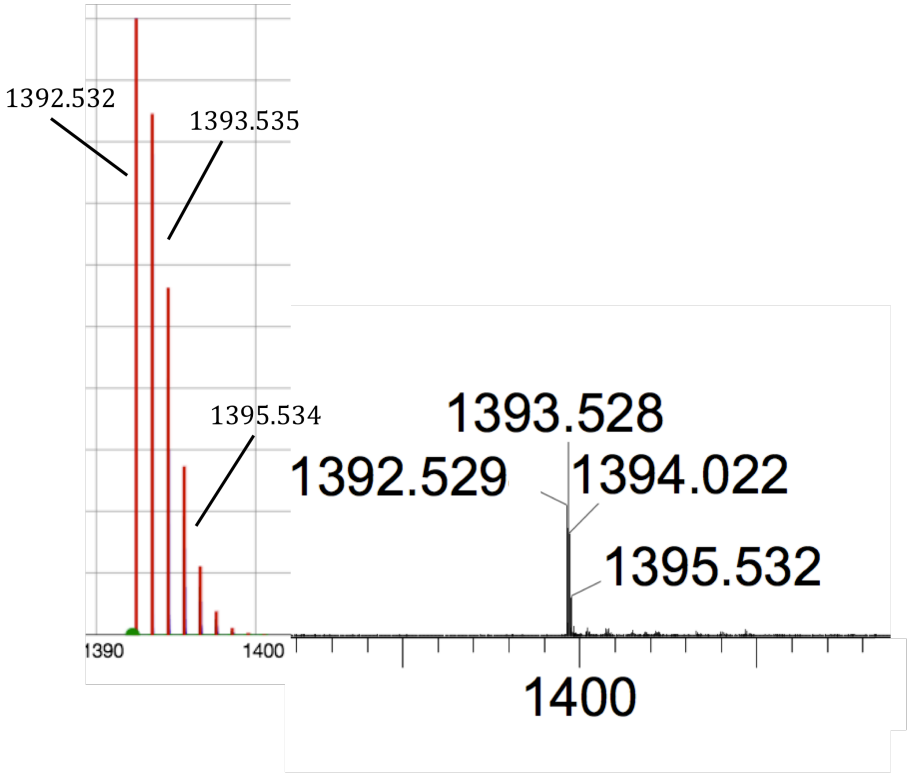

Figure 6.4. Calculated (left) and observed (right) high-resolution electrospray mass spectra of **[NIR-1]**; TOF negative mode.

6.3 Photophysical Characterisation

The photophysical characterisation of **[NIR-1]** and **[NIR-2]** was carried out in water. The absorption spectra of **[NIR-1]** and **[NIR-2]** each show broad absorption bands centred around 776 nm, with a bathochromatically shifted secondary band around 712 nm (*Figure 6.5*). The extinction coefficient of each dye at 776 nm was estimated to be 240,000 M^{-1} cm^{-1}, and is consistent with an intense $\pi \rightarrow \pi*$ transition, representing the $0 \rightarrow 0$ transition in a vibronic progression. The shoulder at 712 nm is also a $\pi \rightarrow \pi*$ transition, but relates to the $0 \rightarrow 1$ or $0 \rightarrow 2$ vibronic transition.[24] The absorption properties of **[NIR-1]** and **[NIR-2]** make them ideal candidates as NMDA receptor-targeted photoacoustic agents, with the maximum wavelength of absorption falling in the optical window where endogenous photoabsorbers are poorly absorbing.

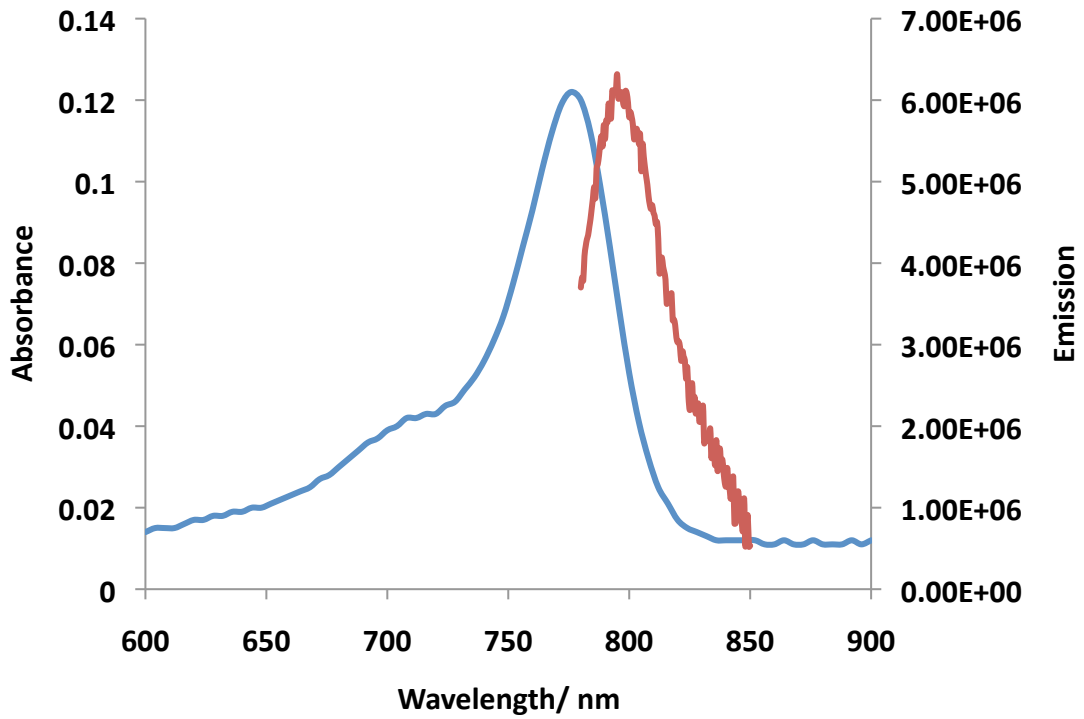

Figure 6.5. Absorption (blue) and emission (red) spectra of **[NIR-1]**. (H_2O, λ_{ex} = 776 nm, λ_{em} = 801 nm, 298 K).

The emission spectra of **[NIR-1]** and **[NIR-2]** were measured following excitation at 776 nm. Again the emission spectra were structurally the same in each case, with one main emission band centred at 801 nm, resulting in a Stokes' shift of 25 nm. Unfortunately, the quantum yields of fluorescence of **[NIR-1]** and **[NIR-2]** were not measured, as this would require the use of a silicon detector, which was unavailable at the time of this work. However, previous literature suggests that similar structures possess a quantum yield between 5-10%.[14]

6.4 Cellular Fluorescence Studies

6.4.1 Cell-Surface Localisation Studies Using Optical Microscopy

The first step in the evaluation of **[NIR-1]** and **[NIR-2]** as NMDA receptor-targeted photoacoustic contrast agents was to determine the localisation profile of the probes on differentiated NSC-34 cells expressing NMDA receptors. Two methods were explored.

The first, performed by Dr Robert Pal, involved using **[NIR-1]** and **[NIR-2]** as FRET acceptors, which were excited using a Eu(III) complex which acted as a FRET donor. Excitation of the Eu(III) complex at 365 nm led to sensitised population of the dye excited state. An overlap of the emission spectrum of the donor and the absorption spectrum of the acceptor leads to excitation of **[NIR-1]** or **[NIR-2]**, providing both donor and acceptor are close in space. This allows emission from the acceptor to be observed. A Stern-Volmer analysis conducted by Martina Delbianco showed that 65% energy transfer could be achieved between the Eu(III) complex, **[Eu.L^{MD}]** (*Scheme 6.5*) and heptamethine cyanine dye, ***95***, demonstrating the feasibility of the experiment.

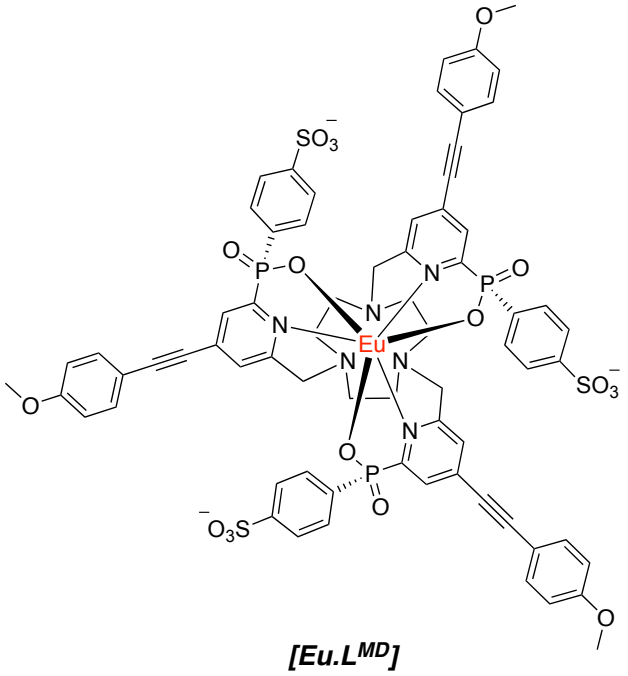

[Eu.L^{MD}]

Scheme 6.5. The structure of **[Eu.L^{MD}]** used as the FRET donor.

Differentiated NSC-34 cells were grown (as described in *chapter 2*) on specially designed microscope slides, comprising a 100 μL flow-through channel. The cells were incubated with a 10 μM solution of either **[NIR-1]** or **[NIR-2]** for 30 minutes (37 °C, 5% CO_2) and washed three times to remove any unbound probe. Finally, the cells were treated with fresh buffer containing 20 μM of the Eu(III) complex, **[Eu.L^{MD}]**, and imaged using a Zeiss Axiovert 200 M inverted microscope. Excitation at 365 nm and visualisation of the emission at 780 nm

demonstrated that both **[NIR-1]** and **[NIR-2]** showed a localisation profile at the cell surface (*Figure 6.6*), with **[NIR-1]** appearing to label the cells more readily than **[NIR-2]**, suggesting a higher affinity for **[NIR-1]** toward the NMDA receptor. Further confirmation of the cell-surface localisation for both probes was achieved through a repeat of the loading experiment detailed above, with a co-incubation of the commercially available cell mask-orange (*Figure 6.6*).

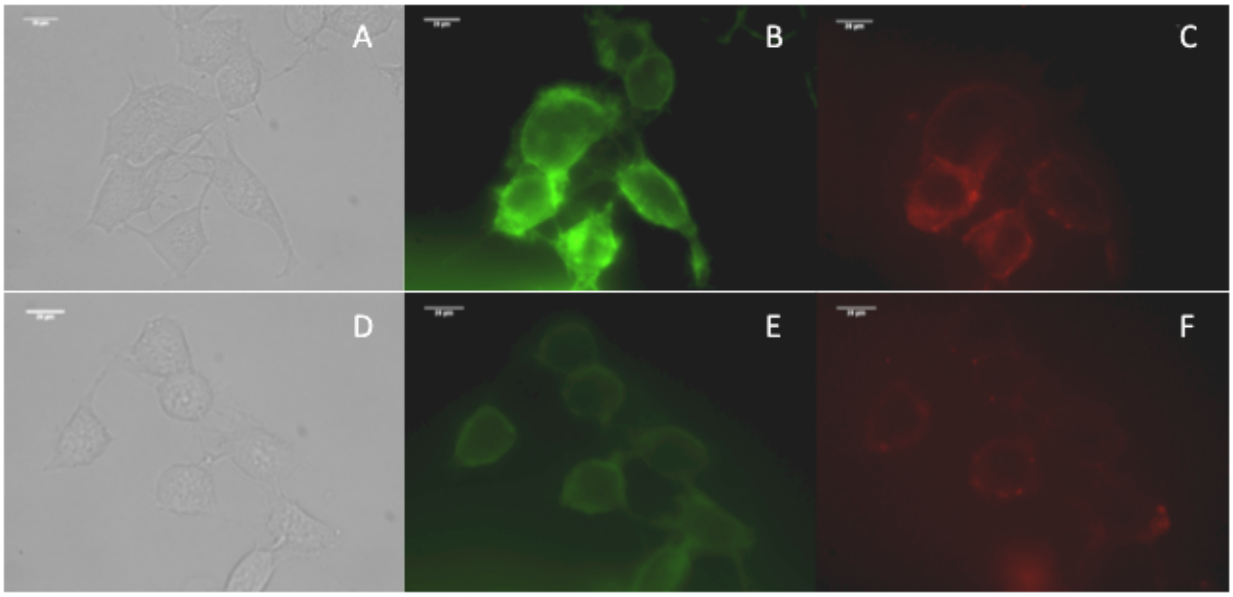

Figure 6.6. Live cell fluorescence microscopy images of differentiated NSC-34 cells following treatment with either **[NIR-1]** or **[NIR-2]** (10 μM, 30 minutes) showing cell surface localisation. (A) Transmission image; (B) visualisation of **[NIR-1]** ($\lambda_{ex}/\lambda_{em}$ = 365/780 nm); (C) visualisation of cell mask orange ($\lambda_{ex}/\lambda_{em}$ = 525/590 nm); (D-F) As images (A-C) but with **[NIR-2]**.

The second method for probe visualisation on differentiated NSC-34 cells was performed by Dr Sven Gottschalk at the institute for biological and medical imaging, Munich. This method involved direct excitation of **[NIR-1]** or **[NIR-2]** upon incubation with differentiated NSC-34 cells (*Figure 6.7*).

Similar to the experiment above, differentiated NSC-34 cells were incubated with a 10 μM solution of either **[NIR-1]** or **[NIR-2]** for 30 minutes, washed to remove any unbound probe and then imaged using epifluorescence microscopy. Again, more signal was detected from the cells treated with **[NIR-1]** (*Figure 6.7A vs B*), suggesting this compound bound with a higher affinity to the cell surface NMDA receptor.

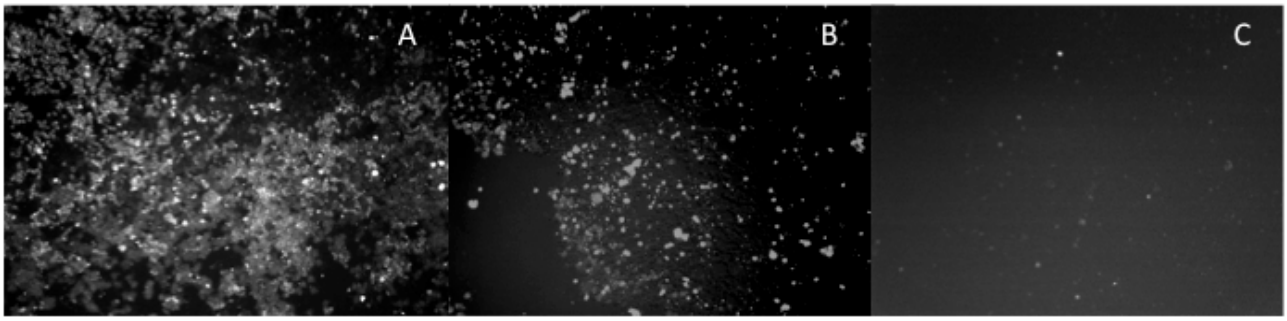

Figure 6.7. Live cell fluorescence microscopy images of differentiated NSC-34 cells ($\lambda_{ex}/\lambda_{em}$ = 780/800 nm). (A) Treatment with **[NIR-1]** (10 μM, 30 minutes); (B) Treatment with **[NIR-2]** (10 μM, 30 minutes); (C) Treatment with compound ***95*** (10 μM, 30 minutes).

In order to confirm that the localisation profiles of **[NIR-1]** and **[NIR-2]** are due to the presence of the NMDA receptor-binding moieties interacting with the receptor and not due to the heptamethine cyanine dye binding non-specifically to the cell membrane, a control experiment was conducted. Differentiated NSC-34 cells were treated with a 10 μM solution of compound ***95*** for 30 minutes. After washing, the cells were imaged which led to no fluorescence signal being observed (*Figure 6.7C*). This demonstrated the lack of non-specific binding of the dye, and suggests that the observed localisation profiles are due to the presence of the NMDA receptor-binding moieties binding to the NMDA receptor, in a similar fashion to what was observed for **[Gd.L$^{11\text{-}12}$]**.

6.4.2 Establishing Cellular Specificity of Binding

A key characteristic needed for these NMDA receptor-targeted photoacoustic contrast agents is to have cellular specificity of binding, meaning that they only bind to cells which express functional NMDA receptors. It was shown that the heptamethine cyanine dye itself does not bind to differentiated NSC-34 cells (*Figure 6.7C*). However, the potential of **[NIR-1]** and **[NIR-2]** to bind to NMDA receptor-negative cells was assessed using NIH 3T3 mouse skin fibroblast cells, which do not express any NMDA receptors. These cells were incubated with a 10 μM solution of either **[NIR-1]** or **[NIR-2]** for 30 minutes (37 °C, 5% CO_2), washed

three times to remove any unbound probe and then treated with fresh buffer containing 20 μM of the Eu(III) complex, **[Eu.L^{MD}]**. No localisation profile of any kind, cell-surface or intracellular, was observed, strengthening the argument of a receptor-mediated localisation effect observed when **[NIR-1]** and **[NIR-2]** were incubated with differentiated NSC-34 cells. These promising results further enhance the potential of **[NIR-1]** and **[NIR-2]** to act as NMDA receptor-targeted photoacoustic contrast agents.

6.4.3 Assessing the Reversibility of Binding

Having demonstrated that **[NIR-1]** and **[NIR-2]** only bind to cells which express NMDA receptors, one further characteristic needed for these probes was to possess the ability to bind at the NMDA receptor in a reversible manner, with a competitive affinity to the endogenous ligand glutamate. Since it was much easier to visualise **[NIR-1]** on the surface of differentiated NSC-34 cells, the fate of this probe after a stimulated 'glutamate burst' was assessed.

Using a similar contrast transfer function experiment to that described in *Chapter 4*, differentiated NSC-34 cells were incubated with a 10 μM solution of **[NIR-1]** for 30 minutes (37 °C, 5% CO_2), washed three times to remove any unbound probe and then treated with fresh buffer containing 20 μM of the Eu(III) complex, **[Eu.L^{MD}]**. The cells were imaged and the average intensity was recorded in triplicate using three cells (*Figure 6.8A*). These cells were then washed with five successive aliquots (V_{tot} = 500 μL) of a glutamate-rich (1 mM) culture medium and then treated with fresh buffer containing 20 μM of the Eu(III) complex, **[Eu.L^{MD}]**. This sequence resulted in a ten-fold drop in fluorescence intensity, compared to the original cell staining experiment (*Figure 6.8B*). Furthermore, when differentiated NSC-34 cells were first treated with a glutamate-rich (1 mM) solution to block the NMDA receptor, washed with fresh buffer and then re-incubated sequentially with both components (10 μM of **[NIR-1]** for 30 mins and 20 μM **[Eu.L^{MD}]** in the medium), the fluorescence signal could be fully recovered to the original value (*Figure 6.8C*).

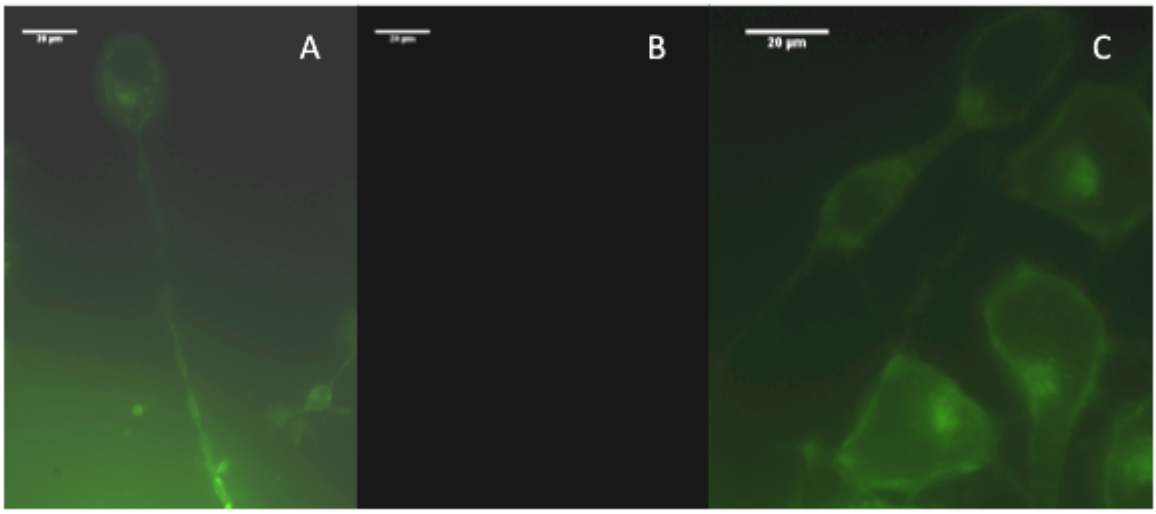

Figure 6.8. (A) Live cell fluorescence microscopy images ($\lambda_{ex}/\lambda_{em}$ = 365/780 nm) of differentiated NSC-34 cells following treatment with **[NIR-1]** (10 μM, 30 minutes); (B) As image (A) but with a post glutamate (1 mM) wash, showing **[NIR-1]** is removed from the cell surface; (C) Cells first treated with a glutamate (1 mM) rich culture media to block the receptor, washed and then re-incubated with both **[NIR-1]** (10 μM, 30 minutes) and the europium complex (20 μM) showing the ability of **[NIR-1]** to compete and bind in the presence of glutamate.

The quality of the images in *figures 6.6 and 6.8* are much worse than those obtained in *chapter 4 and 5*. This is due to the decreased detector sensitivity at 780 nm, resulting in the images being obtained at the detection limit. Nevertheless, these results obtained throughout the fluorescence microscopy studies on the localisation, cellular specificity and reversibility of binding suggest that the probes, **[NIR-1]** and **[NIR-2]**, are binding via their receptor-binding moieties to the cell surface NMDA receptor.

6.5 Photoacoustic Imaging of [NIR-1] and [NIR-2]

6.5.1 Preliminary Evaluation of the Cellular Photoacoustic Signal

Having established sufficient evidence that **[NIR-1]** and **[NIR-2]** can both label the cell surface NMDA receptor on differentiated NSC-34 cells, the ability of the contrast agents to generate a significant photoacoustic signal was evaluated. These experiments were undertaken in Germany, by Dr Sven Gottschalk, using multi-spectral optoacoustic tomography performed on an inVision 256-TF small animal scanner (iThera). Approximately 10 million differentiated NSC-34 cells

were treated with a 10 μM solution of either **[NIR-1]** or **[NIR-2]** for 30 minutes at 37 °C and 5% CO_2. After this time, the cells were washed thoroughly to remove any unbound probe and then re-suspended in a 1:1 mixture of fresh buffer and a 3% agar solution. The presence of the agar solution generated a scattering pattern that mimicked tissue scattering. The cells were then warmed to 37 °C and loaded into short plastic straws. At this temperature, the agar solution solidified and generated a 'stationary solution' of cells from which the phantom MSOT images were acquired. The images were obtained by defining regions of interest from the locations of the straws, scanning the wavelengths between 680-900 nm, using 5 nm intervals and 10 averages per wavelength.

Initial studies showed that **[NIR-1]** clearly labels differentiated NSC-34 cells, generating a large, detectable photoacoustic signal (*Figure 6.9 green*). As a control, cells alone (*Figure 6.9 brown*) and cells treated with the non-targeted heptamethine cyanine dye, ***95*** (*Figure 6.9 cyan*) did not give rise to any observable MSOT signal, suggesting that the receptor-binding moiety of **[NIR-1]** binds to the cell surface NMDA receptor and is responsible for the observed signal.

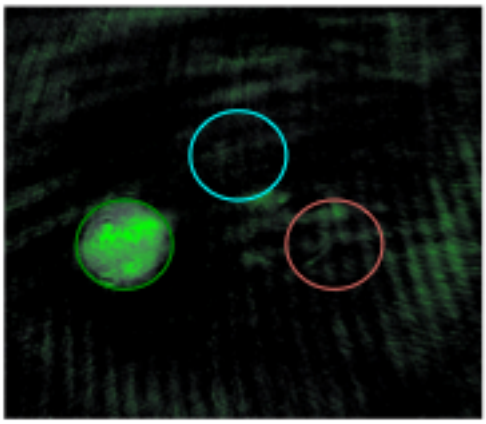

Figure 6.9. Live cell MSOT of differentiated NSC-34 cells under different conditions. (Green) Cells treated with **[NIR-1]** (10 μM, 30 minutes) showing large MSOT signal; (Brown) Cells treated with the non-targeted heptamethine cyanine dye, ***95*** (10 μM, 30 minutes), showing no MSOT signal; (Cyan) Untreated cells showing no MSOT signal.

Figure 6.10 shows the wavelength dependence of the photoacoustic signal of cells treated with **[NIR-1]**. This photoacoustic spectrum clearly resembles the absorbance spectrum of **[NIR-1]** and suggests that this compound should be

observable in an *in vivo* model, in the presence of the endogenous photoabsorbers.

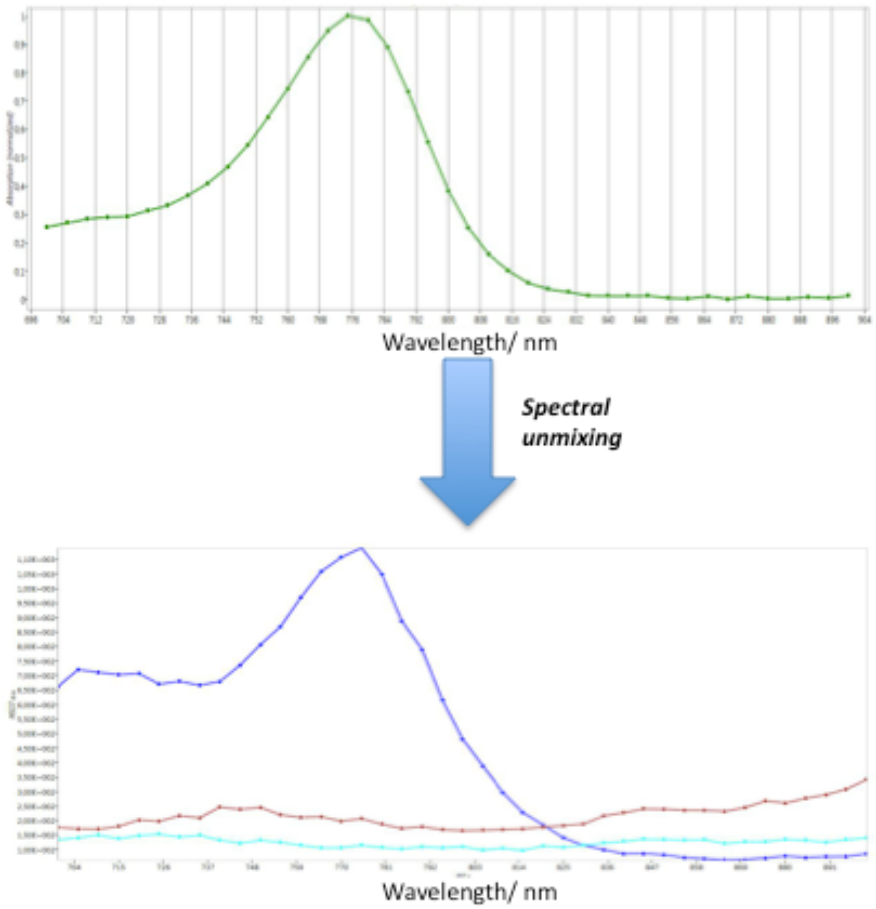

Figure 6.10. (Top) Absorbance spectrum of **[NIR-1]** which is fed into the unmixing algorithm. (Bottom) Wavelength-dependent analysis (photoacoustic spectrum) obtained from the unmixing algorithm of differentiated NSC-34 cells labelled with **[NIR-1]** (10 μM, 30 minutes).

Surprisingly, when the same cell-labelling analysis was performed using **[NIR-2]** (10 μM, 30 minutes), no photoacoustic signal was detected from differentiated NSC-34 cells. Instead, a large signal was observed from the supernatant suggesting that **[NIR-2]** does not bind to the cell surface NMDA receptor. This is a contradiction to the results obtained from the fluorescence microscopy experiments, which despite the signal being weak, demonstrated that **[NIR-2]** was present on the surface of differentiated NSC-34 cells. One possible explanation for this result is that the receptor density during the time of analysis of **[NIR-2]** was low, meaning that **[NIR-2]** could not sufficiently label

differentiated NSC-34 cells. Alternatively, a larger probe concentration may be needed in order to give a detectable photoacoustic signal.

In order to assess the effect of conjugation of the large heptamethine cyanine dye to the NMDA receptor-binding moiety of **[NIR-1]**, a competition experiment was performed to assess the cellular labelling of **[NIR-1]** in the presence of the small molecule antagonist, ifenprodil. Differentiated NSC-34 cells were treated with a 40 μM solution of ifenprodil for 10 minutes, washed to remove any excess antagonist and then incubated with a 20 μM solution of **[NIR-1]** for 30 minutes. After this time, the cells were washed and imaged using MSOT (*Figure 6.11*).

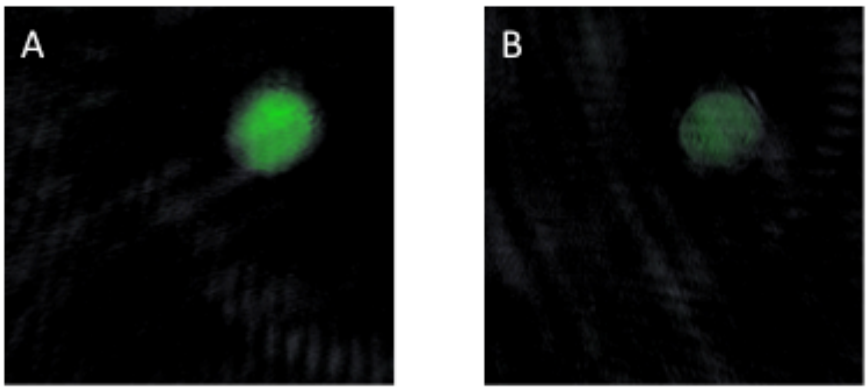

Figure 6.11. Live cell MSOT of differentiated NSC-34 cells under different conditions. (A) Cells treated with **[NIR-1]** (10 μM, 30 minutes) showing large MSOT signal; (B) Cells treated with the NMDA receptor-binding moiety of **[NIR-1]**, ifenprodil (40 μM, 10 minutes), followed by treatment with **[NIR-1]** (20 μM, 30 minutes) showing no a decrease in MSOT signal consistent with lower cellular labelling of **[NIR-1]** in the presence of the small molecule antagonist.

Figure 6.11A shows the large photoacoustic signal observed from the original cell labelling experiment using **[NIR-1]**. However, pre-treating the cells with the NMDA receptor-binding moiety of **[NIR-1]** before loading the cells with **[NIR-1]** resulted in a significantly diminished photoacoustic signal (*Figure 6.11B*). Such behaviour suggests that the presence of the large heptamethine cyanine dye does not affect binding too much and that **[NIR-1]** binds to the same position on the NMDA receptor as the small molecule antagonist, albeit with a weaker affinity, as expected. Such behaviour is similar to that observed when the pentamethine cyanine dye was conjugated to ifenprodil.[11]

Finally, the ability of **[NIR-1]** to be displaced from the NMDA receptor by the natural ligand, glutamate, was demonstrated using MSOT. Approximately 10 million differentiated NSC-34 cells were treated with a 10 μM solution of **[NIR-1]** for 30 minutes (*Figure 6.12A*). This gave a large, detectable photoacoustic signal similar to that detected in *figure 6.9*. The cells were then washed with a glutamate-rich (1 mM) culture medium before being re-suspended and imaged. This resulted in a significantly diminished photoacoustic signal (*Figure 6.12B*), demonstrating the ability of **[NIR-1]** to be displaced following a simulated glutamate burst. This result is in keeping with the findings from the fluorescence microscopy experiments.

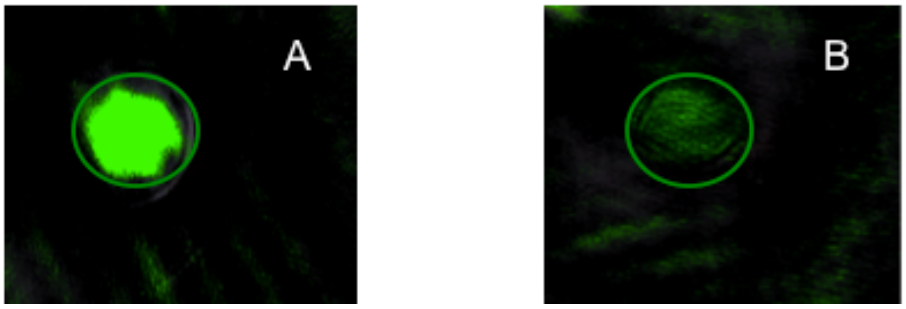

Figure 6.12. Live cell MSOT of differentiated NSC-34 cells under different conditions. (A) Cells treated with **[NIR-1]** (10 μM, 30 minutes) showing large MSOT signal; (B) As image (A) but with a post (1 mM) glutamate wash, showing the ability of **[NIR-1]** to be displaced from the NMDA receptor.

6.5.2 Preliminary *In Vivo* Studies With [NIR-1]

Following the encouraging *in vitro* results of **[NIR-1]**, preliminary *in vivo* studies were carried out by Dr. Sven Gottschalk, at the Institute for Biological and Medical Imaging, Munich, on female athymic nude mice (aged 8 weeks). The contrast agent, **[NIR-1]**, will not be able to enter the brain via blood flow, since such an anionic species of this volume will not be able to penetrate the blood-brain-barrier. Therefore, administration of **[NIR-1]** was undertaken through direct injection into the brain parenchyma of an anaesthetised mouse (oxygen/ 2% isofluorane). The coordinates of the injections were from the Bregma: anterior 1.10 mm and 1.75 mm left or right, with an injection depth of

approximately 2.00 mm, placing the injection inside the M1 motorcortex, which is a region known to possess a high expression of NMDA receptors.[25]

Due to the symmetrical nature of the brain, two injections per mouse could be made, allowing comparative analysis. Initially, 1 μL of a 3.6 mM solution of **[NIR-1]** was injected into the right hemisphere, with the same volume of phosphate buffered saline (PBS) injected into the left hemisphere, to serve as a negative control. The mouse was then loaded into an inVision 256-TF small animal scanner and continuously imaged over a one hour period (*Figure 6.13*).

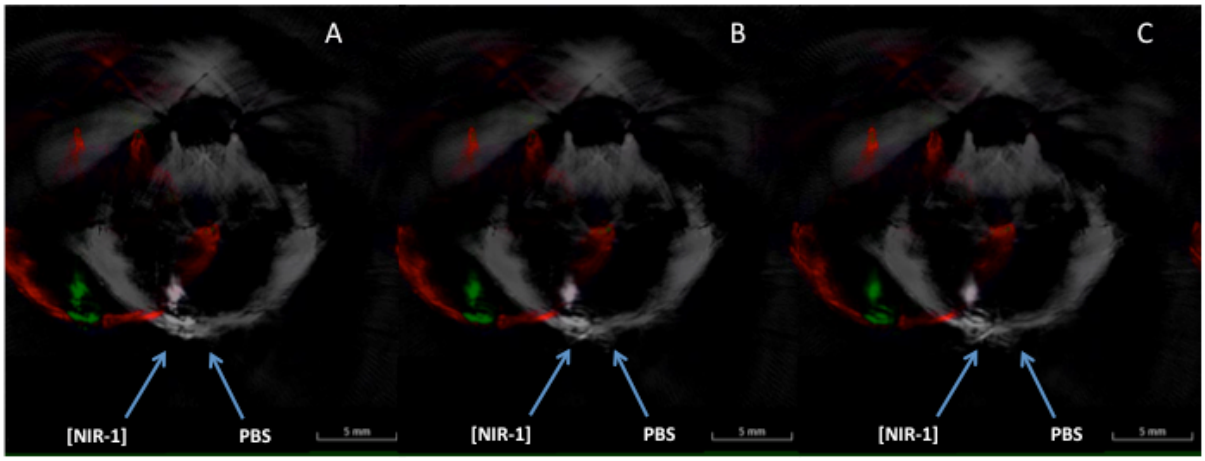

Figure 6.13. *In vivo* imaging by MSOT of the brain of an 8 week old female athymic nude mouse following intracranial injection of **[NIR-1]** (3.6 nmol) or PBS into the right and left hemispheres, respectively. The mouse is lying on its back resulting in right and left being swapped over in MSOT images. Images (A-C) show different slice thicknesses ranging from 11.5, 12.0 and 12.5 mm. Green is the unmixed signal of **[NIR-1]**, red is unmixed signal of oxygenated haemoglobin and grey is the spectrally anatomical image at 776 nm.

In *figure 6.13*, the green signal represents the unmixed photoacoustic signal from **[NIR-1]**, the red is the unmixed photoacoustic signal from oxygenated haemoglobin and the grey is the anatomical image generated through spectral unmixing of the photoacoustic signal at 776 nm. These images show that **[NIR-1]** is readily identified in the presence of endogenous photoabosrbers in the brain of a live mouse. Furthermore, no photoacoustic signal was observed from the PBS injection site, demonstrating that this technique of drilling a hole through the skull and injecting a needle does not generate artefacts that would decrease the signal to noise ratio.

In order to demonstrate that **[NIR-1]** is binding to the cell surface NMDA receptors *in vivo*, a preliminary comparative analysis of the clearance rate of **[NIR-1]** versus the non-targeted heptamethine cyanine dye, ***95***, was undertaken. It was envisaged that if **[NIR-1]** is bound to the cell surface NMDA receptor, it should preferentially be retained in the brain for longer than compound ***95***, showing a slower clearance rate. To investigate this, 1 μL of a 3.6 mM solution of **[NIR-1]** was injected into the right hemisphere, with the same concentration of compound ***95*** injected into the left hemisphere. After the slow injection, the skin above the injection site was sealed and the mouse imaged (*Figure 6.14*).

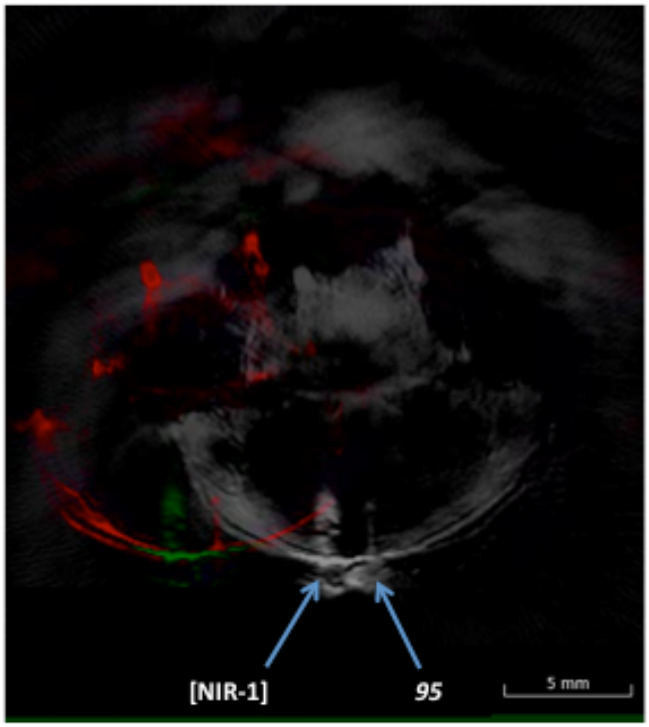

Figure 6.14. *In vivo* imaging by MSOT of the brain of an 8 week old female athymic nude mouse following intracranial injection of **[NIR-1]** (3.6 nmol) or compound ***95*** (3.6 nmol) into the right and left hemispheres, respectively. The mouse is lying on its back resulting in right and left being swapped over in MSOT image. The image clearly shows **[NIR-1]** is detectable whereas compound ***95*** has leaked from the injection site.

Similar to *figure 6.13*, a large signal is easily observed from the injection of **[NIR-1]**, while no signal is detected from compound ***95***. This is surprising considering ***95*** possesses essentially the same absorption properties as **[NIR-1]**. However, due to the large amount of signal around the outside of the injection site of ***95***, it is likely that the injection of compound ***95*** was unsuccessful and the compound leaked out of the site before the wound was sealed. Nevertheless, regions of

interest were defined around the injection site of **[NIR-1]**, and were imaged continuously for 90 minutes. An increase in signal intensity was observed initially, and this decreased slowly over time, which can tentatively be assigned to **[NIR-1]** binding to the cell surface NMDA receptors. However, a much more thorough analysis and comparison to the clearance rate of compound ***95*** is needed in order to fully relate this observation to NMDA receptor binding.

6.6 Conclusions

The initial aim of this chapter was to design, synthesise and evaluate two NMDA receptor-targeted photoacoustic contrast agents. The contrast agents, **[NIR-1]** and **[NIR-2]** are derived from a strongly absorbing heptamethine cyanine dye, conjugated to the non-competitive NMDA receptor antagonist, ifenprodil, and the receptor-binding moiety of **[Gd.L^{12}]**, respectively. These two compounds were fully characterised before analysis of their receptor binding properties.

Two fluorescence microscopy methods were used to study the localisation profiles of **[NIR-1]** and **[NIR-2]** on differentiated NSC-34 cells. Under each set of conditions, the contrast agents were found to localise on the cell surface, consistent with NMDA receptor labelling. Receptor binding was further established in a control experiment, where no localisation profile was observed when NMDA receptor-negative cells were treated with solutions of **[NIR-1]** or **[NIR-2]**. Finally, the most promising contrast agent, **[NIR-1]**, was found to bind to differentiated NSC-34 cells in a reversible manner in the presence of the natural ligand glutamate.

The cellular labelling ability of **[NIR-1]** and **[NIR-2]** was also assessed by measuring the cellular photoacoustic signal using MSOT on differentiated NSC-34 cells. The contrast agent **[NIR-1]** demonstrated a large and detectable photoacoustic signal, whereas **[NIR-2]** did not appear to label cells efficiently. This was surprising based on the results from the fluorescence microscopy experiments, but may be explained by either a reduction in the NMDA receptor density at the time of imaging, or due to the probe concentration/affinity being

too low. In either case this would result in **[NIR-2]** being unable to label cells efficiently well.

Conjugation of the relatively large heptamethine cyanine dye to the NMDA receptor antagonist, ifenprodil, did not appear to alter receptor binding properties. A competition experiment whereby differentiated NSC-34 cells were pre-treated with ifenprodil before loading **[NIR-1]** resulted in a decrease in cellular photoacoustic signal. This suggested that **[NIR-1]** binds in the same place on the NMDA receptor as ifenprodil, but with a lower affinity, as would be expected.

Finally, preliminary *in vivo* studies were carried out through direct injection of **[NIR-1]** into the primary motorcortex of female athymic nude mice. The photoacoustic signal was easily identified and an anatomical image of the brain generated from the signal at 776 nm, using MSOT. This promising result was extended slightly by a preliminary study of the probe clearance rate. Upon injection an initial increase in photoacoustic signal could be observed, which slowly decreased over time. This could tentatively be assigned to **[NIR-1]** binding to the cell surface NMDA receptors and then being displaced over time and removed from the region of interest. Only further analysis and comparison of the clearance rate to that of the non-targeted heptamethine cyanine dye, ***95***, will allow a better understanding of the dynamics of NMDA receptor binding.

6.7 References

1. M. L. James and S. S. Gambhir, *Physiol. Rev.*, 2012, **92**, 897-965.
2. V. Ntziachristos and D. Razansky, *Chem. Rev.*, 2010, **110**, 2783-2794.
3. B. Cox, *Introduction to Biomedical Photoacoustic Imaging, Eur. Soc. Mol. Imag.*, Presentation, 2013.
4. A. G. Bell, *Am. J. Sci.*, 1881, 305.
5. A. Rosencwaig, *Science*, 1973, **181**, 657-658.
6. M. S. Patterson, B. Chance and B. C. Wilson, *Appl. Opt.*, 1989, **28**, 2331-2336.
7. P.-C. Li, C.-R. C. Wang, D.-B. Shieh, C.-W. Wei, C.-K. Liao, C. Poe, S. Jhan, A.-A. Ding and Y.-N. Wu, *Opt. Express*, 2008, **16**, 18605-18615.
8. M. Eghtedari, A. Oraevsky, J. A. Copland, N. A. Kotov, A. Conjusteau and M. Motamedi, *Nano Lett.*, 2007, **7**, 1914-1918.
9. A. De La Zerda, C. Zavaleta, S. Keren, S. Vaithilingam, S. Bodapati, Z. Liu, J. Levi, B. R. Smith, T.-J. Ma, O. Oralkan, Z. Cheng, X. Chen, H. Dai, B. T. Khuri-Yakub and S. S. Gambhir, *Nat. Nano*, 2008, **3**, 557-562.
10. I. J. Reynolds and R. J. Miller, *Mol. Pharmacol.*, 1989, **36**, 758-765.
11. P. Marchand, J. Becerril-Ortega, L. Mony, C. Bouteiller, P. Paoletti, O. Nicole, L. Barré, A. Buisson and C. Perrio, *Bioconjugate Chem.*, 2011, **23**, 21-26.
12. K. Williams, *Mol. Pharmacol.*, 1993, **44**, 851-859.
13. W. A. Kinney, M. Abou-Gharbia, D. T. Garrison, J. Schmid, D. M. Kowal, D. R. Bramlett, T. L. Miller, R. P. Tasse, M. M. Zaleska and J. A. Moyer, *J. Med. Chem.*, 1998, **41**, 236-246.
14. M. Y. Berezin, K. Guo, W. Akers, J. Livingston, M. Solomon, H. Lee, K. Liang, A. Agee and S. Achilefu, *Biochem.*, 2011, **50**, 2691-2700.
15. F. M. Hamann, R. Brehm, J. Pauli, M. Grabolle, W. Frank, W. A. Kaiser, D. Fischer, U. R. Genger, and I. Hilger, *Mol. Imag.*, 2011, **10**, 258-269.
16. M. Lopalco, E. N. Koini, J. K. Cho and M. Bradley, *Org. Biomol. Chem.*, 2009, **7**, 856-859.
17. R. B. Mujumdar, L. A. Ernst, S. R. Mujumdar, C. J. Lewis and A. S. Waggoner, *Bioconjugate Chem.*, 1993, **4**, 105-111.
18. G. A. Reynolds and K. H. Drexhage, *J. Org. Chem.*, 1977, **42**, 885-888.
19. S. A. Hilderbrand, K. A. Kelly, R. Weissleder and C.-H. Tung, *Bioconjugate Chem.*, 2005, **16**, 1275-1281.
20. L. Strekowski, M. Lipowska and G. Patonay, *J. Org. Chem.*, 1992, **57**, 4578-4580.
21. Q. Li, J. Tan and B.-X. Peng, *Molecules*, 1997, **2**, 91-98.
22. S. Lou and G. C. Fu, *J. Am. Chem. Soc.*, 2010, **132**, 1264-1266.
23. B. L. Chenard, I. A. Shalaby, B. K. Koe, R. T. Ronau, T. W. Butler, M. A. Prochniak, A. W. Schmidt and C. B. Fox, *J. Med. Chem.*, 1991, **34**, 3085-3090.
24. D. S. Pisoni, L. Todeschini, A. C. A. Borges, C. L. Petzhold, F. S. Rodembusch and L. F. Campo, *J. Org. Chem.*, 2014, **79**, 5511-5520.
25. O. v. B u. Halbach and R. Dermietzel, *Neurotransmitters and Neuromodulators*, Wiley-VCH Verlag GmbH & Co. KGaA, 2003.

CHAPTER SEVEN

Conclusions and Future Work

7. Conclusions and Future Work

7.1 General Conclusions

At the outset of the project, the objective was to design, synthesise and evaluate a series of contrast agents that specifically targeted the NMDA receptor. Initial work was directed towards the development of NMDA receptor-targeted MRI contrast agents, since this imaging modality is regarded as one of the most powerful for neurological research.

Two groups of NMDA receptor-targeted MRI contrast agents were synthesised. The first generation contrast agents were based on a paramagnetic [Gd.DOTA] core, conjugated via a pendant lysine arm to derivatives of competitive NMDA receptor antagonists derived from the acyclic 3,4-diamino-3-cyclobutene-1,2-dione moiety. Of the four first generation contrast agents, **[Gd.L^{2}]** and **[Gd.L^{4}]** induced large enhancements in cellular relaxation rate (170 and 176%, respectively), upon incubation with a neuronal cell line model.

The surprising result that the most potent NMDA receptor-binding moiety used in **[Gd.L^{3}]** did not induce any enhancement in $R_{1,\text{cell}}$ led to the design of a series of second generation NMDA receptor-targeted MRI contrast agents. Based on the assumption that intramolecular hydrogen bonding was responsible for the lack of receptor binding of **[Gd.L^{3}]**, the receptor-binding moiety was rigidified in a bicyclic structure, so that the conformation was restricted to similar highly potent NMDA receptor antagonists.

Four bicyclic NMDA receptor-binding moieties were synthesised and conjugated to a [Gd.DOTA] core via a glutaric acid linker, giving the complexes, **[Gd.L$^{5\text{-}8}$]**. Unfortunately, upon incubation of these contrast agents with differentiated NSC-34 cells, no significant enhancements in $R_{1,\text{cell}}$ were observed. Since it was envisaged that the second generation receptor-binding moieties should possess a greater receptor affinity, the observation of no relaxation rate enhancement was attributed to the close proximity of the large Gd(III) chelate to the NMDA receptor-binding moiety, restricting receptor binding. Therefore, the chain length of the linker unit was extended to space the receptor-binding moiety further away from the sterically demanding paramagnetic core, generating two

more complexes, **[Gd.L$^{9\text{-}10}$]**. Incubation of **[Gd.L^{9}]** with differentiated NSC-34 cells led to a measureable increase in $R_{1,\text{cell}}$ of 123%.

Of the ten NMDA receptor-targeted MRI contrast agents synthesised, **[Gd.L^{2}]**, **[Gd.L^{4}]** and **[Gd.L^{9}]** gave rise to large enhancements in $R_{1,\text{cell}}$ consistent with an increase in rotational correlation time that is associated with slower molecular tumbling of the receptor-bound complex. In order to further confirm this, derivatives of **[Gd.L^{4}]** and **[Gd.L^{9}]** were synthesised which allowed study of the localisation profile, reversibility and cellular specificity of binding, by optical microscopy. The complexes, **[Gd.L^{11}]** and **[Gd.L^{12}]** (derived from **[Gd.L^{4}]** and **[Gd.L^{9}]**, respectively), were found to reside on the cell surface of differentiated NSC-34 cells and bind specifically to cells which possess NMDA receptor density. The complexes could also bind reversibly at the NMDA receptor after a simulated glutamate burst, with the ability to displace glutamate competitively upon restoration of equilibrium. The complex, **[Gd.L^{12}]**, was found to label cells more readily than **[Gd.L^{11}]**, suggesting that the affinity of the receptor binding moiety of **[Gd.L^{12}]** is higher than the receptor-binding moiety of **[Gd.L^{11}]**. This result demonstrated that the length of the spacer unit between the receptor-binding moiety and the paramagnetic core can have a significant effect on the expected gain in relaxation rate. Taken together, these results suggest that the gadolinium complexes of ***L^{2}***, ***L^{4}*** and ***L^{9}*** are promising MR contrast agents for reporting or monitoring NMDA receptor density, and possess the ability to report on synaptic glutamate activity.

Following the success achieved with the two-component optical imaging probes, **[Gd.L^{11}]** and **[Gd.L^{12}]**, it was reasoned that a single component optical imaging contrast agent may be more desirable and could potentially replace standard radiolabelled ligands in biological assays. A new complex, **[Eu.L^{13}]**, was designed and synthesised based on the europium complex of a 9-*N*-3-tris-arylalkynylpyridyl ligand with a pendant lysine arm, conjugated to the NMDA receptor-binding moiety of **[Gd.L^{12}]**. The localisation profile of **[Eu.L^{13}]** on differentiated NSC-34 cells was studied using live-cell laser scanning confocal microscopy. Disappointingly, there was no cell-surface localisation and only a small degree of complex internalisation was observed. The internalisation mechanism was found to be non-receptor mediated and it is reasonable to

assume that the localisation of **[Eu.L^{13}]** is dictated by the large nature of the parent Eu(III)-complex and not by the relatively small NMDA receptor-binding moiety.

Chapter 6 described the development of two NMDA receptor-targeted contrast agents for photoacoustic imaging. The contrast agents were based on conjugation of the non-competitive NMDA receptor antagonist, ifenprodil, or the receptor-binding moiety of **[Gd.L^{12}]**, to a strongly absorbing heptamethine cyanine dye. The cellular labelling ability of **[NIR-1]** and **[NIR-2]** on differentiated NSC-34 cells was first assessed by fluorescence microscopy. Under two separate sets of conditions, the contrast agents were found to reside on the cell surface, consistent with NMDA receptor labelling. Further fluorescence microscopy experiments demonstrated that **[NIR-1]** and **[NIR-2]** only label cells that express functional NMDA receptors, and that **[NIR-1]** can bind in a reversible manner after a simulated glutamate burst. Such behaviour is consistent with **[NIR-1]** and **[NIR-2]** binding to the cell-surface NMDA receptor.

The cellular labelling ability of **[NIR-1]** and **[NIR-2]** was also assessed by measuring the photoacoustic signal using MSOT on differentiated NSC-34 cells. Whilst incubation of **[NIR-1]** generated a large and detectable cellular photoacoustic signal consistent with the fluorescence microscopy results, **[NIR-2]** did not appear to label differentiated NSC-34 cells at all. Although this contradictive result for **[NIR-2]** was surprising, **[NIR-1]** was further evaluated *in vivo*. Direct injection of **[NIR-1]** into the primary motorcortex of female athymic nude mice resulted in a large, detectable photoacoustic signal, which only slowly decreased over time. Despite these being preliminary studies, the results gained so far are promising and can tentatively be assigned to **[NIR-1]** binding to the cell-surface NMDA receptors in a mouse brain.

7.2 Future Work

The cellular labelling ability ($R_{1,\text{cell}}$ enhancements), cellular specificity and reversibility of binding of **[Gd.L^{2}]**, **[Gd.L^{4}]** and **[Gd.L^{9}]** make these complexes very promising as NMDA receptor-targeted MRI contrast agents. It is difficult to envisage improvements in their receptor-binding properties without moving to a

completely new receptor-binding moiety. However, it may be possible to improve the relaxation rate enhancement of **[Gd.L^{9}]** towards similar enhancements gained by **[Gd.L^{2}]** and **[Gd.L^{4}]**. Optical microscopy studies suggest that **[Gd.L^{9}]** possesses the receptor-binding moiety with the highest affinity and so the lower $R_{1,cell}$ enhancement may be due to the chain length of the linker unit. By reducing the length of the linker in **[Gd.L^{9}]**, such that receptor-binding is not inhibited and rotational motion remains coupled, an optimal linker unit may increase the $R_{1,cell}$ enhancement.

It is also recognised that **[Gd.L^{9}]** is present as a racemic mixture when incubated with differentiated NSC-34 cells. The stereochemical preference for ligand binding is partially described in *chapter 1*, and it is envisaged that one enantiomer of **[Gd.L^{9}]** might exhibit a higher NMDA receptor affinity than the other. Therefore, it may be worthwhile to separate the two enantiomers of the precursor amine and evaluate the derived complexes in terms of their ability to induce enhancements in $R_{1,cell}$.

A considerable amount of progress has been made over the last three years and the next step in assessment of **[Gd.L^{2}]**, **[Gd.L^{4}]** and **[Gd.L^{9}]** as potential NMDA receptor-targeted MR contrast agents is to evaluate these complexes *in vivo*. As these complexes will be unable to penetrate the blood-brain-barrier, direct injection of the contrast agent into regions of the brain expressing high NMDA receptor-density, to create a steady-state local concentration, will allow real-time monitoring of probe-receptor binding during application of an external stimulus. Furthermore, by using an appropriate animal model, these contrast agents have the potential to report upon diseased states where NMDA receptor density is decreased or receptor binding is inhibited.

A second area of future development is to modify the complex, **[Eu.L^{13}]**, such that the NMDA receptor-binding moiety will dictate the localisation profile of the complex. One possible way is by changing the conjugation point of the receptor-binding moiety (*Scheme 7*). Positioning the receptor-binding moiety at the periphery of the arylalkynylpyridyl chromophores may increase receptor binding and limit the degree of non-specific protein binding leading to complex internalisation.

The complex, **[Eu.L^{MD}]**, was used as a FRET donor to excite **[NIR-1]** and **[NIR-2]** in the fluorescence microscopy experiments in *chapter 6*. This complex was observed everywhere in the cell culture medium and did not bind to, or be taken up by, differentiated NSC-34 cells. Therefore, elaboration of the triazacyclononane core of this complex with a pendant lysine arm, conjugated to an NMDA receptor-binding moiety, may give rise to a Eu(III)-complex which has the ability to label the NMDA receptor of differentiated NSC-34 cells (*Scheme 7*). Providing one of these complexes is successful, they have the potential to replace standard radiolabelled ligands, or two component immunoflourescence ligands, used in biological assays.

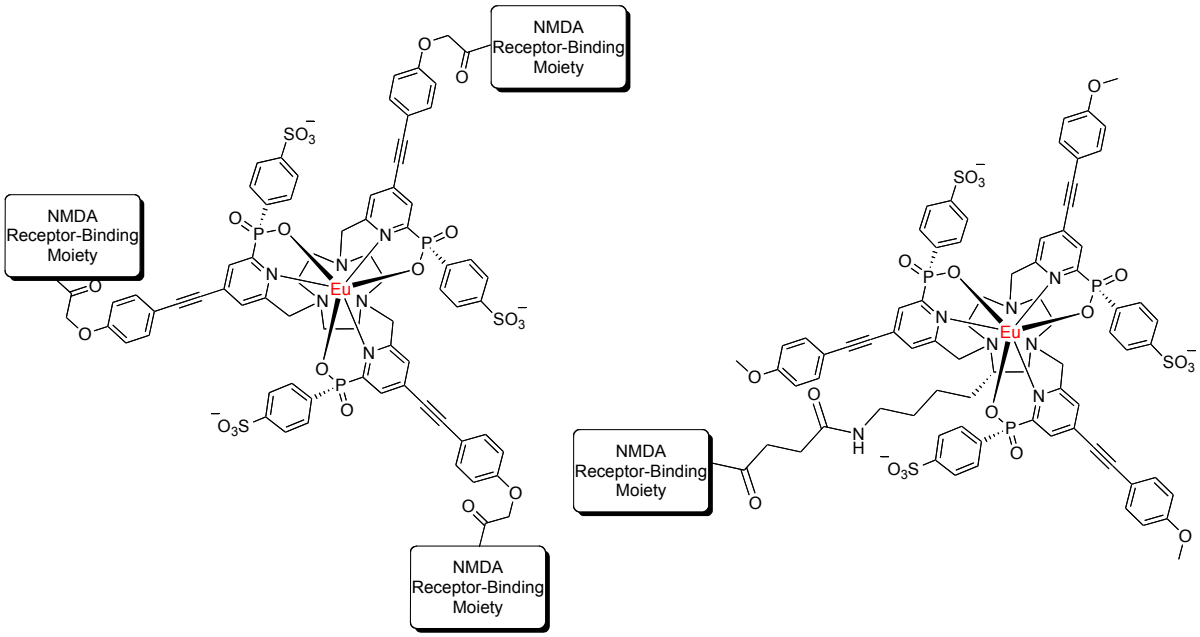

Scheme 7.

The final area in which future work should be concentrated is in the further evaluation of the photoacoustic contrast agents, more specifically, **[NIR-1]**. Preliminary studies have shown that **[NIR-1]** generates a large photoacoustic signal and can be easily detected *in vivo*. However, a more detailed analysis of the clearance rate of **[NIR-1]** in comparison to that of a non-targeted photoacoustic probe is needed to allow for a better understanding of the dynamics of NMDA receptor binding. Again, **[NIR-1]** and **[NIR-2]** are expected to be unable to penetrate the blood-brain-barrier. However, they could find use beyond basic

neuroscience research in diseased-based circumstances, when the blood-brain-barrier is damaged.

7.3 Final Thoughts

Detection and imaging of neuronal transmission and monitoring receptor activity is of prime importance in cognitive neuroscience. Despite the achievements of neuroscientists over the passed twenty to thirty years, this is yet to be realised for the NMDA receptor. The area of molecular imaging is rapidly growing and advances in instrument technology are allowing progress to this end. Nevertheless, it is apparent from this thesis that there is not one ultimate technique that suits all needs. Instead, there are several molecular imaging modalities to choose from depending on what you wish to visualise, and a greater insight is often achieved through using a variety of complementary imaging techniques. Therefore, the development of a chemical toolbox that provides imaging agents for several modalities is highly desirable, not only for NMDA receptor imaging, but for neuronal imaging in general.

CHAPTER EIGHT

Experimental

8. Experimental

8.1 Experimental Procedures

8.1.1 General Procedures

All solvents used were laboratory grade and anhydrous solvents, when required, were freshly distilled over the appropriate drying agent. Water was purified by the 'PuriteSTILLplus' system, with conductivity of ≤ 4 μS cm^{-1}. All reagents used were purchased from commercial suppliers (Acros, Aldrich, Fluka, Merck and Strem) and were used without further purification unless otherwise stated. Reactions requiring anhydrous conditions were carried out using Schlenk line techniques under an atmosphere of argon.

Thin layer chromatography was performed on neutral aluminium sheet silica gel plates (Merck Art 5554) and visualised under UV irradiation (254 nm), or using specific reagent staining. Preparative column chromatography was performed using silica gel (Merck Silica Gel 60, 230-400 mesh).

^{1}H, ^{13}C and ^{31}P NMR spectra were recorded in commercially available deuterated solvents on a Varian Mercury-400 (^{1}H 399.960, ^{13}C 100.572), Bruker Avance-400 (^{1}H 400.052, ^{13}C 100.603 and ^{31}P 161.91), Varian Inova-500 (^{1}H 499.722, ^{13}C 125.671,), Appleby VNMRS-600 (^{1}H 599.832, ^{13}C 150.828), or Varian VNMRA-700 (^{1}H 699.731, ^{13}C 175.948 and ^{31}P 283.26) spectrometer. All chemical shifts are given in ppm and all coupling constants are three-bond, unless otherwise stated, and are reported in Hz.

Low-resolution electrospray mass spectra (LR-MS) were recorded on a Fisons VG Platform II, Waters Micromass LCT or Thermo-Finnigan LTQ FT instrument operating in positive or negative ion mode as stated, with MeOH or MeCN as the carrier solvent. High-resolution electrospray mass spectra (HR-MS) were recorded using the Thermo-Finnigan LTQ FT mass spectrometer.

Reverse phase HPLC was performed at 298 K on a Perkin Elmer system, comprising a Perkin Elmer Series 200 pump, Perkin Elmer Series 200 auto-sampler, Perkin Elmer Series 200 UV/Vis detector and Perkin Elmer Series 200 fluorescence detector. Either an XBridge C18 column, 4.6 x 100 mm, i.d. 5 µm (flow rate 2 mL/minute) or an XBridge C18 column, 19 x 100 mm, i.d. 5 µm (flow rate 17 mL/ minute) was used with run times varying between 20 and 30 minutes. Solvent systems comprising gradient elusions of H_2O (0.1% FA)/ MeOH (0.1% FA) or 25 mM triethylammonium acetate buffer (pH 7)/ MeCN were used.

Melting points were recorded using a Gallenkamp (Sanyo) apparatus and are uncorrected.

Relaxivity measurements were carried out at 310 K, 60 MHz (1.4 T) on a Bruker Minispec mq60 instrument. The mean value of three independent measurements was recorded and averaged. The relaxivities of the compounds were calculated as the slope of the function shown in *equation 8*,

$$\frac{1}{T_{1,obs}} = \frac{1}{T_{1,d}} + r_1\left[Gd.L^n\right] \qquad (8)$$

where $T_{1,obs}$ is the measured T_1, $T_{1,d}$ is the diamagnetic contribution of the solvent (calculated to be 4000 ms) and $[Gd.L^n]$ is the concentration in mM of the appropriate Gd^{3+} complex (n = 1 - 12).

The apparent binding constant for the interaction of the Gd^{3+} complexes with Human Serum Albumin (HSA) was calculated using *equation 8.1*:

$$[X] = \frac{\frac{(R-R_0)/(R_1-R_0)}{K} + [Gd.L^n] * \frac{(R-R_0)}{(R_1-R_0)} - [Gd.L^n] * \left(\frac{(R-R_0)}{(R_1-R_0}\right)^2}{1 - \frac{(R-R_0)}{(R_1-R_0)}} \qquad (8.1)$$

$$K = \frac{[GdX]}{[X_f][Gd_f]}$$

where: [X]: the total concentration of HSA in the solution; [Gd.L^n]: the total concentration of the complex; K: the binding constant; *R*: relaxation rate of a given concentration of X; R_0: the initial relaxation rate; R_1: final relaxation rate; [Gd.X]: the concentration of the HSA- coordinated complex; [X_f]: the concentration of free HSA in the mixture; [Gd_f]: the concentration of the free complex.

All samples for optical analyses were contained in quartz cuvettes with a path length of 1 cm and a polished base. Measurements were recorded at 298 K. UV/Vis absorbance spectra were measured on a Perkin Elmer Lambda 900UV/Vis/NIR spectrometer using FL Winlab software. Samples were measured relative to a reference of pure solvent contained in a matched cell. Emission spectra were measured on a ISA Joblin-Yvon Spex Fluorolog-3 luminescent spectrometer using DataMax v2.20 software. Excitation wavelengths were selected according to the specific measurement. An integration time of 0.5 seconds, increment of 0.5 nm and scitation and emission slit widths of 2.5 and 1.5 nm, respectively, were used throughout. Lifetime measurements were carried out on a Perkin Elmer LS55 luminescence spectrometer.

8.1.2 Cell culture

Cell culture was performed by Dr's Robert Pal or Sven Gottschalk. In short, the NSC-34 cells were cultured in a 1:1 mixture of Dulbecco's modified Eagle's (DMEM) and F12 medium supplemented with fetal bovine serum (FBS, 10% v/v), non essential amino acids (0.5%) and Penicillin/Streptomycin (0.1%). At approximately 90% confluence after 3 healthy passages, cells were sub-cultured into a different growth medium, which contained a mixture of DMEM/Ham's F12 (1:1), FBS (1%), non-essential amino acids (1%) and Penicillin/Streptomycin (0.1%). Cells were allowed to proliferate over a period of several days to allow for the growth of functional NMDA receptors.

NIH-3T3 cells were maintained in an exponential growth as monolayers in an appropriate medium, which was supplemented with 10% fetal bovine serum (FBS) and 1% penicillin and streptomycin. Cells were incubated at 37 °C, 20% average humidity and 5% (v/v) CO_2.

8.1.2.1 Immunofluorescence measurements

NSC-34 cells grown and differentiated for 1 week on surface-modified glass chamber slides (Thermo Scientific Nunc, Denmark) were fixed for 10 min at room temperature with 4% paraformaldehyde (Roti®-Histofix 4%, Roth, Germany). Non-specific antibody binding sites were blocked by incubating for 30 min with 10% (v/v) goat-serum in PBST. Fixed cells were then incubated for 2 hours with the primary antibodies for the NMDA receptor subunits NMDAR-1 or NMDAR-2B (diluted in 1% BSA (Roth, Germany) in PBST) in a humidified chamber at RT. After washing, cells were incubated with secondary antibodies in 1% BSA in PBST in the humidified chamber in the dark. Afterwards cellular DNA was stained with 16.2µM Hoechst 33342 (Merck, Germany) for 15 min and slides were mounted overnight with Mowiol 4-88 (Roth, Germany) containing 50 mg/mL of the anti-bleaching reagent 1,4-diaza-bicyclo[2.2.2]octane (Roth, Germany). Microscopic images were taken on a Zeiss Axiovert 200 M microscope (Germany) using appropriate fluorescence filters and a Zeiss Plan APOCHROMAT 63x/1.4 oil DIC objective. Volocity acquisition and visualisation software 5.2.0 (Perkin Elmer, USA, MA) was used for image capture and analysis. The used antibodies were as follows and all antibodies were obtained from Abcam (UK, Cambridge). Primary antibodies, rabbit polyclonal to NMDAR2B or NMDAR1; secondary antibody, goat polyclonal to rabbit IgG – H&L conjugated to Cy3.

8.1.2.2 Cytotoxicity

IC_{50} values were determined using the MTT assay, which makes use of the conversion of MTT (3-(4,5-dimethylthiazol-2-yl)-2,5-diphenyltetrazolium bromide) to a purple formazan product by the mitochondrial dehydrogenase of

viable cells. This insoluble formazan was quantified spectrophotometrically upon dissolution in DMSO. Approximately 5 x 10^3 differentiated NSC-34 cells in 100 µL culture medium were seeded into each well of flat-bottomed 96-well plates and allowed to attach overnight. Complex solutions were added to triplicate wells to give final concentrations over a 2-log range. Following 24 h incubation, MTT (1.0 mM) was added to each well, and the plates incubated for a further 4 h. The culture medium was removed, and DMSO (150 µL) was added. The plates were shaken for 20 seconds and the absorbance measured immediately at 540 nm in a microplate reader. IC_{50} values were determined as the drug concentration required to reduce the absorbance to 50% of that in the untreated, control wells, and represent the mean for data from at least three independent experiments

8.1.3 Measurement of Cellular Relaxation Rates at 3 T

Differentiated NSC-34 cells were grown to confluency and trypsinised with Trypsin/EDTA 0.05/0.02% (w/v) (Biochrom AG, Germany), centrifuged and re-suspended to 1 x 10^7 cells/ 500 µL HBSS in 750 µL Eppendorf tubes. A maximum of 20 µL of highly concentrated stock solutions of the compounds were added to give 200 µM solutions; cells were incubated for 45 min. at 37°C, 10% CO_2. Afterwards, cells were centrifuged (300×g, 5 min., RT) and the supernatant was kept for MR- measurements. Cells were washed once with HBSS, centrifuged again (300×g, 5 min., RT) and re-suspended carefully in 500 µL of HBSS. In some experiments the wash-solution was also kept for MR-measurements. Cells were allowed to settle down before making MR-measurements. MR imaging of the cell pellets and supernatants, data analysis and determination of the cellular relaxation rates $R_{1,cell}$ were assessed from the measured T_1 values, according to the literature.

Briefly, MR measurements were performed on a clinical 3T (128 MHz, 21°C) human MR scanner (MAGNETOM Tim Trio, Siemens Healthcare, Germany). Longitudinal relaxation times (T_1) were measured using an inversion recovery sequence to obtain images from a 1 mm thick slice through the samples. The inversion time (T_i) was varied from 23 ms to 3000 ms in about 12-17 steps.

Images were read out with a turbo spin echo technique, acquiring 5 echoes per scan. The repetition time (T_R) was 10.000 ms to ensure complete relaxation. A matrix of 256 x 256 voxels was used over a field-of-view of 110 x 110 mm^2. Six averages per T_i were possible within 18 min.

Fitting to relaxivity curves was done using self-written routines in MATLAB 6.5 R13 (The Mathworks Inc., USA). T_1 relaxation data with varying $t = T_R$ were fitted to $S=S_0(1-a \times \exp(-t/T_1))$. Nonlinear least-squares fitting of three parameters S_0 (initial signal at t=0), T_1 and a was done for each voxel with the Gauss-Newton method (MATLAB function nlinfit). For each fitted parameter, the 95% confidence intervals were calculated (MATLAB functions nlparci, nlpreci) and used as an error estimate of the fitted relaxation times T_1 and S_0. The fit procedure resulted in parameter maps of T_1, S_0 and corresponding error maps σT_1, σS_0.

Circular image-regions in the tubes were defined as Regions Of Interest (ROIs), and the means and distribution width of the relaxation times of voxels in these regions were calculated. An iterative Gaussian fit was used to determine mean and standard deviation (SD) of a distribution with outliers' correction. For this purpose, a distribution histogram was first fitted to a Gaussian to estimate the mean and SD. The tails of the distribution were then discarded by using a threshold of three SDs. A repeated fit proved to be robust and converged to the 'true' Gaussian mean and width of the distribution barring the outliers, observed as a result of the non-linear fit of noisy voxels. The processing of the relaxation data thus resulted in specific $R_1 = 1/T_1$ values for each tube sample, including the standard deviation in the selected ROI ensemble. The ensemble error matched closely the errors of a single-voxel fit, which showed that no further systematic errors were introduced by the image encoding.

8.1.4 Confocal Microscopy and Cell Spectral Imaging

Cell images and co-localisation experiments of **[Gd.L$^{11\text{-}12}$]** and **[Eu.L$^{12\text{-}14}$]** were obtained using a Leica SP5 II microscope. A HeNe laser was used to visualise SA-AF488 fluorescence. The microscope was equipped with a triple channel imaging detector, comprising two conventional PMT systems and a HyD hybrid avalanche

photodiode detector. The latter part of the detection system, when operated in the BrightRed mode, is capable of improving imaging sensitivity above 550 nm by 25%, reducing signal to noise by a factor of 5. The pinhole was always determined by the Airy disc size, calculated from the objective in use (HCX PL APO 63x/1.40 NA LbdBlue), using the lowest excitation wavelength (488 nm). Scanning speed was adjusted to 400 Hz in a bidirectional mode, to ensure both sufficient light exposure and enough time to collect the emitted light from the optical probes (1024 x 1024 frame size, a pixel size of 120 x 120 nm and depth of 0.89 μm). The average image intensity of each phase was assessed as triplicates using 3 cells (excluding the axon) within each image.

Cell Microscopy and spectral imaging of **[NIR-1]** and **[NIR-2]** in cells was achieved using a custom built microscope (modified Zeiss Axiovert 200M), using a Zeiss APOCHROMAT 63x/1.40 NA objective combined with a low voltage 365 nm pulsed UV LED focused, collimated excitation source (1.2W). For rapid spectral acquisition the microscope was equipped at the X1 port with a Peltier cooled 2D-CCD detector (Ocean Optics) used in an inverse 100 Hz time gated sequence. The spectrum was recorded from 400-800 nm with a resolution of 0.24 nm and the final spectrum was acquired using an averaged 10,000 scan duty cycle. Probe lifetimes were measured on the same microscope platform using a novel cooled PMT detector (Hamamatsu H7155) interchangeable on the X1 port. Both the control and detection algorithm were written in LabView2011.

8.1.5 Multispectral Optoacoustic Imaging

In short, a tunable optical parametric oscillator pumped by an Nd:YAG laser allows excitation from 680 nm to 980 nm. Laser pulse duration is below 10 ns and the pulse repetition frequency is 10 Hz. The beam is coupled into a custom fiber bundle that is divided into 10 output arms, allowing even illumination around the circumference of the mouse with a ring-shape pattern. A custom-made piezo composite ultrasonic cylindrically focused transducer array with 256 elements and a central frequency of 5 MHz is used for detection. Transducer array, fiber bundle outputs and sample holder are submerged in a water bath maintained at 34 °C. Samples are placed in a horizontal position

inside a thin polyethylene membrane without direct contact with water. This arrangement allows a convenient acoustic coupling between the sample and the transducer array. In case of imaging mice the animals were kept under isoflurane anesthesia during the whole imaging process.

Differentiated NSC-34 cells were grown to confluency and trypsinised with Trypsin/EDTA 0.05/0.02% (w/v), centrifuged and re-suspended to 2.5 x 10^5 cells/ 250 µL in incubation buffer (HBSS supplemented with 20mM HEPES, pH 7.2) in 750 µL Eppendorf tubes. A maximum of 20 µL of highly concentrated stock solutions of either **[NIR-1]** or **[NIR-2]** were added to give solutions with the desired concentrations. Cells were incubated for 20 minutes at 37 °C, 5% CO_2. Afterwards, cells were centrifuged (300×g, 5 min., RT) and the supernatant was kept for MSOT-measurements. Cells were washed once with HBSS, centrifuged again (300×g, 5 min., RT) and re-suspended carefully in 250 µL of HBSS. The cell-solution was then embedded into an agar phantom for MSOT-imaging. In short, the labeled cells were enclosed within a 3 mm diameter plastic tube embedded into an 2 cm-diameter cylindrical phantom made of 1.3% agar and 1.2% by volume of Intralipid emulsion (Sigma-Aldrich). This mix leads to an optically diffusive medium with acoustic properties similar those of tissue. MSOT imaging was then done in one cross-sectional imaging plane (~200 µm in plane resolution). The phantom images were reconstructed using the interpolated model-matrix inversion. Afterwards, linear spectral unmixing was applied to each set of multiwavelengths images to resolve absorber specific signals. For each pixel the total measured optoacoustic spectrum was fitted to the known spectra of the contrast agent.

8.2 Synthetic Procedures

3-Amino-4-ethoxy-3-cyclobutene-1,2-dione, 1[1]

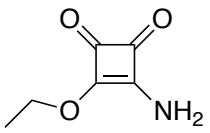

To a solution of 3,4-diethoxy-3-cyclobutene-1,2-dione (888 μL, 6.0 mmol) in anhydrous EtOH (15 mL), was added a solution of NH_3 in EtOH (3.3 mL, 6.6 mmol) and the reaction mixture was stirred at room temperature for 16 hours. EtOH was removed under reduced pressure and the solid residue triturated with cold hexane to reveal the title compound as a white powder (815 mg, 96%). ^{1}H NMR ($CDCl_3$, 400 MHz) δ 1.47 (3H, t, J = 7, $OCH_2C\mathbf{H}_3$), 4.47 (2H, q, J = 7, $OC\mathbf{H}_2CH_3$), 5.83 (2H, s, br, $N\mathbf{H}_2$). ^{13}C NMR ($CDCl_3$, 400 MHz) δ 15.9 ($OCH_2\mathbf{C}H_3$), 70.1 ($O\mathbf{C}H_2CH_3$), 173.4 (C=$\mathbf{C}NH_2$), 179.2 (C=$\mathbf{C}$OEt), 184.4, 189.2 ($\mathbf{C}$O). MS (ES^-) *m/z* 140.1 $[M-H]^-$; $C_6H_7NO_3Na$ requires 164.0315; found 164.0324. R_f = 0.28 (DCM/MeOH, 95:5). M. Pt. 143-145 °C.

tert-Butyl (2-ethoxy-3,4-dioxocyclobut-1-en-1-yl)carbamate, 2

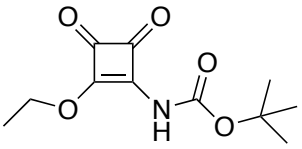

3-Amino-4-ethoxy-3-cyclobutene-1,2-dione (4.76 g, 33.7 mmol) and di-*tert*-butyl-dicarbonate (7.40 mg, 33.9 mmol) were dissolved in dichloromethane (500 mL), to which triethylamine (4.70 mL, 33.7 mmol) was added and the resulting solution stirred at room temperature for 24 h. At this point a further portion of di-*tert*-butyl-dicarbonate and triethylamine were added and stirred again for 24 h. Once no further change was observed by TLC, the reaction was concentrated under reduced pressure to yield a crude orange residue, which was purified by column chromatography (DCM 100%; R_f = 0.6), to give a light yellow solid (4.46

g, 55%). ^{1}H NMR ($CDCl_3$, 400 MHz) δ 1.51 (3H, t, J = 7, $OCH_2C\mathbf{H}_3$), 1.54 (9H, s, $C(C\mathbf{H}_3)_3$), 4.89 (2H, q, J = 7, $OC\mathbf{H}_2CH_3$), 7.53 (1H, s, br, N**H**). ^{13}C NMR ($CDCl_3$, 101 MHz) δ 16.0 ($OCH_2\mathbf{C}H_3$), 28.1 ($C(\mathbf{C}H_3)_3$), 70.8 ($O\mathbf{C}H_2CH_3$), 84.6 ($\mathbf{C}(CH_3)_3$), 149.0 (C=**C**NH), 167.2 (C=**C**OEt), 182.3, 187.1, 187.8 (**C**O). MS (ES^+) *m/z* = 242.1 $[M+H]^+$; $C_{11}H_{15}NO_5$ requires 242.1022; found 242.1023. M. Pt. 163-165 °C.

tert-Butyl 2-((2-((_tert_-butoxycarbonyl)amino)-3,4-dioxocyclobut-1-en-1-yl)amino)acetate, 3

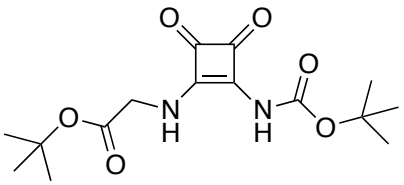

To a solution of *tert*-butyl (2-ethoxy-3,4-dioxocyclobut-1-en-1-yl)carbamate (200 mg, 0.83 mmol) in anhydrous ethanol (10 mL) was added a solution of glycine *tert*-butyl ester hydrochloride (140 mg, 0.83 mmol) and diisopropylethylamine (145 μL, 0.83 mmol) in anhydrous ethanol (2 mL), over a two hour period. The resulting mixture was stirred at room temperature and reaction progress monitored by TLC. Upon consumption of starting materials, the ethanol was removed under reduced pressure and the crude residue purified by column chromatography (DCM/MeOH, 100% to 95:5; R_f = 0.62) to give a light yellow solid (220 mg, 82%). ^{1}H NMR ($CDCl_3$, 400 MHz) δ 1.49 (9H, s, $C(C\mathbf{H}_3)_3$), 1.51 (9H, s, $C(C\mathbf{H}_3)_3$), 4.40 (2H, d, J = 6, $C\mathbf{H}_2$), 7.77 (1H, s, br, N**H**). ^{13}C NMR ($CDCl_3$, 101 MHz) δ 28.1, 28.2 ($C(\mathbf{C}H_3)_3$), 45.7 ($\mathbf{C}H_2$), 83.2, 84.6 ($\mathbf{C}(CH_3)_3$), 151.6 (C=**C**NHBoc), 159.8 (C=**C**$NHCH_2$), 168.3, 171.4, 182.5, 187.2 (**C**O). MS (ES^+) *m/z* = 349.2 $[M+Na]^+$; $C_{15}H_{22}N_2O_6Na$ requires 349.1387; found 349.1376. M.Pt >250 °C.

tert-Butyl 2-((2-((_tert_-butoxycarbonyl)amino)-3,4-dioxocyclobut-1-en-1-yl)(2-methoxy-2-oxoethyl)amino)acetate, 4

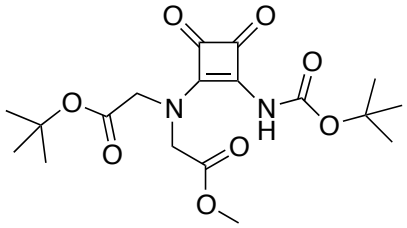

To a solution of *tert*-butyl 2-((2-((*tert*-butoxycarbonyl)amino)-3,4-dioxocyclobut-1-en-1-yl)amino)acetate (100 mg, 0.31 mmol) and NaH (20 mg, 0.50 mmol) in anhydrous DMF (5 mL) was added methylbromoacetate (50 μL, 0.50 mmol). The resulting solution was stirred at 40 °C for 48 hours when the mixture was cooled to room temperature and the solvent removed under reduced pressure. The crude residue was then taken up into EtOAc (20 mL) and H_2O (15 mL) added. The layers were separated and the aqueous portion was extracted with EtOAc (3 x 50 mL). The organic portions were combined, dried over $MgSO_4$, filtered and the solvent removed under reduced pressure. The crude residue was purified by column chromatography (DCM/MeOH, 100% to 95:5 using 0.5% increments; R_f = 0.75) to give a light green viscous oil (116 mg, 94%). ^{1}H NMR ($CDCl_3$, 700 MHz) δ 1.48 (9H, s, C(C**H**$_3$)$_3$), 1.49 (9H, s, C(C**H**$_3$)$_3$, 3.76 (3H, s, C**H**$_3$), 4.42 (2H, d, J = 6, C**H**$_2$CO$_2$^{t}Bu), 4.82 (2H, s, C**H**$_2$CO$_2$Me), 7.84 (1H, br. s, N**H**). ^{13}C NMR ($CDCl_3$, 176 MHz) δ 27.9, 28.2 (C(**C**H$_3$)$_3$), 45.7 (**C**H$_2$CO$_2$^{t}Bu), 47.6 (**C**H$_2$CO$_2$Me), 52.6 (**C**H$_3$), 83.1, 86.7 (**C**(CH$_3$)$_3$), 151.6 (C=**C**NHBoc), 161.3 (C=**C**N(CH$_2$)$_2$), 168.2, 168.9, 171.2, 182.7, 188.0 (**C**O). MS (ES$^+$) *m/z* = 399.3 [M+H]$^+$; $C_{18}H_{26}N_2O_8Na$ requires 421.1584; found 421.1587.

2-((2-(*tert*-Butoxy)-2-oxoethyl)(2-((*tert*-butoxycarbonyl)amino)-3,4-dioxocyclobut-1-en-1-yl)amino)acetic acid, 5

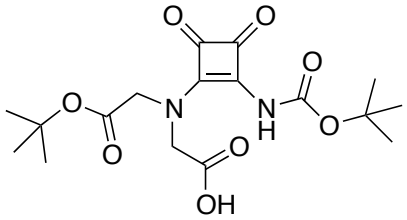

tert-Butyl 2-((2-((*tert*-butoxycarbonyl)amino)-3,4-dioxocyclobut-1-en-1-yl)(2-methoxy-2-oxoethyl)amino)acetate (116 mg, 0.29 mmol) was dissolved in a mixture of THF (3 mL) and methanol (2 mL). To the solution was added LiOH powder (7 mg, 0.29 mmol) as a solution in H_2O (1 mL). The reaction was stirred at room temperature for 1 hour with loss of methyl ester verified by ESI-MS, ^{1}H NMR (loss of methyl singlet at 3.76 ppm) and TLC. At this point, the solvent was evaporated under reduced pressure and the glassy yellow solid taken up into purite H_2O. The pH was adjusted to pH 7 and the solution lyophilized. This revealed *the title compound*, which was used directly in the next step without further purification. ^{1}H NMR (D_2O, 400 MHz) δ 1.36-1.42 (18H, s, C(C**H**$_3$)$_3$), 3.92-4.92 (4H, m, C**H**$_2$NC**H**$_2$). MS (ES$^-$) *m/z* = 403.2 [M-2H+3Li]$^+$.

***tert*-Butyl 2-((2-((*tert*-butoxycarbonyl)amino)-3,4-dioxocyclobut-1-en-1-yl)amino)propanoate, 6**

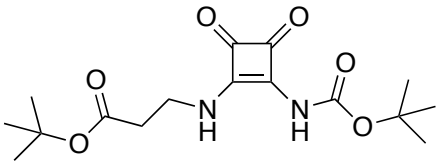

A solution of *tert*-butyl (2-ethoxy-3,4-dioxocyclobut-1-en-1-yl)carbamate (300 mg, 1.24 mmol) in anhydrous ethanol (12 mL) was treated with a solution of *β*-alanine *tert*-butyl ester hydrochloride (226 mg, 1.24 mmol) and diisopropylethylamine (216 μL, 1.24 mmol) in anhydrous ethanol (3mL) over a two hour period. The reaction was then stirred at room temperature and

monitored by TLC. Upon consumption of starting materials, excess ethanol was removed under reduced pressure and the crude residue purified by column chromatography (DCM/MeOH, 100% to 95:5; R_f = 0.52) to give a light yellow solid (332 mg, 79%). ^{1}H NMR ($CDCl_3$, 700 MHz) δ 1.45 (9H, s, C(C**H**$_3$)$_3$), 1.46 (9H, s, C(C**H**$_3$)$_3$, 2.57 (2H, t, J = 7, CH_2C**H**$_2$$CO_2$^{t}Bu), 3.93 (2H, app. q, J = 7, C**H**$_2$$CH_2$$CO_2$^{t}Bu), 7.85 (1H, br. s, N**H**), 8.90 (1H, br. s, N**H**). ^{13}C NMR ($CDCl_3$, 176 MHz) δ 28.0, 28.1 (C(**C**H$_3$)$_3$), 36.9, 39.9 ((**C**H$_2$)$_2$), 81.7, 83.9 (**C**(CH$_3$)$_3$), 152.0 (C=**C**NHBoc), 160.1 (C=**C**NHCH$_2$), 170.4, 171.6, 182.3, 187.0 (**C**O). MS (ES$^+$) *m/z* = 363.3 [M+Na]$^+$; $C_{16}H_{24}N_2O_6Na$ requires 363.1548; found 363.1532. M.Pt >250 °C.

tert-Butyl 2-((2-((*tert*-butoxycarbonyl)amino)-3,4-dioxocyclobut-1-en-1-yl)(2-methoxy-2-oxoethyl)amino)propanoate, 7

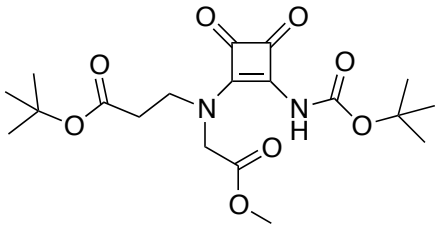

To a solution of *tert*-butyl 2-((2-((*tert*-butoxycarbonyl)amino)-3,4-dioxocyclobut-1-en-1-yl)amino)propanoate (330 mg, 0.97 mmol) and NaH (28 mg, 1.16 mmol) in anhydrous DMF (8 mL) was added methylbromoacetate (110 μL, 1.16 mmol) dropwise. The resulting solution was stirred at 40 °C for 48 hours, at which point the mixture was cooled to room temperature and the solvent removed under reduced pressure. The crude residue was then taken up into EtOAc (20 mL) and H_2O added (15 mL). The layers were separated and the aqueous layer was extracted with EtOAc (3 x 50 mL), with the combined organic portions dried over $MgSO_4$. Filtration and removal of the volatiles under reduced pressure gave a crude residue which was purified by column chromatography (DCM/MeOH, 100% to 95:5 using 0.5% increments; R_f = 0.74) to give a light green viscous oil (280 mg, 71%). ^{1}H NMR ($CDCl_3$, 700 MHz) δ 1.45 (9H, s, C(C**H**$_3$)$_3$), 1.46 (9H, s, C(C**H**$_3$)$_3$), 2.57 (2H, t, J = 7, C**H**$_2$$CH_2$), 3.75 (3H, s, C**H**$_3$), 3.96 (2H, app. q, J = 7, CH_2C**H**$_2$), 4.81 (2H, s, C**H**$_2$$CO_2$Me), 7.93 (1H, br. s, N**H**). ^{13}C NMR

($CDCl_3$, 176 MHz) δ 27.8, 28.1 (C(**C**H_3)$_3$), 36.8, 39.8 (**C**H_2**C**H_2), 47.6 (**C**H_2CO_2Me), 52.6 (**C**H_3), 81.7, 85.4 (**C**$(CH_3)_3$), 151.5 (C=**C**NHBoc), 160.9 (C=**C**N$(CH_2)_2$), 169.0, 170.6, 171.2, 182.3, 188.0 (**C**O). MS (ES^+) *m/z* = 435.7 $[M+Na]^+$; $C_{19}H_{28}N_2O_8Na$ requires 435.1743; found 435.1548.

2-((3-(*tert*-Butoxy)-3-oxopropyl)(2-((*tert*-butoxycarbonyl)amino)-3,4-dioxocyclobut-1-en-1-yl)amino)acetic acid, 8

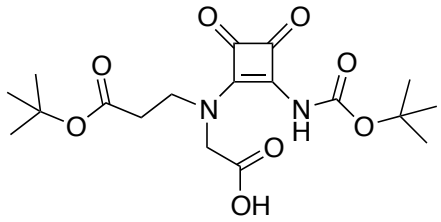

tert-Butyl 2-((2-((*tert*-butoxycarbonyl)amino)-3,4-dioxocyclobut-1-en-1-yl)(2-methoxy-2-oxoethyl)amino)propanoate (154 mg, 0.37 mmol) was dissolved in a mixture of THF (3 mL) and methanol (2 mL). To the solution was added LiOH powder (9 mg, 0.37 mmol) as a solution in H_2O (1 mL). The reaction was stirred at room temperature for 1 hour, with loss of methyl ester verified by ESI-MS, ^{1}H NMR (loss of methyl singlet at 3.75 ppm) and TLC. At this point, the solvent was evaporated under reduced pressure and the glassy yellow solid taken up into purite H_2O. The pH was adjusted to pH 7 and the solution lyophilized. This revealed *the title compound*, which was used directly in the next step without further purification. ^{1}H NMR (D_2O, 400 MHz) δ 1.36-1.42 (18H, s, C(C**H**$_3$)$_3$), 2.54-2.66 (2H, m, C**H**$_2$), 3.50-3.65 (2H, m, C**H**$_2$), 4.08-4.27 (2H, m, C**H**$_2$). MS (ES^+) *m/z* = 415.3 $[M-2H+3Li]^+$.

Diethyl (3-(1,3-diocoisoindolin-2-yl)propyl) phosphonate, 9[2]

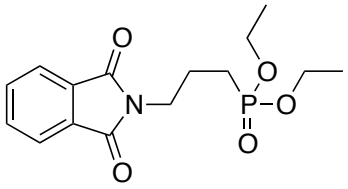

To the solution of potassium phthalamide (2.89 g, 15.61 mmol) and NaH (374 mg, 15.6 mmol) in anhydrous DMF (25 mL) was added diethyl-3-bromopropyl phosphonate (2.0 mL, 10.41 mmol) and the resulting mixture heated to 100 °C for 20 hours. After this time, the mixture was cooled to room temperature and the precipitate filtered. The filtrate was concentrated under reduced pressure to give a light green residue, which was taken up into $CHCl_3$ (30 mL). The chloroform was washed with H_2O (3 x 10 mL) and dried over $MgSO_4$. After filtration, the solvent was removed under reduced pressure to give a light green oil (1.16 g, 34%). ^{1}H NMR ($CDCl_3$, 400 MHz) δ 1.30 (6H, t, J = 7, $P(OCH_2C\mathbf{H}_3)_2$), 1.73-2.03 (4H, m, $PC\mathbf{H}_2C\mathbf{H}_2$), 3.75 (2H, t, J = 7, $P(CH_2)_2C\mathbf{H}_2$), 4.07 (4H, qd, $^3J_{H\text{-}H}$ = 7, $^3J_{H\text{-}P}$ = 3, $P(OC\mathbf{H}_2CH_3)_2$), 7.70-7.73 (2H, m, Ar-**H**), 7.83-7.86 (2H, m, Ar-**H**). ^{13}C NMR ($CDCl_3$, 101 MHz) δ 16.6 (d, ^{3}J = 6, $P(OCH_2\mathbf{C}H_3)_2$), 22.1 (d, ^{2}J = 5, $PCH_2\mathbf{C}H_2CH_2$), 23.6 (d, ^{1}J = 143, $P\mathbf{C}H_2(CH_2)_2$), 38.4 (d, ^{3}J = 20, $P(CH_2)_2\mathbf{C}H_2$), 61.8 (d, ^{2}J = 7, $P(O\mathbf{C}H_2CH_3)_2$), 123.4 , 133.1, 134.2 (Ar-**C**), 168.4 (**C**O). ^{31}P NMR ($CDCl_3$, 162 MHz) δ 29.85. MS (ES^+) *m/z* 326.2 $[M+H]^+$; $C_{15}H_{21}NO_5P$ requires 326.1157; found 326.1160.

Diethyl (3-aminopropyl) phosphonate, 10[2]

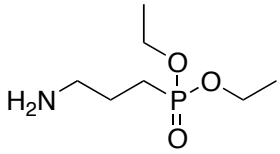

Diethyl (3-(1,3-diocoisoindolin-2-yl)propyl) phosphonate (1.16 g, 3.55 mmol) and hydrazine monohydrate (238 μL, 4.90 mmol) were stirred as a solution in anhydrous ethanol (13 mL) and heated to reflux. After 20 hours, ethanol was

removed under reduced pressure and the white residue that remained was taken up into DCM (15 mL). After sonication, the precipitate was filtered and the filtrate concentrated. To this was added $CHCl_3$ (10 mL), which yielded a second batch of precipitate that was again filtered. The filtrate was concentrated under reduced pressure to yield a green oil (639 mg, 92%). ^{1}H NMR ($CDCl_3$, 400 MHz) δ 1.29 (6H, t, J = 7, P(OCH$_2$C**H**$_3$)$_2$), 1.68-1.86 (4H, m, PC**H**$_2$C**H**$_2$), 2.78 (2H, t, J = 7, P(CH$_2$)$_2$C**H**$_2$N), 3.33 (2H, br. s, N**H**$_2$), 3.99-4.13 (4H, qd, $^3J_{H\text{-}H}$ = 7, $^3J_{H\text{-}P}$ = 3, P(OC**H**$_2$CH$_3$)$_2$). ^{13}C NMR ($CDCl_3$, 101 MHz) δ 16.6 (d, ^{3}J = 6, P(OCH$_2$**C**H$_3$)$_2$), 22.1 (d, ^{1}J = 142, P**C**H$_2$(CH$_2$)$_2$), 26.1 (d, ^{2}J = 5, (PCH$_2$**C**H$_2$CH$_2$), 42.4 (d, ^{3}J = 17, P(CH$_2$)$_2$**C**H$_2$), 61.6 (d, ^{2}J = 7, P(OC**H**$_2$CH$_3$)$_2$). ^{31}P NMR ($CDCl_3$, 162 MHz) δ 31.24. MS (ES$^+$) *m/z* 196.6 [M+H]$^+$; $C_7H_{19}NO_3P$ requires 196.1103; found 196.1120.

tert-Butyl (2-((diethoxyphosphoryl)ethyl)amino)-3,4-dioxocyclobut-1-en-1-yl)carbamate, 11

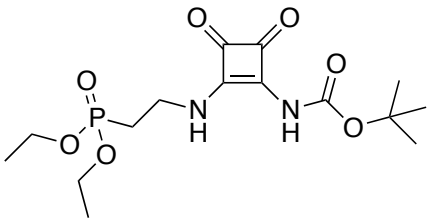

A solution of *tert*-butyl (2-ethoxy-3,4-dioxocyclobut-1-en-1-yl)carbamate (236 mg, 0.98 mmol) in anhydrous ethanol (12 mL) was treated with a solution of diethyl-2-aminoethyl phosphonate oxalate (443 mg, 1.64 mmol) and diisopropylethylamine (570 μL, 3.27 mmol) in anhydrous ethanol (4 mL) over a one hour period. The resulting mixture was allowed to stir at room temperature for 22 hours. After this time, ethanol was removed under reduced pressure to give an orange residue which was purified by column chromatography (DCM/MeOH, 100% to 95:5 using 0.5% increments; R_f = 0.37) to give a light green oil (223 mg, 60%). ^{1}H NMR ($CDCl_3$, 400 MHz) δ 1.30 (6H, t, J = 7, P(OCH$_2$C**H**$_3$)$_2$), 1.45 (9H, s, C(C**H**$_3$)$_3$), 2.07-2.15 (2H, m, PC**H**$_2$CH$_2$), 3.93-4.03 (2H, m, PCH$_2$C**H**$_2$N), 4.11 (4H, qd, $^3J_{H\text{-}H}$ = 7, $^3J_{H\text{-}P}$ = 3, P(OC**H**$_2$CH$_3$)$_2$), 7.76 (1H, t, J = 4, N**H**CH$_2$), 9.23 (1H, br. s, N**H**). ^{13}C NMR ($CDCl_3$, 101 MHz) δ 16.5 (d, ^{3}J = 6, P(OCH$_2$**C**H$_3$)$_2$), 27.8 (d, ^{1}J = 141, NHCH$_2$**C**H$_2$P), 27.9 (C(**C**H$_3$)$_3$), 38.5 (d, ^{2}J = 6, NH**C**H$_2$CH$_2$P), 62.1 (d, ^{2}J = 6, P(O**C**H$_2$CH$_3$)$_2$), 83.7 (**C**(CH$_3$)$_3$), 152.1, 160.4 (**C**=**C**),

171.3, 182.3, 187.1 (**C**O). ^{31}P NMR ($CDCl_3$, 162 MHz) δ 27.06. MS (ES^+) *m/z* = 399.2 $[M+Na]^+$; $C_{15}H_{25}N_2O_7PNa$ requires 399.1297; found 399.1276.

Methyl 2-((*tert*-butoxycarbonyl)amino)-3,4-dioxocyclobut-1-en-1-yl)(2-(diethoxyphosphoryl)ethyl)amino)acetate, 12

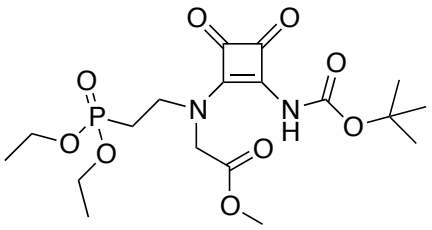

To a solution of methylbromoacetate (75 μL, 0.80 mmol) in anhydrous DMF (3 mL) was added a solution of *tert*-butyl (2-((diethoxyphosphoryl)ethyl)amino)-3,4-dioxocyclobut-1-en-1-yl)carbamate (200 mg, 0.53 mmol) and NaH (19 mg, 0.80 mmol) in DMF (4 mL) dropwise over a period of 10 minutes. The resulting solution was then stirred at 40 °C for 48 hours. Upon no further reaction, as observed by TLC, the DMF was removed under reduced pressure and the resulting residue taken up into EtOAc (10 mL). H_2O (10 mL) was added and the layers separated. The aqueous layer was extracted with EtOAc (3 x 40 mL) and the combined organic fractions dried over $MgSO_4$. The solution was filtered and EtOAc removed under reduced pressure to give the crude residue, which was purified by column chromatography (DCM/MeOH, 100% to 95:5 using 0.2% increments; R_f = 0.31) to give a light green oil (115 mg, 50%). ^{1}H NMR ($CDCl_3$, 400 MHz) δ 1.34 (6H, t, J = 8, $P(OCH_2C\mathbf{H}_3)_2$), 1.47 (9H, s, $C(C\mathbf{H}_3)_3$), 2.09-2.16 (2H, m, $PC\mathbf{H}_2CH_2$), 3.76 (3H, s, $C\mathbf{H}_3$), 3.98-4.08 (2H, m, $PCH_2C\mathbf{H}_2$), 4.09-4.21 (4H, qd, $^3J_{H\text{-}H}$ = 7, $^3J_{H\text{-}P}$ = 3, $P(OC\mathbf{H}_2CH_3)_2$), 4.83 (2H, s, $C\mathbf{H}_2CO_2Me$), 7.89 (1H, br. s, N**H**). ^{13}C NMR ($CDCl_3$, 101 MHz) δ 16.6 (d, ^{3}J = 6, $P(OCH_2\mathbf{C}H_3)_2$), 27.9 (d, ^{1}J = 141, $NHCH_2\mathbf{C}H_2P$), 27.9 ($C(\mathbf{C}H_3)_3$), 38.5 (d, ^{2}J = 6, $NH\mathbf{C}H_2CH_2P$), 47.6 ($\mathbf{C}H_2CO_2Me$), 52.6 ($\mathbf{C}H_3$), 62.2 (d, ^{2}J = 7, $P(O\mathbf{C}H_2CH_3)_2$), 85.2 ($\mathbf{C}(CH_3)_3$), 151.5, 161.0 (**C**=**C**), 168.9, 171.1, 182.4, 187.9 (**C**O). ^{31}P NMR ($CDCl_3$, 283 MHz) δ 27.83. MS (ES^+) *m/z* = 449.3 $[M+H]^+$; $C_{18}H_{29}N_2O_9PNa$ requires 471.1508; found 471.1513.

2-((2-((Tert-butoxycarbonyl)amino)-3,4-dioxocyclobut-1-en-1-yl)(2-(diethoxyphosphoryl)ethyl)amino)acetic acid, 13

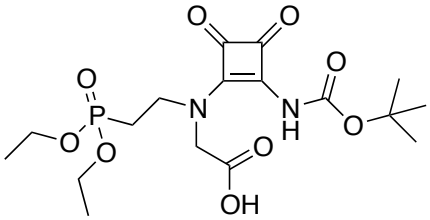

Methyl 2-((*tert*-butoxycarbonyl)amino)-3,4-dioxocyclobut-1-en-1-yl)(2-(diethoxyphosphoryl)ethyl)amino)acetate (185 mg, 0.41 mmol) was dissolved in MeOD (3 mL), to which KOD (39 mg, 0.68 mmol) was added as a solution in D_2O (4 mL). The resulting mixture was stirred at room temperature and reaction profile monitored by TLC, ^1H (loss of methyl singlet at 3.76 ppm) and ^{31}P NMR spectroscopy (no shift in ^{31}P signal). After 1 h, complete conversion of starting material was achieved and the solvent removed under reduced pressure. The solid residue was taken up in purite H_2O (5 mL) and the pH adjusted to about 7 using HCl (0.1 M). The resulting solution was lyophilized to give the product as a light green solid which was used directly in the next step without further purification. ^1H NMR (D_2O, 400 MHz) δ 1.27-1.35 (6H, m, $P(OCH_2C\mathbf{H}_3)_2$), 1.37-1.42 (9H, s, $C(C\mathbf{H}_3)_3$), 2.17-2.31 (2H, m, $PC\mathbf{H}_2CH_2$), 3.53-3.75 (2H, m, $PCH_2C\mathbf{H}_2$), 4.05-4.20 (4H, m, $P(OC\mathbf{H}_2CH_3)_2$), 4.88 (2H, $C\mathbf{H}_2CO_2H$). ^{31}P NMR (D_2O, 162 MHz) δ 30.59. MS (ES^+) *m/z* = 475.2 $[M+K]^+$.

***tert*-Butyl (2-((diethoxyphosphoryl)propyl)amino)-3,4-dioxocyclobut-1-en-1-yl)carbamate, 14**

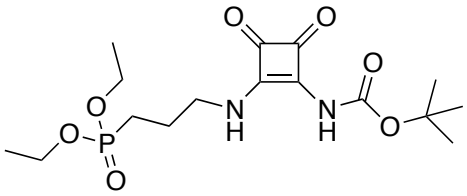

A solution of *tert*-butyl (2-ethoxy-3,4-dioxocyclobut-1-en-1-yl)carbamate (392 mg, 1.62 mmol) in anhydrous ethanol (19 mL) was treated with a solution of diethyl (3-aminopropyl) phosphonate (317 mg, 1.62 mmol) and

diisopropylethylamine (283 μL, 1.62 mmol) in anhydrous ethanol (4 mL) over a one hour period. The resulting mixture was allowed to stir at room temperature for 48 hours. After this time, ethanol was removed under reduced pressure to give an orange residue which was then purified by column chromatography (DCM/MeOH, 100% to 95:5 using 0.5% increments; R_f = 0.35) to give a yellow oil (266 mg, 42%). ^{1}H NMR ($CDCl_3$, 700 MHz) δ 1.33 (6H, t, J = 7, P(OCH$_2$C**H**$_3$)$_2$), 1.51 (9H, s, C(C**H**$_3$)$_3$), 1.79-1.83 (2H, m, PC**H**$_2$(CH$_2$)$_2$), 1.93-1.99 (2H, m, PCH$_2$C**H**$_2$CH$_2$), 3.79 (2H, m, P(CH$_2$)$_2$C**H**$_2$), 4.06-4.15 (4H, qd, $^3J_{H-H}$ = 7, $^3J_{H-P}$ = 3, P(OC**H**$_2$CH$_3$)$_2$), 7.51 (1H, br. s, N**H**), 7.96 (1H, br. s, N**H**). ^{13}C NMR ($CDCl_3$, 176 MHz) δ 16.6 (d, ^{3}J = 5, P(OCH$_2$**C**H$_3$)$_2$), 22.7 (d, ^{1}J = 143, NH(CH$_2$)$_2$**C**H$_2$P), 24.6 (d, ^{2}J = 5, PCH$_2$**C**H$_2$CH$_2$), 28.1 (C(**C**H$_3$)$_3$), 44.4 (d, ^{3}J = 18, NH**C**H$_2$(CH$_2$)$_2$P), 61.9 (d, ^{2}J = 7, P(O**C**H$_2$CH$_3$)$_2$), 84.5 (**C**(CH$_3$)$_3$), 151.8, 159.4 (**C**=**C**), 171.6, 182.1, 187.1 (**C**O). ^{31}P NMR ($CDCl_3$, 283 MHz) δ 30.70. MS (ES$^+$) *m/z* = 391.3 [M+H]$^+$; $C_{16}H_{28}N_2O_7P$ requires 391.1634; found 391.1639.

Methyl 2-((*tert*-butoxycarbonyl)amino)-3,4-dioxocyclobut-1-en-1-yl)(2-(diethoxyphosphoryl)propyl)amino)acetate, 15

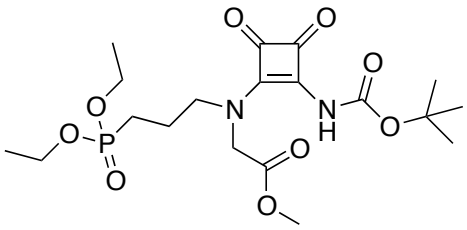

tert-Butyl (2-((diethoxyphosphoryl)propyl)amino)-3,4-dioxocyclobut-1-en-1-yl)carbamate (169 mg, 0.43 mmol) and NaH (15 mg, 0.65 mmol) were dissolved in anhydrous DMF (5 mL) and stirred at room temperature for 15 minutes. After this period, methylbromoacetate (61 μL, 0.65 mmol) was added and the resulting solution stirred at 40 °C for 48 hours. The resulting solution was cooled to room temperature and the solvent removed under reduced pressure. The residue was then taken up in EtOAc (50 mL) and H_2O (30 mL) added. The layers were separated and the aqueous washed with EtOAc (3 x 50 mL). The combined organic portions were dried over $MgSO_4$, filtered and the solvent removed under

reduced pressure to give the crude residue, which was then purified by column chromatography (DCM/MeOH, 100% to 95:5 using 0.2% increments; R_f = 0.43) to give a viscous yellow oil (126 mg, 63%). ^{1}H NMR ($CDCl_3$, 400 MHz) δ 1.31 (6H, t, J = 8, $P(OCH_2C\mathbf{H}_3)_2$), 1.47 (9H, s, $C(C\mathbf{H}_3)_3$), 1.75-1.84 (2H, m, $PC\mathbf{H}_2(CH_2)_2$), 1.89-1.99 (2H, m, $PCH_2C\mathbf{H}_2CH_2$), 3.76 (3H, s, $C\mathbf{H}_3$), 3.80 (2H, m, $P(CH_2)_2C\mathbf{H}_2$), 4.02-4.16 (4H, qd, $^3J_{H\text{-}H}$ = 7, $^3J_{H\text{-}P}$ = 3, $P(OC\mathbf{H}_2CH_3)_2$), 4.82 (2H, s, $C\mathbf{H}_2CO_2Me$), 7.66 (1H, s, br, N**H**). ^{13}C NMR ($CDCl_3$, 101 MHz) δ 16.6 (d, ^3J = 6, $P(OCH_2\mathbf{C}H_3)_2$), 22.7 (d, ^1J = 143, $N(CH_2)_2\mathbf{C}H_2P$), 24.6 (d, ^2J = 5, $PCH_2\mathbf{C}H_2CH_2$), 27.9 ($C(\mathbf{C}H_3)_3$), 44.2 (d, ^3J = 17, $N\mathbf{C}H_2(CH_2)_2P$), 47.6 ($\mathbf{C}H_2CO_2Me$), 52.6 ($\mathbf{C}H_3$), 61.9 (d, ^2J = 7, $P(O\mathbf{C}H_2CH_3)_2$), 85.6 ($\mathbf{C}(CH_3)_3$), 151.6, 160.9 (**C=C**), 168.9, 171.5, 182.3, 187.9 (**C**O). ^{31}P NMR ($CDCl_3$, 162 MHz) δ 29.89. MS (ES^+) *m/z* = 485.2 $[M+Na]^+$; $C_{19}H_{31}N_2O_9PNa$ requires 485.1665; found 485.1647.

2-((2-((*tert*-Butoxycarbonyl)amino)-3,4-dioxocyclobut-1-en-1-yl)(3-(diethoxyphosphoryl)propyl)amino)acetic acid, 16

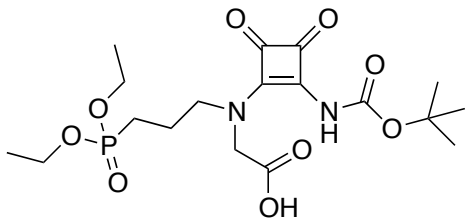

Methyl 2-((*tert*-butoxycarbonyl)amino)-3,4-dioxocyclobut-1-en-1-yl)(2-(diethoxyphosphoryl)propyl)amino)acetate (126 mg, 0.27 mmol) was dissolved in MeOD (3 mL), to which KOD (39 mg, 0.68 mmol) was added as a solution in D_2O (4 mL). The resulting mixture was stirred at room temperature and the reaction profile monitored by TLC, ^{1}H (loss of methyl singlet at 3.76 ppm) and ^{31}P NMR spectroscopy (no shift in ^{31}P signal). After 24 h, complete conversion of starting material was achieved and the solvent removed under reduced pressure. The solid residue was taken up in purite H_2O (5 mL) and the pH adjusted to about 7 using HCl (0.1 M). The resulting solution was lyophilized to give the product as a light green solid which was used directly in the next step without further purification. ^{1}H NMR (D_2O, 400 MHz) δ 1.20-1.34 (6H, m, $P(OCH_2C\mathbf{H}_3)_2$),

1.40-1.44 (9H, s, C(C**H**$_3$)$_3$), 1.78-2.06 (4H, m, (C**H**$_2$)$_2$), 3.36-3.57 (2H, m, C**H**$_2$), 4.07-4.32 (4H, m, P(OC**H**$_2$CH$_3$)$_2$), 4.81 (2H, m, C**H**$_2$). ^{31}P NMR (D_2O, 162 MHz) δ 34.24. MS (ES^+) *m/z* 490.3 $[M+K]^+$.

(S)-2-Bromo-6-(2-phenylcarbamate)hexanoic acid, 17[3]

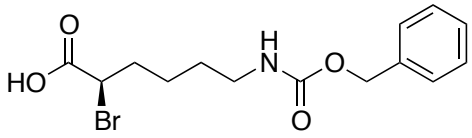

To a stirred solution of H-Lys(Z)-OH (5.0 g, 17.8 mmol), NaBr (5.1 g, 49.0 mmol) and 1M HBr (106 mL) at –5 ˚C, was added a solution of $NaNO_2$ (2.3 g, 33.87 mmol) in H_2O (21 mL) over a period of 40 minutes. The resulting yellow solution was stirred at room temperature overnight. After this period, H_2SO_4 (1.5 mL) was added to the reaction mixture, which was extracted with diethyl ether (3 x 100 mL). The organic phase was washed with brine (1 x 100 mL) and dried over $MgSO_4$. Filtration and removal of the solvent under reduced pressure yielded viscous yellow oil, which was used directly in the next step without further purification.

(S)-tert-Butyl 2-bromo-6-(2-phenylcarbamate)hexanoate, 18[3]

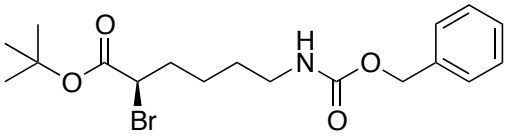

A solution of *(S)*-2-bromo-6-(2-phenylcarbamate)hexanoic acid (5.93 g, 17.3 mmol) in *tert*-butyl acetate (63 mL) and $HClO_4$ in H_2O (74 μL, 0.86 mmol) was stirred at room temperature for 16 hours. Upon completion, H_2O (80 mL) was added and the organic phase separated and washed with H_2O (60 mL) and 5 % Na_2CO_3 (1 x 60 mL). The combined organic fractions were then dried over $MgSO_4$, filtered and the solvent removed under reduced pressure. The sticky residue was then purified by column chromatography (hexane/EtOAc, 70:30; R_f

= 0.42) to give a viscous yellow oil (2.50g, 44% over two steps). ^{1}H NMR ($CDCl_3$, 700 MHz) δ 1.46 (9H, s, C(C**H**$_3$)$_3$), 1.49-1.55 (4H, m, br, C**H**$_2$C**H**$_2$CH$_2$NH), 1.90-2.03 (2H, m, br, CHC**H**$_2$), 3.19 (2H, dd, J = 7, 3, CH$_2$CH$_2$C**H**$_2$NH), 4.08 (1H, t, J = 7, C**H**Br), 4.88 (1H, s, br, N**H**) 5.08 (2H, s, OC**H**$_2$Ph), 7.34 (5H, m, Ar-**H**). ^{13}C NMR ($CDCl_3$, 176 MHz) δ 24.5 (**C**H$_2$CH$_2$CH$_2$NH), 27.8 (C(**C**H$_3$)$_3$), 29.3 (CH$_2$**C**H$_2$CH$_2$NH), 34.5 (CH**C**H$_2$), 40.8 (CH$_2$CH$_2$**C**H$_2$NH), 47.6 (**C**Br), 66.7 (O**C**H$_2$Ph), 82.5 (**C**(CH$_3$)$_3$), 128.2, 128.6, 128.6, 136.7 (Ar-**C**), 156.5, 168.8 (**C**O). MS (ES$^+$) *m/z* 422.2 [M+Na]$^+$; $C_{18}H_{26}NO_4BrNa$ requires 422.0943; found 422.0945.

4,7-Bis-*tert*-butoxycarbonylmethyl-1,4,7,10-tetraaza-cyclododec-1-yl)acetic acid *tert*-butyl Ester, 19[4]

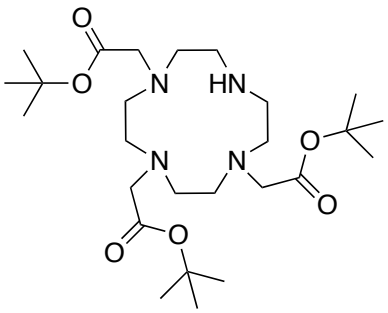

tert-butylbromoacetate (11.6 mL, 78.3 mmol) was added to a stirred solution of 1,4,7,10-tetraazacyclododecane (5.0 g, 28.9 mmol) and $NaHCO_3$ (6.5 g, 78.0 mmol) in anhydrous CH_3CN (190 mL) under an atmosphere of argon. The reaction was stirred overnight at room temperature, at which point the mixture was filtered and the solvent evaporated under reduced pressure. Toluene was added to the residue, which allowed precipitation of the *title compound* as a white solid (8.4 g, 57%). ^{1}H NMR ($CDCl_3$, 400 MHz) δ 1.46 (27H, s, C(C**H**$_3$)$_3$), 2.80-2.93 (12H, m, br, C**H**$_2$), 3.10 (4H, s, br, C**H**$_2$), 3.29 (2H, s, C**H**$_2$CO), 3.37 (4H, s, C**H**$_2$CO), 10.07 (1H, s, N**H**). ^{13}C NMR ($CDCl_3$, 101 MHz) δ 27.2, 28.2 (C(**C**H$_3$)$_3$), 46.5, 47.8, 48.2 (**C**H$_2$), 50.3, 57.2 (**C**H$_2$O), 80.7, 80.9 (**C**(CH$_3$)$_3$), 168.6, 169.5 (**C**O). MS (ES$^+$) *m/z* 515.6 [M+H]$^+$; $C_{26}H_{51}O_6N_4$ requires 515.3803; found 515.3809. M. Pt. 184-185 °C.

_(R)_-tri-_tert_-Butyl-2,2',2''-(10-(1-(_tert_-butoxy)-1oxo-6-(2-phenylacetamido)hexan-2-yl)-1,4,7,10-tetraazacyclododecane-1,4,7-triyl)triacetate, 20

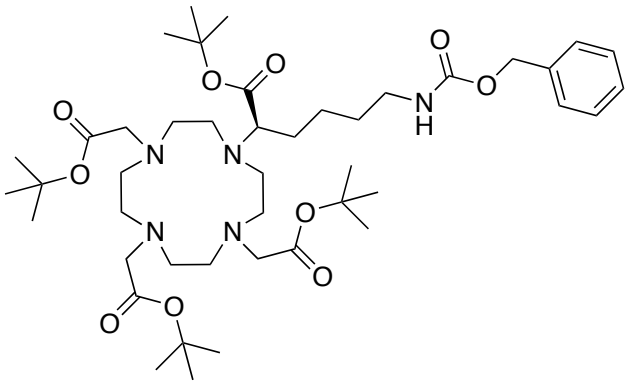

4,7-Bis-*tert*-butoxycarbonylmethyl-1,4,7,10-tetraaza-cyclododec-1-yl)acetic acid *tert*-butyl ester (1.57 g, 3.05 mmol), *(S)*-*tert*-butyl 2-bromo-6-(2-phenylcarbamate)hexanoate (1.41 g, 3.70 mmol) and K_2CO_3 (843 mg, 6.1 mmol) were dissolved in anhydrous acetonitrile (15 mL) and the reaction mixture stirred at 80 °C for 16 hours. Upon completion, the reaction mixture was cooled to room temperature and the potassium salts filtered. The filterate was evapourated under reduced pressure and the resulting orange residue purified by column chromatography (DCM/MeOH, 100% to 90:10 using 1% increments; R_f = 0.40) to yield a light yellow gum (1.51g, 66%). ^{1}H NMR ($CDCl_3$, 600 MHz) δ 1.21-1.39 (4H, m, C**H**$_2$), 1.44 (9H, s, (C**H**$_3$)$_3$), 1.45 (18H, s, (C**H**$_3$)$_3$), 1.46 (9H, s, C(C**H**$_3$)$_3$), 1.51-1.59 (2H, m, C**H**$_2$), 2.07-2.17 (2H, m, C**H**$_2$), 2.26-2.56 (6H, m, C**H**$_2$), 2.73-2.96 (4H, m, C**H**$_2$), 3.05-3.12 (1H, br, m, C**H**), 3.14-3.23 (4H, m, C**H**$_2$), 3.27-3.50 (8H, m, C**H**$_2$O + C**H**$_2$), 5.08 (2H, s, OC**H**$_2$Ph), 7.31-7.35 (5H, m, Ar-**H**). ^{13}C NMR ($CDCl_3$, 151 MHz): δ 22.7 (**C**H$_2$), 27.8, 27.8 (C(**C**H$_3$)$_3$), 27.9 (**C**H$_2$), 28.1 (C(**C**H$_3$)$_3$), 33.6, 40.70, 44.8, 47.3, 50.8, 53.3, 55.6, 55.9 (**C**H + **C**H$_2$), 66.4 (O**C**H$_2$Ph), 81.6, 81.7, 81.8 (**C**(CH$_3$)$_3$), 127.9, 128.4, 128.4,136.6 (Ar-**C**), 156.4, 169.6, 170.4, 172.9 (**C**O). MS (ES$^+$) *m/z* 857.7 [M+Na]$^+$. $C_{44}H_{75}N_5O_{10}Na$ requires 856.5412; found 856.5453.

_(R)_–tri-_tert_-Butyl 2,2',2''-(10-(6-amino-1-(tert-butoxy)-1-oxohexan-2-yl)-1,4,7,10-tetraazacyclododecane-1,4,7-triyl)triacetate, 21

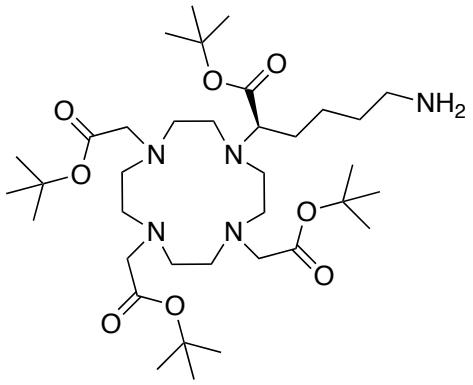

(R)-tri-*tert*-butyl-2,2',2''-(10-(1-(*tert*-butoxy)-1oxo-6-(2-phenylacetamido)hexan-2-yl)-1,4,7,10-tetraazacyclododecane-1,4,7-triyl)triacetate (1.20 g, 1.44 mmol) was dissolved in MeOH (15 mL) to which $Pd(OH)_2$ (10%) was added. The vessel was then loaded onto a Parr hydrogenator (P_{H2}=40 bar) and the reaction mixture agitated over 48 hours. After this period, the mixture was filtered to remove excess catalyst and washed exhaustively with MeOH. The methanolic solution was then evaporated under reduced pressure to yield the title compound as a light grey solid (993 mg, 99%). ^{1}H NMR ($CDCl_3$, 700 MHz) δ 1.43, 1.44, 1.45 (27H, s, C(C**H**$_3$)$_3$), 1.50-1.61 (2H, m, C**H$_2$**), 1.63-1.73 (4H, m, C**H$_2$**), 2.05-2.14 (2H, m, C**H$_2$**), 2.22-2.57 (8H, m, C**H**$_2$), 2.69-3.17 (12H, m, br, C**H**$_2$ + N**H**$_2$), 3.25-3.61 (5H, m, C**H$_2$** + C**H**). ^{13}C NMR ($CDCl_3$, 176 MHz) δ 22.7 (**C**H$_2$), 27.8, 27.8 (C(**C**H$_3$)$_3$), 27.9 (**C**H$_2$), 28.1 (C(**C**H$_3$)$_3$), 33.6, 40.70, 44.8, 47.3, 50.8, 53.3, 55.6, 55.9 (**C**H$_2$), 61.5 (**C**H), 81.6, 82.0, 82.1 (**C**(CH$_3$)$_3$), 171.0, 172.8, 173.0 (**C**O). MS (ES$^+$) *m/z* 700.5 [M+H]$^+$; $C_{36}H_{70}N_5O_8$ requires 700.5224; found 700.5232.

[Conjugate 1], 22

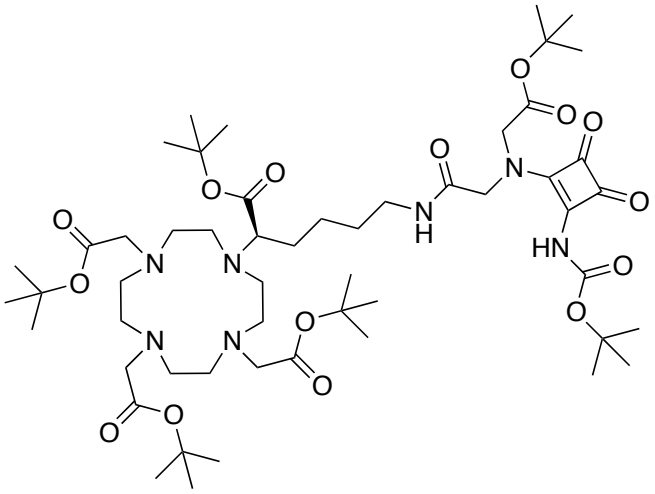

2-((2-(*Tert*-butoxy)-2-oxoethyl)(2-((*tert*-butoxycarbonyl)amino)-3,4-dioxocyclobut-1-en-1-yl)amino)acetic acid (50 mg, 0.13 mmol), EDC (27 mg, 0.14 mmol) and HOBt (19 mg, 0.14 mmol) were dissolved in anhydrous DMF (4 mL) and stirred at room temperature under an atmosphere of argon for 20 minutes. After this period, a pre-stirred solution of *(R)*–tri-*tert*-butyl 2,2',2''-(10-(6-amino-1-(tert-butoxy)-1-oxohexan-2-yl)-1,4,7,10-tetraazacyclododecane-1,4,7-triyl)triacetate (91 mg, 0.13 mmol) and NMM (29 μL, 0.26 mmol) in anhydrous DMF (2 mL) was added dropwise and the resulting solution was stirred at room temperature for a total of 48 hours. After this period, DMF was removed under reduced pressure and the crude oil taken up into EtOAc (50 mL). $NaHCO_3$ (30 mL) was added, the layers were separated and the aqueous layer was washed with EtOAc (3 x 50 mL). The combined organic portions were dried over $MgSO_4$, filtered and the solvent removed under reduced pressure. The crude residue was purified by column chromatography (DCM/MeOH, 100% to 90:10 in 1% increments; R_f =0.26) to yield a viscous yellow oil (26 mg, 19%). ^{1}H NMR ($CDCl_3$, 600 MHz) δ 1.29-1.38 (4H, m, C**H**$_2$), 1.4, 1.4, 1.4, 1.4, 1.4 (54H, 5 x s, (C(C**H**$_3$)$_3$), 1.51-1.57 (2H, m, C**H**$_2$), 2.04-2.14 (4H, m, C**H**$_2$), 2.21-2.37 (4H, m, C**H**$_2$), 2.43-2.55 (4H, m, C**H**$_2$), 2.67-2.90 (4H, m, C**H**$_2$), 2.98-3.78 (11H, m, C**H**$_2$ + C**H**), 4.16-4.35 (2H, m, C**H**$_2$), 7.54-7.86 (2H, br. m, N**H**). ^{13}C NMR ($CDCl_3$, 151 MHz) δ 24.2, 27.6 (**C**H$_2$), 27.7, 27.8, 27.8, 27.9, 27.9, 27.9 (C(**C**H$_3$)$_3$), 39.0, 47.2, 48.0, 48.4, 52.4, 52.61, 53.3, 55.4, 55.7 (**C**H$_2$), 61.2 (**C**H), 81.9, 82.1, 82.6, 82.7, 83.1 (**C**(CH$_3$)$_3$),

151.7, 151.8 (**C**=**C**), 160.4, 160.6, 166.2, 167.6, 170.4, 172.7, 172.7, 172.8 (**C**O). MS (ES^+) *m/z* = 1066.7 $[M+H]^+$; $C_{53}H_{92}N_7O_{15}$ requires 1066.665; found 1066.670.

[Conjugate 2], 23

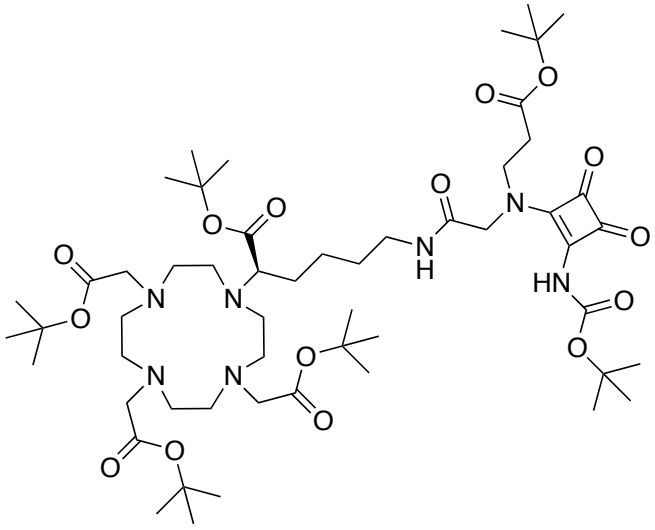

2-((3-(*Tert*-butoxy)-3-oxopropyl)(2-((*tert*-butoxycarbonyl)amino)-3,4-dioxocyclobut-1-en-1-yl)amino)acetic acid (46 mg, 0.12 mmol), EDC (28 mg, 0.14 mmol) and HOBt (19 mg, 0.14 mmol) were dissolved in anhydrous DMF (3 mL) and stirred at room temperature under an atmosphere of argon for 20 minutes. After this period, a pre-stirred solution of *(R)* –tri-*tert*-butyl 2,2',2''-(10-(6-amino-1-(tert-butoxy)-1-oxohexan-2-yl)-1,4,7,10-tetraazacyclododecane-1,4,7-triyl)triacetate (84 mg, 0.12 mmol) and NMM (24 μL, 0.24 mmol) in anhydrous DMF (1.2 mL) was added dropwise and the resulting solution was stirred at room temperature for a total of 48 hours. After this period, DMF was removed under reduced pressure and the crude oil taken up into EtOAc (50 mL). $NaHCO_3$ (30 mL) was added, the layers were separated and the aqueous layer was washed with EtOAc (3 x 50 mL). The combined organic portions were dried over $MgSO_4$, filtered and the solvent removed under reduced pressure. The crude residue was purified by column chromatography (DCM/MeOH, 100% to 90:10 using 1% increments; R_f =0.26) to yield a viscous yellow oil (17 mg, 14%). ^1H NMR ($CDCl_3$, 700 MHz): δ 1.29-1.38 (4H, m, C**H**$_2$), 1.40, 1.40, 1.41, 1.41, 1.44 (54H, s, C(C**H**$_3$)$_3$), 1.51-1.57 (2H, m, C**H**$_2$), 2.04-2.14 (4H, m, C**H**$_2$), 2.21-2.37 (4H, m, C**H**$_2$), 2.43-2.55 (4H, m, C**H**$_2$), 2.59 (2H, t, J = 7, C**H**$_2$$CO_2{}^tBu$), 2.67-2.90 (4H, m,

C**H**$_2$), 2.98-3.78 (11H, m, C**H**$_2$ + C**H**), 4.16-4.35 (2H, m, C**H**$_2$), 7.54-7.86 (2H, br. m, N**H**). ^{13}C NMR ($CDCl_3$, 151 MHz) δ 24.4, 27.9 (**C**H$_2$), 27.9, 28.0, 28.0, 28.1, 28.1, 28.1 (C(**C**H$_3$)$_3$), 34.6, 39.2, 47.4, 48.2, 48.6, 52.6, 52.6, 53.5, 55.6 (**C**H$_2$CO$_2$^{t}Bu), 55.9 (**C**H$_2$), 61.4 (**C**H), 81.9, 82.1, 82.8, 82.9, 83.3 (**C**(CH$_3$)$_3$), 151.9, 152.0 (**C**=**C**), 160.6, 160.8, 166.4, 167.8, 170.6, 172.9, 172.9, 173.0 (**C**O). MS (ES$^+$) *m/z* = 1080.7 [M+H]$^+$; $C_{54}H_{94}N_7O_{15}$ requires 1080.681; found 1080.677.

[Conjugate 3], 24

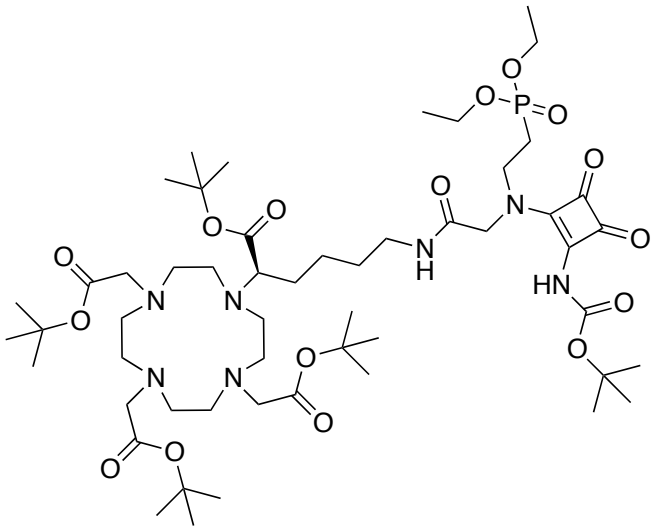

2-((2-((*Tert*-butoxycarbonyl)amino)-3,4-dioxocyclobut-1-en-1-yl)(2-(diethoxyphosphoryl)ethyl)amino)acetic acid (182 mg, 0.42 mmol), EDC (100 mg, 0.50 mmol) and HOBt (70 mg, 0.50 mmol) were dissolved in anhydrous DMF (4 mL) and stirred at room temperature under an atmosphere of argon for 20 minutes. After this period, a pre-stirred solution of *(R)* –tri-*tert*-butyl 2,2',2''-(10-(6-amino-1-(tert-butoxy)-1-oxohexan-2-yl)-1,4,7,10-tetraazacyclododecane-1,4,7-triyl)triacetate (292 mg, 0.42 mmol) and NMM (91 μL, 0.83 mmol) in anhydrous DMF (1.5 mL) was added drop wise and the resulting solution was stirred at room temperature for a total of 48 hours. After this period, DMF was removed under reduced pressure and the crude oil taken up into EtOAc (40 mL). $NaHCO_3$ (30 mL) was added, the layers were separated and the aqueous layer was washed with EtOAc (3 x 50 mL). The combined organic portions were dried over $MgSO_4$, filtered and the solvent removed under reduced pressure. The crude residue was purified by column chromatography (DCM/MeOH 100% to 93:7

using 1% increments; R_f = 0.24) to yield a viscous yellow-brown oil (89 mg, 19%). ^{1}H NMR ($CDCl_3$, 700 MHz) δ 1.23-1.27 (2H, m, **C**H_2), 1.29 (3H, t, J = 7, $P(OCH_2C\mathbf{H}_3)_2$), 1.32 (3H, t, ^{3}J = 7, $P(OCH_2C\mathbf{H}_3)_2$), 1.40, 1.41, 1.42, 1.42, 1.42 (45H, s, $C(C\mathbf{H}_3)_3$), 1.51-1.68 (6H, m, C$\mathbf{H}_2$), 2.06-2.15 (4H, m, C$\mathbf{H}_2$), 2.25-2.39 (4H, m, C$\mathbf{H}_2$), 2.41-2.61 (4H, m, C$\mathbf{H}_2$), 2.70-2.87 (5H, m, C$\mathbf{H}_2$ + C**H**), 3.07-3.43 (10H, m, C$\mathbf{H}_2$), 3.65-3.86 (2H, m, C$\mathbf{H}_2CH_2P$), 3.99-4.16 (4H, m, $P(OC\mathbf{H}_2CH_3)_2$), 7.54-7.86 (2H, br. m, N**H**). ^{13}C NMR ($CDCl_3$, 176 MHz) δ 16.52 (d, ^{3}J = 7, $P(OCH_2\mathbf{C}H_3)_2$), 24.6 (**C**H_2), 27.7(d, ^{1}J = 141, $NCH_2\mathbf{C}H_2P$), 27.8 ($C(\mathbf{C}H_3)_3$), 27.8 (**C**H_2), 27.8 27.9, ($C(\mathbf{C}H_3)_3$), 28.1 (**C**H_2), 29.2 ($C(\mathbf{C}H_3)_3$), 39.1 (**C**H_2), 45.2 (d, ^{2}J = 6, N**C**H_2CH_2P), 47.3, 48.1, 48.5, 52.5, 52.6 , 55.5, 55.7 (**C**H_2), 61.9 (**C**H), 62.1 (d, ^{2}J = 7, $P(O\mathbf{C}H_2CH_3)_2$), 81.9, 82.0, 82.1, 82.7 (**C**$(CH_3)_3$), 151.8, 151.9 (**C**=**C**), 160.5, 160.7, 165.2, 172.8, 172.8, 172.9, 174.9 (**C**O). ^{31}P NMR ($CDCl_3$, 283 MHz) δ 27.28. MS (ES^+) *m/z* = 1139.9 $[M+Na]^+$; $C_{53}H_{96}N_7O_{16}P$ requires 1117.665; found 1117.663.

[Conjugate 4], 25

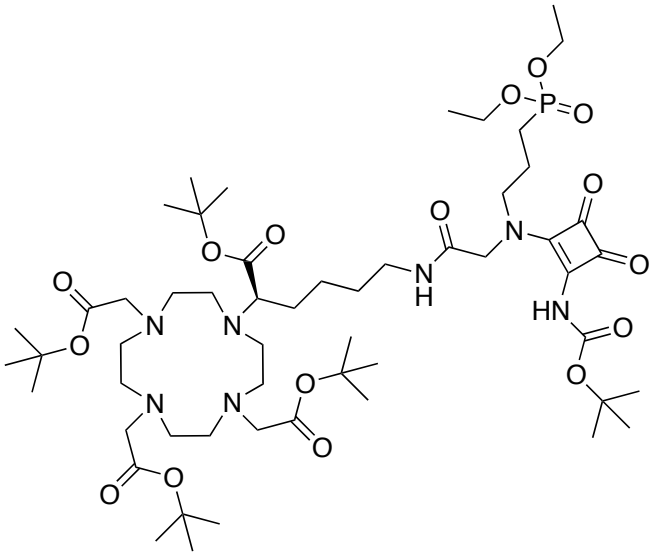

2-((2-((*Tert*-butoxycarbonyl)amino)-3,4-dioxocyclobut-1-en-1-yl)(3-(diethoxyphosphoryl)propyl)amino)acetic acid (75 mg, 0.17 mmol), EDC (40 mg, 0.20 mmol) and HOBt (28 mg, 0.20 mmol) were dissolved in anhydrous DMF (3 mL) and stirred at room temperature under an atmosphere of argon for 20 minutes. After this period, a pre-stirred solution of *(R)* –tri-*tert*-butyl 2,2',2''-(10-(6-amino-1-(tert-butoxy)-1-oxohexan-2-yl)-1,4,7,10-tetraazacyclododecane-

1,4,7-triyl)triacetate, (117 mg, 0.17 mmol) and NMM (37 μL, 0.34 mmol) in anhydrous DMF (1.5 mL) was added drop wise and the resulting solution was stirred at room temperature for a total of 48 hours. After this period, DMF was removed under reduced pressure and the crude oil taken up into EtOAc (40 mL). $NaHCO_3$ (30 mL) was added, the layers were separated and the aqueous layer was washed with EtOAc (3 x 50 mL). The combined organic portions were dried over $MgSO_4$, filtered and the solvent removed under reduced pressure. The crude residue was purified by column chromatography (DCM/MeOH, 100% to 93:7 using 1% increments; R_f = 0.30) to yield a viscous yellow-brown oil (23 mg, 12%). ^{1}H NMR ($CDCl_3$, 700 MHz) δ 1.23-1.27 (2H, m, C**H**$_2$), 1.29 (3H, t, J = 7, P(OCH$_2$C**H**$_3$)$_2$), 1.32 (3H, t, ^{3}J = 7, P(OCH$_2$C**H**$_3$)$_2$), 1.40, 1.41, 1.42, 1.42, 1.42 (9H, s, C(C**H**$_3$)$_3$), 1.51-1.68 (6H, m, C**H**$_2$), 1.89-1.98 (2H, m, C**H**$_2$P), 2.06-2.15 (4H, m, C**H**$_2$), 2.25-2.39 (4H, m, C**H**$_2$), 2.41-2.61 (4H, m, C**H**$_2$), 2.70-2.87 (5H, m, C**H**$_2$ + C**H**), 3.07-3.43 (10H, m, C**H**$_2$), 3.65-3.86 (2H, m, C**H**$_2$), 3.99-4.16 (4H, m, P(OC**H**$_2$CH$_3$)$_2$), 7.54-7.86 (2H, br. m, N**H**). ^{13}C NMR ($CDCl_3$, 176 MHz) δ 16.5 (d, ^{3}J = 7, P(OCH$_2$**C**H$_3$)$_2$), 22.3 (d, ^{2}J = 5, NCH$_2$**C**H$_2$CH$_2$P), 23.1 (d, ^{1}J = 143, N(CH$_2$)$_2$**C**H$_2$P) 24.6 (**C**H$_2$), 27.8 (C(**C**H$_3$)$_3$), 27.8 (**C**H$_2$), 27.8, 27.9, (C(**C**H$_3$)$_3$), 28.1 (**C**H$_2$), 29.2 (C(**C**H$_3$)$_3$), 39.1, 47.3, 48.1, 48.5, 52.5, 52.6 (**C**H$_2$), 56.0 (d, ^{3}J = 17, N**C**H$_2$(CH$_2$)$_2$P), 55.5, 55.7 (**C**H$_2$), 61.9 (**C**H), 61.92 (d, ^{2}J = 7, P(O**C**H$_2$CH$_3$)$_2$), 81.9, 82.0, 82.1, 82.7 (**C**(CH$_3$)$_3$), 151.8, 151.9 (**C**=**C**), 160.5, 160.7, 165.2, 172.8, 172.8, 172.9, 174.9 (**C**O). ^{31}P NMR ($CDCl_3$, 283 MHz) δ 30.18. MS (ES$^+$) *m/z* = 1153.7 [M+Na]$^+$; $C_{54}H_{97}N_7O_{16}$PNa requires 1153.661; found 1153.657.

[Gd.L^1]

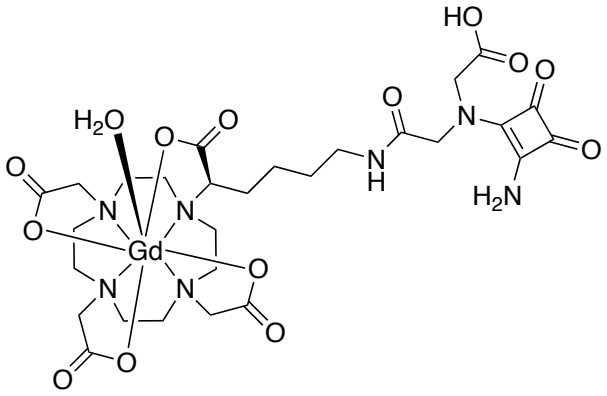

22 (26 mg, 0.02 mmol) was dissolved in DCM (1 mL) with stirring. To this was added trifluoroacetic acid (1 mL) and the resulting solution was stirred at room temperature overnight. Complete removal of the protecting groups was verified by ESI-MS, at which point the excess solvent was removed under reduced pressure. The residue was repeatedly re-dissolved in DCM (2 mL) and the solvent removed under reduced pressure to remove excess TFA. This process yielded **L^1** as a brown solid. MS (ES$^+$) *m/z* 685.7 [M+H]$^+$. **L^1** (13 mg, 0.02 mmol) was dissolved in purite H_2O (1 mL) and the pH adjusted to about 5.5 by the addition of NaOH (0.1 M). $GdCl_3.6H_2O$ (11.5 mg, 0.031 mmol) was added as a solution in H_2O (0.5 mL) and the reaction mixture stirred at 60 °C overnight. The pH of the solution was periodically checked and adjusted to 6.5 by addition of NaOH/HCl (0.1 M). Upon completion, excess gadolinium was removed by the addition of Chelex-100™ with stirring. The Chelex trap was filtered and the complex eluted with excess H_2O. Removal of the water by lyophilisation gave the complex as a light yellow solid. HR-MS (ES$^-$) $C_{28}H_{37}{}^{157}GdN_7O_{13}$ requires 837.1690 [M-2H]$^-$; found 837.1695. r_{1p} = 5.2 mM^{-1}s^{-1} (60 MHz, 310K).

[Gd.L²]

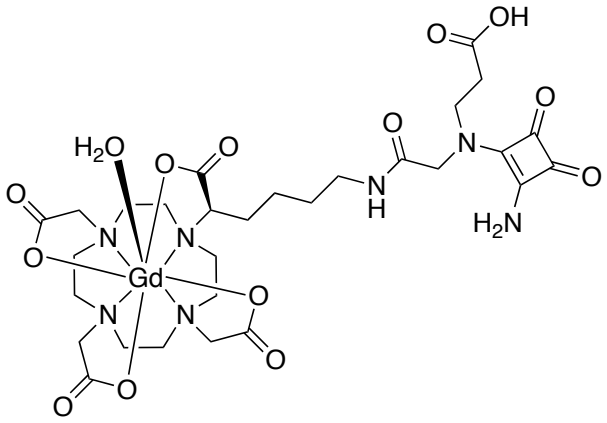

23 (17 mg, 0.02 mmol) was dissolved in DCM (1 mL) with stirring. To this was added trifluoroacetic acid (1 mL) and the resulting solution was stirred at room temperature overnight. Completion of the reaction was verified by ESI-MS at which point the excess solvent was removed under reduced pressure. The residue was repeatedly re-dissolved in DCM (2 mL) and the solvent removed under reduced pressure to remove excess TFA. This process yielded the product as a light-brown solid. MS (ES^+) *m/z* 700.5 $[M+H]^+$. **L²** (14 mg, 0.02 mmol) was dissolved in purite H_2O (1 mL) and the pH adjusted to 5.5 by the addition of NaOH (0.1 M). $GdCl_3.6H_2O$ (11.5 mg, 0.031 mmol) was added as a solution in H_2O (0.5 mL) and the reaction mixture stirred at 60 °C overnight. The pH of the solution was periodically checked and adjusted to 6.5 by addition of NaOH/HCl (0.1 M). Upon completion, excess gadolinium was removed by the addition of chelex-100™ with stirring. The chelex trap was filtered and the complex eluted with excess H_2O. Removal of the water by lyophilisation gave the complex as a light yellow solid. HR-MS (ES^-) $C_{29}H_{39}{}^{157}GdN_7O_{13}$ requires 851.1932 $[M-2H]^-$; found 851.1909. r_{1p} = 5.3 $mM^{-1}s^{-1}$ (60 MHz, 310K).

[Gd.L³]

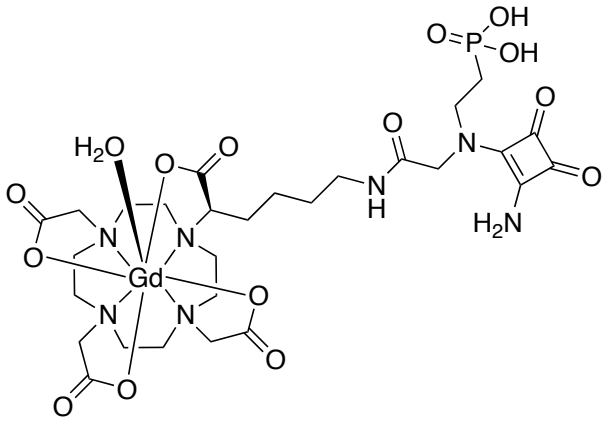

24 (10 mg, 9 μmol) was dissolved in DCM (1 mL) with stirring. To this was added trifluoroacetic acid (1 mL) and the resulting solution was stirred at room temperature for overnight. Loss of *tert*-butyl and BOC groups was verified by ESI-MS ($[M+H]^+$; m/z =791.5) at which point the excess solvent was removed under reduced pressure. The residue was repeatedly re-dissolved in DCM (2 mL) and the solvent removed under reduced pressure to remove excess TFA. This process yielded the phosphonate ethyl ester as a light-brown solid. This residue was dissolved in DMF (1 mL) to which bromotrimethylsilane (20 μL, 0.15 mmol) was added dropwise. The resulting mixture was heated to 60 °C overnight until complete deprotection. The solvent was removed under reduced pressure, before the residue redissolved in H_2O, the pH adjusted to 6 and the aqueous washed with diethyl ether (x3). The solvent was removed by lyophilisation to give **L³** as a light brown solid. MS (ES^+) *m/z* 735.0 $[M+H]^+$. **L³** (7 mg, 9 μmol) was dissolved in purite H_2O (1 mL) and the pH adjusted to 5.5 by the addition of NaOH (0.1 M). $GdCl_3.6H_2O$ (4 mg, 10 μmol) was added as a solution in H_2O (0.5 mL) and the reaction mixture stirred at 60 °C overnight. The pH of the solution was periodically checked and adjusted to 6.5 by addition of NaOH/HCl (0.1 M). Upon completion, excess gadolinium was removed by the addition of chelex-100™ with stirring. The chelex trap was filtered and the complex eluted with excess H_2O. Removal of the water by lyophilisation gave the complex as a light yellow solid. HR-MS (ES^-) $C_{28}H_{42}{}^{157}GdN_7O_{14}P$ requires 887.1697 $[M-2H]^-$; found 887.1686. r_{1p} = 4.7 $mM^{-1}s^{-1}$ (60 MHz, 310K).

[Gd.L⁴]

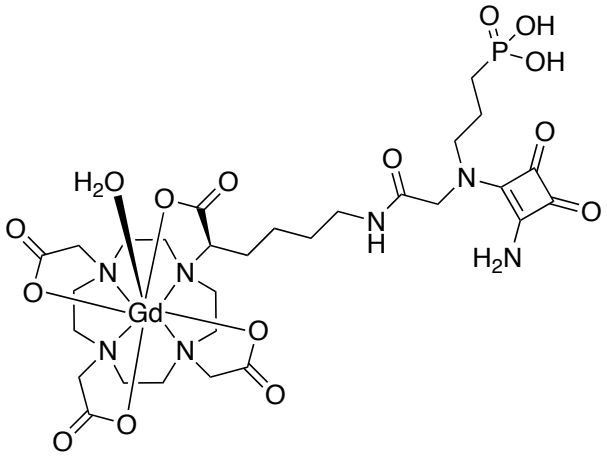

25 (10 mg, 9 μmol) was dissolved in DCM (1 mL) with stirring. To this was added trifluoroacetic acid (1 mL) and the resulting solution was stirred at room temperature for overnight. Loss of *tert*-butyl and BOC groups was verified by ESI-MS ($[M+H]^+$; m/z = 806.0) at which point the excess solvent was removed under reduced pressure. The residue was repeatedly re-dissolved in DCM (2 mL) and the solvent removed under reduced pressure to remove excess TFA. This process yielded the phosphonate ethyl ester as a light-brown solid. This residue was dissolved in DMF (1 mL) to which bromotrimethylsilane (20 μL, 0.15 mmol) was added dropwise. The resulting mixture was heated to 60 °C overnight until complete deprotection. The solvent was removed under reduced pressure, before the residue redissolved in H_2O, the pH adjusted to 6 and the aqueous washed with diethyl ether (x3). The solvent was removed by lyophilisation to give **L⁴** as a light brown solid. MS (ES^+) *m/z* 750.0 $[M+H]^+$. **L⁴** (7 mg, 9 μmol) was dissolved in purite H_2O (1 mL) and the pH adjusted to 5.5 by the addition of NaOH (0.1 M). $GdCl_3.6H_2O$ (4 mg, 10 μmol) was added as a solution in H_2O (0.5 mL) and the reaction mixture stirred at 60 °C overnight. The pH of the solution was periodically checked and adjusted to 6.5 by addition of NaOH/HCl (0.1 M). Upon completion, excess gadolinium was removed by the addition of chelex-100™ with stirring. The chelex trap was filtered and the complex eluted with excess H_2O. Removal of the water by lyophilisation gave the complex as a light yellow solid. HR-MS (ES^-) $C_{29}H_{44}{}^{155}GdN_7O_{14}P$ requires 898.1809 $[M-2H]^-$; found 898.1788. r_{1p} = 4.8 $mM^{-1}\,s^{-1}$ (60 MHz, 310K).

(3-Amino-2-hydroxypropyl)carbamic Acid 1,1-dimethylethyl ester, 26[5]

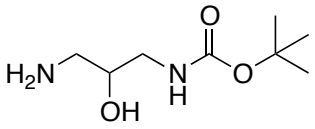

A solution of 1,3-diamino-2-hydroxypropane (5.0 g, 55.5 mmol) in anhydrous acetonitrile (50 mL) was maintained at room temperature and treated with a solution of di-*tert*-butyl dicarbonate (4.04 g, 18.5 mmol) in anhydrous acetonitrile (20 mL) over a 2 hour period with vigorous stirring. The resulting suspension was left to stir overnight. After a period of 18 hours, the reaction mixture was concentrated and the residue re-dissolved in brine (50 mL). The pH was adjusted to 5 by treatment with HCl (1 N), the mixture was washed with dichloromethane (3 x 50 mL) and made basic (pH 12) by the addition of NaOH solution (2.5 M). The product was extracted using $CHCl_3$ (5 x 100 mL), and the combined organic layers dried over $MgSO_4$, filtered and concentrated to yield a white solid (1.23 g, 34%). ^{1}H NMR (400 MHz, $CDCl_3$) δ 1.43 (9H, s, C(C**H**$_3$)$_3$), 2.42-2.72 (3H, m), 2.78-2.92 (2H, m), 3.01-3.15 (1H, m), 3.20-3.35 (1H, m), 3.56-3.72 (1H, m), 5.05 (1H, br, s). ^{13}C NMR (125 MHz, $CDCl_3$) δ 28.4 (C(**C**H$_3$)$_3$), 44.1, 44.5 (**C**H$_2$), 71.0 (**C**OH), 79.5 (**C**(CH$_3$)$_3$), 156.7 (**C**O). MS (ES$^+$) *m/z* 191.1 [M + H]$^+$; $C_8H_{19}N_2O_3$ requires 191.1396; found 191.1392. M. Pt. 78-80 °C [Lit. 77-79 °C].

(3-((2-(Diethoxyphosphinyl)ethyl)amino)-2-hydroxypropyl)carbamic acid 1,1-dimethylethyl ester, 27[6]

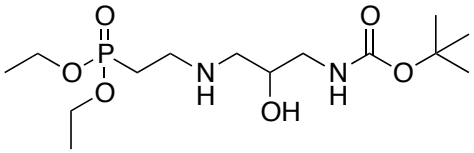

A solution of (3-amino-2-hydroxypropyl)carbamic acid 1,1-dimethylethyl ester (1.20 g, 6.26 mmol), sodium carbonate (995 mg, 9.39 mmol) and diethyl (2-bromoethyl)phosphonate (1.8 mL, 9.92 mmol) in anhydrous ethanol (23 mL) was boiled under reflux for 16 hours until no further reaction was observed by

TLC. The mixture was concentrated under reduced pressure before being partitioned between DCM/H_2O (1:1, 30 mL). The organic portion was separated and the aqueous layer was extracted with DCM (3 x 25 mL). The combined organic fractions were dried over $MgSO_4$, filtered and concentrated, allowing the crude residue to be purified by column chromatography (DCM/MeOH, 100% to 90:10 using 1% increments; R_f = 0.42) to give a colourless oil (975 mg, 44%). ^{1}H NMR (400 MHz, $CDCl_3$) δ 1.31 (6H, t, J = 7, P(OCH$_2$C**H**$_3$)$_2$), 1.42 (9H, s, C(C**H**$_3$)$_3$), 2.08 (2H, dt, $^2J_{H-P}$ = 18, $^3J_{H-H}$ = 7, PC**H**$_2$CH$_2$), 2.63 (1H, dd, J = 12, 8), 2.78 (1H, dd, J = 12, 3), 2.91-3.05 (2H, m, PCH$_2$C**H**$_2$), 3.05-3.14 (1H, m), 3.32-3.34 (1H, m), 3.68 (3H, br, s), 3.79-3.86 (1H, m, C**H**), 4.03-4.16 (4H, qd, $^3J_{H-H}$ = 7, $^3J_{H-P}$ = 3, P(OC**H**$_2$CH$_3$)$_2$). ^{13}C NMR (101 MHz, $CDCl_3$) δ 16.6 (d, ^{3}J = 6, P(OCH$_2$**C**H$_3$)$_2$), 25.7 (d, ^{1}J = 140, NHCH$_2$**C**H$_2$P), 28.5 (C(**C**H$_3$)$_3$), 43.2 (d, ^{2}J = 5, NH**C**H$_2$CH$_2$P), 44.3, 51.9 (**C**H$_2$), 62.1 (d, ^{2}J = 7, P(O**C**H$_2$CH$_3$)$_2$), 68.5 (**C**OH), 79.6 (**C**(CH$_3$)$_3$), 156.8 (**C**O). ^{31}P NMR ($CDCl_3$, 162 MHz) δ 30.73. MS (ES$^+$) *m/z* 355.2 [M + H]$^+$; $C_{14}H_{32}N_2O_6P$ requires 355.1998; found 355.2001.

(3-((2-(Diethoxyphosphinyl)ethyl)(2-ethoxy-3,4-dioxo-1-cyclobuten-1-yl)amino)-2-hydroxypropyl)carbamic acid 1,1-Dimethylethyl Ester, 28[6]

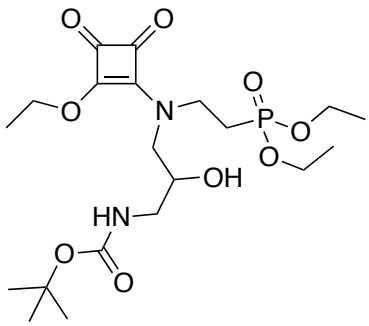

To a solution of 3,4-diethoxy-3-cyclobutene-1,2-dione (368 μL, 2.49 mmol) in anhydrous ethanol (13 mL), was added a solution of (3-((2-(diethoxyphosphinyl)ethyl)amino)-2-hydroxypropyl)carbamic acid 1,1-dimethylethyl ester (882 mg, 2.49 mmol) in anhydrous ethanol (5 mL) over 30 minutes. The resulting solution was stirred under argon at room temperature and the progress of the reaction was monitored by TLC. After 16 hours, the solution was concentrated under reduced pressure, and the crude residue was

purified by column chromatography (DCM/MeOH, 100% to 90:10 using 1% increments; R_f = 0.28) to give a colourless viscous oil as a pair of rotamers (777 mg, 65%). ^{1}H NMR (400 MHz, $CDCl_3$) δ 1.21 (6H, t, J = 7, ($P(OCH_2C\mathbf{H}_3)_2$), 1.27-1.36 (12H, m, $C(C\mathbf{H}_3)_3$ + $OCH_2C\mathbf{H}_3$), 1.98-2.17 (2H, m, $PC\mathbf{H}_2CH_2$), 2.89-3.91 (8H, m, $C\mathbf{H}_2$ + C**H** + O**H**), 3.94-4.04 (4H, m, $P(OC\mathbf{H}_2CH_3)_2$), 4.58-4.67 (2H, m, $OC\mathbf{H}_2CH_3$), 5.42 (1H, br, N**H**). ^{13}C NMR (101 MHz, $CDCl_3$) δ 15.7 ($OCH_2\mathbf{C}H_3$), 16.3 (d, ^{3}J = 6, $P(OCH_2\mathbf{C}H_3)_2$), 25.6 (d, ^{1}J = 140, $NCH_2\mathbf{C}H_2P$), 28.2 ($C(\mathbf{C}H_3)_3$), 44.0 ($N\mathbf{C}H_2CH_2P$), 45.2, 53.5 ($\mathbf{C}H_2$), 62.0 (d, ^{2}J = 7, $P(O\mathbf{C}H_2CH_3)_2$), 69.5 (**C**OH), 69.7 ($O\mathbf{C}H_2CH_3$), 79.4 ($\mathbf{C}(CH_3)_3$), 156.7 (**C**O), 172.5, 176.6 (**C**=**C**), 182.6, 188.4 (**C**O). ^{31}P NMR ($CDCl_3$, 162 MHz) δ 26.28. MS (ES^+) *m/z* 479.1 $[M+H]^+$; $C_{20}H_{36}N_2O_9P$ requires 479.2158; found 479.2156.

(2-(4-Hydroxy-8,9-dioxo-2,6-diazabicyclo[5.2.0]non-1(7)-en-2-yl)ethyl)phosphonic Acid diethyl ester, 29[6]

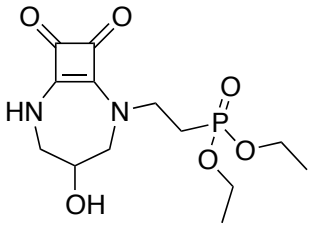

To a solution of (3-((2-(diethoxyphosphinyl)ethyl)(2-ethoxy-3,4-dioxo-1-cyclobuten-1-yl)amino)-2-hydroxypropyl)carbamic acid 1,1-dimethylethyl ester (777 mg, 1.63 mmol) in anhydrous dichloromethane (2 mL) was added TFA (2 mL) dropwise, and the resulting solution was stirred at room temperature for 1 hour. The reaction was complete after this period, as indicated by TLC, and the solvents were removed under reduced pressure. The residue was re-dissolved in dichloromethane and the volume was reduced. This process was repeated 5 times to ensure complete removal of excess TFA. The TFA salt was dissolved in anhydrous ethanol (8 mL) to which a solution of diisopropylethylamine (1.13 mL, 6.52 mmol) in anhydrous ethanol (24 mL) was added over a 1 hour period. The resulting solution was heated to reflux for 18 hours, until no further reaction was observed by TLC. At this point, the solvent was removed and the crude

residue was purified by column chromatography (DCM/MeOH, 100% to 90:10 using 1% increments; R_f = 0.40) to give a white solid (488 mg, 90%). ^{1}H NMR (400 MHz, $CDCl_3$) δ 1.32 (6H, 2 x t, J = 7, ($P(OCH_2C\mathbf{H}_3)_2$), 2.11-2.31 (2H, m, $PC\mathbf{H}_2CH_2$), 3.39 (1H, d, J = 14, C**H**), 3.55 (1H, d, J = 14, C**H**), 3.61-3.77 (5H, m, $C\mathbf{H}_2$ + $PCH_2C\mathbf{H}_2$ + O**H**), 4.04-4.14 (4H, m, $P(OC\mathbf{H}_2CH_3)_2$), 4.16-4.19 (1H, m, C**H**), 4.29-4.42 (1H, m, $PCH_2C\mathbf{H}_2$), 7.58 (1H, s, N**H**). ^{13}C NMR (101 MHz, $CDCl_3$) δ 16.5 (d, ^{3}J = 6, $P(OCH_2\mathbf{C}H_3)_2$), 25.8 (d, ^{1}J = 140, $NCH_2\mathbf{C}H_2P$), 45.3 (d, ^{2}J = 5, $N\mathbf{C}H_2CH_2P$), 53.7, 57.6 ($\mathbf{C}H_2$), 62.3 (d, ^{2}J = 7, $P(O\mathbf{C}H_2CH_3)_2$), 68.2 (**C**OH), 168.4, 168.5 (**C**=**C**), 180.8, 182.1 (**C**O). ^{31}P NMR ($CDCl_3$, 162 MHz) δ 27.4. MS (ES^+) *m/z* 333.1 $[M+H]^+$; $C_{13}H_{22}N_2O_6P$ requires 333.1216; found 333.1209. M. Pt. 167-169 °C.

Benzyl *tert*-butyl(2-hydroxypropane-1,3-diyl)dicarbamate, 30

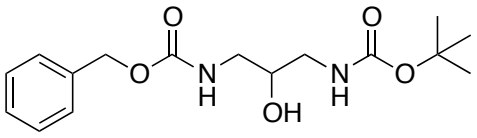

To a solution of (3-amino-2-hydroxypropyl)carbamic acid 1,1-dimethylethyl ester (1.28 g, 6.72 mmol) in anhydrous dichloromethane (43 mL) was added benzyl chloroformate (1.05 mL, 7.39 mmol) and diisopropylethylamine (1.29 mL, 7.39 mmol) at 0 °C. The resulting solution was stirred under argon at this temperature for 30 mins before being allowed to warm to room temperature and stirred overnight. After complete consumption of starting materials has been revealed by TLC, the reaction mixture was concentrated and the crude residue purified by column chromatography (DCM/MeOH, 100% to 95:5 using 1% increments R_f = 0.26) to give a pale green oil (1.64 g, 75%). ^{1}H NMR (400 MHz, $CDCl_3$) δ 1.43 (9H, s, $C(C\mathbf{H}_3)_3$), 3.06-3.35 (4H, m, 2 x $NHC\mathbf{H}_2$), 3.76 (1H, quin, J = 6, C**H**), 5.09 (2H, s, $C\mathbf{H}_2Ph$), 5.14 (1H, br, O**H**), 5.49 (2H, br, N**H**), 7.29-7.38 (5H, m, Ar-**H**). ^{13}C NMR (101 MHz, $CDCl_3$) δ 28.5 ($C(\mathbf{C}H_3)_3$), 43.7, 44.1 ($\mathbf{C}H_2$), 67.1 ($\mathbf{C}H_2Ph$), 70.9 (**C**OH), 80.1 ($\mathbf{C}(CH_3)_3$), 128.2, 128.3, 128.7, 136.5 (Ar-**C**), 157.4, 157.6 (**C**O). MS (ES^+) *m/z* 347.2 $[M+Na]^+$; $C_{16}H_{24}N_2O_5Na$ requires 347.1583; found 347.1593.

11,11-Dimethyl-3,9-dioxo-1-phenyl-2, 10-dioxa-4,8-diazadodecan-6-yl methylsulfonate

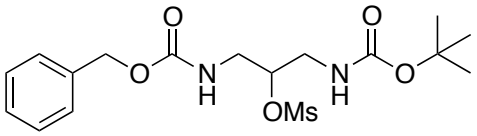

Benzyl *tert*-butyl(2-hydroxypropane-1,3-diyl)dicarbamate (907 mg, 2.80 mmol) was dissolved in anhydrous dicholormethane (16 mL), to which triethylamine (430 μL, 3.08 mmol) and methanesulfonyl chloride (238 μL, 3.08 mmol) were added at 0 °C. The resulting solution was stirred at this temperature for 5 minutes before being warmed to room temperature for a further 1 hour until complete conversion of the starting material was observed by ESI-MS. The solvent was removed under reduced pressure and the residue was partitioned between brine and DCM (30 mL, 1:1). The organic portion was separated and the aqueous layer was extracted with dichloromethane (3 x 30 mL). The combined organic portions were dried over $MgSO_4$, filtered and reduced to give a colourless oil (1.20 g, 100%). ^{1}H NMR (400 MHz, $CDCl_3$) δ 1.43 (9H, s, C(C**H**$_3$)$_3$), 3.04 (3H, s, SO_2C**H**$_3$), 3.22-3.59 (4H, m, 2 x NHC**H**$_2$), 4.68 (1H, br, N**H**), 5.10 (2H, s, C**H**$_2$Ph), 5.13 (1H, m, C**H**), 5.55 (1H, br, N**H**), 7.31-7.38 (5H, m, Ar-**H**). MS (ES$^+$) *m/z* 403.1 [M+H]$^+$.

Benzyl *tert*-butyl (2-azidopropane-1,3-diyl)dicarbamate, 31

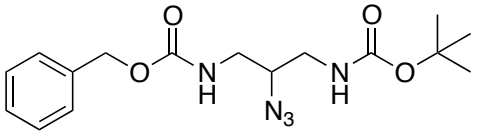

To a solution of the mesylate (1.20 g, 2.93 mmol) in anhydrous dimethylformamide (13 mL) was added NaN_3 (580 mg, 8.93 mmol) at room temperature. After addition, the cloudy mixture was heated to 60 °C under a stream of argon for 20 hours. Once no further conversion of starting materials has been revealed by ESI-MS, the mixture was cooled and the solvent was removed under reduced pressure. The residue was partitioned between

EtOAc/H_2O (40 mL, 1:1) and the organic portion was retained. The aqueous was extracted with EtOAc (3 x 40 mL) and the combined organic portions were dried over $MgSO_4$, filtered, concentrated to give the crude residue which was purified by column chromatography (hexane/EtOAc, 90:10 to 70:30 using 5% increments; R_f = 0.51) to give a colourless oil (605 mg, 59%). ^{1}H NMR (400 MHz, $CDCl_3$) δ 1.44 (9H, s, C(C**H**$_3$)$_3$), 3.07-3.28 (2H, m, C**H**$_2$), 3.31-3.49 (2H, m, C**H**$_2$), 3.66 (1H, quin, J = 6, C**H**), 5.04 (1H, br, N**H**), 5.11 (2H, s, C**H**$_2$Ph), 5.46 (1H, br, N**H**), 7.28-7.39 (5H, m, Ar-**H**). ^{13}C NMR (101 MHz, $CDCl_3$) δ 28.4 (C(**C**H$_3$)$_3$), 40.9, 41.3 (**C**H$_2$), 60.9 (**C**N$_3$), 67.2 (**C**H$_2$Ph), 80.2 (**C**(CH$_3$)$_3$), 128.2, 128.4, 128.7, 136.4 (**C**-Ar), 156.4, 156.9 (**C**O). MS (ES$^+$) *m/z* 372.1 [M+Na]$^+$; $C_{16}H_{23}N_5O_4Na$ requires 372.1648; found 372.1626.

tert-Butyl (3-amino-2-azidopropyl)carbamate, 32

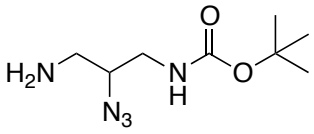

Benzyl *tert*-butyl (2-azidopropane-1,3-diyl)dicarbamate (605 mg, 1.73 mmol) was dissolved in anhydrous glyme (40 mL) to which a solution of $Ba(OH)_2$ in H_2O (0.15 M, 20 mL) was added. The resulting solution was heated to 80 °C under argon, and the reaction progress monitored by ESI-MS and TLC. After 48 hours, the reaction was cooled to room temperature and the solvent removed under reduced pressure. The residue was partially dissolved in brine and the pH adjusted to 5 using HCl (1 N). The aqueous portion was washed with dichloromethane (2 x 100 mL) before adjusting the pH to 12 using NaOH solution (2.5 M). The product was extracted with copious amounts of $CHCl_3$ (5 x 100 mL), dried over $MgSO_4$, filtered and concentrated to give a colourless oil (257 mg, 69%). ^{1}H NMR (400 MHz, $CDCl_3$) δ 1.45 (9H, s, C(C**H**$_3$)$_3$), 1.56 (2H, br. s) 2.76 (1H, dd, J = 13, 7, CH**H**NHCO), 2.88 (1H, dd, J = 13, 5, C**H**HNH), 3.20 (1H, dt, J = 13, 7, C**H**HNH$_2$), 3.35 (1H, dt, J = 13, 5 CH**H**NH$_2$), 3.50-3.60 (1H, m, C**H**), 4.89 (1H, br, N**H**). ^{13}C NMR (101 MHz, $CDCl_3$) δ 28.5 (C(**C**H$_3$)$_3$), 42.1, 43.4 (**C**H$_2$), 64.7

(**C**H), 78.4 (**C**(CH_3)$_3$), 156.6 (**C**O). MS (ES^+) *m/z* 216.1 $[M+H]^+$; $C_8H_{18}N_5O_2$ requires 216.1461; found 216.1458.

***tert*-Butyl (2-azido-3-((2-(diethoxyphosphoryl)ethyl)amino)propyl)carbamate, 33**

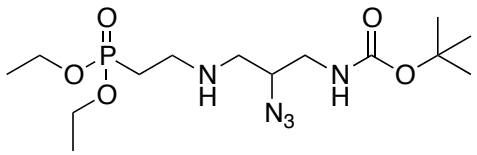

A solution of *tert*-butyl (3-amino-2-azidopropyl)carbamate (257 mg, 1.20 mmol), sodium carbonate (191 mg, 1.80 mmol) and diethyl (2-bromoethyl)phosphonate (345 μL, 1.90 mmol) in anhydrous ethanol (5 mL) was boiled under reflux for 16 hours until no further reaction was observed by TLC. The mixture was concentrated under reduced pressure, before being partitioned between DCM/H_2O (1:1, 30 mL). The organic portion was separated and the aqueous extracted with dicholormethane (3 x 25 mL). The combined organic layer was dried over $MgSO_4$, filtered and concentrated, allowing the crude residue to be purified by column chromatography (DCM/MeOH, 100% to 90:10 using 1% increments; R_f = 0.48) to give a colourless oil (147 mg, 32%). ^{1}H NMR (400 MHz, $CDCl_3$) δ 1.28 (6H, t, J = 7, P(OCH_2C**H**$_3$)$_2$), 1.39 (9H, s, C(C**H**$_3$)$_3$), 1.72 (1H, br, N**H**), 1.92 (2H, dt, $^2J_{H\text{-}P}$ = 18, $J_{H\text{-}H}$ = 7, PC**H**$_2$CH$_2$), 2.62 (1H, dd, J = 12, 6, C**H**H), 2.71 (1H, dd, J = 12, 6, CH**H**), 2.78-2.94 (2H, m, PCH$_2$C**H**$_2$), 3.13 (1H, dt, J = 14, 7, C**H**H), 3.29 (1H, dt, J = 14, 7, CH**H**), 3.56-3.67 (1H, m, C**H**), 4.03-4.16 (4H, qd, $^3J_{H\text{-}H}$ = 7, $^3J_{H\text{-}P}$ = 3, P(OC**H**$_2$CH$_3$)$_2$), 5.14 (1H, br, N**H**). ^{13}C NMR (101 MHz, $CDCl_3$) δ 16.5 (d, ^{3}J = 6, P(OCH$_2$**C**H$_3$)$_2$), 26.7 (d, ^{1}J = 140, NHCH$_2$**C**H$_2$P), 28.4 (C(**C**H$_3$)$_3$), 42.47 (**C**H$_2$), 43.4 (d, ^{2}J = 4, NH**C**H$_2$CH$_2$P), 50.4 (**C**H$_2$), 61.7 (d, ^{2}J = 7, P(O**C**H$_2$CH$_3$)$_2$), 61.8 (**C**N$_3$), 79.7 (**C**(CH_3)$_3$), 156.0 (**C**O). ^{31}P NMR ($CDCl_3$, 162 MHz) δ 31.29. MS (ES^+) *m/z* 380.2 $[M+H]^+$; $C_{14}H_{31}N_5O_5P$ requires 380.2063; found 380.2054.

tert-Butyl (2-azido-3-((2-(diethoxyphosphoryl)ethyl)(2-ethoxy-3,4-dioxocyclobut-1-en-1-yl)amino)propyl)carbamate, 34

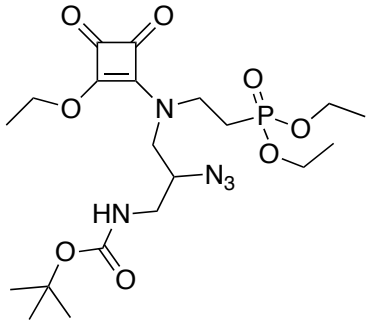

To a solution of 3,4-diethoxy-3-cyclobutene-1,2-dione (47 μL, 0.32 mmol) in anhydrous ethanol (1 mL), was added a solution of *tert*-butyl (2-azido-3-((2-(diethoxyphosphoryl)ethyl)amino)propyl)carbamate (147 mg, 0.32 mmol) in anhydrous ethanol (2.5 mL) over 30 minutes. The resulting solution was stirred under argon at room temperature and the progress of the reaction followed by TLC. After 48 hours, the solution was concentrated under reduced pressure and the crude residue purified by column chromatography (DCM/MeOH, 100% to 97:3 using 0.5% increments; R_f = 0.26) to give a colourless oil, observed as a pair of rotamers (133 mg, 83%). ^{1}H NMR (400 MHz, $CDCl_3$) δ 1.25 (6H, t, J = 7, P(OCH$_2$C**H**$_3$)$_2$), 1.35 (9H, s, C(C**H**$_3$)$_3$), 1.38 (3H, t, J = 7, OCH$_2$C**H**$_3$), 1.98-2.14 (2H, m, PC**H**$_2$CH$_2$), 3.05-3.39 (2H, m, C**H**$_2$), 3.45-3.96 (5H, m, C**H**$_2$C**H** + PCH$_2$C**H**$_2$), 3.98-4.10 (4H, m, P(OC**H**$_2$CH$_3$)$_2$), 4.69 (2H, q, J = 7, OC**H**$_2$CH$_3$), 5.29 (1H, br, N**H**). ^{13}C NMR (101 MHz, $CDCl_3$) δ 15.7 (OCH$_2$**C**H$_3$), 16.3 (d, ^{3}J = 6, P(OCH$_2$**C**H$_3$)$_2$), 26.0 (d, ^{1}J = 140, NCH$_2$**C**H$_2$P), 28.3 (C(**C**H$_3$)$_3$), 42.1 (**C**H$_2$), 45.2 (N**C**H$_2$CH$_2$P), 50.9 (**C**H$_2$), 60.96 (**C**N$_3$), 62.0 (d, ^{2}J = 7, P(O**C**H$_2$CH$_3$)$_2$), 70.0 (O**C**H$_2$CH$_3$), 79.8 (**C**(CH$_3$)$_3$), 155.9 (**C**O), 172.4, 177.2 (**C**=**C**), 182.8, 188.2 (**C**O). ^{31}P NMR ($CDCl_3$, 162 MHz) δ 27.38. MS (ES$^+$) *m/z* 526.1 [M+Na]$^+$; $C_{20}H_{34}N_5O_8PNa$ requires 526.2043; found 526.2027.

Diethyl (2-(4-azido-8,9-dioxo-2,6-diazabicyclo[5.2.0]non-1(7)-en-2-yl)ethyl)phosphonate, 35

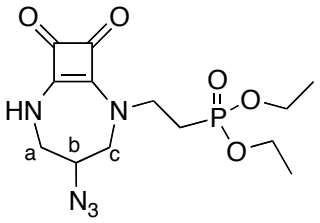

To a solution of *tert*-butyl (2-azido-3-((2-(diethoxyphosphoryl)ethyl)(2-ethoxy-3,4-dioxocyclobut-1-en-1-yl)amino)propyl)carbamate (133 mg, 0.26 mmol) in anhydrous dichloromethane (1 mL) was added TFA (1 mL), and the resulting solution stirred at room temperature for 1 hour. Reaction was observed to be complete after this period, as indicated by TLC, and the solvents were removed under reduced pressure. The residue was re-dissolved in dichloromethane and evaporated to dryness. This process was repeated 5 times to ensure complete removal of excess TFA. The TFA salt was dissolved in anhydrous ethanol (3 mL) to which a solution of triethylamine (145 μL, 1.04 mmol) in anhydrous ethanol (2 mL) was added over a 20 minute period. The resulting solution was heated to reflux for 18 hours, until no further reaction was observed by TLC. At this point, the solvent was removed under reduced pressure and the crude residue purified by column chromatography (DCM/MeOH, 100% to 90:10 using 1% increments; R_f = 0.21) to give a colourless oil (77 mg, 83%). ^{1}H NMR (700 MHz, $CDCl_3$) δ 1.30 (6H, 2 x t, J = 7, P(OCH$_2$C**H**$_3$)$_2$), 2.12-2.23 (2H, m, PC**H**$_2$CH$_2$), 3.49 (1H, dd, J = 14, 7, H^c(axial)), 3.55 (1H, d, J = 14, H$^{c/a}$(eq)), 3.64 (1H, d, J = 14, H$^{c/a}$(eq)), 3.67 (1H, ddd, J = 14, 7, 4, H^a(axial)), 3.86-4.12 (7H, m, C**H** + NC**H**$_2$CH$_2$P + P(OC**H**$_2$CH$_3$)$_2$), 8.18 (1H, br, s, NH). ^{13}C NMR (176 MHz, $CDCl_3$) δ 16.5 (d, ^{3}J = 6, P(OCH$_2$**C**H$_3$)$_2$), 25.9 (d, ^{1}J = 140, NCH$_2$**C**H$_2$P), 45.9 (N**C**H$_2$CH$_2$P), 48.7, 56.0 (**C**H$_2$), 59.4 (**C**N$_3$), 62.2 (dd, ^{2}J = 7, P(O**C**H$_2$CH$_3$)$_2$), 167.7, 168.1 (**C**=**C**), 180.8, 182.4 (**C**O). ^{31}P NMR ($CDCl_3$, 243 MHz) δ 26.78. MS (ES$^+$) *m/z* 358.1 [M+H]$^+$; $C_{13}H_{21}N_5O_5P$ requires 358.1280; found 358.1269.

Diethyl (2-(4-amino-8,9-dioxo-2,6-diazabicyclo[5.2.0]non-1(7)-en-2-yl)ethyl)phosphonate, 36

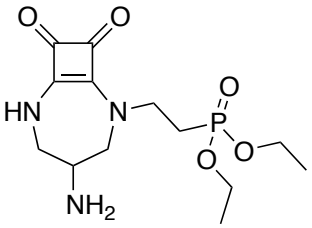

To a solution of diethyl (2-(4-azido-8,9-dioxo-2,6-diazabicyclo[5.2.0]non-1(7)-en-2-yl)ethyl)phosphonate (71 mg, 0.2 mmol) in anhydrous THF (4 mL) was added H_2O (100 μL) and PPh_3 (78 mg, 0.3 mmol). The suspension was stirred under argon at 60 °C and over time, became a clear solution. After stirring for 16 hours, the solvent was removed under reduced pressure and the crude residue partitioned between DCM and H_2O (10 mL, 1:1). The aqueous layer was separated and washed twice with DCM (10 mL), before lyophilisation yielded a white solid (65 mg, 99%). ^{1}H NMR (400 MHz, MeOD) δ 1.34 (6H, t, J = 7 P(OCH$_2$C**H**$_3$)$_2$), 2.31 (2H, dt, $J_{H\text{-}P}$ = 18, $J_{H\text{-}H}$ = 7, PC**H**$_2$CH$_2$), 3.48-3.66 (5H, m, C**H** + C**H**$_2$), 3.98-4.07 (2H, m, NC**H**$_2$CH$_2$P), 4.09-4.19 (4H, qd, $^3J_{H\text{-}H}$ = 7, $^3J_{H\text{-}P}$ = 3, P(O**C**H$_2$CH$_3$)$_2$). ^{13}C NMR (101 MHz, MeOD) δ 16.7 (d, ^{3}J = 6, P(OCH$_2$**C**H$_3$)$_2$), 25.5 (d, ^{1}J = 140, NCH$_2$**C**H$_2$P), 46.4 (N**C**H$_2$CH$_2$P), 51.1 (**C**H), 52.3 (**C**H$_2$), 58.0 (**C**H$_2$), 63.6 (d, ^{2}J = 7, P(O**C**H$_2$CH$_3$)$_2$), 169.2, 169.6 (**C**=**C**), 182.7, 182.9 (**C**O). ^{31}P NMR (162 MHz, MeOD) δ 30.97. MS (ES$^+$) *m/z* 332.1 [M+H]$^+$; $C_{13}H_{23}N_3O_5P$ requires 332.1375; found 332.1362. M. Pt > 250 °C.

Methyl 2-((azido-3-((*tert*-butoxycarbonyl)amino)propyl)amino)acetate, 37

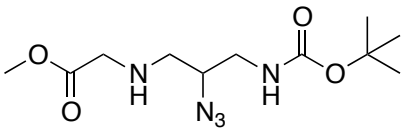

A solution of *tert*-butyl (3-amino-2-azidopropyl)carbamate (395 mg, 1.84 mmol), sodium carbonate (293 mg, 2.76 mmol) and methyl bromoacetate (275 μL, 2.91 mmol) in anhydrous ethanol (8 mL) was boiled under reflux for 16 hours until no further reaction was observed by TLC. The mixture was concentrated under reduced pressure before being partitioned between DCM/H_2O (1:1, 30 mL). The

organic portion was retained and the aqueous layer was extracted with dicholormethane (3 x 25 mL). The combined organic fractions were dried over $MgSO_4$, filtered and concentrated, allowing the crude residue to be purified by column chromatography (DCM/MeOH, 100% to 90:10 using 1% increments R_f = 0.41) to give a colourless oil (178 mg, 34%). ^{1}H NMR (400 MHz, $CDCl_3$) δ 1.39 (9H, s, C(C**H**$_3$)$_3$), 1.85 (1H, br, N**H**), 2.63 (1H, dd, J = 12, 7, C**H**H), 2.76 (1H, dd, J = 12, 5, CH**H**), 3.13 (1H, dt, J = 14, 7, C**H**H), 3.31 (1H, dt, J = 14, 5, CH**H**), 3.39 (2H, s, C**H**$_2$), 3.57-3.65 (1H, m, C**H**), 3.68 (3H, s, C**H**$_3$) 5.09 (1H, br, N**H**). ^{13}C NMR (101 MHz, $CDCl_3$) δ 28.4 (C(**C**H$_3$)$_3$), 42.4 (**C**H$_2$), 50.5, 50.6 (**C**H$_2$), 51.9 (**C**H$_3$), 62.0 (**C**N$_3$), 79.7 (**C**(CH$_3$)$_3$), 156.0, 172.7 (**C**O). MS (ES$^+$) *m/z* 288.2 $[M+H]^+$; $C_{11}H_{22}N_5O_4$ requires 288.1672; found 288.1670. [Transesterification from the solvent meant the ethyl ester was also present $C_{12}H_{24}N_5O_4$ requires 302.2; found 302.2].

Methyl 2-((azido-3-((*tert*-butoxycarbonyl)amino)propyl)(2-ethoxy-3,4-dioxocyclobut-1-en-1-yl)amino)acetate, 38

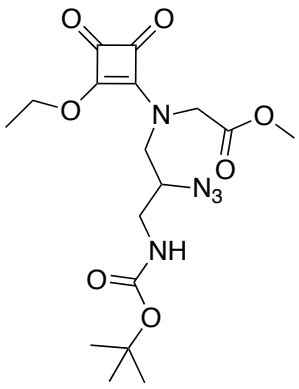

To a solution of 3,4-diethoxy-3-cyclobutene-1,2-dione (45 μL, 0.31 mmol) in anhydrous ethanol (0.5 mL), was added a solution of methyl 2-((azido-3-((*tert*-butoxycarbonyl)amino)propyl)amino)acetate (88 mg, 0.31 mmol) in anhydrous ethanol (2.5 mL) over 30 mins. The resulting solution was stirred under argon at room temperature and the progress of the reaction followed by TLC. When no further reaction was observed by TLC, the solution was concentrated under reduced pressure. The crude residue was then purified by column chromatography (DCM/MeOH, 100% to 95:5 using 0.5% increments; R_f = 0.58) to give a colourless oil as a pair of rotamers (89 mg, 70%). ^{1}H NMR (400 MHz, $CDCl_3$) δ 1.41 (9H, s, C(C**H**$_3$)$_3$), 1.43 (3H, t, J = 7, OCH$_2$C**H**$_3$), 3.10-3.43 (3H, m,

C**H**$_2$), 3.50-3.70 (1H, m, C**H**$_2$), 3.77 (3H, s, C**H**$_3$), 3.79-3.91 (1H, m, C**H**), 4.14-4.28 (1H, m, C**H**$_2$), 4.44-4.56 (1H, m, C**H**$_2$), 4.73 (2H, q, J = 7, OC**H**$_2$CH$_3$), 5.13 (1H, br, N**H**). ^{13}C NMR (101 MHz, $CDCl_3$) δ 15.8 (OCH$_2$**C**H$_3$), 28.4 (C(**C**H$_3$)$_3$), 42.0, 51.9, 52.0 (**C**H$_2$), 52.9 (**C**H$_3$), 61.2 (**C**N$_3$), 70.3 (O**C**H$_2$CH$_3$), 80.1 (**C**(CH$_3$)$_3$), 155.9 (**C**O), 168.8 (**C**=**C**) , 173.2 (**C**O), 177.8 (**C**=**C**), 183.2, 188.3 (**C**O). MS (ES$^+$) *m/z* 434.0 [M+Na]$^+$; $C_{17}H_{25}N_5O_7Na$ requires 434.1652; found 434.1649. [The ethyl ester was also present $C_{18}H_{27}N_5O_4Na$ requires 448.1; found 448.1].

Methyl 2-(4-azido-8,9-dioxo-2,6-diazabicyclo[5.2.0]non-1(7)-en-2-yl)acetate, 39

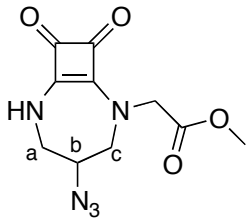

To a solution of methyl 2-((azido-3-((*tert*-butoxycarbonyl)amino)propyl)(2-ethoxy-3,4-dioxocyclobut-1-en-1-yl)amino)acetate (89 mg, 0.22 mmol) in anhydrous dichloromethane (1 mL) was added TFA (1 mL), and the resulting solution stirred at room temperature for 1 hour. Reaction was complete after this period, as indicated by TLC, and the solvents were removed under reduced pressure. The residue was re-dissolved in dichloromethane and again reduced under reduced pressure. This process was repeated 5 times to ensure complete removal of excess TFA. The TFA salt was dissolved in anhydrous ethanol (3 mL) to which a solution of triethylamine (120 μL, 0.868 mmol) in anhydrous ethanol (1.5 mL) was added over a 20 minute period. The resulting solution was heated under reflux for 18 hours, until no further reaction was observed by TLC. At this point, the solvent was removed under reduced pressure and the crude residue purified by column chromatography (DCM/MeOH, 100% to 90:10 using 1% increments; R_f = 0.42) to give a colourless oil (46 mg, 80%). ^{1}H NMR (700 MHz, DMSO-d_6) δ 3.44-3.49 (1H, d, J = 14, **H**^{a}(eq)), 3.56-3.61 (2H, m, **H**$^{a/c}$ (ax)), 3.63 (1H, d, J = 14, **H**^{c} (eq)), 3.69 (3H, s, C**H**$_3$), 4.34 (1H, m, CH), 4.40 (1H, d, J = 17, C**H**$_2$CO$_2$Me), 4.67 (1H, d, J = 17, C**H**$_2$CO$_2$Me), 8.69 (1H, br, N**H**). ^{13}C NMR (176 MHz, DMSO-d_6) δ 47.7 (**C**^{a}), 50.8 (**C**H$_2$CO$_2$Me), 52.2 (**C**H$_3$), 55.7 (**C**^{c}), 58.8 (**C**N$_3$),

167.9, 168.5 (**C**=**C**), 169.0, 181.3, 181.4 (**C**O). MS (ES$^+$) *m/z* 266.1 [M+H]$^+$; $C_{10}H_{12}N_5O_4$ requires 266.0889; found 266.0902. [The ethyl ester was also present $C_{11}H_{14}N_5O_4$ requires 280.1; found 280.1].

Methyl 2-(4-amino-8,9-dioxo-2,6-diazabicyclo[5.2.0]non-1(7)-en-2-yl)acetate, 40

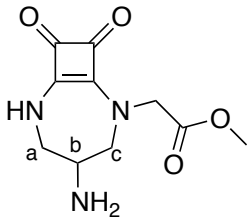

To a solution of methyl 2-(4-azido-8,9-dioxo-2,6-diazabicyclo[5.2.0]non-1(7)-en-2-yl)acetate (43 mg, 0.15 mmol) in anhydrous THF (3.5 mL) was added H_2O (200 µL) and PPh_3 (60 mg, 0.23 mmol). The suspension was stirred under argon at 60 °C and over time, became a clear solution. After stirring for 16 hours, the solvent was removed under reduced pressure and the crude residue partitioned between DCM and H_2O (10 mL, 1:1). The aqueous layer was separated and washed twice with DCM (10 mL), before lyophilisation yielded a white solid (34 mg, 92%). ^{1}H NMR (600 MHz, DMSO-d_6) δ 2.06-2.48 (2H, br, N**H**$_2$), 3.11-3.18 (2H, m, **H**$^{a/c}$), 3.23-3.28 (1H, m, H^b), 3.32-3.40 (2H, m, **H**$^{a'/c'}$), 3.69 (3H, s, C**H**$_3$), 4.48 (1H, d, J = 17, C**H**$_2$CO$_2$Me), 4.54 (1H, d, J = 17, C**H**$_2$CO$_2$Me), 8.58 (1H, br, N**H**). ^{13}C NMR (151 MHz, DMSO-d_6) δ 51.2 (**C**H$_2$CO$_2$Me), 51.6 (**C**H), 51.9 (**C**H$_2$), 52.2 (**C**H$_3$) 58.8 (**C**H$_2$), 167.5, 168.2, (**C**=**C**), 169.4, 181.3, 181.6 (**C**O). MS (ES$^+$) *m/z* 240.0 [M+H]$^+$; $C_{10}H_{14}N_3O_4$ requires 240.0984; found 240.0979. M. Pt > 250 °C.

[The ethyl ester was also present $C_{11}H_{16}N_3O_4$ requires 254.1140; found 254.1140].

Methyl 3-((2-azido-3-((*tert*-butoxycarbonyl)amino)propyl)amino)propanoate, 41

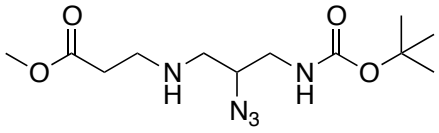

A solution of *tert*-butyl (3-amino-2-azidopropyl)carbamate (200 mg, 0.93 mmol), diisopropylethylamine (243 μL, 1.4 mmol) and methyl-3-bromopropionate (102 μL, 0.93 mmol) in anhydrous DMF (8 mL) was stirred at room temperature for 48 hours until no further reaction was observed by TLC. The mixture was concentrated under reduced pressure before being partitioned between EtOAc/H_2O (1:1, 30 mL). The organic portion was separated and the aqueous extracted with EtOAc (3 x 25 mL). The combined organic layer were dried over $MgSO_4$, filtered and concentrated, allowing the crude residue to be purified by column chromatography (DCM/MeOH, 100% to 94:6 using 1% increments; R_f = 0.47) to give a yellow oil (220 mg, 79%). ^{1}H NMR (400 MHz, $CDCl_3$) δ 1.43 (9H, s, C(C**H**$_3$)$_3$), 1.50 (1H, br, N**H**), 2.77 (2H, dd, J = 12, 7, C**H**$_2$), 2.89 (2H, dd, J = 12, 5, C**H$_2$**), 3.09 (2H, t, J = 6, C**H**$_2$), 3.36 (2H, t, J = 6, C**H**$_2$), 3.71 (3H, s, C**H**$_3$), 4.02 (1H, m, C**H**), 5.19 (1H, br, N**H**). ^{13}C NMR (101 MHz, $CDCl_3$) δ 28.4 (C(**C**H$_3$)$_3$), 32.5, 42.0, 44.8, 49.5 (**C**H$_2$), 52.3 (**C**H$_3$), 59.6 (**C**N$_3$), 80.4 (**C**(CH$_3$)$_3$), 156.5, 172.4 (**C**O). MS (ES$^+$) *m/z* 302.2 [M+H]$^+$; $C_{12}H_{24}N_5O_4$ requires 302.1828; found 302.1831.

Methyl 3-((2-azido-3-((*tert*-butoxycarbonyl)amino)propyl)(2-ethoxy-3,4-dioxocyclobut-1-en-1-yl)amino)propanoate, 42

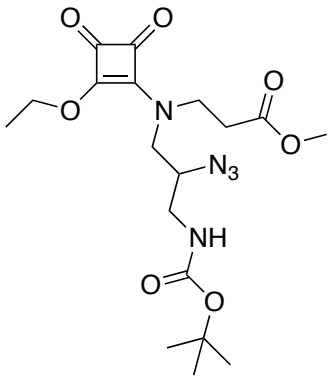

To a solution of 3,4-diethoxy-3-cyclobutene-1,2-dione (102 μL, 0.68 mmol) in anhydrous ethanol (1 mL), was added a solution of methyl 3-((2-azido-3-((*tert*-butoxycarbonyl)amino)propyl)amino)propanoate (206 mg, 0.68 mmol) in anhydrous ethanol (5 mL) over 30 mins. The resulting solution was stirred under argon at room temperature and the progress of the reaction followed by TLC. When no further reaction was observed by TLC, the solution was concentrated under reduced pressure. The crude residue was then purified by column chromatography (DCM/MeOH, 100% to 95:5 using 0.5% increments; R_f = 0.59) to give a colourless oil as a pair of rotamers (234 mg, 81%). ^{1}H NMR (400 MHz, $CDCl_3$) δ 1.41 (9H, s, C(C**H**$_3$)$_3$), 1.43 (3H, t, J = 7, OCH$_2$C**H**$_3$), 2.66 (2H, t, J = 7, CH$_2$C**H**$_2$CO$_2$Me), 3.08-3.57 (3H, m, C**H**$_2$), 3.66 (3H, s, C**H**$_3$) 3.71-4.07 (4H, m, C**H**$_2$C**H**), 4.75 (2H, q, J = 7, OC**H**$_2$CH$_3$), 5.09 (1H, br, N**H**). ^{13}C NMR (101 MHz, $CDCl_3$) δ 15.9 (OCH$_2$**C**H$_3$), 28.4 (C(**C**H$_3$)$_3$), 33.9, 42.2, 46.2, 51.1 (**C**H$_2$), 52.1 (**C**H$_3$), 61.2 (**C**N$_3$), 70.1 (O**C**H$_2$CH$_3$), 80.1 (**C**(CH$_3$)$_3$), 155.9 (**C**O), 171.2 (**C**=**C**) , 172.7 (**C**O), 177.4 (**C**=**C**), 183.0, 188.4 (**C**O). MS (ES$^+$) *m/z* 851.1 [2M+H]$^+$; $C_{36}H_{55}N_{10}O_{14}$ requires 851.3899; found 851.3918.

Methyl 3-(4-azido-8,9-dioxo-2,6-diazabicyclo[5.2.0]non-1(7)-en-2-yl)propanoate, 43

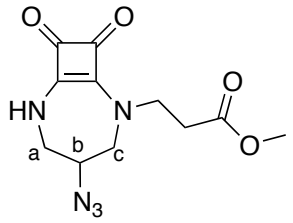

To a solution of methyl 3-((2-azido-3-((*tert*-butoxycarbonyl)amino)propyl)(2-ethoxy-3,4-dioxocyclobut-1-en-1-yl)amino)propanoate (78 mg, 0.18 mmol) in anhydrous dichloromethane (1 mL) was added TFA (1 mL), and the resulting solution stirred at room temperature for 1 hour. Reaction was complete after this period, as indicated by TLC, and the solvents were removed under reduced pressure. The residue was re-dissolved in dichloromethane and again concentrated under reduced pressure. This process was repeated 5 times to ensure complete removal of excess TFA. The TFA salt was dissolved in anhydrous ethanol (2 mL) to which a solution of triethylamine (102 μL, 0.736 mmol) in anhydrous ethanol (1.5 mL) was added over a 20 minute period. The resulting solution was heated to reflux for 18 hours, until no further reaction was observed by TLC. At this point, the solvent was removed and the crude residue purified by column chromatography (DCM/MeOH, 100% to 90:10 using 1% increments; R_f = 0.52) to give a colourless oil (42 mg, 82%). ^{1}H NMR (700 MHz, DMSO-d_6) δ 2.69 (2H, overlapping dt, J = 14, 7, C**H**$_2$CO$_2$Me), 3.40 (1H, dd, J = 14, 7, **H**^{a}(eq)), 3.55 (1H, ddd, J = 14, 7, 4, **H**^{a}(axial)), 3.57-3.59 (2H, br, m, **H**^{c} (ax/eq)), 3.60 (3H, s, C**H**$_3$), 3.86 (1H, dt, J = 14, 7, C**H**$_2$CH$_2$CO$_2$Me), 3.94 (1H, dt, J = 14, 7, C**H**$_2$CH$_2$CO$_2$Me), 4.31 (1H, m, C**H**), 8.53 (1H, br, N**H**). ^{13}C NMR (176 MHz, DMSO-d_6) δ 33.0 (**C**^{e}), 45.9 (**C**H$_2$CH$_2$CO$_2$Me), 47.5 (**C**^{a}), 51.5 (**C**H$_3$), 54.4 (CH$_2$**C**H$_2$CO$_2$Me), 58.9 (**C**N$_3$), 167.7, 168.3 (**C**=**C**), 171.1, 180.9, 181.0 (**C**O). MS (ES$^+$) *m/z* 280.1 [M+H]$^+$; $C_{11}H_{14}N_5O_4$ requires 280.1046; found 280.1067.

Methyl 3-(4-amino-8,9-dioxo-2,6-diazabicyclo[5.2.0]non-1(7)-en-2-yl)propanoate, 44

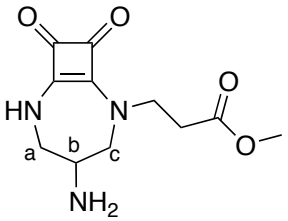

To a solution of methyl 3-(4-azido-8,9-dioxo-2,6-diazabicyclo[5.2.0]non-1(7)-en-2-yl)propanoate (38 mg, 0.14 mmol) in anhydrous THF (3 mL) was added H_2O (100 µL) and PPh_3 (54 mg, 0.20 mmol). The suspension was stirred under argon at 60 °C and over time, became a clear solution. After stirring for 16 hours, the solvent was removed under reduced pressure and the crude residue partitioned between DCM and H_2O (10 mL, 1:1). The aqueous layer was separated and washed twice with DCM (10 mL), before lyophilisation yielded a white solid (34 mg, 99%). ^{1}H NMR (700 MHz, DMSO-d_6) δ 1.78-2.18 (2H, br, N**H**$_2$), 2.69 (2H, overlapping dt, J = 14, 7, C**H**$_2$CO$_2$Me), 3.11 (2H, m, **H**^{a}), 3.21 (1H, dd, J = 14, 7, **H**^{c}(axial)), 3.27-3.31 (1H, m, **H**^{b}), 3.36 (1H, d, J = 14, **H**^{c}(eq)), 3.59 (3H, s, C**H**$_3$), 3.87 (1H, dt, J = 14, 7, C**H**$_2$CH$_2$CO$_2$Me), 3.92 (1H, dt, J = 14, 7, C**H**$_2^{d'}$), 8.53 (1H, br, N**H**). ^{13}C NMR (176 MHz, DMSO-d_6) δ 32.9 (CH$_2$**C**H$_2$CO$_2$Me), 46.2 (**C**H$_2$CH$_2$CO$_2$Me), 51.5 (**C**H$_3$), 51.6 (**C**H), 51.8 (**C**H$_2$), 58.8 (**C**H$_2$), 167.3, 168.0 (**C**=**C**), 171.3, 180.1, 181.2 (**C**O). MS (ES$^+$) *m/z* 254.1 [M+H]$^+$; $C_{11}H_{16}N_3O_4$ requires 254.1141; found 254.1166. M. Pt > 250 °C.

***tert*-Butyl (2-azido-3-((3-(diethoxyphosphoryl)propyl)amino)propyl)carbamate, 45**

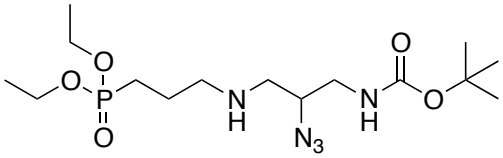

A solution of *tert*-butyl (3-amino-2-azidopropyl)carbamate (395 mg, 1.84 mmol), sodium carbonate (293 mg, 2.76 mmol) and diethyl-3-bromopropyl

phosphonate (560 μL, 2.91 mmol) in anhydrous ethanol (8 mL) was boiled under reflux for 16 hours until no further reaction was observed by TLC. The mixture was concentrated under reduced pressure before being partitioned between DCM/H_2O (1:1, 30 mL). The organic portion was separated and the aqueous extracted with dicholormethane (3 x 25 mL). The combined organic fractions were dried over $MgSO_4$, filtered and concentrated, allowing the crude residue to be purified by column chromatography (DCM/MeOH, 100% to 92:8 using 1% increments; R_f = 0.35) to give a colourless oil (396 mg, 55%). ^{1}H NMR (400 MHz, $CDCl_3$) δ 1.31 (6H, t, J = 7, P(OCH$_2$C**H**$_3$)$_2$), 1.43 (9H, s, C(C**H**$_3$)$_3$), 1.71-1.86 (5H, m, PC**H**$_2$C**H**$_2$CH$_2$ + N**H**), 2.66 (1H, dd, J = 12, 7, C**H**H), 2.69 (2H, m, PCH$_2$CH$_2$C**H**$_2$), 2.71 (1H, dd, J = 12, 5, CH**H**), 3.17 (1H, dt, J = 14, 7, C**H**H), 3.33 (1H, dt, J = 14, 5, CH**H**), 3.63-3.72 (1H, m, C**H**), 4.02-4.15 (4H, qd, $^3J_{H-H}$ = 7, $^3J_{H-P}$ = 3, P(OC**H**$_2$CH$_3$)$_2$), 5.01 (1H, br, N**H**). ^{13}C NMR (101 MHz, $CDCl_3$) δ 16.6 (d, ^{3}J = 6, P(OCH$_2$**C**H$_3$)$_2$), 23.0 (d, J = 5, NCH$_2$**C**H$_2$CH$_2$P), 23.4 (d, ^{1}J = 143, NHCH$_2$**C**H$_2$P), 28.5 (C(**C**H$_3$)$_3$), 42.6 (**C**H$_2$), 50.0 (d, ^{2}J = 18, N**C**H$_2$CH$_2$CH$_2$P), 50.8 (**C**H$_2$), 61.7 (d, ^{2}J = 7, P(O**C**H$_2$CH$_3$)$_2$), 61.9 (**C**N$_3$), 79.9 (**C**(CH$_3$)$_3$), 156.1 (**C**O). ^{31}P NMR ($CDCl_3$, 162 MHz) δ 32.01. MS (ES$^+$) *m/z* 394.2 [M+H]$^+$; $C_{15}H_{32}N_5O_5P$ requires 394.2219; found 394.2215.

tert-Butyl (2-azido-3-((3-(diethoxyphosphoryl)propyl)(2-ethoxy-3,4-dioxocyclobut-1-en-1-yl)amino)propyl)carbamate, 46

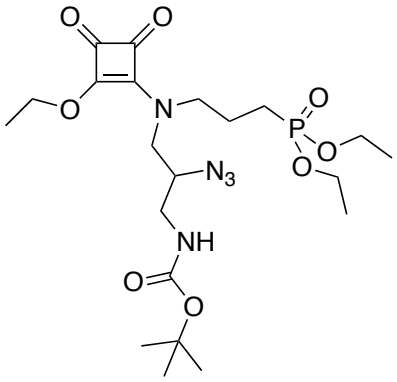

To a solution of 3,4-diethoxy-3-cyclobutene-1,2-dione (152 μL, 1.03 mmol) in anhydrous ethanol (1 mL), was added a solution of *tert*-butyl (2-azido-3-((3-(diethoxyphosphoryl)propyl)amino)propyl)carbamate (396 mg, 1.0 mmol) in anhydrous ethanol (7 mL) over 30 mins. The resulting solution was stirred

under argon at room temperature and the progress of the reaction followed by TLC. After no further reaction was observed by TLC, the solution was concentrated under reduced pressure. The crude residue was then purified by column chromatography (DCM/MeOH, 100% to 95:5 using 0.5% increments; R_f = 0.44) to give a colourless oil as a pair of rotamers (417 mg, 79%). ^{1}H NMR (700 MHz, $CDCl_3$) δ 1.32 (6H, t, J = 7, $P(OCH_2C\mathbf{H}_3)_2$), 1.44 (9H, s, $C(C\mathbf{H}_3)_3$), 1.46 (3H, t, J = 7, $OCH_2C\mathbf{H}_3$), 1.65-1.96 (4H, m, $PC\mathbf{H}_2\mathbf{C}H_2CH_2$), 3.11-3.42 (2H, m, $C\mathbf{H}_2$), 3.48-3.89 (5H, m, $C\mathbf{H}_2C\mathbf{H}$ + $PCH_2CH_2C\mathbf{H}_2$), 4.03-4.15 (4H, m, $P(OC\mathbf{H}_2CH_3)_2$), 4.75-4.80 (2H, m, $OC\mathbf{H}_2CH_3$), 5.04 (1H, br, N**H**). ^{13}C NMR (175 MHz, $CDCl_3$) δ 16.0 ($OCH_2\mathbf{C}H_3$), 16.6 (d, ^{3}J = 6, $P(OCH_2\mathbf{C}H_3)_2$), 22.3 (d, ^{2}J = 5, $NCH_2\mathbf{C}H_2CH_2P$), 22.6 (d, ^{1}J = 143, $NCH_2CH_2\mathbf{C}H_2P$), 28.4 ($C(\mathbf{C}H_3)_3$), 42.2 ($\mathbf{C}H_2$), 50.6 (d, ^{3}J = 18, $N\mathbf{C}H_2CH_2CH_2P$), 50.8 ($\mathbf{C}H_2$), 61.1 ($\mathbf{C}N_3$), 62.0 (d, ^{2}J = 7, $P(O\mathbf{C}H_2CH_3)_2$), 70.2 ($O\mathbf{C}H_2CH_3$), 80.3 ($\mathbf{C}(CH_3)_3$), 156.0 (**C**O), 172.7, 177.2 (**C**=**C**), 182.9, 188.5 (**C**O). ^{31}P NMR ($CDCl_3$, 283 MHz) δ 30.14. MS (ES^+) *m/z* 518.1 $[M+H]^+$; $C_{21}H_{37}N_5O_8P$ requires 518.2380; found 518.2375.

Diethyl (3-(4-azido-8,9-dioxo-2,6-diazabicyclo[5.2.0]non-1(7)-en-2-yl)propyl)phosphonate, 47

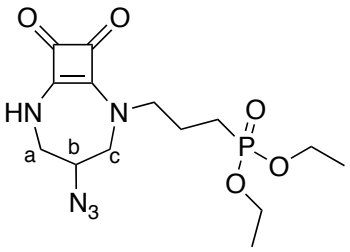

To a solution of *tert*-butyl (2-azido-3-((3-(diethoxyphosphoryl)propyl)(2-ethoxy-3,4-dioxocyclobut-1-en-1-yl)amino)propyl)carbamate (201 mg, 0.39 mmol) in anhydrous dichloromethane (1 mL) was added TFA (1 mL), and the resulting solution stirred at room temperature for 1 hour. Reaction was complete after this period, as indicated by TLC, and the solvents were removed under reduced pressure. The residue was re-dissolved in dichloromethane and again reduced under reduced pressure. This process was repeated 5 times to ensure complete removal of excess TFA. The TFA salt was dissolved in anhydrous ethanol (5 mL) to which a solution of triethylamine (218 μL, 1.56

mmol) in anhydrous ethanol (2 mL) was added over a 20 minute period. The resulting solution was heated to reflux for 18 hours, until no further reaction was observed by TLC. At this point, the solvent was removed under reduced pressure and the crude residue purified by column chromatography (DCM/MeOH, 100% to 90:10 using 1% increments; R_f = 0.26) to give a colourless oil (126 mg, 87%). ^{1}H NMR (400 MHz, $CDCl_3$) δ 1.30 (6H, t, J = 7, P(OCH$_2$C**H**$_3$)$_2$), 1.69-2.01 (4H, m, PC**H**$_2$C**H**$_2$CH$_2$), 3.49 (1H, dd, J = 13, 7, H^c(axial)), 3.52-3.62 (3H, m, H$^{c/a}$(eq), H^a(axial)), 3.71-4.11 (7H, m, C**H** + NC**H**$_2$CH$_2$CH$_2$P + P(OC**H**$_2$CH$_3$)$_2$), 8.16 (1H, br, s, NH).). ^{13}C NMR (101MHz, $CDCl_3$) δ 16.5 (d, ^{3}J = 6, P(OCH$_2$**C**H$_3$)$_2$), 21.8 (d, ^{2}J = 5, NCH$_2$**C**H$_2$CH$_2$P), 22.2 (d, ^{1}J = 143, NCH$_2$CH$_2$**C**H$_2$P), 48.5 (**C**H$_2$), 51.3 (d, ^{3}J = 18, N**C**H$_2$CH$_2$CH$_2$P), 55.3 (**C**H$_2$), 59.5 (**C**N$_3$), 62.0 (d, ^{2}J = 7, P(O**C**H$_2$CH$_3$)$_2$), 167.6, 168.6 (**C**=**C**), 180.9, 182.2 (**C**O). ^{31}P NMR ($CDCl_3$, 162 MHz) δ 30.80. MS (ES$^+$) *m/z* 372.1 [M+H]$^+$; $C_{14}H_{23}N_5O_5P$ requires 372.1437; found 372.1436.

Diethyl (3-(4-amino-8,9-dioxo-2,6-diazabicyclo[5.2.0]non-1(7)-en-2-yl)propyl)phosphonate, 48

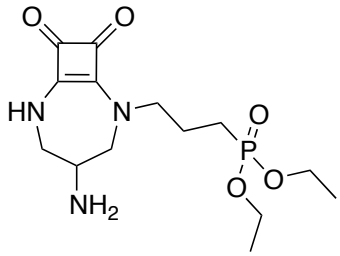

To a solution of diethyl (3-(4-azido-8,9-dioxo-2,6-diazabicyclo[5.2.0]non-1(7)-en-2-yl)propyl)phosphonate (179 mg, 0.48 mmol) in anhydrous THF (10 mL) was added H_2O (250 μL) and PPh_3 (189 mg, 0.72 mmol). The suspension was stirred under argon at 60 °C and over time, became a clear solution. After stirring for 16 hours, the solvent was removed under reduced pressure and the crude residue partitioned between DCM and H_2O (20 mL, 1:1). The aqueous layer was separated and washed twice with DCM (10 mL), before lyophilisation yielded a white solid (155 mg, 94%). ^{1}H NMR (700 MHz, DMSO-d_6) δ 1.23 (6H, t, J = 7 P(OCH$_2$C**H**$_3$)$_2$), 1.72-1.81 (4H, m, PC**H**$_2$C**H**$_2$CH$_2$), 3.23-3.38 (2H, br, N**H**$_2$), 3.39-3.77 (7H, m, C**H**$_2$ **+** C**H**), 3.95-4.01 (4H, qd, $^3J_{H\text{-}H}$ = 7, $^3J_{H\text{-}P}$ = 3, P(O**C**H$_2$CH$_3$)$_2$), 8.57 (1H, s, N**H**). ^{13}C NMR (176 MHz, DMSO-d_6) δ 16.3 (d, ^{3}J = 6, P(OCH$_2$**C**H$_3$)$_2$), 21.3 (d,

^{2}J = 5, $NCH_2\mathbf{C}H_2CH_2P$), 21.5 (d, ^{1}J = 143, $NCH_2CH_2\mathbf{C}H_2P$), 47.9, 50.3 (**C**H), 50.7 (d, ^{3}J = 18, $N\mathbf{C}H_2CH_2CH_2P$), 54.8 (**C**H_2), 61.0 (d, ^{2}J = 7, $P(O\mathbf{C}H_2CH_3)_2$), 167.9, 168.4 (**C**=**C**), 181.2, 181.4 (**C**O). ^{31}P NMR (162 MHz, DMSO-d_6) δ 31.27. MS (ES^+) *m/z* 346.1 $[M+H]^+$; $C_{14}H_{25}N_3O_5P$ requires 346.1532; found 346.1550. M. Pt > 250 °C.

(*S*)-2-Bromo-pentanedioic acid 5-benzyl Ester, 49[7]

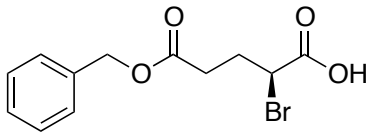

A solution of $NaNO_2$ (5.50 g, 80.1 mmol) in H_2O (50 ml) was added dropwise over 30 min to a stirred solution of (*S*)-glutamic acid 5-benzyl ester (10.0 g, 42.1 mmol) and NaBr (16.0 g, 116 mmol) in 1 M HBr (250 ml), cooled at –5 °C. After 10 hours, conc. H_2SO_4 (5 ml) was slowly added to the reaction mixture, which was then extracted with diethyl ether (3 x 300 ml). The combined organic extracts were washed with brine (200 ml), dried over Na_2SO_4, filtered and the filtrate concentrated under reduced pressure. The crude material was purified by column chromatography on silica (Hexane/EtOAc, 100% to 80:20 utilizing 1 % EtOAc increments; R_f = 0.25) to yield a yellow oil (7.40 g, 58 %). ^{1}H NMR (700 MHz, $CDCl_3$) δ 2.30 (1H, m, C**H₂**CHBr), 2.42 (1H, m, C**H₂**CHBr), 2.60 (2H, m, C**H₂**CH_2CHBr), 4.41 (1H, dd, J = 9, 5, C**H**), 5.14 (2H, s, OC**H**$_2$Ph), 7.33-7.39 (5H, m, Ar-**H**). ^{13}C NMR (176 MHz, $CDCl_3$) δ 29.7 (**C**H_2CH_2CHBr), 31.6 (**C**H_2CHBr), 44.2 (**C**H), 66.9 (O**C**H_2Ph), 128.4, 128.5, 128.6, 128.7, 128.8, 135.8 (Ar-**C**), 172.1, 173.4 (**C**O). MS (ES^+) *m/z* 323.2 $[M+H]^+$.

(*S*)-2-Bromo-pentanedioic acid 5-benzyl ester 1-*tert*-butyl ester, 50[7]

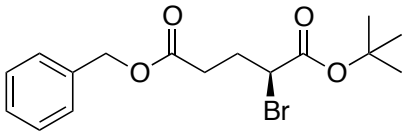

A solution of (*S*)-2-bromo-pentanedioic acid 5-benzyl ester (2.00 g, 6.85 mmol) in *tert*-butyl acetate (25 ml) and $HClO_4$ in H_2O (70 %, 0.34 mmol) was stirred at rt, for 16 h. H_2O (35 ml) was added to the reaction mixture, and the organic phase separated. The organic phase was washed with H_2O (25 ml), followed by 5 % Na_2CO_3 (25 ml). The solvent was removed under reduced pressure to yield a yellow coloured oil (2.15 g, 88 %). ^{1}H NMR (700 MHz, $CDCl_3$) δ 1.47 (9H, s, C(C**H**$_3$)$_3$), 2.25-2.30 (1H, m, **CH$_2$**CHBr), 2.36-2.42 (1H, m, **CH$_2$**CHBr), 2.55 (2H, m, **CH$_2$**CH_2CHBr), 4.23 (1H, dd, J = 9, 5, C**H**), 5.12 (2H, s, OC**H**$_2$Ph), 7.31-7.36 (5H, m, Ar-**H**). ^{13}C NMR (76 MHz $CDCl_3$) δ 27.9 (C(**C**H_3)$_3$), 29.9 (**C**H_2CH), 31.8 (**C**H_2CH_2), 46.9 (**C**H), 66.7 (**C**H_2Ph), 82.8 (**C**$(CH_3)_3$), 128.4, 128.5, 128.6, 128.7, 128.8, 136.0 (Ar-**C**), 168.5, 172.2 (**C**O). MS (ES$^+$): *m/z* 379.0 $[M+Na]^+$; $C_{16}H_{21}O_{10}{}^{79}BrNa$ requires 379.0521; found 379.0517.

(*R*)-5-Benzyl 1-*tert*-butyl 2-[4,7,10-tris(2-*tert*-butoxy-2-oxoethyl)-1,4,7,10-tetraazacyclododecan-1-yl]pentanedioate, 51[8]

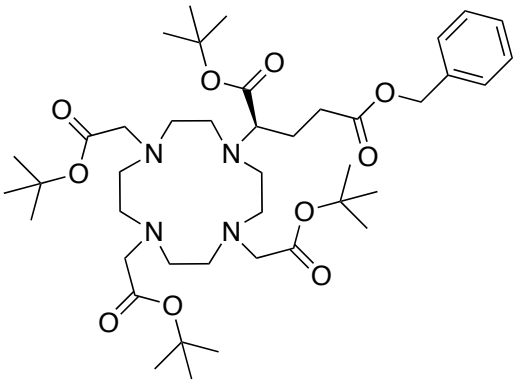

A solution of tri-*tert*-butyl 2,2',2''-(1,4,7,10-tetraazacyclododecane-1,4,7-triyl)triacetate (2 g, 3.89 mmol) and K_2CO_3 (0.81 g, 5.83 mmol) in anhydrous MeCN (50 mL) was stirred at room temperature under an inert atmosphere for

30 min. (*S*)-5-Benzyl 1-*tert*-butyl 2-bromopentanedioate (1.66 g, 4.67 mmol) was added in one aliquot and the reaction mixture was heated at reflux overnight**.** The completion of reaction was verified by TLC, at which point the solution was filtered, concentrated under reduced pressure, re-dissolved in CH_2Cl_2 (80 ml) and washed with water (3 x 50 ml). The organic layer was evaporated under reduced pressure and the residue purified by column chromatography (100% DCM, to 90:10 DCM/MeOH; R_f = 0.30) to give an off-white hygroscopic solid (1.6 g, 52%). ^{1}H NMR (400 MHz, $CDCl_3$) δ 1.43 (9H, s, C(C**H**$_3$)$_3$), 1.46 (18H, s, C(C**H**$_3$)$_3$), 1.47 (9H, s, C(C**H**$_3$)$_3$), 1.99-2.97 (20H, br. m, C**H**$_2$), 3.12-3.54 (7H, m, COC**H** + COC**H**$_2$), 5.10 (2H, s, OC**H**$_2$Ph), 7.23-7.41 (5H, m, Ar-**H**). ^{13}C NMR (101 MHz, $CDCl_3$) δ 26.4, 28.1, 28.9 (C(C**H**$_3$)$_3$), 30.4, 53.6, 54.3, 56.2, 56.6, 57.9, 58.0 (**C**H$_2$), 66.5 (O**C**H$_2$Ph), 69.3 (**C**H), 78.1, 78.2, 83.3 (**C**(CH$_3$)$_3$), 128.3, 128.4, 128.6, 135.7 (Ar-**C**), 171.7, 171.8, 173.8, 174.9 (**C**O). MS (ES$^+$): *m/z* 791.5 [M+H]$^+$; $C_{42}H_{70}N_4O_{10}$ requires 791.5170; found 791.5165.

(*R*)-5-*tert*-Butoxy-5-oxo-4-[4,7,10-tris(2-*tert*-butoxy-2-oxoethyl)-1,4,7,10-tetraazacyclododecan-1-yl]pentanoic acid, 52[8]

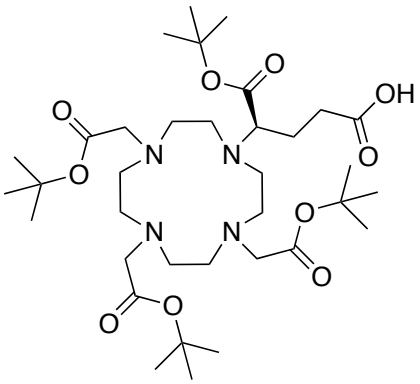

A solution of (*R*)-5-benzyl 1-*tert*-butyl 2-[4,7,10-tris(2-*tert*-butoxy-2-oxoethyl)-1,4,7,10-tetraazacyclododecan-1-yl]pentanedioate (677 mg, 0.86 mmol) and Pd-C (10%) in MeOH (10 mL), was agitated at room temperature, under H_2 (40 psi), in a Parr apparatus for 6 h. The reaction mixture was filtered through celite and the filtrate evaporated under reduced pressure, to give the free acid as a hygroscopic solid (530 mg, 88%). ^{1}H NMR (400 MHz, $CDCl_3$) δ 1.27 (9H, s, C(C**H**$_3$)$_3$), 1.28 (18H, s, C(C**H**$_3$)$_3$), 1.29 (9H, s, C(C**H**$_3$)$_3$), 1.86-2.16 (4H, m, C**H**$_2$C**H**$_2$CO), 2.18-3.18 (16H, br. m, C**H**$_2$), 3.23 (4H, s, COC**H**$_2$), 3.24 (2H, s, COC**H**$_2$),

3.27-3.35 (1H, m, COC**H**), 3.67 (1H, s, O**H**). ^{13}C NMR (101 MHz, $CDCl_3$) δ 27.6, 27.7, 27.9, 28.0 (C(C**H**$_3$)$_3$), 33.7, 49.7, 52.5, 55.3, 55.6, 56.0, 60.1 (**C**H$_2$), 69.6 (**C**H), 81.7, 82.0, 82.5 (**C**(CH$_3$)$_3$), 171.2, 172.6, 175.2, 176.0 (**C**O). MS (ES$^+$): *m/z* 701.1 [M+H]$^+$; $C_{35}H_{65}N_4O_{10}$ requires 701.4701; found 701.4704.

(*R*)-4-((6-*tert*-Butoxy)-6-oxo-5-(4,7,10-tris(2-(*tert*-butoxy)-2-oxoethyl)-1,4,7,10-tetraazacyclododecan-1-yl)hexyl)amino)-4-oxobutanoic acid, 53

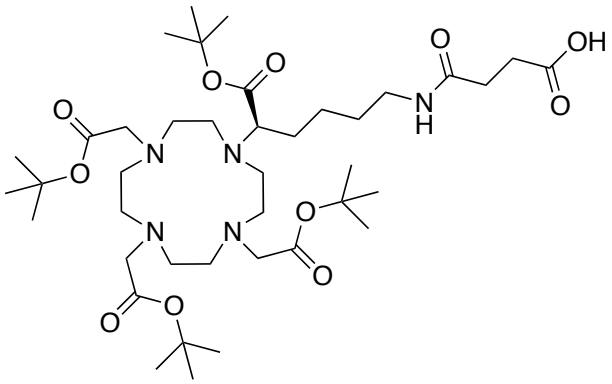

To a pre-stirred solution of (*R*)-tri-*tert*-butyl 2,2',2''-(10-(6-amino-1-(*tert*-butoxy)-1-oxohexan-2-yl)-1,4,7,10-tetraazacyclododecane-1,4,7-triyl)triacetate (325 mg, 0.46 mmol) and diisopropylethylamine (160 μL, 0.92 mmol) in anhydrous DMF (3 mL), was added succinic anhydride (46 mg, 0.46 mmol) and the resulting solution stirred at room temperature and the reaction monitored by ESI-MS. After 16 hours, the solvent was removed under reduced pressure and the crude residue purified by column chromatography (DCM/MeOH, 100% DCM to 87:13; R_f = 0.32) to give a yellow gum (228 mg, 62%). ^{1}H NMR (600 MHz, $CDCl_3$) δ 1.34 (9H, s, C(C**H**$_3$)$_3$), 1.35 (18H, s, C(C**H**$_3$)$_3$), 1.36 (9H, s, C(C**H**$_3$)$_3$), 1.41-1.64 (6H, m), 1.96-2.06 (3H, m), 2.11-2.27 (4H, m), 2.37-2.54 (7H, m), 2.65-2.80 (6H, m), 2.83-2.96 (3H, m), 3.10-3.20 (2H, m), 3.21-3.31 (3H, m), 3.32-3.33 (1H, m), 8.27-8.83 (1H, br. s, O**H**), 8.85 (1H, br.s, N**H**). ^{13}C NMR (151 MHz, $CDCl_3$) δ 24.5 (**C**H$_2$), 26.5, 27.7, 27.8, 27.8 (C(**C**H$_3$)$_3$), 28.8, 30.0, 31.8, 39.1, 44.5, 47.1, 48.0, 48.3, 48.4, 52.4, 52.5, 53.5, 55.4, 55.6, 55.7 (**C**H$_2$), 61.1 (**C**H), 81.9, 82.0, 82.0 (**C**(CH$_3$)$_3$)172.5, 172.7, 174.4, 174.8, 175.1 (**C**O). MS (ES$^+$) *m/z* 800.4 [M+H]$^+$; $C_{40}H_{74}N_5O_{11}$ requires 800.5385; found 800.5366.

[Conjugate 5], 54

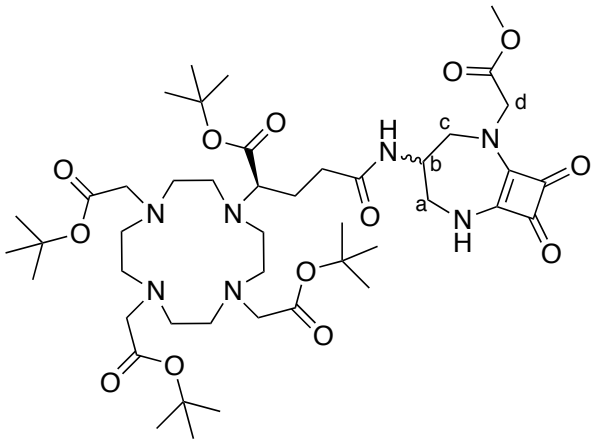

(*R*)-5-*tert*-Butoxy-5-oxo-4-[4,7,10-tris(2-*tert*-butoxy-2-oxoethyl)-1,4,7,10-tetraazacyclododecan-1-yl]pentanoic acid (108 mg, 0.16 mmol), EDC (36 mg, 0.19 mmol) and HOBt (25 mg, 0.19 mmol) were dissolved in anhydrous DMF (2 mL) and stirred at room temperature under an atmosphere of argon for 20 minutes. After this period, a pre-stirred solution of methyl 2-(4-amino-8,9-dioxo-2,6-diazabicyclo[5.2.0]non-1(7)-en-2-yl)acetate (37 mg, 0.16 mmol) and NMM (34 μL, 0.31 mmol) in anhydrous DMF (2 mL) was added dropwise and the resulting solution stirred at room temperature until complete consumption of the starting materials was indicated by ESI-MS. After this period, the solvent was removed under reduced pressure and the crude oil taken up into EtOAc (20 mL). Saturated $NaHCO_3$ (20 mL) was added, the layers were separated and the aqueous was washed with EtOAc (3 x 40 mL). The combined organic portions were dried over $MgSO_4$, filtered and the solvent removed under reduced pressure. The crude residue was purified by column chromatography (DCM/MeOH, 100% to 90:10 in 1% increments; R_f =0.39) to yield a brown viscous oil. This product was characterised as a pair of diastereoisomers (33 mg, 26%). ^{1}H NMR (600 MHz, $CDCl_3$) δ 1.41-1.43 (36H, overlapping s, C(C**H**$_3$)$_3$), 1.77-1.89 (1H, m), 1.94-2.13 (4H, m), 2.17-2.38 (4H, m), 2.43-2.69 (7H, m), 2.70-2.86 (4H, m), 2.88-3.08 (3H, m), 3.26-3.58 (6H, m), 3.69 (3H, s, C**H**$_3$), 3.81-3.97 (2H, m, **H**^{c}), 4.31-4.52 (2H, C**H**$_2^d$), 4.57-4.70 (1H, m, C**H**NH), 7.66 (1H, br, N**H**), 8.59 (1H, br, N**H**). ^{13}C NMR (151 MHz, $CDCl_3$) δ 27.9, 28.0 (overlapping C(**C**H$_3$)$_3$), 35.4, 44.5, 47.2 (**C**^{d}), 48.5, 48.7, 49.8, 50.1 (C**H**NH), 52.4, 52.6, 52.8 (**C**H$_3$), 55.6, 55.9, 60.8 (**C**H), 82.0, 82.1, 82.2, 82.6 (**C**(CH$_3$)$_3$), 168.1, 168.6 (**C**=**C**), 171.9, 172.6,

172.8, 172.9, 173.6, 175.3, 182.3, 182.3 (**C**O). MS (ES$^+$) *m/z* 922.4 [M+H]$^+$; $C_{45}H_{76}N_7O_{13}$ requires 922.5501; found 922.5526. [The ethyl ester was also present $C_{46}H_{78}N_7O_{13}$ requires 936.5658; found 936.5686].

[Conjugate 6], 55

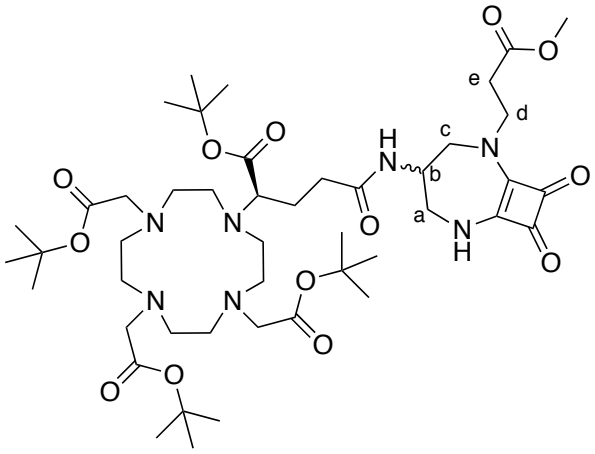

(*R*)-5-*tert*-Butoxy-5-oxo-4-[4,7,10-tris(2-*tert*-butoxy-2-oxoethyl)-1,4,7,10-tetraazacyclododecan-1-yl]pentanoic acid (94 mg, 0.13 mmol), EDC (31 mg, 0.16 mmol) and HOBt (22 mg, 0.16 mmol) were dissolved in anhydrous DMF (2 mL) and stirred at room temperature under an atmosphere of argon for 20 minutes. After this period, a pre-stirred solution of methyl 3-(4-amino-8,9-dioxo-2,6-diazabicyclo[5.2.0]non-1(7)-en-2-yl)propanoate (34 mg, 0.13 mmol) and NMM (30 μL, 0.27 mmol) in anhydrous DMF (1.5 mL) was added dropwise and the resulting solution stirred at room temperature until complete consumption of the starting materials was revealed by ESI-MS. After this period, the solvent was removed under reduced pressure and the crude oil taken up into EtOAc (20 mL). Saturated $NaHCO_3$ (20 mL) was added, the layers were separated and the aqueous fraction washed with EtOAc (3 x 40 mL). The combined organic portions were dried over $MgSO_4$, filtered and the solvent removed under reduced pressure. The crude residue was purified by column chromatography (DCM/MeOH, 100% to 90:10 in 1% increments; R_f = 0.37) to yield a brown viscous oil. This product was characterised as a pair of diastereoisomers (33 mg, 26%). ^{1}H NMR (600 MHz, $CDCl_3$) δ 1.42-1.44 (36H, overlapping s, C(C**H**$_3$)$_3$), 1.82-1.93 (1H, m), 1.95-2.11 (4H, m), 2.17-2.27 (3H, m), 2.34-2.41 (1H, m), 2.49-2.58

(4H, m), 2.60-2.70 (5H, m, C**H**$_2^e$ + C**H**$_2$), 2.71-2.78 (2H, m), 2.78-2.85 (2H, m), 2.89-2.99 (3H, m), 3.29-3.38 (2H, m), 3.40-3.52 (4H, m, **H**^{a} + C**H**), 3.64 (3H, s, C**H**$_3$), 3.77-3.87 (2H, m, **H**^{c}), 3.94 (1H, dt, J = 14, 7, C**H**$_2^d$), 4.03 (1H, dt, J = 14, 7, C**H**$_2^{d'}$), 4.13-4.19 (1H, m, C**H**NH), 7.72 (1H, br, N**H**), 8.70 (1H, br, N**H**). ^{13}C NMR (151 MHz, $CDCl_3$) δ 27.9, 28.0 (overlapping C(**C**H$_3$)$_3$), 33.8 (**C**^{e}), 35.3, 45.6, 47.2 (**C**^{d}), 48.2, 48.7, 49.8, 50.2 (C**H**NH), 51.2 (**C**H$_3$), 52.8, 55.6, 55.9, 56.4, 60.8 (**C**H), 82.0, 82.1, 82.1, 82.2 (**C**(CH$_3$)$_3$), 167.7, 167.9 (**C**=**C**), 171.4, 172.6, 172.8, 172.9, 173.5, 175.3, 181.2, 182.0 (**C**O). MS (ES$^+$) *m/z* 936.6 [M+H]$^+$; $C_{46}H_{78}N_7O_{13}$ requires 936.5658; found 936.5672.

[Conjugate 7], 56

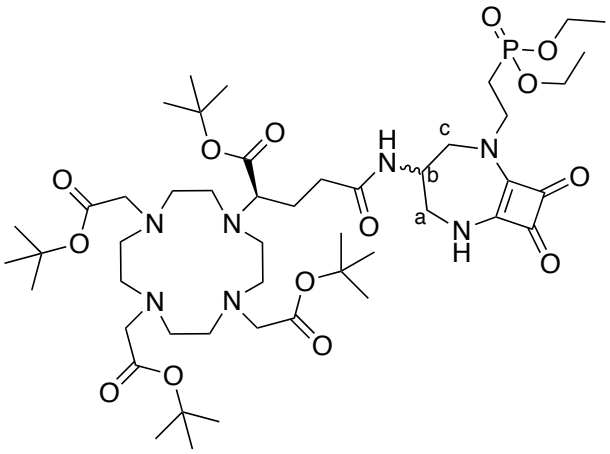

(*R*)-5-*tert*-Butoxy-5-oxo-4-[4,7,10-tris(2-*tert*-butoxy-2-oxoethyl)-1,4,7,10-tetraazacyclododecan-1-yl]pentanoic acid (138 mg, 0.20 mmol), EDC (45 mg, 0.24 mmol) and HOBt (32 mg, 0.24 mmol) were dissolved in anhydrous DMF (3 mL) and stirred at room temperature under an atmosphere of argon for 20 minutes. After this period, a pre-stirred solution of diethyl (2-(4-amino-8,9-dioxo-2,6-diazabicyclo[5.2.0]non-1(7)-en-2-yl)ethyl)phosphonate (65 mg, 0.20 mmol) and NMM (43 μL, 0.39 mmol) in anhydrous DMF (2 mL) was added dropwise and the resulting solution stirred at room temperature until complete consumption of the starting materials was revealed by ESI-MS. After this period, the solvent was removed under reduced pressure and the crude oil taken up into EtOAc (30 mL). Saturated $NaHCO_3$ (30 mL) was added, the layers were separated and the aqueous was washed with EtOAc (3 x 50 mL). The combined organic

portions were dried over $MgSO_4$, filtered and the solvent removed under reduced pressure. The crude residue was purified by column chromatography (DCM/MeOH, 100% to 90:10 in 1% increments; R_f =0.41) to yield a brown viscous oil. This product was characterised as a pair of diastereoisomers (42 mg, 21%). ^{1}H NMR (600 MHz, $CDCl_3$) δ 1.28 (6H, t, J = 7, $P(OCH_2C\mathbf{H}_3)_2$), 1.39, 1.40, 1.41, 1.42 (36H, s, $C(C\mathbf{H}_3)_3$), 1.77-2.08 (5H, m), 2.12-2.14 (2H, m, $PC\mathbf{H}_2CH_2$), 2.16-2.25 (3H, m), 2.35 (1H, m), 2.45-2.56 (4H, m), 2.57-2.66 (3H, m), 2.66-2.87 (6H, m), 2.90-2.99 (2H, m), 3.28-3.34 (2H, m), 3.39-3.50 (4H, m, $\mathbf{H}^c$, $\mathbf{H}^a$, $C\mathbf{H}CO_2{}^t$Bu) 3.71-3.78 (1H, m, $\mathbf{H}^c$), 3.81-3.89 (2H, m, $PCH_2C\mathbf{H}_2$), 4.01-4.12 (4H, m, $P(OC\mathbf{H}_2CH_3)_2$), 4.14-4.20 (1H, m, $\mathbf{H}^b$), 7.64 (1H, br, N**H**), 7.84 (1H, br, N**H**). ^{13}C NMR (151 MHz, $CDCl_3$) δ 16.5 (d, ^{3}J = 6, $P(OCH_2\mathbf{C}H_3)_2$), 25.6 (d, ^{1}J = 140, $NCH_2\mathbf{C}H_2P$), 27.9, 28.0 (overlapping $C(\mathbf{C}H_3)_3$), 35.1, 44.5, 47.1, 48.1, 48.6 ($\mathbf{C}H_2$), 49.7 ($\mathbf{C}^b$), 50.0 (d, J = 16, $PCH_2\mathbf{C}H_2$), 52.6, 52.7, 52.8, 55.6 ($\mathbf{C}H_2$), 55.8 ($\mathbf{C}^a$), 56.3 ($\mathbf{C}^c$), 60.7 ($\mathbf{C}$H), 62.0 (d, ^{2}J = 7, $P(O\mathbf{C}H_2CH_3)_2$), 81.9, 82.0, 82.1, 82.6 ($\mathbf{C}(CH_3)_3$), 167.6, 167.8 (**C**=**C**), 172.6, 172.8, 172.9, 173.4, 175.3, 181.3, 182.0 (**C**O). ^{31}P NMR (162 MHz, $CDCl_3$) δ 26.78. MS (ES^+) *m/z* 1014.1 $[M+H]^+$; $C_{48}H_{85}N_7O_{14}P$ requires 1014.589; found 1014.593.

[Conjugate 8], 57

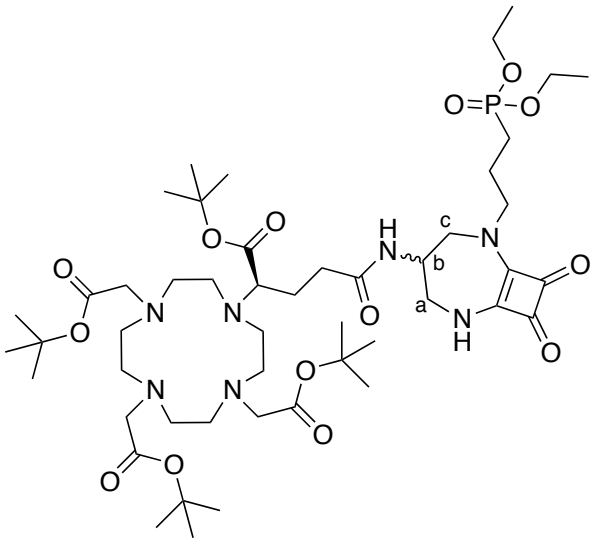

(*R*)-5-*tert*-Butoxy-5-oxo-4-[4,7,10-tris(2-*tert*-butoxy-2-oxoethyl)-1,4,7,10-tetraazacyclododecan-1-yl]pentanoic acid (138 mg, 0.20 mmol), EDC (45 mg, 0.24 mmol) and HOBt (32 mg, 0.24 mmol) were dissolved in anhydrous DMF (3

mL) and stirred at room temperature under an atmosphere of argon for 20 minutes. After this period, a pre-stirred solution of diethyl (3-(4-amino-8,9-dioxo-2,6-diazabicyclo[5.2.0]non-1(7)-en-2-yl)propyl)phosphonate (68 mg, 0.20 mmol) and NMM (43 μL, 0.39 mmol) in anhydrous DMF (2 mL) was added dropwise and the resulting solution stirred at room temperature until complete consumption of the starting materials was revealed by ESI-MS. After this period, the solvent was removed under reduced pressure and the crude oil taken up into EtOAc (30 mL). Saturated $NaHCO_3$ (30 mL) was added, the layers were separated and the aqueous was washed with EtOAc (3 x 50 mL). The combined organic portions were dried over $MgSO_4$, filtered and the solvent removed under reduced pressure. The crude residue was purified by column chromatography (DCM/MeOH, 100% to 90:10 in 1% increments; R_f =0.41) to yield a brown viscous oil. This product was characterised as a pair of diastereoisomers (57 mg, 28%). ^{1}H NMR (700 MHz, $CDCl_3$) δ 1.27 (6H, t, J = 7, $P(OCH_2C\mathbf{H}_3)_2$), 1.40, 1.40, 1.41, 1.42 (36H, s, $C(C\mathbf{H}_3)_3$), 1.66-1.74 (2H, m, $PC\mathbf{H}_2CH_2CH_2$), 1.81-1.89 (3H, m, $PCH_2C\mathbf{H}_2CH_2$ + C**H**H), 1.96-2.09 (4H, m), 2.15-2.23 (3H, m), 2.32-2.40 (1H, m), 2.45-2.56 (4H, m), 2.59-2.64 (3H, m), 2.70-2.76 (2H, m), 2.76-2.82 (2H, m), 2.87-2.97 (3H, m), 3.28-3.35 (2H, m), 3.36-3.38 (1H, m), 3.40-3.44 (1H, m), 3.46-3.54 (2H, m), 3.61-3.68 (1H, m), 3.72-3.77 (1H, m, **H**^{c}) 3.79-3.87 (2H, m, $PCH_2CH_2C\mathbf{H}_2$), 3.99-4.07 (4H, m, $P(OC\mathbf{H}_2CH_3)_2$), 4.13-4.19 (1H, m, **H**^{b}), 7.56 (1H, br, N**H**), 8.85 (1H, br, N**H**). ^{13}C NMR (176 MHz, $CDCl_3$) δ 16.6 (d, ^{3}J = 6, $P(OCH_2\mathbf{C}H_3)_2$), 22.0 (d, ^{2}J = 5, $NCH_2\mathbf{C}H_2CH_2P$), 22.9 (d, ^{1}J = 143, $NCH_2CH_2\mathbf{C}H_2P$), 27.9, 28.0 (overlapping $C(\mathbf{C}H_3)_3$), 35.3, 38.7, 44.5, 47.1, 48.4, 50.2 (**C**HNH), 51.5 (d, ^{3}J = 16, $N\mathbf{C}H_2CH_2CH_2P$), 52.8, 55.6, 55.9, 56.2, 60.7 (**C**H), 61.7 (overlapping d, ^{2}J = 7, $P(O\mathbf{C}H_2CH_3)_2$), 82.0, 82.1, 82.1, 82.3 ($\mathbf{C}(CH_3)_3$), 167.4, 167.8 (**C**=**C**), 172.6, 172.8, 172.9, 173.4, 175.3, 181.4, 181.8 (**C**O). ^{31}P NMR (283 MHz, $CDCl_3$) δ 30.85. MS (ES^+) *m/z* 1028.5 $[M+H]^+$; $C_{49}H_{87}N_7O_{14}P$ requires 1028.605; found 1028.606.

[Conjugate 9], 58

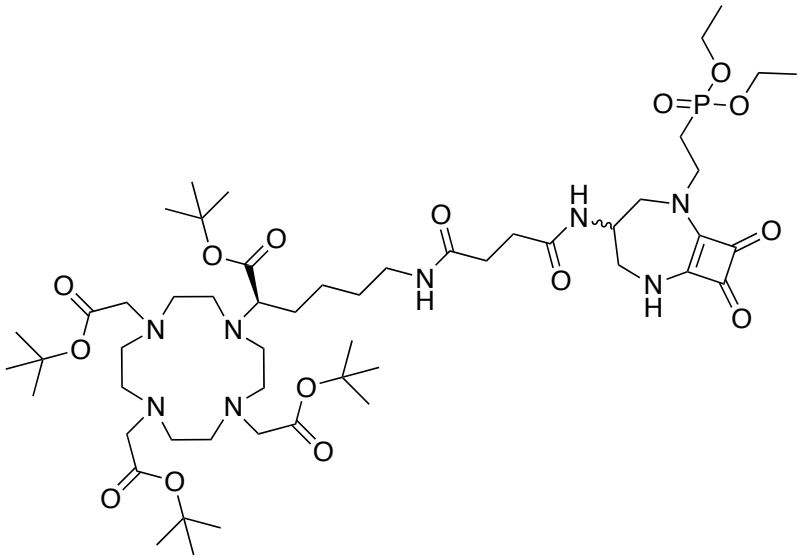

(*R*)-4-((6-*Tert*-butoxy)-6-oxo-5-(4,7,10-tris(2-(*tert*-butoxy)-2-oxoethyl)-1,4,7,10-tetraazacyclododecan-1-yl)hexyl)amino)-4-oxobutanoic acid (168 mg, 0.21 mmol), EDC (48 mg, 0.25 mmol) and HOBt (34 mg, 0.25 mmol) were dissolved in anhydrous DMF (3 mL) and stirred at room temperature under an atmosphere of argon for 20 minutes. After this period, a pre-stirred solution of diethyl (2-(4-amino-8,9-dioxo-2,6-diazabicyclo[5.2.0]non-1(7)-en-2-yl)ethyl)phosphonate (70 mg, 0.21 mmol) and NMM (46 μL, 0.42 mmol) in anhydrous DMF (1.0 mL) was added dropwise and the resulting solution stirred at room temperature until complete consumption of the starting materials was revealed by ESI-MS. After this period, the solvent was removed under reduced pressure and the crude oil taken up into EtOAc (30 mL). Saturated $NaHCO_3$ (30 mL) was added, the layers were separated and the aqueous layer was washed with EtOAc (3 x 30 mL). The combined organic portions were dried over $MgSO_4$, filtered and the solvent removed under reduced pressure. The crude residue was purified by column chromatography (DCM/MeOH, 100% to 85:15 in 1% increments; R_f =0.22) to yield a brown viscous oil. This product was characterised as a pair of diastereoisomers (52 mg, 22%). ^{1}H NMR (700 MHz, $CDCl_3$) δ 1.30 (6H, dt, J = 7, 3, $P(OCH_2C\mathbf{H}_3)_2$), 1.42, 1.42, 1.43 (36H, s, $C(C\mathbf{H}_3)_3$), 1.49-1.69 (6H, m), 1.96-2.06 (2H, m), 2.11-2.18 (2H, m, $PC\mathbf{H}_2CH_2$), 2.19-2.28 (2H, m), 2.47-2.64 (9H, m), 2.71-2.86 (4H, m), 2.93-3.08 (5H, m), 3.11-3.25 (4H, m),

3.30 (1H, d, J = 14, **H**$^{c/a}$ (eq)), 3.35 (2H, dd, J = 14, 7, **H**^{c} (axial)), 3.42-3.48 (2H, m), 3.74 (1H, ddd, J = 14, 7, 4, **H**^{a} (axial)), 3.78-3.82 (1H, m, **H**$^{c/a}$ (eq)), 3.86-3.94 (2H, m, $PCH_2C\mathbf{H}_2$), 4.04-4.14 (4H, m, $P(OC\mathbf{H}_2CH_3)_2$), 4.15-4.19 (1H, m, **H**^{b}), 7.46 (1H, br, N**H**), 7.96 (1H, br, N**H**), 8.67 (1H, br, N**H**). ^{13}C NMR (176 MHz, $CDCl_3$) δ 16.5 (d, ^{3}J = 6, $P(OCH_2\mathbf{C}H_3)_2$), 25.0 (**C**H_2), 25.5 (d, ^{1}J = 140, $NCH_2\mathbf{C}H_2P$), 26.7 (**C**H_2), 27.9, 28.0, 28.0 (overlapping $C(\mathbf{C}H_3)_3$), 29.4, 33.0, 38.8, 44.7, 45.7, 47.3 (**C**H_2), 48.2 (d, J = 16, $PCH_2\mathbf{C}H_2$), 48.5 (**C**H_2), 49.5 (**C**^{b}), 50.2, 52.7, 52.8, 55.7 (**C**H_2), 55.9 (**C**^{a}), 56.2 (**C**^{c}), 61.3 (**C**H), 62.1 (d, ^{2}J = 7, $P(O\mathbf{C}H_2CH_3)_2$), 82.0, 82.0, 82.0, 82.1, 82.1, 82.1 (**C**$(CH_3)_3$), 167.8, 167.9 (**C**=**C**), 172.7, 172.9, 173.0, 173.3, 173.3, 175.6, 181.5, 182.0 (**C**O). ^{31}P NMR (283 MHz, $CDCl_3$) δ 27.02. MS (ES^+) *m/z* 1113.0 $[M+H]^+$; $C_{53}H_{94}N_8O_{15}P$ requires 1113.658; found 1113.653.

[Conjugate 10], 59

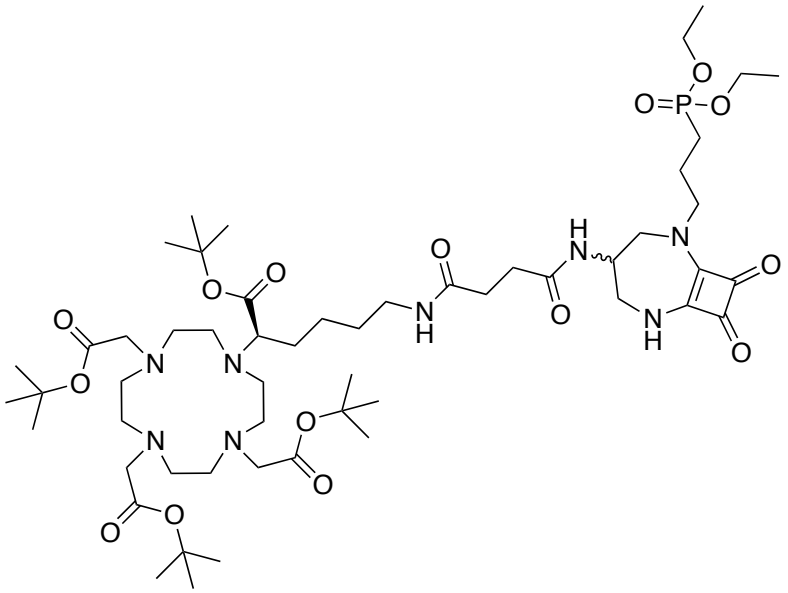

(*R*)-4-((6-*Tert*-butoxy)-6-oxo-5-(4,7,10-tris(2-(*tert*-butoxy)-2-oxoethyl)-1,4,7,10-tetraazacyclododecan-1-yl)hexyl)amino)-4-oxobutanoic acid (144 mg, 0.18 mmol), EDC (41 mg, 0.22 mmol) and HOBt (29 mg, 0.22 mmol) were dissolved in anhydrous DMF (2 mL) and stirred at room temperature under an atmosphere of argon for 20 minutes. After this period, a pre-stirred solution of diethyl (3-(4-amino-8,9-dioxo-2,6-diazabicyclo[5.2.0]non-1(7)-en-2-yl)propyl)phosphonate (62 mg, 0.18 mmol) and NMM (40 μL, 0.36 mmol) in anhydrous DMF (1.5 mL) was added dropwise and the resulting solution stirred

at room temperature until complete consumption of the starting materials was revealed by ESI-MS. After this period, the solvent was removed under reduced pressure and the crude oil taken up into EtOAc (30 mL). Saturated $NaHCO_3$ (30 mL) was added, the layers were separated and the aqueous layer was washed with EtOAc (3 x 30 mL). The combined organic portions were dried over $MgSO_4$, filtered and the solvent removed under reduced pressure. The crude residue was purified by column chromatography (DCM/MeOH, 100% to 85:15 in 1% increments; R_f =0.35) to yield a brown viscous oil. This product was characterised as a pair of diastereoisomers (60 mg, 22%). ^{1}H NMR (700 MHz, $CDCl_3$) δ 1.27 (6H, dt, J = 7, 3, $P(OCH_2C\mathbf{H}_3)_2$), 1.41, 1.41, 1.42 (36H, s, $C(C\mathbf{H}_3)_3$), 1.47-1.69 (6H, m), 1.69-1.77 (2H, m, $PC\mathbf{H}_2CH_2CH_2$), 1.82-1.89 (2H, m, $PCH_2C\mathbf{H}_2CH_2$), , 2.04-2.10 (2H, m) 2.21-2.26 (2H, m), 2.46-2.64 (9H, m), 2.71-2.85 (4H, m), 2.91-3.07 (5H, m), 3.10-3.25 (4H, m), 3.29 (1H, d, J = 14, $\mathbf{H}^{c/a}$ (eq)), 3.34 (2H, dd, J = 14, 7, $\mathbf{H}^{c}$ (axial)), 3.37-3.43 (2H, m), 3.47 (1H, ddd, J = 14, 7, 4, $\mathbf{H}^{a}$ (axial)), 3.70-3.74 (1H, m, $\mathbf{H}^{c/a}$ (eq)), 3.75-3.81 (2H, m, $PCH_2CH_2C\mathbf{H}_2$), 4.01-4.08 (4H, m, $P(OC\mathbf{H}_2CH_3)_2$), 4.15-4.19 (1H, m, $\mathbf{H}^{b}$), 7.56 (1H, br, N**H**), 7.99 (1H, br, N**H**), 8.64 (1H, br, N**H**). ^{13}C NMR (176 MHz, $CDCl_3$) δ 16.5 (d, ^{3}J = 6, $P(OCH_2\mathbf{C}H_3)_2$), 22.8 (d, ^{1}J = 140, $P\mathbf{C}H_2CH_2CH_2$), 24.9 ($\mathbf{C}H_2$), , 26.7 ($\mathbf{C}H_2$), 27.9, 27.9, 28.0, 28.0 (overlapping $C(\mathbf{C}H_3)_3$), 29.4, 33.0, 38.8, 44.7, 45.7, 47.3 ($\mathbf{C}H_2$), 48.5 (d, J = 16, $PCH_2\mathbf{C}H_2CH_2$), 48.6 ($\mathbf{C}H_2$), 49.7 ($\mathbf{C}^{b}$), 50.2 ($\mathbf{C}H_2$), 51.5 (d, ^{3}J = 16, $PCH_2CH_2\mathbf{C}H_2$), 52.7, 52.8, 55.6 ($\mathbf{C}H_2$), 55.9 ($\mathbf{C}^{a}$), 55.9 ($\mathbf{C}^{c}$), 61.3 ($\mathbf{C}$H), 61.8 (d, ^{2}J = 7, $P(O\mathbf{C}H_2CH_3)_2$), 82.0, 82.0, 82.0, 82.1, 82.1, 82.1 ($\mathbf{C}(CH_3)_3$), 167.6, 168.1 (**C**=**C**), 172.7, 172.9, 173.0, 173.2, 173.3, 175.5, 181.5, 181.8 (**C**O). ^{31}P NMR (283 MHz, $CDCl_3$) δ 30.91. MS (ES^+) *m/z* 1127.3 $[M+H]^+$; $C_{54}H_{96}N_8O_{15}P$ requires 1127.673; found 1127.673.

[Gd.L^5]

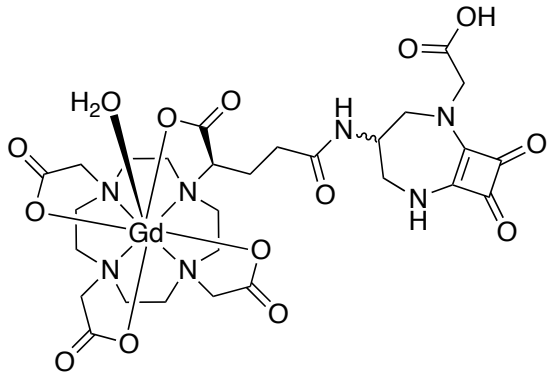

54 (10 mg, 0.01 mmol) was dissolved in MeOH (200 μL) with stirring. To this solution was added NaOH (0.5 mg) dissolved in H_2O (2.5 M) and the resulting solution stirred at room temperature overnight. Complete removal of the methyl/ethyl ester groups was verified by ESI-MS at which point the solvent was removed under reduced pressure. The residue was completely dried under high vacuum before being suspended in DCM (1 mL), to which trifluoroacetic acid (1 mL) was added. The resulting yellow solution was stirred at room temperature overnight. Complete removal of the *tert*-butyl ester groups was verified by ESI-MS, at which point excess solvent was removed under reduced pressure. The residue was repeatedly re-dissolved in DCM (2 mL) and the solvent removed under reduced pressure to remove excess TFA. This process yielded **L^5** as a pale-brown solid. MS (ES$^+$) *m/z* 684.7 $[M+H]^+$. The residue, **L^5**, as its protonated salt, (6.8 mg, 0.01 mmol) was dissolved in H_2O (0.5 mL) and the pH adjusted to about 5.5 by the addition of NaOH (0.1 M). $GdCl_3.6H_2O$ (4.8 mg, 0.013 mmol) was added as a solution in H_2O (0.5 mL) and the reaction mixture stirred at 60 °C overnight. The pH of the solution was periodically checked and maintained between 5-6 by the addition of NaOH/HCl (0.1 M). Upon completion of complexation, excess gadolinium was removed by the addition of Chelex-100™ with stirring. The Chelex trap was filtered and the complex eluted with excess H_2O. Removal of the water by lyophilisation gave the complex as a white solid that was purified by RP-HPLC. HR-MS (ES$^+$) $C_{28}H_{39}{}^{154}GdN_7O_{13}$ requires 835.1815 $[M+2H]^+$; found 835.1820. r_{1p} = 4.9 $mM^{-1}s^{-1}$ (60 MHz, 310K). RP-HPLC: t_R = 7.1 mins [2-30% MeOH in H_2O over 10 mins].

[Gd.L^6]

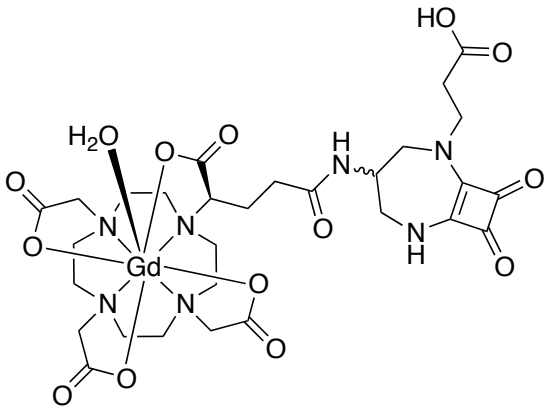

55 (10 mg, 0.01 mmol) was dissolved in MeOH (200 μL) with stirring. To this was added NaOH (0.5 mg) as a solution in H_2O (2.5 M) and the resulting solution stirred at room temperature overnight. Complete removal of the methyl ester was verified by ESI-MS, at which point the solvent was removed under reduced pressure. The residue was completely dried under high vacuum before being suspended in DCM (1 mL), to which trifluoroacetic acid (1 mL) was added. The resulting yellow solution was stirred at room temperature overnight. Complete removal of the *tert*-butyl ester groups was verified by ESI-MS, at which point excess solvent was removed under reduced pressure. The residue was repeatedly re-dissolved in DCM (2 mL) and the solvent removed under reduced pressure to remove excess TFA. This process yielded the protonated salt of **L^6** as a pale-brown solid. MS (ES$^+$) *m/z* 698.3 [M+H]$^+$. The salt of **L^6** (7.5 mg, 0.01 mmol) was dissolved in H_2O (0.5 mL) and the pH adjusted to about 5.5 by the addition of NaOH (0.1 M). $GdCl_3.6H_2O$ (4.8 mg, 0.013 mmol) was added as a solution in H_2O (0.5 mL) and the reaction mixture stirred at 60 °C overnight. The pH of the solution was periodically checked and maintained between 5-6 by the addition of NaOH/HCl (0.1 M). Upon completion of complexation, excess gadolinium was removed by the addition of Chelex-100™ with stirring. The Chelex trap was filtered and the complex eluted with excess H_2O. Removal of the water by lyophilisation gave the complex as a white solid that was purified by RP-HPLC. HR-MS (ES$^+$) $C_{29}H_{41}{}^{154}GdN_7O_{13}$ requires 849.1965 [M+2H]$^+$; found

849.1956. r_{1p} = 4.5 $mM^{-1}s^{-1}$ (60 MHz, 310K). RP-HPLC: t_R = 7.1 mins [2-30% MeOH in H_2O over 10 mins].

[Gd.L^7]

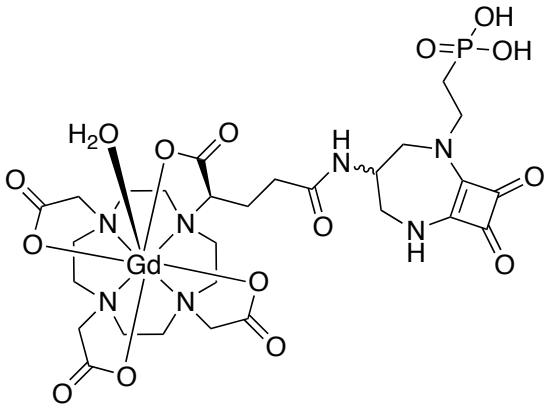

56 (10 mg, 9 μmol) was dissolved in DCM (1 mL) with stirring. To this solution was added trifluoroacetic acid (1 mL) and the resulting solution stirred at room temperature for overnight. Removal of the *tert*-butyl ester groups was verified by ESI-MS, at which point the excess solvent was removed under reduced pressure. The residue was repeatedly re-dissolved in DCM (2 mL) and the solvent removed under reduced pressure to remove excess TFA. This process yielded the phosphonate ethyl ester as a light-brown solid. This residue was dissolved in DMF (1 mL) to which bromotrimethylsilane (13 μL, 0.08 mmol) was added dropwise. The resulting mixture was heated to 60 °C overnight until complete deprotection had occurred, as indicated by ESI-MS. The solvent was removed under reduced pressure, before the residue redissolved in H_2O. The pH was adjusted to 6 and the aqueous phase washed with DCM (3 x 3 mL) and diethyl ether (3 x 3 mL). The aqueous solvent was then removed by lyophilisation to give the protonated salt of **L^7** as a light brown solid. MS (ES^+) *m/z* 734.9 $[M+H]^+$. The salt of **L^7** (7.2 mg, 9 μmol) was dissolved in H_2O (0.5 mL) and the pH adjusted to 5.5. $GdCl_3.6H_2O$ (4.4 mg, 12 μmol) was added as a solution in H_2O (0.5 mL) and the reaction mixture stirred at 60 °C overnight. The pH of the solution was periodically checked and maintained between 5 and 6 by the addition of NaOH/HCl (0.1 M). Upon completion of complexation, excess

gadolinium was removed by the addition of Chelex-100™ with stirring. The Chelex trap was filtered and the complex eluted with excess H_2O. Removal of the water by lyophilisation gave the complex as a white solid that was purified by RP-HPLC. HR-MS (ES^+) $C_{28}H_{42}{}^{157}GdN_7O_{14}P$ requires 888.1767 $[M+2H]^+$; found 888.1763. r_{1p} = 5.8 $mM^{-1}s^{-1}$ (60 MHz, 310K). RP-HPLC: t_R = 7.3 mins [2-30% MeOH in H_2O over 10 mins].

[Gd.L^8]

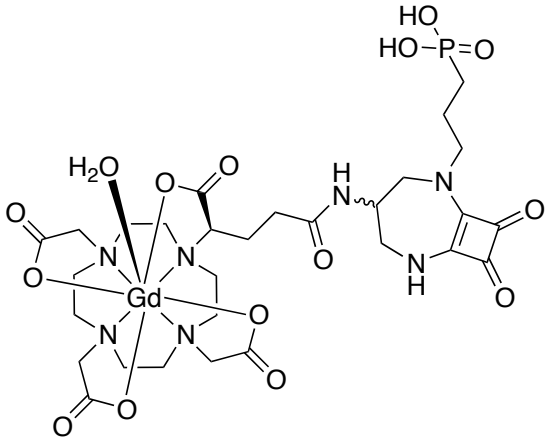

57 (17 mg, 0.02 mmol) was dissolved in DCM (1 mL) with stirring. To this solution was added trifluoroacetic acid (1 mL) and the resulting solution stirred at room temperature for overnight. Removal of the *tert*-butyl ester groups was verified by ESI-MS, at which point the excess solvent was removed under reduced pressure. The residue was repeatedly re-dissolved in DCM (2 mL) and the solvent removed under reduced pressure to remove excess TFA. This process yielded the phosphonate ethyl ester as a light-brown solid. This residue was dissolved in DMF (1 mL) to which bromotrimethylsilane (18 μL, 0.13 mmol) was added dropwise. The resulting mixture was heated to 60 °C overnight until complete deprotection had occurred, as indicated by ESI-MS. The solvent was removed under reduced pressure, before the residue re-dissolved in H_2O. The pH was adjusted to 6 and the aqueous phase washed with DCM (3 x 3 mL) and diethyl ether (3 x 3 mL). The aqueous solvent was then removed by lyophilisation to give the protonated salt of **L^8** as a light brown solid. MS (ES^+) *m/z* 748.7 $[M+H]^+$. The salt of **L^8** (12.5 mg, 0.017 mmol) was dissolved in H_2O (0.5 mL) and the pH adjusted to 5.5. $GdCl_3.6H_2O$ (6.8 mg, 0.018 mmol) was added

as a solution in H_2O (0.5 mL) and the reaction mixture stirred at 60 °C overnight. The pH of the solution was periodically checked and maintained between 5 and 6 by the addition of NaOH/HCl (0.1 M). Upon completion of complexation, excess gadolinium was removed by the addition of Chelex-100™ with stirring. The Chelex trap was filtered and the complex eluted with excess H_2O. Removal of the water by lyophilisation gave the complex as a white solid that was purified by RP-HPLC. HR-MS (ES^+) $C_{29}H_{44}{}^{154}GdN_7O_{14}P$ requires 899.1893 $[M+2H]^+$; found 899.1891. r_{1p} = 5.2 $mM^{-1}s^{-1}$ (60 MHz, 310K). RP-HPLC: t_R = 7.5 mins [2-30% MeOH in H_2O over 10 mins].

[Gd.L^9]

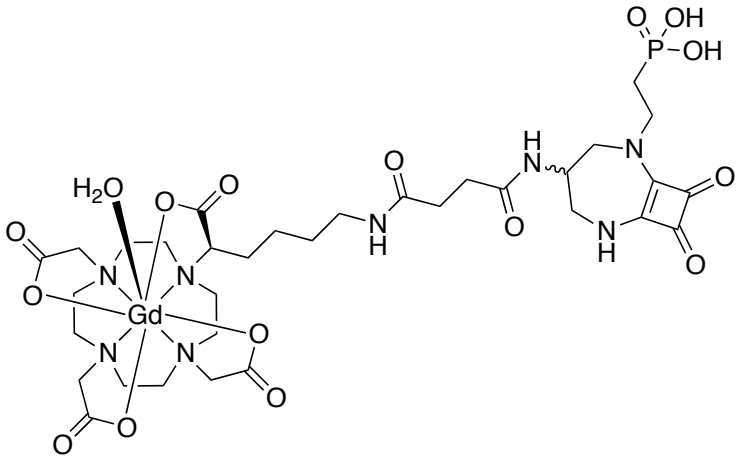

58 (15 mg, 0.013 mmol) was dissolved in DCM (1 mL) with stirring. To this solution was added trifluoroacetic acid (1 mL) and the resulting solution stirred at room temperature for overnight. Removal of the *tert*-butyl ester groups was verified by ESI-MS, at which point the excess solvent was removed under reduced pressure. The residue was repeatedly re-dissolved in DCM (2 mL) and the solvent removed under reduced pressure to remove excess TFA. This process yielded the phosphonate ethyl ester as a light-brown solid. This residue was dissolved in DMF (1 mL) to which bromotrimethylsilane (14 μL, 0.104 mmol) was added. The resulting mixture was heated to 60 °C overnight until complete deprotection of the phosphonate ethyl ester groups was verified by ESI-MS. The solvent was removed under reduced pressure and the residue re-dissolved in H_2O. The pH was adjusted to 6 and the aqueous phase washed with DCM (3 x 3

mL) and diethyl ether (3 x 3 mL). The aqueous solvent was then removed by lyophilisation to give the protonated salt of **L⁹** as a light brown solid. MS (ES^+) *m/z* 833.7 $[M+H]^+$. The salt of **L⁹** (10.8 mg, 0.013 mmol) was dissolved in H_2O (1.0 mL) and the pH adjusted to 6.0. $GdCl_3.6H_2O$ (5.79 mg, 0.016 mmol) was added as a solution in H_2O (0.5 mL) and the reaction mixture stirred at 60 °C overnight. The pH of the solution was periodically checked and maintained between 5 and 6 by the addition of NaOH/HCl (0.1 M). Upon completion of complexation, excess gadolinium was removed by the addition of Chelex-100™ with stirring. The Chelex trap was filtered and the complex eluted with excess H_2O. Removal of the water by lyophilisation gave the complex as a white solid that was purified by RP-HPLC. HR-MS (ES^+) $C_{33}H_{51}{}^{154}GdN_8O_{15}P$ requires 984.2420 $[M+2H]^+$; found 984.2433. r_{1p} = 5.0 mM^{-1} s^{-1} (60 MHz, 310K). RP-HPLC: t_R = 7.8 mins [2-30% MeOH in H_2O over 10 mins].

[Gd.L¹⁰]

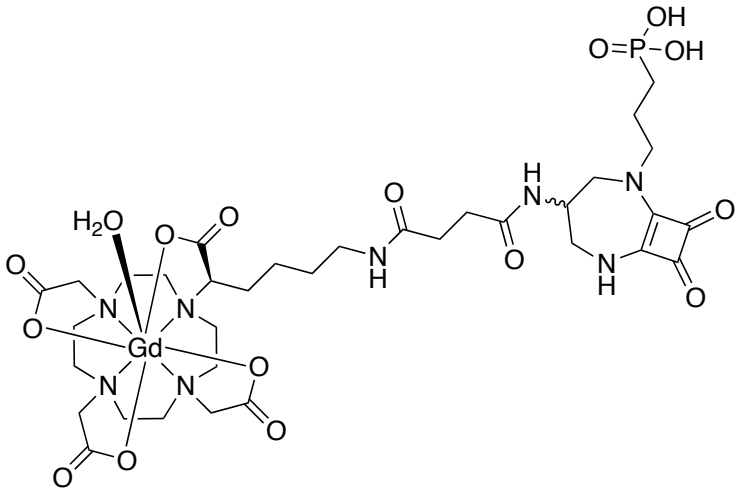

59 (10 mg, 0.01 mmol) was dissolved in DCM (1 mL) with stirring. To this soution was added trifluoroacetic acid (1 mL) and the resulting solution stirred at room temperature for overnight. Removal of the *tert*-butyl ester groups was verified by ESI-MS, at which point the excess solvent was removed under reduced pressure. The residue was repeatedly re-dissolved in DCM (2 mL) and the solvent removed under reduced pressure to remove excess TFA. This process yielded the phosphonate ethyl ester as a light-brown solid. This residue was dissolved in DMF (1 mL) to which bromotrimethylsilane (10 μL, 0.07 mmol) was

added dropwise. The resulting mixture was heated to 60 °C overnight until complete deprotection was indicated by ESI-MS. The solvent was removed under reduced pressure, before the residue re-dissolved in H_2O. The pH was adjusted to 6 and the aqueous phase washed with DCM (3 x 3 mL) and diethyl ether (3 x 3 mL). The aqueous solvent was then removed by lyophilisation to give the protonated salt of **L10** as a light brown solid. MS (ES^+) *m/z* 847.8 $[M+H]^+$. The salt of **L10** (7.6 mg, 0.01 mmol) was dissolved in H_2O (1 mL) and the pH adjusted to 6. $GdCl_3.6H_2O$ (4.0 mg, 0.011 mmol) was added as a solution in H_2O (0.5 mL) and the reaction mixture stirred at 60 °C overnight. The pH of the solution was periodically checked and maintained between 5 and 6 by the addition of NaOH/HCl (0.1 M). Upon completion of complexation, excess gadolinium was removed by the addition of Chelex-100™ with stirring. The Chelex trap was filtered and the complex eluted with excess H_2O. Removal of the water by lyophilisation gave the complex as a white solid that was purified by RP-HPLC. HR-MS (ES^+) $C_{34}H_{53}{}^{158}GdN_8O_{15}P$ requires 1002.261 $[M+2H]^+$; found 1002.267. r_{1p} = 5.2 mM^{-1} s^{-1} (60 MHz, 310K). RP-HPLC: t_R = 7.8 mins [2-30% MeOH in H_2O over 10 mins].

[Eu-DOTAGlu]

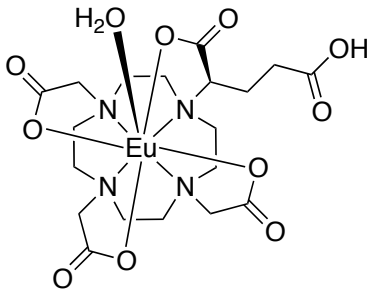

(*R*)-5-*tert*-Butoxy-5-oxo-4-[4,7,10-tris(2-*tert*-butoxy-2-oxoethyl)-1,4,7,10-tetraazacyclododecan-1-yl]pentanoic acid (25 mg, 0.036 mmol) was dissolved in DCM (1 mL) and trifluoroacetic acid (1 mL) was added. The mixture was stirred at room temperature overnight. After this time, the solvents were removed under reduced pressure and the residue that remained dissolved in DCM, which was again removed under reduced pressure. This process was repeated three

times in order to ensure complete removal of excess TFA. Confirmation of ester deprotection was gained through ^{1}H NMR analysis before the residue dissolved in H_2O (3 mL). The pH was adjusted to 6.5 and $EuCl_3$ (15.7 mg, 0.043 mmol) added. The reaction was heated to 60 °C for the progress monitored by ESI-MS. Upon completion after 4 hours, excess europium was removed through chelation to Chelex-100™ resin. The Chelex trap was filtered and the complex eluted with excess H_2O. Removal of the water by lyophilisation gave the complex as a white solid (15.7 mg, 70%). HR-MS (ES^+) $C_{19}H_{29}{}^{153}EuN_4O_{10}$ requires 626.1096 $[M+H]^+$; found 626.1102.

1,4,7,10-Tetraazacyclododecane-1,7-dicarboxylic acid dibenzyl ester, 60[7]

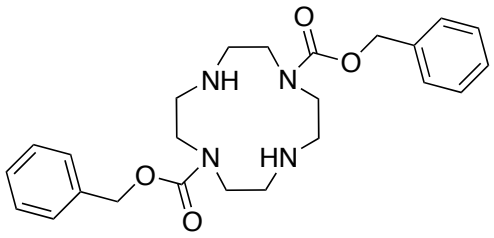

1,4,7,10-Tetraazacyclododecane (2.5 g, 14.5 mmol) was dissolved in a solution of distilled H_2O:dioxane (25:10, 35 mL), followed by addition of disodium hydrogen phosphate (7.0 g, 49.3 mmol). The pH of the solution was adjusted to 2.5 by careful addition of conc. HCl. Benzyl chloroformate (5.0 mL, 35.0 mmol) in dioxane (10 mL) was added dropwise over a period of 2 hours and the solution left to stir for a further 18 hours at room temperature, yielding a colourless solution with a white precipitate. The solvent was evaporated under reduced pressure and the residue dissolved in H_2O (100 mL), followed by adjustment of the pH to 7 by addition of conc. KOH (aq). The aqueous phase was extracted with Et_2O (2 x 100 mL), followed by CH_2Cl_2 (2 x 100 mL). The organic phases were combined, dried over $MgSO_4$, filtered, and the solvent removed under reduced pressure to give a clear oil. The oil was repeatedly washed with Et_2O to yield a white solid (4.20 g, 64 %). ^{1}H NMR (500 MHz, $CDCl_3$) δ 2.07 (2H, br. s, N**H**), 2.80–3.14 (8H, m, C**H**$_2$ ring), 3.42–3.81 (8H, m, C**H**$_2$), 5.16 (4H, s, OC**H**$_2$Ph), 7.30–7.38 (10H, m, Ar-**H**). ^{13}C NMR (125 MHz, $CDCl_3$) δ 48.0, 50.8 (**C**H_2), 67.4, 68.1 (**C**H_2Ph),

128.3, 128.7, 128.9, 129.1, 136.1 (Ar-**C**), 156.3, 156.4 (**C**O). MS (ES$^+$) *m/z* 441.5 $[M+H]^+$; $C_{24}H_{33}N_4O_4$ requires 441.2502; found 441.2514. M.pt. 115-117 °C.

4,10-Bis-*tert*-butoxycarbonylmethyl-1,4,7,10-tetraazacyclododecane-1,7-dicarboxylic acid dibenzyl ester, 61[7]

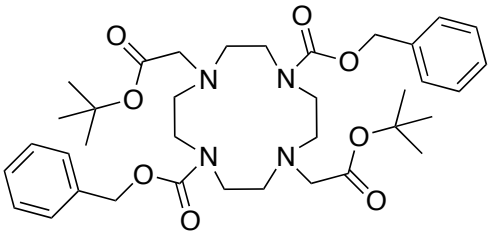

1,4,7,10-Tetraazacyclododecane-1,7-dicarboxylic acid dibenzyl ester (2.6 g, 5.83 mmol) and *tert*-butyl bromoacetate (1.93 mL, 13.1 mmol) were dissolved in anhydrous CH_3CN (25 mL) followed by the addition of Cs_2CO_3 (5.7 g, 17.5 mmol). The mixture was stirred under reflux for 18 hours. The cesium salts were filtered, and the solvent removed under reduced pressure. The resulting dark yellow oil was purified by column chromatography (DCM/MeOH, 100% to 98:2; R_f = 0.58) to yield a light yellow oil (2.81 g, 69 %). ^{1}H NMR (400 MHz, $CDCl_3$) δ 1.42 (18H, s, C(C**H**$_3$)$_3$), 2.76- 2.96 (8H, br. s, C**H**$_2$), 3.14- 3.49 (12H, C**H**$_2$ + C**H**$_2$CO), 5.12 (4H, s, OC**H**$_2$Ph), 7.27- 7.37 (10H, m, Ar-**H**). ^{13}C NMR ($CDCl_3$, 176 MHz) δ 28.0 (C(**C**H$_3$)$_3$), 46.7- 46.9 (br., **C**H$_2$ ring), 54.2- 54.5 (br., **C**H$_2$ ring), 55.9 (**C**H$_2$CO), 66.8 (O**C**H$_2$Ph), 80.7 (**C**(CH$_3$)$_3$), 127.7, 127.8, 128.0, 128.3, 128.5, 136.8 (Ar-**C**), 156.3, 170.4 (**C**O); MS (ES$^+$) *m/z* 669.7 $[M+H]^+$; $C_{36}H_{53}N_4O_8$ requires 669.3858; found 669.3860.

(7-*tert*-Butoxycarbonylmethyl-1,4,7,10-tetraazacyclododec-1-yl)-acetic acid *tert*-butyl ester, 62[7]

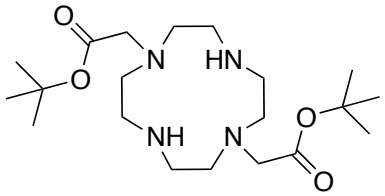

4,10-Bis-*tert*-butoxycarbonylmethyl-1,4,7,10-tetraazacyclododecane-1,7-dicarboxylic acid dibenzyl ester (2.81 g, 4.21 mmol) was dissolved in absolute

ethanol (20 mL) to which $Pd(OH)_2/C$ (10%) was added. The mixture was agitated in a Parr hydrogenation apparatus (40 psi) for 3 days. The catalyst was filtered and the ethanol removed under reduced pressure to yield a viscous yellow oil (1.67 g, 99 %). ^{1}H NMR (500 MHz, $CDCl_3$) δ 1.45 (18H, s, C(C**H**$_3$)$_3$), 2.71 (8H, br. s, C**H**$_2$), 2.82 (8H, br. s, C**H**$_2$), 3.31 (4H, s, C**H**$_2$CO). ^{13}C NMR (125MHz, $CDCl_3$) δ 27.3 (C(**C**H$_3$)$_3$), 51.8, 53.4 (**C**H$_2$), 82.7 (**C**(CH$_3$)$_3$), 171.9 (**C**O). MS (ES$^+$) *m/z* 401.6 $[M+H]^+$; $C_{20}H_{41}N_4O_4$ requires 401.3122; found 401.3121.

_(R)_-Di-*tert*-butyl 2,2'-(4-(6-(((benzyloxy)carbonyl)amino)-1-(*tert*-butoxy)-1-oxohexan-2-yl)-1,4,7,10-tetraazacyclododecane-1,7-diyl)diacetate, 63[9]

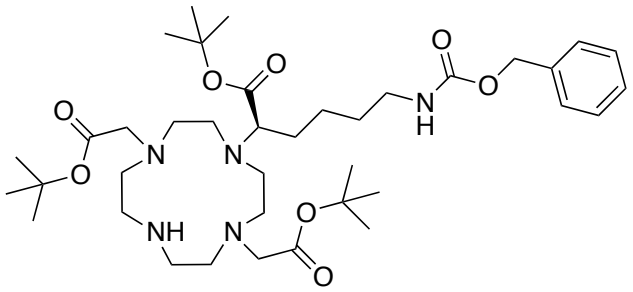

(7-*tert*-Butoxycarbonylmethyl-1,4,7,10-tetraazacyclododec-1-yl)-acetic acid *tert*-butyl ester (1.64 g, 4.08 mmol), *(S)-tert*-butyl 2-bromo-6-(2-phenylacetamido)hexanoate (1.47 g, 3.67 mmol) and Na_2CO_3 (389 mg, 3.67 mmol) were stirred as a solution in anhydrous acetonitrile (17 mL) at 80 °C for 16 hours. Completion of the reaction was verified by TLC, at which point the sodium salts were filtered and the filtrate reduced. The crude orange oil was purified by column chromatography on silica gel (DCM/MeOH, 100% to 90:10 using 1% increments; R_f = 0.44) to give a colourless oil which solidified on standing (1.34 g, 51%). ^{1}H NMR (600 MHz, $CDCl_3$) δ 1.22–1.38 (2H, m, C**H**$_2$), 1.44 (18H, s, C(C**H**$_3$)$_3$), 1.46 (9H, s, C(C**H**$_3$)$_3$), 1.50–1.71 (4H, m, C**H**$_2$), 2.72–2.85 (4H, m, C**H**$_2$), 2.92–3.16 (12H, br, m, C**H**$_2$), 3.18–3.24 (1H, m, C**H**), 3.25–3.30 (2H, m, C**H**$_2$), 3.35 (4H, s, C**H**$_2$), 5.08 (2H, s, C**H**$_2$), 7.26–7.36 (m, 5H, Ar-**H**), 9.54 (br. S, 2H, N**H**). ^{13}C NMR (151 MHz, $CDCl_3$) δ 23.9, 28.1, 28.2 (C(**C**H$_3$)$_3$), 29.3, 30.1, 40.5 (**C**H$_2$), 45.6, 48.6, 50.0, 56.1 (**C**H$_2$), 56.4 (**C**H$_2$CO$_2$^{t}Bu), 61.9 (**C**HCO$_2$^{t}Bu), 66.1 (Ar-**C**H$_2$CO),

81.6, 81.7 (**C**(CH_3)$_3$), 127.7, 127.8, 128.3, 136.9 (Ar-**C**), 156.6, 170.1, 171.4 (**C**O). MS (ES$^+$) *m/z* 720.6 [M+H]$^+$; $C_{38}H_{66}N_5O_8$ requires 720.4911; found 720.4940.

_(R)_-5-benzyl 1-_tert_-butyl 2-(7-(_(R)_-6(((benzyloxy)carbonyl)amino)-1-(_tert_-butoxy)-1-oxohexan-2-yl)-4,10-bis(2-(_tert_-butoxy)-2-oxoethyl)-1,4,7,10-tetraazacyclododecan-1-yl)pentanedioate, 64[10]

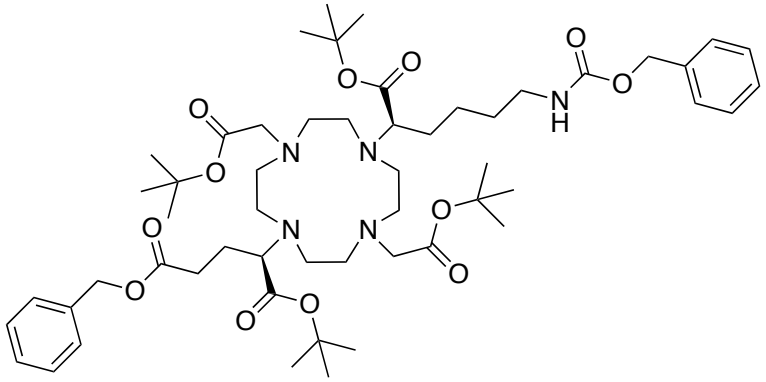

(R)-Di-*tert*-butyl 2,2'-(4-(6-(((benzyloxy)carbonyl)amino)-1-(*tert*-butoxy)-1-oxohexan-2-yl)-1,4,7,10-tetraazacyclododecane-1,7-diyl)diacetate (1.34 g, 1.87 mmol), K_2CO_3 (517 mg, 3.74 mmol) and *(S)-tert*-butyl 2-bromo-5-(2-phenylacetamido)pentanoate (801 mg, 2.24 mmol) were stirred as a solution in acetonitrile (20 mL) at 60 °C for 48 hours. The completion of the reaction was verified by TLC and the mixture cooled to room temperature, filtered and the filtrate concentrated under reduced pressure. The crude orange residue was then purified by column chromatography (DCM/MeOH, 100% to 93:7 utilizing 1% increments; R_f = 0.4) to give a green oil (596 mg, 32%). ^{1}H NMR (700 MHz, $CDCl_3$) δ 1.22–1.36 (4H, m, C**H**$_2$), 1.39 (9H, s, C(C**H**$_3$)), 1.41 (18H, s, C(C**H**$_3$)), 1.44 (9H, s, C(C**H**$_3$)), 1.59–1.73 (2H, m, C**H**$_2$), 2.04–2.12 (1H, m, C**H**), 2.25–2.75 (12H, m, C**H**$_2$), 2.96–3.19 (8H, m, C**H**$_2$), 3.26–3.31 (2H, m, C**H**$_2$), 3.34–3.35 (1H, m, C**H**), 3.46 (4H, m, C**H**$_2$), 5.04 (2H, s, OC**H**$_2$Ph), 5.06 (2H, s, OC**H**$_2$Ph), 5.15 (1H, s, N**H**), 7.25–7.35 (10H, m, Ar-**H**). ^{13}C NMR (176 MHz, $CDCl_3$) δ 24.4, 26.5, 27.7, 27.72 (C(**C**H$_3$)$_3$), 27.8, 28.1, 29.9, 32.6, 40.6, 55.6, 55.9, 56.4, 59.8 (**C**H$_2$), 61.2(**C**H$_2$CO$_2$^{t}Bu), 66.3, 67.6 (**C**HCO$_2$^{t}Bu), 68.4, 69.3 (O**C**H$_2$Ph), 81.7, 81.9, 82.4 (**C**(CH_3)$_3$), 127.9, 128.2, 128.3, 128.4, 128.6, 135.6, 136.5 (Ar-**C**), 156.4, 172.9, 173.4, 174.6, 175.1 (**C**O). MS (ES$^+$) *m/z* = 996.5 [M+H]$^+$; $C_{54}H_{86}N_5O_{12}$ requires 996.6273; found 996.6293.

_(R)_-4-(7-(_(R)_-6-(((benzyloxy)carbonyl)amino)-1-(_tert_-butoxy)-1-oxohexan-2-yl)-4,10-bis(2-(_tert_-butoxy)-2-oxoethyl)-1,4,7,10-tetraazacyclododecan-1-yl)-5-(_tert_-butoxy)-5-oxopentanoic acid, 65

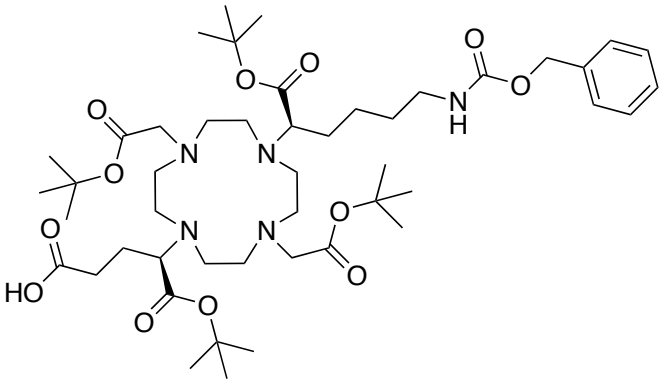

(R)-5-benzyl 1-*tert*-butyl 2-(7-(*(R)*-6(((benzyloxy)carbonyl)amino)-1-(*tert*-butoxy)-1-oxohexan-2-yl)-4,10-bis(2-(*tert*-butoxy)-2-oxoethyl)-1,4,7,10-tetraazacyclododecan-1-yl)pentanedioate (196 mg, 0.20 mmol) was dissolved in anhydrous THF (3 mL) and NaOH (17 mg, 0.40 mmol) was added as a solution in water (1 mL). The light yellow solution was stirred at room temperature and the progress of the reaction monitored by TLC. Upon complete conversion of the starting material, the solvent was removed under reduced pressure to give a yellow solid which was dried fully on a high vacuum line before being used directly in the next step without further purification (181 mg, 100%). ^{1}H NMR (400 MHz, $CDCl_3$) δ 1.28–1.39 (2H, m, C**H**$_2$), 1.40 (9H, s, C(C**H**$_3$)), 1.41 (18H, s, C(C**H**$_3$)), 1.42 (9H, s, C(C**H**$_3$)), 1.69-1.78 (4H, m, C**H**$_2$,), 2.14–2.22 (1H, m, C**H**), 2.27–2.88 (12H, m, C**H**$_2$), 2.92–3.39 (8H, m, C**H**$_2$), 3.42–3.51 (2H, m, C**H**$_2$), 3.49-3.55 (1H, m, C**H**), 3.67 (4H, s, C**H**$_2$), 4.63 (1H, s, COO**H**), 5.01 (2H, s, OC**H**$_2$Ph), 7.15–7.33 (5H, m, Ar-**H**). ^{13}C NMR (101 MHz, $CDCl_3$) δ 22.5, 24.6, 26.9 (C(**C**H$_3$)$_3$), 27.2, 27.3, 30.2, 31.5, 39.6, 53.8, 54.9, 55.4, 58.3 (**C**H$_2$), 59.0 (**C**H$_2$CO$_2$^{t}Bu), 63.4, 66.9 (**C**HCO$_2$^{t}Bu), 67.9 (O**C**H$_2$Ph), 80.4, 80.8, 80.9 (**C**(CH$_3$)$_3$), 125.9, 127.2, 127.4, 141.0 (Ar-**C**), 155.6, 171.6, 174.9, 175.5, 179.1 (**C**O). MS (ES$^+$) *m/z* = 906.6 [M+H]$^+$; $C_{47}H_{80}N_5O_{12}$ requires 906.5803; found 906.5763.

tert-Butyl (2-(5-((3a*S*, 4*S*, 6a*R*)-2-oxohexahydro-1*H*-thieno[3,4-*d*]imidazol-4-yl)pentanamido)ethyl)carbamate, 66[11]

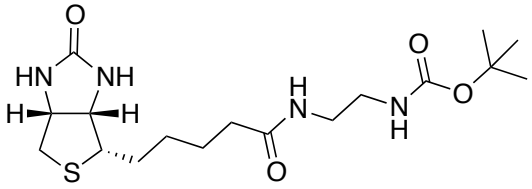

A suspension of D-biotin (300 mg, 1.23 mmol), N-Boc-1,2-diaminoethane (236 mg, 1.48 mmol) and EDC (307 mg, 1.60 mmol) in a solution of anhydrous MeOH (3 mL) and anhydrous acetonitrile (9 mL), was stirred for 5 hour at room temperature. Upon no further reaction, as verified by TLC, the mixture was concentrated under reduced pressure. The crude residue was then re-suspended in MeOH (25 mL) and filtered. The filtrate was concentrated and the crude product was purified by column chromatography (DCM/MeOH, 100% to 90:10; R_f = 0.64) to give a white solid (170 mg, 36%). ^{1}H NMR (400 MHz, MeOD) δ 1.27-1.29 (2H, m, C**H**$_2$), 1.34 (9H, s, C(C**H**$_3$)$_3$), 1.46-1.69 (4H, m, C**H**$_2$), 2.11 (2H, t, J = 7, C**H**$_2$CO), 2.61 (1H, d, J = 12, SCH**H**), 2.83 (1H, dd, J = 12, 5, SC**H'**H), 3.05 (2H, m, NHCH$_2$C**H**$_2$NHBOC), 3.09-3.18 (3H, m, NHC**H**$_2$CH$_2$NHBOC + SC**H**), 4.21 (1H, dd, J = 8, 4, C**H**), 4.41 (1H, dd, J = 8, 4, C**H**). ^{13}C NMR (400 MHz, MeOD) δ 26.8, 28.8, 29.5 (**C**H$_2$), 29.8 (C(**C**H$_3$)$_3$), 36.8 (**C**H$_2$CO), 37.4, 40.5 (NH**C**H$_2$), 41.0 (**C**H$_2$), 57.0 (**C**H-biotin chain), 61.6, 63.3 (**C**H), 80.2 (**C**(CH$_3$)$_3$), 158.5, 166.1, 176.4 (**C**O). MS (ES$^+$) *m/z* 409.7 [M+Na]$^+$; $C_{17}H_{30}N_4O_4SNa$ requires 409.1885; found 409.1883. M.Pt. 96-98 °C.

_N_-(2-Aminoethyl)-5-((3a_S_, 4_S_, 6a_R_)-2-oxohexahydro-1_H_-thieno[3,4-_d_]imidazol-4-yl)pentanamide, 67[11]

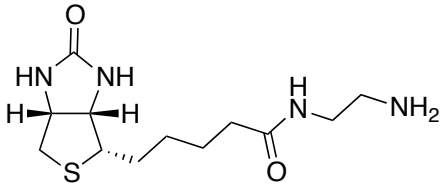

tert-Butyl (2-(5-((3a*S*, 4*S*, 6a*R*)-2-oxohexahydro-1*H*-thieno[3,4-*d*]imidazol-4-yl)pentanamido)ethyl)carbamate (155 mg, 0.4 mmol) was dissolved in anhydrous DCM (1 mL) to which anhydrous TFA (1 mL) was added with stirring. The solution was stirred at room temperature for 1 hour, before the solvent was removed under reduced pressure. The crude residue that remained was repeatedly re-dissolved in DCM and removed under reduced pressure to facilitate the removal of excess TFA. Drying under high vacuum gave the TFA salt as a light yellow oil (115 mg, 100%) which was used directly in the next step without further purification. ^{1}H NMR (400 MHz, D_2O) δ 1.14-1.29 (2H, m, C**H**$_2$), 1.35-1.61 (4H, m, C**H**$_2$), 2.14 (2H, t, J = 7, C**H**$_2$CO), 2.62 (1H, d, J = 12, SCH**H**), 2.82 (1H, dd, J = 12, 5, SC**H**H), 2.98 (2H, t, J = 6, NHCH$_2$C**H**$_2$NH$_2$), 3.13-3.20 (1H, m, SC**H**), 3.34 (2H, t, J = 6, NHC**H**$_2$CH$_2$NH$_2$), 4.27 (1H, dd, J = 8, 4, NC**H**), 4.46 (1H, dd, J = 8, 4, NC**H**). MS (ES$^+$) *m/z* 287.6 [M+H]$^+$; $C_{12}H_{23}N_4O_2S$ requires 287.1542; found 287.1533.

di-*tert*-Butyl 2,2'-(4-((*R*)-6-(((benzyloxy)carbonyl)amino)-1-(*tert*-butoxy)-1-oxohexan-2-yl)-10-((*R*)-1-(*tert*-butoxy)-1,5-dioxo-5-((2-5-((3a*S*,4*S*,6a*R*)-2-oxohexhydro-1H-thieno[3,4-*d*]imidazol-4-yl)pentanamido)ethyl)amino)pentan-2-yl)-1,4,7,10-tetraazacyclododecane-1,7-diyl)diacetate, 68

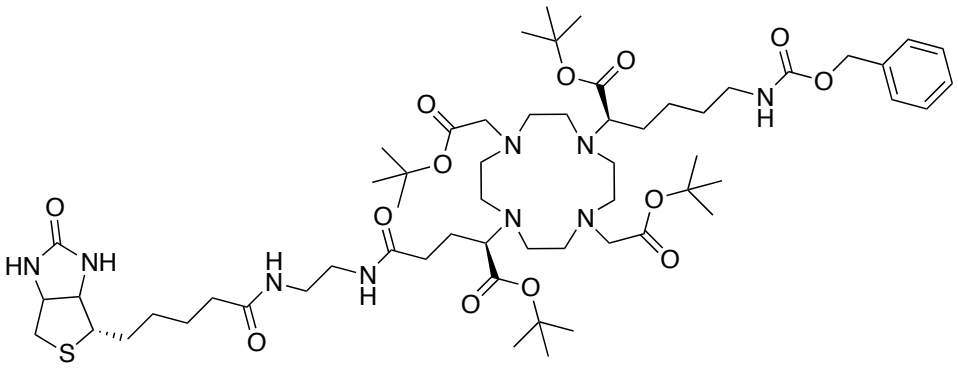

A solution of *(R)*-4-(7-(*(R)*-6-(((benzyloxy)carbonyl)amino)-1-(*tert*-butoxy)-1-oxohexan-2-yl)-4,10-bis(2-(*tert*-butoxy)-2-oxoethyl)-1,4,7,10-tetraazacyclododecan-1-yl)-5-(*tert*-butoxy)-5-oxopentanoic acid (181 mg, 0.2 mmol), EDC (46 mg, 0.24 mmol) and HOBt (32 mg, 0.24 mmol) in anhydrous DMF (1 mL) were stirred under argon at room temperature for 15 minutes. To the mixture was added a solution of *N*-(2-Aminoethyl)-5-((3a*S*, 4*S*, 6a*R*)-2-oxohexahydro-1*H*-thieno[3,4-*d*]imidazol-4-yl)pentanamide (57.5 mg, 0.2 mmol) and NMM (44 μL, 0.4 mmol) in anhydrous DMF (0.7 mL) dropwise over 5 minutes. The resulting mixture was stirred at room temperature overnight, before a second addition of the coupling reagents (EDC 46 mg, 0.24 mmol; HOBt 32 mg, 0.24 mmol). The reaction mixture was again stirred overnight at room temperature. Upon no further reaction by ESI-MS, the DMF was removed under reduced pressure and the residue taken up into EtOAc (30 mL). The organic phase was washed with saturated $NaHCO_3$ (30 mL) and the aqueous repeatedly extracted with EtOAc (3 x 30 mL). The combined organics were washed with brine (40 mL), dried over $MgSO_4$, filtered and evaporated. The crude residue was then purified by column chromatography (DCM/MeOH/NH_4OH, 100% to 80:18:2; R_f = 0.13) to give a viscous brown oil (70 mg, 30 %). ^{1}H NMR (600 MHz, $CDCl_3$) δ 1.32-1.56 (41H, m, C(C**H**$_3$)$_3$, C**H**$_2$), 1.57-1.69 (5H, m, C**H**$_2$), 1.70-1.90 (3H, m, C**H**$_2$), 2.09-2.25 (4H, m, C**H**$_2$), 2.49-2.67 (6H, m, C**H**$_2$), 2.68-2.77 (6H, m, C**H**$_2$),

2.78-2.92 (6H, m, C**H**$_2$), 3.04-3.23 (9H, m, C**H**$_2$), 3.23-3.41 (5H, m, C**H**$_2$), 4.27 (1H, dd, J = 8, 5, NHC**H**CH$_2$S), 4.45 (1H, dd, J = 8, 5, NHC**H**CH$_2$S), 5.06 (2H, s, OC**H**$_2$Ph), 5.89 (1H, br. s, N**H**), 6.51 (1H, br. s, N**H**), 7.28-7.35 (5H, m, Ar-**H**). ^{13}C NMR (151 MHz, $CDCl_3$) δ 23.6, 25.6, 27.9, 28.0 (**C**H/**C**H$_2$), 28.2, 28.3, 28.4 (C(**C**H$_3$)$_3$), 29.7, 29.9, 33.3, 35.9, 39.4, 40.6, 41.0, 49.5, 50.0, 50.7, 53.0, 53.2, 55.7, 56.7 (**C**H/**C**H$_2$), 60.3, 61.8 (**C**H$_2$CO$_2$^{t}Bu), 63.5, 64.5 (**C**HCO$_2$^{t}Bu), 66.6 (O**C**H$_2$Ph), 80.9, 81.0, 81.1 (**C**(CH$_3$)$_3$), 128.1, 128.2, 128.5, 136.8 (Ar-**C**), 156.6, 164.1, 171.3, 172.5, 173.0, 173.9, 175.4 (**C**O). MS (ES$^+$) *m/z* = 1174.7 [M+H]$^+$; $C_{59}H_{100}N_9O_{13}S$ requires 1174.716; found 1174.719.

[Conjugate 11], 69

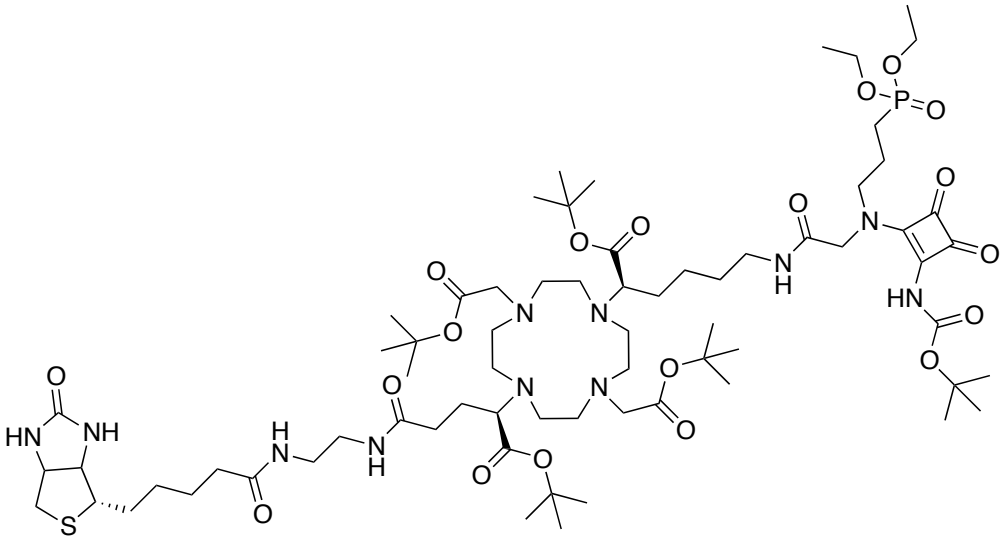

Di-*tert*-Butyl 2,2'-(4-((*R*)-6-(((benzyloxy)carbonyl)amino)-1-(*tert*-butoxy)-1-oxohexan-2-yl)-10-((*R*)-1-(*tert*-butoxy)-1,5-dioxo-5-((2-5-((3a*S*,4*S*,6a*R*)-2-oxohexhydro-1H-thieno[3,4-*d*]imidazol-4-yl)pentanamido)ethyl)amino)pentan-2-yl)-1,4,7,10-tetraazacyclododecane-1,7-diyl)diacetate (70 mg, 0.06 mmol) was dissolved in MeOH (10 mL) to which $Pd(OH)_2$ (20 mg) was added. The vessel was then loaded onto a Parr hydrogenator (P_{H2}=40 bar) and the reaction mixture agitated over 72 hours. After removal of the CBz protecting group (MS (ES$^+$) *m/z* 520.9 [M+2H]$^{2+}$), the mixture was filtered to remove excess palladium and washed excessively with MeOH. The amine residue was then evaporated to dryness. A solution of the amine (62 mg, 0.06 mmol) and NMM (13 μL, 0.12 mmol) in anhydrous DMF (1 mL) were then added dropwise over 5 minutes to a

pre-stirred solution of 2-((2-((*tert*-Butoxycarbonyl)amino)-3,4-dioxocyclobut-1-en-1-yl)(3-(diethoxyphosphoryl)propyl)amino)acetic acid (28 mg, 0.06 mmol), EDC (14 mg, 0.07 mmol) and HOBt (10 mg, 0.07 mmol) in anhydrous DMF (1 mL). The resulting mixture was stirred at room temperature overnight, before a second addition of the coupling reagents (EDC 14 mg, 0.07 mmol; HOBt 10 mg, 0.07 mmol). The reaction mixture was again stirred overnight at room temperature. Upon no further reaction by ESI-MS, the DMF was removed under reduced pressure and the residue taken up into EtOAc (20 mL). The organic phase was washed with saturated $NaHCO_3$ solution (20 mL) and the aqueous repeatedly extracted with EtOAc (3 x 20 mL). The combined organics were washed with saturated brine (30 mL), dried over $MgSO_4$, filtered and evaporated. The crude residue was then purified by RP-HPLC to give the desired compound as a brown film (5 mg, 6%). ^{1}H NMR (700 MHz, $CDCl_3$) δ 1.22-1.54 (53H, br.), 1.62-2.48 (35H, br.), 2.70-3.51 (22H, br.), 4.10 (4H, br.). ^{31}P NMR (283 MHz, $CDCl_3$) δ 30.49. MS (ES$^+$) *m/z* = 736.3 $[M+2H]^{2+}$; $C_{69}H_{121}N_{11}O_{19}SP$ requires 736.422; found 736.420.

[Gd.L^{11}]

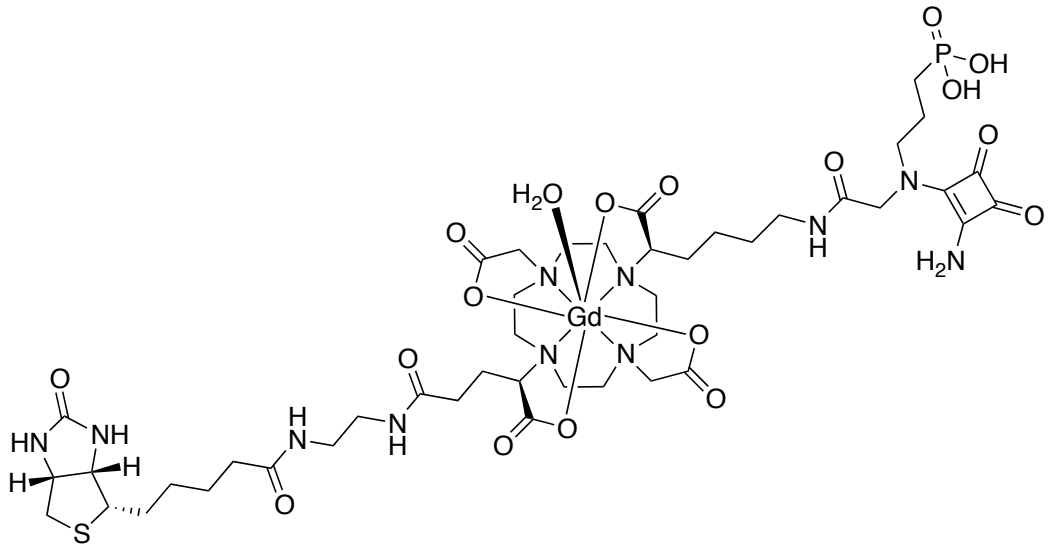

To a solution of ***69*** (5 mg, 0.003 mmol) in anhydrous THF (1 mL), was added a solution of KOH (1 mg, 0.02 mmol) in H_2O (200 μL) and the resulting mixture heated to 60 °C for 4 hours. After this period, the solvent was removed under reduced pressure to give the crude residue. Removal of the phosphonate ethyl

esters was verified by ESI-MS ($[M+2K]^{2+}$; m/z = 745.5). The free phosphonic acid was then partially dissolved in DCM (1 mL) to which TFA (1 mL) was added. The resulting yellow solution was stirred at room temperature overnight before removal of the solvent under reduced pressure. The crude product was re-dissolved in DCM and concentrated under reduced pressure. This process was repeated 3 times to yield **L^{11}** ($[M+2H]^{2+}$ m/z = 545.1). The residue was then dissolved in H_2O (1 mL) and the pH adjusted to 5.5 by the addition of NaOH (0.1M). $GdCl_3.6H_2O$ (2 mg, 5.4 μmol) was added as a solution in H_2O (0.2 mL) and the reaction mixture stirred at 60 °C overnight. The pH of the solution was periodically checked and adjusted to 5.5 by the addition of NaOH/HCl (0.1 M). Upon completion, excess gadolinium ions were removed by the addition of chelex-100™ with stirring. The Chelex trap was filtered and the complex eluted with excess H_2O. Removal of the water by lyophilisation gave the complex as a light yellow solid that was purified by RP-HPLC. HR-MS (ES^+) $C_{44}H_{69}{}^{157}GdN_{11}O_{17}PSK_2$ requires 440.672 $[M+H+2K]^{3+}$; found 440.671. r_{1p} = 7.2 $mM^{-1}s^{-1}$ (60 MHz, 310K). RP-HPLC: t_R = 15.9 mins [2-30% MeOH in H_2O over 10 mins].

(*S*)-2-Bromo-pentanedioic acid 5-methyl ester, 70

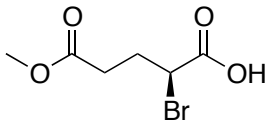

A solution of $NaNO_2$ (6.11 g, 88.5 mmol) in H_2O (50 ml) was added dropwise over 30 min to a stirred solution of (*S*)-glutamic acid 5-methyl ester (7.50 g, 46.5 mmol) and NaBr (13.2 g, 128.1 mmol) in 1 M HBr (276 mL), cooled at –5 °C. After 10 h, conc. H_2SO_4 (5 ml) was slowly added to the reaction mixture, which was then extracted with diethyl ether (3 x 300 ml). The combined organic extracts were washed with brine (200 ml), dried over Na_2SO_4, filtered and the filtrate concentrated under reduced pressure. The crude material was purified by column chromatography on silica (hexane/EtOAc, 100% to 80:20 utilizing 1 % increments; R_f = 0.20) to yield a yellow oil (4.35 g, 42 %). ^1H NMR (400 MHz,

$CDCl_3$) δ 2.27-2.32 (1H, m, C**H₂**CHBr), 2.38-2.43 (1H, m, C**H₂**CHBr), 2.57-2.65 (2H, m, C**H₂**CH_2CHBr), 3.69 (3H, s, C**H**$_3$), 4.41 (1H, dd, J = 9, 5, C**H**). ^{13}C NMR (176 MHz, $CDCl_3$) δ 29.7 (**C**H_2CH_2CHBr), 31.6 (**C**H_2CHBr), 44.2 (**C**H), 52.0 (**C**H_3), 172.1, 173.4 (**C**O). MS (ES^+) *m/z* 246.8 $[M + Na]^+$.

(*S*)-2-Bromo-pentanedioic acid 5-methyl ester 1-*tert*-butyl ester, 71

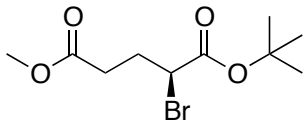

A solution of (*S*)-2-bromo-pentanedioic acid 5-methyl ester (2.94 g, 13.1 mmol) in *tert*-butyl acetate (47 ml) and $HClO_4$ in H_2O (70 %, 0.34 mmol) was stirred at room temperature, for 16 h. H_2O (35 ml) was added to the reaction mixture, and the organic phase separated. The organic phase was washed with H_2O (25 ml), followed by 5 % Na_2CO_3 (25 ml). The solvent was removed under reduced pressure to yield a yellow coloured oil (2.58 g, 70 %). ^{1}H NMR (400 MHz, $CDCl_3$) δ 1.47 (9H, s, C(C**H**$_3$)$_3$), 2.20-2.25 (1H, m, **CH₂**CHBr), 2.30-2.35 (1H, m, **CH₂**CHBr), 2.47-2.55 (2H, m, **CH₂**CH_2CHBr), 3.69 (3H, s, C**H**$_3$), 4.23 (1H, dd, J = 9, 5, C**H**). ^{13}C NMR (76 MHz $CDCl_3$) δ 27.9 (C(**C**H_3)$_3$), 29.9 (**C**H_2CH), 31.5 (**C**H_2CH_2), 46.8 (**C**H), 52.0 (**C**H_3), 82.8 (**C**$(CH_3)_3$), 168.4, 172.7 (**C**O). MS (ES^+) *m/z* 303.5 $[M+H]^+$; $C_{10}H_{17}O_4{}^{79}$BrNa requires 303.0208; found 303.0223.

(*R*)-1-*tert*-Butyl 5-methyl 2-(7-((*R*)-6-(((benzyloxy)carbonyl)amino)-1-(*tert*-butoxy)-1-oxohexan-2-yl)-4,10-bis(2-(*tert*-butoxy)-2-oxoethyl)-1,4,7,10-tetraazacyclododecan-1-yl)pentandioate, 72

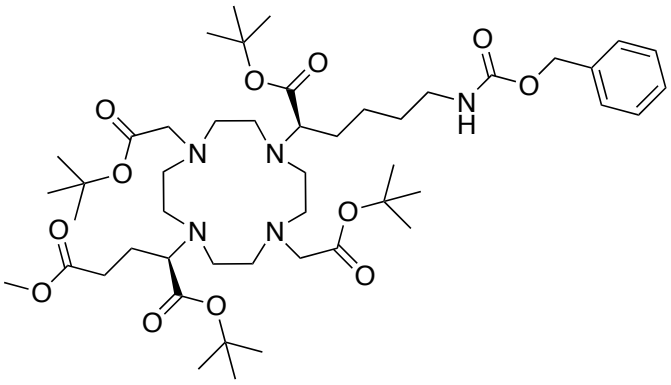

(*R*)-di-*tert*-butyl 2,2'-(4-(6-(((benzyloxy)carbonyl)amino)-1-(*tert*-butoxy)-1-oxohexan-2-yl)1,4,7,10-tetraazacyclododecane-1,7-diyl)diacetate (1.35 g, 1.87 mmol), K_2CO_3 (310 mg, 2.24 mmol) and (*S*)-2-bromo-pentanedioic acid 5-methyl ester 1-*tert*-butyl ester (631 mg, 2.24 mmol) were stirred as a solution in acetonitrile (20 mL) at 60 °C for 48 hours. Completion of reaction was verified by ESI-MS, at which point the mixture was cooled to room temperature, filtered and the filtrate concentrated under reduced pressure. The crude orange residue was then purified by column chromatography (DCM/MeOH, 100% DCM to 93:7 utilising 1% increments; R_f = 0.41) to give a dark yellow oil (571 mg, 33%). ^{1}H NMR (700 MHz, $CDCl_3$) δ 1.36 (9H, s, C(C**H**$_3$)$_3$), 1.37 (18H, s, C(C**H**$_3$)$_3$), 1.38 (9H, s, C(C**H**$_3$)$_3$), 1.43–1.50 (4H, m, C**H**$_2$), 1.54–1.63 (2H, m, C**H**$_2$), 1.64-1.78 (2H, m, C**H**$_2$), 1.84-1.93 (2H, m, C**H**$_2$), 2.38-2.52 (2H, br. m, C**H**$_2$), 2.52-2.61 (4H, br. m), 2.62-2.86 (12H, m, C**H**$_2$), 3.06-3.19 (6H, m), 3.57 (3H, s, C**H**$_3$), 5.00 (2H, s, OC**H**$_2$Ph), 5.17 (1H, s, N**H**), 7.21–7.31 (5H, m, Ar-**H**). ^{13}C NMR (176 MHz, $CDCl_3$) δ 27.7, 27.8 (**C**H$_2$), 28.2, 28.3, 28.3 (C(**C**H$_3$)$_3$), 30.4, 32.1, 40.5, 40.7, 44.1, 44.5, 47.1, 47.2, 48.7, 48.8 (**C**H$_2$), 51.4 (CH$_2$), 52.9 (**C**H$_3$), 55.8, 56.0, 59.7 (**C**H$_2$ ring), 61.1 (**C**H$_2$CO$_2$^{t}Bu), 63.2, 63.4 (**C**HCO$_2$^{t}Bu), 66.3 (O**C**H$_2$Ph), 81.8, 81.9, 82.0, 82.5 (**C**(CH$_3$)$_3$), 127.8, 127.9, 128.0, 128.4 (Ar-**C**), 172.8, 172.9, 173.3, 174.0, 174.6, 175.1 (**C**O). MS (ES$^+$) *m/z* 920.8 [M+H]$^+$; $C_{48}H_{82}N_5O_{12}$ requires 920.5782; found 920.5801.

4-(((*R*)-5-(4,10-Bis(2-(*tert*-butoxy)-2-oxoethyl)-7-((*R*)-1-(*tert*-butoxy)-5-methoxy-1,5-dioxopentan-2-yl)-1,4,7,10-tetraazacyclododecan-1-yl)-6-(*tert*-butoxy)-6-oxohexyl)amino)-4-oxobutanoic acid, 73

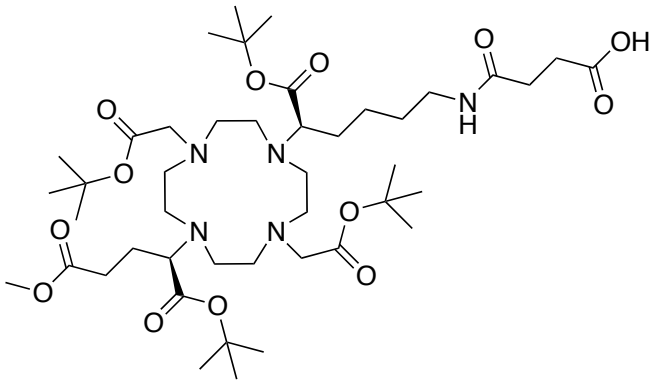

(*R*)-1-*tert*-Butyl 5-methyl 2-(7-((*R*)-6-(((benzyloxy)carbonyl)amino)-1-(*tert*-butoxy)-1-oxohexan-2-yl)-4,10-bis(2-(*tert*-butoxy)-2-oxoethyl)-1,4,7,10-tetraazacyclododecan-1-yl)pentandioate (279 mg, 0.30 mmol) was dissolved in absolute ethanol (10 mL) to which $Pd(OH)_2/C$ (10%) was added. The mixture was agitated in a Parr hydrogenation apparatus (40 psi) overnight. The catalyst was filtered and the ethanol removed under reduced pressure to yield the free amine. The amine was then dissolved in anhydrous DMF (3.5 mL) and diisopropylethylamine (98 μL, 0.56) was added. To this solution was added succinic anhydride (28 mg, 0.28 mmol) and the resulting mixture stirred at room temperature for 16 hours until complete reaction as verified by ESI-MS. The solvent was removed under reduced pressure and the crude residue that remained purified by column chromatography (DCM/MeOH, 100% to 87:13 in 1% increments; R_f =0.43) to yield a brown, viscous oil (160 mg, 60% over 2 steps). ^{1}H NMR (700 MHz, $CDCl_3$) δ 1.42 (9H, s, C(C**H**$_3$)$_3$), 1.44 (18H, s, C(C**H**$_3$)$_3$), 1.49 (9H, s, C(C**H**$_3$)$_3$), 1.51-1.68 (6H, m), 2.06-2.66 (16H, m), 2.67-3.08 (10H, m), 3.14-3.37 (6H, m), 3.62 (3H, s, C**H**$_3$), 7.75 (1H, br, N**H**), 8.15 (1H, br, O**H**). ^{13}C NMR (176 MHz, $CDCl_3$) δ 27.9, 27.9 (**C**H$_2$), 28.0, 28.0, 28.2, 28.3 (C(**C**H$_3$)$_3$), 29.1, 30.7, 32.3, 39.1, 38.8, 44.2, 46.9, 47.3, 48.7, 50.6, 51.7 (**C**H$_2$), 51.8 (**C**H$_3$), 52.7, 52.8, 56.0, 56.1 (**C**H$_2$), 56.4 (**C**H$_2$CO$_2$^{t}Bu), 59.8, 61.2 (**C**HCO$_2$^{t}Bu), 82.1, 82.2, 82.7, 83.6 (**C**(CH$_3$)$_3$), 172.9, 173.1, 173.5, 174.0, 174.8, 174.9, 175.4 (**C**O). MS (ES$^+$) *m/z* 886.7 [M+H]$^+$; $C_{44}H_{80}N_5O_{13}$ requires 886.5753; found 886.5742.

(2*R*)-1-*tert*-Butyl 5-methyl 2-(4,10-bis(2-(*tert*-butoxy)-2-oxoethyl)-7-((2*R*)-1-(*tert*-butoxy)-6-(4-((2-(2-(diethoxyphosphoryl)ethyl)-8,9-dioxo-2,6-diazabicyclo[5.2.0]non-1(7)-en-4-yl)amino)-4-oxobutanamido)-1-oxohexan-2-yl)-1,4,7,10-tetraazacyclododecan-1-yl)pentanedioate, 74

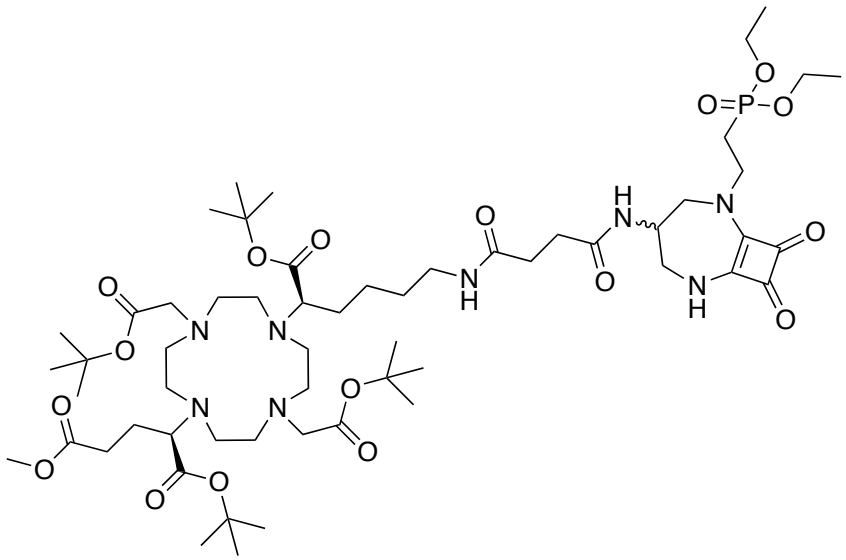

4-(((*R*)-5-(4,10-Bis(2-(*tert*-butoxy)-2-oxoethyl)-7-((*R*)-1-(*tert*-butoxy)-5-methoxy-1,5-dioxopentan-2-yl)-1,4,7,10-tetraazacyclododecan-1-yl)-6-(*tert*-butoxy)-6-oxohexyl)amino)-4-oxobutanoic acid (157 mg, 0.18 mmol), EDC (41 mg, 0.22 mmol) and HOBt (29 mg, 0.22 mmol) were dissolved in anhydrous DMF (2 mL) and stirred at room temperature under an atmosphere of argon for 20 minutes. After this period, a pre-stirred solution of diethyl (2-(4-amino-8,9-dioxo-2,6-diazabicyclo[5.2.0]non-1(7)-en-2-yl)ethyl)phosphonate (59 mg, 0.18 mmol) and NMM (41 μL, 0.36 mmol) in anhydrous DMF (1.0 mL) was added dropwise and the resulting solution stirred at room temperature until complete consumption of the starting materials was revealed by ESI-MS. After this period, the solvent was removed under reduced pressure and the crude oil taken up into EtOAc (30 mL). Saturated $NaHCO_3$ solution (30 mL) was added, the layers separated and the aqueous washed with EtOAc (3 x 30 mL). The combined organic portions were dried over $MgSO_4$, filtered and the solvent removed under reduced pressure. The crude residue was purified by column chromatography (DCM/MeOH, 100% to 85:15 in 1% increments; R_f =0.25) to yield a yellow viscous oil (50 mg, 23%). ^{1}H NMR (700 MHz, $CDCl_3$) δ 1.32 (6H, dt, J = 7, 3,

P($OCH_2C\mathbf{H}_3)_2$), 1.43 (36H, s, C($C\mathbf{H}_3)_3$), 1.44-1.46 (4H, m), 1.56-1.66 (2H, m), 1.75-1.84 (2H, m), 1.90-1.98 (2H, m), 2.12-2.19 (2H, m, P$C\mathbf{H}_2CH_2$), 2.42-2.51 (2H, m), 2.54-2.65 (7H, m), 2.66-2.74 (5H, m), 1.76-2.87 (8H, m), 3.10-3.13 (1H, m), 3.15-3.19 (3H, m), 3.21-3.24 (3H, m), 3.33 (1H, d, J = 14, $\mathbf{H}^{c/a}$ (eq)), 3.50 (1H, d, J = 14, $\mathbf{H}^{c}$ (axial)), 3.64 (3H, s, $C\mathbf{H}_3$), 3.69-3.79 (2H, m, $PCH_2C\mathbf{H}_2$), 3.90 (1H, dd, J = 14, 7, $\mathbf{H}^{a}$ (axial)), 4.05-4.14 (4H, m, P($OC\mathbf{H}_2CH_3)_2$), 4.25-4.29 (1H, m, $\mathbf{H}^{b}$). ^{13}C NMR (176 MHz, $CDCl_3$) δ 16.5 (d, ^{3}J = 6, P($OCH_2\mathbf{C}H_3)_2$), 24.0 ($\mathbf{C}H_2$), 25.0 (d, ^{1}J = 140, $NCH_2\mathbf{C}H_2P$), 25.2, 27.9, 27.9, 28.3 ($\mathbf{C}H_2$), 28.3, 28.4, 28.5 (overlapping C($\mathbf{C}H_3)_3$), 30.6, 31.0, 31.4, 31.8, 39.5, 45.2, 48.7 ($\mathbf{C}H_2$), 49.7 (d, J = 16, $PCH_2\mathbf{C}H_2$), 51.5 ($\mathbf{C}^{b}$), 52.9, 53.1, 53.1($\mathbf{C}H_2$), 55.5 ($\mathbf{C}^{a}$), 56.1 ($\mathbf{C}^{c}$), 62.2 (d, ^{2}J = 7, P($O\mathbf{C}H_2CH_3)_2$), 62.5 ($\mathbf{C}$H), 63.2 ($\mathbf{C}H_2CO_2{}^t$Bu), 64.5 ($\mathbf{C}$H), 80.8, 80.8, 80.8, 81.0 ($\mathbf{C}(CH_3)_3$), 168.0, 168.2 ($\mathbf{C}$=$\mathbf{C}$), 171.1, 172.2, 172.5, 173.0, 173.5, 174.4, 177.2, 181.2, 182.2 ($\mathbf{C}$O). ^{31}P NMR (283 MHz, $CDCl_3$) δ 27.26. MS (ES^+) *m/z* 1199.4 $[M+H]^+$; $C_{57}H_{100}N_8O_{17}P$ requires 1199.694; found 1199.693.

[Conjugate 12], 75

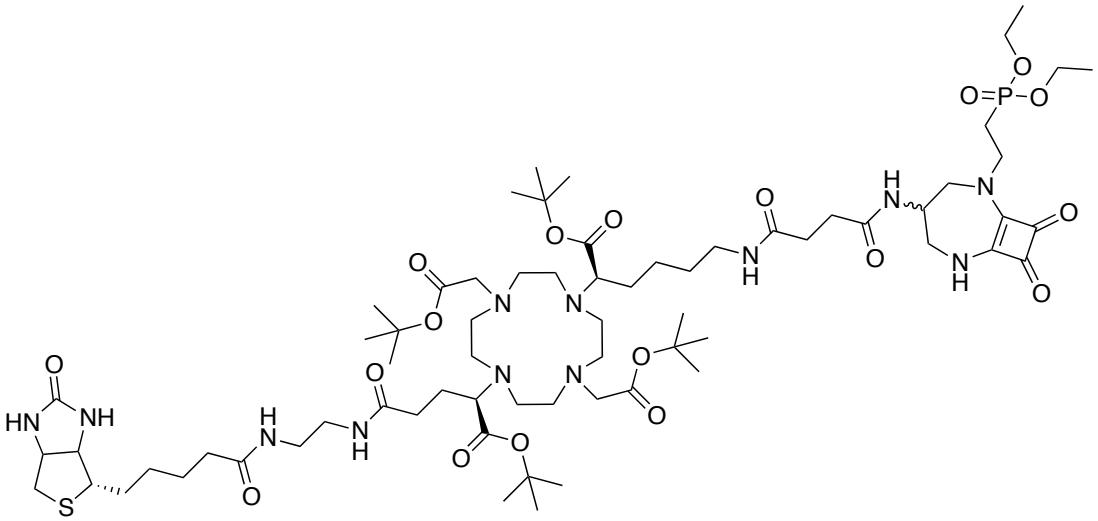

(2*R*)-1-*tert*-Butyl 5-methyl 2-(4,10-bis(2-(*tert*-butoxy)-2-oxoethyl)-7-((2*R*)-1-(*tert*-butoxy)-6-(4-((2-(2-(diethoxyphosphoryl)ethyl)-8,9-dioxo-2,6-diazabicyclo[5.2.0]non-1(7)-en-4-yl)amino)-4-oxobutanamido)-1-oxohexan-2-yl)-1,4,7,10-tetraazacyclododecan-1-yl)pentanedioate (50 mg, 0.042 mmol) was dissolved in methanol (1 mL) and NaOH (2 mg, 0.051 mmol) was added as a solution in H_2O (250 μL). The light yellow solution was stirred at room

temperature and progress of the reaction monitored by ESI-MS. Upon complete hydrolysis of the methyl ester after 1 hour, the solvent was removed under reduced pressure to give a pale yellow solid, which was dried fully on a high vacuum line. This yielded the carboxylic acid (49 mg, 0.042), to which EDC (9.6 mg, 0.050 mmol) and HOBt (6.8 mg, 0.050 mmol) were added and dissolved in anhydrous DMF (1 mL). The mixture was stirred at room temperature under an atmosphere of argon for 20 minutes. After this period, a pre-stirred solution of *N*-(2-Aminoethyl)-5-((3a*S*, 4*S*, 6a*R*)-2-oxohexahydro-1*H*-thieno[3,4-*d*]imidazol-4-yl)pentanamide (12 mg, 0.042 mmol) and NMM (9 μL, 0.083 mmol) in anhydrous DMF (0.5 mL) was added dropwise and the resulting solution stirred at room temperature until complete consumption of the starting materials was revealed by ESI-MS. After this period, the solvent was removed under reduced pressure and the crude oil taken up into EtOAc (15 mL). Saturated $NaHCO_3$ solution (15 mL) was added, the layers separated and the aqueous washed with EtOAc (3 x 20 mL). The combined organic portions were dried over $MgSO_4$, filtered and the solvent removed under reduced pressure. The crude residue was purified by column chromatography (DCM/MeOH/NH_4OH, 100% to 80:15:5; R_f =0.15) to yield a yellow oil (10 mg, 17%). ^1H NMR (700 MHz, $CDCl_3$) δ 1.29-1.37 (6H, m, $P(OCH_2C\mathbf{H}_3)_2$), 1.40-1.51 (40H, m), 1.56-1.75 (5H, m), 2.22-2.80 (20H, m), 2.80-3.51 (31H, m), 3.60-3.93 (5H, m), 5.05-4.15 (4H, m, $P(OC\mathbf{H}_2CH_3)_2$), 4.21-4.52 (3H, m), 7.87-8.51 (3H, m). ^{31}P NMR (283 MHz, $CDCl_3$) δ 27.17. MS (ES^+) *m/z* 727.4 $[M+2H]^{2+}$; $C_{68}H_{118}N_{12}O_{18}PS$ requires 1453.815; found 1453.819.

[Gd.L^{12}]

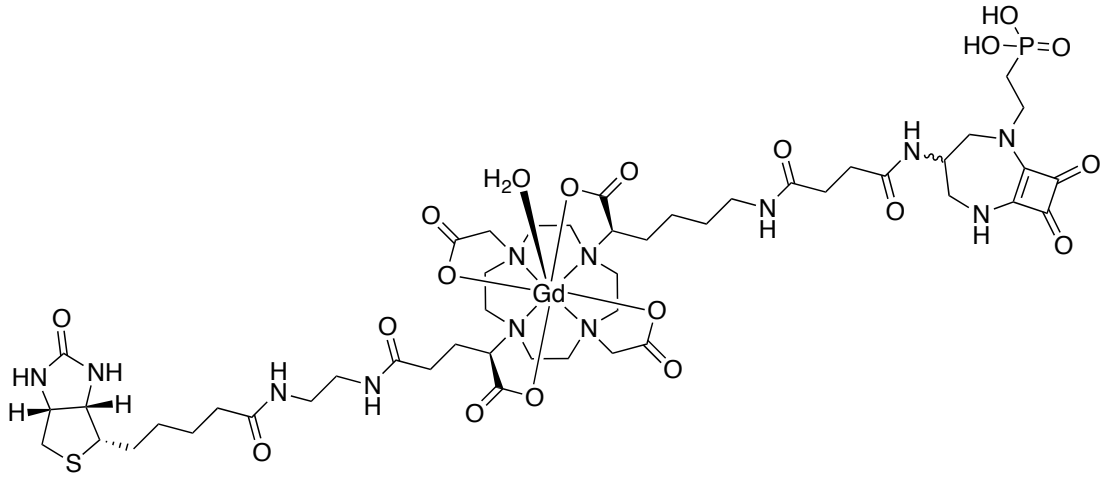

75 (10 mg, 0.007 mmol) was dissolved in DCM (1 mL) with stirring. To this solution was added trifluoroacetic acid (1 mL) and the resulting solution was stirred at room temperature for overnight. Removal of the *tert*-butyl ester groups was verified by ESI-MS, at which point the excess solvent was removed under reduced pressure. The residue was repeatedly re-dissolved in DCM (2 mL) and the solvent removed under reduced pressure to remove excess TFA. This process yielded the phosphonate ethyl ester as a light-brown solid. This residue was dissolved in DMF (0.8 mL) to which bromotrimethylsilane (7 μL, 0.055 mmol) was added dropwise. The resulting mixture was heated to 60 °C overnight until complete deprotection as verified by ESI-MS. The solvent was removed under reduced pressure, before the residue re-dissolved in H_2O. The pH was adjusted to 6 and the aqueous phase washed with DCM (3 x 2 mL) and diethyl ether (3 x 2 mL). The aqueous solvent was then removed by lyophilisation to give the protonated salt of **L^{12}** as a light brown solid. MS (ES$^+$) *m/z* 587.0 $[M+2H]^{2+}$. The salt of **L^{12}** (8.1 mg, 0.007 mmol) was dissolved in H_2O (0.5 mL) and the pH adjusted to 6. $GdCl_3.6H_2O$ (3.1 mg, 0.008 mmol) was added as a solution in H_2O (0.5 mL) and the reaction mixture stirred at 60 °C overnight. The pH of the solution was periodically checked and maintained between 5 and 6 by the addition of NaOH/HCl (0.1 M). Upon completion of comlexation, excess gadolinium was removed by the addition of Chelex-100™ with stirring. The Chelex trap was filtered and the complex eluted with excess H_2O. Removal of the water by lyophilisation gave the complex as a white solid that was purified by

RP-HPLC. HR-MS (ES$^+$) $C_{48}H_{75}{}^{154}GdN_{12}O_{18}PS$ requires 1324.399 $[M+2H]^+$; found 1324.399. r_{1p} = 7.2 mM^{-1} s^{-1} (60 MHz, 310K). RP-HPLC: t_R = 16.7 mins [2-30% MeOH in H_2O over 10 mins].

[2-(4-Hydroxy-8,9-dioxo-2,6-diazabicyclo[5.2.0]non-1(7)-en-2-yl)ethyl]phosphonic acid, 76[6]

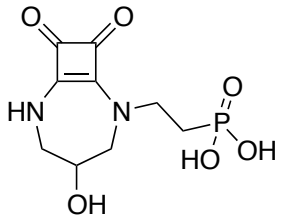

To a solution of (2-(4-hydroxy-8,9-dioxo-2,6-diazabicyclo[5.2.0]non-1(7)-en-2-yl)ethyl)phosphonic acid diethyl ester (59 mg, 0.18 mmol) in anhydrous DCM (3 mL) was added bromotrimethylsilane (188 μL, 1.42 mmol) and the reaction heated to reflux for 30 minutes. After this time, the solvent was removed under reduced pressure and the crude product purified by preparative HPLC to give a white solid (14 mg, 28%). ^{1}H NMR (400 MHz, D_2O) δ 1.86-1.98 (2H, m, PC**H**$_2$CH$_2$), 3.56 (1H, d, J = 14, C**H**), 3.65-3.74 (2H, m, 2 x C**H**), 3.78 (1H, d, J = 14, C**H**), 3.85-3.99 (2H, m, PCH$_2$C**H**$_2$), 4.31-4.36 (1H, m, C**H**). ^{31}P NMR (162 MHz, D_2O) δ 19.28. MS (ES$^+$) *m/z* 277.1 $[M+H]^+$; $C_9H_{14}N_2O_6P$ requires 277.0590; found 277.0588.

(2*S*)-*N*-(2-aminoethyl)-(2,6-diaminohexanamide), 77[12]

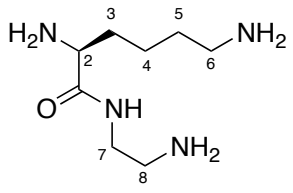

(2*S*)-Lysine ethyl ester hydrochloride (7.0 g, 28 mmol) was added in small portions over 1 h to ethylenediamine (70 mL) at 80 °C, under argon, with continuous stirring. The reaction was heated to 120 °C for 3 hours before the ethylenediamine was removed by distillation under reduced pressure. The

orange oil that remained was taken into aqueous NaOH solution (10 mL, 4 M), the solvent removed and the residue redissolved in MeOH (20 mL). The solution was filtered and the filtrate added to DCM (70 mL) and passed through a pad of celite. The filtrate was evapourated to give a yellow oil (3.9 g, 75%). ^{1}H NMR (400 MHz, $CDCl_3$) δ 1.30-1.46 (10H, m, N**H**$_2$ + **H**^{4} + **H**^{5}), 1.85 (2H, m, **H**^{3}), 2.68 (2H, t, J = 6, **H**^{6}), 2.80 (2H, t, J = 6, **H**^{8}), 3.28 (2H, q, J = 6, **H**^{7}), 3.32-3.35 (1H, m, **H**^{2}), 7.57 (1H, br. s, N**H**). ^{13}C NMR (101 MHz, $CDCl_3$) δ 23.2, 33.5, 35.0 (**C**^{3} + **C**^{4} + **C**^{5}), 41.5, 41.7, 41.9 (**C**^{6} + **C**^{7} + **C**^{8}), 55.2 (**C**^{2}), 188.6 (**C**O). MS (ES$^+$) *m/z* 211.3 [M + Na]$^+$; $C_8H_{20}N_4ONa$ requires 211.1535; found 211.1535.

(5*S*)-3-Azanonane-1,5,9-triamine, 78[12]

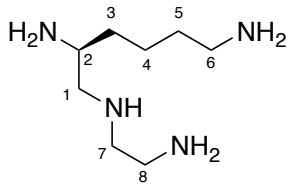

(2*S*)-*N*-(2-Aminoethyl)-(2,6-diaminohexanamide) (3.9 g, 21 mmol) was boiled under reflux (70 °C) in BH_3-THF (100 mL, 100 mmol) for 24 hours. After this time, the reaction was quenched by the slow addition of methanol (100 mL) at 0 °C and the solvent removed under reduced pressure. Reaction completion was confirmed by IR spectroscopy (disappearance of amide carbonyl). The resulting white solid was boiled under reflux overnight in HCl (50 mL, 2 M), at which point evaporation of the solvent under reduced pressure revealed the tetra-hydrochloride salt as a white gum (6.67 g, 100%). ^{1}H NMR (400 MHz, D_2O) δ 1.38-1.73 (6H, m, **H**^{3} + **H**^{4} + **H**^{5}), 2.93 (2H, t, J = 8, **H**^{6}), 3.30-3.38 (6H, m, **H**^{1} + **H**^{7} + **H**^{8}), 3.58-3.64 (1H, m, **H**^{2}). ^{13}C NMR (101 MHz, D_2O) δ 21.5, 26.5, 30.0 (**C**^{3} + **C**^{4} + **C**^{5}), 35.5, 39.2, 45.3, 48.6, 49.3 (**C**^{1} + **C**^{2} + **C**^{6} + **C**^{7} + **C**^{8}). MS (ES$^+$) *m/z* 175.4 [M + H]$^+$; $C_8H_{23}N_4$ requires 175.1923; found 175.1925.

(5*S*)-*N*-(5,9-Diamino-7-azanonyl)benzamide, 79[12]

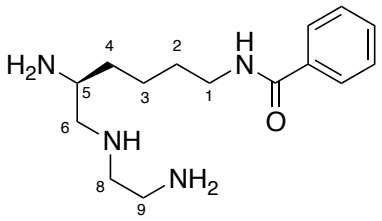

The tetrahydrochloride salt of (5*S*)-3-azanonane-1,5,9-triamine was converted to the free amine by the addition of KOH (to pH 7). The free amine (1.49 g, 8.52 mmol) was dissolved in H_2O (25 mL) and $Cu(CO_3)Cu(OH)_2$ (1.04 g, 4.68 mmol) was added to give an intense blue colour. The mixture was heated to 50 °C for 45 mins before cooling to 0 °C. Benzoyl chloride (1.29 mL, 11.08 mmol) was added dropwise to the cooled solution, whilst the pH was maintained between 8-9 by the addition of KOH. The reaction was allowed to warm to room temperature and the stirring continued for 1 hour. The solution was filtered and the filtrate treated with H_2S for 5 minutes to precipitate a brown solid. This solid was filtered and pale yellow solution was washed with DCM. The aqueous layer was reduced to 50% original volume and the pH was increased to 12. The aqueous solution was repeatedly extracted with DCM and $CHCl_3$, with evaporation of the organic giving a colourless oil (1.02 g, 43%). ^{1}H NMR (400 MHz, $CDCl_3$) δ 1.53-1.67 (11H, m, N**H**$_2$ + **H**^{2} + **H**^{3} + **H**^{4}), 2.38-2.42 (1H, m, **H**^{5}), 2.66-2.72 (6H, m, **H**^{6} + **H**^{8} + **H**^{9}), 2.82 (2H, t, J = 4, **H**^{1}), 6.33 (1H, br.s, N**H**), 7.43-7.80 (5H, Ar-**H**). ^{13}C NMR (101 MHz, $CDCl_3$) δ 22.5, 23.7, 28.7 (**C**^{2} + **C**^{3} + **C**^{4}), 38.7 (**C**^{1}), 40.8, 50.0, 51.6 (**C**^{6} + **C**^{8} + **C**^{9}), 55.6 (**C**^{5}), 125.9, 127.5, 130.3, 133.8 (Ar-**C**), 166.6 (**C**O). MS (ES$^+$) *m/z* 279.1 $[M + H]^+$; $C_{15}H_{27}N_4O$ requires 279.2185; found 279.2190.

(5*S*)-*N*-(5,9-Bistoluene-p-sulphonamido-7-toluene-p-sulphonyl-7-azanonyl)benzamide, 80[12]

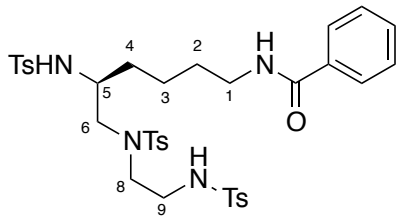

A solution of 4-toluenesulfonyl chloride (2.48 g, 12.99 mmol), in anhydrous DCM (30 mL) was added dropwise to a solution of (5*S*)-*N*-(5,9-diamino-7-azanonyl)benzamide (1.02 g, 3.66 mmol), and triethylamine (2.32 mL, 16.66 mmol) in anhydrous DCM (20 mL), with stirring over a 1 hour period. The resulting solution was stirred at room temperature overnight, after which time the mixture was washed with water (2 x 30 mL). The water layers were combined and extracted with EtOAc (3 x 30 mL) and the combined organic layers concentrated under reduced pressure. The crude residue that remained was then purified by column chromatography (DCM/EtOAc, 100 % to 70:30; R_f = 0.35) to give a white solid (954 mg, 35%). ^{1}H NMR (400 MHz, $CDCl_3$) δ 0.98-1.02 (2H, m, **H**^{3}), 1.35-1.50 (3H, m, **H**^{2} + **H**^{4}), 1.71 (1H, m, **H**^{4}), 2.25 (3H, s, C**H**$_3$), 2.73 (6H, s, C**H**$_3$), 3.04-3.35 (9H, m, **H**^{1} + **H**^{5} + **H**^{6} + **H**^{8} + **H**^{9}), 5.26-2.30 (2H, m, N**H**Ts), 6.48 (1H, br.s, N**H**), 6.90 (2H, m, Ar-**H**), 6.99-7.02 (5H, m, Ar-**H**), 7.42-7.47 (2H, m, Ar-**H**), 7.49-7.54 (1H, m Ar-**H**), 7.70 (2H, d, J = 8, Ar-**H**), 7.75-7.80 (3H, m, Ar-**H**), 7.86 (2H, d, J = 8, Ar-**H**). ^{13}C NMR (101 MHz, $CDCl_3$) δ 20.5 (**C**H$_3$), 27.7, 30.1, 38.0 (**C**^{2} + **C**^{3} + **C**^{4}), 41.7 (**C**^{1}), 50.1, 51.6, 52.4 (**C**^{6} + **C**^{8} + **C**^{9}), 55.0 (**C**^{5}), 126.1, 126.3, 126.4, 127.5, 128.7, 128.8, 129.0, 130.4, 133.3, 135.8, 136.1, 142.6, 143.2 (Ar-**C**), 166.8 (**C**O). MS (ES$^+$) *m/z* 741.4 $[M + H]^+$; $C_{36}H_{45}N_4O_7S_3$ requires 741.2450; found 741.2445. M. Pt. 148-150 °C.

(*S*)-2-(4-Benzamidobutyl)-1,4,7-tris-(toluene-p-sulphonyl)-1,4,7-triazacyclononane, 81[12]

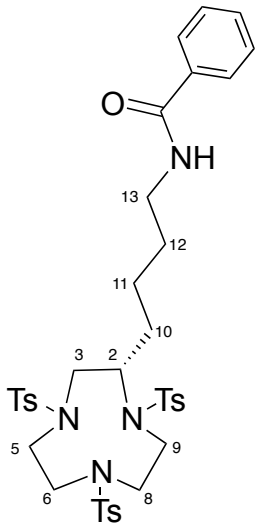

Caesium carbonate (1.38 g, 4.25 mmol) was added to a solution of the tritosylamide (954 mg, 1.29 mmol), in anhydrous DMF (58 mL). A solution of ethylene glycol bis(toluene-p-sulfonate) (526 mg, 1.42 mmol) in anhydrous DMF (25 mL) was added dropwise over a period of 2 hours with stirring. After stirring overnight at room temperature, the reaction was heated to 65 °C for 5 hours. After no further reaction as deduced by ESI-MS, the solvent was removed under reduced pressure and the residue that remained dissolved in $CHCl_3$ (50 mL) and washed with water. The organic layer was dried over $MgSO_4$, filtered and evaporated to give the crude product, which was purified by column chromatography (DCM/EtOAc, 100% to 80:20; R_f = 0.47) to give a white solid (692 mg, 70%). ^{1}H NMR (400 MHz, $CDCl_3$) δ 1.24-1.54 (6H, m, **H**^{10} + **H**^{11} + **H**^{12}), 2.39-2.45 (9H, m, C**H**$_3$), 3.10-3.61 (13H, m, **H**^{2} + **H**^{3} + **H**^{5} + **H**^{6} + **H**^{8} + **H**^{9} + **H**^{13}), 6.59 (1H, s, N**H**), 7.27-2.39 (9H, m, Ar-**H**), 7.60-7.62 (2H, m, Ar-**H**), 7.63-7.67 (2H, m, Ar-**H**), 7.75-7.80 (2H, m, Ar-**H**), 7.83 (2H, d, J = 8, Ar-**H**). ^{13}C NMR (101 MHz, $CDCl_3$) δ 20.5 (**C**H$_3$), 23.0, 28.0, 38.5 (**C**^{10} + **C**^{11} + **C**^{12}), 38.7 (**C**^{13}), 45.3, 49.7, 51.6, 52.7 (**C**^{3} + **C**^{5} + **C**^{6} + **C**^{8} + **C**^{9}), 59.4 (**C**^{2}), 126.0, 126.3, 126.5, 126.6, 126.7, 127.0, 127.5, 128.8, 128.9, 129.0, 130.3, 133.2, 133.4, 133.6, 142.9, 143.1, 143.2 (Ar-**C**), 166.5 (**C**O). MS (ES$^+$) *m/z* 767.0 $[M + H]^+$; $C_{38}H_{47}N_4O_7S_3$ requires 767.2607; found 767.2610. M. Pt. 107-109 °C.

(*S*)-4-(1,4,7-Triazonan-2-yl)butan-1-amine, 82[12]

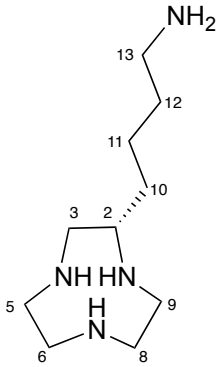

Ammonia (excess) was condensed into a solution of the tritosylamide (692 mg, 0.92 mmol) in a mixture of anhydrous THF (30 mL) and anhydrous EtOH (2.3 mL) whilst stirring under argon at −78 °C. Lithium (400 mg, excess) was added in small portions to the solution and a strong blue colour developed. The solution was slowly warmed to room temperature overnight; during this period the solution turned colourless and the ammonia gas was allowed to evaporate through an anti-suck back apparatus. Water (20 mL) was added to the solution and the solvent was removed. The residue that remained was dissolved directly in HCl solution (7.5 mL, 6 M) and the mixture heated to 100 °C for 72 hours. Upon completion, the reaction was diluted with H_2O (5 mL) and washed with diethyl ether (3 x 15 mL). The aqueous layer was concentrated to give the tetrahydrochloride salt (162 mg, 100%). ^{1}H NMR (400 MHz, D_2O) δ 1.37-1.64 (6H, m, $\mathbf{H}^{10}$ + $\mathbf{H}^{11}$ + $\mathbf{H}^{12}$), 2.87-3.96 (3H, m, $\mathbf{H}^{2}$ + $\mathbf{H}^{13}$), 3.13-3.42 (10H, m, $\mathbf{H}^{3}$ + $\mathbf{H}^{5}$ + $\mathbf{H}^{6}$ + $\mathbf{H}^{8}$ + $\mathbf{H}^{9}$). ^{13}C NMR (101 MHz, D_2O) δ 22.1, 26.5, 30.6, ($\mathbf{C}^{10}$ + $\mathbf{C}^{11}$ + $\mathbf{C}^{12}$), 39.0, 39.1, 39.2, 41.8, 43.2, 46.1 ($\mathbf{C}^{3}$ + $\mathbf{C}^{5}$ + $\mathbf{C}^{6}$ + $\mathbf{C}^{8}$ + $\mathbf{C}^{9}$ + $\mathbf{C}^{13}$), 53.3 ($\mathbf{C}^{2}$). MS (ES$^+$) *m/z* 201.4 $[M + H]^+$; $C_{10}H_{25}N_4$ requires 201.2079; found 201.2068.

(*S*)-*tert*-Butyl (4-(1,4,7-triazonan-2-yl)butyl)carbamate, 83[13]

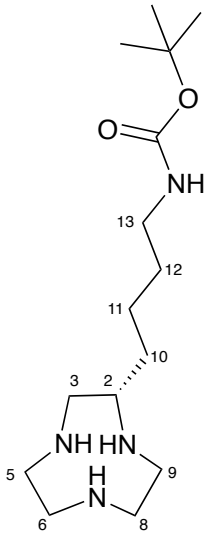

The tetra-hydrochloride salt of (*S*)-4-(1,4,7-triazonon-2-yl)butan-1-amine was converted to the free tetra amine (27 mg, 0.135 mmol) by anion exchange chromatography using DOWEX 1x2-200 resin. The free amine was dissolved in MeOH (2 mL) and $CuCl_2.2H_2O$ (23 mg, 0.135 mmol) was added, resulting in an intense green solution. The mixture was stirred at room temperature under argon for 3 hours, at which point the solvent was removed and the green solid dissolved in H_2O (1.5 mL). A solution of di-*tert*-butyl dicarbonate (59 mg, 0.27 mmol) in dioxane (1.5 mL) was added and the solution stirred at room temperature. After 3 hours, a further equivalent of di-*tert*-butyl dicarbonate was added and the reaction stirred overnight. Upon complete reaction as observed by ESI-MS, the blue solution was treated with H_2S for 5 mins. The brown precipitate was removed by centrifugation and the supernatant washed with DCM. The pH was raised to 11 before exhaustive extraction with DCM/$CHCl_3$. The organic fractions were combined and concentrated to give a colourless oil (15 mg, 37%). ^{1}H NMR (400 MHz, $CDCl_3$) δ 1.35-1.49 (6H, m, **H**^{10} + **H**^{11} + **H**^{12}), 1.47 (9H, s, (C**H**$_3$)$_3$), 2.32-2.37 (3H, m, N**H**), 2.47 (1H, m, **H**^{2}), 2.67-2.89 (10H, m, **H**^{3} + **H**^{5} + **H**^{6} + **H**^{8} + **H**^{9}), 3.08-3.13 (2H, m, **H**^{13}), 6.46 (1H, br, N**H**). ^{13}C NMR (101 MHz, $CDCl_3$) δ 28.6 (C(**C**H$_3$)$_3$), 23.7, 30.4, 33.9 (**C**^{10} + **C**^{11} + **C**^{12}), 40.3 (**C**^{13}), 40.6, 44.3, 45.3, 46.2, 49.9 (**C**^{3} + **C**^{5} + **C**^{6} + **C**^{8} + **C**^{9}), 55.2 (**C**^{2}), 79.3 (**C**(CH$_3$)$_3$), 156.3 (**C**O). MS (ES$^+$) *m/z* 301.1 [M + H]$^+$; $C_{15}H_{33}N_4O_2$ requires 301.2604; found 201.2603.

Methyl 2-(4-ethynylphenoxy)acetate, 84[14]

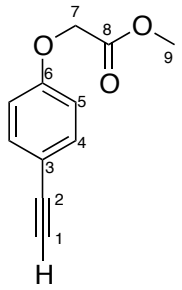

The trimethylsilane-protected alkyne (134 mg, 0.511 mmol) was dissolved in anhydrous THF (2 mL) and triethylammonium dihydrofluoride (833 μL, 5.11 mmol) was added. The mixture was stirred under argon for 24 hours at 35 °C, at which point the solvent was removed under reduced pressure. The crude residue that remained was purified by column chromatography (DCM/Hexane, 70:30; R_f = 0.25) to give a colourless oil (70 mg, 72%). ^{1}H NMR (400 MHz, $CDCl_3$) δ 3.00 (1H, s, **H**^{1}), 3.80 (3H, s, C**H**$_3$), 4.64 (2H, s, C**H**$_2$), 6.85 (2H, d, J = 9, **H**^{5}), 7.43 (2H, d, J = 9, **H**^{4}). ^{13}C NMR (101 MHz, $CDCl_3$) δ 52.5 (**C**^{9}), 65.3 (**C**^{7}), 76.3 (**C**^{1}), 83.4 (**C**^{2}), 114.7 (**C**^{5}), 115.6 (**C**^{3}), 133.8 (**C**^{4}), 158.2 (**C**^{6}), 169.1 (**C**O). MS (ES$^+$) *m/z* 191.9 [M + H]$^+$; $C_{11}H_{11}O_3$ requires 191.0708; found 191.0712.

Methyl 2-(4-((2-(ethoxy(methyl)phosphoryl)-6-(hydroxymethyl)pyridin-4-yl)ethynyl)phenoxy)acetate, 85[14]

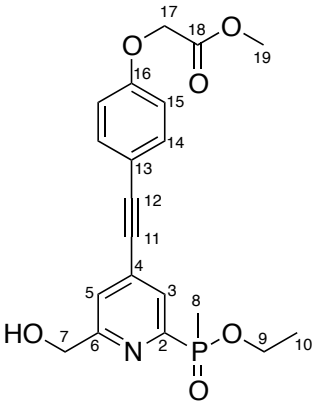

To a stirred degassed solution of ethyl (6-(hydroxymethyl)-4-(bromopyridin-2-yl)(methyl)phosphinate (90 mg, 0.307 mmol) in anhydrous THF (0.8 mL) was added methyl 2-(4-ethynylphenoxy)acetate (70 mg, 0.368 mmol) and

triethylamine (214 μL, 1.535 mmol), and the solution was degassed (freeze-thaw cycle) three times. [1,1-Bis(diphenylphosphino)ferrocene]dichloropalladium(II) (26 mg, 0.031 mmol) and CuI (6 mg, 0.031 mmol) were added and the resulting brown solution was stirred at 65 °C under argon for 18 h. The solvent was removed under reduced pressure and the brown residue was purified by column chromatography (DCM/MeOH, 100% to 97:3 using 0.5% increments; R_f = 0.15) to give a yellow oil (68 mg, 55%). ^{1}H NMR (600 MHz, $CDCl_3$) δ 1.26 (3H, t, J = 7, $OCH_2C\mathbf{H}_3$), 1.76 (3H, d, $^1J_{H\text{-}P}$ = 15, $PC\mathbf{H}_3$), 3.79 (3H, s, $C\mathbf{H}_3$), 3.85-3.87 (1H, m, $OC\mathbf{H}_2CH_3$), 3.99 (1H, br.s, O**H**), 4.07-4.09 (1H, m, $OC\mathbf{H}_2CH_3$), 4.65 (2H, s, $OC\mathbf{H}_2CO$), 4.80 (2H, s, $C\mathbf{H}_2OH$), 6.88 (2H, d, J = 9, $\mathbf{H}^{15}$), 7.45 (2H, d, J = 9, $\mathbf{H}^{14}$), 7.50 (1H, br.s, $\mathbf{H}^5$), 7.98 (1H, br.s, $\mathbf{H}^3$). ^{13}C NMR (151 MHz, $CDCl_3$) δ 13.5 (d, $^1J_{C\text{-}P}$ = 104, PCH_3), 16.5 (d, $^3J_{C\text{-}P}$ = 4, $OCH_2\mathbf{C}H_3$), 52.5 ($\mathbf{C}H_3$), 61.3 (d, $^2J_{C\text{-}P}$ = 5, $O\mathbf{C}H_2CH_3$), 64.3 ($\mathbf{C}H_2OH$), 65.2 ($O\mathbf{C}H_2CO$), 85.6 ($\mathbf{C}^{11}$), 95.7 ($\mathbf{C}^{12}$), 115.0 ($\mathbf{C}^{15}$), 115.1 ($\mathbf{C}^{13}$), 124.2 ($\mathbf{C}^5$), 128.1 (d, $^2J_{C\text{-}P}$ = 22, $\mathbf{C}^3$), 132.9 (d, $^3J_{C\text{-}P}$ =12, $\mathbf{C}^4$), 133.8 ($\mathbf{C}^{14}$), 153.3 (d, $^1J_{C\text{-}P}$ = 155, $\mathbf{C}^2$), 158.8 ($\mathbf{C}^{16}$), 161.0 (d, $^3J_{C\text{-}P}$ = 19, $\mathbf{C}^6$), 168.9 (**C**O). ^{31}P NMR (243 MHz, $CDCl_3$) δ 39.55. MS (ES^+) *m/z* 404.8 $[M + H]^+$; $C_{20}H_{23}NO_6P$ requires 404.1263; found 404.1265.

Methyl 2-(4-((2-(ethoxy(methyl)phosphoryl)-6-((methylsulfonyloxy)methyl)pyridin-4-yl)ethynyl)phenoxy)acetate, 86[14]

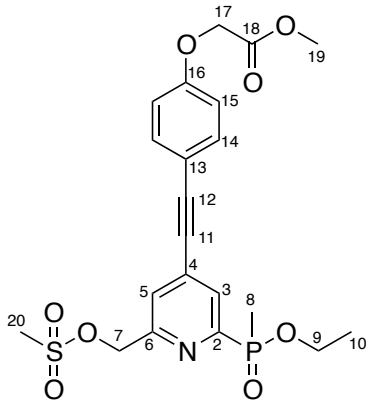

Methyl 2-(4-((2-(ethoxy(methyl)phosphoryl)-6-(hydroxymethyl)pyridin-4-yl)ethynyl)phenoxy)acetate (56 mg, 0.139 mmol) was dissolved in anhydrous THF (2 mL) and cooled to 5 °C. Triethylamine (39 μL, 0.278 mmol) and

methanesulfonyl chloride (16 μL, 0.208 mmol) were added and the mixture was stirred under argon for 90 min. The progress of the reaction was monitored by TLC [DCM/CH_3OH 95:5 v/v, $R_{f(product)}$ = 0.23, $R_{f(reactant)}$ = 0.11]. The solvent was removed under reduced pressure and the residue was dissolved in DCM (30 mL) and washed with saturated aqueous brine solution (30 mL). The aqueous layer was extracted with DCM (3 × 30 mL) and the combined organic layers were dried over $MgSO_4$, and concentrated under reduced pressure to give a yellow oil (66 mg, 100%.). ^{1}H NMR (400 MHz, $CDCl_3$) δ 1.26 (3H, t, J = 7, $OCH_2C\mathbf{H}_3$), 1.76 (3H, d, $^1J_{H\text{-}P}$ = 15, $PC\mathbf{H}_3$), 3.79 (3H, s, $C\mathbf{H}_3$), 3.85-3.87 (1H, m, $OC\mathbf{H}_2CH_3$), 4.07-4.09 (1H, m, $OC\mathbf{H}_2CH_3$), 4.65 (2H, s, $OC\mathbf{H}_2CO$), 5.33 (2H, s, $C\mathbf{H}_2OMs$), 6.88 (2H, d, J = 9, $\mathbf{H}^{15}$), 7.45 (2H, d, J = 9, $\mathbf{H}^{14}$), 7.62 (1H, br.s, $\mathbf{H}^5$), 8.07 (1H, br.s, $\mathbf{H}^3$). ^{31}P NMR (162 MHz, $CDCl_3$) δ 39.04. MS (ES^+) *m/z* 482.2 $[M + H]^+$.

Trimethyl-2,2',2''-(4,4',4''-(*S*,*S*)-6,6',6''-((*S*)-2-(4-(tert-butoxycarbonylamino)butyl)-1,4,7-triazacyclononane-1,4,7-triyl)tris(methylene)tris(2-(ethoxy(methyl)phosphoryl)pyridine-6,4-diyl)tris(ethyne-2,1-diyl)tris(benzene-4,1-diyl)tris(oxy))triacetate, 87[13]

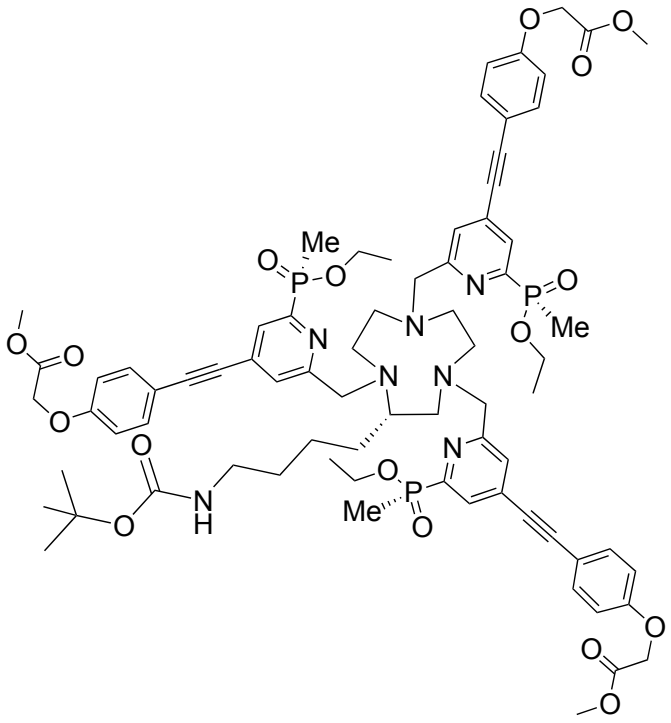

(*S*)-*tert*-Butyl 4-(1,4,7-triazonan-2-yl)butylcarbamate (14 mg, 0.047 mmol) and methyl 2-(4-((2-(ethoxy(methyl)phosphoryl)-6-

((methylsulfonyloxy)methyl)pyridin-4-yl)ethynyl)phenoxy)acetate (66 mg, 0.137 mmol), were dissolved in anhydrous CH_3CN (2 mL) and K_2CO_3 (20 mg, 0.142 mmol) was added. The resulting mixture was stirred under argon for 18 hours at 60 °C and the progress of the reaction monitored by ESI-MS. Upon completion, the reaction was cooled and the solution decanted from the potassium salts. The solvent was removed under reduced pressure and the crude residue purified by column chromatography (DCM/MeOH, 100% to 80:20 using 1% increments; R_f = 0.50) to give a yellow oil (20 mg, 30%). ^{1}H NMR (400 MHz, $CDCl_3$) δ 1.23-1.27 (9H, m, $OCH_2C\mathbf{H}_3$), 1.28-1.45 (6H, m, $C\mathbf{H}_2^{Lysine}$), 1.41 (9H, s, $C(C\mathbf{H}_3)_3$), 1.70-1.85 (9H, m, $PC\mathbf{H}_3$), 2.90-3.12 (13H, m, $C\mathbf{H}_2$ ring + $C\mathbf{H}_2^{Lysine}$), 3.82 (9H, s, $C\mathbf{H}_3$), 3.86-4.12 (12H, m, $OC\mathbf{H}_2CH_3$), 4.67 (6H, s, $OC\mathbf{H}_2CO$), 5.10 (1H, br.s, N**H**), 6.88-6.91 (6H, m, $\mathbf{H}^{14}$), 7.42-7.59 (9H, m, $\mathbf{H}^{11}$ + $\mathbf{H}^{13}$), 7.97-8.04 (3H, m, $\mathbf{H}^{12}$). ^{31}P NMR (162 MHz, $CDCl_3$) δ 39.16. MS (ES^+) *m/z* 1456.4 $[M + H]^+$; $C_{75}H_{93}N_7O_{17}P_3$ requires 1456.584; found 1456.579.

Eu(III) complex of (S)-6,6',6''-(2-(4-(tert-butoxycarbonylamino)butyl)-1,4,7-triazacyclononane-1,4,7-triyl)tris(methylene)tris(4-((4-(carboxymethoxy)phenyl)ethynyl)pyridine-6,2-diyl)tris(methylphosphinate), 88[13]

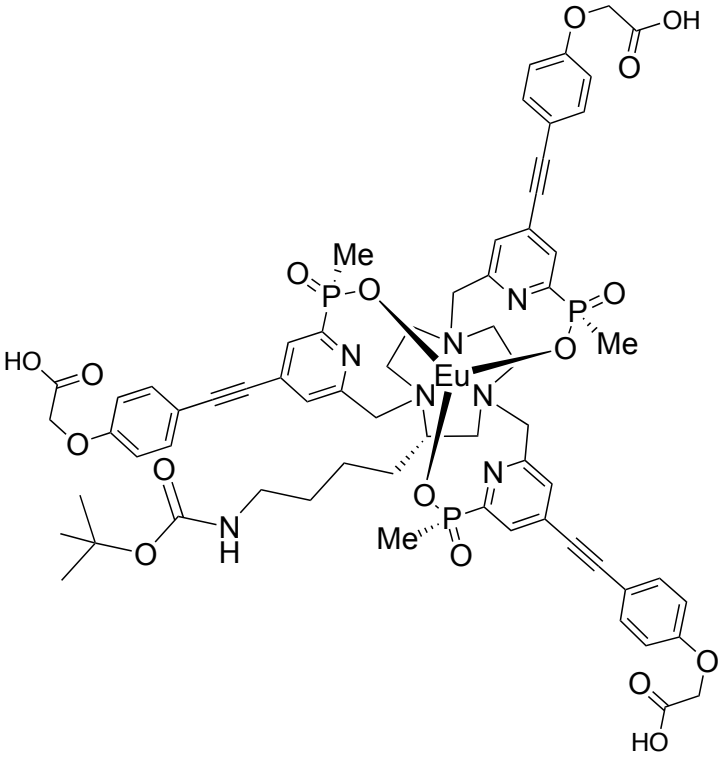

The phosphonate ethyl ester, ***87*** (20 mg, 0.014 mmol) was dissolved in CD_3OD (2 mL) to which KOH (9 mg, 0.137 mmol) was added as a solution in D_2O (1 mL). The mixture was heated to 60 °C and the progress of the reaction was monitored by ^1H and ^{31}P NMR spectroscopy [loss of C**H**$_2$C**H**$_3$ signals; $\delta P_{(product)}$ = 26.35, $\delta P_{(reactant)}$ = 39.16]. After 5 hours, the solution was cooled to room temperature and the pH adjusted to 7 by the addition of HCl (1M). $Eu(OAc)_3.H_2O$ (4.9 mg, 0.015 mmol) was added and the mixture was heated under argon, to 60 °C, overnight. After this time, the solvent was removed under reduced pressure and the product was purified by preparative RP-HPLC to give a white solid (14 mg, 69%). MS (ES^+) *m/z* 741.3 $[M + 2H]^{2+}$. RP-HPLC: t_R = 11.8 mins [2-30% MeOH in H_2O over 10 mins].

Eu(III) complex of (S)-6,6',6''-(2-(4-(tert-butoxycarbonylamino)butyl)-1,4,7-triazacyclononane-1,4,7-triyl)tris(methylene)tris(4-((4-(2-oxo-2-(3-sulfopropylamino)ethoxy)phenyl)ethynyl)pyridine-6,2-diyl)tris(methylphosphinate), 89[13]

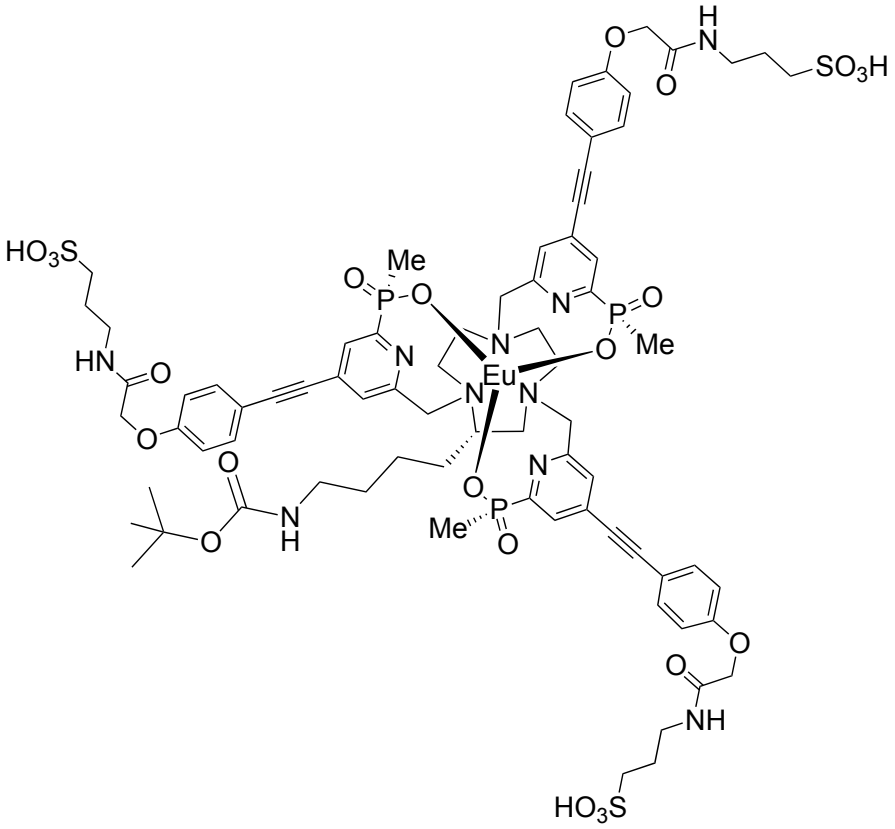

The Eu-complex, ***88*** (14 mg, 0.010 mmol) and 3-amino-1-propanesulfonic acid (8.1 mg, 0.058 mmol) were dissolved in DMSO (2 mL). HATU (10 mg, 0.029 mmol) and diisopropylethylamine (18 μL, 0.097 mmol) were added and the reaction mixture stirred under argon at room temperature and the progress of the reaction was monitored by analytical RP-HPLC. Upon completion after 3 hours, the product was purified by preparative RP-HPLC to give a white solid (13 mg, 73%). MS (ES^+) *m/z* 1844.8 $[M + H]^+$; $C_{75}H_{94}EuN_{10}O_{23}P_3S_3$ requires 1844.408; found 1844.400. RP-HPLC: t_R = 14.8 mins [2-40% MeCN in Triethylammonium Acetate Buffer (25 mM) over 20 mins].

4-((8,9-Dioxo-2-(2-phosphonoethyl)-2,6-diazabicyclo[5.2.0]non-1(7)-en-4-yl)amino)-4-oxobutanoic acid, 90

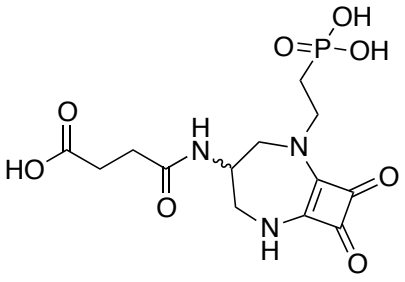

To a solution of diethyl (2-(4-amino-8,9-dioxo-2,6-diazabicyclo[5.2.0]non-1(7)-en-2-yl)ethyl)phosphonate (29 mg, 0.088 mmol) in anhydrous DMF (1.5 mL) was added succinic anhydride (8.5 mg, 0.088 mmol) and diisopropylethylamine (31 μL, 0.178 mmol) and the reaction stirred under argon at room temperature for 1 hour. After this period, bromotrimethylsilane (93 μL, 0.704 mmol) was added and the reaction heated to 60 °C for a further 3 hours. Upon complete removal of the phosphonate ethyl esters, as verified by ESI-MS, the solvent was removed under reduced pressure and the crude residue purified by preparative RP-HPLC to give a white solid (19 mg, 58%). ^{1}H NMR (400 MHz, D_2O) δ 1.88-2.08 (2H, m, PC**H**$_2$CH$_2$), 2.54-2.58 (2H, m, C**H**$_2$CH$_2$CO$_2$H), 2.61-2.65 (1H, m, **H**^{c} (axial)), 3.56 (1H, d, J = 14, **H**$^{c/a}$ (eq)), 3.66-3.74 (4H, m, **H**$^{c/a}$ (eq) + **H**^{a} (axial) + CH$_2$C**H**$_2$CO$_2$H), 3.83-3.98 (2H, m, PCH$_2$C**H**$_2$), 4.34-4.40 (1H, m, C**H**). ^{31}P NMR (162 MHz, D_2O) δ 19.28. MS (ES$^+$) *m/z* 376.1 [M+H]$^+$; $C_{13}H_{19}N_3O_8P$ requires 376.0910; found 376.0909.

[Eu.L^{13}]

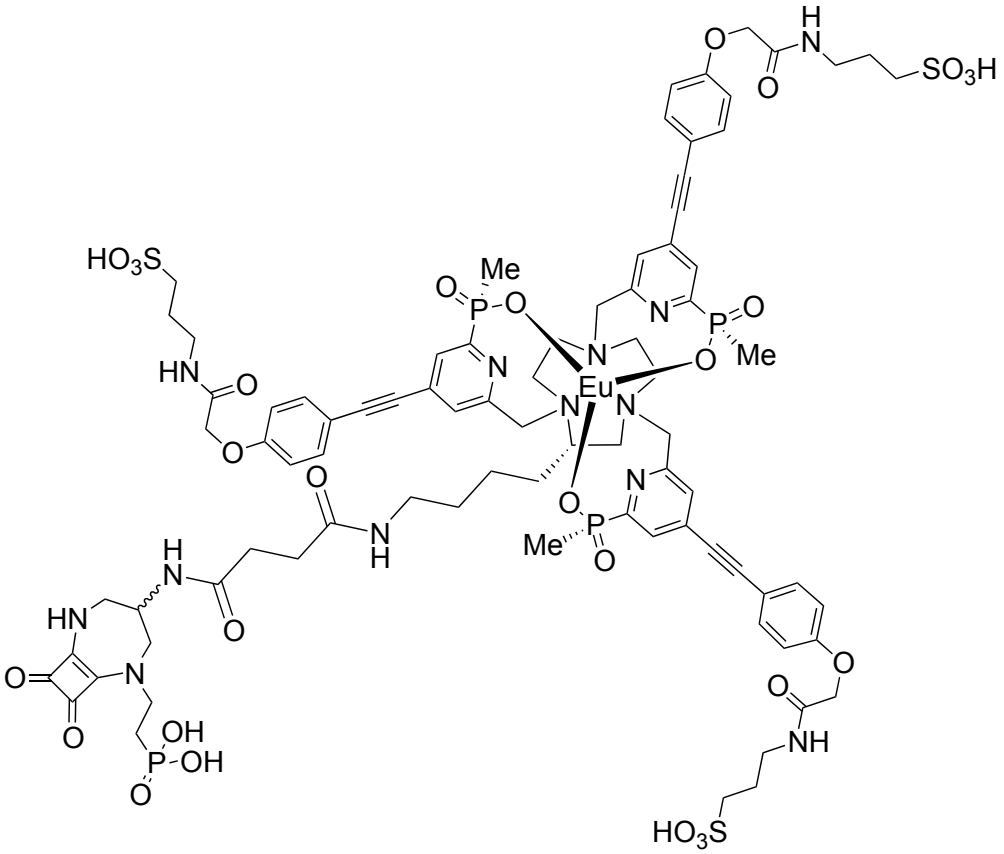

The *N*-Boc-protected Eu-complex, ***89*** (13 mg, 0.007 mmol) was suspended in anhydrous DCM (0.8 mL) and TFA (0.2 mL) was added at 5 °C. The resulting solution was stirred under argon for 20 minutes before the solvents were removed on a high vacuum line. The crude residue was repeatedly re-dissolved in DCM (3 x 2 mL) to remove excess TFA. This process yielded the TFA salt of the Eu-amine complex. The TFA salt of the Eu-amine complex (6.2 mg, 0.004 mmol) was added as a solution in DMSO (0.5 mL) to a pre-stirred solution of 4-((8,9-Dioxo-2-(2-phosphonoethyl)-2,6-diazabicyclo[5.2.0]non-1(7)-en-4-yl)amino)-4-oxobutanoic acid (2 mg, 0.005 mmol), HATU (2 mg, 0.005 mmol) and diisopropylethylamine (2 μL, 0.009 mmol) in anhydrous DMF (0.5 mL). The resulting solution was stirred at room temperature for 24 hours, at which point it was diluted with H_2O and purified by preparative RP-HPLC to give a white solid (4.2 mg, 50%). MS (ES$^+$) *m/z* 1049.7 $[M + 2H]^{2-}$; $[C_{83}H_{100}N_{13}O_{28}P_4S_3Eu]^{2-}$ requires 1049.706; found 1049.707. RP-HPLC: t_R = 14.8 mins [2-40% MeCN in Triethylammonium Acetate Buffer (25 mM) over 20 mins].

[Eu.L^{14}]

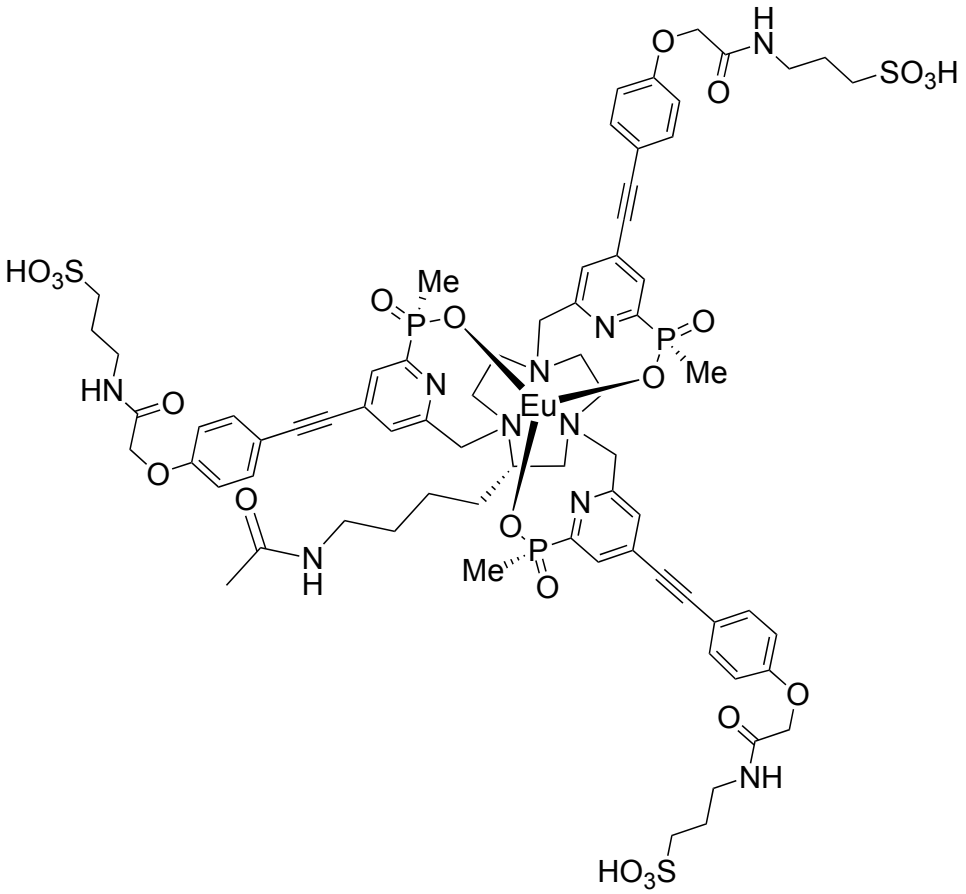

The TFA salt of the Eu-amine complex (2 mg, 0.001 mmol) was added as a solution in DMSO (0.3 mL) to a pre-stirred solution of acetic acid *N*-hydroxy succinimide ester (0.2 mg, 0.001 mmol), and diisopropylethylamine (2 μL, 0.009 mmol) in anhydrous DMF (0.4 mL). The resulting solution was stirred at room temperature for 24 hours, at which point it was diluted with H_2O and purified by preparative RP-HPLC to give a white solid (0.6 mg, 34%). MS (ES$^+$) *m/z* 892.6 [M + H]$^{2-}$; [$C_{72}H_{87}N_{10}O_{22}P_3S_3Eu$]$^{2-}$ requires 892.6792; found 892.6797. RP-HPLC: t_R = 14.7 mins [2-40% MeCN in triethylammonium acetate buffer (25 mM) over 20 mins].

Potassium-2,3,3-trimethyl-3*H*-indole-5-sulfonate, 91[15]

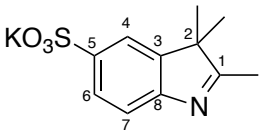

Hydrazinobenzene sulfonic acid (15.0 g, 79.5 mmol) and 3-methyl-2-butanone (25.2 mL, 240 mmol) were dissolved in acetic acid (45 mL) and the mixture heated to reflux for 3 h. After this time, the acetic acid was removed under reduced pressure and the crude residue obtained dissolved in MeOH. This was stirred with a saturated solution of potassium hydroxide in propan-2-ol. The alkaline solution turned yellow and the potassium salt of the sulfoindole precipitated as a pale yellow solid (16.5 g, 75%). ^{1}H NMR (400 MHz, DMSO-d_6) δ 1.24 (6H, s, (C**H**$_3$)$_2$), 2.21 (3H, s, C**H**$_3$), 7.33 (1H, d, J = 8, **H**^{7}), 7.54 (1H, dd, J = 8, 2, **H**^{6}), 7.62 (1H, d, J = 2, H^4). ^{13}C NMR (101 MHz, DMSO-d_6) δ 15.2, 22.51 (**C**H$_3$), 53.2 (**C**(CH$_3$)$_2$), 118.1, 119.2, 125.1, 145.1, 145.2, 153.6 (Ar-**C**), 188.8 (**C**=N). MS (ES$^+$) *m/z* 240.5 [M+H]$^+$; $C_{11}H_{14}NO_3S$ requires 240.0694; found 240.0696. M.Pt > 250 °C.

Potassium 2,3,3-trimethyl-1-(4-sulfonatobutyl)-3*H*-indol-1-ium-5-sulfonate, 92[16]

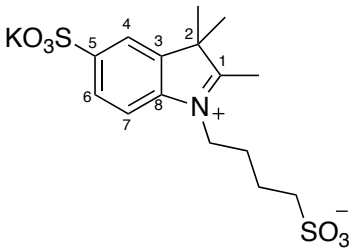

Potassium-2,3,3-trimethyl-3*H*-indole-5-sulfonate (1.68 g, 7.0 mmol) and 1,4-butanesultone were stirred as a solution in toluene (12 mL) under an atmosphere of argon at 100 °C for 12 hours. After this period, the solvent was decanted and the residue triturated with cold propan-2-ol to yield a pink powder (1.73 g, 66%). ^{1}H NMR (400 MHz, D$_2$O) δ 1.62 (6H, s, (C**H**$_3$)$_2$), 1.92 (2H, quin, J = 7, NCH$_2$C**H**$_2$) 2.13 (2H, quin, J = 7, C**H**$_2$CH$_2$SO$_3$), 2.99 (2H, t, J = 7, NC**H**$_2$CH$_2$), 4.56,

(2H, t, J = 7, $CH_2C\mathbf{H}_2SO_3$), 7.93 (1H, d, J = 8, **H**[7]), 8.05 (1H, dd, J = 8, 2, **H**[6]), 8.14 (1H, d, J = 2, H[4]). ^{13}C NMR (101 MHz, D_2O) δ 21.4, 21.5 (**C**H_3), 25.8 ($NCH_2\mathbf{C}H_2$), 47.8 (**C**$H_2CH_2SO_3$), 50.0 ($N\mathbf{C}H_2CH_2$), 55.0 ($CH_2\mathbf{C}H_2SO_3$), 115.9, 120.9, 126.9, 142.6, 142.8, 144.1 (Ar-**C**), 199.3 (**C**=N). MS (ES^+) *m/z* 376.2 $[M+H]^+$; $C_{15}H_{22}NO_6S_2$ requires 376.0889; found 376.0884. M.Pt > 250 °C.

(*E*)-2-Chloro-3-(hydroxymethylene)cyclohex-1-enecarbaldehyde, 93[17]

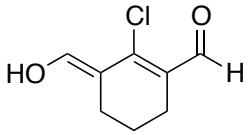

Anhydrous DMF (8 mL, 103 mmol) in anhydrous DCM (8 mL) were cooled in an ice bath to 0 °C and a solution of $POCl_3$ (7.4 mL, 79.1 mmol) in anhydrous DCM (7 mL) was added dropwise with stirring. Cyclohexanone (2.0 g, 21.5 mmol) was then added and the resulting solution heated 80 °C for 3 hours. After this time, the reaction mixture was cooled to room temperature before being poured onto ice and left overnight. The solution was decanted and the resulting yellow crystals dried under vacuum for several hours (1.58 g, 43%). ^{1}H NMR (400 MHz, $CDCl_3$) δ 1.71 (2H, quin, J = 6, $CH_2C\mathbf{H}_2CH_2$), 2.46 (4H, t, J = 6, $C\mathbf{H}_2CH_2C\mathbf{H}_2$), 4.30-4.88 (1H, br. s, C**H**OH), 8.89 (2H, br. s, O**H** and CO**H**). ^{13}C NMR (101 MHz, $CDCl_3$) δ 18.7($CH_2\mathbf{C}H_2CH_2$), 20.4, 23.8 (**C**$H_2CH_2\mathbf{C}H_2$), 24.0 (**C**), 56.9 (**C**), 136.6 (**C**Cl), 190.6 (**C**OH), 197.4 (**C**O). MS (ES^+) *m/z* 173.3 $[M+H]^+$; $C_8H_{10}ClO_2$ requires 173.0369; found 173.0374. M. Pt. 129-131 °C.

4-(2-((*E*)-2-((*E*)-2-Chloro-3-((*E*)-2-(3,3-dimethyl-5-sulfo-1-(4-sulfobutyl)indolin-2-ylidene)ethylidene)cyclohex-1-en-1-yl)vinyl)-3,3-dimethyl-5-sulfo-3*H*-indol-1-ium-1-yl)butane-1-sulfonate, 94[18]

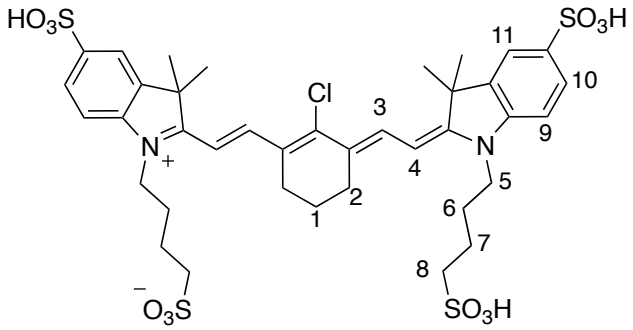

Potassium 2,3,3-trimethyl-1-(4-sulfonatobutyl)-3*H*-indol-1-ium-5-sulfonate (40 mg, 0.11 mmol) and (*E*)-2-chloro-3-(hydroxymethylene)cyclohex-1-enecarbaldehyde (9.2 mg, 0.05 mmol) were dissolved in a mixture of anhydrous butan-1-ol (2.8 mL) and anhydrous benzene (1.2 mL) and heated to 110 °C overnight. After this period, the solvents were removed under reduced pressure and the residue washed with diethyl ether (3 x 5 mL). This gave a green powder, which was dried for several hours and used directly in the next step without further purification (47 mg, 100%). ^{1}H NMR (400 MHz, D_2O) δ 1.61 (12H, s, C**H**$_3$), 1.76-1.97 (10H, m, **H**^{1}, **H**^{6}, **H**^{7}), 2.05-2.18 (4H, m, **H**^{2}), 2.98 (4H, t, J = 7, **H**^{5}), 4.54 (4H, t, J = 7, **H**^{8}), 6.83 (2H, d, **H**^{4}), 7.51-7.61 (2H, m, **H**^{3}), 7.92 (2H, d, J = 8, **H**^{9}), 8.03 (2H, d, J = 8, **H**^{10}), 8.12 (2H, s, **H**^{11}). MS (ES$^-$) *m/z* 885.2 [M-H]$^-$; $C_{38}H_{46}N_2ClO_{12}S_4$ requires 885.1622; found 885.1634. (HPLC) t_R = 13.05 min; λ_{max} (H_2O) 784 nm.

4-(2-((*E*)-2-((*E*)-2-(4-carboxyphenoxy)-3-((*E*)-2-(3,3-dimethyl-5-sulfo-1-(4-sulfobutyl)indolin-2-ylidene)ethylidene)cyclohex-1-en-1-yl)vinyl)-3,3-dimethyl-5-sulfo-3*H*-indol-1-ium-1-yl)butane-1-sulfonate, 95

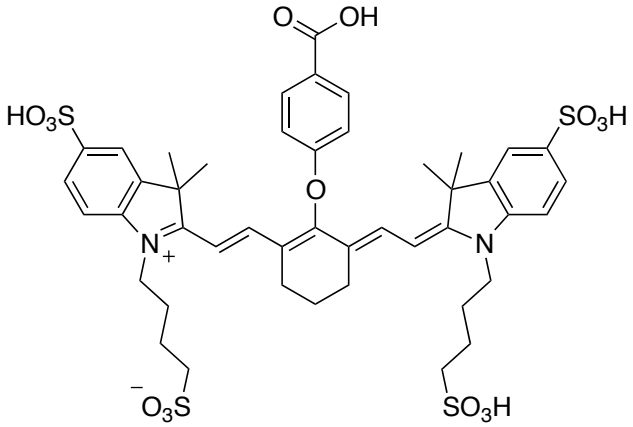

4-hydroxybenzoic acid (15 mg, 0.106 mmol) and NaH (5.1 mg, 0.212 mmol) were stirred as a solution in anhydrous DMF (700 μL) at 0 °C for 15 mins. 4-(2-((*E*)-2-((*E*)-2-chloro-3-((*E*)-2-(3,3-dimethyl-5-sulfo-1-(4-sulfobutyl)indolin-2-ylidene)ethylidene)cyclohex-1-en-1-yl)vinyl)-3,3-dimethyl-5-sulfo-3*H*-indol-1-ium-1-yl)butane-1-sulfonate (47 mg, 0.053 mmol) was added dropwise as a solution in anhydrous DMF (1 mL) and the resulting mixture heated to 70 °C. The progress of the reaction was monitored by analytical RP-HPLC until complete conversion of the starting material was obtained [note: may take several additions of 4-hydroxybenzoic acid and NaH]. Upon completion of the reaction, the solvent was removed under reduced pressure and the crude product purified by preparative RP-HPLC to give a green powder (15 mg, 29%). MS (ES^-) *m/z* 987.1 $[M-H]^-$; $C_{45}H_{51}N_2O_{15}S_4$ requires 987.2172; found 987.2167. λ_{max} (H_2O) 772 nm. RP-HPLC: t_R = 12.5 mins [2-40% MeCN in triethylammonium acetate buffer (25 mM) over 20 mins].

1-(4-(Benzyloxy)phenyl)-2-bromopropan-1-one, 96[19]

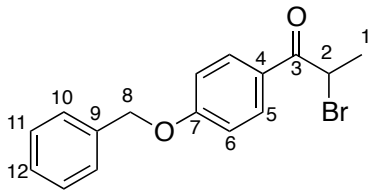

Bromine (512 μL, 10.00 mmol) was added to a solution of 1-(4-(benzyloxy)phenyl)propan-1-one (2.40 g, 10.00 mmol) in diethyl ether (25 mL). The mixture was stirred at room temperature for 30 minutes when a colour change from red to yellow was observed. At this point, the reaction was quenched by the addition of H_2O (10 mL) and the mixture was diluted with Et_2O (25 mL). The organic layer was separated and washed with saturated $NaHCO_3$ solution (30 mL), saturated $Na_2S_2O_3$ (30 mL) and saturated brine (30 mL), before drying over $MgSO_4$. Filtration and evaporation of the solvent gave the crude product, which was purified by column chromatography (DCM/Hexane, 50:50; R_f = 0.33) to give an orange solid (2.61 g, 82%). ^{1}H NMR (400 MHz, $CDCl_3$) δ 1.89 (3H, d, J = 7, C**H**$_3$), 5.15 (2H, s, OC**H**$_2$Ph), 5.26 (2H, q, J = 7, C**H**Br), 7.03 (2H, d, J = 9, H^5), 7.33-7.46 (5H, m, Ar-**H**), 8.02 (2H, d, J = 9, H^6). ^{13}C NMR (101 MHz, $CDCl_3$) δ 20.4, (**C**H$_3$) 41.6 (**C**HBr), 70.4 (O**C**H$_2$Ph), 114.9 (**C**^{6}), 127.2 (**C**^{10}), 127.6 (**C**^{12}), 128.4 (**C**^{11}), 128.8 (**C**^{5}), 131.5 (**C**^{4}), 136.1 (**C**^{9}), 163.2 (**C**^{7}), 192.1 (**C**O). MS (ES$^+$) *m/z* 319.1 [M+H]$^+$; $C_{16}H_{16}{}^{79}BrO_2$ requires 319.0337; found 319.0336. M. Pt. 76-78 °C.

1-(4-(Benzyloxy)phenyl)-2-(4-benzylpiperidin-1-yl)propan-1-one, 97[20]

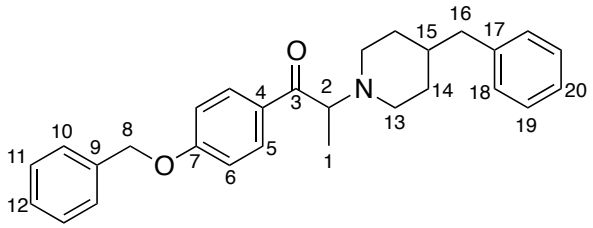

4'-(benzyloxy)-2-bromopropiophenone (2.52 g, 7.91 mmol) and 4-benzyl piperidine (2.78 mL, 15.82 mmol) were stirred as a solution in anhydrous ethanol (11 mL) at 78 °C overnight. Upon no further reaction as observed by TLC, the reaction was concentrated and the white solid that remained triturated with Et_2O. The solid was filtered and the filtrate concentrated and purified by column chromatography (hexane/EtOAc, 50:50; R_f = 0.53) to give a yellow liquid (2.78 g, 84%). ^{1}H NMR (400 MHz, $CDCl_3$) δ 1.27 (3H, d, J = 7, C**H**$_3$), 1.28-1.31 (2H, m, **H**^{14}), 1.45-1.55 (1H, m, **H**^{15}), 1.56-1.68 (2H, m, **H**$^{14'}$), 2.07-2.16 (1H, m, **H**^{13}), 2.34-2.43 (1H, m, **H**^{13}), 2.52 (2H, d, J = 7, C**H**$_2$Ph), 2.78-2.86 (1H, m, **H**^{13}), 2.91-2.98 (1H, m, **H**^{13}), 4.07 (1H, q, J = 7, C**H**CH_3), 5.15 (2H, s, OC**H**$_2$Ph), 7.01 (2H, d, J = 9, H^5), 7.11-7.48 (10H, m, Ar-**H**), 8.13 (2H, d, J = 9, H^6). ^{13}C NMR (101 MHz, $CDCl_3$) δ 11.9 (**C**H_3), 32.5, 32.9 (**C**^{14}), 38.1 (**C**^{15}), 43.3 (C^{16}), 48.8, 51.8 (**C**^{13}), 64.9 (O**C**H_2Ph), 70.2 (**C**HCH_3), 114.4 (**C**^{6}), 125.8 (**C**^{20}), 127.6 (**C**^{10}), 128.2 (**C**^{12}), 128.3 (**C**^{18}), 128.8 (**C**^{19}), 129.2 (**C**^{11}), 129.7 (**C**^{5}), 131.4 (**C**^{4}), 136.4 (**C**^{9}), 140.8 (**C**^{17}), 162.5 (**C**^{7}), 199.6 (**C**O). MS (ES$^+$) *m/z* 414.5 $[M+H]^+$; $C_{28}H_{32}NO_2$ requires 414.2433; found 414.2440.

(1*R*,2*R*)-1-(4-(Benzyloxy)phenyl)-2-(4-benzylpiperidin-1-yl)propan-1-ol, 98[20]

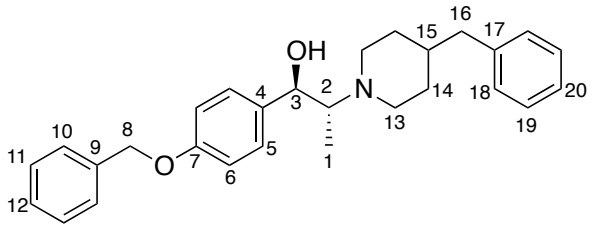

A suspension of $LiAlH_4$ (241 mg, 6.34 mmol) in anhydrous THF (10 mL) was treated with a solution of 1-(4-(Benzyloxy)phenyl)-2-(4-benzylpiperidin-1-yl)propan-1-one (1.31 g, 3.17 mmol) in anhydrous THF (10 mL) at 0 °C over a 10 minute period. The resulting mixture was stirred for a further 2 hours and the reaction progress monitored by ESI-MS. Upon complete reduction, the reaction was quenched by the addition of H_2O (300 μL), NaOH (300 μL, 1M) and finally H_2O (300 μL). The lithium salts were filtered and the solvent reduced to give a white solid (1.00 g, 76%). ^{1}H NMR (400 MHz, $CDCl_3$) δ 0.77 (3H, d, J = 7, C**H**$_3$), 1.26-1.53 (2H, m, **H**^{14}), 1.54-1.64 (1H, m, **H**^{15}), 1.70-1.80 (2H, m, **H**^{14}), 2.09-2.19 (1H, m, **H**^{13}), 2.50-2.65 (2H, m, **H**^{2} + **H**^{13}), 2.61 (2H, d, J = 7, C**H**$_2$Ph), 2.68-2.77 (1H, m, **H**^{13}), 2.84-2.92 (1H, m, **H**^{13}), 4.28 (1H, d, J = 10, **H**^{3}), 5.09 (2H, s, OC**H**$_2$Ph), 5.20-5.47 (1H, br. s, O**H**), 6.98 (2H, d, J = 9, H^5), 7.17-7.49 (12H, m, Ar-**H**). ^{13}C NMR (101 MHz, $CDCl_3$) δ 8.1 (**C**H$_3$), 32.6, 33.1 (**C**^{14}), 38.4 (**C**^{15}), 43.3 (**C**H$_2$Ph), 44.5, 53.0 (**C**^{13}), 66.8 (O**C**H$_2$Ph), 70.2 (**C**HCH$_3$), 73.9 (**C**HOH), 114.8 (**C**^{6}), 126.0 (**C**^{20}), 127.6 (**C**^{10}), 128.0 (**C**^{12}), 128.3 (**C**^{5}), 128.6 (**C**^{18}), 128.7 (**C**^{19}), 129.2 (**C**^{11}), 134.6 (**C**^{4}), 137.2 (**C**^{9}), 140.7 (**C**^{17}), 158.5 (**C**^{7}). MS (ES$^+$) *m/z* 416.2 [M+H]$^+$; $C_{28}H_{34}NO_2$ requires 416.2590; found 416.2589. M. Pt. 117-119 °C.

tert-Butyl (6-(((1*R*,2*R*)-1-(4-(benzyloxy)phenyl)-2-(4-benzylpiperidin-1-yl)propyl)amino)hexyl)carbamate, 99[21]

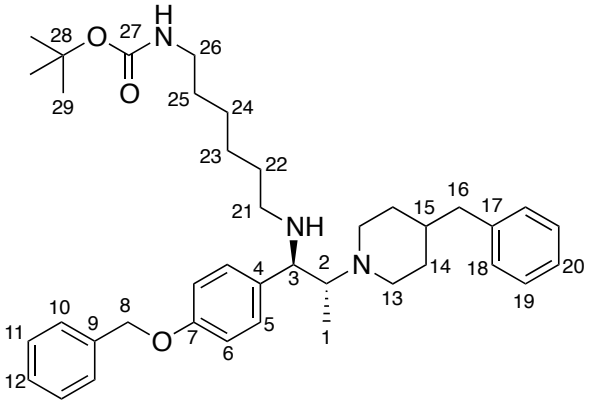

To a stirred solution of *O*-benzylated (*threo*)-ifenprodil (247 mg, 0.595 mmol) in anhydrous THF (7 mL) at 0 °C, was added triethylamine (249 μL, 1.79 mmol) and methansulfonyl chloride (116 μL, 1.50 mmol). The resulting mixture was stirred for 30 mins until complete reaction was confirmed by TLC. To the mesylate was added triethylamine (166 μL, 1.19 mmol) and *N*-Boc-1,6-hexyldiamine (322 mg, 1.49 mmol) and the resulting mixture stirred at room temperature for 24 hours. Upon completion of the reaction as verified by ESI-MS, the reaction mixture was partitioned between DCM (30 mL) and H_2O (30 mL). The layers were separated and the aqueous extracted with DCM (3 x 30 mL). The combined organic portions were washed with sat. $NaHCO_3$ (50 mL) and brine (50 mL), before being dried over $MgSO_4$ and filtered. The solvent was concentrated under reduced pressure and the crude residue purified by column chromatography (DCM/MeOH, 100 to 95:5; R_f = 0.31) to give a white solid (231 mg, 63%). ^{1}H NMR (700 MHz, $CDCl_3$) δ 0.61 (3H, d, J = 7, C**H**$_3$), 1.13-1.33 (4H, m, **H**^{14} + **H**^{24}), 1.37-1.56 (6H, m, **H**^{14} + **H**^{25} + **H**^{23}), 1.44 (9H, s, C(C**H**$_3$)$_3$), 1.48-1.57 (1H, m, **H**^{15}), 1.63-1.73 (2H, m, **H**^{22}), 2.04-2.35 (2H, m, **H**^{21}), 2.39-2.47 (2H, m, **H**^{13}), 2.55 (2H, d, J = 7, C**H**$_2$Ph), 2.66-2.78 (2H, m, **H**^{13}), 3.07-3.12 (2H, m, **H**^{26}), 3.32 (1H, d, J = 9, **H**^{3}), 4.50 (1H, br.m, **H**^{2}), 5.04 (2H, s, OC**H**$_2$Ph), 6.93 (2H, d, J = 9, **H**^{6}), 7.15 (2H, d, J = 9, **H**^{5}), 7.19 (1H, dd, J = 8, 5, **H**^{20}), 7.23-7.30 (4H, m, **H**^{18} +**H**^{19}), 7.32 (1H, dd, J = 8, 5, **H**^{12}), 7.38 (2H, t, J = 8, **H**^{11}), 7.44 (2H, d, J = 8, **H**^{10}). ^{13}C NMR (176 MHz, $CDCl_3$) δ 9.0 (**C**H$_3$), 26.8 (**C**^{24}), 27.1 (**C**^{25}), 27.2 (**C**^{23}), 28.6 (C(**C**H$_3$)$_3$), 30.2 (**C**^{22}), 33.1, 33.2 (**C**^{14}),

38.6 (**C**^{15}), 40.7(**C**^{26}), 43.5 (**C**H_2Ph), 44.5, 47.1 (**C**^{13}), 52.9(**C**^{21}), 63.8 (**C**HCH_3), 65.7 (**C**HNH), 70.2 (O**C**H_2Ph), 79.2 (**C**$(CH_3)_3$), 114.7 (**C**^{6}), 125.9 (**C**^{20}), 127.7 (**C**^{10}), 128.1 (**C**^{12}), 128.3 (**C**^{5}), 128.7 (**C**^{18}), 129.2 (**C**^{19}), 129.6 (**C**^{11}), 133.9 (**C**^{4}), 137.3 (**C**^{9}), 140.9 (**C**^{17}), 156.1 (**C**O), 158.2 (**C**^{7}). MS (ES$^+$) *m/z* 614.0 $[M+H]^+$; $C_{39}H_{56}N_3O_3$ requires 614.4322; found 614.4327. M. Pt. 97-99 °C.

N^1-((1*R*,2*R*)-1-(4-(Benzyloxy)phenyl)-2-(4-benzylpiperidin-1-yl)propyl)hexane-1,6-diamine, 100^{21}

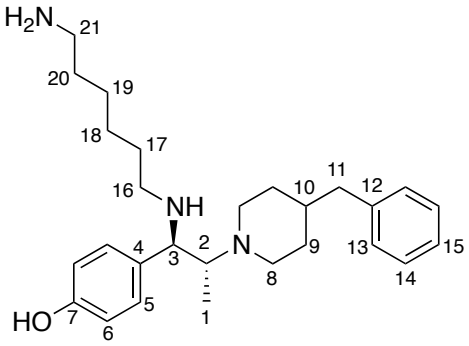

To a solution of *tert*-butyl (6-(((1*R*,2*R*)-1-(4-(benzyloxy)phenyl)-2-(4-benzylpiperidin-1-yl)propyl)amino)hexyl)carbamate (109 mg, 0.180 mmol) in acetic acid (3.3 mL), was added HBr (47% in H_2O, 0.3 mL) and the solution heated to 100 °C overnight. After cooling to room temperature, aqueous NaOH (3M) was added until pH 12. The aqueous layer was extracted with $CHCl_3$ (3 x 20 mL) and the organic dried over $MgSO_4$, filtered and concentrated. The crude residue was then purified by column chromatography (DCM/MeOH, 100 to 85:15; R_f = 0.12) to give a pale yellow solid (24 mg, 32%). ^{1}H NMR (400 MHz, $CDCl_3$) δ 0.59 (3H, d, J = 7, C**H**$_3$), 1.22-1.70 (13H, m, **H**^{9} + **H**^{10} + **H**^{17} + **H**^{18} + **H**^{19} + **H**^{20}), 2.05 (1H, m, **H**^{8}), 2.29-2.48 (3H, m, **H**^{8}), 2.56 (2H, d, J = 7, C**H**$_2$Ph), 2.63-2.75 (5H, m, **H**^{2} + **H**^{16} + **H**^{21}), 3.28 (1H, d, J = 10, **H**^{3}), 3.52-3.89 (4H, m, N**H**$_2$ + N**H** + O**H**), 6.71 (2H, d, J = 9, **H**^{6}), 7.09-7.13 (2H, m, **H**^{5}), 7.14-7.22 (3H, m, **H**^{13} + **H**^{15}), 7.25-7.29 (2H, m, **H**^{14}). ^{13}C NMR (101 MHz, $CDCl_3$) δ 8.9 (**C**H_3), 26.7 (**C**^{18}), 27.2 (**C**^{19}), 29.5 (**C**^{17}), 33.1 (**C**^{20}), 33.3, 33.4 (**C**^{9}), 38.6 (**C**^{10}), 42.0 (**C**^{21}), 43.5 (**C**H_2Ph), 44.4, 47.3 (**C**^{8}), 52.9 (**C**^{16}), 64.1 (**C**HCH_3), 65.7 (**C**HNH), 115.7 (**C**^{6}), 125.9 (**C**^{15}), 128.3 (**C**^{13}), 129.2 (**C**^{5}), 129.6 (**C**^{14}), 132.4 (**C**^{4}), 141.0 (**C**^{12}), 156.6 (**C**^{7}). MS (ES$^+$)

m/z 424.1 $[M+H]^+$; $C_{27}H_{42}N_3O$ requires 424.3328; found 424.3330. M. Pt. 56-58 °C.

tert-Butyl (6-((2-(2-(diethoxyphosphoryl)ethyl)-8,9-dioxo-2,6-diazabicyclo[5.2.0]non-1(7)-en-4-yl)amino)-6-oxohexyl)carbamate, 101

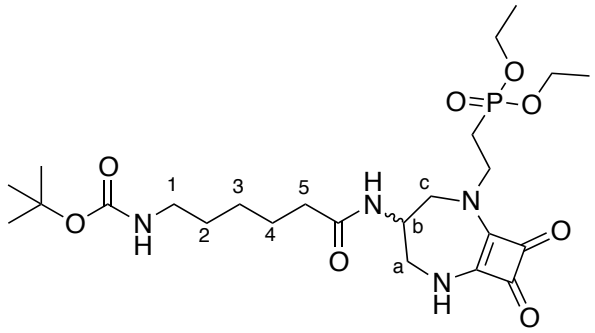

N-Boc-6-aminohexanoic acid (52 mg, 0.22 mmol), EDC (51 mg, 0.264 mmol) and HOBt (36 mg, 0.264 mmol) were dissolved in anhydrous DMF (2 mL) and stirred at room temperature under an atmosphere of argon for 20 minutes. After this period, a pre-stirred solution of diethyl (2-(4-amino-8,9-dioxo-2,6-diazabicyclo[5.2.0]non-1(7)-en-2-yl)ethyl)phosphonate (74 mg, 0.22 mmol) and NMM (48 μL, 0.44 mmol) in anhydrous DMF (1.5 mL) was added drop wise and the resulting solution stirred at room temperature until complete consumption of the starting materials by ESI-MS. After this period, the solvent was removed under reduced pressure and the crude oil taken up into EtOAc (15 mL). $NaHCO_3$ (15 mL) was added, the layers separated and the aqueous fraction washed with EtOAc (3 x 20 mL). The combined organic portions were dried over $MgSO_4$, filtered and the solvent removed under reduced pressure. The crude residue was purified by column chromatography (DCM/MeOH, 100% to 90:10 in 1% increments; R_f =0.25) to give a yellow oil (52 mg, 43%). ^{1}H NMR (700 MHz, $CDCl_3$) δ 1.23-1.29 (2H, m, **H**^{3}), 1.31 (6H, 2 x t, J = 7, $P(OCH_2C\mathbf{H}_3)_2$), 1.40 (9H, s, $C(C\mathbf{H}_3)_3$), 1.42-1.44 (2H, m, **H**^{4}), 1.56-1.63 (2H, m, **H**^{2}), 2.09-2.24 (2H, m, $PC\mathbf{H}_2CH_2$), 2.25-2.34 (2H, m, **H**^{5}), 3.00-3.14 (2H, m, **H**^{1}), 3.20-3.38 (1H, m, **H**^{c}(axial)), 3.51 (1H, d, J = 14, **H**$^{c/a}$(eq)), 3-60-3.73 (2H, m, $PCH_2C\mathbf{H}_2$), 3.87-3.95 (1H, br. m, **H**$^{c/a}$(eq)), 4.02-4.13 (4H, qd, $^3J_{H\text{-}H}$ = 7, $^3J_{H\text{-}P}$ = 3, $P(OC\mathbf{H}_2CH_3)_2$), 4.23-4.39 (2H, m, **H**^{a}(axial) + N**H**), 4.82-4.87 (1H, br. m, **H**^{b}), 7.58 (1H, br. N**H**), 8.01

(1H, br. N**H**). ^{13}C NMR (176 MHz, $CDCl_3$) δ 16.5 (2 x d, ^{3}J = 6, P(OCH$_2$**C**H$_3$)$_2$), 24.7 (d, 1J = 140, P**C**H$_2$CH$_2$), 25.4 (**C**^{3}), 26.4 (**C**^{4}), 28.6 (C(**C**H$_3$)$_3$), 29.8 (**C**^{2}), 35.7 (**C**^{5}), 40.5 (**C**^{1}), 48.6 (**C**^{c}), 49.4, (d, ^{2}J = 16, PCH$_2$**C**H$_2$), 55.3 (**C**^{a}), 62.1 (d, ^{2}J = 7, P(O**C**H$_2$CH$_3$)$_2$), 62.6 (**C**H), 79.1 (**C**(CH$_3$)$_3$), 156.2 (**C**O), 167.6, 168.6 (**C**=**C**), 174.6, 180.6, 182.2 (**C**O). ^{31}P NMR (162 MHZ, $CDCl_3$) δ 27.24. MS (ES$^+$) *m/z* 545.0 [M+H]$^+$; $C_{24}H_{42}N_4O_8P$ requires 545.2740; found 545.2745.

The Boc-group was subsequently hydrolysed in a solution of DCM/TFA (1:1, 2 mL) to give the TFA-salt of the amine (***101.TFA***), which was used directly in the coupling step without further purification. MS (ES$^+$) *m/z* 446.0 [M+H]$^+$.

[NIR-1]

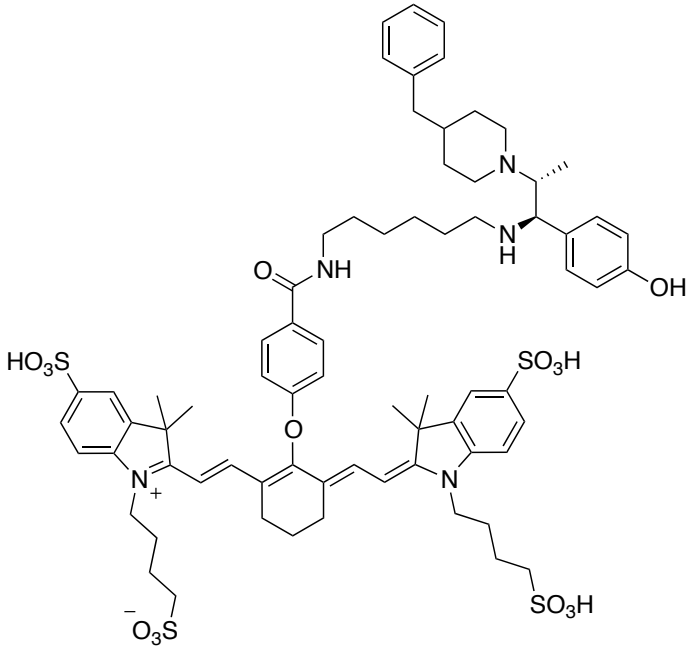

4-(2-((*E*)-2-((*E*)-2-(4-carboxyphenoxy)-3-((*E*)-2-(3,3-dimethyl-5-sulfo-1-(4-sulfobutyl)indolin-2-ylidene)ethylidene)cyclohex-1-en-1-yl)vinyl)-3,3-dimethyl-5-sulfo-3*H*-indol-1-ium-1-yl)butane-1-sulfonate (6.5 mg, 0.0066 mmol) and HATU (3.3 mg, 0.0085 mmol) were dissolved in anhydrous DMF (500 μL) and stirred under argon at room temperature for 10 mins. *N*^{1}-((1*R*,2*R*)-1-(4-(Benzyloxy)phenyl)-2-(4-benzylpiperidin-1-yl)propyl)hexane-1,6-diamine (2.78 mg, 0.0066 mmol) and diisopropylethylamine (2.3 μL, 0.013 mmol) were then added as a solution in anhydrous DMF (300 μL) and the resulting mixture stirred at room temperature overnight. After this period a second addition of the amine

and coupling reagent were added and stirring continued for a further 5 hours. After no further reaction was observed by analytical RP-HPLC, the solvent was removed under reduced pressure and the crude residue purified by preparative RP-HPLC to give a light green solid (1.5 mg, 16%). MS (ES^-) *m/z* 1392.5 $[M-H]^-$; $C_{72}H_{90}N_5O_{15}S_4$ requires 1392.532; found 1392.529. λ_{max} (H_2O) 776 nm. RP-HPLC: t_R = 18.3 mins [2-40% MeCN in triethylammonium acetate buffer (25 mM) over 20 mins].

[NIR-2]

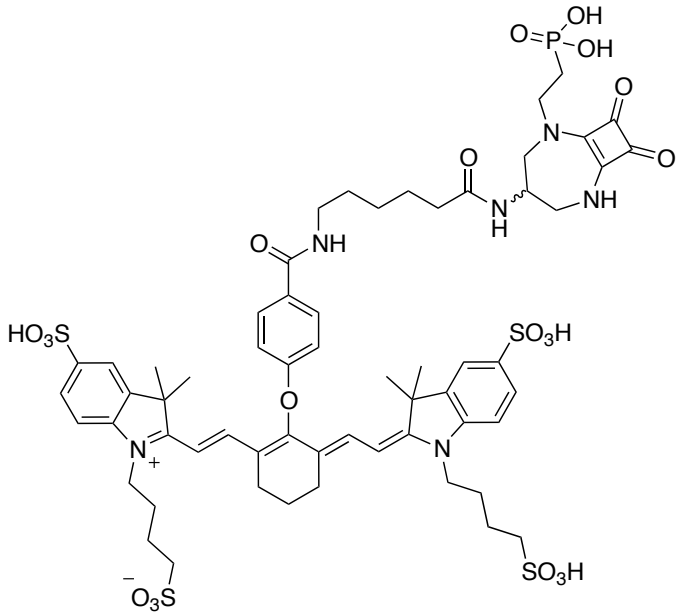

4-(2-((*E*)-2-((*E*)-2-(4-carboxyphenoxy)-3-((*E*)-2-(3,3-dimethyl-5-sulfo-1-(4-sulfobutyl)indolin-2-ylidene)ethylidene)cyclohex-1-en-1-yl)vinyl)-3,3-dimethyl-5-sulfo-3*H*-indol-1-ium-1-yl)butane-1-sulfonate (8.2 mg, 0.0083 mmol) and HATU (4.1 mg, 0.011 mmol) were dissolved in anhydrous DMF (600 μL) and stirred under argon at room temperature for 10 mins. The TFA salt of the amine, ***101.TFA*** (4.6 mg, 0.0083 mmol) and diisopropylethylamine (2.9 μL, 0.017 mmol) were then added as a solution in anhydrous DMF (400 μL) and the resulting mixture stirred at room temperature overnight. After this period a second addition of the amine and coupling reagent were added and stirring continued for a further 5 hours. After no further reaction was observed by analytical RP-HPLC, the solvent was removed under reduced pressure and the crude residue

purified by preparative RP-HPLC to give the phosphonate ethyl ester as a light green solid. The phosphonate ethyl ester (1.7 mg, 0.0012 mmol) was dissolved in anhydrous DMF (300 μL) to which bromotrimethylsilane (1.2 μL, 0.009 mmol) was added. The resulting solution was stirred under argon at 60 °C and the reaction monitored by analytical RP-HPLC. Upon completion after 5 hours, the solvent was removed under reduced pressure and the crude residue purified by preparative RP-HPLC to give a green powder (0.65 mg, 6% over two steps). MS (ES^-) *m/z* 1357.3 $[M-H]^-$; $C_{60}H_{74}N_6O_{20}S_4P$ requires 1357.359; found 1357.358. λ_{max} (H_2O) 776 nm. RP-HPLC: t_R = 17.4 mins [2-40% MeCN in triethylammonium acetate buffer (25 mM) over 20 mins].

8.3 References

1. C.-W. Lee, H. Cao, K. Ichiyama and T. M. Rana, *Bioorg. Med. Chem. Lett.*, 2005, **15**, 4243-4246.
2. P. Bakó, T. Novák, K. Ludányi, B. Pete, T. László and G. Keglevich, *Tetrahedron: Asymmetry*, 1999, **10**, 2373-2380.
3. S. Aime, M. Galli, L. Lattuada, P. Morosini, F. Uggeri, D. Parker and R. Kondareddiar, *Contrast Agents Enodowed With High Relaxivity For Use In Magnetic Resonance Imaging (MRI) Which Contain 1, 4, 7, 10-Tetraazacyclodecan-1, 4, 7-Triacetic Acid Chelating Moiety With Polyhydroxylated Substituents,* IPO WO2006002874, 2006.
4. D. A. Moore, *Org. Synth.*, 2008, 2.
5. W. S. Saari, J. E. Schwering, P. A. Lyle, S. J. Smith and E. L. Engelhardt, *J. Med. Chem.*, 1990, **33**, 97-101.
6. W. A. Kinney, M. Abou-Gharbia, D. T. Garrison, J. Schmid, D. M. Kowal, D. R. Bramlett, T. L. Miller, R. P. Tasse, M. M. Zaleska and J. A. Moyer, *J. Med. Chem.*, 1998, **41**, 236-246.
7. D. Parker, L. Laurent and C. Montgomery, *Pyridyl-aza(thio)xanthone sensitizer comprising lanthanide (III) ion complexing compounds, their luminescent lanthanide (III) ion complexes and use thereof as fluorescent labels*, IPO WO 2010/084090 A1, 2010.
8. A. Mishra, S. Gottschalk, J. Engelmann and D. Parker, *Chem. Sci.*, 2012, **3**, 131-135.
9. S. M. Vibhute, J. Engelmann, T. Verbic, M. E. Maier, N. K. Logothetis and G. Angelovski, *Org. Biomol. Chem.*, 2013, **11**, 1294-1305.
10. A. Mishra, R. Mishra, S. Gottschalk, R. Pal, N. Sim, J. Engelmann, M. Goldberg and D. Parker, *ACS Chem. Neurosci.*, 2013, **5**, 128-137.
11. A. Eisenführ, P. S. Arora, G. Sengle, L. R. Takaoka, J. S. Nowick and M. Famulok, *Bioorg. Med. Chem.*, 2003, **11**, 235-249.
12. A. S. Craig, I. M. Helps, K. J. Jankowski, D. Parker, N. R. A. Beeley, B. A. Boyce, M. A. W. Eaton, A. T. Millican, K. Millar, A. Phipps, S. K. Rhind, A. Harrison and C. Walker, *J. Chem. Soc. Chem. Commun.*, 1989, 794-796.
13. M. Delbianco, V. Sadovnikova, E. Bourrier, G. Mathis, L. Lamarque, J. M. Zwier and D. Parker, *Angew. Chem.*, 2014, Accepted.
14. S. J. Butler, L. Lamarque, R. Pal and D. Parker, *Chem. Sci.*, 2014, **5**, 1750-1756.
15. M. Lopalco, E. N. Koini, J. K. Cho and M. Bradley, *Org. Biomol. Chem.*, 2009, **7**, 856-859.
16. R. B. Mujumdar, L. A. Ernst, S. R. Mujumdar, C. J. Lewis and A. S. Waggoner, *Bioconjugate Chem.*, 1993, **4**, 105-111.
17. G. A. Reynolds and K. H. Drexhage, *J. Org. Chem.*, 1977, **42**, 885-888.
18. S. A. Hilderbrand, K. A. Kelly, R. Weissleder and C.-H. Tung, *Bioconjugate Chem.*, 2005, **16**, 1275-1281.
19. S. Lou and G. C. Fu, *J. Am. Chem. Soc.*, 2010, **132**, 1264-1266.
20. B. L. Chenard, I. A. Shalaby, B. K. Koe, R. T. Ronau, T. W. Butler, M. A. Prochniak, A. W. Schmidt and C. B. Fox, *J. Med. Chem.*, 1991, **34**, 3085-3090.

21. P. Marchand, J. Becerril-Ortega, L. Mony, C. Bouteiller, P. Paoletti, O. Nicole, L. Barré, A. Buisson and C. Perrio, *Bioconjugate Chem.*, 2011, **23**, 21-26.

Appendix

Appendix. List of Key Compounds

1. NMDA Receptor-Targeted MR Contrast Agents

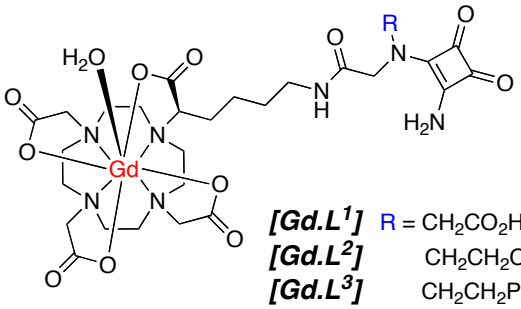

[Gd.L[1]] R = CH_2CO_2H
[Gd.L[2]] $CH_2CH_2CO_2H$
[Gd.L[3]] $CH_2CH_2PO_3H_2$
[Gd.L[4]] $CH_2CH_2CH_2PO_3H_2$

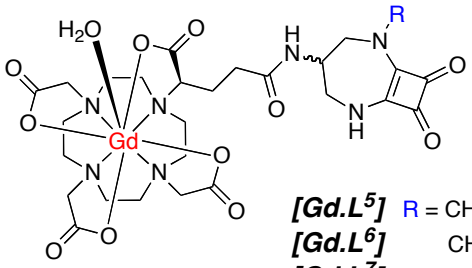

[Gd.L[5]] R = CH_2CO_2H
[Gd.L[6]] $CH_2CH_2CO_2H$
[Gd.L[7]] $CH_2CH_2PO_3H_2$
[Gd.L[8]] $CH_2CH_2CH_2PO_3H_2$

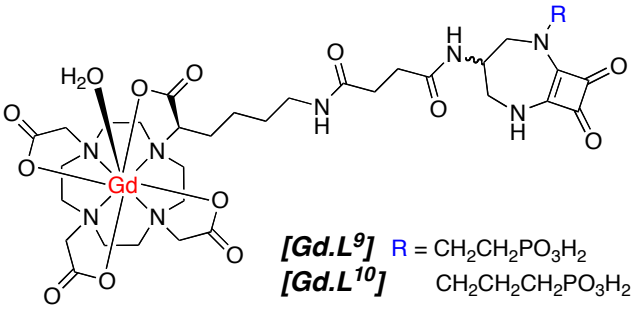

[Gd.L[9]] R = $CH_2CH_2PO_3H_2$
[Gd.L[10]] $CH_2CH_2CH_2PO_3H_2$

2. NMDA Receptor-Targeted Optical Imaging Probes

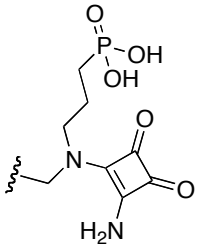

[Gd.L[11]]

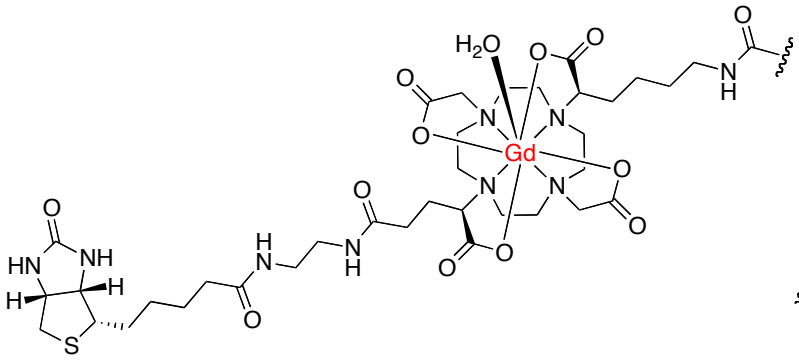

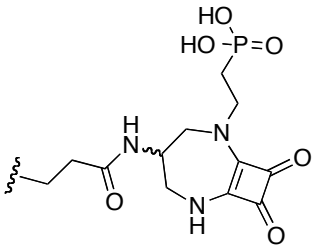

[Gd.L[12]]

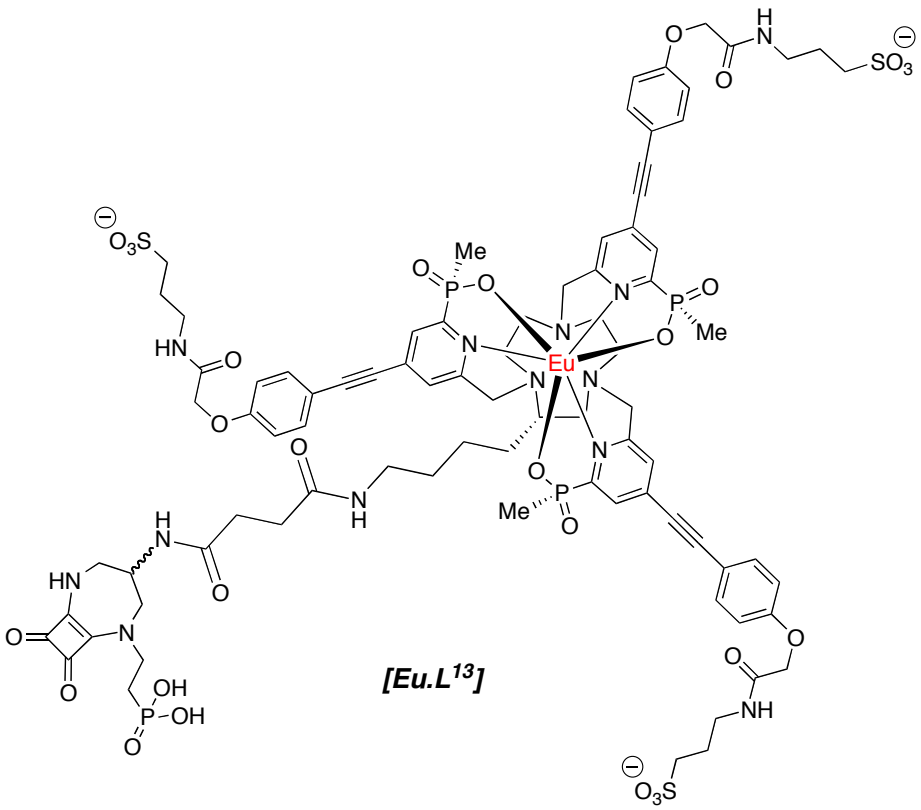

[Eu.L[13]]

3. NMDA Receptor-Targeted Photoacoustic Imaging Agents

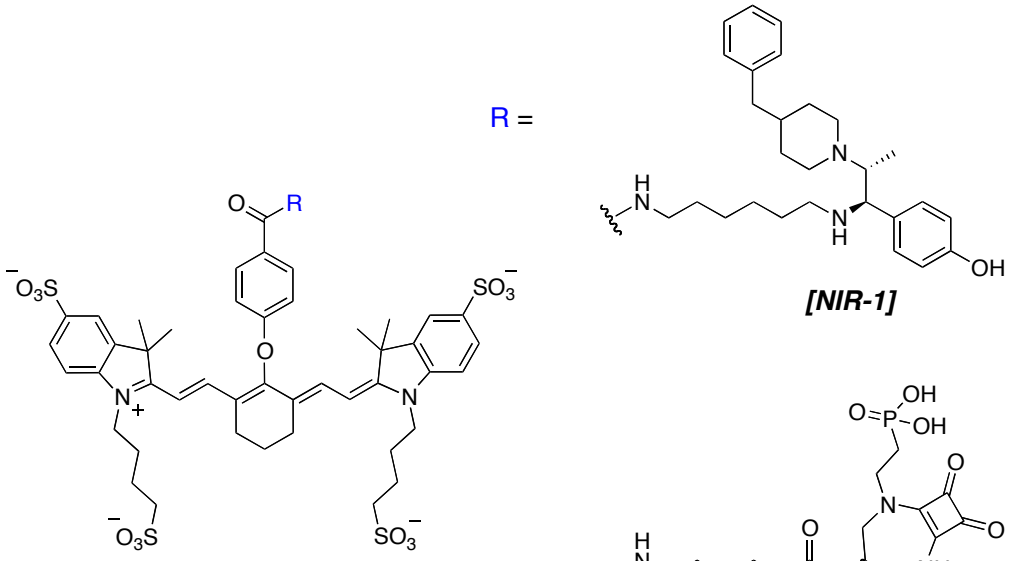

[NIR-1]

[NIR-2]